PROCEEDINGS OF THE

26th International Symposium on Analytical and Environmental Problems

Szeged, Hungary

November 23-24, 2020

University of Szeged

Edited by:
Tünde Alapi
Róbert Berkecz
István Ilisz

Publisher:
University of Szeged, H-6720 Szeged, Dugonics tér 13, Hungary

ISBN 978-963-306-771-0

2020.
Szeged, Hungary

The 26th International Symposium on Analytical and Environmental Problems

Organized by:
SZAB Kémiai Szakbizottság Analitikai és Környezetvédelmi Munkabizottsága

Supporting Organizations
Institute of Pharmaceutical Analysis, University of Szeged
Department of Inorganic and Analytical Chemistry, University of Szeged

Symposium Chairman:
István Ilisz, DSc

Honorary Chairman:
Zoltán Galbács, PhD

Organizing Committee:
István Ilisz, DSc
professor of chemistry
University of Szeged, Institute of Pharmaceutical Analysis
Tünde Alapi, PhD
assistant professor
University of Szeged, Department of Inorganic and Analytical Chemistry
Róbert Berkecz, PhD
assistant professor
University of Szeged, Institute of Pharmaceutical Analysis

Scientific Committee:
István Ilisz, DSc
Tünde Alapi, PhD
Róbert Berkecz, PhD
Daniela Sojic Merkulov, PhD
associate professor
University of Novi Sad, Faculty of Sciences, Department of Chemistry, Biochemistry and Environmental Protection

Lecture Proceedings

EMISSIVE Zn(II) METALLOMESOGEN BASED ON TRIDENTATE TERPYRIDINE LIGAND

Adelina A. Andelescu[1], Benoît Heinrich[2], Emilie Voirin[2], Evelyn Popa[1], Massimo La Deda[3], Giuseppe Di Maio[3], Otilia Costişor[1], Bertrand Donnio[2], Elisabeta I. Szerb[1,*]

[1]Institutul de Chimie "Coriolan Drăgulescu", B-dul. Mihai Viteazu nr. 24, 300223-Timişoara, România.
szella73@gmail.com
[2]Institut de Physique et Chimie des Matériaux de Strasbourg, 23 Rue du Loess, Strasbourg, 67034, France
[3]Dipartimento di Chimica e Tecnologie Chimiche, Universita della Calabria, via P. Bucci, Cubo 14/C, 87036 Arcavacata di Rende, Italy

Abstract
A low temperature liquid crystal based on luminescent terpyridine Zn(II) complex is presented. The induction of the mesomorphic properties was achieved using a lipophilic gallate unit as ancillary ligands. The mesomorphic properties were investigated by polarised optical microscopy (POM), differential scanning calorimetry (DSC), thermogravimetric analysis (TA) and X-ray scattering (SWAXS) of bulk materials, while the optical properties of the complex were investigated in solution and in condensed liquid crystalline states.

Introduction
Metallomesogens (metal-containing liquid crystals) combine the supramolecular ordering of liquid crystals with the properties imparted by the metal centre (magnetic, electrical, optical and electro-optical),**[1]** thus leading to advanced materials with potential applications in optoelectronics.**[2,3]** Due to their excellent light emitting efficiencies and high thermal stabilities, Zn(II) complexes are of particularly high interest.**[4]** On this background, we report the synthesis and characterization of a terpyridine (tpy) Zn(II) liquid crystal.

Experimental
The structural characterization of the compounds was realized by employing a variety of analytical and spectroscopic methods: elemental analysis, Nuclear Magnetic Resonance - NMR, Fourier-Transform Infrared - FT-IR, and Ultraviolet–visible - UV-Vis spectroscopies. The thermal behaviour and liquid-crystalline properties were investigated by polarised optical microscopy (POM), differential scanning calorimetry (DSC), thermogravimetric analysis (TGA) and small- and wide-angle X-ray scattering (SWAXS). Photophysical investigations were carried out in different solvents and condensed states.

Results and discussion
The ligand **L_tpy [5]** and precursor **AgGal [6]** were obtained following reported procedures. The reaction of **L_tpy** with $ZnCl_2$ afforded the neutral complex **Zn_1**, whereas the final complex **Zn_2** was obtained by the displacement of the chlorine ligands with AgGal lipophilic unit,**[7]** as described in Scheme 1.

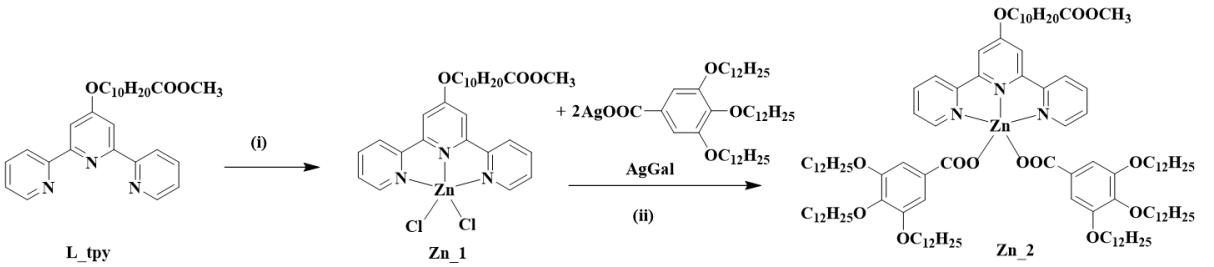

Scheme 1. Synthesis of Zn(II) complexes: (i) $ZnCl_2$, MeOH/$CHCl_3$, r. t., 1.5 hours; (ii) $CHCl_3$, r. t., 2 hours.

The neutral pentacoordinated complex **Zn_2** self-assembles in a columnar hexagonal phase already at room temperature, as determined by POM, DSC and SWAXS analysis.
The absorption and emission properties were studied in dichloromethane solutions. Both complexes resulted to be fluorescent, with an emission quantum yield of 6.4 % for **Zn_1** and 24.5 % for **Zn_2**. Also, both complexes presented emission in condensed state at room temperature.
The luminescent properties of the liquid crystalline **Zn_2** were also measured in condensed states at various temperatures and found to be kept in the liquid crystalline states, but lost in the isotropic states due to the increase of the vibrational modes by increasing the temperature.

Conclusion

A luminescent liquid crystal based on Zn(II) metal centre was obtained by a straightforward synthetic approach, using a lipophilic gallate derivative as ancillary ligand. The complex was found to be luminescent in solution and in condensed states. In the mesophase, **Zn_2** emits showing a broad band whose maximum depends on the temperature.

Acknowledgements

M. LD and G. DM acknowledge the help granted by Regione Calabria (POR Calabria FESR 2014/2020-Azione 1.2.2) through the MERAVIGLIE project. B.D. and B.H. thank the CNRS and University of Strasbourg for support. A.A.A. P.E, E.I.S. and O.C. acknowledge the Romanian Academy, Program 4. A.A.A. is grateful for an “Ion Heliade Radulescu” mobility scholarship.

References

[1] B. Donnio, D.W. Bruce, Struct. Bonding 95 (1999) 193.
[2] X. Wu, G. Xie, C.P. Cabry, X. Xu, S.J. Cowling, D.W. Bruce, W. Zhu, E. Baranoff, Y. Wang, J. Mater. Chem. C 6 (2018) 3298.
[3] X. Wu, M. Zhu, D.W. Bruce, W. Zhu, Y. Wang, J. Mater. Chem. C 6 (2018) 9848.
[4] A. Crispini, M. Ghedini, D. Pucci, Beilstein J. Org. Chem. 5 (2009) 54.
[5] U.S. Schubert, S. Schmatloch, A. Precup, Des. Monomers Polym. 5 (2002) 211.
[6] E. I. Szerb, D. Pucci, A. Crispini, M. La Deda, Mol. Cryst. Liq. Cryst. 573 (2013) 34.
[7] A.A. Andelescu, B. Heinrich, M.A. Spirache, E. Voirin, M. La Deda, G. Di Maio, E.I. Szerb, B. Donnio, O. Costisor, Chem. Eur. J. 26 (2020) 4850.

HIGH-PERFORMANCE LIQUID CHROMATOGRAPHIC ENANTIOSEPARATION OF SOME AMINO CMOPOUNDS WITH PHARMACEUTICAL RELEVANCE ON ION-EXCHANGER-BASED CHIRAL STATIONARY PHASES

Attila Bajtai[1], Dániel Tanács[1], Enikő Forró[2], Ferenc Fülöp[2], Wolfgang Lindner[3], Antal Péter[1], István Ilisz[1]

[1]Institute of Pharmaceutical Analysis, Interdisciplinary Excellence Centre, University of Szeged, H-6720 Szeged, Somogyi utca 4, Hungary
[2]Institute of Pharmaceutical Chemistry, Interdisciplinary Excellence Centre, University of Szeged, H-6720 Szeged, Eötvös u. 6, Hungary
[3]Department of Analytical Chemistry, University of Vienna, Währingerstrasse 38, 1090 Vienna, Austria
e-mail: bajtai@pharm.u-szeged.hu

New, pharmacologically interesting chiral amino compounds, namely, tetrahydroisoquinoline (THIQ)- and tetrahydro-*β*-carboline (TH*β*C)-core containing alkaloids ([1, 2], Figure 1) have been separated by high-performance liquid chromatography on novel strong cation exchangers and *Cinchona* alkaloid-based zwitterionic (ZWIX(+)™ and ZWIX(−)™) ion-exchanger stationary phases. Separation of the stereoisomers was optimized by investigating the effects of the composition of the bulk solvent, the impact of the counter- and co-ion concentration and the influence of the temperature on the chromatographic behaviour. In addition, the relationship between the compound's structure and the chromatographic parameters were also investigated. Experiments were performed in the temperature range 10–50 °C. Thermodynamic parameters were calculated from plots of lnα versus 1/T. The separations were generally enthalpy-controlled, but entropy-controlled separation was also observed. The enantiomer elution order was determined in all cases and most of the time was observed to be opposite on the ZWIX(+)™ and ZWIX(−)™ columns. Our results contribute to a better understanding of the enantiorecognition mechanism of chiral bases with chiral zwitterionic and cation-exchanger selectors.

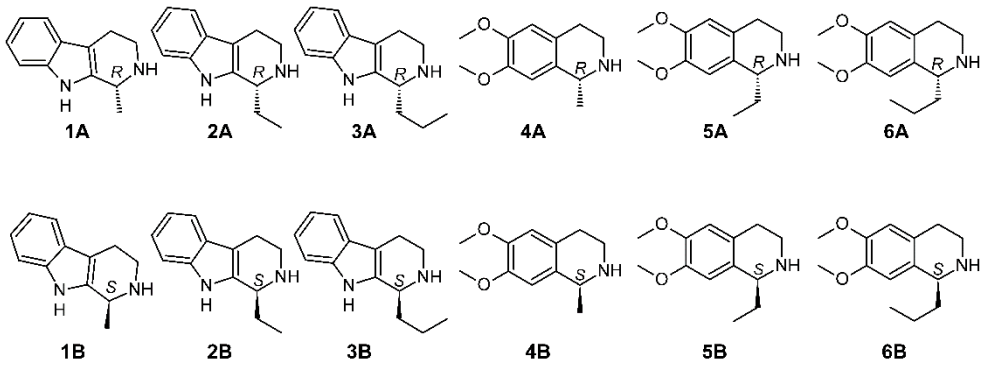

Figure 1. Structure of analytes

Acknowledgements

SUPPORTED BY THE ÚNKP-20-3 - NEW NATIONAL EXCELLENCE PROGRAM OF THE MINISTRY FOR INNOVATION AND TECHNOLOGY FROM THE SOURCE OF THE NATIONAL RESEARCH, DEVELOPMENT AND INNOVATION FUND.

References

[1] B. Kovács; R. Megyesi; E. Forró; F. Fülöp *Tetrahedron: Asymmetry* 2017, 28, 1829-1833.
[2] B. Kovács; E. Forró; F. Fülöp *Tetrahedron*, 2018, 74, 6873-6877.

RECOGNITION OF RENEWABLE ENERGY AMONG BUSINESS STUDENTS

László Berényi[1], Nikolett Deutsch[2]

[1]Institute of Management Science, University of Miskolc, H-3515 Miskolc-Egyetemváros, Hungary
[2]Department of Strategy and Project Management, Corvinus Business School, Corvinus University of Budapest, No. 8. Fővám Square, H-1093 Budapest, Hungary
e-mail: szvblaci@uni-miskolc.hu

Abstract
Using renewable energy sources is in the mainstream of environmental protection, including climate change. Non-professional opinions in the field are essential to explore for enhancing the acceptance and utilization level. This paper shows the evaluation of Hungarian business students (n=632) about renewable energy sources and their utilization. The results show that the students feel that the use of renewable energy lags behind the EU level, but there is a trust in convergence in the medium term.

Introduction
Energy dependence is a complex social and technical challenge of the present age [1]. Forcing the use of renewable energy sources is beneficial to climate, but technical problems and availability must be managed [2], including the local access to them [3]. Moreover, there are human aspects to consider. The lack of knowledge and social acceptance [4] may deflect the use of technically right solutions.
EU has embraced the topic that gives legal justification for development and research efforts. The renewable energy directives [5-6] require the EU to fulfill at least 20% of its total energy needs with renewables by 2020 (at least 10% for each member country) and 32% for 2030. The statistics [7] show a remarkable increase in renewable energy use, but the target vales seem to be ambitious. In the case of Hungary, a decline can be detected (Figure 1). Among others, this result draws attention to comprehensive research on renewable energy use. The problem goes far beyond one study; our paper aims to contribute to a better understanding of the possible development directions.

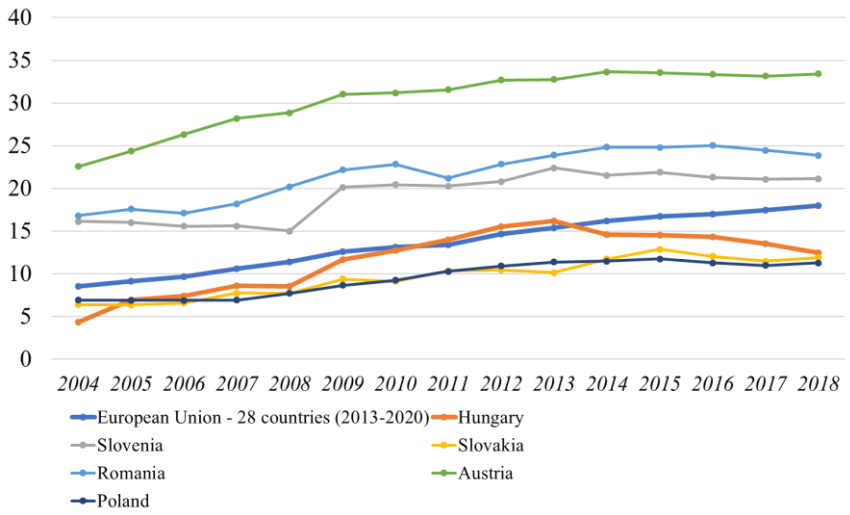

Figure 1. Share of renewable energy in gross final energy consumption in some countries
Source: based on [7]

Experimental

Data collection is performed by a voluntary online survey among higher education students between 2018 and 2019. The research sample includes 563 respondents who are studying business. 61.6% of them are females, and 38.4% are males. 54.2% of the respondents are studying bachelor or higher vocational students, 45.8% of them are at the master level. There are students without any work experience (38.4%), others with internship experience (20.4%) and employees (41.2%). It is to note that the responses are collected from business students of various Hungarian universities, but the representativeness of the sample structure is not ensured. Despite a large number of responses, the generalization of the results and conclusions are limited.

The presented results are based on two items of the survey. It includes a list of some energy sources (Figure 2) and asks to mark whether the respondents consider it as renewable or not. This part of the survey allows us to check the knowledge level and non-professional opinions about the perception of renewable characteristics. Besides, there are four questions formulated with a 5-point scale evaluation about the present and future position of renewable energies:

- Q1: How do you think we currently use renewable energy sources compared to other European countries? (1: much less, 5: in a much greater extent);
- Q2: Do you think people would pay more for energy if it were definitely from a 'green' source? (1: surely not, 5: surely yes);
- Q3: How much do you agree with the statement that people are increasingly striving to save energy in their everyday lives? (1: not at all, 5: fully agree);
- Q4: Do you think that in 10-15 years, we will use renewable energy sources compared to other European countries? (1: much less, 5: in a much greater extent).

The mean values of the responses represent the results of the evaluation.

Results and discussion

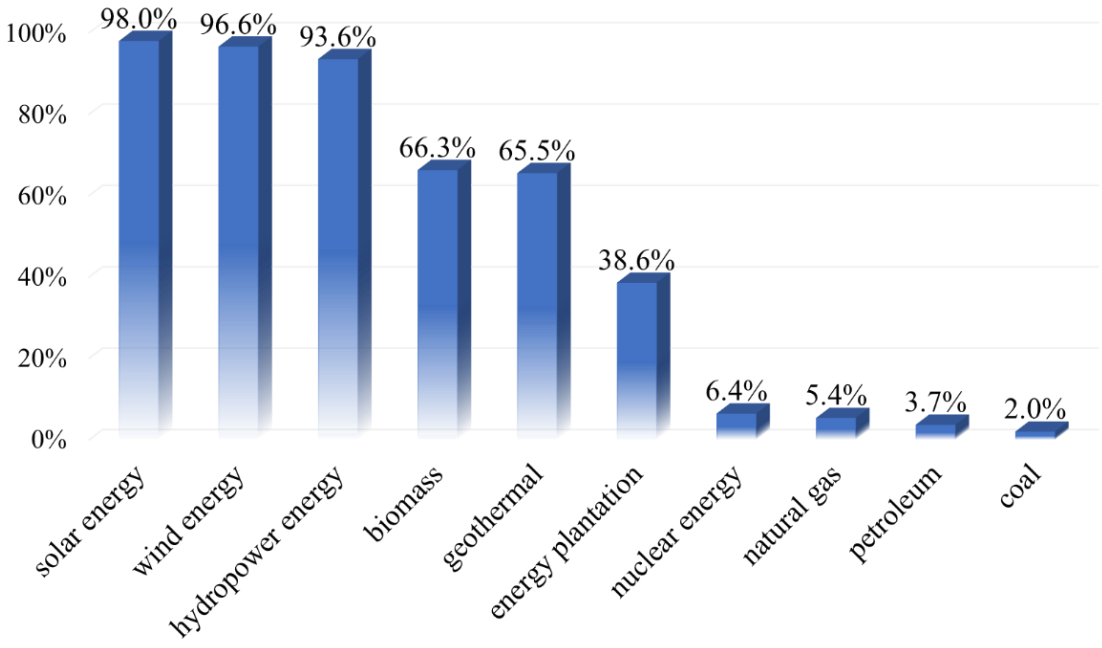

Figure 2: Evaluation of renewable characteristic of energy sources (marked by % of the sample)

The items of energy sources include both evident and questionable items. Compared to the professional opinion about the renewable characteristic, the results show some differences (Figure 2). Nuclear energy (6.4%) and natural gas (5.4%) are considered renewable by a small but remarkable minority. The results of solar, wind, and hydropower energy are in line with professional opinions. Biomass (66.3%) and geothermal (65.5%) energy sources are less

considered renewable. Energy plantations (38.6%) represent a surprisingly low share, especially that about half of the respondents marked it who marked biomass.
According to the evaluation of the present and future of renewable energy, ANOVA tests were conducted in order to check the grouping effect of gender, level of studies, and work experience. The analysis found significant effects in 2 of 12 cases (Table 1) by the non-parametric Kruskal-Wallis test. Various statistical tests were run for finding clustering the results to draw up characteristic patterns of opinions and to develop targeted strategies, but the outcomes were not significant or interpretable.

Table 1: Significant differences by grouping factors

Item	Factor	Mean values	Kruskal-Wallis H	d_f	sig.
How much do you agree with the statement that people are increasingly striving to save energy in their everyday lives?	Level of Studies	$x_{bachelor}$ =3.10 x_{master}=3.34	8.274	1	.004
How do you think we currently use renewable energy sources compared to other European countries?	Work experience	x_{none}=2.03 $x_{employee}$=1.84 $x_{internship}$=2.02	6.709	2	.035

Other results are presented for the entire sample (Figure 3). The mean values of the responses suggest that the students are critical to present, but hey have trust in the future. They think that the use of renewable energy sources will reach the EU level that in 10-15 years. Paying for greener energy does not seem to be an acceptable way; saving energy received a higher mean value.

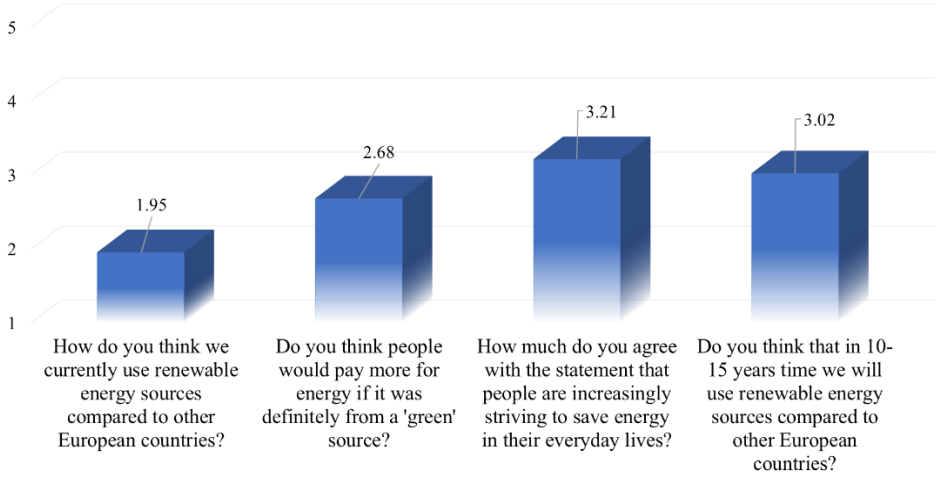

Figure 3: Mean values of evaluation (5-point scale)

Consequently, it is also worth examining the distribution of the evaluations due to the medium level of mean values (Table 2 and Figure 4). The present use of renewables compared to the EU is evaluated rather worse by 78.7% of the respondents, while 2.7% think that Hungary has a better performance. According to the future, the ratio of skeptics (evaluated 1 or 2) is 26.8%, while there are 28.9% optimists in the sample.

Table 2: Distribution of evaluations on the 5-point scale (% of the sample)

	1	2	3	4	5
How do you think we currently use renewable energy sources compared to other European countries?	30.17	48.55	18.07	2.60	0.61
Do you think people would pay more for energy if it were definitely from a 'green' source?	11.79	34.76	29.71	21.29	2.45
How much do you agree with the statement that people are increasingly striving to save energy in their everyday lives?	5.36	17.76	34.61	35.07	7.20
Do you think that in 10-15 years, we will use renewable energy sources compared to other European countries?	5.51	21.29	44.26	23.74	5.21

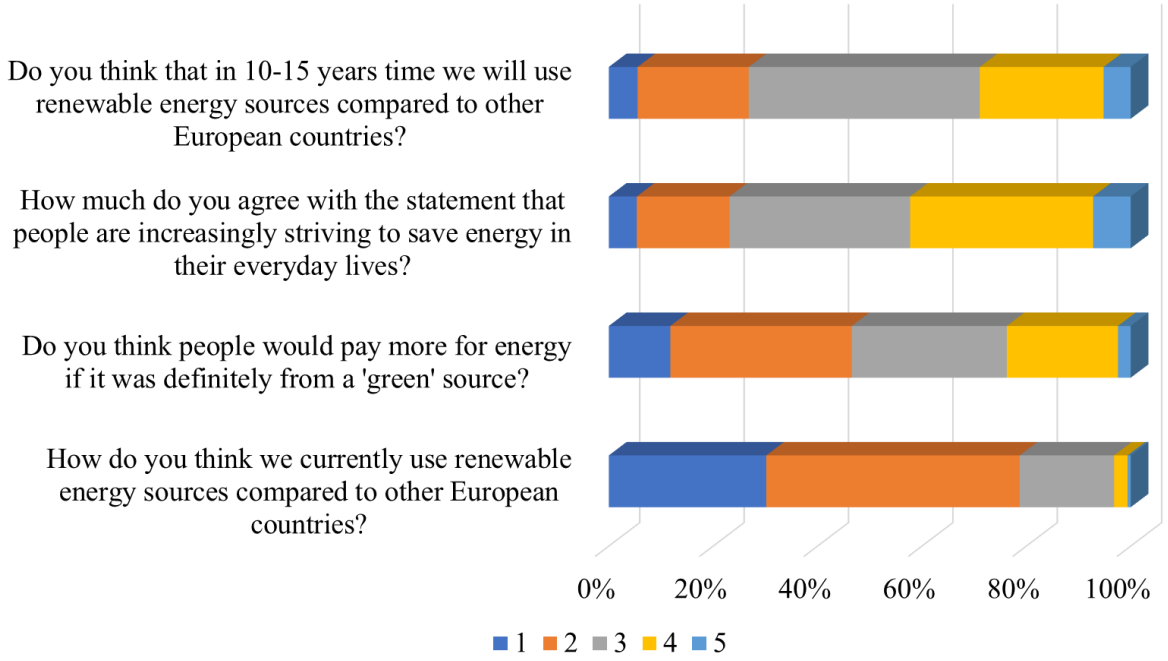

Figure 4: Distribution of evaluations on the 5-point scale (% of the sample)

Those who think that people would pay more for green energy represent 23.7% of the sample, while 46.6% consider still the opposite. At the same time, 42.3% rather trust that people will strive to save energy. This suggests that 'saving' covers both energy and cost-saving by the students.

The correlation between the responses (Table 3) shows weak and medium level but significant results. The highest value (0.372) is found between the present and the future use of renewable energy sources. Future use significantly correlates with strive to save energy (0.206) and willingness to pay more for green energy with strive to save it (0.217).

Table 3: Spearman's correlation between the questions

		Q1	Q2	Q3	Q4
Q1 (present use)	*Corr. Coef.*		.113**	.121**	.372**
	Sig. (2-tailed)		0.004	0.002	0.000
Q2 (pay more for green energy)	*Corr. Coef.*	.113**		.217**	.141**
	Sig. (2-tailed)	0.004		0.000	0.000
Q3 (strive to save energy)	*Corr. Coef.*	.121**	.217**		.206**
	Sig. (2-tailed)	0.002	0.000		0.000
Q4 (future use)	*Corr. Coef.*	.372**	.141**	.206**	
	Sig. (2-tailed)	0.000	0.000	0.000	
**: correlation is significant at the 0.01 level (2-tailed)					

Conclusion

Professional and non-professional (student) opinions are not entirely overlapped. While solar, wind, and hydropower energy are considered renewable by most students, geothermal energy, biomass, and especially energy plantation are already in the background. A conclusion for teaching and education is given by the results that a higher emphasis should be given to the technical issues of renewable energy.

The positive approach to the future improvement in using renewable energies and convergence to the EU level is encouraging, but an essential experience of the survey is that progress is rather supported by energy savings than paying more for greening. Since business students are expected to become company decision-makers in the near future, consequently, their opinions and attitudes are prognostic.

References

[1] P. Högselius, A. Kaijser, Energy dependence in historical perspective: The geopolitics of smaller nations. Energy Policy 127 (2019) 438-444.

[2] V.V. Quaschning, Renewable Energy and Climate Change, 2nd edition, Wiley, Hoboken, 2019, pp. 351.

[3] L. Berényi, Z. Birkner, N. Deutsch, A Multidimensional Evaluation of Renewable and Nuclear Energy among Higher Education Students, Sustainability, 12, 2020, 1449.

[4] M. Wolsink, Contested environmental policy infrastructure: Socio-political acceptance of renewable energy, water, and waste facilities. Environmental Impact Assessment Review 30 (2010) 302-311.

[5] Directive 2009/28/EC of the European Parliament and of the Council of 23 April 2009 on the promotion of the use of energy from renewable sources and amending and subsequently repealing Directives 2001/77/EC and 2003/30/EC

[6] Directive (EU) 2018/2001 of the European Parliament and of The Council of 11 December 2018 on the promotion of the use of energy from renewable sources

[7] Share of renewable energy in gross final energy consumption (T2020_31). Available online: https://ec.europa.eu/eurostat/databrowser/view/t2020_31/default/table?lang=en (accessed on 10 07 2020).

AMMONIA TRANSPORT ACCIDENT EXPOSURE ANALYSIS

Jovana Bondžić[1], Maja Petrović[1]

[1]*Department of Environmental Engineering and Occupational Safety and Health, Faculty of Technical Sciences, University of Novi Sad, Trg Dositeja Obradovića 6, Novi Sad, Serbia*
e-mail: jovanasimic@uns.ac.rs

Abstract
Anhydrous ammonia proved its efficiency and has been used extensively in the food and processing industry as a refrigerant. Between production and utilization locations it is necessary to organize transport of this substance. Due to its physicochemical properties, there is a possibility for the endangering population and environment in urban areas if the tank traffic accident occurs during the transport. Therefore, this research analyses exposure to ammonia transport accidents through the use of two software applications.

Introduction
Ammonia is, under normal conditions, a colorless gas with a pungent odor [1]. It is lighter than air and soluble in water. In industry, ammonia is used in pure form, without water and is called anhydrous ammonia. It can be liquefied under pressure, or at a temperature below its boiling point. Its boiling point, under atmospheric pressure, is -33,3℃. The low boiling point and the ability to absorb a large amount of heat enable the use of ammonia as a refrigerant. As industrial refrigerant ammonia has been used extensively since chlorofluorocarbons evolved as less toxic refrigerants. Still, it is widely used in industrial refrigeration, because of its low cost and high efficiency. Ammonia is toxic with an 8-hour exposure limit of 25 ml/m^3 and a 15-minute exposure limit of 35 ml/m^3 [2]. The flammable limit of ammonia is between 16-27% by volume [3], while the auto-ignition temperature is 651℃.

In the Republic of Serbia, anhydrous ammonia is produced in HIP Azotara Pančevo, and it is transported to the locations of use by road in tanks. Considering the physicochemical characteristics of ammonia, in the case of an accidental release during transport in populated areas, the human population and environment could be exposed to the toxic and flammable impact of ammonia. In this research, for the exposure analysis of ammonia transport accident, two software ALOHA and Quantum GIS (QGIS) were used. A case study was developed for ammonia release from a tanker truck in the urban area of Novi Sad for three possible hazard scenarios.

Experimental
The quantity of ammonia transported criss-cross the Republic of Serbia differs according to demands, therefore, there is an expectancy of a small tank with ammonia to be driven through the urban area of Novi Sad. Considering the probability of traffic accidents during the transport of ammonia, a location with a high traffic frequency was chosen for the experimental analysis. Based on the ammonia properties, three possible scenarios were identified: dispersion of toxic vapor cloud, ignition of vapor cloud and explosion of the vapor cloud. For the determination of dispersion for each scenario, ALOHA (Areal Locations of Hazardous Atmospheres) software, as a hazard modeling program, was used.

ALOHA is a computer program designed to model chemical releases for emergency responders and planners [4]. It allows user to enter details about a real or potential chemical release, and then it will generate threat zone estimates for various types of hazards such as toxic release

dispersion, flammable area of the gas cloud, vapor cloud explosion, BLEVE (Boiling Liquid Expanding Vapor Explosion), jet fire, etc. For the purpose of this research, hazard scenarios were modeled in ALOHA based on input parameters' values listed in Table 1.

Table 1. Input parameters' values for hazard model in ALOHA software

Location, time		Tank parameters		Atmospheric parameters	
Latitude:	45° 14.873' N	Diameter:	1,4 m	Wind speed:	1,1 m/s
Longitude:	19° 50.189' E	Length:	3,6 m	Wind direction:	S
Date:	9.11.2020.	Orientation:	horizontal	Cloud cover:	70 %
Time:	2 p.m.	Mass in the tank:	2500 kg	Air Temperature:	13 °C
		Rupture diameter:	5 cm	Stability class:	E
				Humidity:	86%

The results of the simulation experiments were obtained in the form of graphs showing the threat zones. Threat zones represent the area within which the ground-level exposure exceeds the user-specified level of concern at some time after the beginning of a release [5]. ALOHA will display up to three threat zones, yellow, orange and red, overlaid on a single picture. Using ALOHA's KML export feature, outputs were imported into the Quantum GIS project in order to analyze the overall spatial context of the accident.

Quantum GIS is a user-friendly and open-source Geographic Information System that enables viewing, editing, and analysis of geospatial data. It supports numerous vector, raster, and database formats and functionalities [6]. It is suitable for representing objects from the real system on the spatial model.

Results and discussion

Two of three possible hazard scenarios simulated within the experiment gave results that exceed user-specified levels of concern (LOC). Level of Concern is a threshold value of a hazardous impact (toxicity, flammability, or overpressure) above which a threat to people or property may exist.

For the Toxic Area of Vapor Cloud scenario, Acute Exposure guideline Level (AEGL) was used as a LOC. In Figure 1a, it can be seen that all three LOCs were exceeded in this scenario. In the red zone, it is predicted that the population exposed to more than 1 000 ppm concentration of ammonia could experience life-threatening health effects or death. In the orange zone, people could experience irreversible or other serious, long-lasting adverse health effects or an impaired ability to escape. In the yellow zone, the effects are not disabling and are temporary.

Flammable Area of Vapor Cloud scenario uses 60% of LEL (Lower Explosive Limit) as a LOC for a red zone and 10% of LEL as a LOC for a yellow zone. Both concentrations were exceeded as it is shown in Figure 1b. If there is an ignition source, fire hazard could occur between 90 000 and 15 000 ppm ammonia concentration in the air.

Comparing two graphs it can be noticed that far more area will be endangered in the case of toxic than flammable exposure. In order to analyze the exposed population and property both graphs were imported into the QGIS project (Figure 2). In addition, OpeenStreet Map was used as a base map layer in the project. By visual examination of both scenarios represented within the spatial model, it can be concluded that significant urban areas could be exposed to the hazard of this type. The most vulnerable objects detected in both exposed zones are primary, secondary

and higher schools because of high frequency of children presented during the whole day. Also, it should be emphasized that a primary school for children with disabilities will be exposed within the red zone of both scenarios.

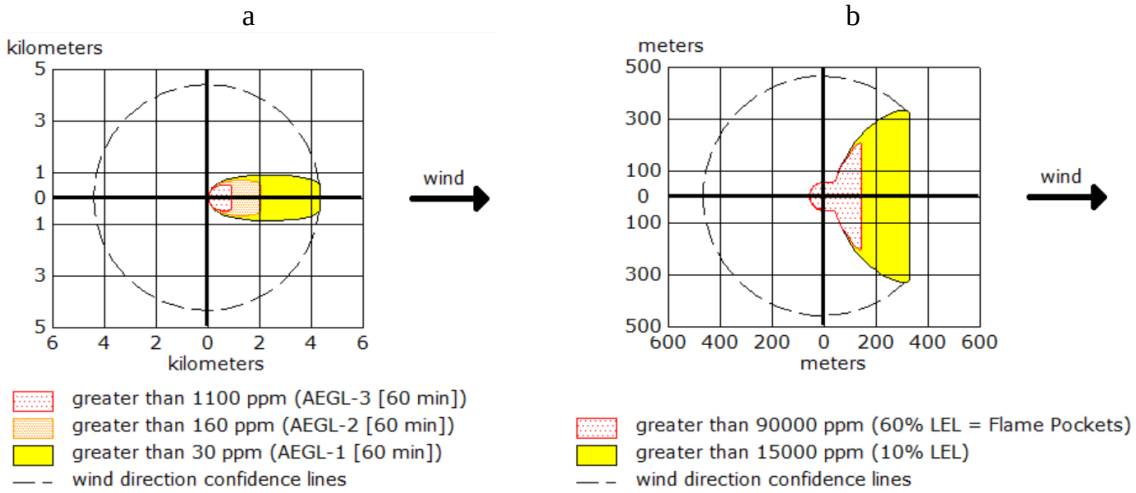

Figure 1. Results obtained by ALOHA software: a – Toxic area; b – Flammable area

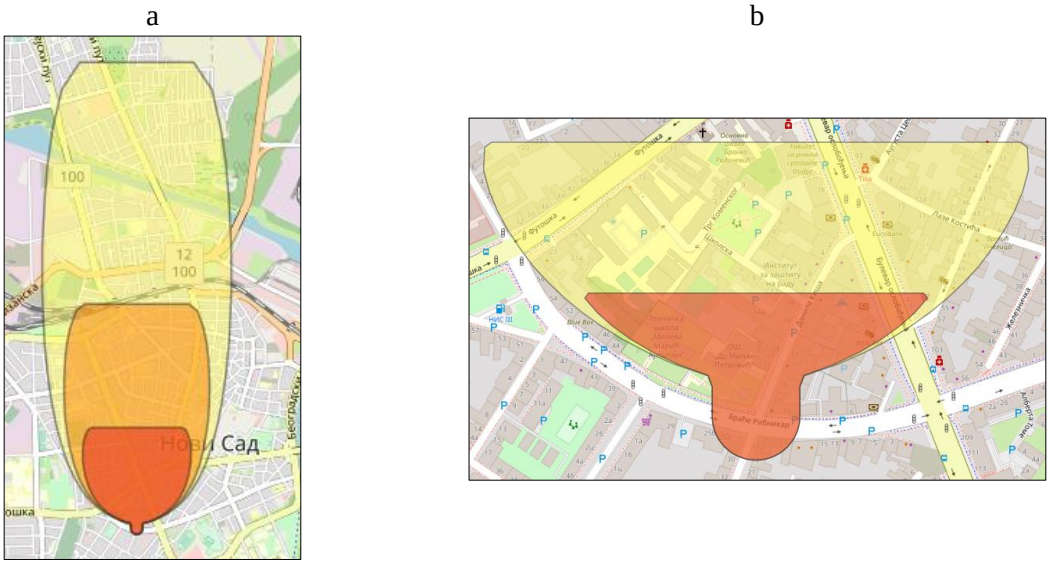

Figure 2. Results imported into QGIS project: a – Toxic area; b – Flammable area

Conclusion

The described method for the analysis of potential accidental situations during the transport of toxic substances enables responders to generate necessary information almost immediately and to conduct appropriate reactions promptly. Therefore, it is extremely important to analyze hazards that could occur in the populated areas in advance, to be as prepared as possible for the unwanted consequences to people and the environment.

References

[1] Janković Z., 2016. Razvoj modela za proračun rizika u logističkim sistemima opasnih materija. PhD thesis. Faculty of Technical Sciences, University of Novi Sad

[2] Eckhoff R., 2016. Explosion Hazards in the Process Industries, Chapter Three - Boiling Liquid Expanding Vapor Explosions (BLEVEs), University of Bergen, Norway

[3] HIP Azotara, 2010. MSDS, Available at: http://hip-azotara.rs/wp-content/uploads /2016/10/amonijak-sr.pdf. (Accessed 10th November 2020)
[4] NOAA, 2020. Available at: https://response.restoration.noaa.gov/sites/default/files/aloha.pdf (Accessed 11th November 2020)
[5] QGIS, 2020. Available at: https://qgis.org/en/site/about/index.html (Accessed 12th November 2020)
[6] Jones, R., W. Lehr, D. Simecek-Beatty, R. Michael Reynolds. 2013. ALOHA® (Areal Locations of Hazardous Atmospheres) 5.4.4: Technical Documentation. U. S. Dept. of Commerce, NOAA Technical Memorandum NOS OR&R 43. Seattle, WA: Emergency Response Division, NOAA. 96 pp.

STRUCTURAL AND MAGNETIC PROPERTIES OF THREE 1D COPPER(II) COORDINATION POLYMERS

Ildiko Buta[1*], Peter Lönnecke[2], Evamarie Hey-Hawkins[2], Marius Andruh[3], Otilia Costisor[1]

[1]Romanian Academy ''Coriolan Dragulescu" Institute of Chemistry, 24 Mihai Viteazu Bvd., 300223-Timisoara, Romania
[2]Leipzig University, Faculty of Chemistry and Mineralogy, Institute of Inorganic Chemistry, Johannisallee 29, 04103 Leipzig, Germany
[3]University of Bucharest, Faculty of Chemistry, Inorganic Chemistry Laboratory, 23 Dumbrava Rosie Str, 020464-Bucharest, Romania
e-mail: ildiko_buta@acad-icht.tm.edu.ro

Abstract

The design of coordination polymers is controlled by the nature of the ligands and metal ions involved [1]. The electronic structure, size and stereochemical preference of the metal ion, along with the number and the relative position of the coordinating groups of the ligand, determine the dimensionality and topology of the resulting compounds [2].

Here, we report three coordination polymers, $^{1}_{\infty}[Cu_3L_2(NO_3)]NO_3 \cdot 2MeOH \cdot 2H_2O$ (**1**), $^{1}_{\infty}[Cu_3L_2(N_3)]CH_3COO$ (**2**) and $^{1}_{\infty}[Cu_3L_2(H_2O)](ClO_4)_2$ (**3**), based on the Schiff base H_2L (H_2L = N,N'-bis[(2-hydroxybenzilideneamino)propyl]piperazine). X-ray single-crystal analysis shows that compounds **1** and **2** are isostructural and crystallize in orthorombic system, space group, $P2_12_12_1$, while complex **3** crystallizes in a monoclinic system, space group $P2_1/c$. Compounds **1**-**3** consist of trinuclear complex entities, $[Cu_3L_2]^{2+}$, connected via different bridges, nitrato (**1**), azido (**2**) and phenoxido (**3**), depending on the nature of the counterion. The cryomagnetic measurements showed weak ferro- (**1**) and antiferromagnetic (**2** and **3**) interactions between the copper(II) ions (Figure 1).

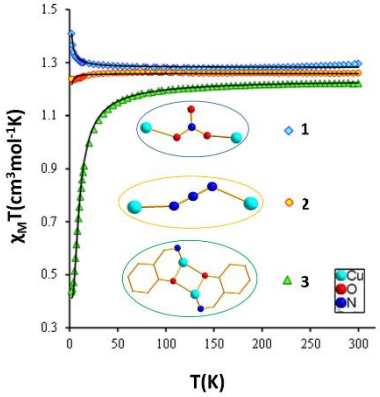

Figure 1. $\chi_M T$ vs T curves for compounds **1**-**3**

Acknowledgements

We thank the Romanian Academy, Institute of Chemistry "Coriolan Dragulescu" (Project 4.1.3) for financial support.

References

[1] F.A.A. Paz, J. Klinowski, S.M.F. Vilela, J.P.C. Tomé, J.A.S. Cavaleiro, J. Rocha, Chem. Soc. Rev. 41 (2012) 1088.
[2] W.L. Leong, J.J. Vittal, Chem. Rev. 111 (2011) 688.

COULD HUMIC SUBSTANCES BE GOOD ANTIOXIDANTS?

A. Csicsor[a], E. Tombácz[b]

[a]Hymato Products Ltd., H-8225 Szentkirályszabadja, Kossuth u 33., Hungary
[b]University of Pannonia, Soós Ernő Water Technology Research and Development Center, H-8800 Zrínyi M. str. 18. Nagykanizsa, Hungary
email: csicsor.attila@gmail.com

Abstract

Humic substances (HS) are natural macromolecules that can be found everywhere (e.g., soils, waters, air, peat, coal deposits) in the environment. Humic substances (HS) are natural organic colloids built up randomly from the decay products of plant originated biomass in humification process. [1]

In today's modern world, processed foods, medicines, cosmetics, and electro smog produce so much free radical in living organisms that antioxidants taken from the outside will become increasingly important to neutralize this increased load.

Antioxidants are substances that inhibit the oxidation in a broader sense oxidation retardants. The most important physiological role of antioxidant substances is to deactivate the free radicals continuously formed in the Szent-Györgyi-Krebs cycle, and to counteract the radicals with different oxidizing properties that enter the body from the outside.

There are well known antioxidants like vitamin-C; vitamin-A; flavonoids; resveratrol, ect. These antioxidants like flavonoid and the resveratrol are formed in plants. The reason plants produce these materials is to protect themselves for the effect of the UV radiation. When the UV light beam hits the plant it produces free radicals. By producing antioxidant molecules the plants can protect themself from this effect [2].The reason we think that the humic substances could be great antioxidant is this. Because they are formed from plant residues. So these materials are like the essence of the decomposed plant. [3]. Humic acid also has antioxidant properties via phenolic and polyphenolic hydroxyl groups, and behaves as free radical scavengers. Secondary substituents on the polyphenolic structure that support the electron-donating ability of phenolic OH groups by inductive and mesomeric effects also enhance the antioxidant property. [4]

First of all we extracted different fractions (humic acid, fulvic acid and hymatomelic acid) from a raw material the Leonardite. Then we measured the antioxidant capacity of these fractions. Although it is not an easy task. We measured the total phenol content (TPC) of the samples. We used gallic acid as a reference molecule. The values are as follows: while gallic acid (GS) gave 982 mg/g TPC, the values of fulvic acid 9 mg/g TPC and hymatomelic acid 52 mg/g TPC are much lower. We also measured the antioxidant capacity by the DPPH and CUPRAC methods, and the values were as follows. For the DPPH radical scavenging activity for the fulvic acid was 20,4 % for the hymatomelic 31,4 % in an interval concertation from 0-1 mg/ml. From the results we can conclude that humic substances has antioxidant, free radical inhibitory effects.

References

[1] *Stevenson, F.J.* Humus Chemistry: Genesis, Composition, Reactions, *Wiley, New York, 1994, pp. 188-210.*

[2] *Gould, K. S., and Lister, C. (2006).* "Flavonoid functions in plants," in Flavonoids: Chemistry, Biochemistry and Applications, eds Ø. M. Anderson and K. R. Markham (Boca Raton: CRC Press), 397–442.

[3] *Şeyda Karadirek at al. (2016):* Determination of total antioxidant capacity of humic acids using CUPRAC, Folin-Ciocalteu, noble metal nanoparticle- and solid-liquid extraction-based methods, DOI: 10.1016/j.talanta.2016.03.006

[4] *O.V. Smirnova, at al. (2012):* Antioxidant and pro-oxidant activity of ascorbic and humic acids in radical-chain oxidation processes, Russ. J. Appl. Chem. 85 (2012) 252-255. DOI: https://doi.org/10.1134/S1070427212020164

POULTRY WASTEWATER TREATMENT USING *PORPHYRIDIUM* SPP.

Zamfira Dincă[1], Anamaria Iulia Török[1], Ana Moldovan[1,2], Emilia Neag[1], Cecilia Roman[1]

[1]INCDO-INOE 2000, Research Institute for Analytical Instrumentation, 67 Donath Street, 400293, Cluj-Napoca, Romania
[2]Technical University, Faculty of Materials and Environmental Engineering, 103-105 Muncii Boulevard, 400641 Cluj-Napoca, Romania
e-mail: emilia.neag@icia.ro

Abstract

Wastewater contains various nutrients that can be used by microalgae for their growth. Microalgae are capable of removing nitrogen, phosphorus, heavy metals, as well as some toxic compounds from wastewater [1]. Microalgae species must present the ability to adapt in wastewater and the capability of growing to high cell density [2]. Several species, such as *Chlorella vulgaris, Nannochloropsis* spp., *Rhizoclonium* spp., *Scenedesmus intermedius* were used for wastewater treatment, while few studies reported the potential of *Porphyridium* spp., a red microalgae, to grow in wastewater [3].

The main objective of the present study was to investigate the capability of the marine microalgae, *Porphyridium* spp. to grow in poultry wastewater containing heavy metals and other contaminants in various concentrations. The composition of wastewater was determined before and after the microalgae cultivation, in order to monitor the ability of *Porphyridium* spp. to reduce the metals concentration. The initial pH of the wastewater as a growth medium was 6.6. After ten days of growth period, the pH value increased up to 8.6 suggesting that the *Porphyridium* spp. adapted to the new conditions. Also, the conductivity of the medium increased to 8.2 mS/cm after treatment compared with the initial value (before treatment) of 0.73 mS/cm. The highest removal efficiency exceeded 98 % in case of Al, followed by 95 % in case of Zn, 92 % for Fe and 90 % for B, while the lowest removal efficiency of 7 % was obtained for Mg. The results revealed a removal percentage of 41 % for Cd, 67 % for Cr, 54 % for Co, 10 % for Cu, 44 % for Mn, 30 % for Ni, 7 % for Mg, 79 % for Si, 8 % for K and 67 % for Ca. However, *Porphyridium* spp. exhibited low biomass productivity after wastewater treatment, compared with the control biomass grown in modified F/2 (Guillard's) medium. Even if the growth rate was low compared to the control, poultry wastewater has the potential to be used as an alternative growth medium for microalgae with simultaneous uptake of the metals and organic contaminants.

Acknowledgements

This work was funded by the Core Program, under the support of ANCS, project no. PN 19-18.01.01 (contract no. 18N/08.02.2019).

References

[1] N. Abdel-Raouf, A.A. Al-Homaidan, I.B.M. Ibraheem, Saudi J. Biol. Sci. 19 (2012) 257–275.
[2] W. Zhou, B. Hu, Y. Li, M. Min, M. Mohr, Z. Du, P. Chen, R. Ruan, Appl. Biochem. Biotechnol. 168 (2012) 348–363.
[3] H.B. Ulusoy Erol, M. L. Menegazzo, H. Sandefur, E. Gottberg, J.Vaden, M. Asgharpour, C.N. Hestekin, J.A. Hestekin, Energies 13, 2020, 3194.

IMPROVING THE PERFORMANCE OF THE POLYSULFONE MEMBRANES INDUCED BY THE PRESENCE OF IONIC LIQUIDS: RHEOLOGICAL INVESTIGATIONS

Adina Maria Dobos[1], Mihaela Dorina Onofrei[1], Lavinia Lupa[2], Anca Filimon[1]

[1]"Petru Poni" Institute of Macromolecular Chemistry, Aleea Grigore Ghica Voda 41 A, 700487 Iasi, Romania
[2]University Politehnica Timisoara, Faculty of Industrial Chemistry and Environmental Engineering, 6 Vasile Parvan Blv, 300223, Timisoara, Romania
e-mail: necula_adina@yahoo.com

Abstract

The various environmental problems of air or water pollution recently are trying to be solved by membrane technology. For this reason, finding the right compounds to obtain reverse osmosis, nanofiltration, and ultrafiltration membrane with improved properties is always a challenge for the researchers. In this context, the polysulfones containing quaternary ammonium side groups (PSFQ) are considered to be suitable for a wide range of applications from environmental field as result of their specific properties, such as hydrophylicity, flexibility and film forming capability. However, experience in the operation of polysulfonic membrane shows that there are some problems caused by membrane fouling. Thus, the aim is to improve their performance by mixing them with ionic liquids. In the obtaining process of ionic liquids-based membranes these could act as carrier of the final product which leads to the increasing of the membrane functionality and selectivity. For the present study two types of ionic liquids were chosen to be mixed in various rations (0.03 – 0.25wt.) with PSFQ: trihexyltetradecylphosphonium chloride (Cyphos) (ILp) and methyltrialkylammonium chloride, Aliquat 336 (ILq). The flow behavior of these mixtures was analyzed by rheology, in order to obtain information concerning the flexibility, conformation and also, to identify the specific interactions (Figure 1). Based on these parameters were established the compatibility of compounds and implicitly, the optimal composition of the used ionic liquids, aspects which will allow the obtaining of membranes suitable for treatment or water purification.

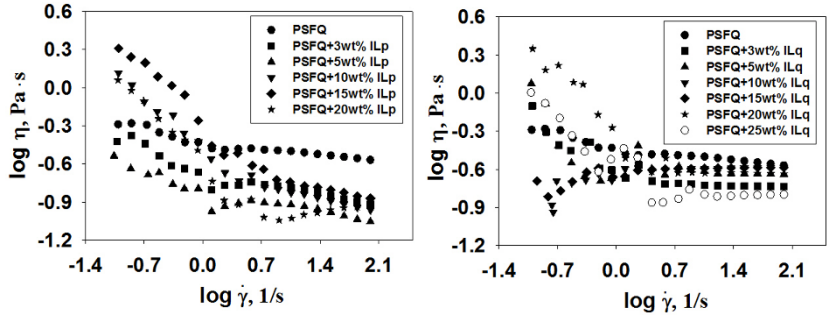

Figure 1. Log–log plots of dynamic viscosity *vs.* shear rate for PSFQ/ILp and PSFQ/ILq at different mixing ratio

As is observed from Figure 1, the two ionic liquids act like as plasticizers, manifesting a thinning behavior, visualized by a decrease of the dynamic viscosity of blends compared with pure solution of PSFQ. The obtained results are useful in identifying of the most suitable mixing ratio of PSFQ/ILp and PSFQ/ILq blends that will have an impact on membranes obtaining with the performance required by water purification technology.

Acknowledgements

This work was supported by a grant of the Romanian Ministry of Education and Research, CCCDI - UEFISCDI, project number PN-III-P2-2.1-PED-2019-3013, within PNCDI III.

MODELING THE FUNCTIONALIZED POLYSULFONE FIBERS BY THE ELECTROSPINNING PROCESS AND CONTROL OF SOLUTIONS PARAMETERS

Anca Filimon[1], Niculae Olaru[1], Florica Doroftei[1]

[1] *"Petru Poni" Institute of Macromolecular Chemistry, Aleea Grigore Ghica Voda 41 A, 700487 Iasi, Romania*
e-mail: capataanca@yahoo.com

Abstract

Industrial activities and increase of population worldwide have led to severe water and air contamination that result in major environmental concerns and cause adverse health effects. The development of nanostructured materials by electrospinning technique destine for use in environmental applications is considered to be of importance in the effective removal of water and air contaminants. Among those, long and continuous polymer fibers with tunable properties (e.g., high surface-to-volume ratio, high porosity and permeability), and tailored functionalities are highly promising in environmental applications (e.g., in water remediation and in air filtration processes). In this context, one of the most versatile polymeric materials is functionalized polysulfones (e.g., quaternized polysulfones, PSFQ) that have found industrial and medical applications as advanced membranes due to many useful characteristics, such as hydrophilicity, antimicrobial properties, higher permeability, and better separation. Therefore, the solutions of the functionalized polysulfone, with a tunable density of quaternary ammonium functional groups, were processed by electrospinning to create new fibrous materials that can modulate membrane properties. In the present study the relationship between processable solution properties and morphological aspects was assessed by scanning electron microscopy (SEM) technique (Figure 1). Images were conducted to visualize and compare the differences in morphology and characteristics of nanofibers attribute to the effects of the structural features of PSFQ and concentrations of the solution used in electrospinning process.

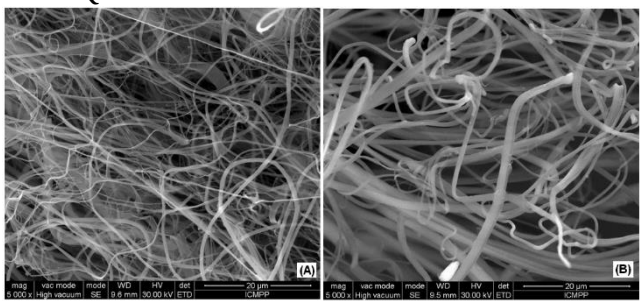

Figure 1. SEM images of PSFQ fibers obtained in N,N-dimethylformamide (DMF) at the polymer concentration of 40% (A) and 45 % (B), respectively.

The results have shown that the morphology of fibers formed with different forms and dimensions can be attributed to the combined effects of the solution parameters associated with polymer and solvent properties (concentrations, viscosity, boiling point of the solvents, and the surface tension) and also, processing parameters related with the operation of electrospinning apparatus and environmental parameters (temperature, humidity, and local atmospheric conditions). Therefore, the combining these factors assure the PSFQ fibers performance in terms of morphological and surface characteristics and implicitly, the possibility of fibrous material applicability in environmental field.

Acknowledgements

This work was supported by a grant of the Romanian Ministry of Education and Research, CCCDI - UEFISCDI, project number PN-III-P2-2.1-PED-2019-3013, within PNCDI III.

CHARACTERIZATION OF NATURAL ZEOLITE (CLINOPTILOLITE) AS ONE OF THE HIGH CATION EXCHANGE CAPACITY GEOPOLYMER MATERIAL

Nenad Grba[1], Marina Šćiban[2], Dejan Krčmar[1], Sanja Panić[2], Mirjana Petronijević[2], Slaven Tenodi[1], Đurđa Kerkez[1], Kristiana Zrnić Tenodi[1], Dragan Radulović[3] and Božo Dalmacija[1]

[1]University of Novi Sad, Faculty of Sciences, Department of Chemistry, Biochemistry and Environmental Protection, Trg Dositeja Obradovica 3, Novi Sad, Serbia,
[2]Faculty of Technology, University of Novi Sad, Novi Sad, Bulevar cara Lazara 1, Serbia
[3]Institute for Technology of Nuclear and other Mineral Raw Materials, Franse d' Esperea 86, Belgrade, Serbia
e-mail: nenad.grba@dh.uns.ac.rs

Abstract

The aim of this research is to subject one of the specific and locally used natural zeolite (clinoptilolite) from Vranjska Banja, Serbia with high cation exchange capacity. Mineralogical - X-Ray Diffraction Analysis (XRD), Scanning electron microscopy (SEM) and energy dispersive X-ray spectroscopy (EDS) and determination of cation exchange capacity (CEC) were investigated. Results showed homogenous structure with dominant clinoptilolite - heulandite type zeolites as most abundant minerals. The important aspect of this research is possibility of wider usage of natural zeolite-clinoptilolite due to cost-efficiency aspects of this natural material that can be exploited in large amount from several Serbian deposits e.g. "Zlatokop" (Vranjska Banja) and "Igroš Vidojević" (Brus), Serbia. The present of higher, but also extremely concentration of heavy metals in Pannonian, Internal Dinarides and wider European region lead us to boost novel high performance but economically viable techniques. The starting points are geochemical characterization of novel geo- materials before further water-treatment implementation.

Introduction

Natural zeolites are hydrated aluminosilicate minerals with valuable physicochemical properties, such as cation exchange, molecular sieving, catalysis and sorption. In the past decades, natural zeolites have found a variety of applications in adsorption, catalysis, building industry, agriculture, soil remediation, and energy. The use of natural zeolites for environmental applications is gaining new research interests mainly due to their properties and significant worldwide occurrence. Natural zeolite have also been reported for removal of anions and organics from water systems [1, 2, 3]. These materials are abundant and low-cost resources and have been found in many areas of the world. In this paper we will examine the characterization of zeolite (clinoptilolite) from the territory of the Republic Serbia.

The aim of this work is to determine the consistent, homogenity and high CEC capacity for local and economicly most affordable materilas in order to be use on fileds investigations on groundwater and industrial wastewater most suitable purification/remediation material in order to recommend it for best avaible water treatment technology as main adsorbent.

The need for new geomaterial with high to superhigh cation exchange capacity (CEC) have been stated in many scientific papers and fields investigations [1]. The aim of this study is to characterizes zeolites from the investigated area of Serbia, in this case specific geochemical composition from natural zeolite (clinoptiolite) from Vranjska Banja, Serbia.

Experimental

The primary sample of zeolite, natural zeolite (clinoptiolite) from Vranjska Banja, Serbia ca. 1 kg, was prepared and dried by Standard methods for sample preparation (SRPS B.B8.080.) in Dryer - "Binder" (sample distributor Jones). The sample was analyzed for mineralogical - XRD analysis, SEM/EDS and determination of CEC. XRD and SEM analysis of the matrices were done in order to elucidate the microscopic structures and morphology of surfaces and CEC analysis will show specific content of exchangeable cations in clinoptilolite sample. Examination of the mineral composition of the sample was investigated by X-ray automatic powder diffractometer PHILIPS, model PW-1710. X-ray diffraction analysis was used to determine and monitor the phase composition of the sample. The intensities of diffracted CuKα X-rays radiation (λ=1.54178Å) were measured at room temperature at intervals of 0,02 °2θ and a time of 1 s in the range from 4 do 65 °2θ. The X-ray tube was loaded with a voltage of 40 kV and a current of 30 mA, while the slots for directing the primary and diffracted beam were 1° and 0.1 mm. Method for determination of exchangeable cations Ca^{2+}, Mg^{2+}, Na^{+} and K^{+} and cation exchange capacity was DM 10-0/40.

Results and discussion

The sample was examined by X - ray diffraction on a polycrystalline sample (powder). The diffractogram of the tested sample is presenting the clinoptilolite - heulandite type zeolites as most aboundant minerals.

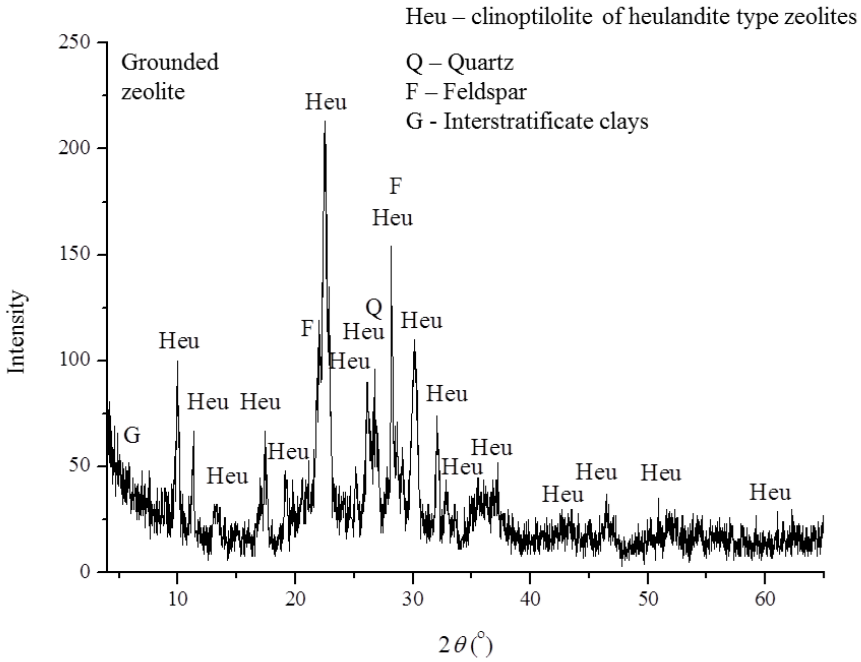

Figure 1. The diffractogram of the clinoptilolite (natural zeolites) from Vranjska Banja

The presence of the following minerals was determined in the analyzed sample: clinoptilolite-heulandite type zeolites, feldspar, quartz, interstarted clays, carbonates and mica. The most common minerals are zeolite and then feldspar, while quartz is significantly less common. Of the feldspar, plagioclase is predominantly represented, relative to K-feldspar. Semiquantitative share crystalline phases (minerals) is as follows: zeolites ≈ 85%, feldspars ≈ 10%, clays ≤ 5%, quartz 2-3%. Carbonates, respectively calcite and mica are present in the trace.

The next important targeted analysis of sample surfaces is Scanning electron microscopy (SEM) and energy dispersive X-ray spectroscopy (EDS) method and results can be seen from Figure 2. The SEM-micrograph shoves from several to tents micrometers semi-homogenius structure and macro/meso-porosity. The brighter areas in the crystallites represent feldspar and darker areas clinoptilolite as in study from [4].

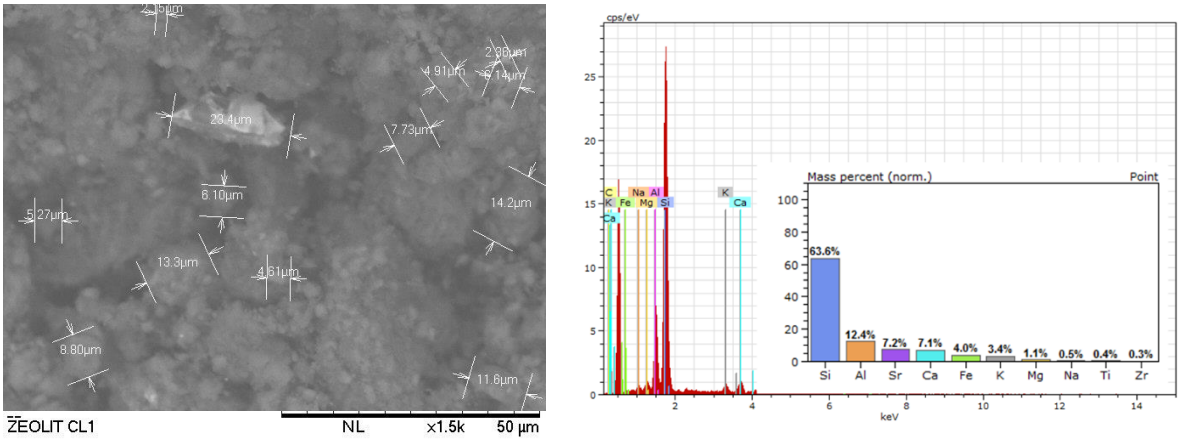

a) b)

Figure 2. SEM-micrograph (a) and (b) EDS spectrum of the natural zeolite (clinoptilolite) sample

Generally, the important ratio for clasification of zeolite from clinoptilolite type is Si/Al and according to the EDS analysis it was round 5.3 and accordingly higher then prescribed value of 4.5 [2] for this type. Additinaly, previous studies support this examination with also similar Ca, Fe, K, Mg and Na content (Table 1) and similar chemical composition on globescale[1].

Table 1. Results of EDS analysis from natural zeolite (clinoptilolite) from Vranjska Banja, Serbia compared with other related zeolites (clinoptilolite) samples

Element	[norm. wt.%]	[norm. wt.%][4]	[norm. wt.%][3]
Silicon	**69.98**	**65.63**	70.90
Aluminium	**13.19**	**12.97**	12.40
Calcium	7.49	3.08	2.54
Iron	4.19	1.48	1.21
Potassium	3.57	1.33	4.46
Magnesium	1.12	1.41	0.83
Sodium	0.44	0.95	0.28
CEC (meq/g)	1.2	/	1.6–1.8

The results of determining the content of exchangeable cations are shown in Table 2:

Table 2. Results of determining the content of variable cations of zeolite samples (meq/100g)

Sample/ions	**Na^+**	**K^+**	**Ca^{2+}**	**Mg^{2+}**	**$\Sigma_{cations}$**
Natural zeolite (clinoptilolite) from Vranjska Banja, Serbia	2,53	48,47	68,61	3,36	**122,97**

Due to many study observed in paper from Wang and Peng, 2008 the CEC value could clasify this zeolite as higher in the class with high potential for local but also comercial near region used as adsorbent with superhigh cation exchange capacity regarding previous [4,5] but also ongoing and future studies.

Conclusion

This research shows good potential and high CEC capacity of zeolite (clinoptilolite) from Vranjska Banja, Serbia. Future application will be based on this geochemical scaning of clinoptilolite as potentialy well structure and geo-chemicaly powerful purification material.

Acknowledgements

The authors acknowledge financial support of the Ministry of Education, Science and Technological Development of the Republic of Serbia (Grant No. 451-03-68/2020-14/200125 and No. 451-03-68/2020-14/200134) and the Innovation Fund of the Republic of Serbia (Grant No. 5717). The authors also acknowledge PhD Goran Kitić and MSc Jovana Stanojev from BioSense Institute (Novi Sad, Serbia), for the technical support from SEM/EDS analysis.

References

[1] S. Wang, Y. Peng: Natural zeolites as effective adsorbents in water and wastewater treatment, Chemical Engineering Journal 156 1 (2010) 11-24.
[2] C. Orha, F. Manea, A. Popi, G. Burtica, I. Fazakas Todea: Materials with Antibacterial Properties, Rev. Chim. (Bucuresti) 59 (2008) 173–177.
[3] S.K. Alpat, O. Ozbayrak, S. Alpat, H. Akcay: Journal of Hazardous Materials 151 (2008) 213–220.
[4] Š. C. Stefanović, N. Z. Logar, K. Margeta, N. No. Tušar, I. Arčon, K. Maver, J. Kovač, V. Kaučič: Microporous and Mesoporous Materials, 105 3 (2007) 251-259
[5] Z. T. Sekulić, A.S. Daković, M. Kragović, M.A. Marković, B. Ivosević and B.M. Kolonja: Hemijska Industrija, 67 (2013) 4.

PREPARATIVE PURIFICATION OF OCHRATOXIN A BY LIQUID-LIQUID CHROMATOGRAPHY

Zsófia Hegedüs[1,2], Dominik Szabó[1], Csaba Vágvölgyi[1], András Szekeres[1]

[1]University of Szeged, Faculty of Science and Informatics, Departement of Microbiology, Közép fasor 52. Szeged H-6726
[2]Doctoral School in Biology, Faculty of Science and Informatics, University of Szeged, Szeged, Hungary
e-mail: hegedus.zsofia95@gmail.com

Abstract
Ochratoxin A is an important mycotoxin, produced by different *Aspergillus* and *Penicillium* species hence there are strict regulations on its level in foods and feeds. Qualitative and quantitative measurements of this compound require relatively high amounts of pure ochratoxin A as a standard. This large amount of pure compound can be obtained by purifying the fermentation medium of the producing microorganisms. Liquid-liquid chromatography (LLC) seems to be a suitable method, which is becoming more common in the purification of natural compounds.

Introduction
Mycotoxins are toxic secondary metabolites produced by certain filamentous fungi. Among them ochratoxins have outstanding importance due to their high-level toxicity, which could cause remarkable problems in food and feed industry [1,2]. One of the most important member of this metabolite group is ochratoxin A, which was classified as possible human carcinogen (group 2B) by IARC [3]. In food safety laboratories, numerous methods are available for measuring these compounds from various matrices [4-6] requiring relatively high amounts of pure ochratoxins as standard compounds for both qualification and quantification. Generally, the chemical synthesis of ochratoxins can be accomplished with low yield [7], but higher amount of pure compound can be obtained by the purification of the fermentation environment of the producer microorganisms. Liquid-liquid chromatography may be a suitable method, whose application is becoming frequently used in the purification of natural compounds [8,9]. One of the technical implementations of this technique is the Centrifugal Partiton Chromatography (CPC), which was applied in our work for the separation of ochratoxins from the fermentation product and from each other.

Experimental
Aspergillus albertensis (SZMC 2107) was cultivated on yeast extract, sucrose media in dark at 28 °C. The incubation time and the sucrose content of the culture media was optimized for maximum ochratoxin production. For sample preparation a three-step acid-base extraction was used with ethyl acetate and sodium-bicarbonate as solvents. The crude extract was dispensed into 1,5 ml vials and were evaporated to dryness. For solvent system testing numerous three- and four-component biphasic systems were examined with the “Shake-flask” method. The selected systems were assembled and mixed in a test tubes, thereafter equal volumes of the phases were added to the vials containing the extract. The concentrations in the upper- and lower phase were measured by HPLC-UV technique. Partition coefficients (P) and separation factors (α) were calculated based on the concentrations, and the best system was selected for the purification procedure. During instrumental optimization suitable flow direction, flow rate and rotational speed was chosen. The purity of ochratoxin A and B in the collected fractions was calculated based on the areas of HPLC-UV chromatogram on 333 nm.

Results and discussion

At the beginning of our work the cultivation parameters of *Aspergillus albertensis* (SZMC 2107) were optimized. The maximum amount of ochratoxin A was measured after an incubation period of 8 days on liquid media containing 2 % yeast extract and 15 % sucrose. The crude extract obtained after liquid-liquid extraction contained ochratoxin A (OTA), ochratoxin B (OTB) and 9 major impurities. The extract was used for solvent system testing to find an appropriate biphase for the purification. Several compositions of one quaterner (hexane-ethyl-acetate-methanol-water) and 19 different type ternary systems were studied. The distribution coefficients and the separation factors of both OTA and OTB were in the proper range in a hexane-isopropanol-water system. After instrumental optimization the separation was carried out in ascendent mode at 10 ml/min flow rate and 2000 rpm rotational speed. The purities of OTA and OTB were more than 99% and 55 %, respectively.

Conclusion

The separation of ochratoxin A and B was accomplished using Centrifugal Partition Chromatography with the purities of more than 99 % and 55 %, respectively. Based on the results the developed method may be suitable for large scale purification of ochratoxin A in high purity, which is required for quantitative and qualitative measurements. Further investigation is necessary in order to increase the purity of OTB, and to confirm the purities by HR-MS and NMR techniques.

Acknowledgements

This work was supported by the Hungarian Scientific Research Fund by grants NKFI K-115690 and this work was connected to the project GINOP-2.3.2-15-2016-00012. The infrastructural background was established with the support of GINOP-2.3.3-15-2016-00006.

References

[1] Miraglia, M., De Dominicis, A., Brera, C., Corneli, S., Cava, E., Menghetti, E., and Miraslia, E. (1995). Ochratoxin a levels in human milk and related food samples: An exposure assessment. Nat. Toxins 3, 436–444.

[2] Duarte, S.C., Pena, A., and Lino, C.M. (2010). A review on ochratoxin A occurrence and effects of processing of cereal and cereal derived food products. Food Microbiology 27, 187–198.

[3] IARC. Ochratoxin A. In IARC Monographs on the Evaluation of Carcinogenic Risk to Humans: Some Naturally Occurring Substances; Food Items and Constituents, Heterocyclic Aromatic Amines and Mycotoxins; IARC: Lyon, France, 1993; Volume 56, 489–521.

[4] Valenta, H. (1998). Chromatographic methods for the determination of ochratoxin A in animal and human tissues and fluids. Journal of Chromatography A 815, 75–92.

[5] Aboul-Enein, H.Y., Kutluk, Ö.B., Altiokka, G., and Tunçel, M. (2002). A modified HPLC method for the determination of ochratoxin A by fluorescence detection: Determination of ochratoxin A. Biomed. Chromatogr. 16, 470–474.

[6] Li, J., Liu, X., Han, S., Li, J., Xu, Q., Xu, H., Wang, Y., Liu, F., and Zhang, Z. (2012). Analysis of Ochratoxin A in Wine by High-Resolution UHPLC-MS. Food Anal. Methods 5, 1506–1513.

[7] Kraus, G.A. (1981). A facile synthesis of ochratoxin A. J. Org. Chem. 46, 201–202.

[8] Endre, G., Hegedüs, Z., Turbat, A., Škrbić, B., Vágvölgyi, C., and Szekeres, A. (2019). Separation and Purification of Aflatoxins by Centrifugal Partition Chromatography. Toxins 11, 309.

[9] Szekeres, A., Lorántfy, L., Bencsik, O., Kecskeméti, A., Szécsi, Á., Mesterházy, Á., and Vágvölgyi, Cs. (2013). Rapid purification method for fumonisin B1 using centrifugal partition chromatography. Food Additives & Contaminants: Part A 30, 147–155.

THE MECHANOCHEMICAL IMPLEMENTATION OF THE ENVIRONMENTALLY FRIENDLY ASYMMETRIC TRANSFER HYDROGENATION OF KETONES

Vanessza Judit Kolcsár,[1]* György Szőllősi[2]

[1]*Department of Organic Chemistry, University of Szeged, Dóm tér 8, Szeged, 6720, Hungary,*
[2]*MTA-SZTE Stereochemistry Research Group, Dóm tér 8, Szeged, 6720, Hungary*
**Corresponding author: kolcsar.vanessza@chem.u-szeged.hu*

Abstract

Optically pure compounds are essential in the synthesis of pharmaceuticals, fragrances and pesticides. Asymmetric catalytic reactions are the most favorable methods to achieve high conversions and enantiomeric excesses in fast reactions, using only catalytic amount of the chirality sources. Hydrogenations and transfer hydrogenations are well-studied procedures to obtain optically pure chiral alcohols. The transfer hydrogenation is convenient, as it ensures the possibility to use a hydrogen donor compound instead of hydrogen gas to provide the necessary H atom. In the past few decades several synthetic chiral compounds were used as the ligand of the catalyst complex, however these days more environmentally friendly implementations are favored. The use of natural chiral compounds would provide great opportunities to carry out asymmetric catalytic reactions using less organic solvents and producing less hazardous waste.

In our previous studies, we have developed an asymmetric catalytic system for the transfer hydrogenation of prochiral ketones using an *in situ* prepared Ru-chitosan complex in aqueous media. The catalyst prepared using the readily and easily available, biodegradable and inexpensive biopolymer provided good result in the transfer hydrogenation of various prochiral ketones in aqueous-phase reactions. In order to increase the preparative value of this method for preparing optically pure alcohols, we decided to use mechanical energy transmission instead of conventional thermally activated reactions carried out in magnetically stirred batch reactors. With the former method the reaction time can be reduced, as well as the volume of the used solvent and the produced waste. After the optimization of the reaction conditions in the transfer hydrogenation of 4-chromanone, we examined the reaction of various ketones and the obtained results were compared with those reached in reactions carried out conventionally. All the examined ketones were transformed in similar degrees and the chiral alcohols were obtained in high enantiomeric excesses (ee). The reactions were scaled up as well, to prepare the optically enriched compounds in mmol quantities.

Introduction and aims

During the last few decades the protection of the environment, the application of sustainable and economical solutions play major role in science. Although the synthesis of optically pure compounds is well studied and successful as well, researchers have to develop greener and more sustainable methods to meet the standards of the environmental regulations. Optically pure compounds are widely used in pharmaceuticals, agrochemicals, flavors and fragrances. Asymmetric catalytic transfer hydrogenations are convenient methods to transform prochiral unsaturated compounds into essential optically pure chemicals. Large variety of chiral complexes have been developed to catalyze these reactions [1]. Although excellent results were achieved, synthetic ligands do not meet the requirements of the recent economic and ecologic trends.

The use of chiral ligands from natural sources became essential, to develop new, economically and environmentally advantageous methods. Shell food industry produces great volume of chitin as waste, which could be further used in catalysis. In alkali solution chitin can

be deacetylated to obtain chitosan [2], which may replace the expensive, synthetic ligands. Due to the presence of the free amino groups, this biopolymer is able to form complexes with metal cations to catalyze several types of organic transformations [3]. Furthermore, it can be used in aqueous media as a result of its hydrophilic character. In our previous studies, we used chitosan as a chiral ligand to *in situ* form Ru-chitosan complex in aqueous media, which catalyzed the asymmetric transfer hydrogenations of prochiral ketones. Using this method several phenyl ethanol derivatives, cyclic and heterocyclic alcohols and even amino alcohols were obtained with high conversions (90-99%) and enantioselectivities (ee: 88-97%). Based on the results achieved in the reactions of different ketones we reached to numerous conclusions about the secondary bonds formed between the complex and the ketones in the transition state. We have also examined the pre-prepared Ru-chitosan complex, which gave identical results even after several months' of storage. The NMR and IR characterization of the complex provided enough information to determine the possible structure of the complex and that of the transition state [4,5].

Although, the use of the natural ligand gave excellent results, similar to the synthetic compounds, the mechanochemical implementation could open new opportunities to the development of greener, more sustainable methods [6,7]. Our aim was to investigate the transfer hydrogenation of prochiral ketones catalyzed by a chiral Ru-chitosan complex prepared from unmodified, commercially available chitosan in aqueous solvents, using a mixing mill to provide the necessary energy for the reaction. We chose the transfer hydrogenation of 4-chromanone to determine the optimal reaction conditions, then we planned to implement the method to other, previously studied prochiral compounds as well. Practical use is essential in science, so our goals included the scale-up of the reactions as well.

Experimental

The prochiral ketones, the hydrogen donor (HCOONa), the metal precursor ([Ru(*p*-cymene)Cl]$_2$Cl$_2$) and the chitosan were obtained from commercial sources and were used as received. Transfer hydrogenations were carried out in closed 10 mL ZrO_2 grinding jars with grinding balls made from the same material with the diameter of 3; 5; 12 and 15 mm (Figure 1.). In a typical run all the compounds were measured into to the jars, then the necessary amount of balls was counted and added to the system. The mixture then was mixed in a Retsch Mixing Mill MM 400 instrument at the chosen frequency for the desired time. When the reaction was completed 2 mL ethyl acetate was added into the jar to dissolve the organic compounds from the ZrO_2 surfaces. The system then was washed 2 times with 1 mL ethyl acetate. The organic phases were combined, then filtered to remove the solid remnants. The products were analyzed by GC-MSD and GC-FID using chiral capillary columns, and NMR spectroscopy. The products of the serial and the scale up measurements were easily purified by column chromatography using desired mixture of hexane and ethyl acetate as eluent, or in the cases of the solid products recrystallization from pure hexane was also efficient.

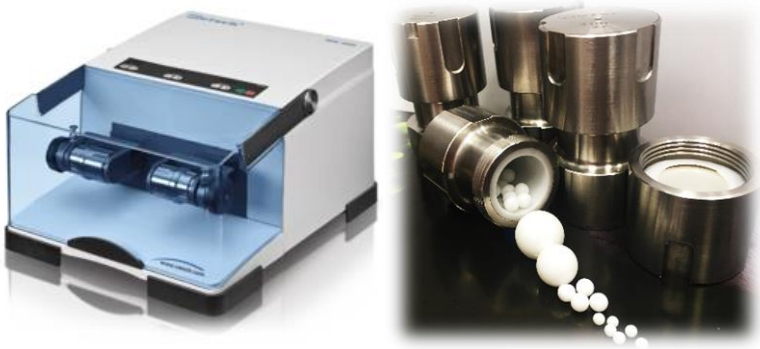

Figure 1. Retsch Mixing Mill MM400 Instrument, and the used ZrO_2 grinding jars and balls

Results and discussion

First, based on the results of our previous studies the transfer hydrogenation of 4-chromanone was carried out in the new catalytic system. The optimization of the instrument parameter such as the size and the quantity of the balls, the used frequency and the reaction time led us to the conclusion that 100 grinding balls with 3 mm diameter, at 30 Hz gave the best result after 120 min of reaction time (Figure 2.). Then the reaction parameters – the volume of solvent, the amount of the hydrogen donor and the catalyst – were optimized. 0.2 mL water/^{i}PrOH gave the best result with 10 eq. of HCOONa and 5% catalyst. We would like to stress out that under these conditions we were able to decrease significantly the reaction time, from 48 h to 2 h, thus, the turn-over frequency (TOF) has increased twenty-fourfold (from 0.41 h^{-1} to 10 h^{-1}).

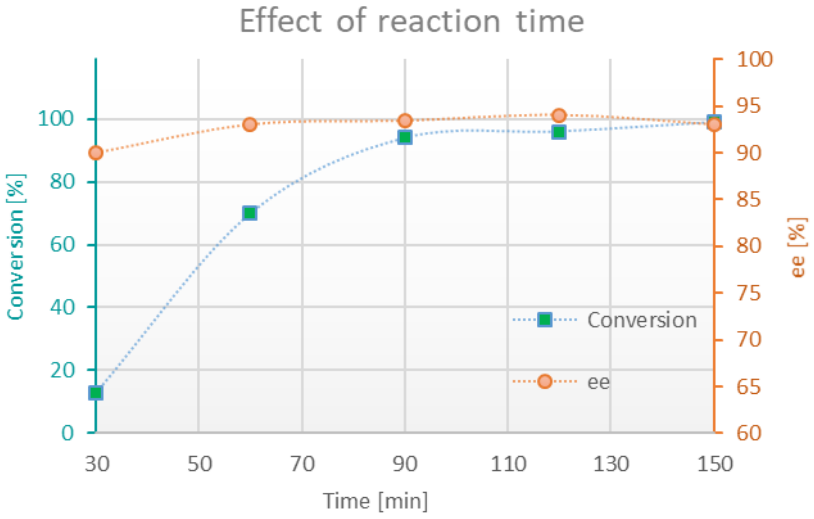

.

Figure 2. The effect of reaction time. 100 grinding balls with 3 mm diameter, 30 Hz, 0.2 mL solvent, 2 eq. hydrogen donor, 5% catalyst

Next we examined the possibility of scale up by adding 1 mmol 4-chromanone to the system. In this case the reaction was slower, and at the same frequency the amount of the solvent, the catalyst and the hydrogen donor had to be increased to achieve 98 % conversion with 91 % ee. Although, the amount of the catalyst and the hydrogen donor had to be increased, to our delight the reaction required less equivalents of these components as compared to the ketone than in the serial measurements.

In our following experiments, other ketones were used in the catalytic system. Further compounds – 7 acetophenone derivatives, 9 cyclic ketones and 10 heterocyclic ketones – were chosen based on the results obtained in our previous studies [4,5]. Although the above conditions were set for the transfer hydrogenation of 4-chromanone, some of the prochiral ketones' reactions were slower in the magnetically stirred reactions. Based on this observation further optimizations were needed in the reaction of some of these compounds. Following these optimizations all of the desired chiral alcohols were obtained with excellent conversion (90-99,9 %) in this catalytic system (Figure 3.). As our previous studies showed, the enantiomeric excess highly depends on the structure of the prochiral ketones. In this system all the achieved ee values were similar to the ee obtained in our previous experiments carried out in batch system using magnetic stirring (67-96%). A few percent of decrease can be observed. Probably the heat produced by repetitive impact energy causes the faster degradation of the catalyst complex or the racemization of the product. This effect was known from previous, high temperature

measurements, although, in the mechanochemial reactions it didn't seem to be as significant as in the magnetically stirred ones.

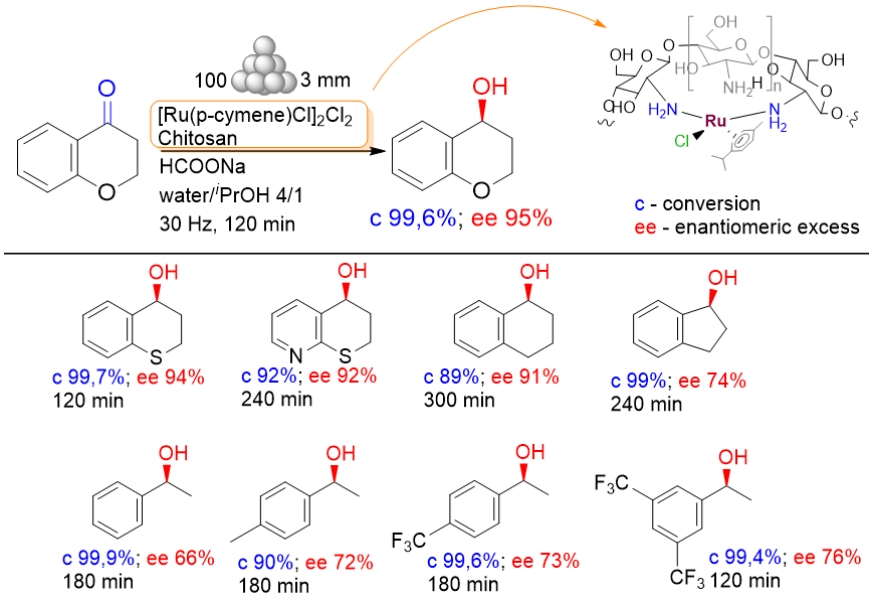

Figure 3. The transfer hydrogenation of 4-chromanone with the previously determined catalyst structure and a few examples of starting compounds with the achieved conversions and ee values

Conclusions

In summary, we have developed a sustainable and green method, using the biopolymer chitosan as a chiral ligand to *in situ* form a Ru complex in aqueous catalytic system, in which high enantioselectivities were obtained in the asymmetric transfer hydrogenation of prochiral ketones by mechanical energy transmission in a mixing mill. The enantiomeric excess and conversion values were similar to the values achieved in magnetically stirred reactions, although significantly less solvent and shorter reaction times were necessary. In consequence, the TOF of the catalyst could be increased twenty-fourfold. The product alcohols were easily separable from the reaction mixture and were purified by column chromatography or recrystallization. The latter method has many advantages, such as greener and less organic solvent was used during the work-up process. The reaction was easily scaled-up in this system. Accordingly, with this new system optically pure alcohols can be obtained with the use of natural chiral ligand in aqueous media using mechanical energy transmission following an environmentally benign procedure.

Acknowledgements

The authors thank the financial support of the Ministry of Human Capacities through grants 20391-3/2018/FEKUSTRAT and NTP-NFTÖ-20 (V. J. Kolcsár).

References

[1] Catalytic Methods in Asymmetric Synthesis (Ed.: I. Ojima), John Wiley & Sons, Hoboken, NJ 3rd ed. (2010)
[2] K. Kurita, K. Tomita, S. Ishii, S.-I. Nishimura, K. Shimoda, J. Polym. Sci. Part A 31 (1993) 485-491.
[3] Á. Molnár, Coord. Chem. Rev. 388 (2019) 126-171.

[4] Gy. Szőllősi, V. J. Kolcsár, ChemCatChem. 11 (2019) 820-830.
[5] V. J. Kolcsár, F. Fülöp, Gy. Szőllősi, ChemCatChem. 11 (2019) 2725-2732.
[6]M. Pérez-Venegas, E. Juaristi, ACS Sustainable Chem. Eng. 8 (2020) 8881-8893.
[7] G.-W. Wang, Chem. Soc. Rev. 42 (2019) 7668-7700.

PHOSPHORAMIDE CHIRAL CATALYSTS FOR ENVIRONMENTALLY FRIENDLY ASYMMETRIC ORGANOCATALYTIC PROCESSES

Viktória Kozma[1], György Szőllősi[2]

[1]Department of Organic Chemistry, University of Szeged, 6720 Szeged, Dóm tér 8, Hungary
[2]MTA-SZTE Stereochemistry Research Group, 6720 Szeged, Dóm tér 8, Hungary
e-mail: kozma.viktoria92@gmail.com

Abstract

Phosphoramides and thiophosphoramides were prepared from optically pure 1,2-diamines and were used as chiral organocatalysts in the asymmetric Michael additions of different Michael-donors to *N*-substituted maleimides. The 1,2-diphenylethane-1,2-diamine derived thiophosphoramide, which could be prepared in good yield in a one-step procedure, was found to be excellent catalyst in the addition of aldehydes to various maleimide derivatives. Products resulted in reactions of ketones with maleimides were also obtained in high yields and enantioselectivities. The thiophosphoramide derivative was efficient in the asymmetric conjugate addition of other carbonyl compounds, such as □-diketones and □-keto esters, as well. Investigations of these reactions led to valuable conclusions as concerns the structural requirements of the catalyst and reactants needed for obtaining high activities and stereoselectivities. Due to the low catalyst amount and the solvent applied, these reactions could be carried out in a more environmentally benign way as with the previously used chiral organocatalysts.

Introduction

Extremely significant economic advantages of asymmetric catalytic processes have led to the explosive development of chiral enantioselective catalysts [1,2]. Most of the widely used catalysts are transition metal complexes, which raises some concerns. For example, the toxicity of transition metals is a significant disadvantage of these methods, as their removal from the final product is challenging for technological processes in most of the cases. In the last few decades, a new field of research has emerged and led to a solution in catalyst development, the so-called organocatalysis. Nowadays, this area is in the forefront of the modern chemical research. Its name also suggests that it uses small organic molecules called “microenzymes” that do not need metals at all in catalytic processes. The most significant results of organocatalysis were in the field of asymmetric reactions. These catalysts are widely applied in C-C coupling reactions, C-N and C-O bond formations, reductions and oxidations.

One of the most important asymmetric C-C coupling reaction is the Michael addition [3-5], a highly efficient method for connecting small molecules to create new chiral centers in a stereospecific step. Asymmetric Michael additions are widely applied for preparing optically pure fine chemicals. Many donors and acceptors can be used, allowing the synthesis of a wide variety of products. Maleimides – as Michael-acceptors – have significant application possibilities in asymmetric organocatalysis. One of the easiest way to prepare enantioenriched succinimide compounds is the direct Michael addition of nucleophiles to maleimides. The presence of succinimide moiety can be seen in natural products and clinical drugs [6], being part of pharmaceuticals used in the treatment of epilepsy [7], depression [8], neurodegenerative disease and HIV [9]. The promising results of previous studies also demonstrate that further research aimed at producing optically pure succinimides and their testing may be important in the future.

In the present work, our aim was to study the applicability of newly synthesized phosphoramide catalysts in various asymmetric Michael additions [10]. We determined the

optimal reaction conditions (temperature, reaction time, amount of solvent and reagent) for each reaction to achieve the best enantioselectivities and conversions.

Experimental

Optically pure 1,2-diamines and the chloro(thio)phosphate derivatives were purchased from Sigma-Aldrich and used as received. Carbonyl compounds, a few *N*-substituted maleimides and the other donors and acceptors were commercial products and were used without purification. Solvents, reagents and additives of analytical grades were used in all reactions. To prepare new maleimides we purchased analytical grade primary amines and maleic anhydride.

The catalysts were prepared in one or in three-step preparation methods. In the one-step method a solution of 1,2-diphenylethane-1,2-diamine and equivalent amount of Et_3N in dry CH_2Cl_2 was flushed with N_2 and cooled to 0°C. To this solution *O,O'*-diethyl chlorothiophosphate dissolved in dry CH_2Cl_2 was added dropwise in 2 h. Following one day, water was added and the product was extracted in CH_2Cl_2 followed by purification by flash chromatography. In the three-step method first we had to protect one of the amino group of the diamine and after phosphorylation of the free amine in the third step we removed the protecting group to obtain the appropriate catalyst. Maleimides were synthesized from maleic anhydride and the corresponding primary amine using sodium acetate and acetic anhydride in one day at 70°C. The crude products were purified by flash chromatography. Catalytic Michael additions were performed in vials with magnetic stirring. The chiral catalyst was dissolved in the given solvent, followed by the addition of a maleimide derivative and 2-3 equivalents of nucleophile. The mixture was stirred at the indicated temperature. After the given times the products were extracted with ethyl acetate and analyzed.

Products resulted in the Michael additions were analyzed by GC-MSD and GC-FID using chiral capillary columns. Larger scale experiments were also carried out and the resulted products were purified by column chromatography for determination of the isolated yields. The pure compounds were characterized by ^{1}H- and ^{13}C-NMR spectroscopy. For identification of the newly prepared organocatalysts and for mechanistic investigations the ESI-MS spectra were recorded.

Results and discussion

Initially we have attempted to prepare phosphoramides and thiophosphoramides from optically pure (*R,R*)-1,2-cyclohexanediamine or (*S,S*)-1,2-diphenylethane-1,2-diamine by a one-step procedure using *O,O'*-diethyl(thio)phosphoric chlorides (Scheme 1). This method was successful using 1,2-diphenylethane-1,2-diamines, however, in reactions of 1,2-cyclohexanediamines low yields were obtained. Thus, the three-step procedure was applied to reach satisfactory yields with the latter diamines.

With these optically pure diamine derivatives in hand we started our catalytic studies by testing them as organocatalysts in the asymmetric conjugate addition of isobutyraldehyde to *N*-benzylmaleimide leading to the succinimide derivative shown in Scheme 2. Phosphoramide and thiophosphoramide having cyclohexane backbone were highly active catalysts in the test reaction, assuring complete conversion of the maleimide in one hour at room temperature (rt). Product resulted in good yield and in 94% *ee*'s. The organocatalysts with 1,2-diphenylethane scaffold were less active as compared with the previous catalysts at room temperature in three days. However, high *ee* (>99%) was obtained. Higher conversion, without altering the *ee* value, was reached in one day by increasing the reaction temperature to 70°C.

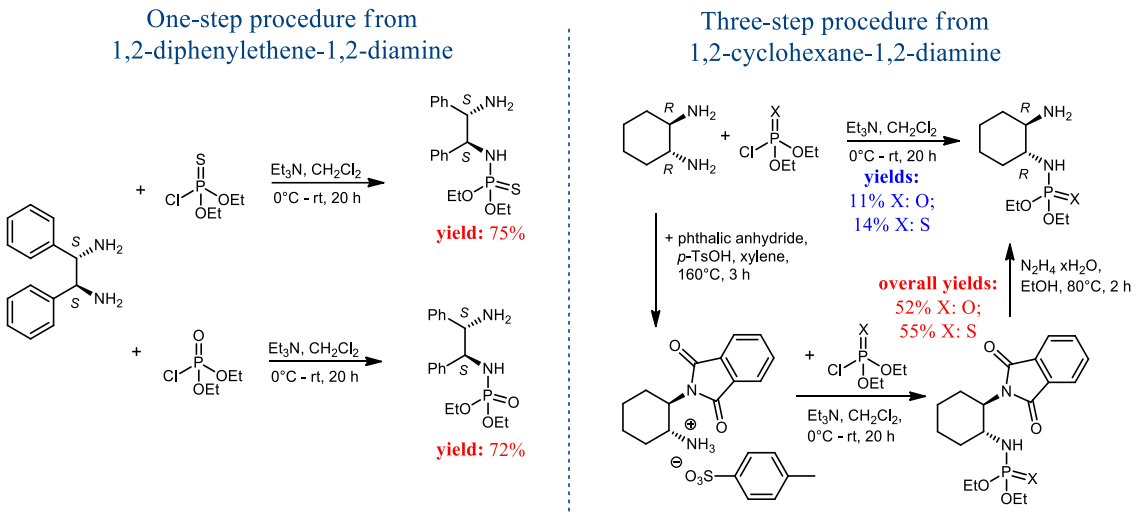

Scheme 1. Preparation of (thio)phosphoramides from optically pure C2-symmetric 1,2-diamines.

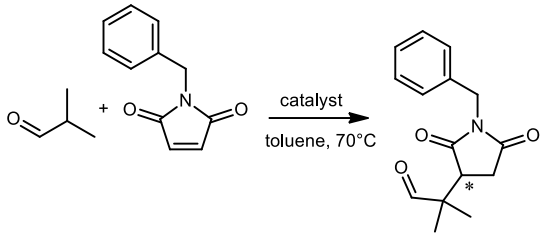

conv: 99%; **ee:** >99%

Scheme 2. The selected test reaction.

Owing to the excellent performance of thiophosphoramide derived from 1,2-diphenylethane-1,2-diamine we have examined the possibility of decreasing the organocatalyst amount. Although, 1.6 mol% was enough to obtain over 60% conversion in one day at 70°C, 2.5 mol% catalyst was necessary for close to complete transformation of the *N*-benzylmaleimide. However, high *ee* value (99%) was obtained even with the lower amount of catalyst.

After studying the test reaction, we began to investigate the use of various carbonyl compounds – simple aldehydes and ketones – as Michael donors in reactions with maleimide derivatives. Similar results were obtained with various aldehydes; however, the products resulted in low diastereomeric ratios in case two chiral centers were formed in the reaction. Reaction in which ketones were used as nucleophiles also proceeded excellently, as illustrated by results obtained using acetone under similar conditions as employed in reactions of aldehydes (Scheme 3.). In these reactions, almost complete transformations of various maleimides were reached and the products resulted in high optical purities.

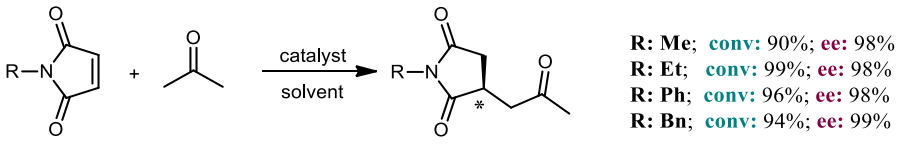

Scheme 3. Michael addition of acetone to maleimide derivatives.

The applicability of the thiophosphoramide derivative was also investigated in other asymmetric conjugate additions, such as those of □-diketones and □-keto esters to maleimides. The conjugate addition of ethyl-2-fluoroacetoacetate and acetylacetone to different *N*-alkyl or

N-benzyl maleimides afforded the corresponding Michael adducts in good yields and excellent enantioselectivities as shown on Scheme 4. With the latter donor, we obtained slightly lower values in each reaction. Contrary to aldehyde nucleophiles, beside high ee values, the reactions of ethyl-2-fluoroacetoacetate also afforded good diastereomeric ratios.

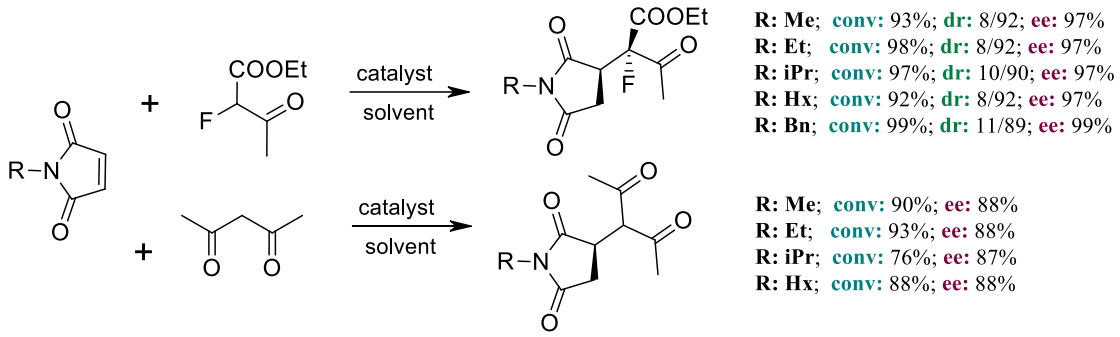

Scheme 4. Michael addition of a □-keto ester and a □-diketone to maleimides.

We also applied the organocatalyst in other Michael additions. Reactions of carbonyl compounds to □-nitrostyrene and that of nitromethane to □,□-unsaturated ketones were also investigated. In each case it was necessary to optimize the reaction conditions. High conversions and *ee* values were reached in these reactions with the (thio)phosphoramide catalysts. Furthermore, high yields were obtained in all reactions, which were carried out in 1 mmol of maleimide derivatives.

Conclusion

Our research aimed at tuning the structure of chiral C_2-symmetric diamines derived bifunctional organocatalysts for application in the asymmetric Michael addition of several Michael acceptors and donors, by using (thio)phosphoramide moieties as hydrogen-bond donor groups. It was found that phosphoramides and especially thiophosphoramides are really efficient in the investigated reactions. Although the thiophosphoramide having cyclohexane backbone gave complete transformations in a much shorter time, the enantioselectivities obtained were lower than those obtained with catalysts bearing diphenylethane backbone. The use of 1,2-diphenylethane-1,2-diamine derived thiophosphoramide, which could be prepared in good yields in a one-step procedure, afforded optically pure products in high yields and also allowed the use of low amount, down to 2.5 mol%, of catalyst. The applicability of the thiophosphoramide derivative was investigated in several asymmetric conjugate additions to various maleimides. With this organocatalyst, high conversions and enantioselectivities can be achieved in these Michael additions, thus provided and environmentally benign procedure of preparing optically pure succinimides needed in the pharmaceutical industry.

Acknowledgements

The authors thank the financial support of the Ministry of Human Capacities through grants 20391-3/2018/FEKUSTRAT and NTP-NFTÖ-20 (V. Kozma).

References

[1] *Catalytic Asymmetric Synthesis*, I. Ojima, (Eds.); 3rd ed., John Wiley & Sons: Hoboken, New Jersey, **2010**.
[2] *Asymmetric Catalysis on Industrial Scale: Challenges, Approaches and Solutions*, H. U. Blaser, E. Schmidt, (Eds.); Wiley-VCH, Weinheim, **2004**.
[3] *Asymmetric Organocatalysis – From Biomimetic Concepts to Applications in Asymmetric Synthesis*, A. Berkessel, H. Gröger, (Eds.); Wiley-VCH, Weinheim, **2005**.

[4] *Organocatalytic Enantioselective Conjugate Addition Reactions, A Powerful Tool for the Stereocontrolled Synthesis of Complex Molecules*, J. L. Vicario, D. Badía, L. Carrillo, E. Reyes, (Eds.); RSC Publishing, Cambridge, **2010**.
[5] U. Scheffler, R. Mahrwald, *Chem. Eur. J.* **2013**, *19*, 14346-14396.
[6] A. Avila, R. Chinchilla, E. Gómez-Bengoa, C. Nájera, *Tetrahedron Asymmetry*, **2013**, *24*, 1531-1535.
[7] K. Das Sarma, J. Zhang, Y. Huang, J.G. Davidson, *Eur. J. Org. Chem.*, **2006**, 3730-3737.
[8] D.M. Barnes, S.J. Wittenberger, J. Zhang, J. Ji, M.G. Fickes, M.A. Fitzgerald, S.A. King, H.E. Morton, F.A. Plagge, M. Preskill, S.H. Wagaw, J. Am. Chem. Soc., **2002**, *124* 13097–13105.
[9] D.A. Nugiel, A. Vidwans, C.D. Dzierba, *Bioorganic Med. Chem. Lett*., **2004**, *14*, 5489–5491.
[10] V. Kozma, F. Fülöp, Gy. Szőllősi, *Adv. Synth. Catal.*, **2020**, *362*, 2444-2458.

"SMART" MOLECULAR ENGINEERING OF METALLOMESOGENS BASED ON Pt(II) TERPYRIDINE COORDINATION COMPLEXES

Evelyn Popa[1], Benoît Heinrich[2], Adelina A. Andelescu[1], Massimo La Deda[3], Giuseppe di Maio[3], Emilie Voirin[2], Bertrand Donnio[2] and Elisabeta I. Szerb[1,*]

[1]Institutul de Chimie "Coriolan Drăgulescu", B-dul. Mihai Viteazu nr. 24, 300223, Timișoara, România
szella73@gmail.com
[2]Institut de Physique et Chimie des Matériaux de Strasbourg, 23 Rue du Loess, Strasbourg, 67034, France
[3]Dipartimento di Chimica e Tecnologie Chimiche, Universita della Calabria, via P. Bucci, Cubo 14/C, 87036 Arcavacata di Rende, Italy

Abstract
A series of ionic tetracoordinated Pt(II) complexes based on terpyridine ligand were synthesized and characterized. Their chemical structures were engineered by using counterions of different coordination strengths and dimensions, namely non-coordinating BF_4, weakly coordinating bulky gallate units, and small and strongly coordinating chlorine (Cl). The complexes containing lipophilic gallate units exhibit low temperature liquid crystalline properties. The mesomorphic properties were investigated by polarized optical microscopy (POM), differential scanning calorimetry (DSC) and X-ray diffraction studies (SWAXS). Photophysical properties were determined in solution and condensed states.

Introduction
In recent years, a particular interest has been granted to Pt(II) terpyridine (*tpy*) complexes, which, due to the rapid progress in the area of structure/reactivity/interaction with biomolecules such as DNA and proteins, present a great potential to expand the applications of this family of coordination compounds in biomedical fields[1]. Moreover, some ionic Pt(II) complexes with *tpy* or functionalised *tpy* ligands were showed to be good candidates for obtaining luminescent supramolecular assemblies both in liquid crystalline phases and gels,[2-6] owing to the extended aromatic region that favours π–π stacking and short Pt···Pt distances[7]. Herein we report the synthesis of new Pt(II) coordination complexes whose molecular structures are engineered by using ligands and counterions of different coordination strength. The gallate unit was decorated with three long alkyl chains, hence liquid crystalline properties were obtained for the resulting species.

Experimental
Synthesis and characterization of Pt(II) terpyridine complexes
The ligand **L** and complexes **Pt_1-4** were structurally analysed by means of spectroscopic (Nuclear Magnetic Resonance - 1D and 2D NMR, Fourier-Transform Infrared - FT-IR) and analytic (elemental analysis) investigations that confirmed their structure and purity. The ionic character of the complexes was evidenced by conductivity measurements in solution.

Results and discussion
Due to the Pt(II) ion straightforward coordination chemistry, both neutral and ionic species with different coordination environment depending on the coordination strength of ligands were obtained.

Complex **Pt_1** was synthesized adapting a procedure reported by Annibale *et al*. [8] Complex **Pt_3**, with BF_4 as counterion, was obtained by reacting complex **Pt_1** with an excess of NH_4BF_4.

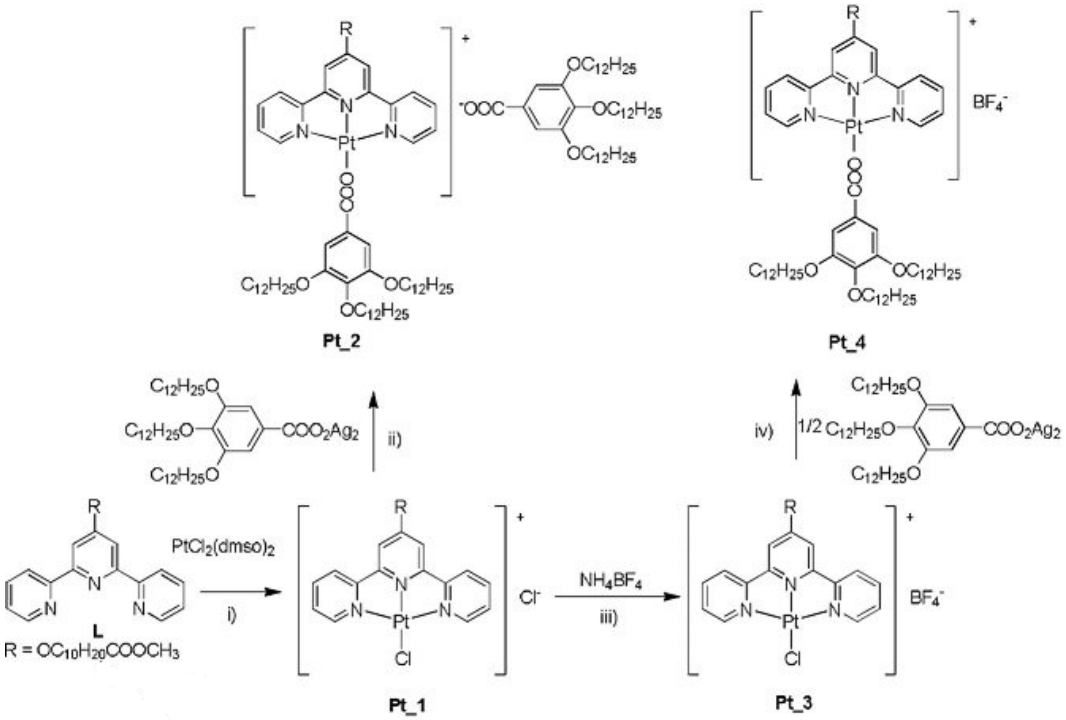

Scheme 1. Synthesis of Pt(II) complexes: i) MeOH, ΔT, 1.5 h; ii) $CHCl_3$/MeOH 1:1, r.t., 2 h; iii) $CHCl_3$/MeOH 1:1, r.t., 1 h; iv) $CHCl_3$/acetone 1:5, r.t., 2 h;

Complexes **Pt_1** and **Pt_3** were used as precursors in reaction with Ag(Gal), which is known as a mildly coordinating anion. The proposed chemical structures of Pt(II) complexes are supported by IR and accurate 1D and 2D NMR spectroscopy. Also, the ionic character of the Pt(II) complexes was evidenced in solution by conductivity measurements.[9]
The mesomorphic properties of the complexes **Pt_1-4** were first assessed by POM observations. As expected, complexes **Pt_1** and **Pt_3** did not possess liquid crystalline behaviour, melting at temperatures greater than 250°C, accompanied by decomposition. Complexes **Pt_2** and **Pt_4** containing the lipophilic gallate unit exhibit low temperature liquid crystalline properties, investigated by accurate POM, DSC and SWAXS measurements. Moreover, the photophysical properties of the Pt(II) complexes will be presented in both solution and condensed states.

Conclusion

Coordination complexes based on square-planar Pt(II) metal ions with luminescent properties are promising functional materials for various display and biomedical applications and there are still relatively few examples reported, which leaves space for the design of new metal–ligand systems to control the phase type, transition temperatures and thermal stability as well as to improve their luminescence in the mesophases.[10] The use of lipophilic gallate unit was shown to be a winning strategy to induce mesomorphic properties, complex **Pt_4** organizing into an original $LamCol_r$ mesophase of *p2mg* symmetry. In case of **Pt_2**, an erratic behaviour was observed, owing to the thermal dissociation of the gallate counterion, resulting in the co-existence of two or more species by varying temperature. However, the presence of bulky gallate groups resulted detrimental for the luminescence of the Pt(II) complexes. The sensitivity

of the metal ion to the molecular environment however is a potentially good property to be exploited in sensing applications.

Acknowledgements

This research was partially supported by Regione Calabria (POR Calabria FESR 2014/2020-Azione 1.2.2) through the MERAVIGLIE project. E.V, B.D. and B.H. thank the CNRS and University of Strasbourg for support. P.E., A.A.A and E.I.S. acknowledge the Romanian Academy, Program 4. E.I.S also acknowledges the support from the Romanian Academy and from the CNRRA bilateral project 2020–2022 (prot. n. 0088276 from 09/12/2019).

References

[1] X. Wu, M. Zhu, D.W. Bruce, W. Zhu, Y. Wang, J. Mater. Chem. C. 6 (2018) 9848–9860.
[2] F. Camerel, R. Ziessel, B. Donnio, C. Bourgogne, D. Guillon, M. Schmutz, C. Iacovita, J.-P. Bucher, Angew. Chem. Int. Ed. 46 (2007) 2659–2662; Angew. Chem. 119 (2007) 2713–2716.
[3] A.Y.-Y. Tam, K.M.-C. Wong, G. Wang, V.W.-W. Yam, Chem. Commun. (2007) 2028–2030.
[4] A.Y.-Y. Tam, V.W.-W. Yam, Chem. Soc. Rev. 42 (2013) 1540–1567.
[5] Y. Chen, C.-M. Che, W. Lu, Chem. Commun. 51 (2015) 5371–5374.
[6] K. Li, G.S.M. Tong, Q. Wan, G. Cheng, W.-Y. Tong, W.-H. Ang, W.-L. Kwong, C.-M. Che, Chem. Sci. 7 (2016) 1653–1673.
[7] J.A.G. Williams, *Top. Curr.Chem.* 281 (2007) 205–268.
[8] G. Annibale, M. Brandolisio, B. Pitteri, Polyhedron 14(3) (1995) 451–453.
[9] W.J. Geary, Coord. Chem. Rev. 7 (1971) 81–122.
[10] A.A. Andelescu, B. Heinrich, M.A. Spirache, E. Voirin, M. La Deda, G. Di Maio, E.I. Szerb, B. Donnio, O. Costisor, Chem. Eur. J. 26 (2020) 4850 – 4860.

DEVELOPING NEW ECOLOGICAL MATERIAL WITH APPLICATIONS IN CONSTRUCTION INDUSTRY AND POLLUTION REDUCTION

Florina-Stefania Rus[1], Stefan Novaconi[1], Madalina Ivanovici[1,2], Paulina Vlazan[1]

[1]*National Institute for Research and Development in Electrochemistry and Condensed Matter, Department of Condensed Matter, Strada Profesor Doctor Aurel Păunescu Podeanu 144, Timișoara 300569*
[2]*Politehnica University of Timisoara, Piata Victoriei 2, Timisoara 300006*
e-mail: rusflorinastefania@gmail.com

Abstract

The photocatalytic activity of TiO_2 incorporated foam glass obtained from glass waste from household activities with $CaCO_3$ waste from the marble industry samples was studied by evaluating their ability to degrade organic pollutants in aqueous solutions under the action of simulated solar radiation and using UV-VIS spectroscopy as a simple method to monitor dye concentrations over time. Organic dye has been selected as the reference substance for degradation experiments because the dyes are stable at high temperatures and light and are reported as a major source of pollution, especially for the aquatic environment generated by effluents, mostly in textile industry. Given the characteristics of glass foam combined with current requirements in environmental protection to develop smart materials to combat climate change caused by environmental pollution, this study aimed to expand the application potential of cellular glass by functionalizing it with a material with properties photocatalytic in order to degrade various pollutants in the atmosphere.

Introduction

Cellular glass is a material that presents an interesting combination of properties of interest that makes it a valuable and future material in the field of construction. The study focused on broadening the application potential of cellular materials by functionalizing them with material that have photocatalytic properties to degrade some pollutants. In this regard, the materials were activated with TiO_2 photocatalyst [1]. The material with embedded TiO_2 was subjected to photocatalytic studies and their ability to degrade pollutants under the action of simulated solar radiation was evaluated. A Methylene Blue (MB) dye was selected as the reference substance to be degraded. Activation of cellular glass to obtain photocatalytic properties was achieved by depositing in its volume. Cellular glass was obtained by capitalizing on household glass waste as a base material and $CaCO_3$ waste. The characterization of activated cell glass was performed by investigating the properties using the following analysis techniques: Raman spectroscopy), SEM-EDAX, X-ray diffraction, thermogravimetric analysis, UV-VIS spectroscopy, confocal 3D laser scanning microscopy and photocatalytic activity.

Experimental

Cellular glass was obtained by exploiting glass waste from household activities as a basic material and $CaCO_3$ waste (5%) from the marble industry as a foaming agent. The glass and marble waste were ground and passed through a sieving system until a powder granulation of 0.036 mm was obtained.

In order to introduce the photoactive compound in the volume of the cell glass, the sol-gel synthesis was applied as a method of obtaining TiO_2. Thus TiO_2 nanoparticles in concentration of 1% were introduced from the beginning of the synthesis together with glass waste, $CaCO_3$ (powder) and ethylene glycol in order to obtain pills, to which two heat treatments were applied: 200°C for 2 h and 850°C for 30 minutes, performed in a SNOL-type

furnace with a heating rate of 5°C/minute for 30 minutes. During the heat treatment, CO_2 bubbles resulted from the thermal decomposition process of $CaCO_3$, the generated gas leading to the formation of pores in the obtained pills and implicitly to the formation of cell glass.

To determine the photocatalytic activity the same equipment was used as in ours previouse paper [2] but instead of Rhodamine B as dye, we used this time Methylene Blue while adsorption-desorption balance between the sample and the dye was 12 hours. to identify and understand the factors and how they influence the results obtained in photocatalytic studies 1 cm diameter cell glass activated with 1% TiO_2 was immersed in aqueous solution of MB, followed by exposure for 2 hours to simulated solar radiation, using different concentrations of solutions. Thus, in table 1 are presented the working conditions and the results obtained for different concentrations of Methylene Blue.

Sample	Colorant concentrations	Conditions used	Adsorbtion Efficiency	Total Removal of Methylene Blue after Adsorbtion and Photocatalysis
Foam glass with 1% TiO_2	20 ml MB solution, concentration 2.5 mg L^{-1}	12h without stirring + 20 minutes stirring before exposure to radiation	66.82%	86.34%
Foam glass with 1%TiO_2	20 ml MB solution, concentration 5 mg L^{-1}	12 h + 20 minutes stirring before exposure to radiation	28.44%	64.51%

Results and discussion

In the Figures 1 with 20X and 2 at 10X magnification by associating 2D images with 3D ones, the deposition of TiO_2 particles is also confirmed outside the pores of the foam glass.

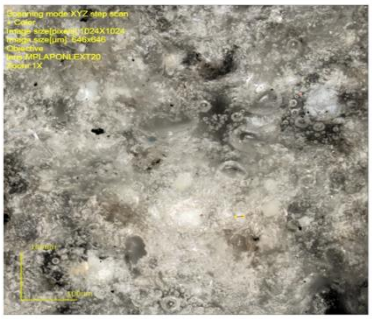

a)

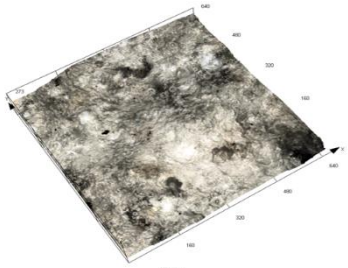

b)

Figure 1. (a) - 2D image of glass foam with 1% TiO_2 (b) 3D image of glass foam with 1% TiO_2 performed at 20X magnification

The surface roughness value at the scale of 20x was calculated on an area of 393289 μm^2, surface of 545240 μm^2 and volume of 914 μm^3 as 4.23 µm.

Figure 2. (a) - 2D image of glass foam with 1% TiO_2 (b) 3D image of glass foam with 1% TiO_2 performed at 10X magnification

For the figure 2 recorded at 10X the surface roughness value was 6.066 µm and calculated on an area of 1625368 µm², surface of 3025017 µm² and volume of 178 µm³.

Thus, considering the simplicity of monitoring the concentration of organic dye in aqueous solutions using UV-VIS spectroscopy but also their stability, photocatalytic studies were performed using Methylene Blue (MB) in different concentrations.

The adsorption and photoactivity of the as-prepared foam glass activated with TiO_2 photocatalyst was tested by the degradation of Methylene Blue (MB) under sunlight radiation at two concentrations of Methylene Blue 2.5 mg/L in figure 3 a) and 5 mg/L in figure 3b).

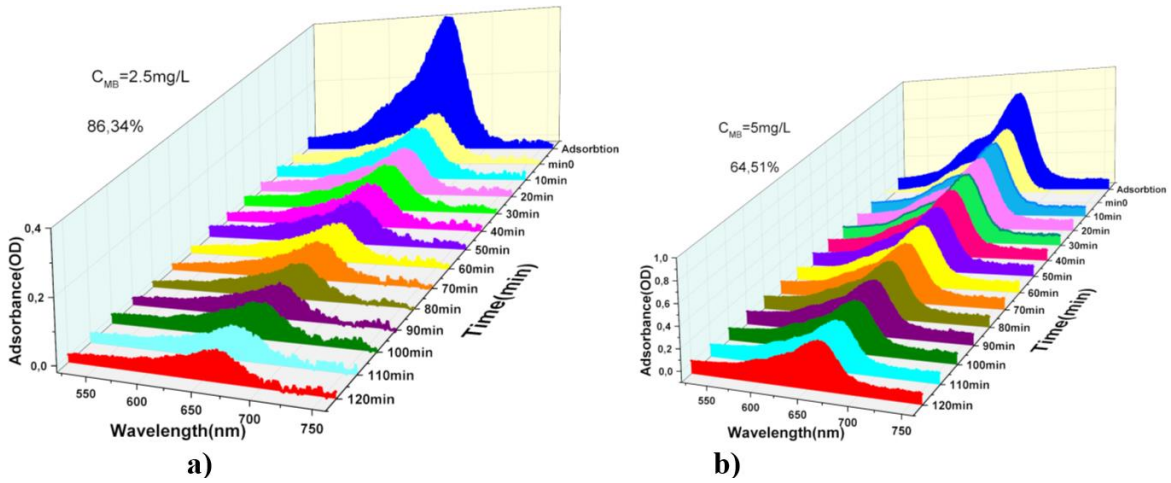

Figure 3. Photocatalytic activity in time of foam glass with 1% TiO_2 at 2.5 mg/L and 5 mg/L concentration of MB

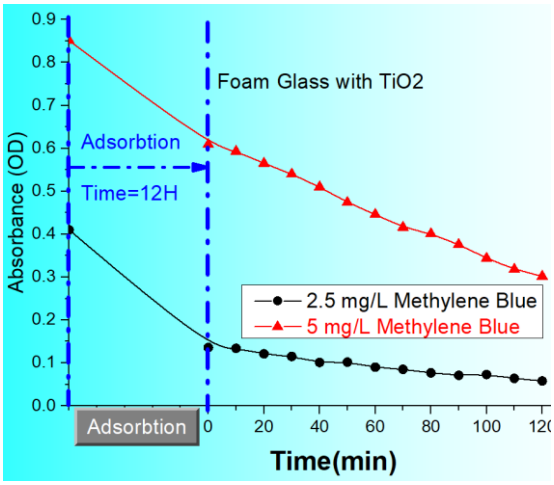

Figure 4. Removal of MB from aqueous solution by: TiO_2 activated cellular glass at 2.5 mg/L (marked with black), and 5 mg/L (marked with red) during adsorption and visible-light exposure

The new photocatalyst was able to reduce the concentration of MB by 88.34% where the initial concentration was 2.5 mg/L and 64.51% where the initial concentration was 5 mg/L.

Conclusion

The photocatalytic efficiency was evaluated by monitoring the discolouration of Methylene Blue applied to the surface of the foam glass obtained by capitalizing on household glass waste as a base material and $CaCO_3$ waste which were then exposed to solar simulator. The adsorption and photoactivity of the as-prepared foam glass activated with TiO_2 photocatalyst was tested at two concentrations of Methylene Blue with great efficiency of dye removal in both cases 88.34% and 64.51% which demonstrates that the ability of the tested samples to remove the dye by adsorption and degradation during photocatalysis is influenced by the solution concentration. Given the characteristics of glass foam combined with current requirements in environmental protection to develop smart materials to combat climate change caused by environmental pollution, this study proved that functionalized glass with TiO_2 can be used as a construction material with photocatalytic properties in order to degrade various pollutants in the atmosphere with great efficiency rate.

Acknowledgements

This work was supported by a grant of the Romanian Ministery of Research and Innovation, CCCDI–UEFISCDI, project number PN-III-P1-1.2-PCCDI-2017-0391/CIA_CLIM-Smart buildings adaptable to the climate change effects, within PNCDI-III.

References

[1] M. Pelaez, N.T. Nolan, S.C. Pillai, M.K. Seery, P. Falaras, A.G. Kontos, P.S.M. Dunlop, J.W.J. Hamilton, J.A. Byrne, K. O'shea, M.H. Entezari, D.D. Dionysiou, Applied Catalysis B, Environmental (2010);

[2] M. Ivanovici, P. Vlazan, S. D. Novaconi, and F. S. Rus, AIP Conference Proceedings 2218, 030013 (2020);

ARSENIC UPTAKE IN TOMATO AND CABBAGE IRRIGATED WITH ARSENIC-CONTAMINATED WATER

Sirat Sandil[1], Victoria Vetesi[1], Peter Dobosy[2], Mihaly Ovari[2], Anna Fuzy[3], Gyula Zaray[1,2]

[1]Cooperative Research Centre of Environmental Sciences, Eötvös Loránd University, Pázmány Péter sétány 1/A, H-1117 Budapest, Hungary
[2]MTA Centre for Ecological Research, Danube Research Institute, Karolina út 29-31, H-1113 Budapest, Hungary
[3]MTA Centre for Agricultural Research, Institute for Soil Sciences and Agricultural Chemistry, Herman Ottó út 15, H-1022 Budapest, Hungary
e-mail: sirat29@gmail.com

Abstract
Arsenic uptake by tomato (*Solanum lycopersicum* L.) and cabbage (*Brassica oleraceae* L. var. capitata L.) plants was studied by cultivating the plants in different soil types and irrigating them with water containing arsenic at concentrations of 0.05 and 0.2 mg As L^{-1}.

Introduction
The presence of arsenic in the agricultural soil or in groundwater used for irrigation causes abiotic stress to the plants cultivated in them. It leads to decrease in biomass production, yield, changes nutritional quality of the food, and alters the soil quality. The transfer of arsenic in soil–plant systems is a major pathway for human exposure to arsenic. As uptake by vegetables depends on the type of vegetable and the available arsenic species (Huang et al., 2006). Ground water in Hungary has naturally occurring arsenic in the range of 1-174 μg L^{-1} (Varsanyi et al., 2006), which is greater than the recommended 10 μg L^{-1} WHO standard, and this water is utilized for irrigation purpose.

Experimental
Arsenic uptake by tomato and cabbage was studied in sand, sandy silt, and silt soil by applying irrigation water containing As at concentrations 0.05 and 0.2 mg L^{-1}. Arsenic was supplied in the form of sodium arsenate. Pre-geminated seeds were grown in a pot-soil system in open greenhouse, supplied with Hoagland's nutrient solution and irrigated weekly. Arsenic accumulation in root, shoot, and fruit was analyzed at the fruiting or mature stage. The pseudo-total As concentration was determined in aqua-regia extract and the plant-available As concentration was determined by ammonium acetate-EDTA method (Lakanen and Ervio, 1971).
Upon harvest plant samples were thoroughly washed and dried at 40°C for 48hrs. The dry homogenized samples were digested in a microwave-assisted acidic digestion system using 7 cm^3 67 % nitric acid and 3 cm^3 30 % hydrogen-peroxide. The resultant solutions were diluted with deionized water up to 25 cm^3. Concentration of As was determined by inductively coupled plasma mass spectrometer.

Results and discussion
- The As content of the sand, sandy silt, and silt soil was 4.32, 6.15, and 9.02 mg kg^{-1}, respectively.
- The As concentration in plant is dependent on the plant-available As and not on the total soil As.

- Increase in As concentration of the irrigation water caused an increase in the As accumulation in the plant, and in both plants maximum As concentration was found in the roots and minimum in the leaf or fruit.
- Vegetables grown in sandy soil had the maximum As concentration and minimum biomass productivity.
- As accumulation in edible part was higher in cabbage.

Conclusion

The FAO-WHO recommended maximum tolerable daily intake limit of As is 2 μg kg^{-1} body weight. Considering this both plants grown in irrigation water containing up to 0.2 mg As L^{-1} are safe for consumption, but cabbage contributes a high amount of As in the diet. It is advised to cultivate plants at 0.05 mg As L^{-1} treatment and in silt soil to maintain an ideal biomass production and minimize As in the edible part.

Acknowledgements

This work was supported by the Hungarian Scientific Research Foundation (NVKP_16-1-2016-0044) granted to GZ and the Stipendium Hungaricum scholarship to SS.

References

[1] Huang R., Gao S., Wang W., Staunton S. and Wang G. (2006), Soil arsenic availability and the transfer of soil arsenic to crops in suburban areas in Fujian Province, southeast China, Science of the Total Environment, 368, 531–54.

[2] Varsanyi, I. Kovacs, L.O. (2006), Arsenic, iron and organic matter in sediments and groundwater in the Pannonian Basin, Hungary, Appl. Geochem. 21(6), 949-962.

POLY (VINYLIDENE FLUORIDE)/TIO_2-CNT NANOCOMPOSITE ULTRAFILTRATION MEMBRANES FOR WASTEWATER TREATMENT

Elias Jigar Sisay[1,2*], Ákos Fazekas[2], Zsuzsanna László[2,3]

[1]Doctoral School of Environmental Sciences, University of Szeged, Hungary.H-6720, Rerrich B. tér 1.
[2]Department of Process Engineering, Faculty of Engineering, University of Szeged, H-6725 Szeged, Moszkvai krt. 9.
[3]Institute of Environmental Science and Technology, University of Szeged, H-6720, Tisza Lajos Blvd. 103, Szeged, Hungary
**eliasjig@gmail.com, fazekas.akos92@gmail.com,zsizsu@mk.u-szeged.hu*

Abstract

Nowadays incorporation of nano-materials into polymers becoming a focus research area in membrane separation and purification technology. The fabricated nano-composite polymers offers an increased hydrophilicity and photo-catalytic benefits. However, the main advantages of each type of the nano-materials are limited. In this study ultra-filtration polymer nano-composite membranes were prepared using TiO_2 and CNT. Our recent work aims to examine the effect of TiO_2 and CNT on filtration properties of PVDF membrane. The contact angle of the neat membrane was78º, which could be lowered in case of the modified membranes of PVDF-TiO_2 and PVDF-TiO_2-CNT to 57.9 º and 64.63 º respectively. This implies that TiO_2 and CNT made the PVDF membrane hydrophilic due to their functional groups. It was found that the modification reduces the filtration resistance and enhances the flux. The water flux (L/m^2h) for neat PVDF membrane, PVDF-TiO_2 and TiO_2-CNT- PVDF was 67.22, 82.94 and 81.07 respectively. Neat PVDF membrane shows higher filtration resistance than TiO_2-PVDF and TiO_2-CNT-PVDF membrane. The irreversible foaling for neat PVDF was higher than the modified membranes. Regeneration of the fouled modified membranes by UV irradiation was possible.BSA and COD rejection was promising. The neat PVDF membrane rejects 99.84% BSA and 99.83% COD. The modified PVDF-TiO_2 also rejects 97.58% BSA and 99.74% COD while PVDF-TiO_2–CNT showed a rejection of 97.46% BSA and 97.05% COD. Relatively better regeneration of the fouled membrane was observed in the presence of CNT. The reasons for this phenomenon could be due to the reduction in recombination of electrons/holes and enhancement of photo-catalytic activity of TiO_2 by CNT as it sinks electrons/ holes. These results may offer significant new findings which are useful to development of modified membrane.

Keywords: nano-material, polymer, photo-catalytic nano-composite membranes, hydropholicity

1. Introduction

Nowadays, membrane separation technology has attracted interest due to the ease of operation and integration with other processes, reliable contaminant removal without production of any harmful by-products and low cost[1].Ultrafiltration (UF) membranes have received considerable attention because of the efficient rejection of bacteria, colloidal matter, protein, suspended particles, organic compounds, and better purification and concentration of food and paper products in industrial separation processes[2].

Among the polymeric materials, polyvinylidene fluoride (PVDF) is used widely in UF because of its superior properties such as high mechanical strength, excellent chemical resistance and

better thermal stability[3].However hydrophobic nature and low surface energy of PVDF membranes leads it to be fouled easily by natural organic matter (NOM), protein and oily wastewater, results a decline in flux and negatively impact production efficiency by reducing the longevity of a membrane and increasing the energy costs [4].An increase in membrane hydrophilicity seems to be a promising strategy to overcome membrane fouling. Recently, antifouling and self-cleaning membrane fabrication that has maximum permeate and long membrane life time is a focus research area in membrane separation and purification technology [5].

Titanium dioxide (TiO_2) nanoparticle is considered to be superior over other due to its excellent physical and chemical properties, availability, high photocatalytic activity, desirable hydrophilic and potential antifouling properties[6]. However the photocatalytic activity of TiO_2 is restricted by the recombination of the photogenerated electron-hole pairs [7].

Carbon nanotubes (CNTs) have attracted a considerable attention due to outstanding properties, such as unique mechanical (stiffness and flexibility), large specific surface area, high thermal and electrical conductivities [8]. They offer a large surface area support for TiO_2 particles due to the unique texture/morphology and adsorption capacity of CNTs. It also serves as an electron scavenger and significantly hinder the recombination of electrons and holes [8]. However, these photocatalysts have been conducted in the form of powders. In this paper, the preparation of $TiO_2$and CNT-TiO2 -PVDF composite membrane with various ratios by phase inversion is reported.

2. Experimental design

2.1 Preparation of modified PVDF membrane and filtration

Ultra-filtration membranes (17.5 wt% (polymer + NPs)and 82.5wt% (solvent)) were prepared with a phase-inversion process.. The fabricated membranes were cut into the desired cross-sectional area corresponding to the ultra-filtration (UF) dead-end cell experiments. The membrane filtration experiments were using1g/L bovine serum albumin (BSA) [9].

2.2.Analytical methods

Membrane contact angle. The water contact angle of the prepared membrane was measured manually by the sessile drop method (Data physics Contact Angle System OCA15Pro, Germany)**.** Standard potassium-dichromate oxidation method was the technique used to determine COD in our experiment.BSA concentrations in feed and permeate solutions were measured using a spectrometer(Hitachi Co., U-2000, Japan) at a 280 nm. Water and permeate fluxes of the neat and modified membranes were compared, organic content (COD: chemical oxygen demand), and protein rejection were investigated. Fouling resistance parameters including total fouling resistance (Rt), reversible fouling resistance (Rr) and irreversible fouling resistance (Rir) were calculated to study the fouling of the membranes process in detail through the resistances-in-series model [10].

3. Results and discussion

Water contact angle measurements

Contact angles were measured to study the surface hydrophilicity of the PVDF membrane, and the contact angles formed by distilled water on the surface of pristine and modified PVDF membrane were calculated using mean of six sample points..The contact angles of the neat PVDF, PVDF-TiO_2 and PVDF-CNT were72.23º, 57.9 º and 64.63º respectively. This implies that TiO_2 and CNT made the PVDF membrane very hydrophilic due to their functional groups.

A similar study by Hossein et al. [11] indicated hydrophilicity improvement of neat PVDF membrane by nanoparticles.

Filtration of BSA solution

In order to check the fouling mitigation ability of modified membranes protein (BSA) solutions were filtered and filtration resistances were calculated through the use of Eqs. (4)–(7). The membrane resistance (*RM*), irreversible resistances (*Rirrev*), reversible resistances (*Rrev*) and total resistances (*RT*) are presented in Figure 1. Pristine membrane shows the highest filtration resistance. It was found that the modification significantly decrease the membrane resistance.

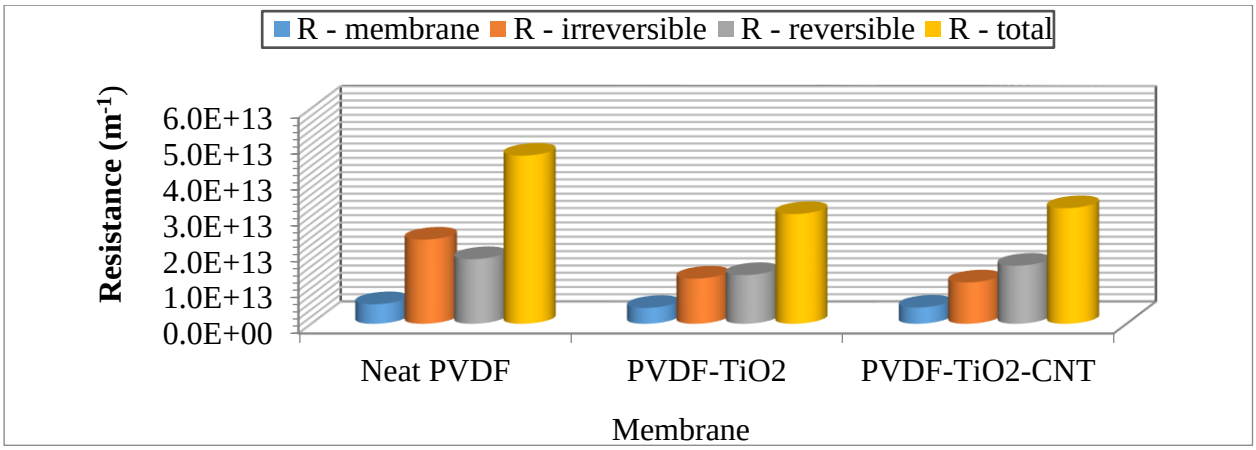

Figure 1. Filtration resistances by pristine and modified membranes

Unlike the neat membrane, reversible fouling of modified membranes were more than irreversible fouling, this can be explained by low contact angle. Our results are in accordance with the earlier observations [12].

Rejection

The BSA and COD rejections of the pristine and modified membranes are illustrated in Fig. 5. The neat PVDF membrane rejects about 98.88% BSA and 99.83% COD. The modified PVDF-TiO_2 also rejects 97.58% BSA and 99.74% COD while PVDF-TiO_2–CNT showed a rejection of 97.46% BSA and 97.05% COD. It was found that the modified membranes shows almost similar BSA and COD rejection as neat PVDF membrane this could be due to the formation of larger pores by nanoparticles [5].

Regeneration of BSA fouled membrane

Regeneration of fouled modified membranes can be achieved by 3 hours UV radiation (λ_{max} = 360 nm) light exposure. The extent of flux restoration for PVDF-TiO_2 a bit lower than PVDF-TiO_2-CNT. The reasons for this phenomenon could be due to the reduction in recombination of electrons/ holes and enhancement of photo-catalytic activity of TiO_2 by CNT as it sinks electrons/ holes [8].

4. Conclusion

This work investigates the effects of TiO_2-CNT incorporated PVDF polymeric membranes on the rejection of a model protein, bovine serum albumin (BSA) solution. Pristine PVDF and TiO_2-CNT- PVDF and TiO_2-PVDF membrane are fabricated by phase inversion method. Phase inversion is a simple and economical strategy method used to fabricate membranes. The membrane modification produced hydrophilic membrane surface, as was proven by contact

angle measurements on pristine and modified PVDF membranes. TiO_2-CNT- PVDF and TiO_2-PVDF membrane revealed a better water flux than the neat PVDF membrane. Neat PVDF membrane shows higher filtration resistance than TiO_2-CNT- PVDF and TiO_2-PVDF membrane. The irreversible foaling is higher for neat PVDF than the modified membranes. Regeneration of the fouled modified membranes by UV irradiation is possible. However 3 hours UV exposure is not enough to achieve the original flux which requires further investigation. A little more flux restoration is observed for TiO_2-CNT- PVDF than TiO_2-PVDF membrane. The reasons for this phenomenon could be due to the reduction in recombination of electrons/ holes and enhancement of photo-catalytic activity of TiO_2 by CNT as it sinks electrons/ holes.

5. Acknowledgements

The authors would appreciate the financial support of the Hungarian Science and Research Foundation (2017-2.3.7-TÉT-IN-2017-00016) the Hungarian State and the European Union (EFOP-3.6.2-16-2017-00010).

6. References

1. Gong, Y. W., Zhang, H. X., & Cheng, X. N. Treatment of dairy wastewater by two-stage membrane operation with ultrafiltration and nanofiltration. Water Science and Technology(2012), 65(5), 915–919.
2. Ayyaru, S., & Ahn, Y.-H. Application of sulfonic acid group functionalized graphene oxide to improve hydrophilicity, permeability, and antifouling of PVDF nanocomposite ultrafiltration membranes. Journal of Membrane Science (2017), 525, 210–219. doi:10.1016/j.memsci.2016.10.048
3. Chang, X., Wang, Z., Quan, S., Xu, Y., Jiang, Z., & Shao, L. Exploring the synergetic effects of graphene oxide (GO) and polyvinylpyrrodione (PVP) on poly(vinylylidenefluoride) (PVDF) ultrafiltration membrane performance.Applied Surface Science (2014).., 316, 537–548.
4. Chang, Y. R., Lee, Y. J., & Lee, D. J. Membrane fouling during water or wastewater treatmentsCurrent research updated.Journal of the Taiwan Institute of Chemical Engineers(2018), 0, 1–9.
5. Farahani, M. H. D. A., &Vatanpour, V. A comprehensive study on the performance and antifouling enhancement of the PVDF mixed matrix membranes by embedding different nanoparticles: Clay, functionalized carbon nanotube, SiO2 and TiO_2.Separation and Purification Technology(2018), 197, 372–381.
6. Leong, S., Razmjou, A., Wang, K., Hapgood, K., Zhang, X., & Wang, H. TiO 2 based photocatalytic membranes(2014). : A review, 472, 167–184.
7. Zouzelka, R., Kusumawati, Y., Remzova, M., Rathousky, J., &Pauporté, T. Photocatalytic activity of porous multiwalled carbon nanotube-TiO_2 composite layers for pollutant degradation. Journal of Hazardous Materials, 317(2016), 52–59.
8. Selvaraj,M.,Hai,.,Banat,F., and Abu,M. Journal of ater Process Engineering Application and prospects of carbon nano-structured materials in water treatment: A review.Journal of Water Process Engineering,33(2020),100-996.
9. Hou L., Wang Z. & Song P. A precise combined complete blocking and cake filtration model for describing the flux variation in membrane filtration process with BSA solution. Journal of Membrane Science, 542(2017) 186–194.
10. Vatanpour, V., Yekavalangi, M. E., &Safarpour, M. Preparation and characterization of nanocomposite PVDF ultrafiltration membrane embedded with nanoporous SAPO-34 to improve permeability and antifouling performance. Separation and Purification Technology (2016)., 163, 300–309.
11. Hossein M., Abadi D. & Vatanpour V.. Separation and Purification Technology A

comprehensive study on the performance and antifouling enhancement of the PVDF mixed matrix membranes by embedding different nano particulates : Clay, functionalized carbon nanotube, SiO 2 and TiO 2, 197(2018).372–381.

12. Ismail N., Lau W.J., Ismail A.F. , & Goh.Preparation P. and Characterization of Polysulfone/Polyphenylsulfone/Titanium Dioxide Composite Ultrafiltration Membranes for Palm Oil Mill Effluent Treatment. Jurnal Teknologi)(2013), 65(4)

ANALYTICAL POSSIBILITIES OF CARBON NANOTUBE BUCKYPAPERS DOPED BY GOETHITE

I. Y. Tóth[1] and Á. Kukovecz[1]

[1]*Department of Applied and Environmental Chemistry, University of Szeged, Interdisciplinary Excellence Centre, H-6720, Szeged, Rerrich Béla tér 1, Hungary*
e-mail: ildiko.toth@chem.u-szeged.hu

Abstract
The evaporation of liquids from porous films is a very complex phenomenon, which can be followed by simultaneous weight monitoring, electric resistance measurement, infrared imaging and contact angel measurement. The appropriate evaluation of these measurement results can carry both quantitative and qualitative analytical information. The aim of our recent work is to demonstrate this opportunity through the example of the evaporation of simple solvents from porous buckypapers prepared from non-functionalized carbon nanotubes (*nf*-CNT) doped by goethite.

Introduction
Recent developments in nanotechnology have highlighted the importance of the classical topics of wetting, droplet spreading and evaporation due to their pronounced effect in technological applications (*e.g.*, air/fuel premixing, micro-fluidics, oil recovery, etc.) [1,2]. Multiple phenomena take place simultaneously when a liquid droplet contacts a porous surface: wetting, spreading, capillary filling, gravity induced convective flow, adsorption, evaporation from the surface, evaporation from the pores, etc. The evaporation of a sessile droplet can be studied by several experimental methods: transmission electron microscopy, environmental scanning electron microscopy, contact angle measurement, high speed camera recordings, thermal imaging, just to name a few. The evaporation of sessile droplets can be followed by an equipment assembled at the Department of Applied and Environmental Chemistry, University of Szeged: this equipment can guide simultaneous weight monitoring, electric resistance measurement and infrared imaging at a controlled temperature (typically at 50 °C). There are several experimental results characteristic for the evaporation process, the most important ones being the total evaporation time, time of evaporation only from the surface, full width at half maximum of the time-dependent mass and resistance curves, evaporation rate, initial area of the droplet, and the wetted area at the moment of total evaporation from the surface, etc. [3-5]. The main goal of this work was to demonstrate the analytical possibilities of the mass and resistivity measurements and IR videos through the example of sessile droplet evaporation (acetone, methanol, ethanol, water) from porous buckypapers (BP) prepared from *nf*-CNT and doped by goethite.

Experimental
Materials: The multiwall **carbon nanotubes** were synthesized by 2 h of catalytic chemical vapor deposition from a C_2H_4:N_2 (30:300 cm^3/min) gas mixture at 650 °C over Fe,Co/Al_2O_3 catalyst (metal loading: 2.5-2.5 m/m%). The synthesized materials were purified by repeating 4 h of refluxing in 10 mol/dm^3 aqueous NaOH, then 4 h in cc. HCl solution four times. The **goethite** nanomaterials were prepared by oxidation-precipitation method from water based solution of $FeCl_2$, precipitated by NaOH solution and oxidized by $NaNO_3$. The synthesis was performed at room temperature and under normal atmosphere. The yellow product was purified by centrifugation. The *nf*-CNTs and goethite were converted into **buckypaper** (BP) by filtering 70 cm^3 of their 0.1 g/dm^3 suspensions through a 0.45 μm nominal pore diameter Whatmann

nylon membrane filter. The *nf*-CNTs (6.3 mg) and goethite (0.7 mg) were suspended by 40 min ultrasonication in N,N-dimethylformamide [3,4]. The schematic of the BP synthesis is presented in Fig. 1.

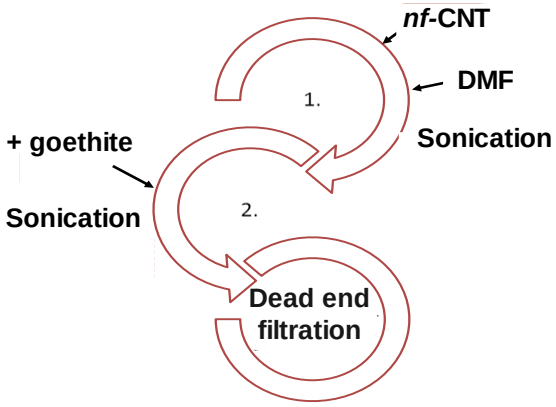

Figure 1. Schematic of the buckypaper synthesis.

Methods:

Electrophoretic mobilities of the CNTs and goethite nanomaterials were measured in a Nano ZS (Malvern) apparatus with a 4 mW He−Ne laser source (λ = 633 nm) using disposable zeta cells (DTS 1070) at 25 ± 0.1 °C. The zeta-standard of Malvern (−55 ± 5 mV) was used for calibration and the samples were diluted to give an optimal intensity. To get comparable data, the dispersions were homogenized in an ultrasonic bath for 10 s, after which 2 min relaxation was allowed. The effect of pH variation were studied at 10 mM NaCl. The Smoluchowski equation was applied to convert electrophoretic mobilities to electrokinetic potential values. The accuracy of the measurements was ±5 mV.

Liquid droplet evaporation (acetone, methanol, ethanol, water) was studied from the buckypaper film. The droplets (5 μL, 50 °C) were instilled with an Eppendorf Xplorer electronic pipette on the surface of the porous films. The temperature, the electric resistance and weight variations could be simultaneously monitored by the equipment assembled at the Department of Applied and Environmental Chemistry, University of Szeged. Buckypaper was placed onto a purpose-built sample holder and kept in place by a top piece that had a 1.4 cm diameter circular opening in it for placing the liquid droplet. The setup included a type K thermocouple in contact with the non-wetted part of the BP. The distance between the porous film and the heater was 1 cm. Data from the thermocouple was fed back to the temperature controller that maintained a base BP temperature of 50 ± 0.5 °C by continuously adjusting the heater power using fuzzy logic control. The sample holder was placed on a Sartorius Cubis microbalance with 0.01 mg readability and the weigh variation during droplet evaporation was recorded. For thermal imaging a FLIR A655sc infrared (IR) camera was used. This unit has a thermal sensitivity of 30 mK, an accuracy of ±2 °C for temperatures up to 650 °C at 640x480 resolution. Its uncooled microbolometer detector has a spectral range of 7.5-14.0 μm. The IR camera is equipped with a 2.9x (50 μm) IR close-up lens, with 32x24 mm field of view and 50 μm spatial resolution. The recorded images are transferred to a PC with FLIR ResearchIR Max software. Sessile droplet evaporation movies were acquired at maximum resolution with 50 Hz frame rate. Each CNT film's emissivity (ε_{film}) was determined by calibration at the initial film temperature (25 °C) with a black electrical tape (ε = 0.95). During liquid surface evaporation the temperature was determined by taking into account the emissivity of the liquid (ε_L = 0.95); after surface evaporation, the emissivity of the wetted film was calculated as the average between the emissivities of the studied liquid and the porous film. The sample holder plastic plate with the 0.7 cm radius gap in the center was equipped with two copper electrical connections at the opposite edges of the gap on the bottom of the sheet. The BP was fixed to

the bottom of the plastic section with magnetic clips. The copper electrodes were contacted to the source meter by 0.3 mm diameter copper wires. The rigidity of these wires did not affect the balance because of the large inertia of the whole assembly mounted on the balance plate. This was confirmed by independent experiments before the evaporation profile (electrical resistance variation as a function of time) measurements. The computer recorded the electrical resistance of the buckypaper as measured by a Keithley 2612A Source Meter. Before the measurements, the BP film was mounted in the assembly and heating at initial temperature was applied until the electrical resistance and the sample weight both stabilized. Then all three recordings (resistivity, IR imaging and sample weight) were started a few seconds before dropping. The evaporation was studied by dropping a single droplet of a selected solvent to the center of the BP film and simultaneously recording the IR video, the mass and electrical resistance until they returned to their original values. The schematic of the equipment is presented in Fig. 2. The ambient air temperature and the relative humidity of the ambient atmosphere were kept constant (at 25 °C and 55 RH%, respectively) [3-5].

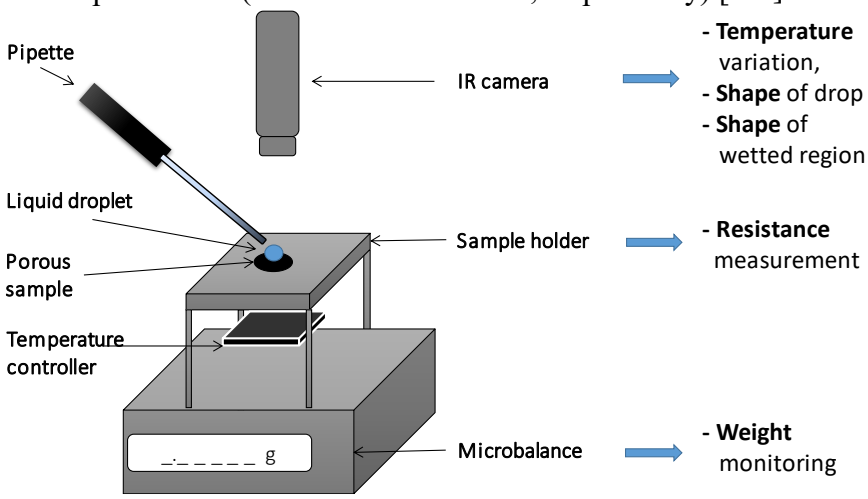

Figure 2. Evaporation monitoring equipment schematic.

Results and discussion

The zeta potential of *nf*-CNTs and goethite nanomaterilas are plotted as a function of pH in Fig. 3. The isoelectric point (IEP, at which the net charge of CNT is zero) is at pH~3 for *nf*-CNT and at pH~4.5 for goethite. The values of zeta potential shift to more negative region with the increasing pH.

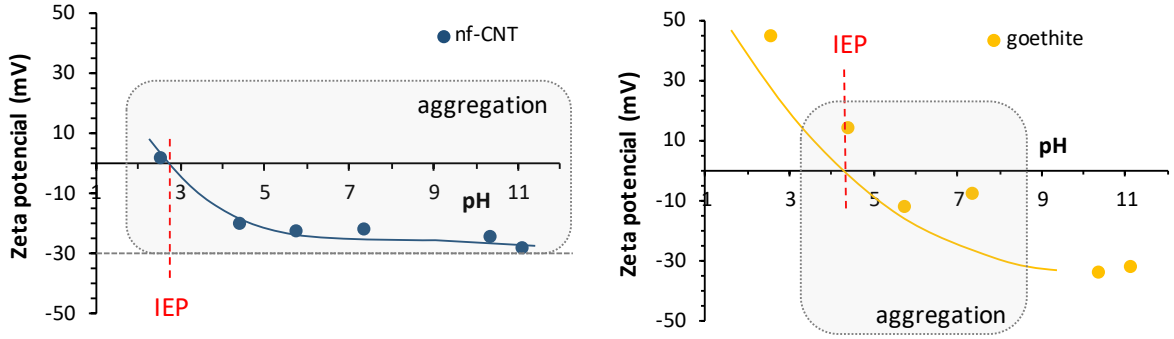

Figure 3. The pH dependent zeta potential of *nf*-CNT and goethite (10 mM NaCl, 25°C).

In general at the moment we drop the liquid on the buckypaper film (t_0), the liquid starts to diffuse immediately into the pores of the BP, but a part of it remains spread on the surface of the film. The evaporation of this liquid from the surface takes place together with the diffusion. Once all liquid evaporates from the surface, namely the primary surface evaporation is complete (t_s), liquid is left only in the pores. The solvent gradually evaporates from the pores as well. The

complete evaporation of the solvent (t_t) was confirmed by the fact that the mass and the resistivity of the buckypaper returned to the baseline.

One typical mass variation is illustrated in Fig. 4. where t_0 marks the time when the drop was instilled. The mass of the BP increased as soon as the solvent was dropped to the film and this is followed by a quasi-linear weight decrease. Once the primary surface evaporation is complete (t_s), the mass of the buckypaper decreases as linear (within experimental error) functions of time due to the continuous evaporation of the solvent. The total evaporation time (t_t) was at the moment when the mass of the BP returned to the baseline. At the linear weight decreasing ranges, the rate of evaporation (-dm/dt) is constant. The change of -dm/dt value suggests the change of the dominant evaporation process, *e.g.*, evaporation of the droplet sitting on the surface of the BP, evaporation of the condensed water from the porous system or the evaporation of the adsorbed water from the microscopical surface of the porous system (see the linear ranges in Fig. 4.). From this measurement, the typical experimentally determined data are the shape of the curve: m_{max}, area, FWHM; t_s and t_t, evaporation rate -dm/dt and its change. These are characteristic for the measured system and can be used to identify them [3-6].

The weight variation during the evaporation of acetone, methanol, ethanol and water from the surface of *nf*-CNT doped by goethite can be seen in Fig. 5. It is clear that the more volatile solvents evaporate faster than water.

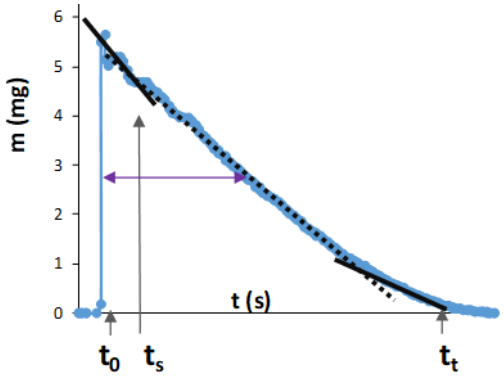

Figure 4. Weight variation of a BP as a functions of time during the evaporation process.

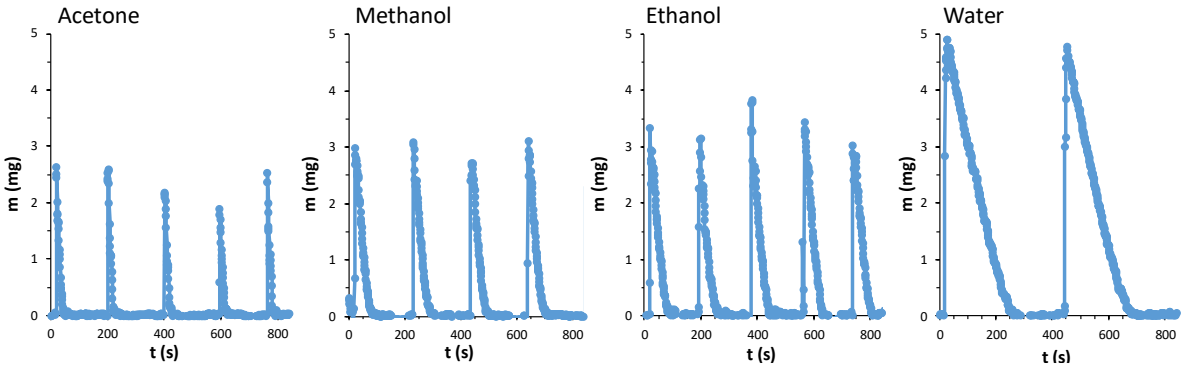

Figure 5. Evaporation of acetone, methanol, ethanol and water from *nf*-CNT buckypaper doped by goethite (5 µL, 50°C).

The IR videos were evaluated at selected representative moments, such a typical series of images is shown in Fig. 6. It is possible to determine the spot area and average temperature of the drop (S_d, T_d) and of the wetted region (S_w, T_w) as a function of time. Some data extracted from weight and resistivity variation and from infrared videos are characteristic for the evaporation of the selected liquid/solid system: surface evaporation time (t_s), total evaporation time (t_t), evaporation rate (-dm/dt) and its change, FWHM values of the curves, initial area of

the drops ($S_{d(t0)}$), area of the wetted region at t_s ($S_{w(ts)}$), etc. Some of these data are collected in Table 1.

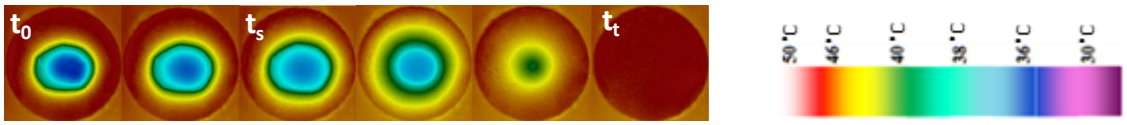

Figure 6. Images exported pro rata from the IR video correspond to t_0, t_s, t_t and several representative intermediate times (*nf*-CNT doped by goethite, 5 µL EtOH, 50°C).

Table 1. Some data extracted from m and R variation and from IR videos recorded during the evaporation of different solvents from the surface of *nf*-CNT doped by goethite (5 µL, 50°C).

	$t_{t(m,R)}$	$t_{s(R)}$	**FWHM$_{(m)}$**	**FWHM$_{(R)}$**	$S_{d(t0)}$	$S_{w(ts)}$
acetone	29 s	6 s	7 s	15 s	-	-
methanol	66 s	9 s	24 s	37 s	-	-
ethanol	83 s	5 s	29 s	47 s	3.3 mm^2	63.4 mm^2
water	227 s	18 s	89 s	87 s	5.4 mm^2	72.2 mm^2

Conclusion

The weight monitoring of the evaporation of liquids from porous films can provide information about the mechanism of wetting and vaporization which is a significant area of the basic researches. Furthermore, it can be proved by using appropriate statistical methods (*e.g.*, matrix of Pearson correlation coefficients, hierarchical cluster analysis, functional analysis, etc.), that the experimentally determined characteristic values are specific for the physical properties of the solvents, and they are also dependent on the quality of the solid materials, therefore, they can be used for qualitative chemical analysis via the estimation of physical properties. The results allow us to presume the possibility of this experimental setup and theoretical approach for a potential future application in the field of analytics.

Acknowledgements

We thank Gábor Veress and István Sütő for the technical contribution during the measurements. Financial support from the Hungarian National Research, Development and Innovation Office through the GINOP-2.3.2-15-2016-00013 “Intelligent materials based on functional surfaces−from syntheses to applications” project is acknowledged. I.Y. Toth also acknowledge the support by the János Bolyai Research Scholarship of the Hungarian Academy of Sciences and the Ministry of Human Capacities, Hungary through the grant ÚNKP-19-4 New National Excellence Program.

References

[1] D. Bonn, et al., Mod. Phys. 81(2) (2009) 739−804.
[2] H.Y. Erbil, Adv. Colloid Interface Sci. 170(1-2) (2012) 67−86.
[3] G. Schuszter, et al., Mic. Mes. Mat. 209 (2015) 105–112.
[4] E.S. Bogya, et al., Carbon 100 (2016) 27–35.
[5] I.Y. Tóth, et al., J. Mol. Liquids 305 (2020) 112826

STUDYING BEER DEALCOHOLIZATION BY REVERSE OSMOSIS

Áron Varga[1,2,3], † Edit Márki[1], Eszter Bihari-Lucena[1,2,4], Márta Ladányi[5], Beatrix Szabó-Nótin[6], András Koris[1]

[1]Department of Food Engineering, Szent István University, H-1118 Budapest, Ménesi út 44., Hungary
[2]Department of Food Chain Management, Szent István University, H-1118 Budapest, Villányi út 29–43., Hungary
[3]Pécs Brewery, H-7624 Pécs, Alkotmány utca 94., Hungary
[4]Department of Brewing and Distilling, Szent István University, H-1118 Budapest, Ménesi út 45., Hungary
[5]Department of Biometrics and Agricultural Informatics, Szent István University, H-1118 Budapest, Villányi út 29-43., Hungary
[6]Department of Food Preservation, Szent István University, H-1118 Budapest, Villányi út 29-43., Hungary
e-mail: mr.aron.varga@gmail.com

Abstract

The production of low-alcohol beer (LAB) or alcohol-free beer (AFB) is important because of several reasons. In this research, pale lager beer samples were dealcoholized by reverse osmosis (RO) at a temperature of 15 ± 1 °C. Alfa Laval RO99 membrane with 0.05 m^2 active surface was used for dealcoholization processes. Flux values were measured during the separations. Dynamic viscosity values and ethanol content of beer and permeate samples were measured. Initial flux values were determined by linear regression. Initial ethanol flux ($J_{EtOH\,0}$) values were calculated from initial flux values and ethanol content values. 2^P type full factorial experimental design was applied, the two factors were the following: Transmembrane Pressure (TMP): 10, 20, 30 bar and Retentate Flow Rate (Q): 120, 180, 240 L hr^{-1}. $J_{EtOH\,0}$ was considered as a response of the full factorial experimental design. The effect sizes of the significant parameters were calculated. The global maximum of the objective function was found with self-developed Grid Search code. The best fitted linear function was as follows:

$J_{EtOH\,0} = 80.871 + 41.094 \times x_{TMP}$

The effect size of the significant parameter was the following: TMP: 1.20. The optimal value of the factor amounted to TMP = 30 bar. The predicted $J_{EtOH\,0}$ under the above condition was 121.965 g m^{-2} hr^{-1}. The detailed method in this study can be implemented by breweries.

Introduction

The scope of this research is to study beer dealcoholization (BDA) by reverse osmosis (RO).

There can be several reasons for low-alcohol beer (LAB) or alcohol-free beer (AFB) production. The reasons are the following: increase in the overall production by introduce new products in countries with highly competative markets; provide beer consumers with products prior or during their activites (driving motor vehicles, operating machinery, doing sports) or under conditions (pregnancy, medication) irreconcilable with alcohol consumption; penetrate beverage markets in countries, where alcohol consumption is forbidden for religious reasons [1]. There are different methods for LAB or AFB production. One of the groups of the methods are the membrane separation processes. Membrane separation processes provide promising alternatives for separating the alcohol after the fermentation process and include such advantages as lower energy consumption, no chemical additives, and operation at mild temperatures, therefore reducing the impact of heat on the product [2]. In this research, a membrane separation process for BDA is investigated, namely RO. The most important

parameters of the BDA by RO are the permeate flux and the ethanol concentration in the permeate. These parameters can be combined into one parameter: ethanol flux [3].
The goals of this research are to determine the analytical parameters of beer and permeate samples (ethanol content values for the physical modelling); to determine the hydrodynamic parameters of the membrane separations for the (physical modelling); to calculate the ethanol flux values of the membrane separations for the response (physical modelling) of the experimental design; to analyse the experimental design (mathematical modelling) of the membrane separations (parameter and effect size estimation); to optimize the objective function (the mathematical model) extracted from the analysis of the experimental design.

Experimental

Beers

0.5 L canned Soproni Klasszikus pale lager beers (HEINEKEN Hungária, Hungary) with 4.5% (V/V) ethanol content were used during beer dealcoholization by reverse osmosis.

Membrane

RO99 flat sheet polyester membrane (Alfa Laval, Sweden) with 0.05 m^2 active surface was used for dealcoholization processes.

Membrane separation process

Dealcoholization experiments were performed according to the experimental design at a temperature of 15 ± 1 °C. Flux values were measured during the separations.

Analytical parameters

Dynamic viscosity values of beer and permeate samples were measured with Physica MCR 51 Rheometer (Anton-Paar Hungary, Hungary) with DG27 double gap concentric cylinder measurement system. Ethanol content values of beer and permeate samples were measured with Alcolyzer Plus (Anton-Paar, Austria).

Linear regression

Based on a linear model, initial flux values were determined by regression in IBM SPSS Statistics 25 software (IBM, USA).

Hydrodynamic parameters

Initial ethanol flux values were calculated from initial flux values and ethanol content values.

Modelling

2^P type full factorial experimental design was applied, the two factors were the following: Transmembrane Pressure (TMP): 10, 20, 30 bar and Retentate Flow Rate (Q): 120, 180, 240 L hr^{-1}. Initial ethanol flux ($J_{EtOH\,0}$) was considered as a response of the full factorial experimental design. Factors were coded to standard values (x): –1, 0, 1. The results of the experimental design were analyzed in R 3.5.1 software (R Foundation for Statistical Computing, Austria) using RcmdrPlugin.DoE package (R Foundation for Statistical Computing, Austria) and RStudio 1.2.1335 software (RStudio, USA). The non-significant parameters were eliminated. The effect size of the significant parameter was calculated. Normality of residuals was accepted by Shapiro-Wilk normality test ($p = 0.72$). The global maximum of the objective function was found with self-developed Grid Search code in Scilab 6.1.0 software (ESI Group, France).

Results and discussion

The best fitted linear function that describes the relation between factors and response was as follows:

$J_{EtOH\ 0} = 80.871 + 41.094 \times x_{TMP}$

The non-significant parameters (Q and interaction) were eliminated. Model accuracy and determination coefficients of the objective function were also significant ($F(1;5) = 143.1$; $p < 0.001$; Multiple $R^2 = 0.97$; Adjusted $R^2 = 0.96$). The effect size of the significant parameter was the following: TMP: 1.20. The optimal value of the factor amounted to TMP = 30 bar. The predicted $J_{EtOH\ 0}$ under the above condition was 121.965 g m^{-2} hr^{-1}.

Conclusion

According to the analysis of the experimental design, TMP had significant effect, while Q had no significant effect on $J_{EtOH\ 0}$ with the given parameters. Furthermore, there was no significant interaction between the factors. This means that the commercial breweries should only focus on the optimization of TMP. BDA by RO can be performed with lowest required Q, which results in lower energy consumption. The lower energy consumption is important because of environmental and economic issues. Furthermore, TMP had interactive effect on $J_{EtOH\ 0}$. Based on the results of the optimization, the highest $J_{EtOH\ 0}$ could be achieved with the highest TMP. Thus, commercial breweries should set the TMP at this level. In a later exercise, beers with different alcohol and extract content could be dealcoholized by RO.

Acknowledgements

This work was supported by the Szent István University, Doctoral School of Food Sciences; the European Union and co-financed by the European Social Fund [grant number EFOP-3.6.3-VEKOP-16-2017-00005]. We would like to say thanks to Szent István University, Department of Brewing and Distilling; Szent István University, Department of Food Preservation for supporting the research. The beer samples were provided by SPAR Magyarország, Hungary.

References

[1] T. Brányik, D.P. Silva, M. Baszczyňski, R. Lehnert, J.B. Almeida E Silva, A review of methods of low alcohol and alcohol-free beer production, Journal of Food Engineering. 108 (2012) 493–506. https://doi.org/10.1016/j.jfoodeng.2011.09.020.

[2] A. Ambrosi, N.S.M. Cardozo, I.C. Tessaro, Membrane Separation Processes for the Beer Industry: A Review and State of the Art, Food and Bioprocess Technology. 7 (2014) 921-936. https://doi.org/10.1007/s11947-014-1275-0.

[3] P. Russo, L. Liguori, D. Albanese, A. Crescitelli, M. Di Matteo, Investigation of osmotic distillation technique for beer dealcoholization, Chemical Engineering Transactions. 32 (2013) 1735–1740. https://doi.org/10.3303/CET1332290.

NOVEL COBALT COMPLEXES WITH GLYOXIMES: SYNTHESIS, PHYSICO-CHEMICAL ANALYSIS AND BIOLOGICAL STUDY

Csaba Várhelyi jr.[1], Roland Szalay[2], György Pokol[3,4], Firuţa Goga[1], Péter Huszthy[3], János Madarász[3], Melinda Simon-Várhelyi[1], Róbert Tötös[1], Alexandra Avram[1]

[1] Faculty of Chemistry and Chemical Engineering, "Babeş-Bolyai" University, RO-400 028 Cluj-N., Arany János str. 11, Romania
[2] Institute of Chemistry, "Eötvös Loránd" University, H-1117 Budapest, Pázmány Péter str. 1/a, Hungary
[3] Faculty of Chemical Technology and Biotechnology, Budapest University of Technology and Economics, H-1111 Budapest, Műegyetem rkp. 3, Hungary
[4] Research Centre for Natural Sciences, H-1117 Budapest, Magyar tudósok körútja 2, Hungary
e-mail: ifj.varhelyi.cs@gmail.com

Abstract

Azomethine derivatives have several applications, especially as reagents for the determination of transition metal ions. Furthermore these ligands and their cobalt complexes were also reported to possess biological activities, such as antimicrobial, anti-tubercular, anticonvulsant, anti-inflammatory, anti-proliferative activities as well as antifungal inhibition potential [1]. Another reason for using metal-containing compounds as structural scaffolds is related to the kinetic stability of their coordination spheres in the biological environment. Metallic ions have been shown to play important role in the biological activity of different compounds in such away that, in some cases, activity is enhanced or only takes place in the presence of these ions [2].

In our research new cobalt(III) complexes were synthesized with α-glyoximes, azides, amines, thiocyanate and halogens, such as $[Co(Me\text{-}propyl\text{-}GlyoxH)_2(N_3)(amine)]$, $[Co(Me\text{-}pentyl\text{-}GlyoxH)_2(N_3)(amine)]$, $[Co(Et\text{-}propyl\text{-}GlyoxH)_2(N_3)(amine)]$, $[Co(Et\text{-}propyl\text{-}GlyoxH)_2(Br)(amine)]$, $[Co(Et\text{-}propyl\text{-}GlyoxH)_2(SCN)(amine)]$, $H[Co(Et\text{-}propyl\text{-}GlyoxH)_2(SCN)_2]$, $[Co(phenyl\text{-}Me\text{-}GlyoxH)_2(amine)_2]I$, $[Co(Et\text{-}propyl\text{-}GlyoxH)_2(amine)_2]I$, $[Co(Et\text{-}Bu\text{-}GlyoxH)_2(amine)_2]I$, where GlyoxH = mono deprotonated glyoxime, and the used amines: imidazole, 3-hydroxy-aniline, lepidine, 3,5-dimethyl-pyridine, di(*n*-butyl)-amine, diisopropyl-amine, 2-amino-pyrimidine, diphenyl-amine, 2-picoline, 3-picoline. The Co(II)-acetate salt dissolved in water and mixed with the glyoxime alcoholic solution was oxidized by air bubbling, then the corresponding diamines and the other complexing agents were added.

The molecular structure of our products was investigated by IR, UV–VIS spectroscopy, mass spectrometry (MS), thermoanalytical measurements (TG-DTG-DTA), and powder XRD. The biological activity, like antimicrobial effect, was studied for a few bacteria.

Introduction

The importance of metal compounds in medicine dates back to the 16th century, with reports on the therapeutic use of metals or metal-containing compounds in the treatment of cancer. Metal ions are often electron deficient species whereas most biological molecules (proteins and DNA) are electron rich molecules, consequently, there is a general tendency for metal ions to bind to and interact with many important biological molecules. Several metal ions also have high affinity towards small molecules, e.g. O_2, that are crucial to life. These considerations alone have fueled much of the past and current interest in developing novel means to use metals or metal-containing agents to modulate biological systems [3].

Some Co-glyoximato complexes show antibacterial activity. The B_{12}-vitamine molecule, which is used in the treatment of pernicious anemia, is also regarded as a Co(III)-glyoxime coordiantion compound. Some other cobalt complexes are also used in analytical chemistry and moreover, they act as catalysts in water-splitting reaction for hydrogen generation [4].

In this paper we report the synthesis, characterization and biological evaluation of some Co(III) complexes with glyoximes, amines and other ligands.

Experimental

Used materials: $Co(OAc)_2$, Me-propyl-GlyoxH_2, Me-pentyl-GlyoxH_2, Et-propyl-GlyoxH_2, phenyl-Me-GlyoxH_2, Et-Bu-GlyoxH_2, imidazole, 3-hydroxy-aniline, lepidine, 3,5-dimethyl-pyridine, $(n\text{-Bu})_2NH$, diisopropyl-amine, 2-amino-pyrimidine, diphenyl-amine, 2-picoline, 3-picoline, sodium azide, potassium thiocyanate, potassium bromide, potassium iodide, EtOH.

Methods:

- *Synthesis of [Co(GlyoxH)$_2$(N$_3$)(amine)] type complexes*

0.005 mol Me-propyl-GlyoxH_2 or Me-pentyl-GlyoxH_2 or Et-propyl-GlyoxH_2 was dissolved in 20 ml EtOH then added to an aqueous solution of 0.0025 mol $Co(OAc)_2$ with 5 ml water. To oxidize Co(II) to Co(III) air was bubbled into the mixture for 2–3 hours, then 0.0025 mol NaN_3 dissolved in 5 ml water and 0.0025 mol amine (imidazole, 3-hydroxy-aniline, lepidine, 3,5-dimethyl-pyridine, di(*n*-butyl)-amine or diisopropylamine) dissolved in 5 ml EtOH were added. The obtained solutions were heated for 2–3 hours on water bath. After cooling the crystalline complexes were filtered out, washed with EtOH–water mixture (1:1), and then dried on air. One example is shown below:

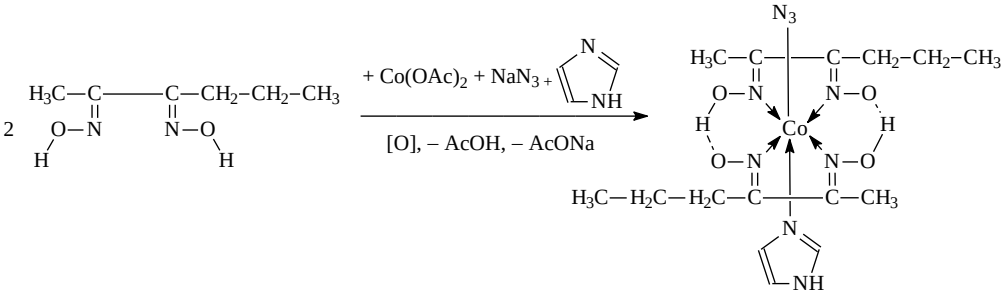

- *Synthesis of [Co(GlyoxH)$_2$(SCN)(amine)] and [Co(GlyoxH)$_2$Br(amine) type complexes*

The syntheses are similar to the procedure above, however, KSCN or KBr was used instead of NaN_3. Examples for the reactions are shown below:

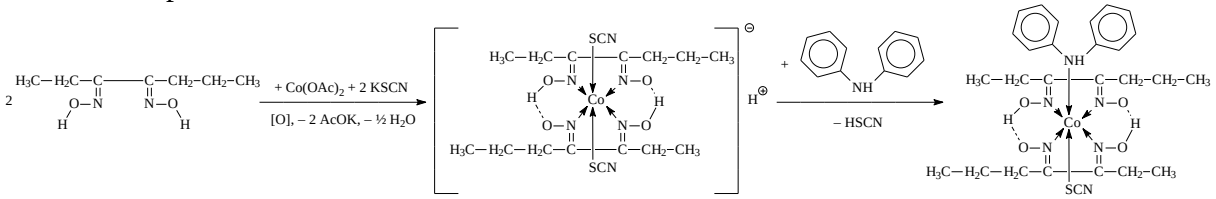

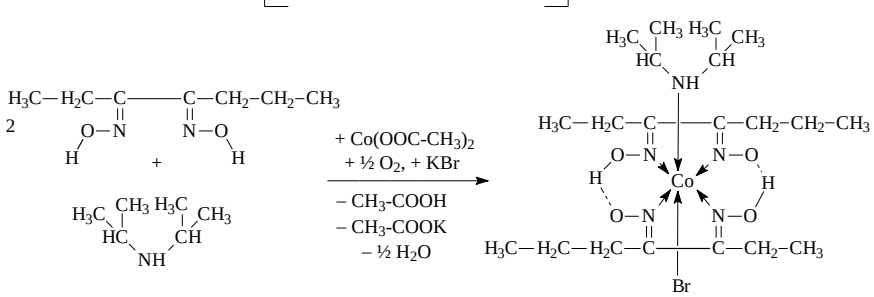

- *Synthesis of [Co(GlyoxH)$_2$(amine)$_2$]$^+I^-$ type complexes*

0.005 mol phenyl-Me-GlyoxH_2 or Et-propyl-GlyoxH_2 was dissolved in 20 ml EtOH was added to the aqueous solution of 0.0025 mol $Co(OAc)_2$ with 5 ml water. Air was bubbled into the

mixture for 2–3 hours, then 0.005 mol amine (3-hydroxy-aniline, di(*n*-butyl)-amine, 2-amino-pyrimidine, diphenyl-amine, 2-picoline or 3-picoline) dissolved in 5 ml EtOH was added. The obtained solutions were heated for 2–3 hours on water bath. In the final step 0.0025 mol KI solved in 10 ml water was added. After cooling the crystalline complexes were filtered out, washed with EtOH–water mixture (1:1), and then dried on air. One example is shown below:

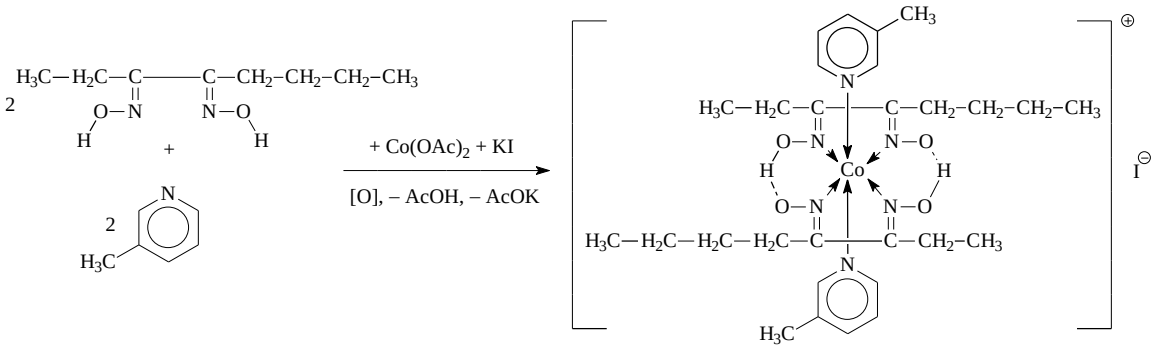

Results and discussion

Microscopic characterization and the yield of prepared complexes are presented in Table 1.

Table 1. Microscopic characterization, calculated molecular weight and the yield of prepared complexes.

Nr.	Compound	Calc. mol. weight	Yield (%)	Microscopic characterization
1.	[Co(Me-Pr-GlyoxH)$_2$(N$_3$)(imidazole)]	455.36	53	Dark brown triangle-based prisms
2.	[Co(Me-Pr-GlyoxH)$_2$(N$_3$)(3-hydroxy-aniline)]	496.41	95	Dark brown triangle-based prisms (microcrystals)
3.	[Co(Me-Pr-GlyoxH)$_2$(N$_3$)(lepidine)]	530.47	60	Dark brown triangle-based prisms
4.	[Co(Me-Pr-GlyoxH)$_2$(N$_3$)(3,5-dimethyl-pyridine)]	494.43	34	Brown triangle-based prisms
5.	[Co(Me-pentyl-GlyoxH)$_2$(N$_3$)((n-Bu)$_2$NH)]	572.63	16	Dark brown triangle-based prisms
6.	[Co(Me-pentyl-GlyoxH)$_2$(N$_3$)(diisopropyl-amine)]	544.58	29	Brown triangle-based prisms (microcrystals)
7.	[Co(Et-Pr-GlyoxH)$_2$Br(diisopropyl-amine)]	554.41	86	Brown triangle-based prisms (microcrystals)
8.	[Co(Et-Pr-GlyoxH)$_2$Br((n-Bu)$_2$NH)]	582.46	14	Dark brown triangle-based prisms (microcrystals)
9.	[Co(Et-Pr-GlyoxH)$_2$(SCN)(diphenyl-amine)]	600.62	20	Black needle-like triangle-based prisms
10.	H[Co(Et-Pr-GlyoxH)$_2$(SCN)$_2$]	491.49	3	Brown triangle-based prisms
11.	[Co(phenyl-Me-GlyoxH)$_2$((n-Bu)$_2$NH)$_2$]I	798.68	7	Dark brown triangle-based prisms (microcrystals)
12.	[Co(phenyl-Me-GlyoxH)$_2$(3-hydroxy-aniline)$_2$]I	758.45	3	Dark brown triangle-based prisms (microcrystals)
13.	[Co(phenyl-Me-GlyoxH)$_2$(3-picoline)$_2$]I	726.45	50	Dark brown triangle-based prisms

14.	[Co(phenyl-Me-GlyoxH)$_2$ (2-amino-pyrimidine)$_2$]I	730.40	12	Dark brown triangle-based prisms (microcrystals)
15.	[Co(Et-Pr-GlyoxH)$_2$ (2-amino-pyrimidine)$_2$]I	690.42	26	Dark brown triangle-based prisms
16.	[Co(Et-Pr-GlyoxH)$_2$ (2-picoline)$_2$]I	686.47	15	Dark brown triangle-based prisms (microcrystals)
17.	[Co(Et-Bu-GlyoxH)$_2$ (t-Bu-amine)$_2$]I	674,54	15	Dark brown triangle-based prisms (microcrystals)
18.	[Co(Et-Bu-GlyoxH)$_2$ (3-amino-1-propanol)$_2$]I	678.49	1	Black triangle-based prisms (microcrystals)
19.	[Co(Et-Bu-GlyoxH)$_2$ (3-amino-pyrimidine)$_2$]I	716.50	28	Brown laminar crystals
20.	[Co(Et-Bu-GlyoxH)$_2$ (3-picoline)$_2$]I	714.52	1	Dark brown triangle-based prisms

Infrared spectroscopic study

The mid-IR spectra were recorded with a Bruker Alpha FTIR spectrometer (Platinum single reflection diamond ATR), at room temperature, in the wavenumber range of 4000–400 cm^{-1}, and the far-IR range of 650–150 cm^{-1}, respectively, on a Perkin–Elmer System 2000 FTIR spectrometer, with a resolution of 4 cm^{-1}. The samples were measured in solid state (in powder form) and in polyethylene pellets, respectively. The data of the most characteristic IR bands for the selected complexes are presented in Table 2.

Table 2. IR data of the selected complexes.

Comp. / cm^{-1}	**1**	**2**	**3**	**7**	**8**	**9**	**10**	**14**	**15**	**16**
ν_{O-H}	3735 m	3567 w	3649 w	3649 w	3649 w	3406 m	-	3405 m	3487 w	3526 w
ν_{N-H}	3649 m	3446 w	3566 w	3447 w	3566 w	3382 s	3446 w	3204 w	3293 w	3385 w
ν_{C-H}	2970 m	2969 s	2927 s	2929 s	2955 s	2964 w	2960 s	2920 w	2928 s	2927 s
ν_{N3}	2359 m 2018 s	2360 m 2032 vs	2359 m 2013 vs	-	-	-	-	-	-	-
$\nu_{S-C\equiv N}$	-	-	-	-	-	2066 m	2108 s	-	-	-
$\nu_{C=C}$	1739 vs	1740 vs	1739 vs	1740 vs	1739 vs	-	-	1629 m	1638 m	1637 m
$\nu_{C=N}$	1559 s	1559 vs	1558 vs	1558 vs	1558 vs	1582 s	1556 vs	1577 vs	1552 vs	1549 vs
δ_{CH2}	1457 s	1457 s	1457 s	1456 s	1457 s	1457 s	1456 s	1444 s	1455 s	1455 s
δ_{CH3}	1373 vs	1373 vs	1374 s	1373 vs	1374 vs	1307 s	1376 s	1360 s	1365 m	1376 m
ν_{N-O}	1217 vs	1217 vs	1216 vs	1217 vs	1217 vs	1220 m	1227 vs	1241 vs	1188 vs	1186 vs
ν_{N-OH}	1105 s	1112 s	1106 vs	1107 vs	1107 s	1149 m	1113 vs	1119 vs	1108 vs	1107 vs
τ_{O-H}	978 s	1041 s	1034 s	1034 s	1034 s	1084 m	1036 s	966 vs	1004 s	1004 s
γ_{C-H}	752 m	764 m	748 m	747 m	747 m	741 vs	747 m	744 vs	747 s	748 s
ν_{Co-N}	516 s	516 m	529 m	528 m	528 s	504 s	505 s	556 s	538 s	530 m
ν_{Co-S}	-	-	-	-	-	470 s	472 s	-	-	-
ν_{Co-Br}	-	-	-	409 m	398 m	-	-	-	-	-

(Abbreviations: vs = very strong, s = strong, m = medium, w = weak)

Mass spectrometry

Mass spectra of the samples were recorded using electrospray ionization (ESI). In the spectra we could detect the molecular ions and some decomposition fragments.

Thermoanalytical measurements (TG-DTG-DTA)

Thermal measurements were performed with a 951 TG and 910 DSC calorimeter (DuPont Instruments), in Ar or N_2 at a heating rate of 10 $Kmin^{-1}$ (sample mass of 4–10 mg).

The thermal stability of complexes is limited at 90–120 °C. In the case of $[Co(GlyoxH)_2(N_3)(amine)]$ type complexes the first decomposition step is belonging to the leaving amine group, then the azide group is lost. Subsequently, the decomposition of glyoxime groups takes place which is accompanied by big exothermic peaks. This behavior can be explained with the presence of oxygen in the molecule. In the case of $[Co(GlyoxH)_2Br(amine)]$ type complexes the decomposition mechanism is similar, unlike azide, here bromine leaves. In the case of $[Co(GlyoxH)_2(amine)_2]^+I^-$ type complexes the iodide ion leaves at 30–190 °C, then the amine and glyoxime groups are lost. The general decomposition mechanisms are the followings:

$$[Co(GlyoxH)_2N_3(amine)] \rightarrow [Co(GlyoxH)_2N_3] \rightarrow [Co(GlyoxH)_2] \rightarrow [Co(GlyoxH)] \rightarrow Co_2O_3$$

$$[Co(GlyoxH)_2Br(amine)] \rightarrow [Co(GlyoxH)_2Br] \rightarrow [Co(GlyoxH)_2] \rightarrow [Co(GlyoxH)] \rightarrow Co_2O_3$$

$$[Co(GlyoxH)_2(amine)_2]^+ I^- \rightarrow [Co(GlyoxH)_2(amine)_2] \rightarrow [Co(GlyoxH)_2(amine)] \rightarrow$$
$$\rightarrow [Co(GlyoxH)_2] \rightarrow [Co(GlyoxH)] \rightarrow Co_2O_3$$

Powder X-ray diffraction measurements

The crystal structure of the complexes was studied with powder XRD measurements, carried out on a PANalytical X'pert Pro MPD X-ray diffractometer. As being novel compounds their diffractograms can not found in the Cambridge database.

UV–VIS spectroscopy

The electronic spectra were recorded with Jasco V-670 Spectrophotometer in 10% EtOH/water solutions containing substrate in 10^{-4} mol/dm^3 concentration. Using Sörensen buffer solutions the electronic spectra were also recorded as a function of pH, and then the acidity constants were calculated too. The obtained values were between $1.2 \cdot 10^{-11} – 1.1 \cdot 10^{-10}$.

Biological study

The antimicrobial effects of complexes were studied for Serratia Marcescens Gram-negative bacteria. The observation was made with the disk method. The complexes were dissolved in DMSO in 100 mmol/l concentration. In the case of $[Co(Me\text{-}Pr\text{-}GlyoxH)_2(N_3)(lepidine)]$ antibacterial effect was observed with 30 µl solution. The inhibition zone was 46.66 mm.

Conclusion

In this work new cobalt complexes were synthesized and characterized with physico-chemical methods. Thermal decomposition mechanism was monitored with thermoanalytical measurements. Antibacterial activity was also investigated.

Acknowledgement

The authors wish to express their thankfulness to the "Domus Hungarica Foundation" of Hungary for the several fellowships provided to Csaba Várhelyi jr.

References

[1] A. Barakata, S.M. Solimanb, M. Alia, A. Elmarghanya, A.M. Al-Majida, S. Yousufd, Z. Ul-Haqe, M.I. Choudharyd, A. El-Faham, *Inorganica Chimica Acta* 503 (2020) 119405

[2] N.A. Mathews, A. Jose, M.R.P. Kurup, *Journal of Molecular Structure* 1178 (2019) 544

[3] R. Huang, A. Wallqvist, D.G. Covell, *Biochemical Pharmacology* 69 (2005) 1009

[4] A.K. Renfrew, E.S. O'Neill, T.W. Hambley, E.J. New, *Coordination Chemistry Reviews* 375 (2018) 221

APPLICATION OF HIGH POWER UV LEDs IN HETEROGENEOUS PHOTOCATALYSIS

Máté Náfrádi, Tamás Hlogyik, Luca Farkas, Tünde Alapi

Department of Inorganic and Analytical Chemistry, University of Szeged, H-6720 Szeged, Dóm tér 7, Hungary
e-mail: nafradim@chem.u-szeged.hu

Abstract

In our work, we designed and built a photochemical reactor with High Power LED light sources, and then tested its operation by heterogeneous photocatalytic decomposition of coumarin. The UV-LEDs emitting at a wavelength of 367(±10) nm were built into a frame with air-cooling elements. A well-controlled electrical power source was used to control and regulate the light output of the LEDs. The photon flux was measured at different electric power inputs, and was found to be linearly dependent on electrical power. Coumarin was used to test the new photoreactor during heterogeneous photocatalysis using TiO_2 and ZnO as photocatalysts. At low photon flux the UV-LEDs outperformed a fluorescent mercury-vapor lamp in terms of efficiency and power consumption, but their usage at high electric input is not favorable.

Introduction

Advanced Oxidation Processes (AOPs) are a possible solution to some emerging environmental problem, such as the elimination of organic pollutants from waters. Several AOPs include the use of UV light, like O_3/UV, UV/Cl_2, photo-Fenton reactions, or heterogeneous photocatalysis. Generally the used light sources are mercury-vapor lamps, but these have some drawbacks, like fragility and hazardous waste production. In the last few years, with the advances in optoelectronics the application of Light Emitting Diodes (LEDs) emitting in the UV region gained more and more popularity. With the application of High Power LEDs the mercury vapor lamps emitting in the 300-400 nm region can be replaced with other UV light sources. UV-LEDs emitting in the UV-C region (260-290 nm) are already available, but their power-efficiency is still relatively low (1-5 %). Due to the further improvements they might also provide a good alternative for mercury vapor lamps emitting UV-C photons (254 nm) [1,2].

UV LEDs that emit at 300-400 nm are especially useful for heterogeneous photocatalysis, since the most frequently used catalysts, TiO_2 and ZnO can be excited with light having wavelength shorter than 390 nm. Due to the absorption of photons having appropriate energy (~3.2 eV), excited conduction band electrons (e_{cb}^-) and valence band holes (h_{vb}^+) form, and they initiate the transformation of organic compounds via charge transfer or hydroxyl radicals (HO•) based reactions. UV-LEDs have already been used in the last few years with good efficiency to transform various pollutants in aqueous media [3-5].

The goal of this current study was to plan, and build a new photoreactor equipped with high power UV-LEDs, and test it for use in the field of heterogeneous photocatalysis. The effect of electric input, and the distance between the reactor wall and light sources were investigated. The photon flux absorbed by the treated solution was determined with actinometry. To test the light sources during heterogeneous photocatalysis, TiO_2 and ZnO as photocatalysts, and coumarin (COU) as a model compound were used. The formation of the hydroxylated product of COU, 7-hydroxy-coumarin (7-HO-COU) allows the estimation of HO• formation rates [6].

Experimental

The Vishay (VLMU3510-365-130) high power UV-LEDs emitting at 367 nm wavelength were supplied by Distrelec Hungary. The LEDs use InGaN die, and are equipped with a high purity silicone lens. Their typical opening voltage is 4.0 V, and they have a radiant power of 690 mW (with a typical 2000 mW power consumption). They have been soldered to star shaped metal core printed circuit boards (MCPCB) supplied by Meodex. Due to the high amount of heat generated by the LEDs, 0.70 K/W aluminum heat sinks were used to convey the heat. An AX-3005DBL-3 laboratory power supply (maximum output is 5.0 A / 30.0 V) was used to provide and precisely control the electrical power needed to operate the light sources. The irradiated solution was held in a 200 cm^3 cylindrical glass reactor that can be bubbled with gas from a porous glass filter at the bottom. Depending on the measurements, N_2 (99.995 %) or synthetic air was used.

The photon flux of the light sources were measured using ferrioxalate actinometry, as described by Hatchard and Parker [7]. 1.0×10^{-2} M Fe(III)-Oxalate solutions were irradiated, the released Fe(II) was measured using 0.2 % phenanthroline. The absorbance of Fe(II)-phenanthroline complex was measured at 510 nm using UV-Vis spectrophotometry (Agilent 8453) in a quartz cuvette with 0.20 cm optical path length. The solutions were bubbled during the measurements with N_2 (99.995 % purity).

The photocatalytic measurements were performed in the previously described UV-LED system, or in a 500 cm^3 glass reactor irradiated using a 15 W mercury vapor lamp emitting between 300-400 nm (GCL303T5/UVA, LightTech) as a reference. Before the measurements, the suspensions were saturated with synthetic air, and they were stirred in the dark for 30 minutes. The samples taken were centrifuged at 15000 RPM, and filtered through a 0.22 µm syringe filter. The experiments were started with turning on the light sources. During the photocatalytic experiments suspensions of TiO_2 (Aeroxide P25) and ZnO (Sigma Aldrich) were irradiated. COU concentration was 5.0×10^{-4} M, its concentration was determined via UV-Vis spectrophotometry at 277 nm. The formation of 7-HO-COU was measured using fluorescence spectroscopy (Hitachi F-4500), the excitation wavelength was 345 nm, while the detection was performed at 455 nm wavelength. Reaction rates were determined from the initial linear part of the kinetic curves (up to 15 % transformation of COU).

Results and discussion

As the first part of the current work, the new LED reactor was planned, and built. The 12 pieces of UV-LEDs were soldered according to their manual to the MCPCB stars. Two LEDs were fastened to each heat sinks, the adequate heat conductivity was provided by thermal paste. The two LEDs on one heat sink was connected in series, and the six parts were connected in parallel, resulting in 8.0 V maximum applicable voltage and 3.0 A maximum applicable current. The six heat sinks are fastened to an aluminum base, their distance from the glass reactor can be changed from 1.25 to 4.25 cm (Fig. 1).

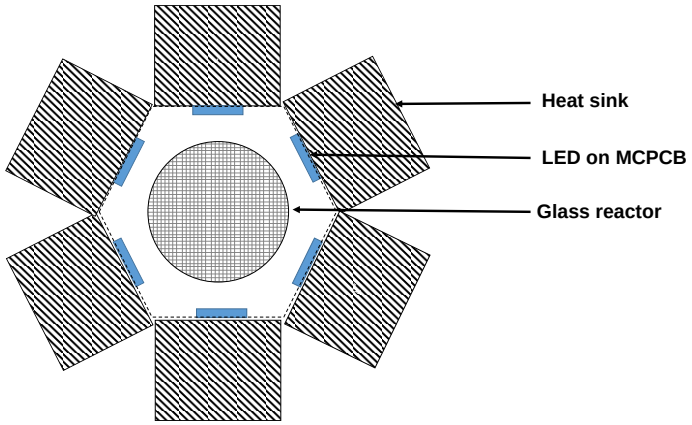

Figure 1. Schematic setup of the reactor (top view), with the LEDs

The reactor was tested using ferrioxalate actinometry to determine the photon flux, and compare it to the mercury vapor lamp. The measurements were performed with different electrical parameters, from 3.39 to 20.77 W. The voltages were set to constant 8.0 V (6.8(±0.1) V measured when turned on), and the current was changed from 0.5 to 3.0 A. The absorbance of the Fe(II)-phenanthroline complex was measured at 510 nm according to literature [7], and the photon flux was calculated from the slope of the line fitted (Figure 2/A). The light emission of UV-LEDs showed very good linearity as a function of electrical energy consumption. The photon flux of the mercury-vapor lamp was also determined (Figure 2/B), and we can see the much greater efficiency of the LED light sources, as they provide ~60 % more photons at similar electric power consumption.

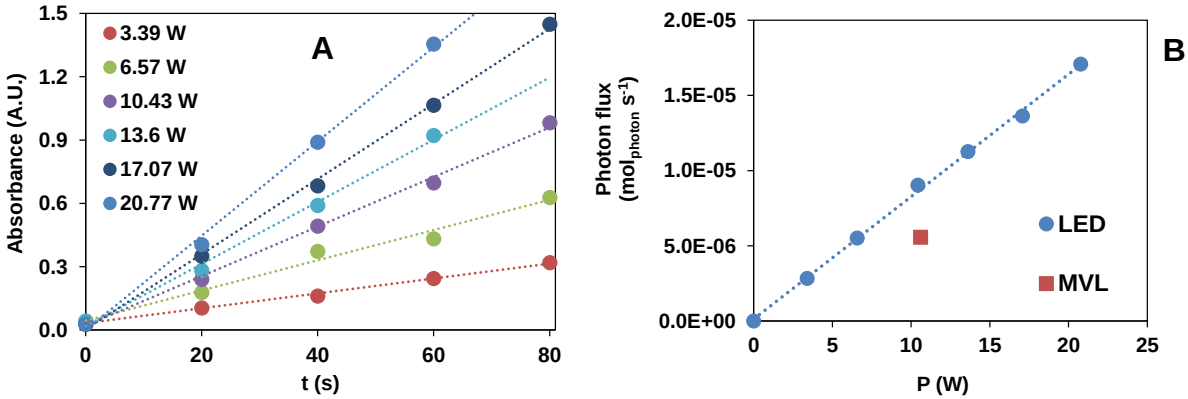

Figure 2. The absorbance values measured at 510 nm as a function of irradiation time at different electric power output (A), and the calculated photon flux of the LEDs compared with the Hg-vapor lamp (B)

The effect of the distance (r) between the LEDs and the glass reactor on the photon flux was also determined at constant power input (13.6 W). The photon flux was reduced with the distance from the light source. Therefore the best option is to use the light sources at the closest position (r = 1.25 cm). The possibility to irradiate a larger volume via changing the distance and using a reactor having a larger diameter is an advantage of this reactor setup.

The LED reactor was tested using TiO_2 P25 Aeroxide and ZnO photocatalysts and COU, as model compound. The hydroxylated product of COU, 7-HO-COU only form during reactions with HO•, therefore it can be used to determine the formation rate of HO• [6]. First, the optimal catalyst concentration was determined, since it greatly depends on the reactor size and design, and light intensity. 5.0×10^{-4} M solutions of COU was irradiated in the presence of

TiO_2 and ZnO. The LEDs were operated at 13.6 W (photon flux = 5.63×10^{-5} mol_{photon} sec^{-1} dm^{-3}). The reaction rate of COU did not change above 0.5 g dm^{-3} catalyst load (Fig. 3/A), similarly to the formation rates of 7-HO-COU, it even started to lower at high (1.5 g dm^{-3}) ZnO dosage (Fig. 3/B), probably because of the increased light scattering. During further experiments, 1.0 g dm-3 catalyst concentration was used, to exclude the contribution of direct photolysis.

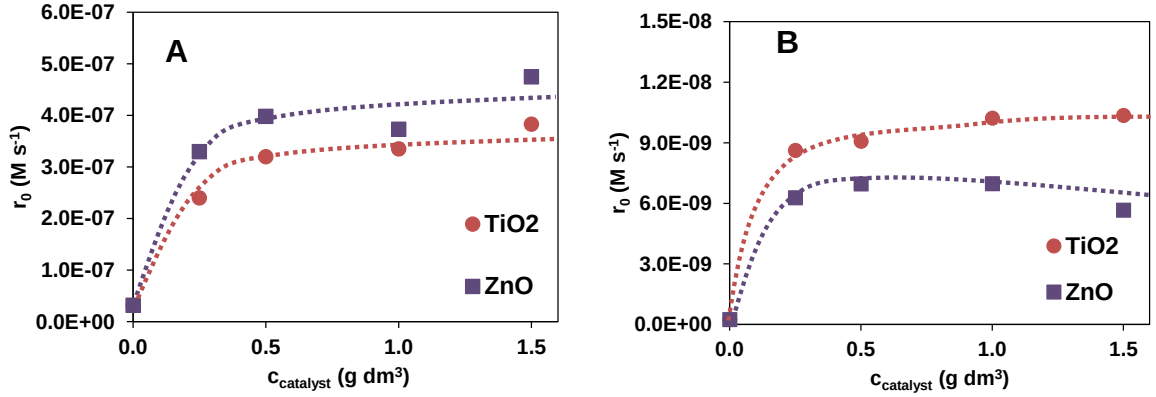

Figure 3. The transformation rate of COU (A), and the formation rate of 7-HO-COU (B) as a function of catalyst concentration

The reaction rates of COU, and the formation rates of 7-HO-COU were determined at different photon fluxes by varying the electric power input (3.07 - 21.14 W) of the LEDs. Although the photon flux increased linearly with electric power input, in the presence of catalysts the reaction rates of COU increased according to a saturation curve (Fig. 4/A). The formation rate of HO• showed a similar tendency (Fig. 4/B). The apparent photonic efficiencies can be calculated using the photon flux determined via actinometry. With the increase of the photon flux the photonic efficiency of the transformation of COU reduced from 1.5 % to 0.5 %.

In the case of measurements with the Hg-vapor lamp similar photonic efficiencies were measured (1.1 %). The results have been corrected according to the different reactor volumes. If we take these into account then the difference is negligible, therefore the cost-efficiency of the two light sources is similar (Fig. 4).

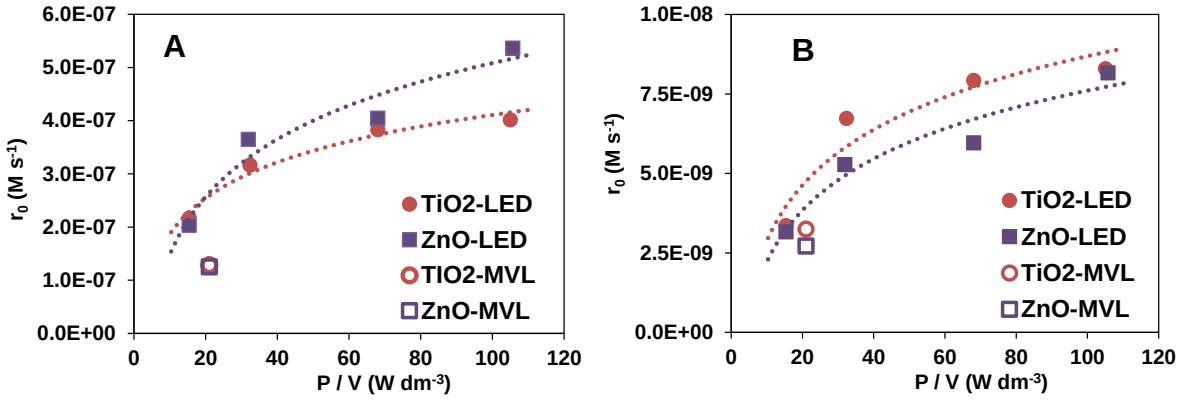

Figure 4. The transformation rate of COU (A), and the formation rate of 7-HO-COU (B) in the case of LEDs and Hg-vapor lamp as a function of electrical power used

Conclusions

The constructed high power UV-LED based photoreactor setup was highly efficient, and well customizable for use with either photolytic of photocatalytic applications. Overall, we can conclude, that the use of LED light sources for photochemical applications is highly favorable

due to their power efficiency, and customizability. The operation of the LEDs is especially cost-effective in the case of lower electric energy input.

Acknowledgements
This work was supported by the János Bolyai Research Scholarship of the Hungarian Academy of Sciences, and new national excellence program of the Ministry for Innovation and Technology (ÚNKP-20-3-SZTE 548, and ÚNKP-20-5-SZTE 639). This work was sponsored by the National Research, Development and Innovation Office-NKFI Fund OTKA, project number FK132742.

References
[1] C. Casado, R. Timmers, A. Sergejevs, C.T. Clarke, D.W.E. Allsopp, C.R: Bowen, R. van Grieken, Marugán, J, Chemical Engineering Journal, **327**, (2017) 1043–1055.
[2] M. Khademalrasool, M. Farbod, M.D. Talebzadeh, Journal of Science: Advanced Materials and Devices, **1**(3), (2016) 382–387.
[3] M.R. Eskandarian, H. Choi, M. Fazli, M.H. Rasoulifard, Chemical Engineering Journal, **300**, (2016) 414–422.
[4] N. Jallouli, L.M Pastrana-Martínez, A.R. Ribeiro, N.F.F. Moreira, J.L. Faria, O. Hentati, A.M.T. Silva, M. Ksibi, Chemical Engineering Journal, **334**, (2018) 976–984.
[5] G. Heydari, J. Hollman, G. Achari. C.H. Langford, Water, **11,** (2019) 621.
[6] Louit, G., Foley, S., Cabillic, J., Coffigny, H., Taran, F., Valleix, A., Renault, J.P., Pina, S., Radiation Physics and Chemistry **72,** (2005) 119–124.
[7] C. G. Hatchard, C. A. Parker, Proc. Royal Soc. A, **235,** (1956) 518-536.

ULTRAHIGH-PERFORMANCE LIQUID CHROMATOGRAPHIC ENANTIOSEPARATION OF SOME β^2-AMINO ACIDS

Dániel Tanács[1], Ferenc Fülöp[2], Antal Péter[1], István Ilisz[1]

[1]Institute of Pharmaceutical Analysis, Interdisciplinary Excellence Centre, University of Szeged, H-6720 Szeged, Somogyi utca 4, Hungary
[2]Institute of Pharmaceutical Chemistry, Interdisciplinary Excellence Centre, University of Szeged, H-6720 Szeged, Eötvös u. 6, Hungary

β-Amino acids have an extra carbon atom between the amino and carboxylic groups. This difference in the structure can cause various effects in β-amino acid-containing peptides, both in the structure [1] and in the stability in an organism. For example, these β-amino acids have different susceptibility to hydrolysis or enzymatic degradation than their α analogs [2]. Monosubstituted β-amino acids can be subdivided into β^2- and β^3-amino acids, depending upon the position of the side-chain on the 3-aminoalkanoic acid skeleton.
Literature data relate mainly to the separation and identification of β^3-amino acid enantiomers and are summarized in several review papers [3-5]. However, relatively few data are available for the separation of β^2-amino acid enantiomers. Recently core-shell particles (superficially porous particles, SPPs) and sub-2 μm fully porous particles have been proven to provide high-throughput and effective separations of a variety of chiral molecules in ultrahigh-performance liquid chromatography (UHPLC). Macrocyclic glycopeptide based stationary phases are known for their highly selective amino acid and peptide separations and there are readily available SPPs with covalently bonded teicoplanin, teicoplanin aglycone and vancomycin.
In this study we used 2.7 μm SPPs bonded with macrocyclic glycopeptides to investigate the enantiomeric separation of 19 β^2-amino acids. We found that the teicoplanin and teicoplanin aglycone-based stationary phases were effective in the enantiomeric separation for all of the examined β^2-amino acids. We also studied the effect of different solvent mixtures and the effect of the nature of buffers and effect of their concentrations.

References

[1] D.F. Hook, F. Gessier, C. Noti, P. Kast, D. Seebach, Probing the proteolytic stability of β-peptides containing α-fluoro-and α-hydroxy-β-amino acids, Chem. BioChem. 5 (2004) 691.
[2] M.-I. Aguilar, A.W. Purcell, R. Devi, R. Lew, J. Rossjohn, A.I. Smith, P. Perlmutter, β-Amino acid-containing hybrid peptides—new opportunities in peptidomimetics, Org. Biomol. Chem. 5 (2007) 2884.
[3] I. Ilisz, A. Péter, W. Lindner, State-of-the-art enantioseparations of natural and unnatural amino acids by high-performance liquid chromatography. TRAC Trends. Anal. Chem. 81 (2016) 11-22.
[4] I. Ilisz, A. Bajtai, W. Lindner, A. Péter, Liquid chromatographic enantiomer separations applying chiral ion-exchangers based on Cinchona alkaloids. J. Pharm. Biomed. Anal. 159 (2018) 127-152.
[5] I. Ilisz, T. Orosz, A. Péter, High-performance liquid chromatography enantioseparations using macrocyclic glycopeptide-based chiral stationary phases – An Overview. in Ed. G.K. Scriba, Chiral Separations: Methods and Protocols, Methods in Molecular Biology 1985, 2019, pp. 201-237.

THE MOST COMMON SYNTHETIC CANNABINOIDS IN THE LAST YEAR; FOCUSING ON THEIR METABOLITES IN BIOFLUIDS

Tímea Körmöczi[1], Éva Sija[2], Róbert Berkecz[1]

[1]*Institute of Pharmaceutical Analysis, University of Szeged, H-6720 Szeged, Somogyi utca 4, Hungary*
[2]*Department of Forensic Medicine, University of Szeged, H-6724 Szeged, Kossuth Lajos sgt. 40, Hungary*
e-mail: kormoczi.timea@pharm.u-szeged.hu

Abstract

Designer drugs are getting popular among teenagers and young adult is a serious problem. Synthetic cannabinoids (SCs) are the most rapidly growing group of designer drugs that mimic the natural cannabinoid effects. SCs have hundreds of street names (*synthetic marijuana, fake weed, Spice, K2 etc.)* and these products are sold in packages containing saturated various plants crumb. Unfortunately, these drugs can be easily overdosed due to their significantly higher binding affinities to the CB1 and CB2 cannabinoid receptors than Δ9-tetrahydrocannabinol as the main active ingredient of cannabis.

The consumption of SCs is verified in urine and blood samples with ultra-high performance liquid chromatography coupled to tandem mass spectrometer (UHPLC-MS/MS) technique. In most cases, it is not enough to detect only the mother compounds for confirmation of SCs consumption, due to their rapid metabolism. The most seized SCs by the police in recent months were **5F-MDMB-PICA** and **4F-MDMB-BICA**.

Our study aimed to quantitatively determine these new SCs and their main metabolites in biological samples (urine and blood) by developed targeted UHPLC-MS/MS method. In general, the concentration of the metabolites was significantly higher than the mother compound. Thus, it is necessary to identify metabolites to prove the fact of consumption.

Acknowledgements

This research was supported by the EU-funded Hungarian grant EFOP 3.6.1-16-2016-00008.

Xe*-EXCIMER LAMP VERSUS LOW PRESSURE MERCURY VAPOR LAMP – THE COMPARISON OF THE EFFICIENCY OF 185 nm WITH 172 nm RADIATION, BASED ON H_2O_2 FORMATION AND COUMARIN OXIDATION

Tünde Alapi, Luca Farkas, Daniele Scheres Firak

Department of Inorganic and Analytical Chemistry, University of Szeged, H-6720 Szeged, Dóm tér 7, Hungary
Email: alapi@chem.u-szeged.hu

Abstract

VUV photolysis is a widely used method for producing high purity water by efficiently removing organic substances present in low concentrations. This process is based on the direct photolysis of water, which results in the formation of HO• and •H radicals. In the case of photo-initiated Advanced Oxidation Processes (AOPs), such as VUV photolysis, the lamp type determines the effectiveness. There are two types of light sources commonly used in VUV photolysis: the low-pressure mercury vapor (LPMV) lamps and the Xe* excimer lamp. In this work, the efficiency of the low-pressure mercury vapor (LPM) lamp, which emits at 254 and 185 nm (UV/$VUV_{185\ nm}$ lamp), and the Xe* excimer lamp, which emits at 172 nm ($VUV_{172\ nm}$) photons, were compared. The comparison of the efficiency of the VUV light sources was based on the formation of H_2O_2 in the case of the pure water as well as on the transformation of coumarin (COU) and formation of its hydroxylated product, umbelliferone (7-HO-COU).

Introduction

The VUV photolysis is mainly used and investigated for the elimination and mineralization of various organic pollutants in aqueous solutions [1,2]. Organic and inorganic molecules or ions have high absorption coefficients in the VUV region. However, in aqueous solutions, the VUV radiation is absorbed almost exclusively by water because its concentration (55.5 mol dm^{-3}) highly exceeds those of the dissolved compounds. Absorption of the VUV radiation results in the homolysis and, with lower quantum yield, the photochemical ionization of water molecules:

$$H_2O + h\nu\ (<190\ nm) \rightarrow H\bullet + HO\bullet$$
$$H_2O + h\nu\ (<200\ nm) \rightarrow [e^-,H_2O^+] + H_2O \rightarrow [e^-,H_2O^+] + (H_2O) \rightarrow e_{aq}^- + HO\bullet + H_3O^+$$

There are some characteristic differences between the 185 and 172 nm VUV light irradiated solutions, which are the consequence of the extremely high absorption coefficient and low penetration depth of the 172 nm VUV light.

Table 1. *The molar absorption coefficient and the penetration depth of 185 and 172 nm VUV light in water and the quantum yields of the formation of reactive species [3-5]*

	absorption coefficient (cm^{-1})	penetration depth in water (mm)	quantum yield	
			Φ(•OH)/ Φ(H•)	Φ(e_{aq}^-)
172 nm	**550**	**0.036**	**0.42**	**0.05**
185 nm	**1.53**	**11**	**0.33**	**0.05**

The extremely low penetration depth of 172 nm photons results in a very thin (0.04 mm) photoreaction zone containing high concentrations of primary radicals. The carbon-centered

radicals, formed by the reaction of organic substances with H• and HO•, react immediately with dissolved O_2 and form organic peroxyl radicals. As a result, an O_2-depleted layer is formed next to the lamp wall.

The VUV photon flux of the Xe-excimer lamp generally highly exceeds that of the low-pressure mercury vapor lamps that emits both 254 nm and 185 nm photons. Although several authors published results about the efficiency of the low-pressure mercury-vapor lamp for the elimination of organic substances from waters [6-9], the studies about the Xe-excimer lamp [10], especially the comparison of these two light sources [5] , are quite rare.

Experimental

For the $VUV_{172\ nm}$ radiation, a Xe_2* excimer lamp (Radium Xeradex^{TM}, 130 mm long, 46 mm diameter, 20 W) was used, which was centred in a high purity silica quartz envelope (53 mm diameter), able to transmit the 172 nm light. The aqueous solution was circulated continuously (375 mL min^{-1}) between the reactor and the reservoir. A double walled, water-cooled reactor was used, and the temperature was set to 25 ± 0.5 °C. Samples were taken from the reservoir. The volume of the treated solution was 500 mL, the thickness of the irradiated water layer was 5 mm.

The low-pressure mercury vapour (LPMV) lamp ($UV/VUV_{185\ nm}$ lamp GCL307T5VH/CELL, 227 mm arc length, produced by LightTech) was used for the UV/VUV (254 nm/185 nm) photolysis. The $UV/VUV_{185\ nm}$ lamp's envelope was made of synthetic quartz to be able to transmit the $VUV_{185\ nm}$ photons. The volume of the treated solution was 500 mL, the thickness of the irradiated water layer was 20 mm.

In the case of $VUV_{172\ nm}$ and $UV/VUV_{185\ nm}$ photolysis, O_2 or N_2 gas was bubbled continuously through the solution. Coumarine (Sigma-Aldrich, ≥98,5%) solutions were made in ultrapure Milli-Q water (MILLIPORE Milli-Q Direct 8/16).

The transformation of coumarin (COU) was followed by a spectrophotometer (Agilent 8453). The concentration was determined from the absorbance of the solution at 277 nm. Fluorescence spectroscopy (Hitachi F4500) was applied to determine the concentration of umbelliferone (7-HO-COU). The wavelength of excitation was 387 nm. The determination of its concentration was based on the intensity of the emitted fluorescence light at 455 nm.

The concentration of H_2O_2 was measured with a cuvette test by Merck, with a 0.015 - 6.00 mg dm^{-3} measuring range.

Results and discussion

In the case of the VUV photolysis, the 172 nm and 185 nm VUV light is absorbed by water to form reactive species, such as hydrogen radicals (H•), hydroxyl radicals (HO•), and, with a lower yield, hydrated electrons (e_{aq}^-) [2]. The VUV flux of light sources determines their efficiency in terms of radical formation and consequently the removal of organic matter from water.

The VUV photon flux was determined with methanol actinometry [11], and was found to be 32 times higher for the excimer lamp (1.04×10^{-5} mol_{photon} s^{-1}) than for the LPM lamp (3.23×10^{-7} mol_{photon} s^{-1}). The UV photon flux was 3.70×10^{-6} mol_{photon} s^{-1}.

The recombination of primer radicals results in the formation H_2O, H_2 and H_2O_2 [12]:

$2\ HO• \rightarrow H_2O_2$	$k = 4.0\times10^9 – 2.0\times10^{10}$ $dm^3\ mol^{-1}\ s^{-1}$
$2\ H• \rightarrow H_2$	$k= 1.0\times10^{10}$ $dm^3\ mol^{-1}\ s^{-1}$
$HO• + H• \rightarrow H_2O$	$k = 2.4\times10^9$ $dm^3\ mol^{-1}\ s^{-1}$

In the presence of dissolved O_2, the reaction of O_2 with H• hinders the recombination of primary radicals [12]:

$$H\bullet + O_2 \rightarrow HO_2\bullet \qquad k = 2.1\times10^{10}\ dm^3\ mol^{-1}\ s^{-1}$$
$$O_2 + e_{aq}^- \rightarrow O_2\bullet^- \qquad k = 2.0\times10^{10}\ dm^3\ mol^{-1}\ s^{-1}$$

The further reactions of $HO_2\bullet$ and $O_2\bullet^-$ also produce H_2O_2 [13]:

$$HO_2\bullet + H_2O \leftrightharpoons H_3O^+ + O_2\bullet^- \qquad pK_a = 4.8$$
$$O_2\bullet^- + HO_2\bullet + H_2O \rightarrow O_2 + H_2O_2 + HO^- \qquad k = 9.7\times10^7\ dm^3\ mol^{-1}\ s^{-1}$$

At first, the H_2O_2 concentration and its formation rate were determined and compared in the case of both lamps, in O_2 saturated and O_2-free Milli-Q waters. In O_2 saturated waters, the rate of H_2O_2 formation was about twice as high, while the equilibrium concentration was almost 50-fold higher in the 172 nm irradiated solution than in the 254/185 nm irradiated Milli-Q water. This result reflects well the nearly 30-fold higher VUV photon flux of the Xe*-excimer lamp. In the case of 172 nm VUV photolysis, the formation rate and equilibrium concentration of H_2O_2 in O_2-free solution was about 20% of the values determined in O_2-saturated water. There was no H_2O_2 formation in O_2-free water for irradiation at 254/185 nm.

Table 2. *The initial transformation rates and equilibrium concentration of H_2O_2 determined in Milli-Q water*

		O_2 saturated Milli-Q water	**O_2-free Milli-Q water**
Xe-excimer lamp, 172 nm	r_0 *(×10^{-8} mol dm^{-3} s^{-1})*	**10.53**	**2.85**
	c_{eq} *(×10^{-6} mol dm^{-3})*	**102**	**19**
LPMV lamp 254/185 nm	r_0 *(×10^{-8} mol dm^{-3} s^{-1})*	**4.83**	**-**
	c_{eq} *(×10^{-6} mol dm^{-3})*	**2.1**	**-**

The transformation of COU is negligible in 254 nm irradiated solutions, its transformation is due to the reaction with HO• ($k = 6.9\times10^9\ mol^{-1}\ dm^3\ s^{-1}$) and H• ($k = 2.5\times10^9\ mol^{-1}\ dm^3\ s^{-1}$) [14], in both UV/VUV_{185nm} and VUV_{172nm} irradiated solutions. Although the reaction of dissolved O_2 with H• inhibits the transformation of COU via H• initiated reaction, it has no negative effect in the 172 irradiated solution, and increased the transformation rate by 20% in the UV/VUV_{185nm} irradiated solution. Dissolved O_2 generally has a positive effect on the radical based transformation of organic substances due to the formation of organic peroxyl radical (R-COO•) from carbon-centered radicals (R-C•). The formation of R-COO• opens up a new pathway for the transformation of organic substances and hinders the backward reactions. In terms of COU transformation rate, it is likely that the negative and positive effects of O_2 are compensated for each other.

The formation of 7-HO-COU starts with the addition of HO• to the aromatic part of COU. From the carbon-centered radical, there are two possibilities of the 7-HO-COU formation: without dissolved O_2 the reaction of two carbon-centered radical results in the formation of hydroxylated product and COU (Fig. 1). However, in the presence of O_2, 7-HO-COU is formed exclusively through organic peroxyl radicals (Fig. 2). Consequently, the dissolved O_2 highly enhances the formation of hydroxylated products, such as 7-HO-COU.

Taking into account the different photon fluxes, we compared the efficiency of photolysis at 172 nm and 185 nm in the transformation of COU and formation of 7-HO-COU. Despite the photon flux more than 30 times higher, the conversion rate of COU was only 5-6 times higher, while the formation rate of 7-HO-COU was only 2-3 times higher in the case of the excimer lamp compared to the LPMV lamp. It has to be mention that, in 172 nm irradiated aqueous solutions of organic substances, due to the extremely high HO• concentration close to the wall of the lamp, an O_2-depletion layer forms. Thus, the positive effect of O_2 via peroxyl radical formation is less pronounced.

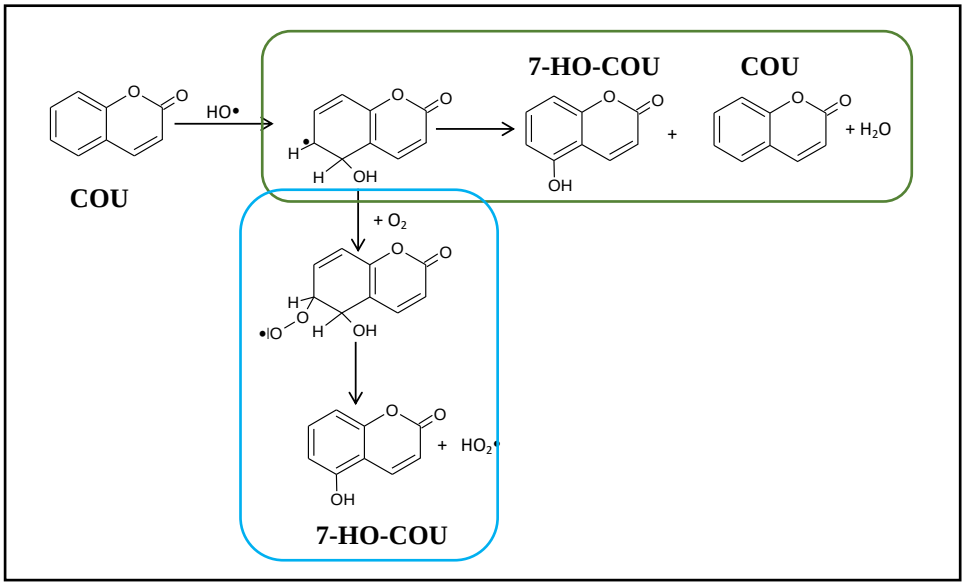

Fig. 1 *The HO• initiated formation of 7-HO-COU from COU in the presence (light blue frame) and absence (dark green frame) of O_2*

Table 3. The initial transformation rate of COU and the formation rate of 7-HO-COU in UV/VUV$_{185nm}$ and VUV$_{172nm}$ radiated solutions (c_0^{COU} = 1.0×10^{-4} M)

The effect of dissolved O_2				
	UV/VUV$_{185nm}$		**VUV$_{172\ nm}$**	
VUV photon flux φ (mol_{photon} s^{-1})	**3.23×10^{-7}**		**1.04×10^{-5}**	
	O_2	**N_2**	**O_2**	**N_2**
r_0^{COU} *(×10^{-8} mol dm^{-3} s^{-1})*	**3.77**	**3.12**	**20.2**	**19.5**
Φ (r_0^{COU}/ φ)	**0.23**	**0.38**	**0.039**	**0.038**
$r_0^{7\text{-HO-COU}}$ *(×10^{-9} mol dm^{-3} s^{-1})*	**1.03**	**0.29**	**2.53**	**9.60**
$r_0^{COU}{}_{O2}$/ $r_0^{COU}{}_{N2}$	**1.21**		**1.04**	
$r_0^{7\text{-HO-COU}}{}_{O2}$/ $r_0^{7\text{-HO-COU}}{}_{N2}$	**3.58**		**2.63**	
Comparison of the VUV$_{172nm}$/VUV$_{185\ nm}$ photolysis				
	O_2		**N_2**	
$r_0^{COU}{}_{172nm}/r_0^{COU}{}_{185nm}$	**5.36**		**6.25**	
$r_0^{COU}{}_{172nm}/r_0^{COU}{}_{185nm}$	**2.46**		**3.33**	

The quantum yield of the COU transformation was one magnitude lower for VUV$_{185\ nm}$ photolysis than VUV$_{172\ nm}$ photolysis (Table 3.). The reason is probably the extreme inhomogeneity of the 172 nm irradiated aqueous solutions of organic substances.

Conclusion

In this work, we compared the efficiencies of two VUV light sources, the low-pressure mercury vapor lamp (UV/VUV185nm) and the Xe-excimer lamp (VUV172nm). The H_2O_2 concentration formed in the 185 and 172 nm Milli-Q irradiated waters well reflects the almost 30-fold higher VUV photon flux of the Xe * -excimer lamp. The high photon flux and the low penetration depth of VUV light at 172 nm causes extreme inhomogeneity in VUV photolysis of an aqueous solution of organic matter. This inhomogeneity is the reason why the apparent quantum yield of the COU transformation is one order of magnitude lower in the 172 nm irradiated solution than with 185 nm irradiation.

Acknowledgements

This publication was supported by the János Bolyai Research Scholarship of the Hungarian Academy of Sciences, and new national excellence program of the Ministry for Innovation and Technology (ÚNKP-20-5-SZTE-639 and ÚNKP-20-3-SZTE-459). The authors thanks the financial support from the project Hungarian Scientific Research Fund (NKFI contract number FK132742)

References

[1] Alapi, T. Schrantz., K.; Arany, E., Kozmér Zs., Chapter 3: Vacuum UV radiation-driven processes, in Advanced Oxidation Processes for Water Treatment, Editor: Stefan, M.I., 2017. IWA Publishing

[2] Oppenländer, T., *Photochemical Purification of Water and Air*. 2003. Wiley-VCH, Weinheim

[3] Weeks, J. L., Meaburn, G. M. A. C., Gordon, S., Radiation Research, 1963. 19(3), 559–567.

[4] Heit, G., Braun, A. M., Water Sci. Technol., 1997. 35(4), 25–30.

[5] Al-Gharabli, S., Engeßer, P., Gera, D., Klein, S., Oppenländer, T., Chemosphere, 2016. 144, 811–815.

[6] Rozsa, G.; Nafradi, M.; Alapi, T.; Schrantz, K.; Szabo, L.; Wojnarovits, L.; Takacs, E.; Tungler, A Appl. Cat. B-Environ. 250. 429-439

[7] Rozsa, G; Fazekas, A; Nafradi, M; Alapi, T; Schrantz, K; Takacs, E; Wojnarovits, L; Fath, A; Oppenlander, T. Environ. Sci. and Poll. Res. 26(23) 23268-23278

[8] Geng, C; Liang, ZJ; Cui, FY; Zhao, ZW; Yuan, C; Du, JY; Wang, C., Chem. Eng. J. 2020. 383. Article number 123145

[9] Arany E., Szabó R.K., Apáti L., Alapi, T., Ilisz, I., Mazellier, P., Dombi, A., Gajda-Schrantz, K., J. Hazard. Mater., 2013. 262, 151–157.

[10] Oppenlander, T. J. Environ. Eng. and Sci. 2007. 6(3) 253-264

[11] Heit, G., Neuner, A., Saugy, P.-Y., Braun, A. M., J. Phys. Chem. A, 1998. 102 (28), 5551–5561.

[12] NDRL/NIST solution kinetics database on the web, https://kinetics.nist.gov/solution/

[13] Bielski, B. H. J. Cabelli, D. E., Arudi, L.R., J. Phys. Chem. Ref. Data, 1985. 14 (4), 1041–1100.

[14] Náfrádi, M., Farkas, L., Alapi, T., Hernádi, K., Kovács, K., Wojnárovits, L., Takács, E. Radiat. Phys. Chem., 2020. 170, 108610

Poster Proceedings

LEACHATE QUALITY ASSESSMENT OF PROTECTED WATER BODIES IN SERBIA AND CROATIA

Tijana Adamov[1], Mladenka Novaković[1], Nevena Živančev[1], Ivan Špánik[2], Ivana Mihajlović[1], Maja Petrović[1]

[1]University of Novi Sad, Faculty of Technical Sciences, Department of Environmental Engineering and Occupational Safety and Health, Trg Dositeja Obradovića 6, 21000 Novi Sad, Serbia
[2]Institute of Analytical Chemistry, Faculty of Chemical and Food Technology, STU, Radlinského 9, 812 37 Bratislava, Slovakia
e-mail: majadjogo@uns.ac.rs

Abstract
Modern agricultural production can not be imagined without the use of pesticides and, if their use is improper, it could lead to continuous introduction of pesticide residues to different environmental media. Water pollution which originates from agricultural activities is a common problem in both observed countries, Serbia and Croatia. The paper provides evaluation of leachate water quality of protected water bodies, Tompojevački ritovi, Croatia, and Lake Zobnatica, Serbia, with the results of detected pesticide residues and other relevant organic micropollutants.

Introduction

Nowadays, the use of pesticides on crops is a necessity, conditioned by the need to preserve yields. Until 2020, over 400 pesticide active ingredients were registered for use in Serbia in the form of 1076 plant protection products, for use on seeds, soil, aboveground parts of plants, fruits or in any other way.

Glyphosate is a versatile herbicide that has been used for more than 40 years to easily, safely and effectively control problematic weeds. Since its introduction in 1974, glyphosate-based products have become the most widely used herbicides in the world due to their ability to control a wide range of weeds, great economic and environmental benefits and a strong safety profile. During the 1990s, the combination of glyphosate with glyphosate-resistant crops led to the transformation of agriculture in many parts of the world and the beginning of the era of modern agricultural biotechnology [1,2,3]. Glyphosate is currently approved for use in over 130 countries, and the current world amount is estimated at about 600 kilotons per year. Glyphosate is especially used in the production of soybeans, corn, potatoes and cotton that are genetically modified to tolerate glyphosate [4].

Glyphosate-based herbicides pollute drinking water sources through rainwater, surface runoff, and infiltration into groundwater, thereby adding drinking water, bathing water, and washing water as possible everyday routes of exposure for humans [1,2,3].

Poor water quality of protected water bodies in Serbia and Croatia is not the only cause of biodiversity loss in wetlands, but often makes surface waters inadequate for irrigation. The main objectives of the study were to provide information about water quality through determination of main physicochemical parameters and pesticides distribution and other relevant organic micropollutants identified in leachates from the wetland area Tompojevački ritovi and Lake Zobnatica.

Experimental

The selected leachate samples were collected near agricultural fields from Lake Zobnatica surrounding area (Republic of Serbia) and wetlands of Tompojevački ritovi (Croatia).

Leachate samples for physicochemical parameters analysis were collected in 1 L bottles, plastic and glass. On site, collected water samples were stabilized by the addition of concentrated nitric acid until pH value was adjusted to 2.

In order to conduct field analysis such as measurement of pH value and dissolved oxygen, Multi 340i multimeter (WTW) was used. The other target parameters were measured under standard laboratory procedures using UV-VIS DR5000 (HACH) spectrophotometer for determination of inorganic ions (orthophosphates, PO_4^{3-} and nitrites, NO_2^-) and chemical oxygen demand (COD). The total organic carbon (TOC) and total nitrogen (TN) were measured on Vario TOC Select (Elementar).

Samples for screening analysis were collected in amber glass 2 L bottles, without stabilization. All samples represent 2-hour composite sample, which is consisted of 8 random samples collected in 2 hours, in 15 minutes intervals, from 1 m depth from the surface. Samples were transported and kept at 4°C until analysis. Samples were prepared by liquid-liquid extraction and analyzed by GC-MS (Shimadzu QP2010Ultra) in SCAN and SIM mode.
The capillary column HP-5MS was used for the analysis. Oven temperature gradient program was set to hold time of 10 minutes on 40 °C, and then increase of 2 °C per minute was adjusted to 300 °C. MSD was used during the analysis in scan mode (m/z 45-600). Helium was used as carrier gas.

Results and discussion

In order to define the origin of leachate pollution, concentration levels of relevant physicochemical parameters at the sampling locations are shown in Table 1.

Table 1. Values of relevant physicochemical parameters at the sampling locations – Lake Zobnatica and Tompojevački ritovi

	pH value	Dissolved O_2 (mg L^{-1})	Orthophosphates PO_4^{3-} (mg L^{-1})	Total N (mg L^{-1})	Other relevant parameters (mg L^{-1})
Lake Zobnatica	> 8,5	< 4	1,7 – 4,5	12,59 – 73,26	0,436 (NO_2^-)
Wetland Tompojevački ritovi	9,5	< 1	7,7 – 10	275,68	79,9 (TOC) 180 (COD)

As presented in Table 1, measured concentration levels of total nitrogen were in range of 12,59 – 73,26 mg L^{-1} while concentration of orthophosphates ranged from 1,7 – 4,5 mg L^{-1}. The influence of the green belt on the reduction of concentration levels of total nitrogen and nitrite was observed [5]. The pH value (higher than 8,5) and concentration of dissolved oxygen (lower than 4 mg L^{-1}) point out anthropogenic activities as possible pollution source. The high level of nitrites concentration (0,436 mg L^{-1}) was detected in one representative sampling point.

The elevated concentration levels of orthophosphate (7,7 – 10 mg L^{-1}) and total nitrogen (275,68 mg L^{-1}), indicate that major pollution sources are implemented agricultural activities resulting

in agricultural runoff. Nitrogen compounds in water are products of organic matter degradation [5]. pH value was greater than 9,5 while measured values of dissolved oxygen were lower than 1 mg L^{-1}. The increased concentration levels for TOC and COD were 79,90 and 180 mg L^{-1}, respectively.

Screening analysis of agricultural runoff water indicated the presence of the following substances shown in Table 2.

Table 2. Comparison of leachate analysis results in Serbia and Croatia

Study (Location)	***Serbia, 2019***	***Croatia, 2019***
Substance		
3-(n-Propylamino)-2,1-benzisothiazole		x
Aminomethyl phosphonic acid (AMPA)	x	
N-Butylbenzenesulfonamide		x
Benzyl butyl phthalate		x
Cholesteryl formate (26-Nor-5-cholesten-3.beta.-ol-25-one)		x
Dibutyl phthalate	x	x
Diisobutyl phthalate	x	x
Diphenyl sulfide	x	
Eicosane	x	
Phenanthrene-D10 (IS)	x	x
Glyphosate (*N*(phosphonomethyl)glycine)		x
2,4-bis(1,1-dimethylethyl)- phenol	x	
Triphenylphosphine oxide		x

Table 2. shows comparison of the obtained results at Lake Zobnatica, Serbia, and Tompojevački ritovi, Croatia. There is a lack of knowledge about distribution of wide range of organic micropollutants in protected water areas. It is much more common to examine the presence of glyphosate and/or AMPA in the leachate of agricultural land, or land treated with agrotechnical measures, than a complete screening analysis. Glyphosate was detected in samples collected from wetlands located in Tompojevački ritovi, Croatia, while it was not detected in samples from Lake Zobnatica, Serbia. However, the glyphosate metabolite aminomethyl phosphonic acid (AMPA) was detected in samples from Lake Zobnatica, and not detected in samples from Tompojevački ritovi. The phthalic acid esters (Dibutyl phthalate (DBP) and Diisobutyl phthalate) were detected in both studied protected areas. DBP is defined as priority pollutant with endocrine disruptor properties. The natural antimicrobial compound, 2,4-bis(1,1-dimethylethyl)-phenol, was detected in study conducted in Serbia.

Due to the presence of the above-mentioned organic substances in leachates, as well as glyphosate and aminomethylphosphonic acid (AMPA), it can be concluded that the contamination of leachates with these substances and herbicide, as well as its metabolite, is due to anthropogenic activity through the usage of agrotechnical measures on the land.

Results of reported research of pesticide residues in protected areas are oriented at their presence in the air and soil or sediment [6, 7], and therefore, the results presented in this paper from the study of water quality in Serbia and Croatia protected areas are valuable and rare.

Conclusion

The results of the study presented in this paper prove that due to the use of glyphosate and glyphosate-based herbicides, its identification in water samples of protected areas is possible, and therefore there is potential for its occurrence in drinking water sources due to incomplete degradation or inadequate usage. Further research should be aimed at establishing a detailed monitoring programs to assess the quality of leachate water media at protected water areas with desirable inclusion of detected organic micropollutants.

Acknowledgements

This research has been supported by the Ministry of Education, Science and Technological Development through the project no. 451-03-68/2020-14/200156: "Innovative scientific and artistic research from the FTS (activity) domain" and the Bilateral project funded by the Ministry of Education, Science and Technological Development (contract no. 337-00-107/2019-09/16).

References

[1] W.A. Battaglin, M.T. Meyer, K.M. Kuivila, J.E. Dietze, J. Am. Water Resour. As. 50 (2014), pp. 275–90.
[2] M.S. Majewski, R.H. Coupe, W.T. Foreman, P.D. Capel, Environ. Toxicol. Chem 33(2014), pp. 1283–93.
[3] R.H. Coupe, S.J. Kalkhoff, P.D. Capel, C. Grégoire, Pest Manag. Sci. 68(2016), pp. 16–30.
[4] M.G. Dill, D.R. Sammons, C.C.P. Feng, F. Kohn, K. Kretzmer, A. Mehrsheikh, M. Bleeke, L.J. Honegger, D. Farmer, D. Wright, A.E. Haupfear, in John Wiley & Sons Inc, Glyphosate: Discovery, development, applications and properties, Hoboken, New Jersey, 2010.
[5] Active Sensor Monitoring Network and Environmental Evaluation for Protection and Wise use of Wetlands and Other Surface Waters. http://senswetlands.ferit.hr/rezultati
[6] S. Wang, T. Steiniche, K.A. Romanak, E. Johnson, R. Quiros, R. Mutegeki, M.D. Wasserman, M. Venier, Environ Sci Technol 53 (2019), pp. 6171-6181.
[7] Y. Sanchez-Palencia, J.E. Ortiz, T. Torres, J. Llamas, J Iber Geol 43 (2017), pp: 539-557.

ADSORPTION REMOVAL OF ANIONIC SURFACE-ACTIVE AGENTS FROM THE WASTE FOUNTAIN SOLUTION

Savka Adamović[1], Vladimir Rajs[1], Aleksandra Mihailović[1], Ivan Pinćjer[1], Ivana Tomić[1]

[1]University of Novi Sad, Faculty of Technical Sciences, Trg Dositeja Obradovića 6, 21000 Novi Sad, Serbia
e-mail: adamovicsavka@uns.ac.rs

Abstract

In the printing industry, surface-active agents are used in printing materials such as printing inks, adhesives and fountain solutions. In printing inks and adhesives, surface-active agents are used as anti-foams. By reducing surface tension, surface-active agents create a binder to better wet and disperse pigments during the production of printing inks [1]. Their primary role during the offset printing process is to reduce the surface tension of the fountain solutions and in such a way accommodate better wetting of the printing plate [2]. Also, surface-active agents can act as emulsifiers because they form and stimulate the production of emulsions between the fountain solution and offset printing inks and participate in the formation of printing and non-printing elements on the offset printing plate [3]. As surface-active agents are included in the emergent substances, according to the Network of reference laboratories, research centers and related organizations for monitoring of emerging environmental substances [4], it is necessary to remove them from the offset effluent and safely dispose of them in the sewage system or a natural recipient.

This paper aims to investigate the removal of the anionic surface-active agents from the waste fountain solution by using adsorption with activated carbon. The removal adsorption efficacy of anionic surface-active agents from the effluent with Norit w35 activated carbon was determined according to the standard SRPS H.Z1.149:1987 method [5] and ASTM D2330-02 method [6] by using a UV/VIS spectrophotometer (GENESYS 10S, Thermo Scientific, USA). At a wavelength of 618 nm, the initial absorbance of the starting effluent and the absorbance of the offset effluent after the adsorption treatment of the waste fountain solution with activated carbon were measured.

For the adsorption treatment, activated carbon masses of 0.375, 0.500, 0.625, and 0.750 g were selected, which corresponded to doses of 15, 20, 25, and 30 g L^{-1}, respectively. The stated masses of Norit w35 activated carbon and 25 mL of waste offset fountain solution were weighed into plastic cuvettes with a volume of 45 mL, respectively. At contact times of 5, 10, 15, 20, and 25 minutes, a mixture of a certain mass of Norit w35 and waste offset effluent was subjected to continuous mixing on a mixer (KS 501 Digital IKA-WERKE, Germany) with a mixing speed of 150 rpm.

After a given contact time, a mixture of a certain mass of Norit w35 (adsorbent) and waste offset fountain solution (adsorbate) was separated by filtration through quantitative cellulose filter paper (Macherei-Nagel, Germany). The absorbances of the filtered samples were measured spectrophotometrically at a wavelength of 618 nm.

The efficiency of adsorption removal (E) of anionic surface-active agents from the waste fountain solution with Norit w35 activated carbon was determined by using the equation:

$$E = ((A_o - A_t) / A_o)\ 100 \qquad (\%)$$

Where: E - adsorption removal efficiency of anionic surface-active agents (%), A_o - absorbance at 618 nm of anionic surface-active agents in the waste fountain solution before the adsorption treatment with Norit w35 activated carbon, and A_t - absorbance at 618 nm of anionic surface-

active agents in the waste fountain solution after the adsorption treatment with a certain dose of Norit w35 activated carbon at a certain adsorption time (t).
The obtained results of the removal of anionic surface-active agents from the waste fountain solution by using Norit w35 activated carbon show the following:

1. It is possible to remove anionic surface-active agents from a waste fountain solution **by** using Norit w35 activated carbon adsorption treatment.

2. With the increase of the dose of Norit w35 activated carbon and the time of adsorption, the efficiency of removing anionic surface-active agents from the waste fountain solution also increases.

3. From an economic point of view, it is desirable that the optimal dose and adsorption time be as low as possible.

4. The operative dose of Norit w35 activated carbon as adsorbent is 25 g L^{-1}.

5. The operative adsorption time of contact between the absorbent (activated carbon) and the adsorbate (anionic surface-active agent) is 10 minutes.

6. The adsorption removal efficiency of anionic surface-active agents from the waste fountain solution is greater than 95% for the defined operational adsorption parameters.

Therefore, the removal efficiency of anionic surface-active agents from the offset effluent of 95.5% is achieved at the adsorption time of 10 minutes, and the dose of 25 g L^{-1} of Norit w35 activated carbon.

Acknowledgements
The authors acknowledge the financial support of the Ministry of Education, Science and Technological Development, Republic of Serbia through the project no. 451-03-68/2020-14/200156: “Innovative scientific and artistic research from the FTS (activity) domain”.

References
[1] M. Prica, S. Adamović, Grafički materijali, 1st ed., FTN Izdavaštvo, Novi Sad, 2017, pp. 96 (In Serbian).
[2] H. Kipphan, Handbook of Print Media-Technologies and Production Methods, Springer-Verlag, Berlin, Germany, 2001, pp. 206.
[3] M. Prica, S. Adamović, Hemija u grafičkom inženjerstvu, 1st ed., FTN Izdavaštvo, Novi Sad, 2019, pp. 294 (In Serbian).
[4] NORMAN - Network of reference laboratories, research centres and related organisations for monitoring of emerging environmental substances, NORMAN Association, 2020, URL: https://www.norman-network.net.
[5] SRPS H.Z1.149:1987: Ispitivanje industrijskih i otpadnih voda - Određivanje sadržaja anjonskih tenzida - Spektrofotometrijska metoda, Institut za standardizaciju Srbije, Republika Srbija, 1987 (In Serbian).
[6] ASTM test method D 2330-02: Standard test method for methylene blue active substances, ASTM International, USA, 2002.

SYNTHESIS OF FLUORESCENT DYES FOR BIOIMAGING

Henrietta Ágoston, Erzsébet Mernyák

Department of Organic Chemistry, University of Szeged, Dóm tér 8, H-6720 Szeged, Hungary
e-mail: hencsike12@gmail.com

Abstract
Super-resolution fluorescence microscopy offers good sensitivity and high temporal resolution for characterizing cellular structures and biomolecules. Red-emittig fluorescent dyes are ideal fluorophores for biomolecule labeling, due to reduced absorbance and autofluorescence of cells in far-red or near-red window. Here we synthesized novel fluorescent dyes based on carbopyronine core. The dyes were synthesized from two fragments based on cyclocondensation and/or Friedel-Crafts alkylation strategies.

Introduction
The majority of the biochemical assays exist based on radioisotope labeling; however, there is an increasing demand for friendlier and greener bioanalytical methods. Fluorescent labeling could serve as a more favorable alternative.[1,2] Nevertheless, the fluorescent labeling might greatly influence the original biological behavior of the biomolecule. The position of labeling, the spacing between the labeled compound and the dye, and the coupling moiety might all determine biological applicability. The ideal fluorophore would have high photostability, far-red excitation and emission wavelenghts, and could be attached to the biomolecule without affecting its original biological function.[3] Here we aimed to synthesize red-emitting dyes based on carbopyronine core.

Results and discussion
The syntheses of the carbopyronine dyes were carried out according to the strategy described on Scheme 1. One fragment was a benzyl alcohol derivative, the other contained the isopropenyl function. The methylene bridges were established via electrophilic aromatic substitution reactions, catalyzed by Lewis- or Brønsted-acids. Functional groups suitable for the late-stage conjugation of the dyes to certain biomolecules were introduced onto the first fragment. The structures of the dyes were characterized by one- and two-dimensional ^{1}H and ^{13}C NMR methods. The conjugation of the fluorophores to neurosteroids is planned in near future.

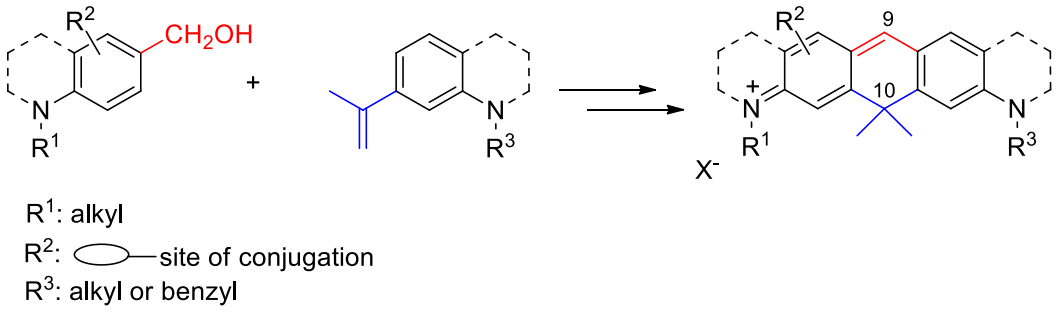

Scheme 1. Synthesis of fluorophores based on carbopyronine core

Conclusion

In conclusion, we have synthesized fluorescent dyes suitable for the labeling of biomolecules. The labeling of neurosteroids with red-emitting dyes allows the investigation of the conjugates by super-resolution fluorescence microscopy in living cells.

Acknowledgements

The work of Erzsébet Mernyák in this project was supported by the János Bolyai Research Scholarship of the Hungarian Academy of Sciences. This work was supported by National Research, Development and Innovation Office-NKFIH through project OTKA SNN 124329. The authors thank the support of project EFOP-3.6.2-16-2017-00005.

References

[1] L. Wang, M.S. Frei, A. Salim, K. Johnsson, J. Am. Chem. Soc., **2019**, *141*, 2770–81.
[2] K. Kolmakov, E. Hebisch, T. Wolfram, L. A. Nordwig, C. A. Wurm, et al. Chemistry **2015**, *21*, 13344–56.
[3] V.N. Belov, S. Stoldt, F. Rüttger, M. John, M., et al. J. Org. Chem. **2020**, *85*, 7267–75.

COMPARISON OF PHENYLUREA PESTICIDES RECOVERY FROM DIFFERENT SOIL TYPES

Milica Baloš[1], Vojislava Bursić[1], Vuković Gorica[2], Rada Đurović-Pejčev[3], Tijana Stojanović[1], Aleksanda Petrović[1], Dušan Marinković[1], Bojana Špirović Trifunović[4], Bojan Konstantinović[1]

[1]*University of Novi Sad, Faculty of Agriculture, Trg Dositeja Obradovića 8, Novi Sad, Serbia,*
[2]*Institute of Public Health, Bulevar despota Stefana 54a, Belgrade, Serbia,*
[3]*Institue of Pesticides and Environmental Protection, Belgrade, Serbia*
[4]*University of Belgrade, Faculty of Agriculture, Nemanjina 6, Zemun, Serbia*
e-mail: cucuzm@yahoo.com

Abstract
The subject of this research work is to determine the recoveries of the studied analytes from the chemical group of phenylurea: isoproturon, diuron and linuron, depending on the physical-chemical soil properties within the validation of multi-residual method for the determination of the herbicide residues in soil by (LC-MS/MS) after QuEChERS extraction of spiked soil samples. The factorial ANOVA did not show any statistical significances regarding the influence of the paired values of different pesticides and soil types. The same result was obtained by the one-way ANOVA calculated for different soil types (p_s=0.151060 for $p<0.05$) and different pesticides (p_p=0.165207 for $p<0.05$) regarding the values of average recoveries. Fishers LSD post hoc test emphasized the homogenity and similarity among average recovery values in both cases.

Keywords: phenylurea, QuEChERS, recovery, soil, LC-MS/MS

Introduction

The use of herbicides in agriculture is a significant factor responsible for the mass production of food. The low degradability of pesticides has led to their presence in water, soil and food. Chemical characteristics of pesticides, such as low solubility in water and high in fats, stability to photo-oxidation and low vapor pressure are the main elements that determine not only the efficiency but also the persistence of pesticides in the environment [1].

The compounds of herbicides can be very persistent in the environment and if they are stable and persist for a long time in soil or water, their application is gradually discontinued or limited in dosage. Phenylurea herbicides are a group of pesticides used to control harmful weeds on agricultural land.

These herbicides are produced and distributed under different names, some of which are: diuron, isoproturon, linuron, buturon, chlortoluron, methiuron, tebuthiuron... These compounds have the ability to inhibit photosynthesis and thus successfully suppress harmful weeds that cause problems on agricultural land. The decomposition of these herbicides in soil can be a slow and problematic process. The decomposition of phenylurea herbicides can be performed under acidic or alkaline conditions and also UV irradiation. Although a large number of phenylureas can be found in agricultural production, little is known about their toxicity, which they can cause with prolonged use. Diuron is a widely used herbicide of all phenylurea herbicides in the whole world. The acute toxicity potential for all phenylureas appears to be low, with oral LD_{50} values typically greater than 1 g/kg [2].

In the normal pH range these herbicides are stable when exposed to hydrolysis and exist as the undissociated form in natural waters. The photochemical degradation of these compounds caused by sunlight is of very little importance. The herbicides from the phenylurea group the

plants adopt via the root and they are quickly translocated to the stems and leaves via xylem. In addition to diurons, linuron and isoproturon have also been widely used in agricultural production for surface application on the leaves of the treated plants.

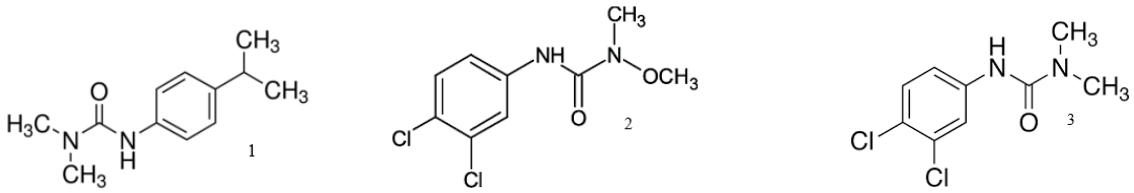

Figure 1. Structural formula of isoproturon (1), linuron (2) and diuron (3)

These compounds inhibit enzymes involved in the Hill reaction and because of that they interrupt the process of photosynthesis. Lewis and Gardiner (1996) have reviewed data on the use and fate and behaviour of these herbicides [3].

The release of linuron into the environment is mainly through machine washing after application, drainage, and accidental spillage as it is widely used in agriculture [4].

The pesticide-soil sorption interaction can include mineral or organic components, and sometimes both of them [5]. The physical and chemical characteristics of the herbicide define the movement of the herbicide towards the target location, the persistence, soil mobility and photostability. Therefore, it is possible to predict which compounds can cause potential problems in the environment [6]. In general, measuring of the trace compounds such as pesticide residues is highly difficult due to time consumption, while the long procedure causes losses of the analytes [7, 8]. The aim of this study was to determine the recoveries of investigated herbicides depending on the physicochemical properties of three different soils. For the extraction of the isoproturon, diuron and linuron, the QuEChERS method was used, followed by liquid chromatography tandem mass spectrometry (LC-MS/MS).

Material and method

The experimental part of the research work, which included the enrichment of the soil samples by the tested pesticides with their extraction, was done at the Department of Phytomedicine and Environmental Protection, Faculty of Agriculture in Novi Sad. The chromatographic separation on LC-MS/MS was performed at the Public Health Institute in Belgrade. The samples of three soil types with different physicochemical characteristics were used (Table 1), in which the presence of pesticide residues (blank samples) was not detected. In order to set the validation parameters, the blank samples were enriched with a certain amount of tested pesticides.

The analytical standards of diuron, linuron and isoproturon were parched from dr. Ehrenstorfer. The stock (≈ 1.0 mg/mL) and working solutions (10 µg/mL) were prepared in acetonitrile (HPLC purity, J.T. Baker). As an internal standards the following were used: (10 µg/mL) carbofuran-D3, atrazine-D5 and isoproturon-D6.

LC-MS/MS analysis. The 6410 Agilent Technologies LC-MS/MS with electrospray ionization was used. The separation was performed using a Zorbax Eclipse XDBC18 column (50 mmx4.6mm id 1.8 µm.) at 25 ºC. The mobile phase (0.4 mL/min): methanol with 0.1% formic acid and 0.1% formic acid in water in the gradient mode. Total run was 30 min. The injection volume was 5 µL. The target ion transition with highest intensity (primary ion transition) was used for the quantitation, whereas the second target ion transition was used for the confirmation.

Table 1. Soil characteristics

Soil	pH (H_2O)	$CaCO_3$ %	Organic matter %	Send 2-0.2 mm %	Send 0.2-0.02 mm %	Powder 0.02-0.002 mm %	Clay <0.002 mm %
1.	8.71	30.6	0.11	1.58	91.7	3.4	3.32
2.	8.16	7.45	3.76	10.25	22.45	25.03	42.27
3.	7.65	1.02	0.88	0. 53	21. 39	29.04	49.04

The instrument uses MassHunter software version B.06.00 for the quantitation and confirmation.
Method validation - recovery was determined according to SANTE/12682/2019 [9]. Recovery was obtained by spiking soil samples in the concentrations 1.0 and 10.0 mg/kg. The limit of detection (LOD) was estimated in the MRM mode analysis as the lowest concentration level that yielded S/N ratio of five.
The pesticides extraction from spiked soil samples was carried out using a modified QuEChERS method [10].
Statistical analyses. In order to determine the statistical differences among the obtained recovery values as the dependent variables and the pesticides and soil types as the independent variables the factorial and one-way factor analysis of variance (ANOVA) were applied using Statistica 13.2 (TIBCO Software Inc. University license).
The calculated differences were tested by Fisher's LSD post-hoc test.

Results and discussions
Before accessing qualitative analysis or the quantification of pesticides it is necessary to set the acquisition parameters of the mass spectrometer - to set the multiple reaction monitoring mode (MRM). MRM-MS sensitivity is dependent upon the appropriate tuning of instrument parameters such as collision energy (CE) and energy of fragmentation (Frag) in order to generate maximal transmission of the pesticide product ions (Table 2).

Table 2. Soil characteristics

Pesticide	Rt (min)	Precursor ion (*m/z*)	Product ion (*m/z*)	Frag (V)	CE (V)
Isoproturon	21.77	207 207	169 72	70 70	15 17
Diuron	22.03	233 233	160 72	70 70	18 25
Linuron	23.56	249 249	182.1 160	120 120	10 20

The obtained recoveries with RSD (%) values are given in the table 3. The obtained RSD values represent the precision of the method.

Table 3. Average recoveries (%)

Pesticide	Soil 1	Soil 2	Soil 3
Isoproturon	97,2 (12,43)	93,3 (4,7)	91,9 (7,45)
Diuron	103,7 (11,72)	99,8 (3,05)	97,2 (7,44)
Linuron	99,7 (12,43)	90,5 (7,23)	86,7 (5,68)

The factorial ANOVA did not show any statistical significances regarding the influence of the paired values of different pesticides and soil types. The same result was obtained by the one-way ANOVA calculated for different soil types (p_s=0.151060 for $p<0.05$) and different pesticides (p_p=0.165207 for $p<0.05$) regarding the values of average recoveries. Fishers LSD post hoc test emphasized the homogenity and similarity among average recovery values in both cases.

Conclusions

The influence of main physicochemical properties of three soils on isoproturon, diuron and linuron recoveries in this matrix were studied applying QuEChERS soil sample preparation followed by the LC-MS/MS determination.

The organic matter and clay content affected the recovery of the studied pesticides. The obtained dependence indicates that with increasing organic matter and clay content (soil 2 and 3), the recoveries were lower than in soil 1.

The applied statistical analyses did not emphasize any statistical differences among pesticides, soil types and obtained recoveries, pointing out the homogenitiy and similarity among obtained data.

Acknowledgements

The authors acknowledge the financial support of the Ministry of Education and Science, Republic of Serbia.

References

[1] Kim J., Smith A. (2001): Distribution of organochlorine pesticides in soils from South Korea, Chemosphere 43, 137-140.

[2] Haye A. (2010): Handbook of Pesticide Toxicology, Chapter 80 - Phenylurea Herbicides; Pages 1725-1731; Oklahoma State University, Oklahoma.

[3] Gardner K., D. Lewis (1996): Anthropology, Development and the Post-Modern Challenge

[4] Department of the Environment, Transport and the Regions (1998): European Marine Sites in England and Wales.

[5] Đurović R., Đorđević T., Bursić V. (2012): Effect of organic matter and clay content in the soil on triazine and organophosphorus pesticides adsorption processes, Annual MGPR Meeting 2012 and International confefrence on food and health safety: Moving towards a sustainable agriculture, Belgrade, Serbia 11-12 October, Book of abstracts, 69.

[6] Konstantinović B. (2011): Fundamentals of Herbology and Herbicides. University of Novi Sad, Faculty of Agriculture.

[7] Ćućuz M., Bursić V., Vuković G., Ćirić V., Zeremski T., Đurović-Pejčev R., Annals of Agronomy (2016) 61.

[8] Baloš M., Bursić V., Vuković G., Đurović-Pejčev R., Zeremski T., Petrović A., Gvozdenac S., Stojanović T. (2019). Carbamate insecticides extraction depending on the soil properties, 25th International Symposium on Analytical and Environmental Problems, Szeged, Hungary, October 7-8, Proceedings, 54-58.

[9] SANTE/12682/2019: Method validation and quality control procedures for pesticide residues analysis in food and feed.
[10] Đurović-Pejčev R., V. Bursić, Zeremski T., J. AOAC Int. 102 (2019) 46.

MORPHOSTRUCTURAL STUDY OF SOME GRAPHENE-BASED AEROGELS FOR SENSORS FABRICATION

Florina Stefania Rus[1], Radu Banica[1], Calin Ladasiu[1]

[1]*National Institute of Research and Development for Electrochemistry and Condensed Matter, 144 Aurel Paunescu-Podeanu, RO-300569 Timisoara, Romania*
e-mail: radu.banica@yahoo.com

Abstract

This paper presents a detailed study of the feature-rich essential properties of the family of two-dimensional graphene flakes, as well as the preparation and properties of graphene-based aerogels. The usefulness of Raman spectroscopy, a versatile tool used to identify and characterize the chemical and physical properties of these graphene flakes and their composites is clearly stated. Furthermore, strategies for the preparation of bulk graphene-based aerogels are also discussed. The properties of nanocomposites were analyzed using XRD and SEM combined with micro Raman spectroscopy, which provides structural and optical information.

Introduction

Altough the X-Ray Diffraction (XRD) and Scanning Electron Microscopy (SEM) spectra can give important information about the composition and structure of graphene aerogels, the Raman spectra can give complementary information that can be corelated with the electrical conductivity of the structure. The Raman spectrum of graphene shows a relative simple structure characterized by two main bands designated as the G and 2D bands (a third band, the D band, can be observed when defects are present in the carbon network). The usefulness of Raman analysis lies in its ability to differentiate between single, double and triple layered graphene. The ratio between the intesities of the specific peaks of graphene – 2D and G was determined. According to the literature, if the ratio is around 2 or above, the recorded spectrum coresponds to a monolayer graphene [1]. The 2D band is always a strong band in graphene even if the D band is not present and the graphene has no defects. This band is also used to determine the thickness of the graphene layer. In contrast to the G-band position method, the method used to determine the thickness of the graphene layers based on the 2D band depends not only on the position of the band but also on the shape of the band [2]. In the case of a double-layered graphene, the interaction of the planes divides the π and π* electronic bands in four structures of parabolic bands (π1, π2, π1*, π2*). The spatial groups theory explains the fact that the laser light excites the electrons as pairs (π1, π1* și π2, π2*) between the four band structures. This gives the maximum 2D dispersivity for the bilayer graphene that can be characterised by four Lorentzian maxima. For the multilayered graphene, the splitting of the electronic bands becomes more complex and more dispersive leading to further widening of the 2D bands [3].

Experimental

The graphene oxide (GO) was prepared using a modified Hümmer method. Briefly, the graphite (supplied by Alfa Aesar, average particle size of 44 μm) was oxidized with H_2O_2 and $KMnO_4$ in the presence of H_2SO_4 and H_3PO_4. After oxidation, the resulting mixture was filtered through a polyester filter. The mixture was then destabilized by the addition of acetone, was separated by centrifugation, and washed with a 30% HCl solution followed by redispersion in water. The process was repeated 5 times without HCl addition until the absence of chlorine ions that were detected by adding a $AgNO_3$ solution. The GO concentration was determined using gravimetric analysis by evaporating in vaccum (< 10 mBar) 5 mL of suspension at 60 ºC for 16

hrs. The suspension was then diluted until the resulting concentration was 2 mg/mL. The precursor used in the aerogels synthesis was a blend of GO1 synthesised according to the above method having a concentration of 0.9 mg/mL, and a Quattro-Type graphene suspension whose concentration was increased to 0.75 mg/ml by centrifugation at 24.000 RPM and redispersed in water [4].

Next, the suspension was freezed at - 196°C then lyophilised using a freeze drier built by the INCEMC collective by modifying the GSL-1500X (MIT Corporation) oven (patent pending invention). The freeze drying took place at a pressure lower than 1 Torr using a vapour trap cooled with liquid nitrogen. The second stage consisted of heating the graphene to 300 ºC in vacuum and maintaining it for 60 minutes at that temperature. The heating speed was 4ºC/min and the forced cooling was done under a stream of cold air to room temperature.

Preparation of the aerogel for the Raman study

The graphene aerogel was pressed on mirror polished silicone substrates cleaned by sonication in alcohol and distilled water. The excess material was extracted several times using adhesive tape until the semi-transparent graphene sheets could be observed [5]. The optical images of the exfoliated graphene flakes were obtained using the 50x and 100x objectives of the Olympus optical microscope. The diffraction spectrum was obtained with the X'Pert Pro MPD difractometer using the Cu (K-α) line and the Raman spectra of the exfoliated graphene were collected using the microRaman system (Olympus BX-51 optical microscope and Andor Shamrock 500i Spectrometer, λ_{ex}=514 nm).

Results and discussion

The XRD diffractogram, the SEM and optical images of the GO sample dried at 30°C for 20 hrs in vacuum at 10 mBar are shown in figure 1.

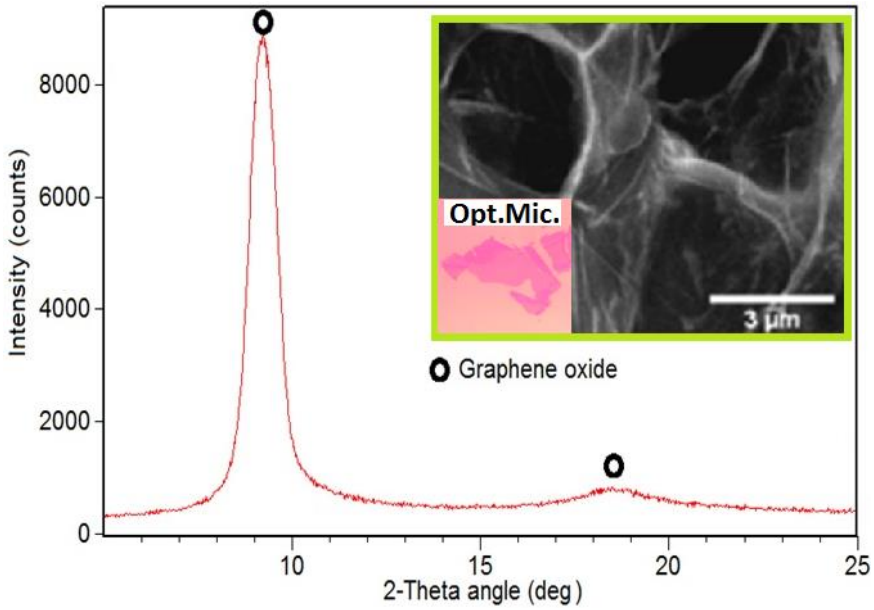

Figure 1. XRD diffractogram and the SEM/Optical image (inset) of the graphene aerogel

The XRD diffractogram shows that the obtained product is pure graphene oxide without traces of graphite.

The G (figure 2a) and 2D (figure 2b) bands of the monolayer graphene with the calculated width at half maximum gives information regarding the number of atomic planes and the density of defects in the carbon atoms plane. The G band around 1585 cm^{-1} in the

graphene spectra is a sharp band and coresponds to the in-plane vibration of the sp^2 hybridized carbon atom that make the graphene sheet. The position of the G band is very sensitive to the number of the layers in the sample [6]. In the case of our samples, in the areas with multiple layers, the G peak shifts to the left from 1584 cm^{-1} (mono-layer) to 1581 cm^{-1} (multi-layer). The 2D vibration is symmetrical having the width reduced to the half of the height (~25 cm^{-1}) and is the best indicator for the monolayer graphene obtained from the aerogel on the silicone substrate. However, the signature of the monolayer graphene is given by the intensity of the 2D band (around 2700 cm^{-1}, value that depends on the excitation wavelenght of the laser) that is at least twice the intensity of the G band (around 1560 cm^{-1}) [7], (figure 2-a, b).

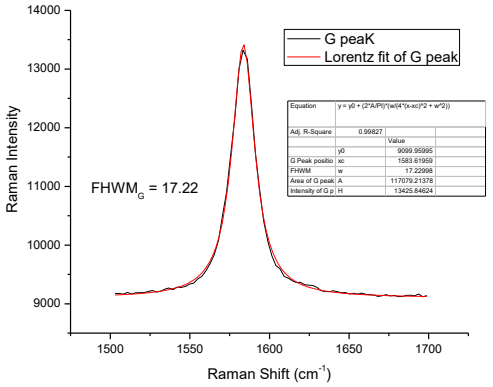

a) Lorentzian deconvolution of G peak for 1 layer graphene

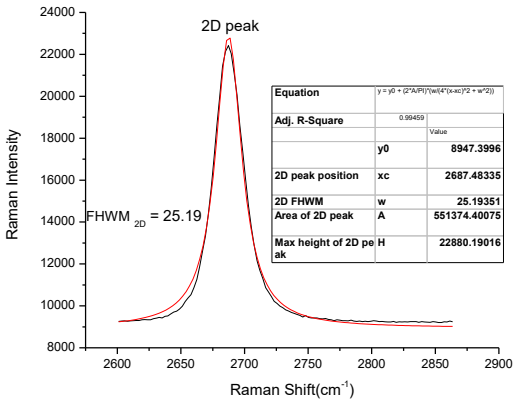

b) Lorentzian deconvolution of 2D peak for 1 layer graphene

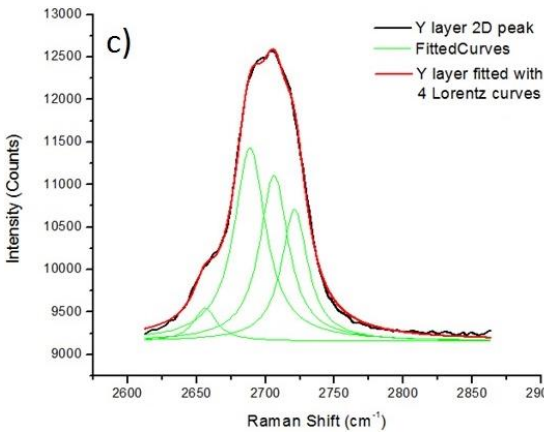

c) Deconvolutions of the 2D band in the sample with different number of layers

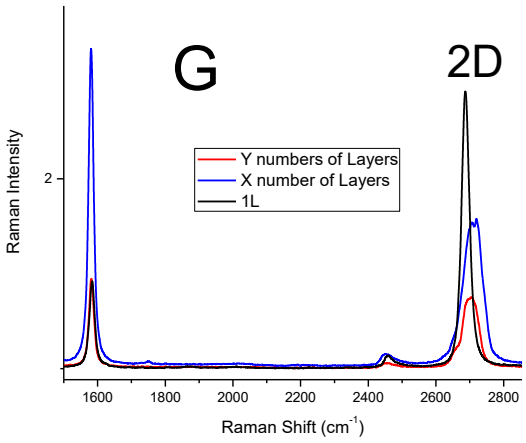

d) Raman Shift for different numers of graphene layers

Figure 2. Raman spectra collected from different areas of the aerogel sample

Based on the above, we suggest that the carbon atom planes were not everywhere fully separated in the sample as it was previously mentioned in literature [8]. This aspect is better seen in the detailed images of the G and 2D bands shown in figure 2c. It can be observed that by adding successive layers of graphene, the 2D band is divided into several overlapping modes and the peak's symmetry decreases with increasing graphene layers in the sample.

The single layer graphene shows a symmetric peak and can be fitted with a single Lorentzian function due to the band structure with a single electron (π) and to the conduction

band (π^*). The full width at half maximum (FWHM) of a single layer is ~ 26.3 cm $^{-1}$[9], close to the value obtained for our samples (25.2 cm^{-1}) (figure 2b).

To determine the exact number of sheets in case of multilayered graphene, more complementary analyses on the same area are necessary such as imaging the area using AFM or STM.

Conclusion

The physicochemical analysis shows that the graphene oxide was successfully synthesized and the graphene aerogel had between one and several graphene layers and that between some of them there is a good electrical bond. The size of the porous mass cells is around 3 μm due to the fast freezing of the dispersion medium preventing the growth of massive ice crystals. Thus, the synthesis method of the aerogel led to a 3D material having probably a good electrical conductivity allowing the charge transfer to the silver nanoparticles that will decorate the aerogel in order to build sensors for H_2S detection.

Acknowledgements

This work was supported by a grant of the Romanian Ministry of Research and Innovation, CCCDI-UEFISCDI, project number PN-III-P1-1.2-PCCDI-2017-0619/Contract 42/2018 "Nanostructured carbon materials for advanced industrial applications", within PNCDI III national research program.

References

[1] L. Zhu, X. Zhao, Y. Li, X. Yu, C. Li, and Q. Zhang,Mater. Chem. Phys. 137 (2013) 984.
[2] V. N. Popov, Journal of Physics: Conference Series 682 (2016) 012013.
[3] S. Karamat, S. Sonuşen, U. Celik, Y. Uysalli, E. Özgönül, A.Y. Oral, Prog. Nat. Sci. Mater. 25 (4) (2015) 291.
[4] C. Mosoarca, D. Ursu, T. Nyari, P. Linul, I. Serbachievici, B. Taranu, R. Banica, Proceedings of the 24th International Symposium on Analytical and Environmental Problems, ISAEP (2018) pp. 248.
[5] A.K. Geim, Rev Mod Phys, 83 (3) (2011), pp. 851.
[6] J. Hodkiewicz, "The Importance of Tight Laser Power Control When Working with Carbon Nanomaterials" Thermo Scientific Application Note AN51948, pp. 2.
[7] J.R. Young, A.I. Kinloch, Graphene and graphene-based nanocomposites. In: Nanoscience:nanostructures through chemistry, vol. 1. The Royal Society of Chemistry; (2013) pp. 156.
[8] J. Wu, M. Lin, X. Cong, H. Liu, & P. Tan, Chemical Society reviews, 47 5, (2018) 1822-1873.
[9] Y. Hao, Y. Wang, L. Wang, Z. Ni, Z. Wang, R. Wang, C.K. Koo, Z. Shen, J.T.L. Thong Small, 6 (2010), pp. 195.

MORPHOLOGICAL AND STRUCTURAL STUDY OF SOME BLACK SEA SHELLS

Cristina Mosoarca, Alexandra Ioana Bucur, Radu Banica, Corina Orha, Maria Poienar, Raul Bucur

National Institute for Research-Development in Electrochemistry and Condensed Matter, no 144 dr A. P. Podeanu, 300569 Timisoara, Romania

e-mail: alexandra.i.bucur@gmail.com

Introduction

Shells are extracellular, calcified structures composed of calcium carbonate crystals and organic material [1]. The primitive crystalline calcium carbonate polymorph for bivalve shells is aragonite. However, while some species are made of aragonite, others are constituted of calcite, and a number of species have both forms. The third calcium carbonate polymorph, vaterite, is also found in bivalves, but it is not common [2].

The purpose of the present study was the collection and identification of some shells from the Black Sea, followed by their grinding and physico-chemical characterization in order to find their structure and composition.

Shells identification

A number of molluscan shells were collected from the Black Sea and examined to determine their species. The examination revealed shell species belonging to various classes, subclasses, families and subfamilies of Mollusca:

- The Mediterranean mussel ***Mytilus galloprovincialis*** may be confused with *Mytilus edulis*, they are often difficult to distinguish. In addition, they may hybridize. However, in *Mytilus galloprovincialis* the umbones turn down, giving the basal line of the shell a concave appearance, the valves are higher and less angular and the mantle edges are darker, becoming blue or purple. All *Mytilus* species have distinctive shells ranging in colouration from black with blue or purplish hues to dark brown and occasionally light brown.
- ***Mya arenaria*** is bivalve with a dirty white or fawn shell with a fawn or light yellow periostracum. The shell is oval in outline, marked by conspicuous concentric lines with dissimilar valves, the right being slightly more convex than the left. The interior of the shell is white with a deep pallial sinus.
- ***Cerastoderma edule*** is thick, equivalve, globular and broadly oval in outline. Shell with 22-28 radiating ribs, crossed by concentric ridges may bear short, flat spines; the surface is off-white, yellowish or brownish. Both valves bear two cardinal teeth.

Experimental

The shells used in this study were collected from the Black Sea and they were identified. The most relevant taxonomic groups are presented in Table 1 [1,2].

Table 1. Identification and classification of molluscan shells collected from the Black Sea

Taxon details	***Mytilus galloprovincialis* (Lamarck, 1819)**	***Mya arenaria* (Linnaeus, 1758)**	***Cerastoderma edule* (Linnaeus, 1758)**
Domain:	Eukaryota	Eukaryota	Eukaryota
Kingdom:	Animalia	Animalia	Animalia
Phylum:	Mollusca	Mollusca	Mollusca
Class:	Bivalvia	Bivalvia	Bivalvia
Subclass:	Autobranchia	Heterodonta	Heterodonta
Order:	Mytilida	Myida	Cardiida

Superfamily:	Mytiloidea	Myoidea	Cardioidea
Family:	Mytilidae	Myidae	Cardiidae
Genus:	Mytilus	Mya	Cerastoderma
Species:	M. galloprovincialis	M. arenaria	C. edule

The samples are numbered in the following order: sample 1 - *Mytilus galloprovincialis;* sample 2 - *Mya arenaria;* sample 3 - *Cerastoderma edule*. Each type is ultrasonicated in distilled water at room temperature, after which the water is drained and the washing is repeated under ultrasound with a different amount of water. After the final rinsing, they are dried for 2 hours at 80°C. After that, the shells are broken one by one by pressing them between 2 steel cylinders with a diameter of about 50 mm at a pressure of 5 tons force (tf) for 30 seconds using the hydraulic press. After breaking, the samples are sieved with sieves of different meshes, of which the fractions: 1) 1-1.6 mm and 2) <200 µm are considered for this study. The obtained powder specimens are characterized in terms of structure by Scanning Electron Microscopy (SEM - Model Inspect S). X-Ray powder diffraction patterns are obtained using an X'Pert PRO MPD diffractometer.

Results and discussion

The structure of the shells was morphological investigated using the scanning electron microscopy, as depicted in figure 1. For the *Mytilus galloprovincialis* fraction 2 sample, the lamellar structure is visible, with well-defined parallel layers, while the other structures are more compact and the layers/lamellas are less well defined.

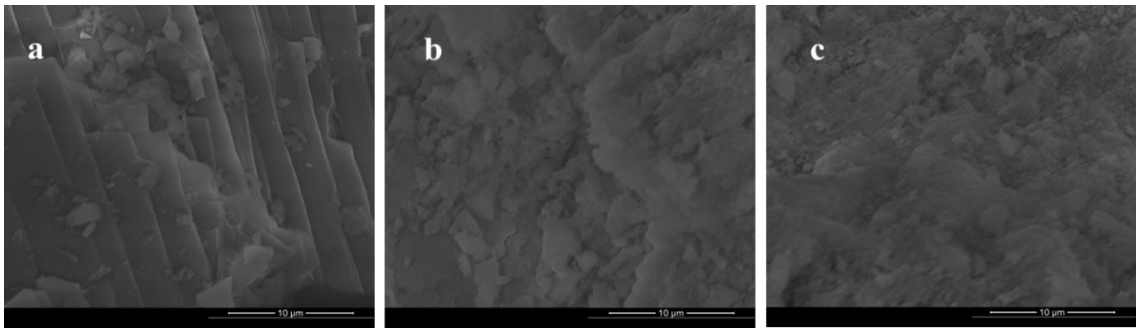

Figure 1. SEM images of a) sample 1 *Mytilus galloprovincialis*, fraction 2; b) sample 2 *Mya arenaria*, fraction 2; c) sample 3 *Cerastoderma edule*. fraction 2

The XRD analysis (Figure 2) was performed in the 2 Theta field 10 - 70 degrees, for fraction 2 (< 200 µm). Ethanol was used for placing the samples on zero background holders. All the samples present a good level of crystallinity, showing intense narrow peaks.

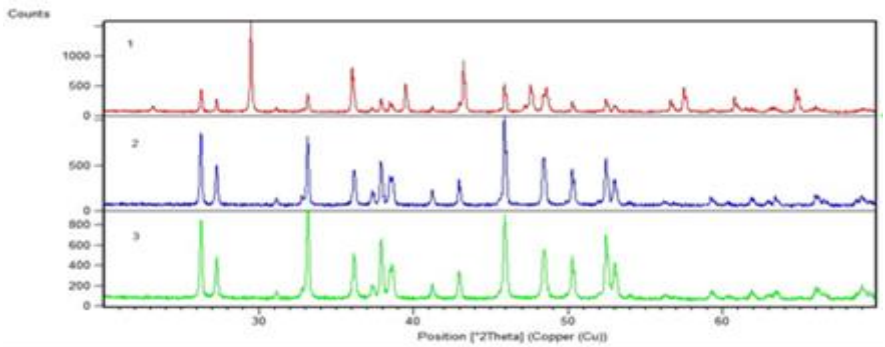

Figure 2. XRD patterns of fraction 1 for samples 1, 2 and 3.

Sample 1 contains aragonite and calcite and the other two specimens contain only aragonite, presenting identical XRD patterns. The identification of peaks belonging to the two phases

present in sample 1 is shown in Figure 3, similar to other results in literature [3].

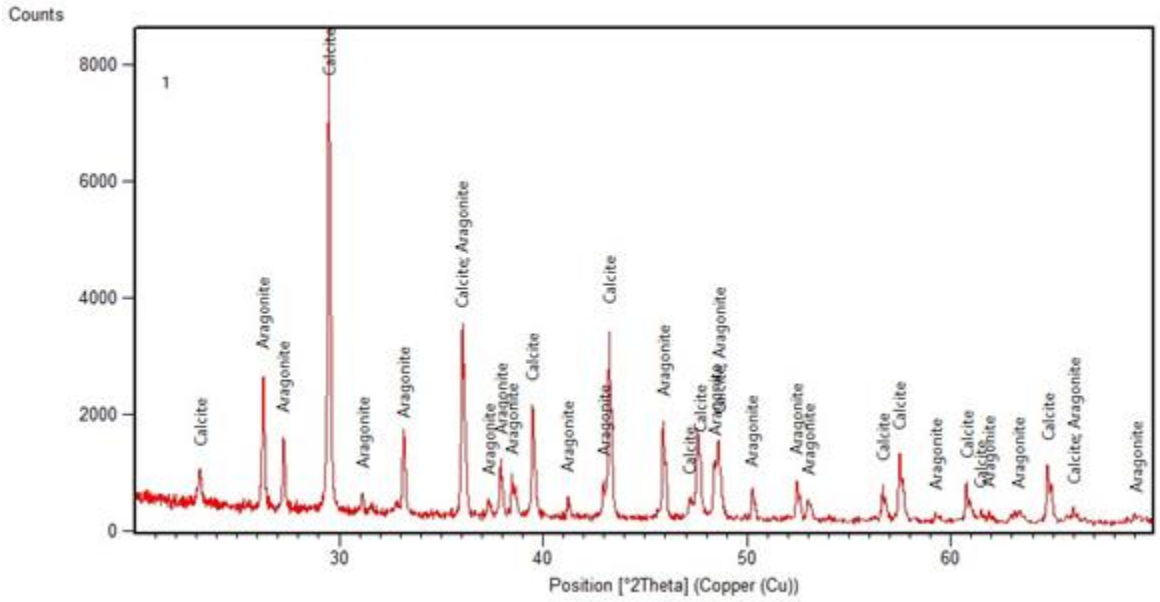

Figure 3. XRD spectrum of sample 1 *Mytilus galloprovincialis,* fraction 1

According to FullProf calculations, sample 1 contains: Phase 1- Aragonite 44.99%; Phase 2- Calcite 55.01%.

Conclusions

Shells collected from the Black Sea and identified in this study belong to the species: *Mytilus galloprovincialis, Mya arenaria and Cerastoderma edule*. Studying their structure and composition, the *Mytilus galloprovincialis* type (brown shells) presents a lamellar structure with well defined parallel layers, while the other two types (white and yellowish) present an inner structure which is less well shaped, compared to the first one. XRD analysis showed that the well defined structure is composed of aragonite and calcite, while the other two types are made of aragonite only. We presume the composition is a major factor in determining the shells outer aspect/color, as well as their properties. We will continue this study in order to find more interesting things and applications for the shells, based on their structure and composition.

Acknowledgements

This work was supported by a grant of the Romanian Ministry of Education and Research, CNCS - UEFISCDI, project number PN-III-P1-1.1-TE-2019-2116, within PNCDI III

References

[1] U. Çevik, N. Damla, A.I. Kobya, V.N. Bulut, C. Duran, G. Dalgıc, R. Bozac, Journal of Hazardous Materials, 160 (2008) 396-401.

[2] G. Soulet, G. Ménot, G. Lericolais, E. Bard, Quaternary Science Reviews, 30 (2011) 1019-1026.

[3] V. Blanco-Gutierrez, A. Demourgues, V. Jubera, M. Gaudon, J. Mater. Chem. C, 2 (2014) 9969-9977.

IN VITRO BEHAVIOR OF TITANIUM DISCS COATED WITH HYDROXYAPATITE

Bogdan-Ovidiu Taranu, Alexandra Ioana Bucur, Paula Svera (m. Ianasi), Corina Orha

National Institute for Research and Development in Electrochemistry and Condensed Matter
no. 144, Dr P.A. Podeanu, Timisoara 300569, Romania
e-mail: alexandra.i.bucur@gmail.com

Abstract

Titanium, one metal with a very wide application range in the dental or orthopaedic fields, and hydroxyapatite (HA), a very versatile and biocompatible ceramic, can be combined to achieve medical implantable devices bearing the advantages of both materials [1, 2].

A new approach for the achievement of HA coated-titanium discs is presented, involving simultaneous precipitation and electrodeposition. One precursor is present in the electrolysis cell and the other precursor is dropwisely added, while an electrochemical potential is applied. The addition order of the precursors was alternated, and the Ti substrate surface modifications were evidenced using various analysis methods. XRD data shows that all the specimens contain HA as the single crystalline phase.

A double ceramic layer configuration is present, with one layer comprised of submicrometric crystals and the second one made up of micrometric constituents. The density of the continuous lower layer is higher, while the upper layer is discontinuous and its density is lower. For both layers the HA crystals are arranged into semi-spherical aggregates.

The roughness observed in AFM results, coupled with data from XRD and SEM analyses, indicates that the HA specimens deposited for longer time periods (4h vs. 1h) are more suited for biointegration.

Since the intended applications concern the dentistry and orthopaedics fields, in vitro tests using artificial saliva solution conducted at 37 °C for 30 and 60 days were followed by XRD and SEM characterizations. Artificial saliva solution was prepared with the same recipe used by Veys-Renaux *et al.* [3]. Results showed the presence of HA throughout the entire testing period, as well as the rapid development of large octacalcium phosphate and dicalcium phosphate crystals. Integrity and resilience of the coatings base layer under corrosive conditions was evidenced by their detachment from the Ti substrate - as opposed to their potential cracking, which would indicate a low corrosion resistance and lack of integrity.

References

1. Cattini, A., Bellucci, D., Sola, A., Pawłowski, L., Cannillo, V.: Suspension plasma spraying of optimised functionally graded coatings of bioactive glass/hydroxyapatite. Surf. Coatings Technol. 236, 118–126 (2013). doi:10.1016/j.surfcoat.2013.09.037
2. Afzal, M.A.F., Kesarwani, P., Reddy, K.M., Kalmodia, S., Basu, B., Balani, K.: Functionally graded hydroxyapatite-alumina-zirconia biocomposite: Synergy of toughness and biocompatibility. Mater. Sci. Eng. C. 32, 1164–1173 (2012). doi:10.1016/j.msec.2012.03.003
3. Veys-Renaux, D., Ait El Haj, Z., Rocca, E.: Corrosion resistance in artificial saliva of titanium anodized by plasma electrolytic oxidation in Na_3PO_4. Surf. Coatings Technol. 285, 214–219 (2016). doi:10.1016/j.surfcoat.2015.11.028

PRELIMINARY STUDIES ON THE SYNTHESIS AND CHARACTERIZATION OF $BaSn(OH)_6$ AS A PRECURSOR FOR PEROVSKITE BARIUM STANNATE CERAMICS

Cristian Casut[1,3], Marinela Miclau[1], Daniel Ursu[1], Nicolae Miclau[2], Iosif Malaescu[3], Alina Zamfir[1,3]

[1] National Institute for Research and Development in Electrochemistry and Condensed Matter, 1 Plautius Andronescu Street, 300224 Timisoara, Romania
[2] Politehnica University Timisoara, Str. PiataVictoriei, nr.2, 300006 Timisoara, Romania
[3] West University of Timisoara, Bulevardul Vasile Pârvan 4, Timişoara 300223 Timisoara, Romania

Functional perovskite oxides may enable entirely new electronic device paradigms, ranging from negative capacitance to charge amplification in phase change devices. A major challenge is the intrinsically poor charge carrier mobility of most perovskite oxides, typically no better than 1^{-10} cm^2 V^{-1} s^{-1} at room temperature.[1] There has been growing interest in perovskite $BaSnO_3$ due to its desirable properties for oxide electronic devices including high electron mobility at room temperature and optical transparency.[2] Because of its high chemical and thermal stability, $BaSnO_3$ can be potentially used at high temperature as a protective coating or catalyst support. The pure compound is an insulator at room temperature and becomes semiconducting when doped with donor impurities such as Sb^{5+} and La^{3+}.[3].

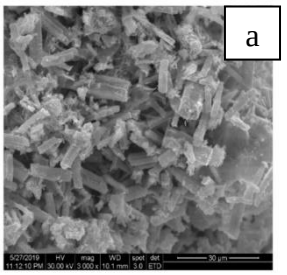

Usually, ceramic powders of $BaSnO_3$ are prepared by solid-state reaction between $BaCO_3$ and SnO_2 at 1000–1200 °C. Polycrystalline materials can be obtained by sintering at 1400–1600 °C, but good densification is difficult to achieve. In this study, we propose using $BaSn(OH)_6$ as precursor for the synthesis of $BaSnO_3$ ceramics. $BaSn(OH)_6$ acicular crystals were obtained by a simple precipitation at 80°C from Na_2SnO_3 and $Ba(NO_3)_2$ aqueous solutions and their transformation in the perovskite like compound $BaSnO_3$ was demonstrated by TG-DTA analysis.

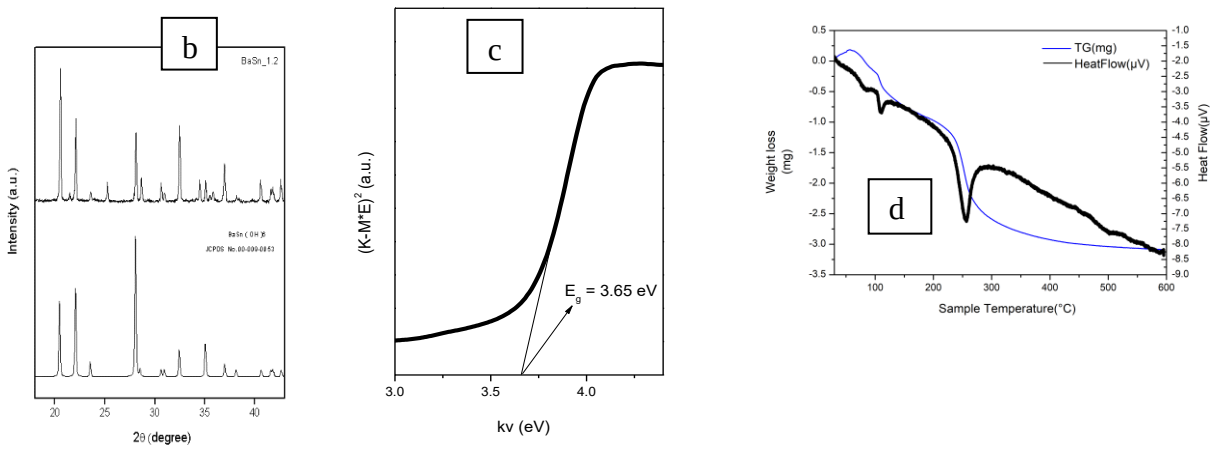

Figure 1: a) SEM image of $BaSn(OH)_6$ b): X-ray diffraction patterns of $BaSn(OH)_6$; c) UV-VIS-NIR of $BaSn(OH)_6$; d) TG-DTA analysis of $BaSn(OH)_6$ in argon

References

1 S. Raghavan, High-mobility BaSnO3 grown by oxide molecular beam epitaxy, APL Mater. 4, 2016

2 M.T. Buscaglia, *Synthesis and characterization of BaSn(OH)6 and BaSnO3 acicular particles*, J. Mater. Res., 2003

3 H. Yun, *Electronic structure of BaSnO3 investigated by high-energyresolution electron energy-loss spectroscopy and ab initio calculations*, Journal of Vacuum Science & Technology, 2018

CHARACTERIZATION OF ANTHOCYANIN EXTRACTS FROM DIFFERENT PLANT MATRICES

Adina Căta[1], Ioana M. C. Ienaşcu[1,2], Mariana N. Ştefănuţ[1]

[1]*National Institute of Research and Development for Electrochemistry and Condensed Matter, 144 Dr. A. P. Podeanu, 300569, Timişoara, Romania*
[2]*"Vasile Goldiş" Western University of Arad, Faculty of Pharmacy, Department of Pharmaceutical Sciences, 86 Liviu Rebreanu, 310045, Arad, Romania*
adina.cata@yahoo.com

Abstract

Anthocyanins represent the largest group of natural water-soluble pigments, including more than 635 different anthocyanins identified in plant tissues [1]. These pigments are well known for their coloring properties but also for their potential health benefits as dietary antioxidants.
The purpose of this study was the preliminary characterization of some anthocyanin extracts from different plant matrices in order to select the most suitable for future studies involving encapsulation in cyclodextrins. Native vegetable sources (fruits, vegetables, flowers) were chosen for the extraction of anthocyanins, namely: black mulberries, black currants, sweet cherries, sour cherries, red onions, red radishes, purple potatoes, wild poppy and red peony. Anthocyanins extraction was carried out with acidified alcohol in ultrasonic condition (59 kHz, 30 min., 25°C). The concentrated extracts were analyzed for anthocyanin content [2], total phenolics [3], and antioxidant capacity [4,5]. The highest anthocyanins content were obtained for the extracts of wild poppy petals (9.031±0.062 mg/g plant material), sweet cherries skins (3.959±0.204 mg/g plant material) and red onion skin (2.714±0.030 mg/g plant material).

Acknowledgements

This work is part of the project PN 19 22 03 01 / 2019-2022 "Supramolecular inclusion complexes of some natural and synthetic compounds with health applications", carried out under NUCLEU Program funded by National Authority for Scientific Research (Romania).

References

[1] J. He, M.M. Giusti, Annual Review of Food Science and Technology, 1, 2010, 163-187.
[2] M.M Giusti., R.E. Wrolstad, Unit F1.2. Anthocyanins. Characterization and Measurement of Anthocyanins by UV-Visible Spectroscopy, Current Protocols in Food Analytical Chemistry, John Wiley & Sons, Inc., 2001, pp. F1.2.1-F1.2.13.
[3] A.L. Waterhouse, Unit I1.1. Polyphenolics. Determination of Total Phenolics, Current Protocols in Food Analytical Chemistry, John Wiley & Sons, Inc., 2002, pp. I1.1.1-I1.1.8.
[4] W. Brand-Williams et al., LWT - Food Science and Technology, 28, 1995, 25-30.
[5] I.F.F. Benzie, J.J. Strain, Analytical Biochemistry, 239, 1996, 70-76.

AIR POLLUTION IN CITY PARKS DURING THE COVID-19 PANDEMIC

Aleksandra M. Cavic[1], Dragan Dj. Solesa[1], Snezana M. Aksentijevic[2], Jelena S. Kiurski[1]

[1]University Business Academy in Novi Sad, Faculty of Economy and Engineering Management in Novi Sad, 21000 Novi Sad, Cvecarska 2, Serbia
[2]Business Technical College, Trg Svetog Save 34, 31000 Uzice, Serbia
e-mail: aleksandra.cavic22@gmail.com

Abstract

The degree of coverage of the urban greenspace area and the factors which affect the concentration of particles in the air in those limited greenspace areas are rarely studied, especially during the Covid-19 pandemic. This paper is based on researching the effects and different impacts of the microclimate parameters on the concentration of particulate matter ($PM_{2.5}$ and PM_{10}) in the studied city parks and their multidisciplinary impact on the most important aspect – The Public Health. In Novi Sad, Serbia, three parks of different sizes and locations have been chosen, depending on the traffic frequency. The measurement results of particle pollution (PM) pointed out the variations of levels of concentration of the PM pollutants, $PM_{2.5}$ particles were in range from 2 to 10 μg/m^3 and PM_{10} were in range from 3 to 12 μg/m^3. Some of the measured values are exceptionally low so it can be concluded that the air was clean. The time of the measurements of the PM pollutants in the parks was in a period from 11a.m to 2 p.m., with temperature oscillation between 15^o-24.3^{o}C and air humidity from 41-50%.

Key words: Air Pollution, Particle Pollution ($PM_{2.5}$ and PM_{10}), City of Novi Sad, Covid-19, City Parks.

Introduction

Particle pollution in air is of course inhalable and as such very harmful for the health of the population, recently experts, legislative and regulatory bodies as well as the civilian sector with the wide public, are pointing out and paying attention to this.

Atmospheric particles (PM – particulate matter) are microscopic suspended particles (in solid or liquid state) in the Earth's Atmosphere. The origin of respirable particles can be natural or anthropogenic, and the composition may include both organic and inorganic particles, such as dust, pollen, soot, smoke and liquid droplets. Particles are differentiated by their size, content and their source. The smaller particles are more dangerous for the respiratory tract because they end up deep in the respiratory system and they cause serious problems with respiratory organs, which can have lethal outcome [1].

Particles that originate from nature are particles which originated from earth, Vulcan eruptions, dust from forests, salts and vegetation, particles which are formed by chemical reactions of various gasses (H_2S, NH_3, NO_X and HC), whereby the already existing particle is being changed in the air or a solid matter product is formed.

Particles of anthropogenic origin are formed in the combustion process, which produces soot from diesel fuel, exhaust gases from motor vehicles, waste gases from industrial facilities where processes take place at high temperatures, waste incineration, as well as from resuspended dust during photochemical reactions, all leading to real urban smog.

Human activity, such as the combustion of fossil fuels in motor vehicles [2], burning of wheat stubbles, power plants, wet cooling towers and other various industrial processes generate significant amounts of particles. Developing countries still use coal as their primary way to heat homes which currently forms about 10% of the total mass of aerosol in the atmosphere [3]. The

increase of environmental consciousness as well as the essential need of every man to have a clean and healthy air has brought us into question during this research, how's the air quality and does the declared epidemic of the virus Covid-19 in Novi Sad affect the air quality and in what way. Considering that the parks are places where people go to relax and to better their psychological and physical state and that the most common visitors of these parks are children and older people, as the most vulnerable groups, this research is completely justified. Especially with the disclosure that the virus Covid-19 is transmitted by droplets [4] and that the parks are ideal places for citizens to visit because of the preventive anti-epidemic measures that can be complied with the physical distance between people and that the public health can be bettered with clean and healthy air. Namely, parks represent the most attractive natural area of the urban ecosystem which gives the urban environment more quality of life and a more esthetically pleasing living environment. It also regulates the urban microclimate and encouraging sustainable urban development which directly affects the public health because the greenery positive influences on the psychological and physical status of man, and it also improves the disturbed city microclimate.

The objective of this research is to determine and compare the differences in pollution of air with the $PM_{2.5}$ and PM_{10} particles in three city parks, which were measured during normal life/work activities in the year 2019 with the values measured during the extraordinary circumstances, because of the Covid-19 epidemic, in the year 2020. The assumption that there would be less air pollution during the Covid-19 epidemic was confirmed, because of the changed and considerably reduced regime of life and work.

Experimental

To measure relevant data regarding the quality of air, relative to the particle pollution $PM_{2.5}$ and PM_{10}, the portable device Aeroqual series 500-monitor was used, which can measure and report changes of the levels of pollution in real time. A non-standard and indicative method was used based on laser and optical sensors. The optical sensor transforms the diffused light into electronic signals which are processed to ensure the measurement of mass – in this case $PM_{2.5}$ and PM_{10} [5]. The device uses a long lasting lithium battery. The display of the device shows the minimum, maximum and average values of the measured gas in ppm or mg/m^3 [6].

Localities: For this research of measured particle pollution $PM_{2.5}$ and PM_{10} three city parks were chosen from which two of them are categorized city parks: Futog Park (FP), Dunav Park (DP) which are classified in category III, they are treated as natural monuments and they are under state protection as a protected park area in an urban construction zone of Novi Sad, and the third Liman Park (LP) which to this day is not covered in categorization [7]. All three parks vary in size, they are located in different parts of the city and they are surrounded by different traffic frequencies and they occupy only 500000 m^2 of a total of 9786416 m^2 of the area of the entire city, which is percentage wise drastically below the world and EU standards. These parks are included with a goal to evaluate the quality of air, to detect possible pollution, to be assessed and compared with the measurements done in 2019, in order to suggest the measurements for further reduction of the pollution of the environment as well as influence an aggressive greening of other public spaces with the building of new city parks.

Results and discussion

Observing the common anthropological meaning of adults and children going to the park, which contributes to the development and maintenance of the physical and psychological health, maintaining vitality, quality of life, relaxing and having fun all of this represents the special pastime activity of adults and children. Those are sets of activities which directly affect the modern man, upgrading physical and psychological public health.

As parks are zones for vacation and recreation mostly outdoors, on them besides the inadequate equipment of urban furniture and greenery a big influence has the ambient air, which in Novi Sad is evidently contaminated in a way that directly or indirectly affects the health of children and adults. A large concentration of the industrial plants located in one place, obsolete technology, dense traffic as well as flouting of environmental laws affect the quality of the green space zones for relaxing and recreation for citizens. Parks in Novi Sad during the Covid-19 epidemic have showed themselves as extremely important like the only way for an easy and available stay in a natural environment, because departures to remote locations in most cases weren't possible due to the limited time windows for getting around. Emissions of the main polluting substances of air in Europe, in the last couple of decades, have went down which shows a positive shift in air quality. However, certain sectors deviate from this positive trend because there was a registered increase in levels of pollution because of fine suspended particles ($PM_{2.5}$), which occur when coal and biomass is burned (in domestic houses and commercial as well as institutional plants), as well as the coarse suspended particles (PM_{10}) which come from industry and transport and are emitted directly into air. Suspended particles represent the deadliest form of air pollution because they have the potential to penetrate deep into the lungs and bloodstream, thereby they can cause benign and malignant transformations in the respiratory system, mutation of DNA, heart attacks and premature death, which with the additional infection caused by the Covid-19 virus, can have an even more complicated and faster course of illness with a larger percentage of lethal outcome. Latest research in Serbia on impact of air pollution on people's health are usually linked to certain cities, such as for example the city Nis [8] and studies on wider areas in Serbia in this field were not carried out. By Regulation of the monitoring conditions and requirements for air quality [9], the limit value of the average daily concentrations of PM_{10} amounts to 50 $\mu g/m^3$ and average yearly to 40 $\mu g/m^3$. Within one year it is allowed for the daily concentration of PM_{10} to be 35 times larger than the limit value.

The measured concentration of particle air pollution in all three city parks in Novi Sad, for PM_{10} total in the range from minimum measured to maximum measured values from 9-12 $\mu g/m^3$, whereas the minimum and maximum values of $PM_{2.5}$ in the range from 2-10 $\mu g/m^3$. Which is considerably below the allowed limit values, and the measured temperature during the measurements was in an interval from 15°-22.8°C, measurements were done from 11 a.m. to 2 p.m. o'clock and the humidity was in the range from 46-50% which is to be expected because of the timing of the measurements with the upwind of medium strength. While the measured concentrations of particle pollution in year 2019 in all three parks in Novi Sad were the same in minimum and maximum values and were about 30 $\mu g/m^3$, which is below the limit daily value for both particle sizes [10].

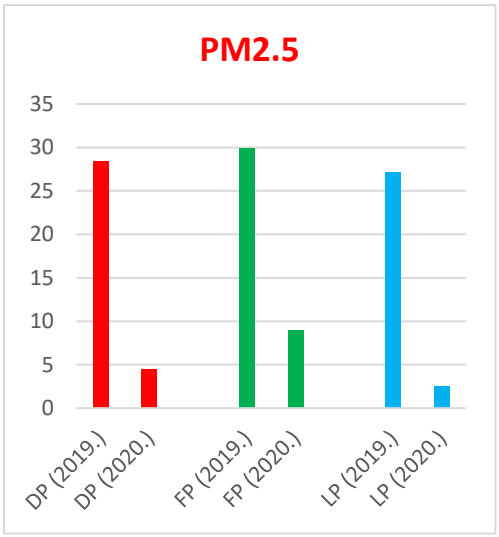

Figure 2 Graphic view of the $PM_{2.5}$ particles concentration in year 2019 and 2020

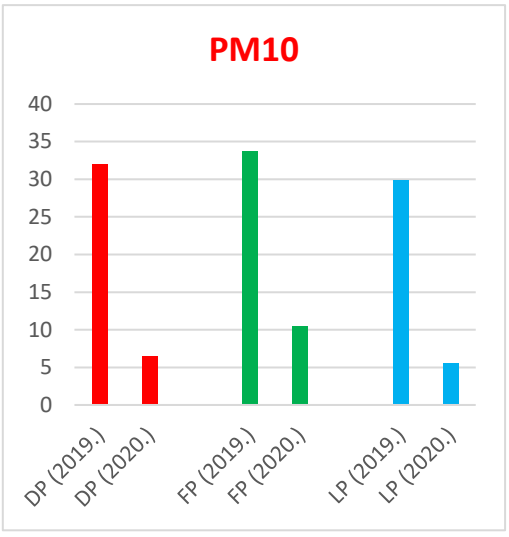

Figure 1 Graphic view of the PM_{10} particles concentration in year 2019 and 2020

Table 1 The reduction of particle pollution during two years of measurements in city parks of Novi Sad

Location	Reduction of $PM_{2.5}$ (%)	Reduction of PM_{10} (%)
Dunav Park	84.15	79.62
Futog Park	69.89	68.84
Liman Park	90.77	81.60

When we compare the average values that were measured in 2019 with the average values that were measured in year 2020, it is concluded that all of the measured values of particle pollution $PM_{2.5}$ and PM_{10} in year 2020 are drastically lower. From Table 1 we can see: Dunav Park $PM_{2.5}$ 84.15% reduction whereas for PM_{10} particles 79.62% reduction, Futog Park seen a smaller reduction with the $PM_{2.5}$ particles seeing a 69.89% reduction whereas for PM_{10} particles 68.84% reduction and Liman Park with the biggest reduction for $PM_{2.5}$ particles for 90.77% whereas PM_{10} particles have seen an 81.60% reduction, Figure 1 and Figure 2.

This comparative data has a large discrepancy if we compare 2019 and 2020 and they show on a noticeable reduction of particle air pollutants in year 2020, which is the consequence of the extraordinary pandemic-epidemic situation which struck the entire World as well as the local. Restrictions in movement and having people stay at home most of the time reduced the dynamic of traffic, people worked less, traveled less and only the most important life activities were done. All of that had an impact on the particle pollution. Of course, temperature, humidity and wind also favor in the reduction of the particle pollution but of course, not to such an extent.

Conclusion

Control of air quality in the city parks of Novi Sad during the Covid-19 pandemic, gives results which are unexpectedly low referent values which are the result of the extraordinary situation caused by the pandemic/epidemic of Covid-19 on the territory of Serbia and the territory of the local government of the city of Novi Sad. With insight in the official data on the status of the economy and employment which is actually in an increase during Covid-19 in the local government of Novi Sad, the low values of particle pollution that were measured in the three green spaces wasn't expected but the measured values direct that the contamination of air was lowered significantly from the products of combustion in motor vehicles in traffic and industry.

This relevant fact of good quality air that was measured in parks during the Covid-19 epidemic could be an incentive for expanding air quality monitoring (stationary or portable) also when life activities get back on their regular state, in order to ensure good and healthy air as an essential requirement for a healthy and safe life of citizens and a bettering of the Public Health as well as a healthy environment for the upcoming generations. It can be concluded that the air is clean and that it is recommended to spend daily more time in green space areas in city parks.

Acknowledgements: The authors acknowledge the financial support of the Provincial Secretariat for Higher Education and Scientific Research, Autonomous Province of Vojvodina, Republic of Serbia, within the Project No. 142-451-3156/2020-03.

References

[1] WHO, Fifty-Third World Health Assembly, 2000, A53/4, 1-10
[2] Omidvarborna H., Kumar A., Kim D-S., Renewable and Sustainable Energy Reviews, 2015, 48: 635–647
[3] NASA (2010) Aerosols: Tiny Particles, Big Impact https://earthobservatory.nasa.gov/Features/Aerosols
[4] WHO, Air quality guidelines for particulate matter, ozone, nitrogen dioxide and sulfur dioxide Summary of risk assessment, 2005, WHO/SDE/PHE/OEH/06.02
[5] Aeroqual (2010) Aeroqual Product catalogue
http://www.aeroqual.com/wp-content/uploads/2010/12/AQL-Product-Catalogue.pdf.
[6] Kiurski J., Solesa D., Ignjatijevic S, Vapa-Tankosic J., Characteristic aero pollutants of the city Novi Sad (in Serbian), Monography, 2019, University Business academy in Novi Sad, Faculty of Economics and Engineering Management in Novi Sad
[7] Monuments of nature (in Serbian), 2018, http://www.pzzp.rs/rs/sr/zastita-prirode/zasticena-podrucja/spomenici-prirode-sp.htm
[8[Nikic D., Bogdanovic D., Nikolic M., Stankovic A., Zivkovic N., Djordjevic A., Environ. Mon. Assess., 2009, 158: 499-506
[9] "Official Gazette RS", No. 11/10, 75/10, 63/13, (in Serbian)
[10] Kiurski S.J., Ralevic M.N., Ignjatijevic D.S., Vapa-Tankosic M.J., Solesa Dj.D., Air Qual Atmos Health, 2019. 12, 955–962, https://doi.org/10.1007/s11869-019-00712-w

MAPPING OF RAINWATER HARVESTING POTENTIAL, A CASE STUDY OF SZEGED, HUNGARY

Ákos Kristóf Csete[1], Ágnes Gulyás[1]

[1]*Department of Climatology and Landscape Ecology, Urban Climate Research Group, University of Szeged, H-6722 Szeged, Egyetem utca 2-6, Hungary*
e-mail: cseteakos@geo.u-szeged.hu

Abstract

In urban environment, rainwater harvesting is a good solution to make the water management sustainable. The rainwater harvesting potential of a whole city gives information to the urban planners about the building possibilities of real collecting systems. In our work, with the help of hydrological modeling we create urban micro-watersheds, which based on the roof of buildings. Our expected results can give a comprehensive picture of rainwater harvesting possibilities in urban areas.

Introduction

In the 21st century one of the most urgent problem is the climate change and its impacts on the whole environmental system. The problem with the effect caused by climate change is the uncertainty. The weather extremes will occur more and more often, and the preparation for their impacts is one of the biggest challenges of the environmental planning. In the urban systems – where the impacts affect many citizens – the changes will also cause serious problems. The artificial pavements and the sewer system alter the hydrological system in urban areas. In addition to these changes in urban areas there are less green surfaces and vegetation cover. Based on these, the hydrological system changed in the cities and the urban planning system needs to be prepared different problems, than natural areas [3]. The first main problem is the occasional too much available water. Heavy rainfalls can cause flooding in cities owing to the impervious pavement, the undersized sewer system and sometimes the obsolete drainage method. The other side of the problems is too less available water in cities [1]. During the long drought period – which is climatic characteristic of the southern part of the Great Hungarian Plain – in the cities the urban vegetation needs irrigation and usually the source of this is potable water, which is not a sustainable solution in long term. Rainwater harvesting can help to reduce the volume of drinking water usage [4].

Study area, methods

The aim of our research is to examine the processes on urban micro-watershed (roofs). The information about these processes (runoff and evaporation on roofs) contribute to create a rainwater harvesting potential map based on a building database. The rainwater harvesting potential map can provide information about the volume of the potentially collectable rainwater. In this study we use the EPA SWMM model, which is one of the widespread storm water management model [2]. The base of the modeling is a building data base, which contains approxametly 15 000 building polygons (Figure 1.). Each polygon represents an urban micro-watershed. Owing to the database it is possible to separate the slope/pitched roof and flat roofs which also allowed us to determine which roofs have the potential to be used as a green roofs to further facilitate efficient rainwater harvesting. Among the geoinformatics database, the model need some meteorological data like daily temperature, windspeed and hourly precipitation.

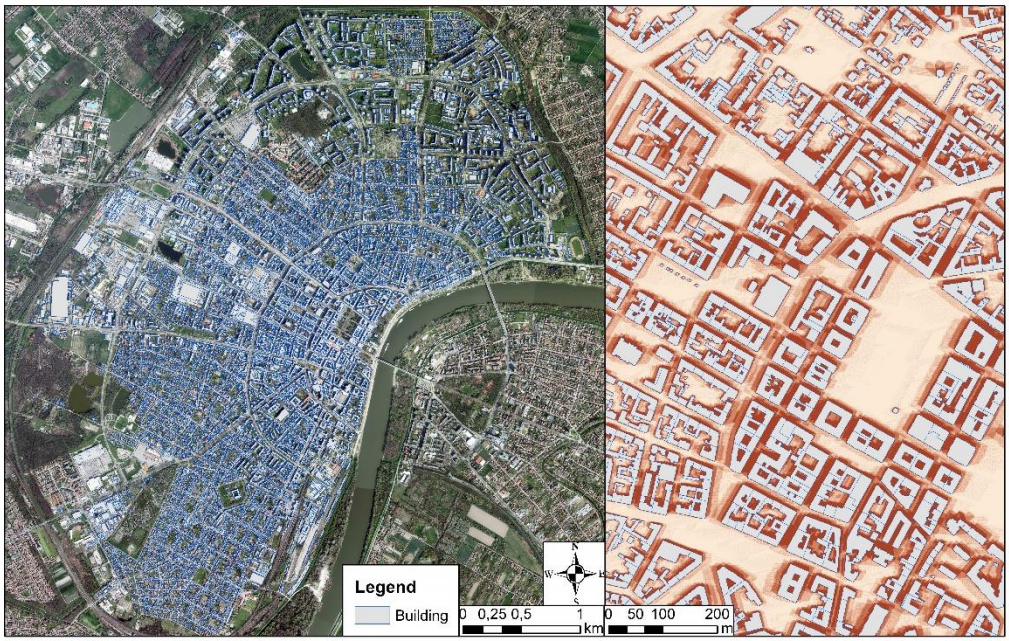

Figure 1. Spatial extent of the building database

Expected results, conclusions

With the help of the modeling processes we can examine both city- and district scale result about the rainwater harvesting possibilities within Szeged. We can also delineate which roofs suitable for to build real rainwater harvesting systems. Based on the whole year meteorological data the result can give information about the seasonal distribution of the collected rainwater and which volume of these water can be used in drought periods. Our results could contribute to the local decision-making processes and give usable data for urban planners to make into greater account the potential of rainwater storage.

Acknowledgements

Supported by the ÚNKP-20-3 - New National Excellence Program of the Ministry for Innovation and Technology from the source of the National Research, Development and Innovation Fund.

References

[1] Fletcher, T.D., Andrieu, H. & Hamel P. 2013 Understanding, management and modelling of urban hydrology and its consequences for receiving waters: A state of the art. Advances in Water Resources, 51, 261-279.

[2]Jayasooriya, V. M., & Ng, A. W. M. (2014). Tools for Modeling of Stormwater Management and Economics of Green Infrastructure Practices: a Review. Water, Air, & Soil Pollution, 225(8), 2055.

[3] Prudencio, L. & Null, S.E 2018 Stormwater management and ecosystem services: a review. Environmental Research Letters, 13, 033002.

[4] Ward, S., Memon F. A., and Butler D. (2010). Rainwater harvesting: model-based design evaluation. Water Science and Technology, 61(1), 85 LP-96.

OPTIMIZED HUMIC PRODUCTS FROM NATURAL SOURCES

A. Csicsor[a], E. Tombácz[b]

[a]Hymato Products Ltd., H-8225 Szentkirályszabadja, Kossuth u 33., Hungary
[b]University of Pannonia, Soós Ernő Water Technology Research and Development Center, H-8800 Zrínyi M. str. 18. Nagykanizsa, Hungary
e-mail: csicsor.attila@gmail.com

Abstract

Humic substances are the biological-chemical-geological decomposition products of the living plant origin matter on the Earth. The biggest part of the terrestrial organic matter (non-living biomass) are humic substances. Humus is the most relevant decomposition product of living matter, so it is the most important media for the reproduction of the continental biomass. Our latest researches shows that these materials can be great antioxidants.[1]

The formation of humic acids in humification processes needs geological times, that is minimum thousands of years. There are many sources of humic substances in nature, like soil, water, organic manure, compost, sapropels, peat, lignite, brown coal, Leonardite.

Our company is engaged in research and production of natural humic substances-based pioneer products. Careful extraction and purification, as well as quality control, are also important in order to produce humic and fulvic acid based products for healthy life. We are producing several humic and fulvic acid based products, as active ingredients for medicines, food supplements and cosmetics.

For our products, we use only contamination free Leonardite deposits in Hungary. The so called standard extraction method of humic substances is based on their alkaline solubility. We extract with sodium hydroxide (NaOH). After the first extraction, the Na-humate solutions may contain some contaminants and sediment that should be removed. The main thing we must first consider is the strict food regulations including heavy metal contaminations and microbiology. Second, we must work according to the GMP (Good Manufacturing Practice) regulations, which is strict in the identification of the active ingredients. [2]

Important question is the analytics and identification of the humic acid fractions. There are no international standards for the analysis of the humic fractions. Our company developed a complex humic-fulvic acid identification and standardization method for the humic substance content of the raw materials and the end products. In our poster, the main extraction process and analytical methods will be shown. [3]

Some application examples of the humic substances are: Huminiqum food supplement containing micronutrients and organic humate and fulvate, Éden chocolate supplemented food, and H.Y. Spray alcoholic hymatomelanic acid extract for skin regeneration.

References

[1] Eladia M. Peña-Méndez, at. al.: Humic substances, compounds of still unknown structure: applications in agriculture, industry, environment, and biomedicine; J. Appl. Biomed. 3: 13.24.

[2] Nelson N. Schwartz at al.: Production of humic acid, United States Patent 3,398,186, Filed Dec. 23, 1963, Ser. No. 332,841 9
[3] Bleam W. (2017). Soil and Environmental Chemistry. Academic Press, Amsterdam.

IMPACT OF THE LAND COVER CHANGE ON THE ABUNDANCE OF FARMLAND BIRDS

Nándor Csikós[1]

[1]*Department of Physical Geography and Geoinformatics, University of Szeged, H-6722 Szeged, Egyetem utca 2, Hungary*
e-mail: csikos@geo.u-szeged.hu

Abstract
The European landscape has been changed in the last decades and this process has different characteristics with different drivers in West and Central East Europe. In this study I analysed the land cover and land use change in two study areas (Hungary, Schleswig-Holstein) and its impact on the abundance data of a representative bird species of European agrarian landscapes, the Eurasian skylark. Generalized Linear Models were used to estimate the land cover effects in R Statistics software. ArcGis 10.3 were used for the spatial data analysis. Arable lands and pastures are habitat areas, while the forests, built up areas and water surfaces are the non-preferred areas of the skylark. According to our findings, the different changes of preferred and non-preferred land cover categories have strong effect on the population of the skylark in country and European scale.

Introduction
The land use and land cover (LULC) of the European landscape have been changed dramatically in the last decades. There are different drivers of the change in West- and Central East Europe, which have effect on the farmland bird fauna [1] abundance. In West Europe (in this case Germany) the main driver was the support of the renewable energies, because the members of the European Union have set up its own climate protection objectives [2,3]. The biogas energy production has the highest impact on the LULC change, because the feeding of the biogas power plants requires lots of material, such as manure and energy crops. In the beginning of the 2000s, Germany has been introduced the new energy law, which support the transformation of the agricultural landscapes into energy landscapes. These changes reshaped the land use, landscape structure, landscape pattern which had strong impact on biodiversity[4–8].
In the Central and East European (CEE) countries, the common agricultural policy of the EU and the land privatisation in the 1990s caused dramatic landscape changes[1,9,10]. In Hungary and other CEE (post- socialist) countries have lands with low soil quality and poor agro-ecological conditions have been abandoned. The land abandonment leads to the arable lands transformations into non cultivated lands, and spontaneous and fast reforestation of grasslands[1,11].
Most of the researches are focusing on parcel scale studies and analysing the land use / crop structure and the abundance of the agricultural fauna. The abundance data of the Eurasian skylark were used to analyse the impact of the LULC change on the agrarian fauna, because this species is one of the most characteristic farmland birds of the European agricultural landscapes. To announce the relationship between the abundance decline of this bird species and regional land cover change in Europe, it is important to identify the skylark preferred and non-preferred land cover types.
In this study I used the EU Corine Land Cover databases as land cover dataset. The Eurasian skylark's abundance data of the Hungarian Common Bird Monitoring database and the ornithological working group of Schleswig-Holstein and Hamburg have been accounted. The following are the objectives of this study: (1) analyse the relationship between the Eurasian

skylark abundance and the LULC categories based on my previous researches, (2) compare the proportion of LULC categories in the study areas and (3) to analyse the LULC categories and LULC change effect on the abundance of the skylark.

Materials and Methods

The basis of my research is the two study areas: At first Hungary, which is located in the Carpathian Basin in Central Europe. The elevation ranges from 77 m to 1014 m. The most common land cover type is agricultural area (61%). The second study area is Schleswig-Holstein Federal state of Germany. This region is surrounded by the Baltic Sea, Denmark and the North Sea. The climate is humid with an average annal temperature of 8.6 °C and mean annual precipitation 878 mm. The main land cover type is also agricultural land (41.5%).

Medium-scale land cover data for the two study areas were extracted from the Corine Land Cover database. It has a scale of 1:100000 and 44 classes of land cover, which 37 are relevant in Germany and 28 in Hungary[12].

The relationship analysis between the Eurasian skylark abundance data and the LULC categories was conducted based on ornithological datasets. In Hungary the Hungarian Common Bird Monitoring Database contains the abundance data and the details of the survey is in the work of Szép & Nagy (2001)[13]. In Schleswig-Holstein, the skylark data were collected by the Ornithological Working Group of Schleswig-Holstein and Hamburg. More details about the survey can be found in the work of Südbeck et. al 2005[14,15].

The impact of the LULC categories on the abundance of skylark were carried out by Generalized Linear Models in R statistics. The details of the model can be found in my previous article Csikós & Szilassi (2020)[16]. I calculated the preferred and non-preferred land cover types' proportion in both study areas and compared them[16,17]. Finally, based on the CLC datasets I analysed the changes of the land cover types. The spatial analyses of the datasets were executed in ArcGis 10.3 software.

Results and discussion

Table 1 shows the results of the Generalized Linear Model, which describe the preferred and non-preferred land cover types of the skylark in both study area. The preferred land cover types are usually covered by low height and low ground cover density plants, which areas suitable for skylark. The non-preferred land cover categories are not suitable areas for skylark, because of the height and density of the plants and the composition of the land use types inside the category[11]. Regarding to the different preferred and non-preferred land cover categories, landscape changes and landscape structure, forced by different environmental, cultural and political drivers, have strong effect on the population of the skylark[1].

Table 1. Results of the Generalized Linear Models based on the study areas, which shows the preferred and non-preferred land cover types of the Eurasian skylark

Hungary		Schleswig-Holstein	
Non-preferred	**Preferred**	**Non-preferred**	**Preferred**
Construction sites	Non-irrigated arable land	Discontinuous urban fabric	Non-irrigated arable land
Green urban areas	Natural grassland	Mixed forest	Pastures
Fruit trees and berry plantations		Water bodies	Natural grassland
Complex cultivation patterns			Inland marshes
Broad-leaved forest			
Coniferous forest			
Inland marshes			

Based on the Table 1. results I calculated and visualised the proportion of the land cover types in both study area, the Figure 1. and explaining most of them. For example, the case of the pastures, in Schleswig-Holstein there are lot of pasture area (proportion and number of patches), because of the dairy production. Discontinuous urban fabric land cover category has higher proportion in Schleswig-Holstein. Complex cultivation patters also unusual land cover category in Schleswig-Holstein, but in Hungary it has a high number of patch, while there is a mixed structure of agriculture, where traditional and intensive farming stand side by side [9]. Because of the different climate conditions, Fruit trees and berry plantations category is rare in Schleswig-Holstein as the Mixed Forest category in Hungary because of the different climatic conditions of the study areas. Figure 2. visualize the spatial characteristics of the preferred and non-preferred land cover types in Hungary and Schleswig-Holstein.

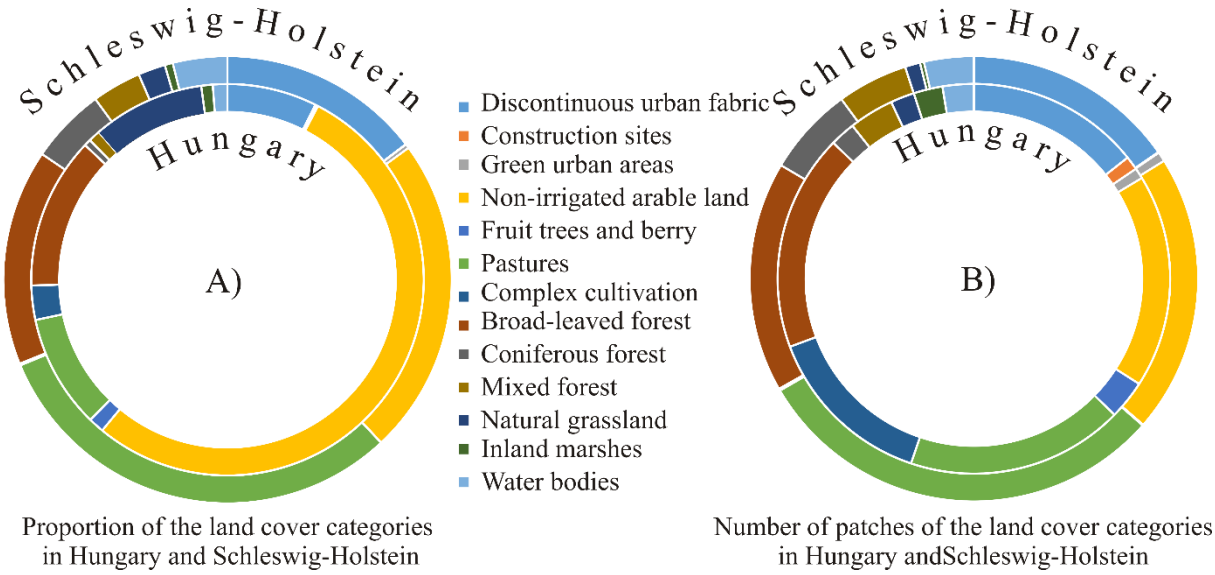

Figure 1. Proportion (A) and number of patches (B) of the land cover categories in Hungary and Schleswig-Holstein

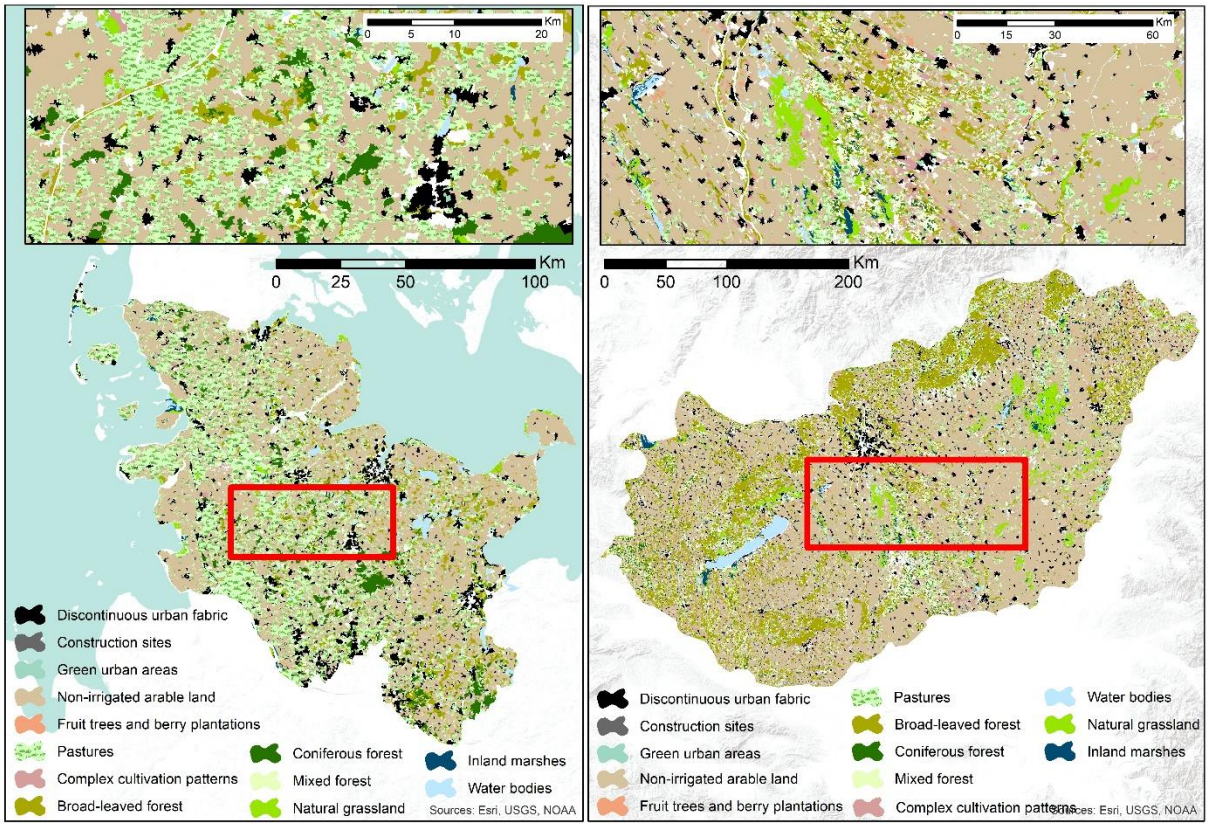

Figure 2. The spatial characteristics of the main land cover categories of Hungary and Schleswig-Holstein

Conclusion

In the last decades, the landscape change in Europe, which has an effect on the population of the agricultural fauna. The Eurasian skylark is an indicator species, so the changes in its population can predict the population changes of other farmland birds. Generalized Linear Models presents different land cover categories as preferred and non-preferred land covers. Landscape changes and landscape structure, influenced by different environmental, cultural and political drivers, have strong effect on the population of the skylark. In a European wide habitat modelling, we have to take under consideration that the certain regions have different environmental and cultural drivers in case of landscape change, which have specific effect on the population of the skylark.

Acknowledgements

This research was funded by the "UNKP-20-3-SZTE-515 NEW NATIONAL EXCELLENCE PROGRAM OF THE MINISTRY FOR INNOVATION AND TECHNOLOGY"

References

1. Tryjanowski, P.; Hartel, T.; Bldi, A.; Szymański, P.; Tobolka, M.; Herzon, I.; Goławski, A.; Konvička, M.; Hromada, M.; Jerzak, L.; et al. Conservation of farmland birds faces different challenges in Western and Central-Eastern Europe. *Acta Ornithol.* **2011**, *46*, 1–12.
2. EU Directive 2009/28/EC of the European parliament and of the council of 23 April 2009 on the promotion of the use of energy from renewable sources and amending and subsequently repealing Directives 2001/77/EC and 2003/30/EC. *Off. J. Eur. Union* **2009**, *52*.

3. EC (European Commission) Optimal use of biogas from waste streams. An assessment of the potential of biogas from digestion in the EU beyond 2020 - European Commission Available online: https://ec.europa.eu/energy/en/studies/optimal-use-biogas-waste-streams-assessment-potential-biogas-digestion-eu-beyond-2020 (accessed on May 9, 2018).
4. Scheftelowitz, M.; Becker, R.; Thrän, D. Improved power provision from biomass: A retrospective on the impacts of German energy policy. *Biomass and Bioenergy* **2018**, *111*, 1–12.
5. Lüker-Jans, N.; Simmering, D.; Otte, A. The impact of biogas plants on regional dynamics of permanent grassland and maize area—The example of Hesse, Germany (2005–2010). *Agric. Ecosyst. Environ.* **2017**, *241*, 24–38.
6. Laggner, B.; Orthen, N.; Osterburg, B.; Röder, N. Ist die zunehmende Biogasproduktion die alleinige Ursache für den Grünlandschwund in Deutschland? – eine Analyse von georeferenzierten Daten zur Landnutzung. *Raumforsch. Raumordn.* **2014**, *72*, 195–209.
7. Schleupner, C.; Link, P.M. Potential impacts on important bird habitats in Eiderstedt (Schleswig-Holstein) caused by agricultural land use changes. *Appl. Geogr.* **2008**, *28*, 237–247.
8. Brandt, K.; Glemnitz, M. Assessing the regional impacts of increased energy maize cultivation on farmland birds. *Environ. Monit. Assess.* **2014**, *186*, 679–697.
9. Báldi, A.; Faragó, S. Long-term changes of farmland game populations in a post-socialist country (Hungary). *Agric. Ecosyst. Environ.* **2007**, *118*, 307–311.
10. Szép, T.; Nagy, K.; Nagy, Z.; Halmos, G. Population trends of common breeding and wintering birds in hungary, decline of long-distance migrant and farmland birds during 1999–2012. *Ornis Hungarica* **2012**, *20*, 13–63.
11. Gil-Tena, A.; De Cáceres, M.; Ernoult, A.; Butet, A.; Brotons, L.; Burel, F. Agricultural landscape composition as a driver of farmland bird diversity in Brittany (NW France). *Agric. Ecosyst. Environ.* **2015**, *205*, 79–89.
12. EEA and ETC-TE CLC Update CLC 2000 Project. Technical Guidelines. Final Version Available online: http://land.copernicus.eu/user-corner/technical-library/techrep89.pdf (accessed on May 9, 2018).
13. Szép, T.; Nagy, K. The GIS UTM Quadrants based Hungarian Bird Monitoring database of the BirdLife Hungary. *Természetvédelmi Közlemények* **2001**, *9*, 31–37.
14. Südbeck, P.; Andretzke, H.; Fischer, S.; Gedeon, K.; Schikore, T.; Schröder, K.; Sudfeldt, C. *Methodenstandards zur erfassung der Brutvögel Deutschlands*; 2005; ISBN 300015261X.
15. Brendt, R.K.; Koop, B.; Struwe-Juhl, B. *Vogelwelt Schleswig-Holsteins*; 2nd ed.; Wachholz Verlag: Neumünster, 2005;
16. Csikós, N.; Szilassi, P. Impact of Energy Landscapes on the Abundance of Eurasian Skylark (Alauda arvensis), an Example from North Germany. *Sustainability* **2020**, *12*, 664.
17. Szilassi, P.; Csikos, N.; Galle, R.; Szep, T. Recent and Predicted Changes in Habitat of the Eurasian Skylark Alauda arvensis Based on the Link between the Land Cover and the Field Survey Based Abundance Data. *Acta Ornithol.* **2019**, *54*, 59.

CSR MOTIVES OF COMPANIES: OPINIONS OF BUSINESS AND STATE SCIENCE STUDENTS

Zsófia Csonka[1], László Berényi[1]

[2]Institute of E-Government, National University of Public Service, H-1083 Budapest, Üllői út 82., Hungary
e-mail: szvblaci@uni-miskolc.hu

Abstract
Corporate social responsibility (CSR) covers both ethical and business considerations in initiatives. There are several concepts and opinions outlined the role of CR in recent decades. A better understanding of opinion patterns can contribute to developing more inclusive strategies in the field. This study compares the opinions of business and state science students about the company's motives for dealing with CSR. The results do not show significant differences by any grouping factors of the research. Nevertheless, cluster analysis explored three different patterns. One of these considers CSR primarily as the tools for solving environmental or social problems; others have a business-oriented approach.

Introduction
There is an enhancing interest in solving environmental and social problems over the past several decades. Corporate Social Responsibility (CSR) and similar concepts cover the contribution of companies to the topic; it became a critical strategic issue. Although the central concept is comprehensive, the diversity of definitions, tools, initiations, and institutes may lead to confusing situations. The coordination efforts of the EU institutions [1-2] are to welcome, but implementation calls for special attention.
Graafland [3] highlights that it is often assumed that the primary and decisive motive of CSR is an extrinsic motive of economic, financial, or strategic self-interest. However, he found that ethical or altruistic reasons become even more decisive. The ethical approach means that a company issues a CSR policy because it perceives CSR as a moral duty [3].
Since companies are for business, the business interest has an essential importance in compliance with stakeholders. This means that CSR cannot be sustainable without favorable business effects. Due to the diversity of company characteristics as well as market profiles, different focuses of CSR can lead to success. A task of education is to give a comprehensive overview of the opportunities and the conditions.
Assuming the comprehensive nature of sustainability and the different approaches in developing even a definition [4], somewhat different opinions may be found between the representatives of different professionals. Understanding these patterns can help to implement both targeted development strategies and general frameworks.

Experimental
A voluntary online survey is designed for higher education students to explore their attitudes and opinions related to corporate social responsibility. Data collection is supported by the EvaSys survey management system in 2020; data analysis is performed with IBM SPSS 24. The paper highlights the students' opinions about the CSR motivations of companies. The respondents are asked to rank six items:

- Attracting and convincing customers;
- Profit-making;
- Because other companies are also doing such a thing;
- Greenwashing and hiding the environmental and social problems;

- Solving ecological and social problems;
- Cost reduction.

The research sample consists of 56 business and 57 state science students who has a clear preference order about the motivations. Table 1 summarizes the sample characteristics.

Table 1. Sample characteristics

		Business	State Science
Sample size (persons)		56	57
gender (%)	female	83.9%	50.1%
	male	16.1%	49.9%
CSR knowledge level (%)	did not study	76.8%	63.2%
	superficial knowledge	17.9%	15.8%
	detailed knowledge	5.3%	21.0%
Average age (years)		22.37	22.30

The goal of the study is to explore the students' opinions in the field and to compare the results between the different studies. The hypothesis of the research can be formulated as business and state science students have different opinions about the companies CSR motivations.
Non-parametric correlation analysis, ANOVA test, and cluster analysis are conducted for checking the hypothesis. Rank order, the mean value of rank sums, and distribution of the rankings represent the average evaluations.
Data collection do not cover the entire population, the sampling is convenient, and the representativeness is not assured. Therefore, the presentation of the results is limited; it can be considered as preliminary research.

Results and discussion

The students consider profit-making and attracting customers as the most important reason for the CSR activities of companies based on the rank orders. State science students ranked attracting and convincing customers the first while business students mostly preferred profit-making. Copying others and greenwashing is at the end of the list in both subsamples (Table 2). Solving environmental and social problems, as well as cost reduction, are in the midfield.

Table 2. Ranking by study type (rank order and mean value of rankings, lower value means more important ranking)

	business		**state science**	
	rank	mean	rank	mean
Profit-making	1.	2.55	2.	2.6
Attracting and convincing customers	2.	2.57	1.	2.42
Solving ecological and social problems	3.	3.46	3.	3.42
Cost reduction	4.	3.84	4.	3.96
Greenwashing and hiding the environmental and social problems	5.	4.27	6.	4.37
Because other companies are also doing such a thing	6.	4.3	5.	4.23

According to the distribution of the rankings (Figure 1), profit orientation has the first-place rankings. However, 25.7% of the respondents rated is as the least important item. Attracting customers is ranked the most important by 23.2% of the business students and the second one by 32.1%, while the ratios are 29.8% and 26.3% among state science students. Although some

differences appear in the opinions by faculty, these are not statistically significant (Table 3). No other grouping factors show significant differences.

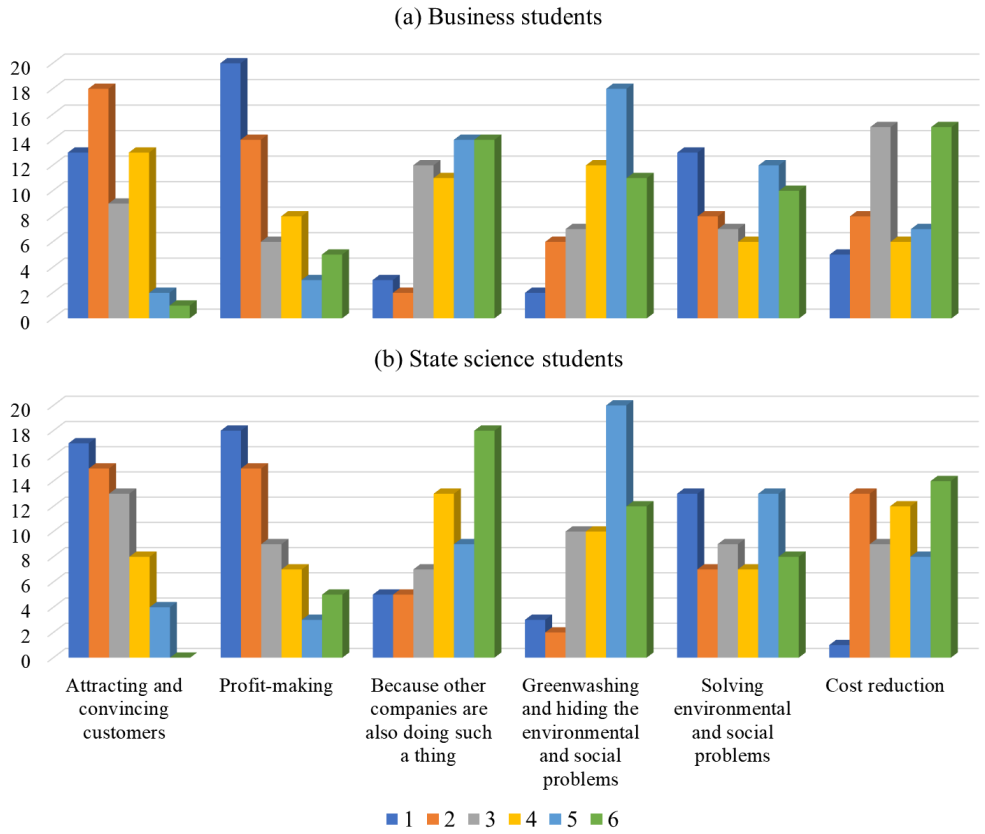

Figure 1. Distribution of the rankings of business (a) and state science (b) students (total sample, 1: the most important, 6: the least important)

Table 3. ANOVA test by studies (Kruskal-Wallis test)

	Kruskal-Wallis H	**d_f**	**Asymp. Sig.**
Attracting and convincing customers	0.393	1	0.531
Profit-making	0.074	1	0.785
Because other companies are also doing such a thing	0.000	1	0.991
Greenwashing and hiding the environmental and social problems	0.162	1	0.687
Solving ecological and social problems	0.025	1	0.875
Cost reduction	0.119	1	0.730

Cluster analysis is conducted to explore patterns of opinions. Three clusters are worth to create (Figure 2). The Kruskal-Wallis test shows significant differences in the views except for the item of greenwashing (Table 4). Cross-tabulation does not show clear patterns by gender, study type, or CSR knowledge level. Since the affiliations by the used grouping factors do not give clear patterns, targeted strategies are not applicable based on this research. However, it is worth to check the patterns of opinions as a basis for further studies.

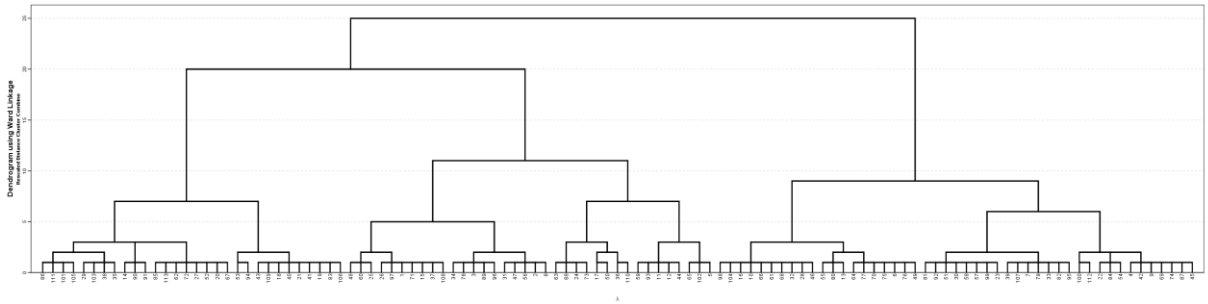

Figure 2. Hierarchical clustering (Ward method)

Table 4. ANOVA test by clusters (Kruskal-Wallis)

	Kruskal-Wallis H	d_f	Asymp. Sig.
Attracting and convincing customers	15.424	2	0.000
Profit-making	45.781	2	0.000
Because other companies are also doing such a thing	31.785	2	0.000
Greenwashing and hiding the environmental and social problems	3.066	2	0.216
Solving environmental and social problems	50.976	2	0.000
Cost reduction	54.589	2	0.000

The patterns of opinions by the cluster analysis are as follows:
Cluster 1: Solving environmental and social problems are considered the most important motives for CSR, followed by cost reduction opportunities. Profit-making is ranked at the end of the list.
Cluster 2: Profit-making and customer-orientation are the most important motives of CSR. The cluster members do not believe that solving environmental and social problems is an important motive of CSR. The opportunities for cost reduction are ranked in the midfield.
Cluster 3: Profit-making is followed by attracting customers as CSR motives. Copying other companies has the most important rank compared to the other clusters. Cost reduction is considered the least important.

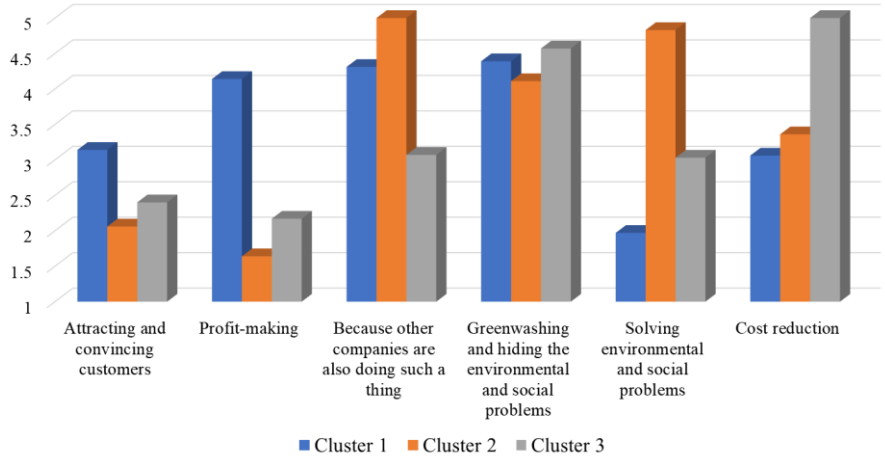

Figure 3. Results by clusters (mean value of the ranks, lower value means more important)

Conclusion

The hypothesis of the research must be rejected. There are no statistically significant differences in the opinions between business and state science students. Nonetheless, the study offers some conclusions. According to the comprehensive goals of sustainability [5], learning about the related issues goes beyond the boundaries of some given faculties. Since each profession may contribute to achieving the goals with different tools, the focus of the critical problems may be nuanced. However, the CSR knowledge level of the sample is poor (Table 1). Boosting CSR education seems to be essential regardless of the lack of its significant grouping nature in this research. The results in attracting and convincing customers (Figure 1) are expected to be more important by business students.

According to Graafland [3] ethical nature issues appear in the personal value systems, but economic interest has a more substantial effect. The cluster analysis explored three patterns of opinions. There are students who believe that CSR is primarily for solving problems and reducing costs. They represent an operational approach to CSR. Another group of students considers CSR as an external tool for enhancing profit through customer-orientation. Solving environmental and social problems are not ranked important among members. A third group represents similar values with higher importance to problems solving. Finding the personal characteristics and relevant grouping factors is the most critical task of continuing the research.

References

[1] European Commission, Reflection Paper Towards a Sustainable Europe by 2030 (2019) COM(2019)22 of 30 January 2019.

[2] D. Kinderman, Global and EU-Level Corporate Social Responsibility: Dynamism, Growth, and Conflict, in: H. Backhaus-Maul, M. Kuncze, S. Nährlich (Eds.), Gesellschaftliche Verantwortung von Unternehmen in Deutschland: Ein Kompendium zur Erschließung eines sich entwickelnden Themenfeldes, Springer, Wiesbaden, 2018, pp. 101-113.

[3] J. Graafland, Motives of CSR, in: S.O. Idowu, N. Capaldi, L. Zu, A.D. Gupta (Eds.), Encyclopedia of Corporate Social Responsibility, Springer, Berlin, 2013, pp. 1722-1728.

[4] J.E. Moore, A. Mascarenhas, J. Bain, S.E Straus, Developing a comprehensive definition of sustainability, Implementation Science. 12 (2017) 110.

[5] UN, Transforming our World: The 2030 Agenda for Sustainable Development (2015) A/RES/70/1.

ARTICHOKE EXTRACT AS CORROSION INHIBITOR FOR CARBON STEEL IN ACID MEDIA

Mircea Laurentiu Dan*, Alin Faur*, Cristian George Vaszilcsin**

**University Politehnica Timişoara, Faculty of Industrial Chemistry and Environmental Engineering, 300223, Parvan 6, Timisoara, Romania*
***INCEMC Timişoara, Dr. A. Paunescu Podeanu 144, 300569,Timisoara, Romania*
e-mail: cristi_vasz@yahoo.com

Abstract

The aim of this investigation is to examine the inhibitory effect of artichoke extract toward the corrosion of carbon steel corrosion in 0.5 M sulfuric acid solution. Potentiodynamic polarization and crhonoamperometry techniques were used in this work to evaluate the inhibition efficiency of the proposed inhibitor in acid solution. Also, Tafel method for the kinetic parameters determination.

Introduction

The use of different types of inhibitors for the control of metals and alloys corrosion process in aggressive environment is the most common method in practice. Many organic compounds were studied to investigate their corrosion inhibition potential. Many organic compounds have been studied to investigate their possibility of use as corrosion inhibitors. Among the organic compounds studied, those that have N, S and O atoms in their structure, have a high efficiency in the inhibiting of corrosion process. The major disadvantages of these compounds are represented by the high price and increased toxicity for living beings. Experimental studies are currently focusing on finding cheap and safe corrosion inhibitors. Currently, several types of plant extracts have become a possible ecological source, readily available and renewable for a wide range of inhibitors. These extracts are rich sources of ingredients - organic compounds - that have a high inhibitory efficiency. In the future, plant extracts are expected to have the real potential to replace, at least partially, synthetic organic and inorganic inhibitors. The mechanism of action of these types of inhibitors, often referred to as green inhibitors, depends on the structure of the active ingredient.

Carbon steel is currently the most common steel used in the industry, as its price is relatively low, while providing acceptable material properties for many applications. However, the permanent challenge is that of low corrosion resistance of this steel, especially in acidic environments. Industrial processes such as acid cleaning, pickling and descaling in the oil and natural gas exploration industries use acid solutions on a large scale and metallic surfaces used in these environments, made of carbon steel are frequently prone to corrosive attack.

References

[1] P. B. Raja, M. G. Sethuraman, Materials Letters, 62 (2008) 113.

[2] P. Mourya, S. Banerjee, M.M. Singh, Corrosion Science 85 (2014) 352.

[3] A. El Bribri, M. Tabyaoui, B. Tabyaoui, H. El Attari, F. Bentiss, Materials Chemistry and Physics, 141 (2013) 240.

[4] N D. K. Singh, S. Kumar, G. Udayabhanu, R. P. John, Journal of Molecular Liquids, 216 (2016) 738.

PHYTOCHEMICAL INVESTIGATION OF *CAREX PRAECOX*

Zsuzsanna Csilla Dávid[1], Norbert Kúsz[1], László Bakacsy[2], Judit Hohmann[1,3], Andrea Vasas[1]

[1]Department of Pharmacognosy, University of Szeged, H-6720 Szeged, Zrínyi utca 9, Hungary
Department of Plant Biology, University of Szeged, H-6726 Szeged, Közép fasor 52, Hungary
[3]Interdisciplinary Centre of Natural Products, University of Szeged, H-6720 Szeged, Eötvös utca 6, Hungary
e-mail: david.zsuzsanna@pharmacognosy.hu

Introduction

Carex praecox belongs to the family Cyperaceae, the third largest family of monocotyledonous plants, containing approximately 100 genera and 5000 species.[1] Several species of the family have been traditionally used as nutritional food or for medicinal purposes, however, the phytochemical and pharmacological investigation of biologically active compounds have been carried out only in the case of a limited number of species. According to the literature data, Cyperaceae species accumulate a variety of secondary metabolites, among them flavonoids, terpenoids, phenolic compounds, steroids, alkaloids and stilbenes.
The aim of our work is to isolate the secondary metabolites of *Carex praecox* followed by the investigation of the pharmacological effects of the pure compounds.

Results and discussion

Dried aerial parts of *C. praecox* were ground and extracted with methanol. After evaporation, the extract was dissolved in 50% methanol and then subjected to solvent–solvent partition with *n*-hexane, chloroform and ethyl acetate. The chloroformic extract was purified by column- and preparative thin layer chromatography, and HPLC methods. The structures of the isolated compounds were determined by a combination of 1D and 2D NMR, and MS measurements. As a result of the preparative work, two novel flavonoids, two novel lignans, an aldehyde and a chromene derivative were identified from the plant.

Conclusion

With the use of diverse chromatographic methods, altogether six compounds have been identified from *C. praecox*, among them four novel metabolites (two flavonoids, two lignans). All compounds have been isolated for the first time from the plant.
Isolation and structure elucidation of further compounds from *C. praecox* are going to be continued. Furthermore, pharmacological studies, especially antibacterial tests will be performed with the pure compounds.

Acknowledgements

This work was supported by the Economic Development and Innovation Operative Program GINOP-2.3.2-15-2016-00012.

References

[1] D.A. Simpson, C.A. Inglis. Kew. Bull. 56 (2001) 257–360.

CHARACTERIZATION OF WASTE-WOOD DERIVED BIO- AND HYDRO-CHAR

Mirjana Petronijević[1], Nataša Đurišić-Mladenović[1], Sanja Panić[1], Igor Antić[1], Predrag Kojić[1], Dragan Govedarica[1], Milan Tomić[2]

[1] University of Novi Sad, Faculty of Technology Novi Sad, 21000 Novi Sad, Bulevar cara Lazara 1, Serbia
[2] University of Novi Sad, Faculty of Agriculture, 21000 Novi Sad, Trg Dositeja Obradovića 8, Serbia
e-mail: natasadjm@tf.uns.ac.rs

Abstract

Carbon materials, such as biochar (BC) and hydrochar (HC) have attracted special attention recently due to the cheap feedstock, wide range of the application possibilities, as well as non-toxicity to the environment. BC and HC could be produced from various biomasses under relatively low reaction temperatures and anoxic conditions [1]. These carbon materials are characterized by a large surface area and porous structure, which makes them a good candidate as a soil conditioner in agriculture [2] and adsorbent important for removal of environmental pollutants [3]. The aim of this work was to compare morphological and chemical characteristics of BC and HC obtained from woody biomass. The BC was synthesized from sawdust of beech and oak wood mixture by pyrolysis at 700°C under atmospheric pressure (Basna doo, Čačak, Serbia). The HC was synthesized by hydrothermal carbonization of wood sawdust at 200°C under auto generated pressure of about 1.5 MPa. The results of gravimetric analysis showed that both BC and HC have very high presence of dry matter (85% BC and 95% HC), of which the largest part is volatile organic matter (78% and 94%, respectively), while the ash content is less than 5%. Both samples are characterized by a heterogeneous surface and a very porous structure determined by scanning electron microscopy (SEM). The pore sizes of BC (5-14 μm) are much higher than the pore size of HC (1-2 μm). Elemental analysis performed by X-ray energy dispersion (EDS) showed that carbon and oxygen are two dominant elements in BC (90% C and 9% O) and HC (76% C and 24% O); potassium and calcium are present in traces in BC , while copper is detected in traces in HC. The gas chromatographic analysis with mass spectrometric detection (GC-MS) of the contents of 12 selected polycyclic aromatic hydrocarbons (PAHs) from a group of 16 EPA PAHs revealed rather similar content of 3-ring and 4-ring compounds in the toluene extracts of both types of char, being the most dominant and representing about 46% and 36% of the total sum, respectively. The most carcinogenic PAHs benzo(a)pyrene and dibenz(ah)anthracene were not detected.

Acknowledgements

This work was supported by the Ministry of Education, Science and Technological Development of Republic of Serbia (Project 451-03-68/2020-14/200134).

References

[1] G. Gascó, J. Paz-Ferreiro, M.L. Álvarez, A. Saa, A. Méndez, Waste Manag. 79 (2018) 395.
[2] Z. Zhang, Z. Zhu, B. Shen, L. Liu, Energy 171 (2019) 581.
[3] X. Tan, Y. Liu, G. Zeng, X. Wang, X. Hu, Y. Gu, et al., Chemosphere 125 (2015) 70.

INVESTIGATION OF ANTIMICROBIAL AGENTS PRODUCED BY GRAM-NEGATIVE BACTERIA

Gábor Endre[1,2], Csenge Kasuba[1], Babett Edit Nagy[1], Dániel Hercegfalvi[1], Mónika Vörös[1] Mónika Varga[1], Csaba Vágvölgyi[1], András Szekeres[1]

[1]University of Szeged, Faculty of Science and Informatics, Departement of Microbiology, Közép fasor 52. Szeged H-6726
[2]Doctoral School in Biology, Faculty of Science and Informatics, University of Szeged, Szeged, Hungary
e-mail: egabcy@gmail.com, andras.j.szekeres@gmail.com

Abstract
Bacterial secondary metabolites are low molecular mass compounds, which are not essential for bacterial growth. These secondary metabolites are produced in the stationary phase of bacterial growth and the produced compounds could have a variety of biological functions. One of these functions are the antibiotic or antimicrobial function that is gaining interest in the microbial community recently.
In this work Gram-negative bacterial strains were cultivated, and their produced secondary metabolites were extracted and tested in antimicrobial plate assays against Gram-positive and Gram-negative bacterial strains as well. The well-known antibiotic, pyrrolnitrin content of the extracts were also determined by HPLC-Quadrupole-Orbitrap MS.

Introduction
Bacterial secondary metabolites are low molecular mass compounds, which are not essential for bacterial growth. They provide many different biological functions for bacteria in nature [1]. There are many compounds that can be considered as secondary metabolites from bacterial sources such as antibiotics [2], enzymes inhibitors [3] and growth promoters [4]. These types of metabolites are produced during the stationary phase of bacterial growth.
Natural antibiotics are compounds that are produced by certain types of bacteria as secondary metabolites [5]. They began to take a wide range of interest especially in the medical and microbiological fields [6,7].

Experimental
Five bacterial strains (*Serratia marcescens*, SZMC 0567; *Serratia plymuthica*, SZMC 24063; *Pseudomonas chlororaphis*, SZMC 24067; *S. plymuthica*, SZMC 24069; *S. plymuthica*, SZMC 24070) were collected from the Szeged Microbial Collection (SZMC).
Strains were cultivated on three different media to get the antimicrobial effects of their secondary metabolites tested. The three media were Czapek-Dox broth (CzDb), glutamate-nitrate medium (GNM) and glutamate-nitrate medium completed with D-tryptophan (GNM+Trp).
Grown cultures were centrifuged and the supernatant was extracted with ethyl-acetate. Organic phases were dried over $MgSO_4$ and were filtered as well as evaporated.
Gained crude extracts were redissolved in 10% methanol (in water (v/v%)) and were centrifuged to get rid of the precipitate. With the solutions antimicrobial microplate assays were performed against three Gram-positive and three Gram-negative bacteria, to get their antimicrobial properties determined. After 24h of incubation, inhibitory rates were calculated.
The pyrrolnitrin content of the crude extracts was determined by HPLC-Quadrupole-Orbitrap MS. 1 mg of each crude extract was redissolved in 1 ml MS grade methanol and was injected

to the HPLC-QOMS. The pyrrolnitrin content was determined by ESTD calibration in the range of 25-500 ng/ml concentration.

Results and discussion

After successful cultivation of the five bacterial strains in three different media the fermentation material was extracted by ethyl-acetate. The antimicrobial activity of the crude extracts was tested against Gram-positive (*Bacillus subtilis*, *Micrococcus luteus* and *Saphylococcus aureus*) and Gram-negative (*Eserichia coli*, *S. marcescens* and *Pseudomonas aeruginosa*) bacteria as well. The experiments resulted that the extracts were active against Gram-positive bacteria and were no growth inhibition against Gram-negative ones. The samples were most active against *B. subtilis* and less active in the cases of *M. luteus* and *S. aureus*. There were two of the cultivated bacteria that might produce high concentrations of antimicrobial agents, because when the extract was in contact with *B. subtilis* inhibitory rates reached above 80%. These bacteria were *S. plymuthica* (SZMC 24063) grown on CzDb and GNM media and *S. plymuthica*, (SZMC 24069) grown on CzDb.

For further investigation a well-known antibiotic compound, the concentration pyrrolnitrin was determined in the crude samples by HPLC-Quadrupole-Orbitrap MS. External standard calibration was carried out in the range of 25-500 ng/ml concentration. It was found that *S. plymuthica* (SZMC 24069) grown on CzDb produced high concentrations of pyrrolnitrin (1687 ng/ml) and *S. plymuthica*, (SZMC 24070) grown on GNM+Trp (868 ng/ml). The pyrrolnitrin production of SZMC 24069 can be correlated to the antimicrobial plate assay, this high concentration of an antibiotic in a solution might cause the growth inhibition of Gram-positive bacteria.

Conclusion

Cultivation of five bacterial strains on three culture media was carried out. The secondary metabolites were successfully extracted from the liquid media. The antimicrobial activity of the crude extracts was tested against Gram-positive and Gram-negative bacteria.

It can be concluded that two bacteria had produced secondary metabolites on certain culture media that are effective against Gram-positive bacteria. The pyrrolnitrin concentrations were also determined by HPLC-Quadrupole-Orbitrap MS , and in one case, the antimicrobial activity can be correlated to the measured high concentration of pyrrolnitrin.

Acknowledgements

SUPPORTED BY THE **ÚNKP-20-4-582** NEW NATIONAL EXCELLENCE PROGRAM OF THE MINISTRY FOR INNOVATION AND TECHNOLOGY FROM THE SOURCE OF THE NATIONAL RESEARCH, DEVELOPMENT AND INNOVATION FUND.

References

[1.] B. Ruiz., Crit. Rev. Microbiol., 2 (2010) 146–167.
[2.] M. O'Neill, Microb. Biotechnol., 46 (1999) 621–657.
[3.] R. K. Pettit, Microb. Biotechnol. 4 (2011) 471–478.
[4.] R. Singh., Biotech. 1 (2017) 1–14.
[5.] M. H. Medema., Res. Suppl. 2 (2011) 339–346.
[6.] S. Nayak, Int. J. Med. Sci. 12 (2016) 2512.
[7.] C. J. Schofield., Nat. Microbiol. 7 (2018) 752–753.

IMPROVED PIEZOELECTRIC PROPERTIES IN (K, Na)NbO_3 LEAD FREE CERAMICS

Bucur Raul Alin, Farkas Iuliana, Bucur Alexandra Ioana

National Institute for Research and Development in Electrochemistry and Condensed Matter, Condensed Matter Department, No. 1 Plautius Andronescu, 300224 Timisoara, Romania.
e-mail: raul_alin_bucur@yahoo.com

Abstract

Piezoelectric ceramics are nowadays used in many applications like medical, communication or aerospace. However, lead oxide based materials are the most widely used ferroelectrics. Because of the toxicity of lead oxide, researchers are now focusing on to substituting this compound with newer, environmental friendly materials [1]. Of considerable interest is the (K,Na)NbO_3 based group of materials (doped potassium sodium niobate), which possesses a relatively high Curie temperature and good piezoelectric properties [2]. Also, the temperature independence of the morphologic phase boundary implies good temperature stability of the piezoelectric and ferroelectric properties [3, 4].

New results related to $GdXO_3$ (where X= Al, Co, Cr, Fe) doped $(K_{0.5}Na_{0.5})NbO_3$ ferroelectrics are presented in this paper. Pure $(K_{0.5}Na_{0.5})NbO_3$ and $(K_{0.5}Na_{0.5})NbO_3$ doped with 0.25, 0.5, 0.75, 1, 2.5, 5 mol% $GdXO_3$ were produced by the conventional solid state synthesis. The ceramics obtained were structurally characterized using x-ray diffraction with a PANalytical X'Pert Pro MPD diffractometer. A morphological phase transition was observed, from orthorhombic to tetragonal crystalline symmetry. The frequency dependence (100 Hz – 5MHz) of the real part of the dielectric constant was studied using a LCR meter TEGAM model 3550. The dielectric constant decreases with the increase off frequency. Such behavior is to be explained based on the dispersion of polarization with frequency. The microstructure of the samples was analyzed using a scanning electron microscope Inspect S - FEI Company. Before piezoelectric measurements, the samples were poled at 60 KV/ cm, at 100 ˚C. A complete set of the piezoelectric constants was obtained using the resonance method with a network analyzer Agilent E5100A. The improvement of the piezoelectric properties is to be related to the decrease of the grain size and the presence of the orthorhombic – tetragonal phase transition. The results show that such materials can be successfully used for new environmental friendly piezoelectric applications.

References

1. J. Rodel, W. Jo, K.T.P. Seifert, E.M. Anton, T. Granzow, D. Damjanovic, J. Am. Ceram. Soc. 92, 1153 (2009).
2. Saito, H. Takao, I. Tani, T. Nonoyama, K. Takatori, T. Homma et al., High performance lead-free piezoelectric materials, Nature 432, 84 (2004) ;
3. L.J. Rigoberto, G.V. Virginia, M.P. Cruz, M.E. Villafuerte-Castrejon, J. Electron. Mater. 44, 2862 (2015).
4. M.D. Maeder, D. Damjanovic, N. Setter, J. Electroceram. 13 (2004) 385.

VOLTAMMETRIC MONITORING OF LACCASE-CATALYSED REACTIONS OF DIFFERENT LIGNINS THROUGH OXIDATIVE COUPLING WITH GLUCOSAMINE

Firuta Ionita Fitigau[1], Cristian George Vaszilcsin[1], Zoltan Urmosi[1]

[1]National Institute of Research-Development for Electrochemistry and Condensed Matter, A. P. Podeanu 144, 300569 Timişoara, Romania
e-mail: fitigau_firuta@yahoo.com

Abstract
The ability of laccase to facilitate grafting hydrophilic compounds, namely glucosamine to lignin in acetone/water mixtures aiming to obtain grafted novel lignin derivatives with new functionalities was assayed by cyclic voltammetry. The oxidation properties registered for the oxidative reactions of syringaldazine lignin model compound with glucosamine evidenced that the reaction scan is direct proportional with the redox potential differences between substrate and laccase. A comparative electrochemical activity of lignins on the GCE in absence and presence of the laccase and glucosamine is presented. From the measurements of the coupling reactions currents it was concluded that the addition of glucosamine can lead to a partial loss of the redox activity of lignin phenolic groups and the co-substrate interaction with the lignin surface groups.

Introduction

Lignin, a highly branched, irregular three-dimensional organic polymer, is the most abundant biopolymer in nature next to cellulose. This natural polymer contains different structures including phenolic and non-phenolic compounds. The applicability of oxidative laccase for both the degradation and the modification of lignin in aqueous media have been intensively studied but limitations still exists due to the low solubility of lignin in media that are compatible with laccase (Cannatelli & Ragauskas, 2016). Organic water-miscible solvents are often required in laccase-catalyzed oxidations because many of the lignin substrates are insoluble in water. Conventionally, the role of fungal laccases in lignin degradation was thought to be limited only to the oxidation of low-redox potential phenolic substructures of the polymer (Johannes & Majcherczyk, 2000).
Due to the low electrochemical reduction potential, laccase can only oxidize the phenolic lignin moiety (<20% of total lignin) and not the non-phenolic aromatic structure (80% of total lignin) (Camarero et al., 1994). Laccase activity on phenols is enhanced by the presence of electron-donating groups at the benzene ring that decrease their electrochemical potentials, thus making them more easily oxidizable. Another factor playing a significant role in the enzymatic catalysis is the pH of the reaction medium and substrate concentration, which affects not only the catalytic activity of laccase, but also the redox potentials of its substrates (Fernández-Sánchez et al., 2002). The purpose of the present study was to evaluate by means of electrochemical techniques the efficiency of laccase in the coupling reactions of four different lignins with glucosamine to obtain modified lignin fractions with potential utilization as biomaterials

Experimental

Lignins

Soda wheat straw lignin (coded SWL) and P1000 soda lignin (coded SGWL) from mixed Sarkanda grass (75%) and wheat straw (25%) were obtained from Greenvalue SA (Lausanne, Switzerland). Organosolv lignin (Alcell) from mixed maple, birch and poplar (hardwoods, coded as OHL) was obtained from Repap Technologies Inc. (Val-ley Forge, PA, USA). Indulin AT, a Kraft lignin from pine (softwood, coded KSL), was obtained from MeadWestvaco

(USA). All lignin samples were previously fractionated by selective extraction at ambient temperature using acetone/water solution of 50% (v/v) acetone.

Laccase

Laccase (Lcc) from *Trametes versicolor* (30.6 U mg^{-1} of solid) were purchased from Sigma-Aldrich (Taufkirchen, Germany. The activity of the laccase was determined by monitoring the oxidation of syringaldazine (Sigma-Aldrich, Taufkirchen, Germany) at 530 nm ($\varepsilon = 65\ mM^{-1}cm^{-1}$) and 25ºC in different acetone: water (v/v) mixtures.

Electrochemical methods

Cyclic voltammetric experiments were performed with a Voltalab 80 PGZ402 potentiostat (Radiometer Analytical, Copenhagen) and controlled by Voltamaster 4 software, version 7.08. All measurements were carried out in a 50-ml thermostated cell, model BEC/EDI, with conventional three electrode configuration. A working glassy carbon electrode (GCE), with a surface diameter of 2.8 mm, was used together with a platinum counter electrode and a saturated calomel reference electrode (SCE), purchased from Radiometer. Before each experiment, the surface of the glassy carbon electrode was polished on a diamond-polishing pad followed by a thorough washing step with distilled water and acetone.

Results and discussion

Cyclic voltammetry of syringaldazine coupling reaction with glucosamine

The oxidation properties registered for the reaction of syringaldazine with glucosamine were demonstrated by cyclic voltammetry, the reaction scan being direct proportional with the redox potential differences between substrate and laccase. The electrochemical oxidation of phenol is known to proceed predominantly via one electron transfer and the formation of polymeric products which lead to electrode fouling (Ivnitski & Atanassov, 2007).

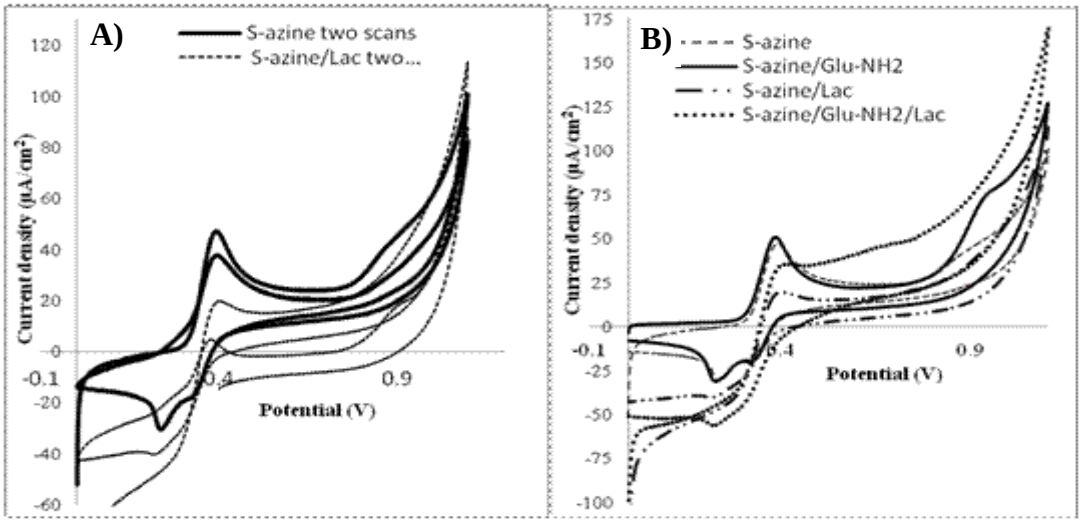

Figure 1. Cyclic voltammograms of A): 0.2 mM syringaldazine (1st and 2nd scan) in acetone/water and 500 mM tartrate buffer (pH 4) in absence (solid line) and presence (dotted line) of T. versicolor laccase immobilized on glassy carbon electrode (GCE); B) 0.2 mM syringaldazine (---), 0.2 mM syringaldazine and glucosamine, 1:2 molar ratio (—), 0.2 mM syringaldazine and laccase immobilised on the GCE (— ··), 0.2 mM syringaldazine, glucosamine (1:2 molar ratio) and laccase immobilised on the GCE (·····). Scan rate: 0.5 mV/s.

In the Figure 1A the two pairs of redox peaks corresponding to syringaldazine reduction and oxidation by laccase two anodic peaks are well observed in the potential area 0.4 V and 0.95 V at a scan rate of 0.5 mV/s. It was assumed (Ivnitski & Atanassov, 2007) that the pair of redox

peaks in low potential area (cathodic peak at 0.32 V and anodic peak at 0.4 V) belongs to the redox process of the T2/T3 center of laccase as being the site for oxygen reduction meanwhile the redox processes at high potentials 0.95 V belongs to T1 copper center. When glucosamine was added in the reaction mixture, the anodic peak decreased more slowly compared with the reaction when only syringaldazine and laccase adsorbed on the electrode surface were present. This could be due to either enzyme inhibition by some products generated in the coupling reaction or by co-substrate inhibition. For the anodic processes the peak potential, E_{a1} is approximatively constant for all the reactions, meanwhile the current peak i_{pa1} decreased for the reactions with laccase being more obvious when no glucosamine was added. In the absence of laccase, the electrochemical parameters corresponding to the first cathodic peak have approximatively the same values, ip_{c1} decreased for laccase mediated reactions the cathodic peak being more evident in the coupling reaction of syringaldazine with glucosamine.

Cyclic voltammetry of lignins coupling reaction with glucosamine

The ability of laccase to facilitate grafting hydrophilic compounds, namely glucosamine to lignin in acetone/water mixtures aiming to obtain grafted novel lignin derivatives with new functionalities was assayed by cyclic voltammetry. Four technical lignins obtained by different isolation technology previously extracted with 50% (v/v) acetone-water mixture were used. To find the compromise conditions at which the substrate is soluble while the enzyme remains active, the reaction was carried out in an 50/50 (v/v) aqueous–acetone mixture with laccase directly adsorbed on the surface of the (glassy carbon electrode) GCE.

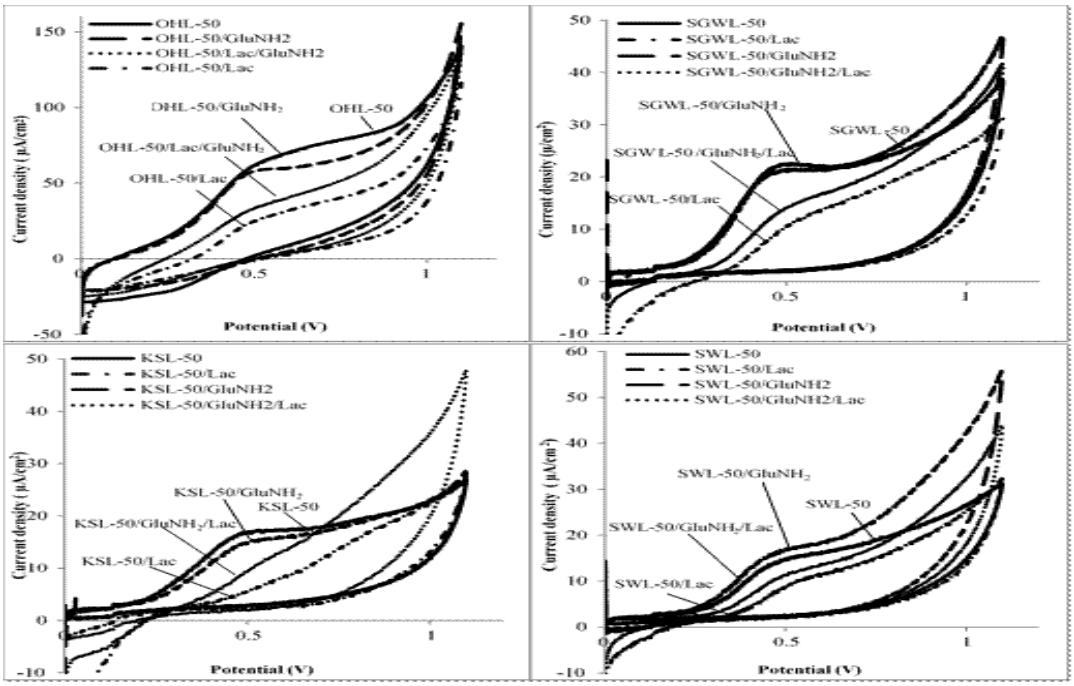

Figure 2. Cyclic voltammograms of coupling reactions of OHL, SGWL, KSL and SWL lignin fractions with glucosamine (1:2.8 total OH_{Ar} : $GluNH_2$ molar ratio) in 50 % (v/v) acetone/water using *T. versicolor* laccase immobilized on glassy carbon electrode (GCE). Scan rate: 0.5 mV/s.

A comparative electrochemical activity of lignins on the GCE in absence and presence of the laccase and glucosamine will be presented in the following. The reactions were performed with the laccase adsorbed on the graphite electrode surface and a remarkable decrease in the redox peak was observed for all studied lignins (Figure 2). Observation of the catalytic activity of laccase confirmed that the in vivo function was retained throughout the immobilization process. All studied lignins presented a redox potential at 480 mV that remain unchanged after the enzymatic treatment. As was expected the intensity of the anodic peak decreased when the GCE

laccase modified electrode was immersed in the reaction mixture as the result of the lignins phenolic group oxidation, the current density being two times smaller than those registered without laccase treatment. With the addition of glucosamine in solution the anodic peak recorded a less pronounced decrease compared with the reaction when only lignin and laccase was present and can be attributed to the partial loss of the redox activity of lignins in presence of glucosamine and the glucosamine interaction with the lignin surface groups.

Conclusion

The absence of the cathodic peaks that were well-defined for syringaldazine reactions are indicating an oxidation process followed by a chemical reaction that quickly removes the generated products. When laccase is adsorbed on graphite, bioelectrocatalytic reduction of oxygen occurs and is observed as a reduction current caused by direct electron transfer from the electrode to the immobilized laccase and then further to molecular oxygen in solution. Small changes in the anodic currents were observed for all the studied lignin when glucosamine was added (Lignin/GluNH2) before catalytic initiation of the reaction with laccase. The studied lignins behave differently in oxidative coupling reactions due to their origin, different extraction methods and the phenolic content. In all cases the redox currents registered for lignin with laccase system in comparison to the reactions without catalyst are significantly reduced.

References

[1] C. Johannes, A. Majcherczyk, J. Biotechnol. 78 (2000) , 193-199.
[2] M.D. Cannatelli, A.J. Ragauskas, Appl. Microbiol. Biotechnol. 100(20) (2016), 8685-8691.
[3] S. Camarero, G. C. Galletti, A. T. Martínez, Appl. Environ. Microbiol. 60 (1994), 4509–4516.
[4] C. Fernández-Sánchez, T. Tzanov, G. M Gübitz, A. Cavaco-Paulo, Bioelectrochem., 58(2002), 149−156.
[5] C.G. Boeriu, F.I. Fitigau, R.J.A. Gosselink, A.E. Frissen, J.H. Stoutjesdijk, F. Peter, Ind. Crops. Prod. 62 (2014), 481 - 490.
[6] D. Ivnitski, P. Atanassov, Electroanalysis 19 (22) (2007), 2307 – 2313.

UV/VIS SPECTRAL SIMULATION OF A SYMMETRICAL DISAZO DIRECT DYE BY THE HARTREE-FOCK APPROXIMATION

Maria Elena Rădulescu-Grad, Simona Funar-Timofei*

Institute of Chemistry Timisoara of the Romanian Academy, Bul. Mihai Viteazu 24, 300223 Timisoara, Romania
e-mail: timofei@acad-icht.tm.edu.ro

Abstract

A disazo direct dye having a symmetrical structure, derived from the 4,4'-diaminostilbene-2,2'-disulfonic acid was previously synthesized and applied to water-based acrylic resins, in coatings. The dye structure was previously experimentally analyzed using the UV/VIS spectroscopy and theoretical Density Functional Theory (DFT) calculations were employed to compare the calculated with the experimental UV/VIS wavelengths. In this paper the molecular dye structure was modeled using the MMFF94 force field and the Hartree-Fock (HF) approach. The UV/VIS spectrum of the minimum energy optimized structure was simulated using the Configuration Interaction Singles (CIS), the Time-Dependent (TD) and the Zerner's Intermediate Neglect of Differential Overlap (ZINDO) methods to evaluate the electronic excitation spectra. The ZINDO approach gave better maximum absorption calculated values compared to the CIS and TD methods, as previously noticed in case of using the DFT approach. A generally good agreement between the experimental and theoretical computed absorption maxima was noticed.

Introduction

Azo dyes are known as the most important class of synthetic, colored organic compounds. They are almost invariably prepared by the diazotization of aromatic amines and by the coupling of the obtained diazonium compounds with phenols, naphthols, arylamines, pyrazolones [1]. They are widely used in textiles, food, pharmaceutical, cosmetic industries, medicine, high-performance technology, etc. [2-7].

The symmetrical disazo direct dye presented in this paper was previously synthesized using 4,4'-diaminostilbene-2,2'-disulphonic acid as middle component and 2,7-dihydroxynaphthalene as coupling component [8]. The objective of this study is to use the Hartree-Fock (HF) approximation to model the structure of this previously synthesized disazo direct dye (**1**) (Fig. 1) in ground state, and the CIS, TD and ZINDO methods for its UV/VIS spectrum simulation. The experimental absorption maxima were compared to the calculated ones.

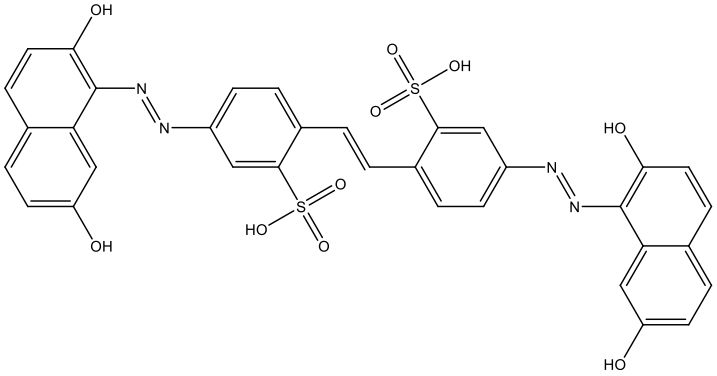

Figure 1. Structure of the disazo direct dye (**1**).

Theoretical structure investigation

The Marvin Sketch program, version 17.18.0, from ChemAxon (Marvin Sketch 17.18.0, 2017, ChemAxon Ltd., http://www.chemaxon.com.) was used to build the structure of the disazo diect dye (**1**). The conformational search was performed using the MMFF94 force field.

The minimum energy conformer thus derived was further geometry optimized in gas phase using the Hartree-Fock (HF) approach [9-11]. The ground state geometrical optimization of the title compound has been performed using the Gaussian 09 package [12]. All optimized structures were characterized as true minima by frequency calculations.

UV/VIS spectra simulation

Ultraviolet spectra analyses of the disazo direct dye (**1**), fully energy optimized in water, used as solvent, have been examined using the Configuration Interaction Singles (CIS) [13], Time-Dependent Systems (TD) [14] and Zerner's Intermediate Neglect of Differential Overlap (ZINDO) [15] methods. Eight singlet excited states were computed for the minimum energy dye conformer. The calculated wavelengths, which are a function of the molar absorption coefficients, were compared with the previously measured experimental data [8].

Results and discussion

The minimum energy conformer of the dye (**1**) derived from MMFF94 calculations was further optimized at the HF/3-21G level in ground state, using the Gaussian 09 program. The following data were obtained: the predicted SCF energy was of -3045.85701481 a.u., the unscaled zero-point correction (ZPE) = 0.575720 (Hartree/Particle); the thermal correction to the enthalpy (Hcorr) = 0.615792; the thermal correction to the Gibbs free energy (Gcorr) = 0.499944. To model the UV/VIS spectrum eight singlet excited states were considered.

The previously reported experimental UV/VIS spectrum in water of the dye (**1**) is characterized by two electronic absorption bands located at 329 nm and 560 nm [8].

The CIS/IEF-PCM(WATER)/3-21G, TD/IEF-PCM(WATER)/3-21G and ZINDO calculations were performed at the HF/3-21G level to simulate the UV/VIS spectrum of the minimum energy conformer of the direct azo dye (**1**) in water. The theoretical UV/VIS transitions were presented by visible absorption maxima and oscillator strengths in Table 1.

Table 1. Calculated CIS, TD and ZINDO absorption maxima and the oscillator strengths of dye (**1**).

Excited state	CIS		TD		ZINDO	
	Wavelength (nm)	Oscillator strength	Wavelength (nm)	Oscillator strength	Wavelength (nm)	Oscillator strength
S1	414	0.000	443	0.000	576	0.000
S2	407	0.000	435	0.000	570	0.000
S3	284	2.539	293	2.301	416	1.593
S4	279	0.079	286	0.026	403	0.012
S5	238	0.284	244	0.176	349	0.072
S6	232	0.261	239	0.164	347	0.069
S7	216	0.354	223	0.314	297	0.342
S8	211	0.008	219	0.014	292	0.057

The simulated UV/VIS spectra of the minimum energy conformer at the HF/3-21G level are presented in Figures 2 to 4. The visible maximum absorption (λ_{max}) value obtained at the HF/3-21G level in the water phase with the ZINDO approach is bigger than the CIS and TD

ones, for the third excited state: λ_{max} (ZINDO) = 416 nm; λ_{max} (TD) = 293 nm; λ_{max} (CIS) = 284 nm. For the seventh excited state, a closer maximum absorption value is noticed for the ZINDO approach, having λ_{max} = 297 nm, compared to the other methods: λ_{max} (TD) = 223 nm and λ_{max} (CIS) = 216 nm. Only the dominant configuration with the oscillator strength value > 0.30 for each excited state was considered. Two distinct low absorption peaks were observed in the CIS and TD simulated spectra, corresponding to lower oscillator strength values. Their presence was not noticed in the experimental UV/VIS spectrum. ZINDO method is considered to have the nearest results to the UV/VIS experimental spectrum.

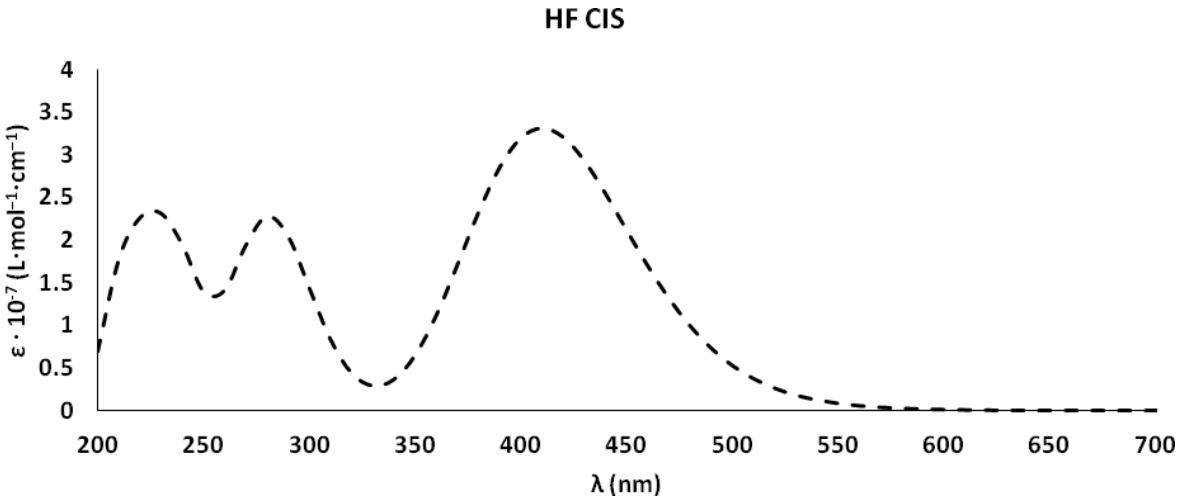

Figure 2. The calculated molar absorption coefficient (ε) versus the wavenumber (λ) of the dye (**1**), using the CIS approach at the HF/3-21G level.

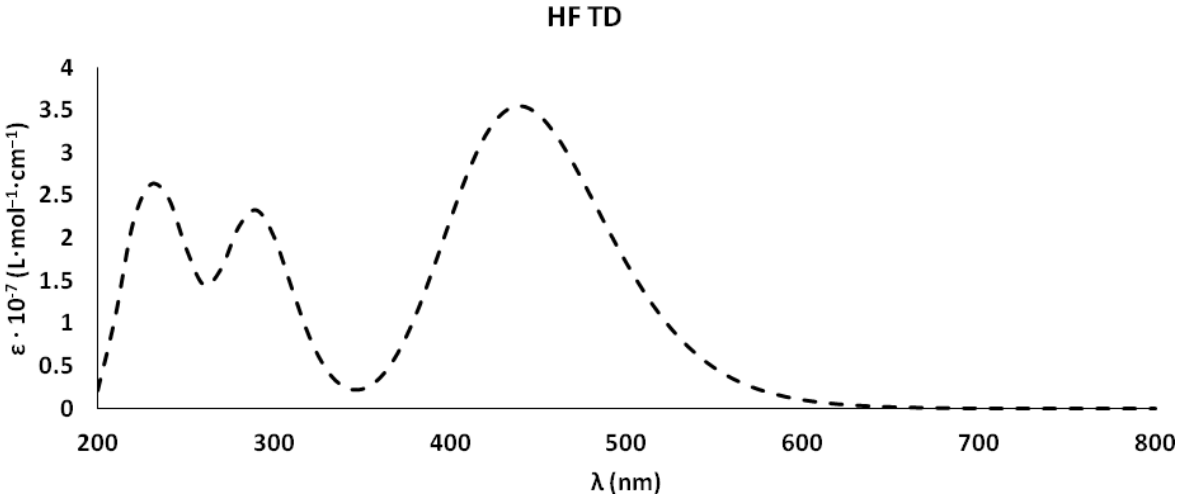

Figure 3. The calculated molar absorption coefficient (ε) versus the wavenumber (λ) of the dye (**1**), using the TD approach at the HF/3-21G level.

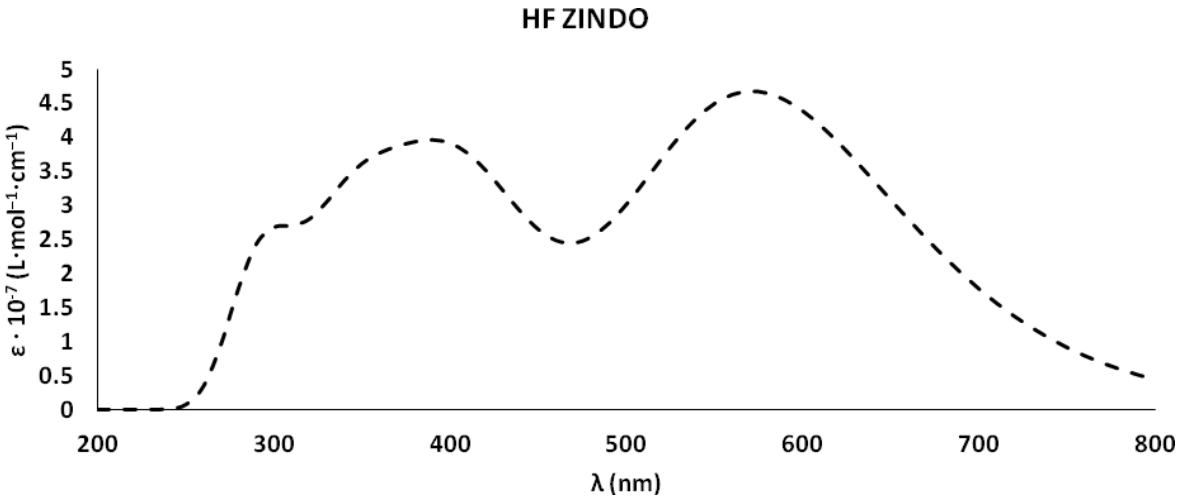

Figure 4. The calculated molar absorption coefficient (ε) versus the wavenumber (λ) of the dye (**1**), using the ZINDO approach at the HF/3-21G level.

Conclusion

The UV/VIS electronic spectrum was simulated for a disazo direct dye structure optimized using the Hartree-Fock approach and the 3-21G basis set. Good agreement between the experimental and ZINDO calculated wavelengths (λ_{max}) values was observed. Better UV/VIS simulation results were achieved using the ZINDO approach and comparable results with the experiment were noticed, compared to the TD and CIS methods, as previously reported for dye structure simulation using the DFT approach [8].

Acknowledgements

This project was financially supported by Projects 1.1 and 2.4 of the Institute of Chemistry of the Romanian Academy. Access to the Chemaxon Ltd. software is greatly acknowledged by the authors.

References

[1] H. Zollinger, Color Chemistry: Synthesis, Properties and Application of Organic Dyes and Pigments, 3rd ed., Wiley-VCH, Weinheim, 2003, pp. 16.
[2] A. Mohammadi, B. Khalili, M. Tahavor, Spectrochim. Acta A Mol. Biomol. Spectrosc. 150 (2015) 799.
[3] K.Yamjala, M.S. Naiar, N.R. Ramisetti, Food Chem. 192 (2016) 813.
[4] N.M. Mallikarjuna, J. Keshavayya, J. King Saud. Univ. Sci. 32 (2020) 251.
[5] F. Vázquez-Ortega, I. Lagunes, Á. Trigos, Dyes. Pigm. 176 (2020) 108248.
[6] D. Akram, I.A. Elhaty, S.S. AlNeyadi, Chem. Data Collect. 28 (2020) 10045.
[7] B. Derkowska-Zielinska, E. Gondek, M. Pokladko-Kowar, A. Kaczmarek-Kedziera, A. Kysil, G. Lakshminarayana, O. Krupka, Sol Energy. 203 (2020) 19.
[8]. M. E. Radulescu-Grad, A. Visa, M. S. Milea, R. I. Lazau, S. Popa, S. Funar-Timofei, J. Mol. Struct. 1217 (2020) 128380.
[9] V.A. Fock, Z. Phys. 61 (1) (1930) 126.
[10] V.A. Fock,. Z. Phys. 62 (11) (1930) 795.
[11] D. R. Hartree, W. Hartree, Proc. Royal Soc. Lond. A. 150 (1935) 9.

[12] Gaussian 09, Revision B.01, M. J. Frisch, G. W. Trucks, H. B. Schlegel, G. E. Scuseria, M. A. Robb, J.R. Cheeseman, G. Scalmani, V. Barone, B. Mennucci, G.A. Petersson, H. Nakatsuji, M. Caricato, X. Li, H. P. Hratchian, A. F. Izmaylov, J. Bloino, G. Zheng, J. L. Sonnenberg, M. Hada, M. Ehara, K. Toyota, R. Fukuda, J. Hasegawa, M. Ishida, T. Nakajima, Y. Honda, O. Kitao, H. Nakai, T. Vreven, J. A. Montgomery, Jr., J. E. Peralta, F. Ogliaro, M. Bearpark, J. J. Heyd, E. Brothers, K. N. Kudin, V. N. Staroverov, T. Keith, R. Kobayashi, J. Normand, K. Raghavachari, A. Rendell, J. C. Burant, S. S. Iyengar, J. Tomasi, M. Cossi, N. Rega, J. M. Millam, M. Klene, J. E. Knox, J. B. Cross, V. Bakken, C. Adamo, J. Jaramillo, R. Gomperts, R. E. Stratmann, O. Yazyev, A. J. Austin, R. Cammi, C. Pomelli, J. W. Ochterski, R. L. Martin, K. Morokuma, V. G. Zakrzewski, G. A. Voth, P. Salvador, J. J. Dannenberg, S. Dapprich, A. D. Daniels, O. Farkas, J. B. Foresman, J. V. Ortiz, J. Cioslowski, D. J. Fox, Gaussian, Inc., Wallingford CT, 2010.
[13] C.D. Sherrill, H.F. Schaefer III, Advances in Quantum Chemistry, P.-O. Löwdin (ed.), Volume 34, Academic Press, San Diego, 1999, pp. 143.
[14] E. Runge, E. K. U. Gross, Phys. Rev. Let., 52(12) (1984) 997.
[15] J. Ridley, M. Zerner, Theor. Chim. Acta, 32 (1973) 111.

TRACEABILITY OF FOOD PRODUCTS AND PHARMACEUTICAL PRODUCTS IN RELATION TO CHEMICAL INVESTIGATION

Mirela Ahmadi-Vincu[1,6], Gabriela Garban[2,6], Florin Muselin[3,6], Robert Ujhelyi[4,6], Zeno Gârban[5,6]

[1]Department of Biochemistry, Faculty of Veterinary Medicine, University of Agricultural Sciences and Veterinary Medicine of Banat "King Michael I of Romania", Calea Aradului No. 119, Timişoara, Romania; [2]Laboratory of Environment and Nutrition, National Institute of Public Health-Branch Timişoara, Romania; [3]Department of Toxicology, Faculty of Veterinary Medicine, University of Agricultural Sciences and Veterinary Medicine of Banat "King Michael I of Romania" Timişoara, Romania; [4]Medical Department, S.C. CaliVita International, Timişoara, Romania; [5]Department of Biochemistry and Molecular Biology (former), Faculty of Food Products Technology, University of Agricultural Sciences and Veterinary Medicine of Banat "King Michael I of Romania" Timişoara; [6]Working Group for Xenobiochemistry, Romanian Academy-Branch Timişoara, Bd. M. Viteazu No. 24, Romania
e-mail: zeno.garban@yahoo.com; mirelaahmadi@gmail.com

Abstract

Approaching issues related to the traceability of food and pharmaceutical products at the 26th International Symposium on Analytical and Environmental Problems, would like to point out the fact that the analytical chemistry investigations and their applications target both natural and processed products in the food and pharmaceutical industry (some raw materials being taken from the environment).

In this context, the paper presents summary data on the traceability systems (integrated and differentiated). Thius, in order to highlight the scientific, technical and economic importance of traceability some data about the identification tools are summarized.

Key words: traceability systems, identification tools

Conceptual aspects

In the domain of food and pharmaceutical products, data on the origin of the raw material, its processing, distribution and location after delivery are of main interest.

The implementation of traceability systems primarily targets food products (e.g. raw materials and processed foods), pharmaceuticals (e.g. drugs obtained by extraction or synthesis) and agrobiological products (e.g. plant growth bioregulators, especially synthetic compounds) - see Pouliot şi Sumner (2010); Cuntroneo et al. (2014); Gârban (2020).

Traceability or product tracing is defined by the Codex Alimentarius Commission as "the ability to follow the movement of a food through specified stage(s) of production, processing and distribution" (http://www.fao.org/fao-who-codexalimentarius).

Globally, traceability issues are specified by the Codex Alimentarius and are "extrapolated" through the use of Information and Communication Technology (ICT). In this way it was possible to establish a Global Traceability Standard (GRS).

It is important to know that xenobiotics (physical, chemical, biological agents) can contribute to the sanitation of the environment with harmful effects in time and space (Walker et al., 1996; Gârban 2020).

The problem of food and pharmaceutical products traceability - in relation to analytical chemistry and environmental issues - is also of interest to nutrivigilence and pharmacovigilance (Ahmadi et al., 2007; Klein and Stark, 2018). Therefore, it is important to know the identifying tools for the products.

Traceability systems

Traceability can be approached in two distinct ways: "in an integrated system" and "in a differentiated system". The specifics of these systems will be briefly discussed below.

Traceability sometimes also involves physico-chemical methods (the called so-called instrumental methods). An example of this is a study undertaken by Zhou et al. (2007) which followed the geographical traceability of samples of propolis from various Chinese provinces. It is known that propolis is used to obtain extracts of nutritional and pharmaceutical interest. The HPLC method and the HPLC-UV methodological tandem were used for this purpose. Chromatographically, rutin, quercetin, kamferol, apigenin, etc. were identified.

1. Traceability in an integrated system

This system involves tracking a specific product in the chain (raw material): raw material-transport-processing-storage-distribution-marketing-consumer (fig. 1).

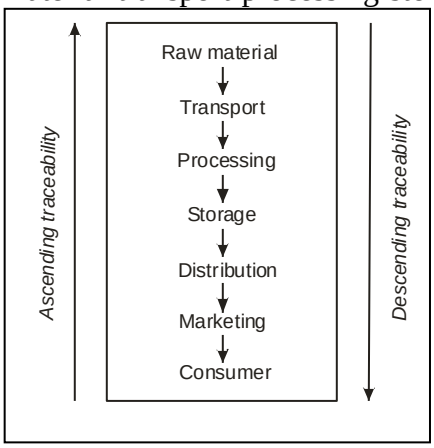

Figure 1. Integrated traceability system

In the integrated traceability system, for product tracking, one can act in two directions (reverse directions) depending of analysis. These are represented by:

□) *Descending (forward) traceability*. It consists of "tracking ahead" and ensures the possibility of locating a product taking into account specific criteria - regardless of where it is in the distribution chain.

□) *Ascending (backward) traceability*. It involves "tracking back" - a circumstance in which one can proceed to identify the origin and characteristics of a product taking into account certain criteria established for distribution points.

2. Traceability in a differentiated system

This system envisages more limited areas pursuing logistics management within the food chain. Within this system, internal traceability and external traceability are distinguished

□) *Internal traceability*. In the case of this type of traceability, a sum of information is considered that interests a certain enterprise / company in the evolution of obtaining the product / food products.

□) *External traceability*. It considers the pursuit of a product along a segment of the food chain, which starts from the finished product obtained by the processor (enterprise / company) to the consumer.

Overall, it can be stated that traceability systems (integrated and differentiated) are of interest to raw material producers, processors, distributors, consumers, but also to the executive power in the state. In this way, coherent measures of socio-economic and medical interest in relation to human nutrition can be ensured.

Identification tools

In order to find out food traceability data different identification tools can be used. A brief description of those tools is of theoretical and applied interest.

A. Barcodes. Encodes information based on numbers represented by a sequence of black and white bars of various sizes. Bar code decryption is done with a scanner. In practice, conditioned by the importance of the marketed product, 8 - 14 digit codes are used for identification (signaling the country, the manufacturer, the product, other details).

B. Radio frequency based benchmarks. In case of *Radio Frequency Identification Devices* (RFID) food data are stored in "electronic circuits" or in "microchips" embedded in plastic material, constituting the so-called "electronic label". For identification there are used various devices operating at radio frequencies ranging between 100 kHz - 2 GHz. These "labels" allow remote data reading.

C. Biological and biochemical tests. The biological and biochemical tests used for identification draw attention to the performance of histology, biochemistry and molecular biology. Although accurate, the application of these methods is limited, due to high costs. Some are mentioned below.

a) Identification of the retinal image. Is based on the recording, with special digital cameras, of the "retinal vascular aspect". This is an attribute of individuality (in this case animals), which is maintained throughout life. It can be applied to live animals transported for slaughter (elsewhere in the world).

b) DNA fingerprint identification. It is based on analyzes specific to molecular biology applied in genetics. In the case of meat and meat products, for example, analyzes based on "DNA fingerprints" can be compared with data on animals from slaughtered lots.There is a great ability to discriminate methods based on molecular biology.

*D. Biodegradable markings.*They are also known as "edible markings" because they are placed directly on the food. They are invisible and is made of an edible substance, e.g. cellulose derivatives. The compound used for labeling is mixed with a certain food ingredient (usually additives). The size of such markings is of the order of 200 μm^2 readable area for a bar code.

E. Markings based on geospatial technology. These include the *Geographic Information System* (GIS) and the *Global Positioning System* (GPS). The latter is a satellite-based radio-positioning system - which contains information and the GPS receiver indicates the location in the field. Marks that use geospatial technology may include the "Quick Response Code", commonly known as the QR Code.Usually, the QR code is a means of storing information in a visual label, which can be read by a device (even a smartphone).

Concluding remarks

1. Traceability systems are of interest to food and pharmaceutical products because they ensure consumer/patient protection by quickly identifying the sources of contamination by government institutions, manufacturers and sellers – throughout the production, processing and distribution chain - and withdrawing the affected product from marketing.

2. In many stages of the entire chain which starts with the raw material, products processing, distribution and saling to consumer (food / medicines) chemical investigations are used.

3. All the identifying tools used in case of food and pharmaceuticl products traceability are based on chemical, physical and biological methods, the ultimate goal being to ensure a fast removal of an affected product from the market for the consumer benefit.

References

[1] Ahmadi Mirela, Avacovici Adina-Elena, Precob V., Sarafolean S., Gârban Z. - *Laboratory handbook, Vol. I. Bioconstituents* (in romanian), Editura Eurobit, Timişoara, 2007.
[2]Cutroneo M. Paola, Isgrň Valentina, Russo Alessandra, Ientile Valentina, Sottosanti Laura, Pimpinella G., Conforti Anita, Moretti U., Caputi P.A., Trifirň G. - Safety Profile of Biological Medicines as Compared with Non-Biologicals: An Analysis of the Italian Spontaneous Reporting System Database, *Drug Safety*, 2014, 37, 961-970.
[3] Gârban Z., Gârban Gabriela – *Human nutrition, Vol.I. Fundamental problems* (in romanian), 3rd edition , Editura orizonturi Universitare, Timişoara, 2003
[4] Gârban Z. - *Quo vadis food xenobiochemistry*, 3rd edition, Editura 3rd edition, Publishing House of the Romanian Academy, Bucharest, 2018 (www.zeno-garban.eu)
[5] Gârban Z. – *Biologically active substances of food, pharmaceutic and agrobiologic interest* (in romanian), Editura ArtPress, Timişoara, 2020
[6] Klein K., Stolk P. - Challenges and Opportunities for the Traceability of (Biological) Medicinal Products, *Drug Safety*, 2018, 41, 911-918.
[7] Pouliot S., Sumner A.D. – *Traceability, Product Recalls, Industry Reputation and Food Safety*, Agricultural Issues Center, University of California, Davis, 2010.
[8] Walker C.H., Hopkin S.P., Sibly R.M., Peakall D.B. (Eds) - in *Principles of Ecotoxicology*, Taylor and Francis, London, 1996.
[9] Zhou J., Li Y., Zhao J., Xue X., Wu L., Chen F. - Geographical traceability of propolis by high-performance liquid-chromatography fingerprints, *Food Chemistry*, 2007, 108(2), 749-759.
[10] *** http://www.fao.org/fao-who-codexalimentarius - accessed August 2020

DETERMINATION OF THE MYCOTOXIN ZEARALENONE IN WATER BY IMMUNOFLUORESCENCE AND TOTAL INTERNAL REFLECTION ELLIPSOMETRY METHODS

Borbála Gémes[1], Eszter Takács[1], Attila Barócsi[2], László Kocsányi[2], László Domján[3], Gábor Szarvas[3], Alexei Nabok[4], András Székács[1]

[1]*Department of Environmental Analysis, Agro-Environmental Research Institute, National Agricultural Research and Innovation Centre, H-1022 Budapest, Herman Ottó u. 15, Hungary.*
[2]*Department of Atomic Physics, Budapest University of Technology and Economics, H-1111 Budapest, Budafoki út 8., Hungary.*
[3]*Optimal Optik Ltd, H-1118 Budapest, Dayka Gábor u. 6/B., Hungary*
[4] *Materials and Engineering Research Institute, Sheffield Hallam University, Harmer Building Level 2, Sheffield S1 1WB, United Kingdom*
e-mail: gemes.borbala.leticia@akk.naik.hu

Abstract

In the scope of project Aquafluosense developing prototypes of fluorescence-based instrumentation for *in situ* measurement of several characteristic parameters of water quality, an immunofluorescent method have been developed for the detection of several environmental xenobiotics, including mycotoxin zearalenone (ZON). ZON, produced by several plant pathogenic *Fusarium* species, has recently been identified as an emerging pollutant in surface water, presenting a hazard to aquatic ecosystems. Due to its physico-chemical properties, detection of ZON at low concentration in surface water is a challenging task. The 96-well microplate-based fluorescent instrument is capable to detect ZON in the concentration range of 0.4–400 ng mL^{-1}. The sensitivity and accuracy of the analytical methods has been demonstrated by comparative assessment with detection by total internal reflection ellipsometry.

Introduction

Through the exhaustion of our global water reserves, water has become an environmental asset of key ecological importance. Water protection is a strategic issue worldwide and is one of the priorities of the European Commission as well. Thus, the EU Water Framework Directive, as one of the key EU policy measures, aims to reach a good status both chemical and ecological, for water bodies in Europe [1]. Within efforts to water conservation, water quality assessment underwent vast advancements driven by emerging water quality problems at a global scale, and by the appearance of novel technologies that allow parallel measurement of water quality parameters at increasing sensitivities.

Project Aquafluosense (NVKP_16-1-2016-0049) [2] aims to develop a new water analysis system for natural and artificial waters, allowing complex, systematic and for main parameters (chlorophyll-a content, chemical and biochemical oxygen demand, total organic carbon, polyaromatic hydrocarbon and certain agricultural pollutants content) *in situ* fluorescence-based assessment and monitoring of water quality, by developing a modular instrument family that can be individually configured for target tasks at each monitoring point.

Mycotoxin zearalenone (ZON) is a well-known food and feed contaminant with serious risk on both livestock and human health. Its occurrence as environmental contaminant is surface water is quite new discovery investigated only in the last decade [3]. The wide occurrence requires effective monitoring systems and analytical technologies. Traditional chromatographic separation e.g., high-performance liquid chromatography (HPLC) [4], thin layer

chromatography (TLC) [5] and liquid or gas chromatography coupled with mass spectroscopy (LC or GC MS) [6] are time consuming technologies requiring special instrumentation. In contrast, immunoanalytical methods allow cost-effective and rapid monitoring [7]. Enzyme-linked fluorescent immunoassays (ELFIA) are simply a variation of colorimetric enzyme-linked immunosorbent assay (ELISA), where the label enzyme converts a substrate into a reaction product fluorescent upon excitation by light of a particular wavelength. In comparison to the colorimetric ELISA, fluorescent immunoassays are more sensitive by widening the dynamic range of the assay and by measuring absorbance and fluorescence in different ways [8]. The fluorescence-based modular water analysis system developed in the frame of the project Aquafluosense utilizes this advantage of fluorescence in water monitoring. Innovative approaches in environmental analysis are sensor technologies that exhibit great sensitivity and specificity. The method of total internal reflection ellipsometry (TIRE) in conjunction with competitive and non-competitive direct label-free immunoassay was successfully applied for detection of low molecular weight ZON [9], thus this study reports comparative assessment of immunfluorescent methods and TIRE sensor technique for determination of ZON.

Experimental

The ZON standard, goat anti-rabbit IgG–HRP (horseradish peroxidase) conjugate as secondary antibody and salts for buffers were purchased from Sigma-Aldrich Inc. (St. Louise, MO, USA). Zearalenone-6'-carboxymethyloxime-bovine serum albumin conjugate (ZON-BSA), immunization in rabbit and serum collection, purification of rabbit anti-ZON IgG as primary antibody were prepared based on literature [10].

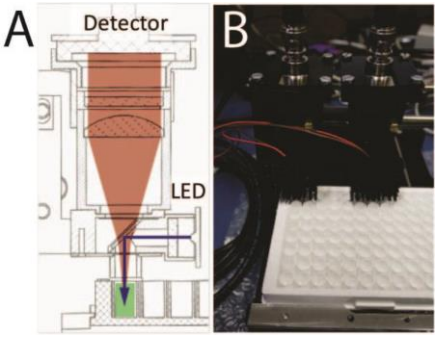

Figure 1. Schematic view of the ELISA plate compatible sensor head (A). Photo of the ELISA plate compatible instrument (B).

Immunoassays were carried out in high capacity 96-well microplates (Nunc, Roskilde, Denmark) for colorimetric assay and in low profile 96-well (white wells for increased fluorescence) PCR plates (Bio-Rad Laboratories, Hercules, CA, USA) with self-designed holder printed by 3D printer by Budapest University of Technology and Economics for ELFIA. QuantaRed Enhanced Chemifluorescent HRP Substrate Kit was used as last step in immunoassays (Thermo Fisher Scientific Inc., Waltham, MA USA). The kit contains 10-acetyl-3,7-dihydroxyphenoxazine (ADHP), a non-fluorescent compound that is dehydrogenated (oxidized) by HRP to resorufin, a highly fluorescent reaction product. Also, resorufin can be measured on a colorimetric plate reader. Absorbances were read by SpectraMax iD3 Multi-Mode Microplate Reader (Molecular Devices, San Jose, CA, USA) at 576 nm wavelength. Relative fluorescent signs were determined by the prototype (Fig 1. A,B) equipped with CREE XPEBGR-L1-0000-00F01 LED (520-535 nm min-max dominant wavelength) as light source and FF01-593/40-25 output filter (peak: 593 nm, width: 40 nm) developed in Aquafluosense project [11].

In an indirect competitive ELISA format, plates were coated with 1 µg/ml bovine serum albumin-ZON conjugate (BSA-ZON) in carbonate buffer (15 mM Na_2CO_3, 35 mM $NaHCO_3$, pH=9,6) overnight at 4°C. Blocking was carried out with 1% gelatine in phosphate buffer saline without Tween20 (137 mM NaCl, 2,7 KCl, 10 mM $Na_2HPO_4x2H_2O$, pH=7.4) at 37°C for 1.5 hours. After 4 times washing 50 µl/well of both ZON dilution series and antiserum (rabbit, dilution 1:1000) were added and incubated at 37°C for 1 hour. After washing 100 µl/well goat anti-rabbit-HRP (dilution 1:7500) were added and incubated for 1 hour at 37°C. The unbound fraction of the labeled secondary antibody was washed out with PBS, and QuantaRed Enhanced Chemifluorescent HRP Substrate Kit was used as substrate to get detectable fluorescence product and color. The process was ended with a stop solution supplied in the fluorescence kit. As this immunoassay is a competitive format, the higher the ZON concentration in the sample, the lower analytical signal is recorded. Assays were performed in triplicates.

Results and discussion

Indirect competitive ELISAs were performed to determine ZON calibration curve and the limit of detection (LOD) was found to be 0.4 ng/ml for ZON, and the detection range was investigated in a concentrations series of 0.004 pg/ml – 2 µg/ml ZON. After the colorimetric assay the liquid phase was transferred with 8-channel pipette to low profile 96-well PCR plate where fluorescence was determined. ZON at concentration of 2000 ng/ml triggered complete inhibition (no free primary antibody remained to connect to BSA-ZON conjugate coated on to the surface of the plate, thus the immunocomplex between the coating antigen and the primary antibody could not be formed), it was applied as background in determination of relative fluorescence sign. Calibration curves and LODs were determined for absorbance and fluorescence (Figure 2.). For comparable representation relative analytical signs are presented.

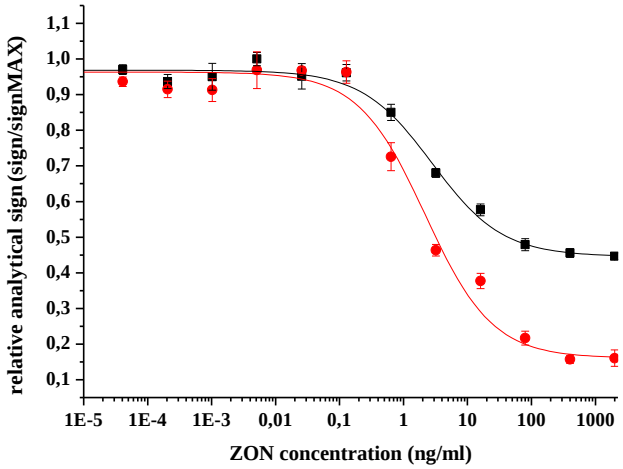

Figure 2. Competitive indirect calibration curves for zearalenone (ZON) determined by absorbance (■) and fluorescence (●).

Different LOD values were calculated for the two analytical signal, LOD = 0.6 and 0.4 ng/ml for visual absorbance and fluorescence detection, respectively. Determination by fluorescence provided a wider and steeper dynamic range, thus ELFIA proved to be a more sensitive method than the corresponding ELISA. Parameters of the sigmoid curves are presented in Table 1. For a colorimetric assay, application of QuantaRed Enhanced Chemifluorescent HRP Substrate Kit with HRP enzyme reaction provided lower LOD than o-phenylenediamine dihydrochloride (OPD) as chromofore (LOD for OPD=0.85 ng/ml).

Table 1. The correlation equation and parameters of sigmoidal calibration curves performed by absorbance and fluorescence detection for zearalenon determination.

Equation for fitting:

$$y = A_2 + (A_1-A_2)/(1 + (x/x_0)^p)^*$$

Adjusted R^2: 0.99037 (absorbance)
0.98804 (fluorescence)

		Value±standard deviation
Absorbance	A_1	0.97±0.01
	A_2	0.45±0.01
	x_0	2.81±0,48
	p	0.79±0.12
Fluorescence	A_1	0.96±0.02
	A_2	0.16±0.03
	x_0	2.20±0.53
	p	0.83±0.19

* A_1: upper platau, A_2: lower platau, x_0: IC_{50}, 50% inhibition, p: power.

Results determined by ELFIA were compared to corresponding results in sensor technology total internal reflection ellipsometry (TIRE) [9]. The sensor surfaces were prepared by a thermal evaporation of layers of chromium (Cr) – 3 nm thick and gold (Au) – 25 nm on standard microscopic glass slides. The Au-surface was modified with mercaptoethyl sodium sulfonate to enhance the negative surface change. For competitive immunoassay, zearalenone-6'-carboxymethyloxime-ovalbumin conjugate (ZON-OVA) was electrostatically immobilized on the Au-surface via a polyallylamine hydrochloride layer. In order to block all the remaining binding sites, an additional adsorption of OVA was carried out. Then a mixture of ZON-specific antiserum and solutions of free ZON (0.01 ng/ml – 10 µg/ml) were injected. The mixtures were pre-incubated for 5 min before injecting (Figure 4). The LOD value for TIRE was 0.01 ng/ml.

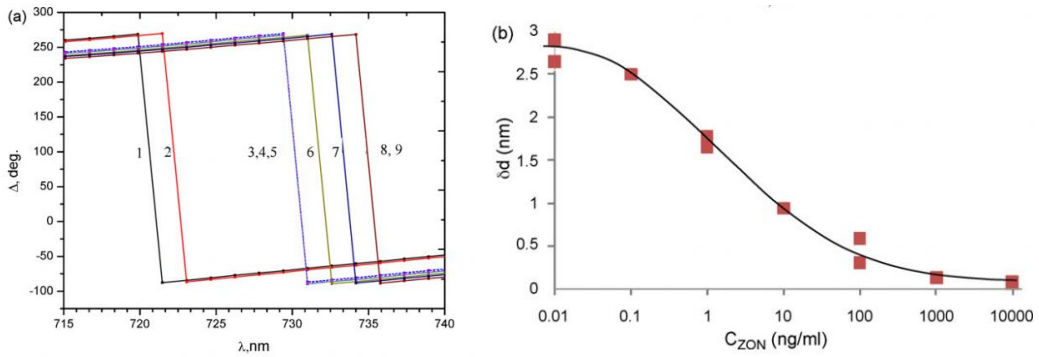

Figure 4. Competitive immunoassay for zearalenone carried out by detection via total internal reflection ellipsometry (TIRE). (a) A typical set of Δ(λ) spectra measured on bare Au surface (1), polyallylamine hydrochloride (2) ZON-OVA conjugate (3), OVA (4), Ab-ZON of from pre-incubated mixtures containing ZON: 100 ng/ml (5), 10 ng/ml (6), 1 ng/ml (7) and 0.1 ng/ml (8). (b) Changes in the adsorbed layer thickness versus the concentration of ZON (in the mixture with Ab-ZON) obtained by fitting the TIRE data.

Conclusion

Within project Aquafluosense, successful development provides a modular instrumentation setup for fluorescence-based determination of several characteristic parameters of water quality. Application of fluorescence, as an analytical signal in an enzyme-linked immunoassay format results in a method of improved sensitivity with a lower LOD value than in the

colorimetric assay. This benefit allows determination of lower pollutant concentrations in surface water, which contributes to a more effective monitoring technique. Although a sensor technology, total internal reflection ellipsometry provides orders of magnitude lower LOD than the immunofluorescent method developed, it is not appropriate for *in situ* determination due to its special laboratory instrumentation need and its limit in number of samples measureable simultaneously. In contrast, the 96-well microplate format in the immunofluorescent determination allows an assay capacity of 25 samples in parallel in triplicates (with standard curves of 7 calibration points).

Acknowledgements

This work was supported by the National Research, Development and Innovation Fund of Hungary within the National Competitiveness and Excellence Program in project NVKP_16-1-2016-0049 “Development of a modular, direct and immunofluorimetry as well as plasma spectroscopy based detector and instrument family for in situ, complex water quality monitoring, and application studies” (Aquafluosense) 2017-2021.

References

[1] European Council, Directive 2000/60/EC of the European Parliament and of the Council, establishing a framework for community action in the field of water policy. Off. J. L327 (2000) 1-73.
[2] *http://aquafluosense.hu*
[3] K. Gromadzka, A. Waśkiewicz, P. Goliński, J. Świetlik, Water Res. 43(4) (2009) 1051-1059.
[4] G.V. Turner, T.D. Phillips, N.D. Heidelbaugh, L.H. Russel, J. Assoc. Off. Anal. Chem. 66 (1983) 102.
[5] P.M. Scott, J.W. Lawrence, W. van Walbeek, Appl. Microbiol. 20 (1970) 839-842.
[6] D.R. Thouvenot, R.F. Morfin, J. Chromatogr. 170 (1979) 165-173.
[7] J.J: Pestka, M.N. Abouzied, Food Technol. 49 (1995) 120-128.
[8] J.R. Lakowicz in: J.R. Lakowicz (Ed.), Springer, Boston, MA., 2006, pp. 623-673.
[9] A. Nabok, A. Tsargorodskaya, M.K. Mustafa, I. Székács, N.F. Starodub, A. Székács, Sens. Actuators B 154 (2011) 232-237.
[10] A. Székács, N Adányi, I. Székács, K. Majer-Baranyi, I. Szendrő, Appl. Optics 48 (2009) B151-158.
[11] D. Csősz, S. Lenk, A. Barócsi, et al., OSA Technical Digest. Optical Society of America (2019), paper JW3A.29.

ADSORPTION KINETICS AND MECHANISM ANALYSIS OF CYAN PRINTING DYE ON POLYETHYLENE MICROPLASTICS

Vesna Gvoić[1], Maja Lončarski[2], Aleksandra Tubić[2], Sanja Vasiljević[2], Dejan Krčmar[2], Jasmina Agbaba[2], Miljana Prica[1]

[1]Department of Graphic Engineering and Design, Faculty of Technical Sciences, University of Novi Sad, Trg Dositeja Obradovića 6, 21000 Novi Sad, Serbia
[2]Department of Chemistry, Biochemistry and Environmental Protection, Faculty of Sciences, University of Novi Sad, Trg Dositeja Obradovića 3, 21000 Novi Sad, Serbia
e-mail: kecic@uns.ac.rs

Abstract

Printing on polymer materials might result with generation of coloured wastewater, enriched with a certain amount of microplastics in a form of polyethylene or polypropylene. In that way, microplastics may acquire the function of carriers of synthetic dyes, heavy metals and other polluting substances. In this paper, kinetics and adsorption mechanism of printing Cyan dye on polyethylene (powdered and granulated), as one of the most common types of microplastics, were investigated. The experiments were performed in a batch mode, in laboratory conditions. Based on the obtained results, a similar adsorption rate degree of selected printing dye was determined on granulated (adsorbed amount was 48.04 μg/g) and powdered material (adsorbed amount was 44.32 μg/g). The adsorption data were fitted well by pseudo-second-order kinetics, while isotherm studies were evaluated using two models: Langmuir and Freundlich. Freundlich and Langmuir equations showed similar performances to fit the solid/liquid distribution of Cyan dye on powdered polyethylene (R^2 = 0.987), whereas Langmuir equation showed slightly better performances for granulated polyethylene than Freundlich equation.

Introduction

Plastic size particles less than 5 mm in diameter, defined as microplastic particles (MPs), are becoming an emerging pollutants due to their ubiquitous interaction with the biotic and abiotic environment. Furthermore, MPs are often added to industrial products, such as dyes, which may be released into the environment after use [1]. The existence of MPs in water bodies has become a concern of researchers in recent years due to their strong sorption capacity for many contaminants: antibiotics [2], polychlorinated biphenyls [3], polycyclic aromatic hydrocarbons [4], heavy metals [5], organochlorine pesticides [6], steroid estrogens [7], etc. Thus, MPs may influence the fate, transport and bioavailability of contaminants in the environment, threatening the ecosystem health. However, little effort has been made to address the adsorptive role of MPs for dyes and the associated underlying interaction mechanisms.

Cyan dye belongs to the group of phthalocyanine dyes, which are characterized by chromophore in a form of four isoindole units linked by nitrogen atoms. It is a derivative of tetrabenzotetraazoporphyrin, complexed with copper metal ion. Due to its high molecular weight and complex structure, phthalocyanine dye is difficult to mineralize. Even discharged into the water bodies with a relatively low concentration, it will be harmful to aquatic organisms [8].

The objectives of this study were to determine adsorption equilibrium and kinetic parameters of Cyan dye on two type of MP particles (powdered (PEp) and granulated (PEg) polyethylene), and to clarify the possible interaction mechanisms between Cyan dye and MPs.

Experimental

Materials. Commercially available MPs in a form of granulated polyethylene (Sigma-Aldrich) and powdered polyethylene (Thermo Fisher Scientific) were used as sorbents. Experiments were performed with Cyan water-based printing dye (C.I.: PB15:3, CAS number: 147-14-8, chemical formula: $C_{32}H_{16}CuN_8$, molar mass: 576.07 g/mol) manufactured by Flint group. The stock solution of Cyan dye was prepared by dissolving 1 g of dye in 1 L of deionized water. The desired concentration of working solution was prepared by diluting stock solution in deionized water.

Adsorption experiments.

Adsorption kinetic experiments of Cyan dye on PEg and PEp particles were conducted in a batch mode, in laboratory conditions. The effect of reaction time on adsorption behavior was conducted in 30 mL solutions with an initial dye concentration of 100 mg/L by adding 30 mg/L of MPs (PEg and PEp). Dye concentration after adsorption experiments were analyzed on UV/VIS spectrophotometer (Genesys 10S, Thermo Fisher) at time intervals of 10 min, 30 min, 1, 2, 3, 4, 5, 6, 24, 36, 48, 72, 96, 144, 192, 264 and 312 h. In order to determine the relationship between adsorption time and adsorption capacity, as well as to analyze the adsorption mechanism of dye on MPs particles, three kinetic models were applied: pseudo-first order, pseudo-second order and Weber-Morris model [1, 9].

Adsorption mechanism of Cyan dye on MPs was evaluated based on the adsorption isotherms, by using seven different initial dye concentrations (1, 5, 25, 50, 100, 150 and 200 µg/L), at a constant sorbent mass of 30 mg. After constant stirring of 72 h, the samples were filtered through a cellulose acetate membrane filter with a porosity of 0.45 µm, and residual dye concentration was determined on a UV/VIS spectrophotometer. The obtained results were analyzed using Freundlich and Langmuir adsorption isotherm models [1].

Results and discussion

Figure 1 shows the adsorption of dye by MPs with increasing reaction time during 312 h. The adsorption of Cyan dye on PEg increased rapidly in first 24 h, then the rate of adsorption slowed down, and equilibrium was reached at 48 h. However, equilibrium between Cyan dye and PEp is established after 72 h.

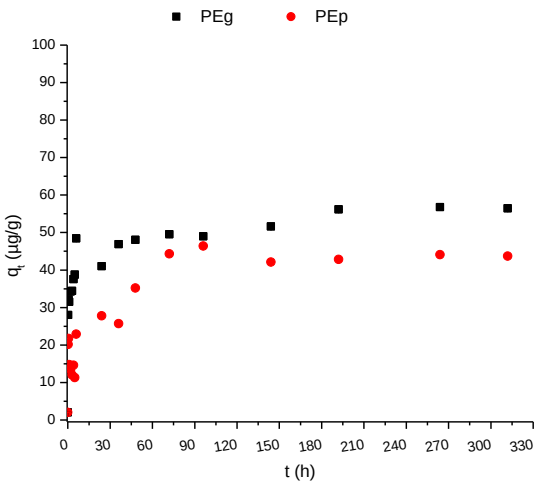

Figure 1. Effects of reaction time on the Cyan adsorption on PEg and PEp

The obtained results indicate that Cyan dye achieved a similar adsorption affinity for both type of MPs, since the adsorbed amount of Cyan on PEg and PEp at equilibrium state were 48.04 µg/g and 44.32 µg/g, respectively. Therefore, the adsorption efficiency is mostly influenced by the type of MPs, while particle size is not crucial.

Three kinetic models were used to describe the adsorption rate and mechanism during adsorption processes of Cyan dye on PEg and PEp: pseudo-first order, pseudo-second order and Weber-Morris model. As shown in Figure 2 and Table 1, the adsorption kinetics were better fitted by pseudo-second-order model (R^2 = 0.958 - 0.999) than pseudo-first-order model (R^2 = 0.332 - 0.606). This indicates that chemisorption was the leading force for the adsorption of dyes on MPs, as well as the adsorption process involves the interaction affinity between sorbents and sorbates [10].

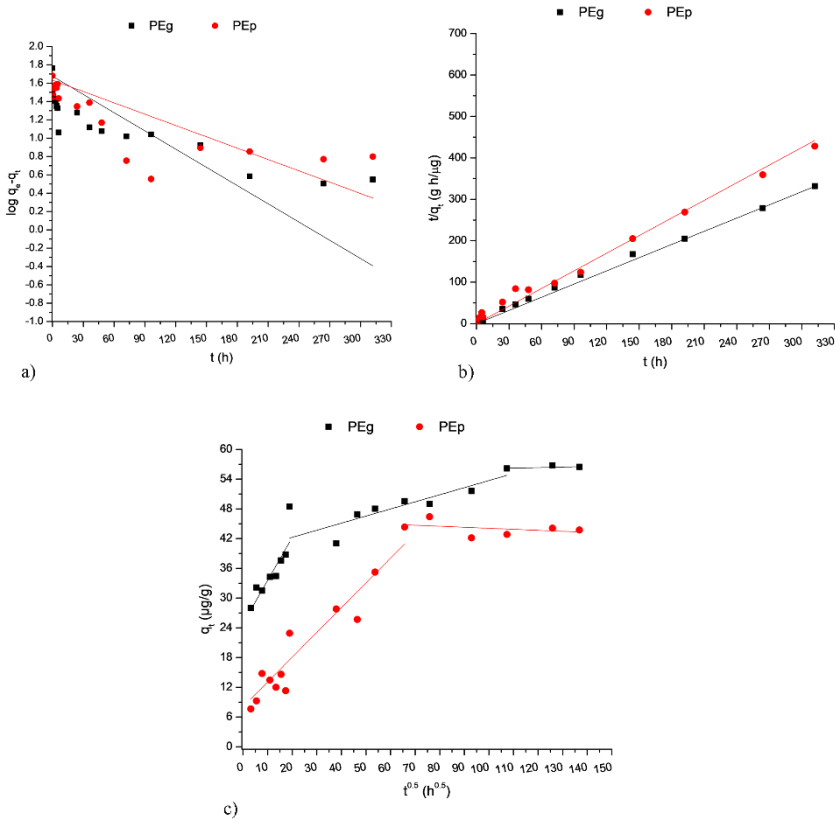

Figure 2. Adsorption kinetic models: (a) pseudo-first-order, (b) pseudo-second-order, (c) Weber-Morris

Table 1. Pseudo-first-order and pseudo-second order kinetic model related parameters

MPs	**Pseudo-first order**			**Pseudo-second order**			
	[a]k_1 (1/h)	[b]q_e (µg/g)	[c]R^2	[d]k_2 (g/µg h)	R^2	[e]q_e (theor.)	q_e (exper.)
PEg	0.00663	5.380	0.332	0.185	0.999	43.200	44.100
PEp	0.00412	5.100	0.606	0.248	0.958	57.100	56.500

[a]k_1 - rate constant of first-order sorption; [b]q_e - adsorption capacity; [c]R^2 - correlation coefficient; [d]k_2 - rate constant of second-order sorption; [e]q_e - equilibrium adsorption coefficient

In order to confirm the validity of the pseudo-second order kinetic model, the experimentally obtained values of the equilibrium adsorption coefficient (q_e experimentally) were compared with theoretical (q_e theoretical) values. Based on the results shown in Table 1, a good agreement is observed, which confirms the fact that Cyan dye adsorption is conducted with chemisorption mechanism on selected types of MPs [11].

In order to explain the complicated adsorption mechanism, including intraparticle diffusion and liquid film diffusion, Weber-Morris kinetic model was used for supplementary interpretation. Based on the results of Weber-Morris kinetic model (Table 2 and Figure 2c) it was determined

that the correlation curves do not pass through the coordinate origin, suggesting that the rate-limiting process was not completely controlled, but probably affected by intraparticle diffusion [12].

Table 2. Weber-Morris kinetic model related parameters

MPs	**[a]K_i (µg/g $h^{1/2}$)**	**[b]C_i (µg/g)**	**R^2**
PEg	0.500	8.086	0.884
	0.020	46.130	0.035
PEp	0.870	24.910	0.850
	0.110	39.400	0.711
	0.090	55.070	0.108

[a]K_i - intraparticle diffusion rate constant;
[b]C_i - thickness liquid film constant

The two-stage and three-stage linear plots in Figure 2c reveal the importance of external mass transfer between the solid and liquid phase, which is explained by the sorbate movement through the aqueous matrix towards the MPs particles, their gradual adsorption on sorbent particles and the establishment of equilibrium state [9]. In that way, adsorption/desorption dynamic equilibrium processes are established for the adsorption of Cyan dye on PEg and PEp particles.

The Langmuir and Freundlich adsorption isotherm models were used to describe the interaction behavior between sorbents and sorbates within the equilibrium states (Figure 3 and Table 3).

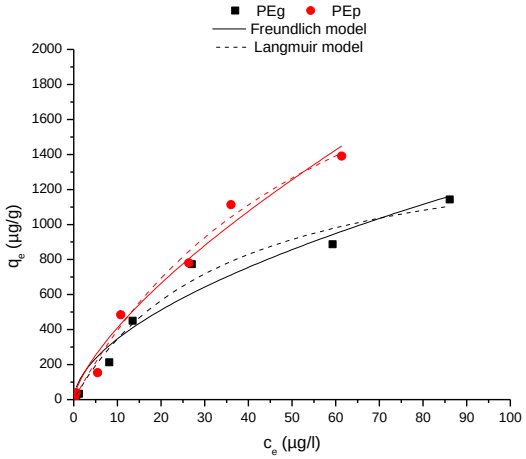

Figure 3. Adsorption isotherms of Cyan dye on PEg and PEp

Table 3. Adsorption isotherms model and related parameters

MPs	**Freundlich model**			**Langmuir model**		
	[a]K_F $(µg/g)/(µg/l)^n$	[b]n	[c]R^2	[d]K_L (l/µg)	[e]q_{max} (µg/g)	R^2
PEg	95.2	0.56	0.947	0.03	1535.9	0.973
PEp	82.7	0.70	0.987	0.02	2874.4	0.987

[a]K_f - Freundlich equilibrium constant; [b]n - adsorption capacity; [c]R^2 - correlation coefficient;
[d]K_L - Langmuir equilibrium constant; [e]q_{max} - maximum adsorption capacity

The Langmuir model achieved a better linear fit for PEg (R^2 = 0.973), indicating that the adsorption occurs on the adsorbent surface with uniform distribution of binding sites. Moreover, the *n* value in Freundlich model is less than 1 for both sorbents, which indicates that the adsorption is chemical process. Furthermore, it was established that adsorption affinity

decreases with covering of available active sites on the MPs surface. Certainly, most adsorption studies preferred to use both of the above isotherm models for data fitting [13].

Conclusion

The present study investigates the adsorption behavior and mechanism of Cyan printing dye on granulated and powdered polyethylene. The adsorption process of dye on microplastics followed the Langmuir isotherm model and the pseudo-second-order kinetics, indicating that monolayer adsorption is mainly controlled by chemical process. Furthermore, Weber-Morris model pointed out to multi-stage adsorption process, revealing that intraparticle diffusion is a limiting factor for the adsorption process. Based on the obtained results, a role of microplastics as a carrier for selected printing dye, if they are released uncontrolled into the environment, is confirmed. Further investigations regarding release of various types of microplastic and printing dyes under different environmental conditions, their interaction and water treatment should be considered.

Acknowledgements

This research has been supported by the Provincial Secretariat for Science and Technological Development, Autonomous Province of Vojvodina through the project: “Synthetic dye removal in the presence of microplastics in advanced water treatment” (Grant No. 142-451-3186/2020-03).

References

[1] H. Li, F. Wang, J. Li, S. Deng, S. Zhang, Chemosphere 264 (2021) 128556.
[2] F. Yu, C. Yang, G. Huang, T. Zhou, Y. Zhao, J. Ma, Sci. Total. Environ. 721 (2020) 137729.
[3] M. A. Fraser, L. Chen, M. Ashar, W. Huang, J. Zeng, C. Zhang, D. Zhang, Ecotox. Environ. Safe. 196 (2020) 110536.
[4] L. Mai, L-J. Bao, L. Shi, L-Y. Liu, E. Y. Zeng, Environ. Pollut. 241 (2018) 834-840.
[5] X. Guo, J. Wang, J. Hazard. Mater. 402 (2021) 123709.
[6] F. Wang, J. Gao, W. Zhai, D. Liu, Z. Zhou, P. Wang, J. Hazard. Mater. 394 (2020) 122517.
[7] B. Hu, Y. Li, L. Jiang, X. Chen, L. Wang, S. An, F. Zhang, J. Hazard. Mater. 400 (2020) 123325.
[8] V. Gvoić, M. Prica, Đ. Kerkez, M. Bečelić-Tomin, A. Kulić Mandić, A. Leovac Maćerak, B. Dalmacija, Acta Periodica Technologica 50 (2019) 77-85.
[9] S. Azizian, J. Colloid. Interface. Sci. 276 (2004) 47-52.
[10] G. Liu, Z. Zhu, Y. Yang, Y. Sun, F. Yu, J. Ma, Environ. Pollut. 246 (2019) 26-33.
[11] Z-Z. Bao, Z-F. Chen, Y. Zhong, G. Wang, Z. Qi, Z. Cai, Sci. Total. Environ. In Press. doi: 10.1016/j.scitotenv.2020.142889.
[12] W. Wang, J. Wang, Chemosphere 193 (2018) 567-573.
[13] T. Huffer, T. Hofmann, Environ. Pollut. 214 (2016) 194-201.

DETECTION OF CHANGES IN SOLUBLE ORGANIC MATTER CONTENT IN MUNICIPAL THICKENED SLUDGE BY DIELECTRIC MEASUREMENTS

Laura Haranghy, Zoltán Jákói, Cecília Hodúr, Sándor Beszédes

University of Szeged Faculty of Engineering, Department of Process Engineering, Moszkvai krt. 9, H-6725 Szeged, Hungary.
e- mail: haranghylaura@gmail.com

Abstract
The dielectric measurement is a rapid and non-destructive method to investigate the physicho-chemical change in the examined materials. Many researches observed the dielectric properties of pure water, different materials from the food industry, but there is less information about the dielectric charachteristic of wastewater and sludge. Our study aims to detect correlation between dielectic constant and SCOD/TCOD parameter, to verify if different microwave irradition treatments can enchance the solubilization of organic matter in municipal sludge. With the detemination of soluble chemical oxygen demand (SCOD) we detect the effects of different microwave irradition treatments on the sludge‘s organic matter solubility. Our results show dielectric measurement is a suitable method to detect the changes in the soluble organic matter content, since there is a strong linear correlation between the dielectric constant (ε‘) and the SCOD/TCOD parameter, which indicates the the solubility of the organic matter.

Introduction
Due to the urbanization, the increasing amount of consumed water quantity, even though the developing wastewater treatment plants, the amount of municipal sludge is increasing. Because of the high cost of operating and treatment proccesses, it should be taken into consideration to utilize the arising amount of sludge. For economic reasons the application of different pre-treatment technologies are required.
Microwave (MW) irradition is a promising pre-treatment method in sludge treatment, as a result of its unique heating mechanism which provides a fast and selective heating ability [1]. Due to its thermal effect it can disrupt the cell wall of pathogene microorganisms, thereby enhance the disposal of sludge. The released cellular fluid contains proteins, carbohydrates and lipids originated from the bacteria presented, which increases the organic matter content of the sludge, therefore it becomes more avaible for the degrading microorganisms [2]. The SCOD/TCOD parameter describes the ratio between the amount of organic matter in the soluble phase and the total chemical oxygen demand of the observed sample.
Dielectric materials, like the municipal sludge can absorbe the microwave interval of the electromagnetic spectrum , and its extent depends on the material properties, structure, temperature and frequency. The dielectric behaviour of a material can be described with certain dielectric properties.
Complex relative permittivity (ε) includes the charachteristics that affect the reflection of electromagnetic waves from the material interface, as well the energy loss that occurs with the absorption of the electromagnetic wave [3]:

$$\varepsilon = \varepsilon' - j \cdot \varepsilon'' \quad (1)$$

The dielectric constant (ε') represents the electrical energy absorption capacity of the dielectrical material, the dielectric loss factor (ε") describes the dissipation ability of the dielectric material and *j* is the imaginary factor.
The product of free space permittivity (ε_0) and the relative permittivity (ε_r') gives the dielectric constant:

$$\varepsilon' = \varepsilon_0 \cdot \varepsilon'_r \quad (2)$$

It has been proven that measuring dielectric properties is a capable way of determine structural and/or molecular changes in the raw material matrix, and such, it is a suitable method todetect the organic matter removal effiency of wastewater treatment proccesses [4]. By the application of this rapid, non-destructive measurement method the efficiency of different pre-treatment processes could be estimated.

Experimental

Municipal thickened sludge samples were being used in our experiments. The samples were pre-treated by microwave irradition with a total energy intensity of 30, 45 and 60 kJ at two different power levels (250 and 500 W), with the corresponding the irradition time of 1-4 minutes. For the microwave treamtments a Labotron 500 laboratory scale microwave equipment was used.

For the dielectric measurments a DAK 3.5 (SPEAG) open-ended coaxial dielectric probe was being used, connected to a ZVL-3 vector network analyser (Rohde&Schwarz). The dielectric properties were measured in the frequency range of 200-2400MHz.

Based on previous studies focusing on the determination of soluble chemical oxygen demand (SCOD), we applied the organic matter fractionation method, i.e. sedimentation, centrifugation (RCF=6000 for 10 minutes) and filtration (0,45μm pore sized PTFE disc filter),which was followed by a colorimetric method (Hanna, COD cuvet test, after 2 hours thermodigestion at 180 °C) to determine the exact values of SCOD

Results and discussion

The aim of our work was to investigate the correlation between the dielectric constant and an indirect parameter, the soluble chemical oxygen demand (SCOD) which expresses the quantity of biodegradable organic matter content in the soluble phase of wastewater sludge for microorganism.

In the first series of the experiments, after the different energy intensity microwave irradition treatments, we measured the dielectric constant (ε‘) in each sample to investigate its frequency dependence:

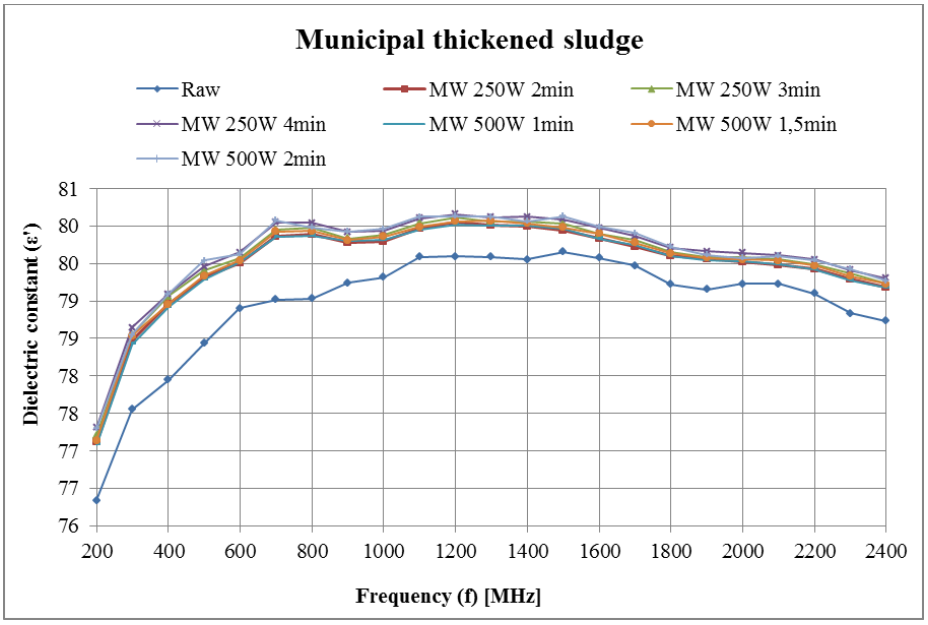

Figure 1. The frequency dependence of the dielectric constant on different MW treatments

In comparison with the raw sample, all different energy intensity MW treatments resulted in higher dielectric constants. The treated samples follow the same tendency and show similar ε‘ values on most of the measuring frequencies. Despite similarity it can be stated that the MW

treatments cause deviation in the dielectric constant. To investigate the extensive effects of the different sludge treatment possibilities on the dielectric constant, further researches are suggested in this topic.

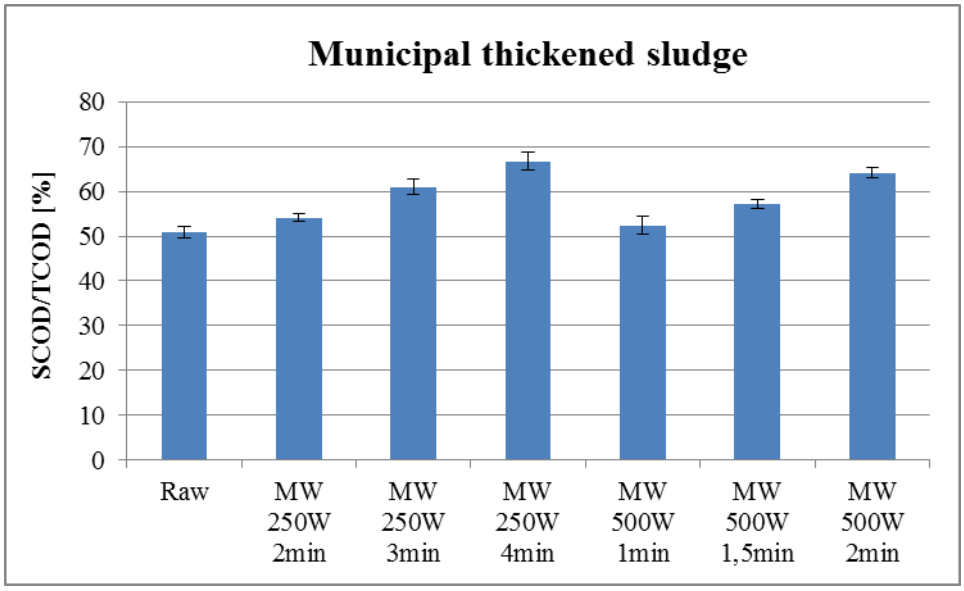

Figure 2. The effect of different MW treatments on SCOD/TCOD.

The SCOD/TCOD results show that the higher energy intensity treatments cause higher solubilition of the organic matter, the effiency grows with the increase of the irradiated energy (Figure 2.). Treatments where lower power level (250W) was applied were more effective than those where it was set at500W.

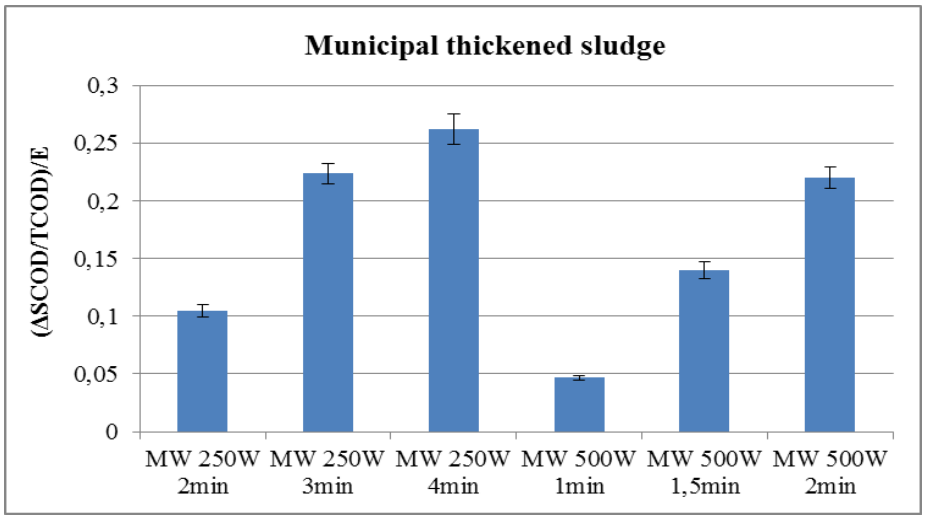

Figure 3. Increase of SCOD/TCOD compared to control sample.

Figure 3. depicts how different treatments affect the SCOD/TCOD parameter in comparison with the raw control. The values was divided by the irradiated energy to create a specific parameter to show the real tendencies of certain treatments. It shows that lower power level (250W) treatments – considering the SD range as well - were observably more effective than the ones which were carried out with the higher level of power (500W) The 250W-4 minutes MW irradition turned out to be the most efficient operational setup, as it resulted in an increase

of more than 50% in regards of the solubility of the organic compounds, compared to the sample which was irradiated for half the time at the same power level.

After the MW irradiaton treatments each sample was cooled to the temperature of 28°C to carry out the dielectric measurements. The results of dielectric measurements show that the dielectric constant at the frequency of 2400 MHz has a linear correlation with the SCOD/TCOD (Figure 4):

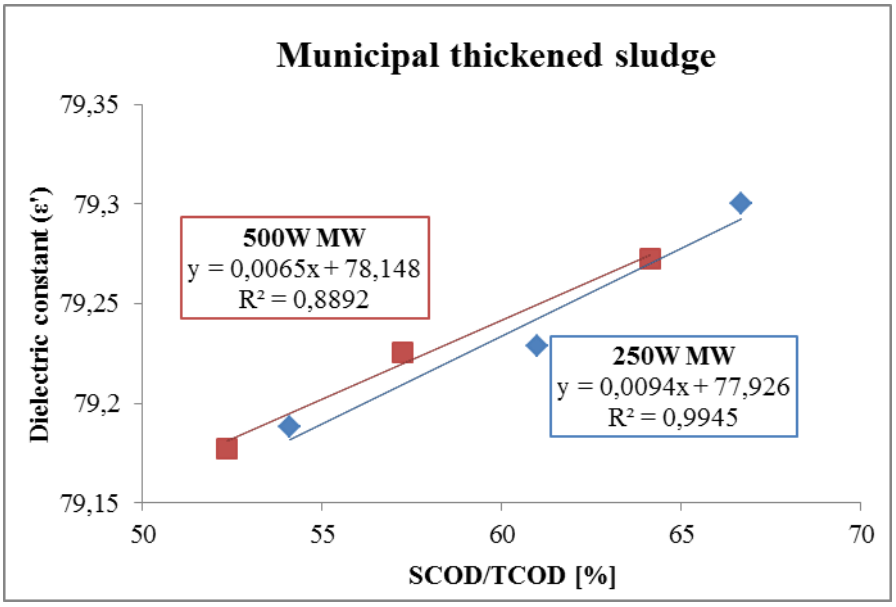

Figure 4. The correlation between SCOD/TCOD and dielectric constant (f = 2400 MHz, temperature of 28°C).

The higher organic matter solubility can be traced back to the degradation effect of the microwave irradition on the solid particales and the macromolecules of the sludge. By detecting the change of the dielectric constant, it can be stated that the irradiation caused flake desintegration in the treated sludge samples [5].

Conclusion

In this study we compared the efficiencies of different energy and power intensity MW treatments on the solubility of organic matter in wastewater sludge samples. Based on our results, microwave irradiation is proved to be an applicable sludge pre-treatment method, since it affects the SCOD/TCOD parameter in a way which indicates that the solubility of the organic compounds of the municipal thickened sludge is enhanced in the soluble phase. In order to gain a more detailed understanding of how microwave irradiation affects the material matrix of sludge, i.e. whether a correlation between biodegradability indicators (e.g. BOD/SCOD) and the MW-enhanced solubility is presented, further researches are recommended.

Our research also focused on to investigate a possible correlation between the dielectric constant (ε‘) and a solubility indicator (SCOD/TCOD). It can be stated that with the application of dielectric measurement the change in the solubility of organic matter can be detected, since the latter and the change of dielectric constant and shows a linear correlation between each other. The application of open-ended coaxial dielectric probe proved to be a promising detection method to estimate the efficiency of various sludge pre-treatment methods.

Acknowledgements

The work was created as part of the project "Sustainable Raw Material Management Thematic Network—RING 2017" EFOP-3.6.2-16-2017-00010 within the Programme SZECHENYI2020, supported by the European Union, co-financed by the European Social Fund. The authors thank the financial support provided by NKFIH/OTKA K-115691 project.

References

[1] Appels L., Houtmeyers S., Degrève J., Impe J.V., Dewil R: Influence of microwave pre-treatment on sludge solubilization and pilot scale semi-continuous anaerobic digestion. *Bioresource Technology*, 2013, 128, 598-603.

[2] Ahn, J.H., Shin, S.G., Hwang S.:Effect of microwave irradiation on the disintegration and acidogenesis of municipal secondary sludge. *Chemical Engineering Journal*, 2009, 153, 145-150.

[3] S. Chandrasekaran, S. Ramanathan, T. Basak: Microwave Material Processing—A Review. *AIChE Journal*, 2012, 58, 2, 330-363.

[4] Jákói Z., Hodúr C., László Z., Beszédes S.: Detection of the efficiency of microwave–oxidation process for meat industry wastewater by dielectric measurement, *Water Science & Technology*, 2018, 78, 10, 2141-2148.

[5] Kovács V.P., Lemmer B., Keszthelyi-Szabó G., Hodúr C., Beszédes S.: Application of dielectric constant measurement in microwave sludge disintegration and wastewater purification processes, *Water Science & Technology*, 2018, 77, 9)ó, 2284-2291.

CHLOROBENZENE COMPOUNDS AS POSSIBLE IMMUNO-DISRUPTOR AGENTS

Péter Hausinger and Krisztián Sepp, Attila Csicsor*, Marianna Radács, Zsolt Molnár and Márta Gálfi

*Institute of Applied Natural Science, Faculty of Education, University of Szeged Hungary, Department of Environmental Biology and Education, Juhász Gyula Faculty of Education, *Faculty of Sciences and Informatics, Ph.D student of Environmental Sciences University of Szeged*

e-mail: galfi.marta@szte.hu, molnar.zsolt.02@szte.hu

Abstract

Dichlorobenzenes are lipophilic, depositable, colorless liquids that appear as an exposure factor because they are continuously present in households, but are also used in agriculture in large quantities in e.g. insecticides and fungicides. As there is a constant interaction between the living systems and its environment and the internal organizational stability of biological systems is controlled by homeostasis, these agents may disrupt the homeostasis, therefore it is especially important to study the effect of these compounds on the immune system.

Introduction

Dichlorobenzenes (DClB) are lipophilic, depositable, colourless liquids (at T = 25 °C, p = 1 atm) with 3 known isomerization states: ortho-dichlorobenzene (1,2-dichlorobenzene; 1,2-DClB), meta-dichlorobenzene (1,3-dichlorobenzene, 1,3-DClB) and para-dichlorobenzene (1,4-dichlorobenzene, 1,4-DClB) [1,2].

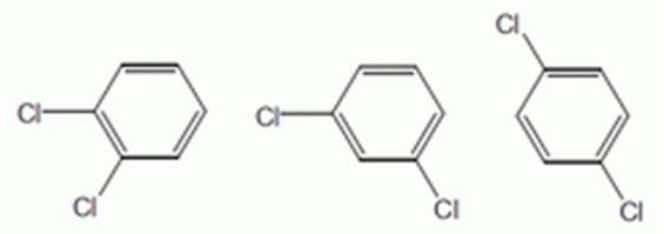

Ortho-DClB meta-DClB para-DClB

Figure 1. Structural formula of ortho-DClB, meta-DClB and para- DClB [1, 2]

DClB can be metabolized in living systems in several ways, e.g. rate of metabolic in human or rat liver: 1,3-DClB → 1,2-DClB → 1,4-DClB. Oral administration of 1,4-DClB, the metabolites in serum were 2,5-dichlorophenyl-methyl-sulfoxide and 2,5-dichlorophenyl-methyl-sulfone [3]. During degradation, para-DClB (PDClB) is hydrolysed to (nephrotoxic) dichlorophenol and then oxidized to dichloro-catechol and dichloro-hydroquinone, which can be further conjugated to glutathione, glucuronic acid and sulfate. These are all hepatotoxic components. 1,4-DClB is less genotoxic [4].

PDClB is a weak antiestrogen via the aryl-hydrocarbon receptor due to estrogen modulation [5]. But sperm destruction, production-reducing and as well as androgenic effects are also known in rats and mice [6]. According to these effects, xenobiotic DClB agents are endocrine disruptor compounds (EDCs). As a fact of exposure, they are very strong because they are constantly present in households (fragrances, fresheners, etc.), but agriculture also uses them in large quantities in insecticides and fungicides, and it is also a raw material in the production of industry and some plastics. The other chlorobenzene (ClB) derivatives are also present in large amounts in the environmental elements, deposited as a function of their stability.

PDClB has become a standard compound of Life Cycle Analysis (LCA) standards, which are the most important basis for environmental safety, and has been used as reference agents in of

Ecotoxicological (ETP) and Human Toxicological Potential (HTP) in impact analyse. These toxicological potentials consistently affect the homeostasis of organisms. The maintenance of human homeostasis, the systemic regulation of psycho-neuroendocrino-immune functions is realised. The dominant element of this is cellular immune function, which is affected by ClB exposures as factors. In this regard, ClBs may be the focus of attention as immune disruptor compounds (IDCs).

Aims

In the present work, we investigated the effects of DClB isomers and hexa-ClB (HClB) on T cell-mediated immunity. We sought to answer the question of whether ClB compounds carry a possible IDC character. Furthermore, did it seem interesting to study why PDClB was chosen by the International Standards as the reference compound?

Methods

In our experiments we used human (♂: 22-34 years) 0 Rh (+) blood group castle samples with healthy physiological parameters, from a portion of heparin (7 IU) anticoagulated blood.
From another part of the heparin blood samples, T lymphocyte transformation activity was tested in whole blood culture. Homogeneous blood samples diluted 10 x in supplemented RPMI-1640 medium were used under sterile conditions in a 96-well plate (p = 5% CO_2, 37 °C). A 180 µl diluted blood sample + 20 µl mitogenic mix (0.1 µg/ml CONA + 1: 1000 PHAP + 0.1 µg/ml PWM) was used as a control. Spontaneous cell transformation was examined in the 180 µl diluted blood sample + 20 µl RPMI-1640 (+suppl.) system. For exposure samples, in the 180 µl RPMI-1640 (+suppl.) diluted blood sample, the test substances (ortho-DClB, meta-DClB, PDClB, HClB) were already present at doses of 0.01 and 0.1 µg/ml, which was supplemented with the +20 µl mitogenic mixture. After 12 and 24 hours of incubation in the treatment protocol, 20 µl of ^{3}H-Thymidine (20 µCi/ml ^{3}H-Thymidine in RPMI-1640) was added to each experimental system for an additional 18 hours.
Evaluation of results:

LySi = stLy cpm / spLY cpm,

in wich:

- Lymphocyte (LY) stimulation index= LySi
- Stimulated Ly transformation cpm (radioactivity)= stLy cpm
- Spontaneous Ly transformation cpm (radioactivity)= spLY cpm

Data were evaluated by ANOVA.

Results

As can be seen from the data in Figure 2, the dose of DClB treatment used inhibited blast transformation.

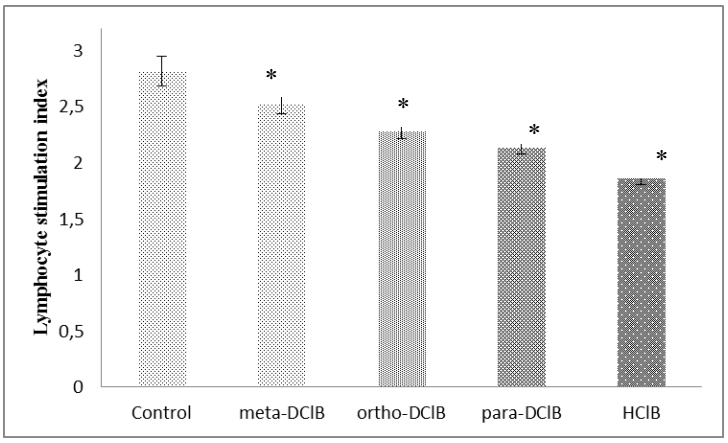

Figure 2. Effects of 0.01 µg/ml DClB isomers on immune function over a 12-hour treatment period (n=5, means±SD, ∗: P<0.001)

It can be seen in the Figure 3, that DClB treatments at a dose of 0.01 µg/ml resulted in a decrease in the lymphocyte stimulation index.

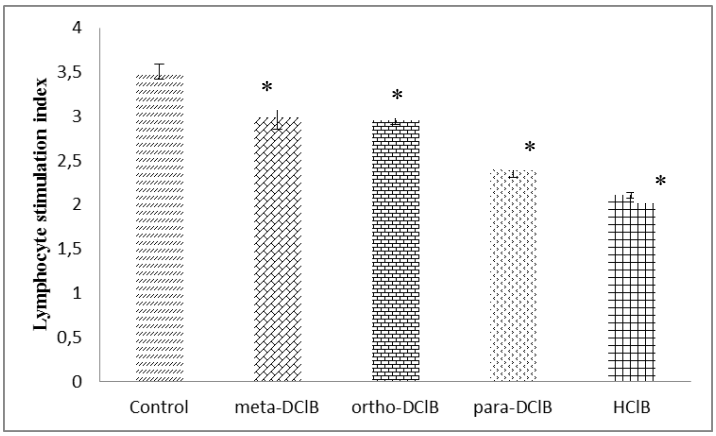

Figure 3. Effects of 0.01 µg/ml DClB isomers on immune function over a 24-hour treatment period (n=5, means±SD, ∗: P<0.001)

In the set experimental protocol, the applied 0.1 µg/ml dose of DClB treatment modulated the blast transformation.

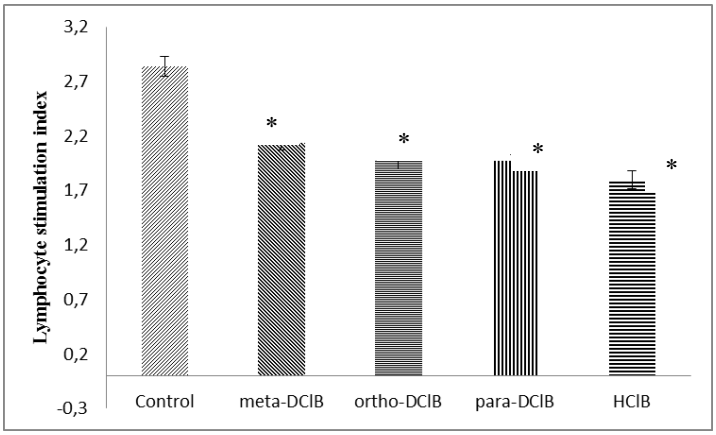

Figure 4. Effect of 0.1 µg/ml DClB isomers on immune function over a 12-hour treatment period (n=5, means±SD, ∗: P<0.001)

Based on the data in Figure 5, the tested DClB isomers significantly reduced the lymphocyte stimulation index during 24-hour treatment.

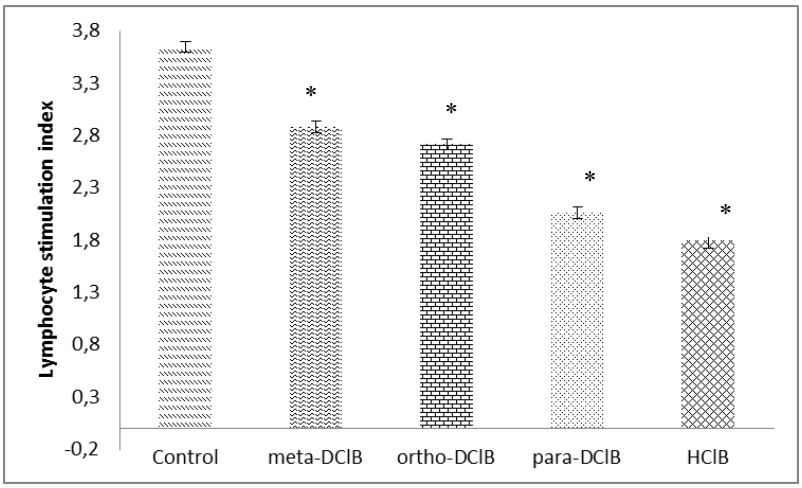

Figure 5. Effect of 0.1 µg/ml DClB isomers on immune function over a 24-hour treatment period (n=5, means±SD, ∗: P<0.001)

Discussion and conclusion

According to our results, in the study of innate immune functions, PDClB proved to be the most potent of the DClB compounds among the DClB isomers, with HClB showing a stronger T-lymphocyte transformation deactivating effect. Because all of the ClB compounds tested were degradative in cellular immunomodulation, these agents could also be treated as IDCs.

Chlorinated benzenes are known to consist of twelve chemicals: one mono-, three di-, three tri-, three tetra-, one penta-, and one hexa-chlorobenzene. Of these, the annual production of 1,4 DClB is the highest in the world [7], and of the DClB compounds, PDClB is the most stable. These two factors: the high xenobiotic presence in society and chemical persistence, combined with lipophilicity, already justify the use of PDClB as a reference compound in the determination of standard toxicity potentials (HTP, ETP).

Acknowledgements

This research was supported by the European Union and the State of Hungary, co-financed by the European Social Fund in the framework of TÁMOP-4.2.4.A/2-11/1-2012-0001 'National Excellence Program', TÁMOP-4.2.6-15/1-2015-0002, TÁMOP-6.1.5-14-2015-0004 and EFOP-3.6.1-16-2016-00008 and EFOP-3.4.3-16-2016-00014.

Reference

[1] USEPA: Ambient Water Quality Criteria Doc: Dichlorobenzenes p.C-14 EPA 440/5-80-039, 1980.

[2] R. Fisher, S. McCarthy, I. G. Sipes, R. P. Hanzlik, K. Brendel, Metabolism of dichlorobenzenes in organ cultured liver slices, Adv Exp Med Biol., 1991, 283, 717-723.

[3] T. Kimura, O. Tanizawa, K. Mori, M. J. Brownstein and H. Okayama, Structure and expression of a human oxytocin receptor. Nature, 1992, 356, 526-529.

[4] US EPA/Office of Pesticide Programs, Reregistration Eligibility Decision (RED) for Para-dichlorobenzene, Health Effects Division Chapter of the Reregistration Eligibility Decision Document (RED). PC Code: 061501, 2007, 11.

[5] O. Takahashi, S. Oishi, M. Yoneyama, A. Ogata, H. Kamimura, Antiestrogenic effect of paradichlorobenzene in immature mice and rats. Arch Toxicol., 2007, 81, 505-17.

[6] O. Takahashi, N. Ohashi, D. Nakae, A. Ogata, Parenteral paradichlorobenzene exposure reduce sperm production, alters sperm morphology and exhibits an androgenic effect in rats and mice. Food Chem Toxicol., 2011, 49, 49-56.
[7] M Morita, Chlorinated benzenes in the environment. Ecotoxicol Environ Saf., 1977, 1, 1-6.

NITROGEN IMPACT ON Cu-Zr-Al(-Ag) BASED MASTER ALLOYS

Petru Hididis [1, a], Mircea Nicolaescu [2, b], Roxana Muntean [1, c], Norbert Kazamer [3, d], Cosmin Codrean [1, e], Viorel-Aurel Serban [1, f]

1"Politehnica" University of Timisoara, P-ta Victoriei, No. 2, Timisoara, Romania
2 National Institute for Research and Development in Electrochemistry and Condensed Matter, no 144 A, Paunescu Podeanu Street, Timisoara, Romania
3 Westfälische Hochschule, Neidenburger Str. 43, 45897 Gelsenkirchen, Germany
[a] petru.hididis@student.upt.ro, [b] mircea.nicolaescu@student.upt.ro, [c] roxana.muntean@upt.ro, [d] norbert.kazamer@w-hs.de, [e] cosmin.codrean@upt.ro, [f] viorel.serban@upt.ro

The use of nitrogen as an alloying element and as a thermochemical treatment called Ønitriding is well known. On the other hand, nitrogen, that is considered as one of the most abundant non-metals from the atmosphere (among oxygen and hydrogen), is considered in metallurgical processes as accompanying chemical element. It is not purposefully inserted in the process and can affect up to 500-2000 ppm of alloys structure and properties. Positive effects of alloying with nitrogen have been recently reported [1-3]. This study is a research on the impact of nitrogen from a controlled atmosphere during production and investigations of Cu-Zr-Al(-Ag) master alloys that are forerunners for glassy alloys with same composition. Producing the master alloys in vacuum resulted in an absence of oxide layer. This allows for an easy diffusion of nitrogen on the master alloys. Effects of nitrogen on the Cu-Zr based ($Cu_{48}Zr_{47}Al_5$ and $Cu_{45}Zr_{45}Al_5Ag_5$) master alloys are investigated. The two button shaped samples were produced using the arc melting technique in an enclosed vacuumed chamber. Microstructural, thermogravimetric (TG) and mechanical investigations were done on both samples. Effects on nitrogen on the master alloys were investigated to observe its impact. To do so, TG analyses were performed in nitrogen atmosphere. The endothermic peaks suggest phase transformation that were later determined by XRD analysis and corresponds to the eutectoid transformation. The high temperature phase B2 CuZr decomposes in a eutectoid manner in two low temperature phases: $Cu_{10}Zr_7$ and $CuZr_2$. Nitrogen has a small atomic radius and a high solubility in some metals (e.g. 25% in Zr) produces an efficient cluster packing structure and thus the nucleation and growth of the crystalline phases can be suppressed and as a result the glass forming ability (GFA) can be improved [3]. Nitrogen presence leads to strong interactions with basic elements of the alloy as reflected by the large positive or negative heat mixing between N-Cu (71 kJ/mol), N-Zr (-78 kJ/mol) and N-Al (63 kJ/mol) binary pairs [3]. This newly formed atomic pairs with strong affinity change the local atom arrangements significantly thus leading to stability of the chemical and topological short-range orderings [3]. This is confirmed by the EDX that shows higher peaks for the Cu, Zr and especially Ag elements after TG. Also results from XRD after TG show strong presence of N_2, ZrN and AlN. Hardness increased on both samples after TG. A fair deduction is that the influence of nitrogen benefits and eases the production of glassy alloys with the same composition. Future studies will establish the optimal interval percent of nitrogen regarding master alloys. These master alloys will allow the production of Cu-Zr based glassy alloys. Such alloys found use in major engineering fields, i.e. consumer electronics, automotive products, medical devices, sporting goods etc. This is a consequence of their distinct mechanical, chemical and technological properties.

References

[1] B. Nabavi, M. Goodarzi, V. Amani, Welding Journal 94(2), 2015, 53s-60s
[2] L. I. D'yachenko, L. V. Fedina, Metal Science and Heat Treatment, Vol. 23, (1981), 668–670
[3] Z. Liu, R. Li, H. Wang, T. Zhang, Journal of Alloys and Compounds 509, (2011), 5033–5037

SYNTHESIS AND CHARACTERIZATION OF SOME N-(4-CHLORO-PHENYL)-2-HYDROXY-BENZAMIDE DERIVATIVES

Ioana M. C. Ienaşcu[1,2], Adina Căta[1], Cristina Moşoarcă[1], Iuliana M. Popescu[3], Mariana N. Ştefănuţ[1]

[1]National Institute of Research and Development for Electrochemistry and Condensed Matter, 144 Dr. A. P. Podeanu, 300569, Timişoara, Romania
[2]"Vasile Goldiş" Western University of Arad, Faculty of Pharmacy, Department of Pharmaceutical Sciences, 86 Liviu Rebreanu, 310045, Arad, Romania
[3]Banat's Agricultural Science University, Faculty of Agriculture, Department of Chemistry and Biochemistry, 119 Calea Aradului, 300645, Timişoara, Romania
imcienascu@yahoo.com

Abstract

Salicylanilides, 2-hydroxy-N-(phenyl)benzamides, represent a group with wide range of biological activities. They have been studied over time on the interest of medicinal chemistry for many interesting effects: act as uncouplers on biomembranes, affect productions of interleukins, regulate an immune response, show analgesic and anti-inflammatory properties, influence ion channels, affect some molecular targets being potentially useful in cancer therapy [1], express moderate hypoglycaemic activity [2], influence the metabotropic glutamate receptors [3]. Also, salicylanilide derivatives are known for their activity against different bacteria, fungi and protozoa, the basic structure is still modulated for antimycobacterial, antifungal and antibacterial activities [1, 4]. Starting from N-(4-chloro-phenyl)-2-hydroxy-benzamide, novel molecules, esters, hydrazides, hydrazones were synthesized under microwave irradiation. The compounds were obtained with good yields (66-97%) after the final purification and were characterized using FTIR, ^{1}H and ^{13}C-NMR. Spectral data unambiguously confirm the proposed structures.

Acknowledgements

This work is part of the project PN 19 22 03 01 / 2019-2022 "Supramolecular inclusion complexes of some natural and synthetic compounds with health applications", carried out under NUCLEU Program funded by National Authority for Scientific Research (Romania).

References

[1] M. Krátký, J.Vinšová, V. Buchta, K. Horvati, S. Bösze, J. Stolaríková, Eur. J. Med. Chem. 45 (2010) 6106.
[2] S.K. Sahu, S.K. Mishra, S.P. Mahapatra, D. Bhatta, C.S. Panda, J. Indian Chem. Soc. 81 (2004) 258.
[3] P.J. Conn, C.W. Lindsley, C.K. Jones, Trends Pharmacol. Sci. 30 (2009) 25.
[4] I.M.C. Ienaşcu, D. Obistioiu, I. Popescu, M.N. Ştefănuţ, G. Osser, C. Jurca, G. Ciavoi, E. Bechir, F. Bechir, A. Căta, Revista de Chimie, 70 (2019), 1496.

PHOTODEGRADATION OF RHODAMINE B BY WO_3/GLASS FOAM VISIBLE-LIGHT THIRD GENERATION PHOTOCATALYST

Madalina Ivanovici[1,2], Florina-Stefania Rus[1], Paulina Vlazan[1], Paula Svera(Ianasi)[1], Stefan Danica Novaconi[1]

[1]National Institute for Research and Development in Electrochemistry and Condensed Matter, 300569 Timisoara, Aurel Paunescu Podeanu Street No. 144, Romania
[2]Politehnica University of Timisoara, 300006 Timisoara, Piata Victoriei No. 2, Romania
e-mail: ivanovicigabriela11@yahoo.com

Abstract

This work focused on the evaluation of the photocatalytic activity of the glass foam, a chemically and physical stable support, coated with WO_3–visible-light photoactive compound for degradation of rhodamine B. In this way, the removal of the rhodamine B in aqueous solution by WO_3/glass foam was compared with the removal of rhodamine B by uncoated glass foam during the experimental stages of the photocatalytic tests: adsorption and visible-light irradiation. The uncoated sample presented no photocatalytic activity, whereas WO_3/glass foam removed approximately 33% of rhodamine B from aqueous solution. Physical and chemical characterization of the photocatalyst was carried out by 3D scanning microscopy and energy dispersive X-ray spectroscopy (EDAX) coupled with scanning electrone microscopy (SEM).

Introduction

Tungsten trioxide is one of the representative visible-light active photocatalyst and also materials based on the WO_3 were developed and investigated for their photocatalytic properties in the visible spectral range as a need to overcome the dependence on the UV electromagnetic radiation [1]. In order to enhance the efficiency and the potential application, research studies were conducted to develop photocatalyst that involve their immobilization on different supports or preparation of films. The advantage of this type of photocalysts (known as the third generation of photocatalysts) compared to nanoparticles, is given by the fact that it is not required an additional procedure for separating the photocatalyst from aqueous solution eliminating the cost and the disadvantages associated with the separation techniques such as incomplete separation and loss of photocatalytic activity. Different supports were involved in designing immobilized photocatalyst including steel, SiO_2, glass, FTO glass, glass foam.

Glass foam is a material which has gained a lot of interest mostly as an insulating material in the construction industry, but the combination of various properties such as chemical and biological stability, porous and rigid structure makes it attractive as an absorber, sound insulator and as support for photocatalysts, suitable for environment application such as water and air purification [2-6].

The aim of the present work was to investigate the ability of WO_3 immobilized on the glass foam to remove rhodamine B (RhB) by a photodegradation process. Considering the chemical stability and the toxicity of the RhB, it has been selected as a substance to degrade and to evaluate the photocatalytic activity of the WO_3 supported on the glass foam.

Experimental section

Different samples were obtained as described in a previous study [7] and involved for a comparative evaluation of photocatalytic properties: glass foam (0.750 g) coated with 0.046 g WO_3 and uncoated glass foam of approximately 0.700 g. The photocatalytic experiments were carried out using UV-VIS spectroscopy by monitoring the absorbance of RhB aqueous solution (20 mL of 1.5 mg L^{-1} initial concentration) at certain time intervals. The photocatalytic

experiments consisted of two subsequent steps: adsorption of the RhB on the samples and the removal of RhB by photodegradation under simulated visible light.

In addition to the photocatalytic evaluation, the samples were characterized for investigation of the porous structure and semi-quantitative chemical composition using 3D scanning microscopy and EDAX spectroscopy coupled with SEM (not presented in the paper).

Results and discussion

The degradation of RhB by the supported WO_3 sample and uncoated glass foam under two hours of visible light irradiation is presented below, in figure 1.

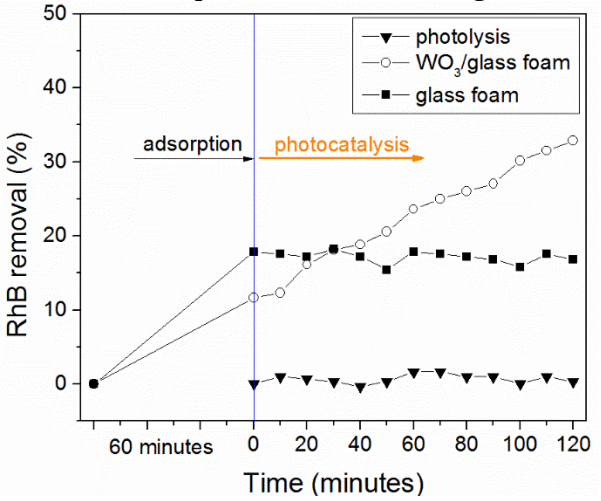

Figure 1. Removal of RhB from aqueous solution by: WO_3 supported on glass foam (marked with ○), glass foam (marked with ■) and with no catalyst (only RhB aqueous solution; marked with ▼) during adsorption and visible-light exposure

It could be noticed that during the photocatalytic experiments, RhB was firstly removed in the adsorption stage (12% for immobilzed photocatalyst –WO_3/glass foam and 17% for the uncoated glass foam) followed by removal of RhB by photodegradation (achieved only by WO_3/glass foam).

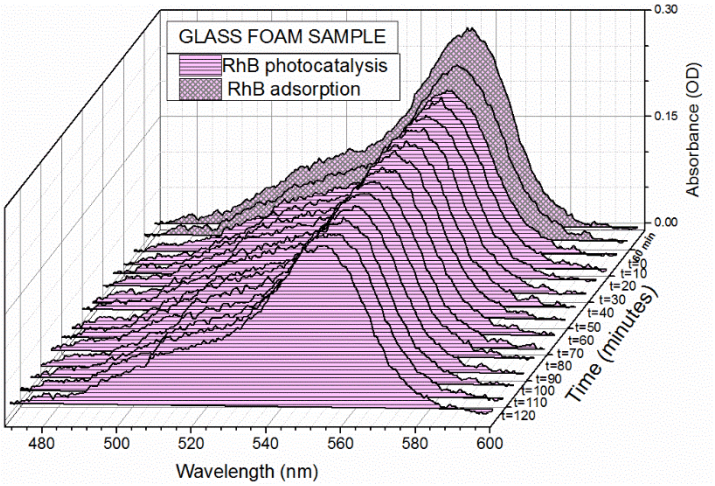

Figure 2. Absorbance decrease of the RhB aqueous solution corresponding to the uncoated glass foam during photocatalytic experiment

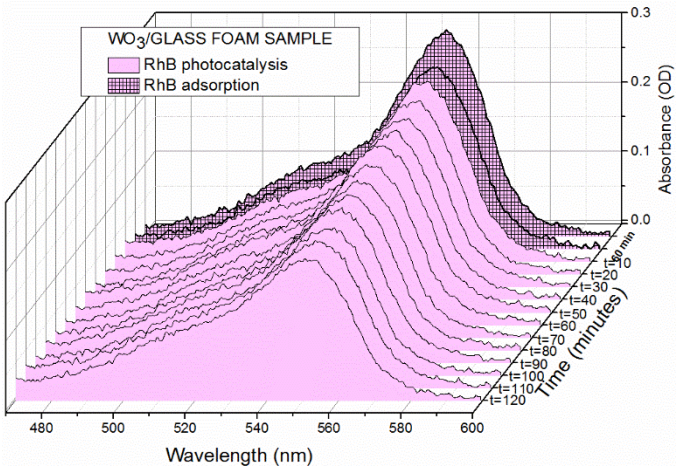

Figure 3. Absorbance decrease of the RhB aqueous solution corresponding to WO_3/glass foam during photocatalytic experiment

As well, the decrease of peak absorbance intensity of the RhB solution for the two samples involved in the study are represented in figure 2 and figure 3. The percent of the RhB removal obtained after adsorption step is higher for the uncoated glass foam even if the mass of the glass foam is lower than the mass of the glass foam used as support, which illustrates that the adsorption may be affected also by other factors including the morphology and the porosity of the glass foam.

The uncoated glass foam presented no photocatalytic activity which emphasize that the photodegradation of RhB for the supported WO_3 sample is given by the WO_3 activity. Moreover, the experiments carried out with uncoated glass foam and with RhB aqueous solution indicated the stability of the RhB under visible light irradiation.

Conclusion

Based on the photocatalytic experiments carried out for the glass foam activated with WO_3 and for the uncoated glass foam, it could be concluded that a higher removal of RhB was achieved by WO_3/glass foam, obtained as a result of both adsorption and photocatalysis process. The removal of RhB given by the photocatalytic properties of the WO_3 was 21% (of total removal of 33%). The uncoated glass foam acted only as an adsorbent, which proved the chemical stability regarding the photocatalytic reaction for RhB degradation.

The photocatalytic activity of the WO_3/glass foam validates the potential for glass foam utilization as a catalyst support dedicated for but not limited to environmental application.

Acknowledgements

This worked was sustained within the project PN-III-P1-1.2-PCCDI-2017-0391/CIA_CLIM-Smart buildings adaptable to the climate change effects, from Romanian Ministery of Research and Innovation, CCCDI–UEFISCDI.

References

[1] P. Dong, G. Hou, X. Xi, R Shao, F. Dong, Environ. Sci. Nano. 4(3) (2017)
[2] H. Anwer, A. Mahmood, J. Lee, K.-H. Kim, J.-W. Park, A. C. K. Yip, Nano. Res. 12 (2019) 955
[3] X. Liu, L. Zhao, K. Domen, K. Takanabe, Mater. Res. Bull. 49 (2014) 58
[4] Q. Xu, X. Li, J. Xu, J. Zeng, RSC Advances 6(57) (2016)
[5] V. Laur, R. Benzerga, R. Lebullenger, L. Le Gendre, G. Lanoë, A. Sharaiha, P. Queffelec, Mater. Res. Bull. 96(2) (2017) 100

[6] R. Lebullenger, S. Chenu, J. Rocherullé, O. Merdrignac-Conanec, F. Cheviré, F. Tessier, A. Bouzaz, S. Brosillon, J. Non-Cryst. Solids 356 (44) (2010) 2562
[7] M. Ivanovici, P. Vlazan, S. D. Novaconi, F. S. Rus, AIP Conference Proceedings 2218(1) (2020)

OPTICAL ENERGY BANDGAP TUNING OF SPINEL ZINC STANNATE BY ERBIUM/YTTERBIUM DOPING

Tamara Ivetić[1], Jelena Petrović[2], Olivera Klisurić[1], Svetlana Lukić-Petrović[1]

[1]University of Novi Sad, Faculty of Sciences, Department of Physics, Trg Dositeja Obradovića 3, 21000 Novi Sad, Serbia
[2]Institute for Electronic Appliances and Circuits, Faculty of Computer Science and Electrical Engineering University of Rostock, Albert-Einstein 2, 18059 Rostock, Germany
e-mail: tamara.ivetic@df.uns.ac.rs

Abstract

This work shows the results of an optical energy bandgap (E_g) investigation supported by scanning electron microscopy (SEM) of spinel-type zinc stannate (Zn_2SnO_4) upon doping with rear earth (RE^{3+}) ions (Er^{3+}, Yb^{3+}). The powder samples are synthesized by a mechanochemical solid-state method with the final annealing step at 1200 °C. The reference Zn_2SnO_4 powder sample bandgap (3.87 eV) turning lower upon doping, precisely to 3.5 eV, and 3.37 eV bandgap values found for Er-doped Zn_2SnO_4 and Er,Yb-codoped Zn_2SnO_4 powder samples, respectively is a confirmation of the successful incorporation of the RE^{3+} ions into the Zn_2SnO_4 host structure. Morphology of the obtained powders shows, in general, the non-uniformly shaped agglomerates, while their particle sizes follow up the bandgap decreasing trend with doping.

Introduction

The ternary zinc tin oxide (ZTO) compound called zinc stannate with inverse spinel structure (Zn_2SnO_4) shows exceptional physicochemical properties that still cause attention in materials science. Its inverse cubic structure belongs to the space group $Fd\bar{3}m$ (No. 227) where the lattice parameter is ~8.65 Å, the Zn^{2+} cations occupy all tetrahedral sites, and the octahedral sites shared by Zn^{2+} and Sn^{4+} cations (Fig. 1). However, ZTO usually exhibits cation disorder when a portion of Sn^{4+} cations, even so, moves to tetrahedral sites.

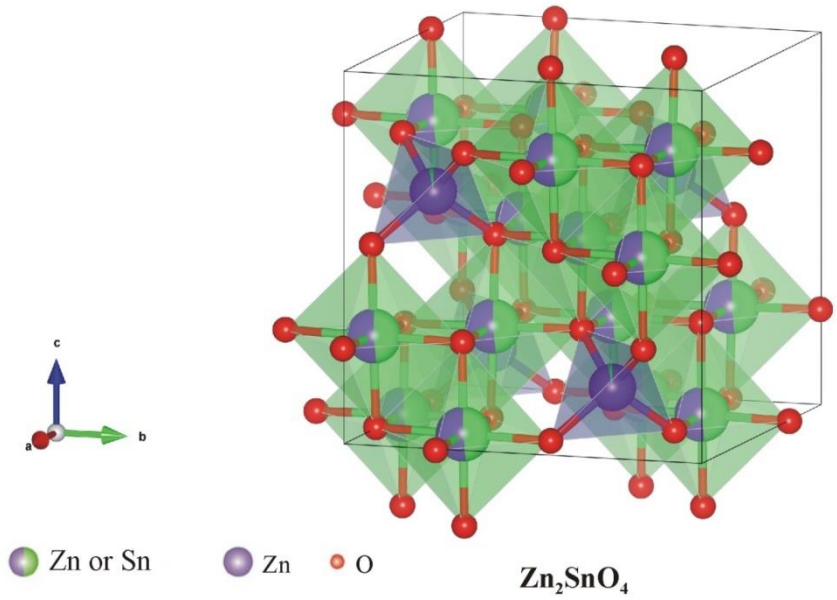

Figure 1. Crystal structure of Zn_2SnO_4.

Zn_2SnO_4 is a transparent n-type semiconductor with high electron conductivity and chemical stability that finds applications in solar cells, sensing, lithium batteries, nanodevices, catalysis [1]. Therefore, the most investigated are its electrical and optical properties dependent upon the type of synthesis method used and the resulting ZTO microstructure.
ZTO was so far successfully synthesized by various methods like high-temperature calcination, mechanical grinding, sol-gel synthesis, hydrothermal/solvothermal, thermal evaporation, with different morphologies obtained, shapes like hollow -cages, -boxes, -tubes and -bowls; and nano -urchins, -flowers, -beads [2].
Reportedly its optical bandgap varies from 3.18 eV to 4.1 eV [3-5] depending on the synthesis method, conditions applied, due to variations in stoichiometry, while 3.6-3.7 eV is its proposed fundamental E_g [6].

Experimental

Synthesis

The non-doped reference Zn_2SnO_4, Er (1 at.%)-doped Zn_2SnO_4 and Er (1 at.%)/Yb (1 at.%)-co-doped Zn_2SnO_4 powder samples were synthesized by a following solid-state method. Starting precursors (ZnO and SnO_2, Sigma-Aldrich, purity 99.9%) mixed in stoichiometric ratio with or without the addition of 1 at.% of Er (Er_2O_3, Sigma-Aldrich, purity 99.9%), and 1 at.% of Er and 1 at.% of Yb (Yb_2O_3, Sigma-Aldrich, purity 99.9%), are milled by Retsch GmbH PM100 at 320 rpm for 160 min and annealed at 1200 °C for 2 hours. For reference, we use the labels ZTO, ZTO:Er, and ZTO:Er,Yb further in the text for the easier marking of un-doped, erbium-doped, and erbium, ytterbium-co-doped Zn_2SnO_4 powder samples, respectively.

Characterization

UV-Vis reflectance was measured using the Ocean Optics QE65000 High-sensitivity Fiber Optic Spectrometer. The microstructure was investigated by scanning electron microscopy (JEOL JSM 7001F).

Results and discussion

Fig. 2 shows that the optical absorption threshold of ZTO redshifts from around 320 nm to ~354 nm and ~368 nm for ZTO:Er and ZTO:Er,Yb powder samples, respectively. The “knees” appearance in the reflectance spectra points to the presence of a secondary phase. Such behavior occurred upon doping in analogous systems [7]. The X-ray diffraction measurements (shown elsewhere [8]) confirmed the presence of the low weights shares of the secondary $Er_2Sn_2O_7$ phase in doped samples. The reflectance measurements (Fig. 2) were used to estimate the optical energy gap of ZTOs by extrapolation of the spectral “knees” using the plots of Kubelka-Munk transformed reflectance spectra for the allowed-direct transitions $[F(R) \cdot h\nu]^2$ *vs*. photon energy ($h\nu$) [4]. For E_g estimated values of reference Zn_2SnO_4, Zn_2SnO_4:Er, and Zn_2SnO_4:Er,Yb samples are 3.87 eV, 3.5 eV, and 3.37 eV, respectively. The lowering of the optical energy bandgap suggests the successful incorporation of RE^{3+} ions into the Zn_2SnO_4 matrix compound structure. The successful RE^{3+} ions incorporation has been confirmed by our recent luminescence report [8], where the up-conversion luminescence of Zn_2SnO_4:Er^{3+},Yb^{3+} powder phosphors was described. The appearance of luminescence emissions shown in Ref. [8] is possible only when the matrix compound (here Zn_2SnO_4) hosts the luminescence activator ions (here RE^{3+} = Er^{3+} and Yb^{3+}) in its crystal lattice.

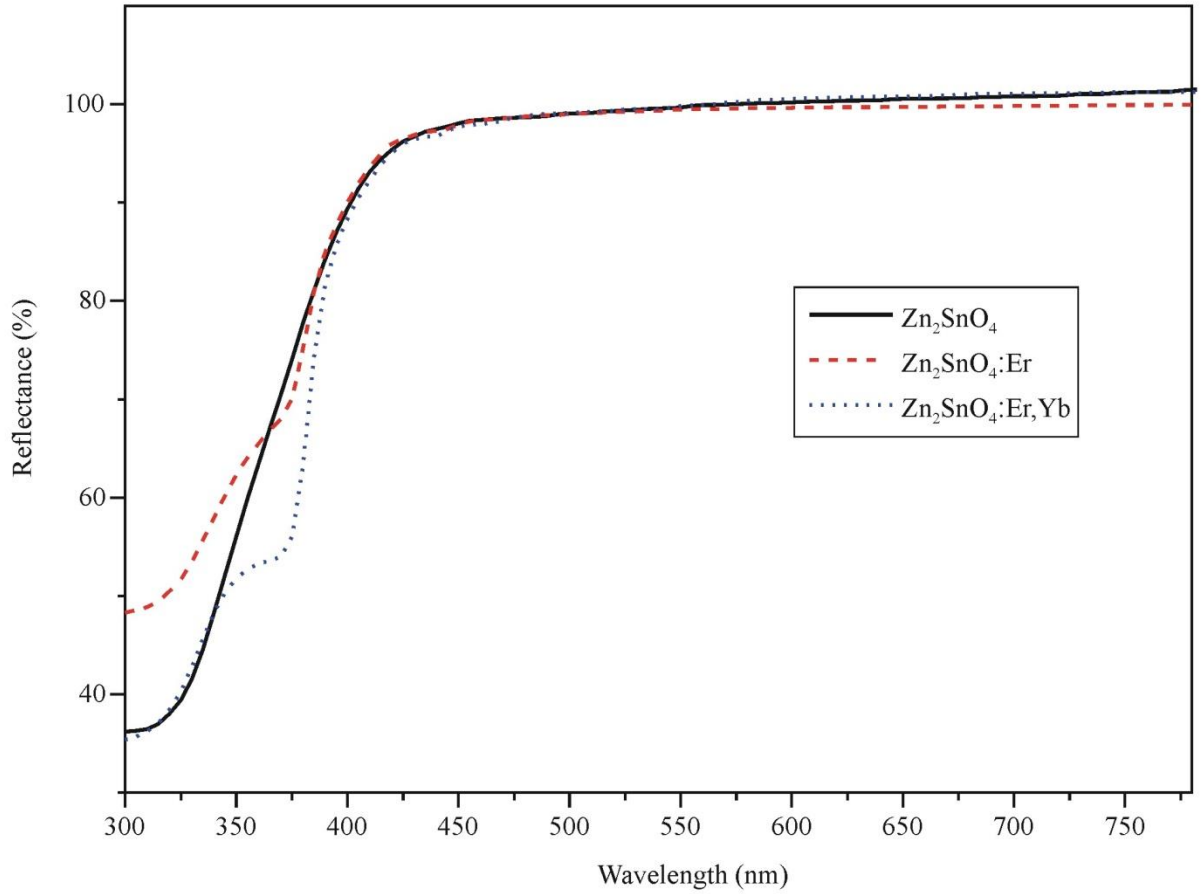

Figure 2. Reflectance spectra of reference ZTO, ZTO:Er and ZTO:Er,Yb powders.

Fig. 3 shows the SEM images of ZTO, ZTO:Er, and ZTO:Er,Yb powder samples. The morphologies consist of non-uniform in shape agglomerates of more or less pasted Zn_2SnO_4 particles with sizes in the range of one to five microns. Doping causes particle sizes to decrease [8].

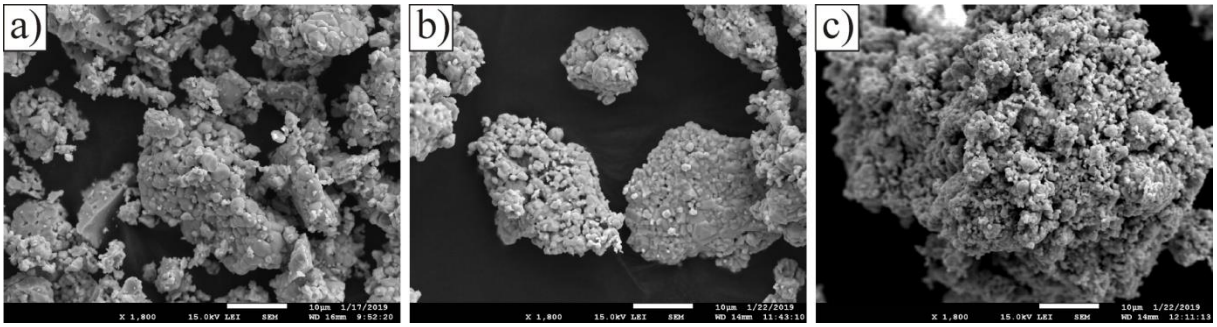

Figure 3. SEM images of a) reference ZTO, b) ZTO:Er, and c) ZTO:Er,Yb powders with × 1,800 magnification.

Conclusion

In this work, we report the potential of band structure tuning of spinel zinc stannate powder by doping with rear earth ions (Er^{3+}, Yb^{3+}) when synthesized using the mechanochemically initiated solid-state reaction method followed by annealing. The optical bandgap characterization points to the successful incorporation of rear-earths into the spinel cubic crystal structure of zinc stannate. The scanning electron microscopy images of the obtained powder

samples showed non-uniformity in shapes of agglomerates with particle size decrease by doping. Our optical measurements report the Zn_2SnO_4 bandgap of 3.87 eV for a direct-allowed transition, and E_g tuning to lower values of 3.5 eV and 3.37 eV when doped with 1 at.% of Er^{3+} ion and co-doped with 1 at.% of Er^{3+} and 1 at.% Yb^{3+} ions, respectively.

Acknowledgements
This work was funded by the Ministry of Education, Science and Technological Development of the Republic of Serbia (Grant No. 451-03-68/2020-14/200125) and financially supported by the German Academic Exchange Service (DAAD) Funding program Research Stays for University Academics and Scientists, 2018 (ID no. 57381327).

References
[1] S. Sun, S. Liang, J. Mater. Chem. A 5 (2017) 20534.
[2] S. Baruah, J. Dutta, Sci. Technol. Adv. Mater. 12 (2011) 013004.
[3] L.T.T. Vien, N. Tu, M.T. Tran, N. Van Du, D.H. Nguyen, D.X. Viet, N.V. Quang, D.Q. Trung, P.T. Huy, Optical Materials 100 (2020) 109670.
[4] T.B. Ivetić, N.L. Finčur, Lj.R. Đačanin, B.F. Abramović, S.R. Lukić-Petrović, Mater. Res. Bull. 62 (2015) 114.
[5] M. Dimitrievska, T.B. Ivetić, A.P. Litvinchuk, A. Fairbrother, B.B. Miljević, G.R. Štrbac, A. Pérez Rodríguez, S.R. Lukić-Petrović, J. Phys. Chem. C 120 (2016) 18887.
[6] M.A. Alpuche-Aviles, Y. Wu, J. Am. Chem. Soc. 131 (2009) 3216.
[7] Lj. Đačanin Far, N. Finčur, T. Ivetić, B. Abramović, D. Štrbac, O. Bosak, S. Lukić-Petrović, Rom. J. Phys. 65 (2020) 601.
[8] T.B. Ivetić, Y. Ding, M. Cvetinov, J. Petrović, O. Klisurić, S. Lukić-Petrović, Yb^{3+} cooperative upconversion luminescence sensitization of Zn_2SnO_4:Er^{3+} powder phosphor, under review.

APPLICATION OF MICROWAVE-ASSISTED FENTON-REACTION FOR ENHANCED ORGANIC MATTER REMOVAL IN WASTEWATER TREATMENT

Zoltán Jákói[1], Laura Haranghy[1], Cecilia Hodúr[1], Sándor Beszédes[1]

[1]*Department of Process Engineering, University of Szeged, H-6725 Szeged, Moszkvai krt. 9, Hungary*
e-mail: jakoiz@mk.u-szeged.hu

Abstract
In our experimental work we focused on the applicability of a novel alternative in wastewater management, i.e. the application of microwave-irradiation assisted Fenton-like process. We wanted to investigate whether the combination of microwave treatment with Fenton's reaction can enhance the organic matter removal in meat industry originated wastewater compared to the standalone oxidative reaction, and if so, to what extent. In our study we also wanted to explore the possibility of using dielectric measurements to determine the change in organic matter content, i.e. to see if there is a connection between the change in COD (chemical oxygen demand) and the dielectric loss tangent (tanδ).

Introduction
Wastewater is produced in larger and larger extent during industrial practice, and contains different – often toxic – organic and inorganic compounds, therefore the proper treatment of it is a necessity before entering into the sewer system or discharge to natural reservoir. Since the composition and quality characteristics of different types of wastewater can vary and is usually challenging to predict, the development of a universal and effective treatment technology would be the most favorable.
Several studies have already shown that advanced wastewater treatment technologies can significantly increase the efficiency of organic matter removal in wastewater samples compared to the conventional technologies [1]. Advanced oxidation processes (AOPs) are a group of these innovative technologies, which standalone Fenton's reaction and the combination of Fenton's reaction and other types of treatments belong to. It has been shown that Fenton and Fenton-like processes can be effectively used in wastewater treatment; since they can significantly reduce the organic content of different types of wastewater, especially in certain combinations (e.g. photo-Fenton or electro-Fenton) [2]. One of the biggest advantages of using Fenton processes is that they can be implemented at ambient temperature and atmospheric pressure, however certain limiting factors are presented as well and should be considered (pH, temperature for instance).
Commonly the main drawback of the application of Fenton reaction is the need for long reaction time. Among the available methods to shorten the time demand of a given process, microwave irradiation has been more and more widely used and investigated. Microwave-assisted Fenton-processes are still quite novel technologies in water and wastewater treatment, however the available preliminary results from different studies are quite promising [3]. In our study we wanted to investigate the effects of microwave-irradiation on the efficiency of Fenton's reaction in the organic matter removal of meat industry wastewater by measuring the COD after the different treatments. Dielectric parameters were also measured to investigate the applicability of dielectric measurements for detection of organic matter removal.

Experimental
For the experiments, meat industry wastewater (MIW) samples were used in a final volume of 100 cm^3. The main characteristics of MIW are presented in Table 1.

Parameter	Unit	Value
COD (chem. ox. demand)	[mg/L]	1612±45
TOC (total organic carbon)	[mg/L]	179 ± 16
TS (total solid)	[w%]	2.1 ± 0.11
pH	[-]	6.7 ± 0.2

Table 1. Main characteristics of MIW

Fenton's and microwave-assisted Fenton's reaction were carried out with different Fe^{2+}/H_2O_2 ratio in order to determine which reagent dosage is the optimal for organic matter removal (i.e. COD decrease) as follows: 300/240 mg/mg, 150/120 mg/mg and 50/40 mg/mg. pH was set at 3.0 before applying the reagents. Each Fenton's reaction were occurring for 2 hours, the reaction was stopped by adding catalase enzyme to the samples in a volume of 400 µl.

Microwave treatments were performed as pre-treatments, i.e. before the Fenton's reaction had occurred. The microwave treatments were carried out in a Labotron 500 laboratory microwave equipment with a magnetron operating at 2450 MHz frequency. The total irradiated energy were varied between 30, 45, 60 and 75 kJ at each experiment. Dielectric measurements were performed with a DAK-3.5 (SPEAG) dielectric probe connected to a ZVL3 (Rhode&Schwartz) type VNA (vector network analyzer) in a frequency range of 200-2400 MHz.

Results and discussion

In the first series of the experiments we investigated the effect of total irradiated microwave energy on the effectiveness of Fenton's reaction in regards of COD. It can be seen that standalone Fenton's reaction (with no MW) was able to reduce the initial COD (1612 mg/L) of the samples by 20-51%, depending on the concentration of the reagents – using 300/240 mg/mg Fe^{2+}/H_2O_2 dosage resulted in the biggest change in COD (Figure 1).

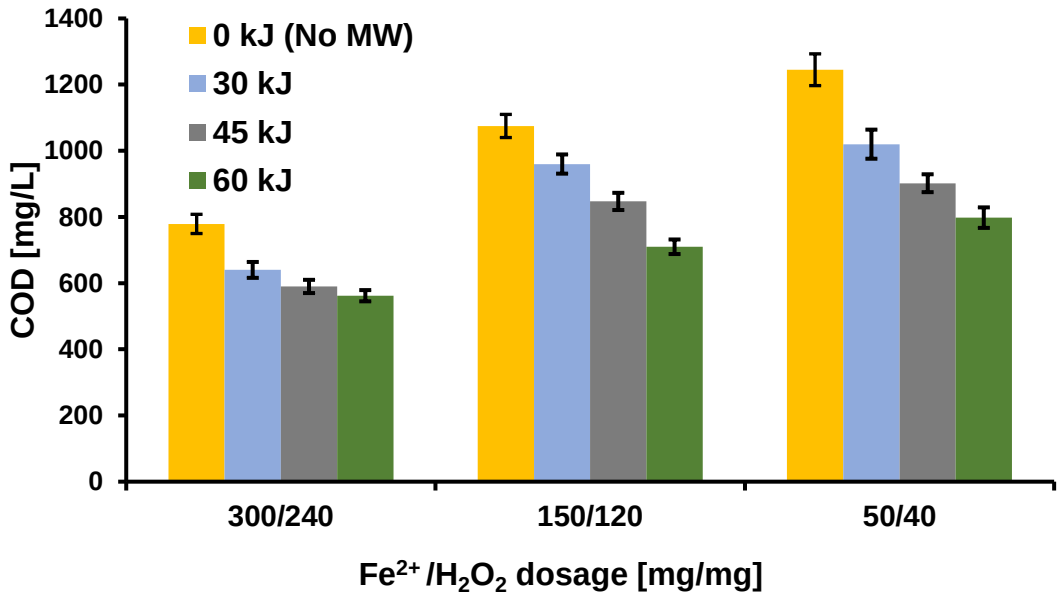

Figure 1. COD change in the function of dosage and total MW energy

The intensification effect of microwave irradiation on Fenton's reaction also depended on the Fe^{2+}/H_2O_2 ratio. It can be concluded that the change of microwave energy intensity has stronger effects at lower reagent-dosage ratios, than that of obtained for higher concentrations. It can be seen that with the combination of MW irradiation during the Fenton process, the absolute need for reagents can be reduced – by applying 60 kJ total irradiated energy with a dosage of 50/40

mg/mg, almost the same COD level could be obtained as with standalone Fenton's reaction with a dosage ratio of 300/240 mg/mg (cf. 798 – 779 mg/L).

In the second half of the experiments we measured the dielectric properties (dielectric constant, dielectric loss factor and dielectric loss tangent) of the differently treated samples to see if any of these constants is applicable to determine the change in COD. Our results verified that there is a strong correlation between the change of dielectric loss tangent (Δtanδ, the ratio of the dielectric constant ε' and dielectric loss factor ε'') and the change of the final COD (ΔCOD) of the MW/Fenton treated samples, with an R^2-value of 0,9602 and 0,9995, respectively. Regarding the effects of treatment the change of concentration of organic matter and the change of the tanδ shows a similar tendency (Figure 2).

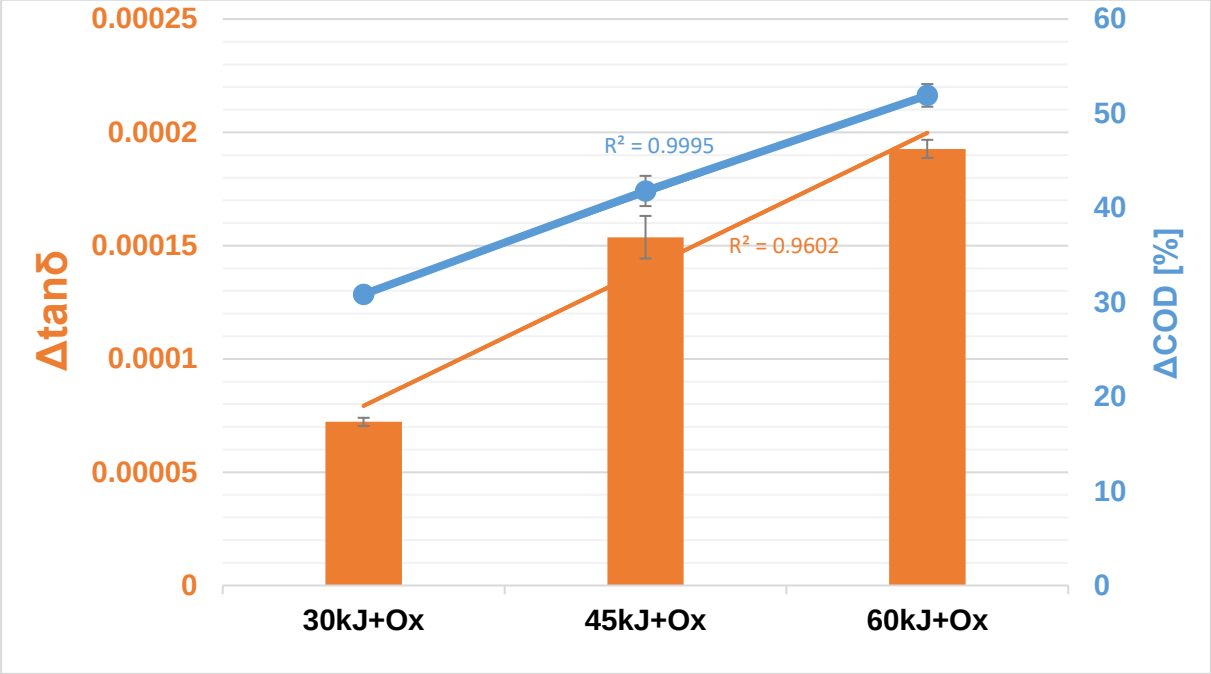

Figure 2. Connection between the change in COD and tanδ (Fe^{2+}/H_2O_2 ratio was fixed at 150/120 mg).

Conclusion

Our experiments focused on the effects of microwave-assisted Fenton's reaction on the organic matter removal in meat industry wastewater samples. Based on the results gained, it can be concluded that microwave-irradiation as a pre-treatment method can increase the efficiency of the oxidation process, and the strength of effect is depending on the concentration of reagents being used. At lower dosage ratio, the effect of MW is stronger, and by applying high total irradiated energy (60 kJ), the need for reagents can be reduced by almost 84% compared to the standalone Fenton's oxidation reaction. Dielectric measurements show that the change in dielectric loss tangent (tanδ) shares a similar tendency with the change in final COD, therefore it is capable of monitoring the changes in organic matter content.

Acknowledgements

The authors are grateful for the financial support provided by the projects EFOP-3.6.2- 16-2017- 00010 – RING 2017; and National Office for Research, Development and Innovation - NKFIH, K115691.

References

[1] H. Zhou, D. W. Smith, Advanced technologies in water and wastewater treatment, Journal of Environmental Engineering and Science, 1 (2002) 4.
[2] Min Xu, Changyong Wu, Yuexi Zhou, in: Ciro Bustillo-Lecompte, Advanced Oxidation Processes – Applications, Trends and Prospects, IntechOpen, 2020, pp. 54-72
[3] Y. Yang, P. Wang, S. Shi, Y. Li, Microwave enhanced Fenton-like process for the treatment of high concentration pharmaceutical wastewater, Journal of Hazardous Materials, 168 (2009).

MICROWAVE-ASSISTED PHOSPHA-MICHAEL ADDITION REACTIONS ON 13α-ESTRANE CORE

Rebeka Jójárt[1], Lili Kóczán[1], Lilla Fajka[1], Sándor Bartha[2], Renáta Minorics[2], István Zupkó[2], Erzsébet Mernyák[1]

[1]Department of Organic Chemistry, University of Szeged, Dóm tér 8, H-6720 Szeged, Hungary
[2]Department of Pharmacodynamics and Biopharmacy, University of Szeged, Eötvös u. 6., H-6720 Szeged, Hungary
e-mail: j.rebeka05@gmail.com

Abstract
Novel 16-modified 13 α-estrone derivatives were synthesized via phospha-Michael addition reactions. Transformations of steroidal α,β-unsaturated ketons were carried out under different conditions in a microwave (MW) reactor. The antiproliferative activities of the newly synthesized compounds against a range of human adherent cancer cell lines (SCC-131, SCC-154, Hela, SiHa, C33A, A2780, MCF-7, MDA-MB-231, T47D) were investigated by means of MTT assays. Certain potent derivatives were identified.

Introduction
Certain substituted estrone derivatives possess anticancer properties. The core-modified 13α-estrone does not possess estrogenic behavior and offers great possibilities concerning selective bioactivities[1]. Certain C-16 modified derivatives display outstanding cell growth-inhibitory action against a range of human adherent cancer cell lines[2]. The microwave assisted phospha-Michael addition of dialkyl phosphites or diarylphosphine oxides to α,β-unsaturated ketones is a known method for the synthesis of organophosphorous compounds[3–5]. It might efficiently be carried out without a catalyst and under short reaction times. Our aim was here to develop a facile and efficient microwave-induced phospha-Michael addition methodology for the synthesis of 16-modified 13 α-estrone derivatives. Investigation of the antiproliferative effect of the newly synthesized 13α-estrone derivatives against a panel of nine human adherent cancer cell lines (SCC-131, SCC-154, Hela, SiHa, C33A, A2780, MCF-7, MDA-MB-231, T47D) was also planned.

Results and discussion
In the first experiments, diphenylphosphine oxide was reacted with the 3-methyl or -benzyl ether of the α,β-unsaturated ketone in acetonitrile, under MW irradiation (Scheme 1). 3-Methyl ether starting compound was completely transformed under 1 h irradiation at 120 °C. In case of the 3-benzyl ether, higher reaction temperature (150 °C) was needed. The reactions of bis(*p*-tolyl)phospine oxide or di(naphthalen-2-yl)phospine oxide as reagents were carried out under the conditions applied for the transformations of benzyl ethers. All the reactions furnished the desired products (in a 2:1 diastereomeric ratio) in high yields. The diastereomers could efficiently be separated by flash chromatography. The structures of the new compounds were confirmed by ^{1}H and ^{13}C and ^{31}P NMR measurements. Certain newly synthesized products displayed substantial antiproliferative action against human adherent cancer cell lines.

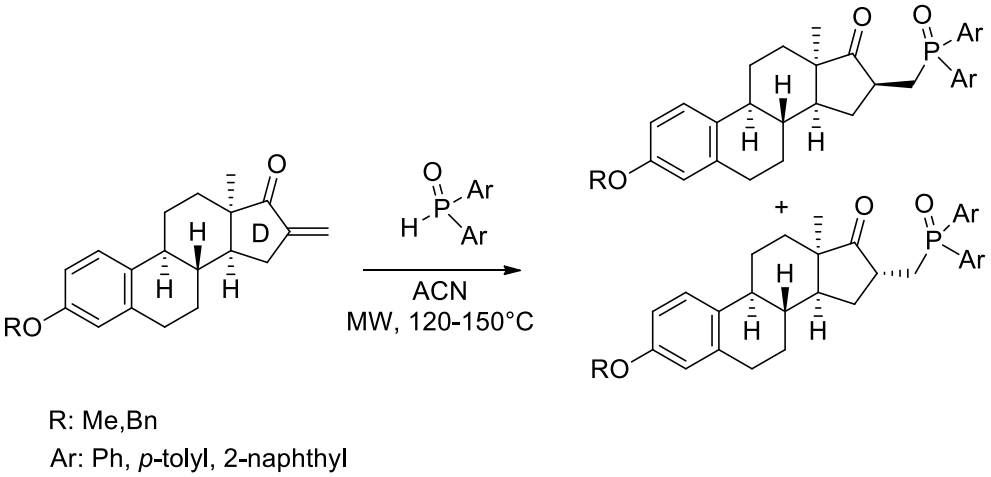

R: Me,Bn
Ar: Ph, *p*-tolyl, 2-naphthyl

Scheme 1. Phospha-Michael additions in the 13 α-estrone series

Conclusion

In conclusion, we have developed an efficient microwave-assisted phospha-Michael addition method for the synthesis of steroidal phosphine oxides. 12 new ring D modified 13α-estrone derivatives have been synthesized. Potent antiproliferative compounds have been identified.

Acknowledgements

The work of Erzsébet Mernyák and Renáta Kanizsainé Minorics in this project was supported by the János Bolyai Research Scholarship of the Hungarian Academy of Sciences. This work was supported by National Research, Development and Innovation Office-NKFIH through project OTKA SNN 124329. The authors thank the support of project EFOP-3.6.2-16-2017-00005 and Ministry of Human Capacities, Hungary grant 20391-3/2018/FEKUSTRAT.

References

[1] D. Ayan, J. Roy, R. Maltais, D. Poirier, J. Steroid Biochem. Mol. Biol. **2011**, *127*, 324-30
[2] E. Mernyák, I. Kovács, R. Minorics, P. Sere, D. Czégány, I. Sinka, J. Wölfling, G. Schneider, Z. Újfaludi, I. Boros, I. Ocsovszki, M. Varga, I. Zupkó . J. Steroid Biochem. Mol. Biol. **2015**, *150*, 123-134.
[3] Mimeau, D.; Delacroix, O.; Join, B.; Gaumont, A.-C. Chimie **2004**, *7*, 845.
[4] Join, B.; Delacroix, O.; Gaumont, A.-C. Synlett **2005**, *12*, 1881.
[5] E. Bálint, J. Takács, L. Drahos, Gy. Keglevich. Heteroatom Chem, **2012**, *23*, 235-240.

APPLICATION OF GRAPHENE QUANTUM DOTS IN HEAVY METALS AND PESTICIDES DETECTION

Slađana Dorontić[1], Olivera Marković[2], Aurelio Bonasera[3], and Svetlana Jovanović[1]

[1]"Vinča" Institute of Nuclear Sciences - National Institute of the Republic of Serbia, University of Belgrade P.O. Box 522, 11001 Belgrade, Serbia
[2]University of Belgrade – Institute of Chemistry, Technology and Metallurgy – National Institute of the Republic of Serbia, Njegoševa 12, 11000, Belgrade, Serbia
[3]Dept. of Physics and Chemistry-Emilio Segrè; (DiFC) - University of Palermo, Consorzio, Interuniversitario Nazionale per la Scienza e Tecnologia dei Materiali (INSTM) - Palermo Research Unit viale delle Scienze, bdg. 17, rm. 1/B6 90128 Palermo (PA) - Italy
e-mail: svetlanajovanovicvucetic@gmail.com

Abstract

Graphene Quantum Dots (GQDs) were produced using electrochemical oxidation of graphite rods. Obtained GQDs were gamma-irradiated in the presence of the N atoms source, ethylenediamine. Both structural and morphological changes were investigated using UV-Vis, X-ray photoelectron and photoluminescence (PL) spectroscopy as well as atomic force microscopy. The ability of both types of dots to change PL intensity in the presence of pesticides such as malathion and glyphosate, as well as copper (II) ions was detected. These preliminary results indicated a high potential of produced GQDs to be applied as non-enzymatic PL sensors for the detection of selected pesticides and metal ions.

Introduction

Graphene quantum dots (GQDs) are round graphene sheets with a diameter below 100 nm and different O-containing functional groups located on the surface and at the edges of dots [1]. Due to a large amount of these functional groups, GQDs are dispersible in water and polar organic solvents. They showed good biocompatibility and low cytotoxicity [2]. Due to the quantum confinement effect and edge sites/defects, GQDs possess stable photoluminescence (PL) and they are resistive to photobleaching [3]. Considering both biocompatibility and photoluminescence, these dots were often investigated for their possible application in the sensing of different ions and molecules [4].

Due to the overuse of pesticides, they are often found in the ground, water, or agricultural products. Pesticides accumulation in the environment leads to their entering into biosystems [5]. Thus, pesticides such as glyphosate and the products of its degradation were detected in human urine in a concentration of 2.63, 1.26, and 0.89 μg/L in samples from Croatia, Belgium, and Malta [6]. Additionally, the pollution of water, air, and ground lead to a high level of heavy metals which are also toxic for animal, humans, and plants [7]. The analytical techniques that are now in-use for pesticides and heavy metal detection request the usage of expensive instruments, highly educated operators, while the analysis often demands time. Thus, there is a need for a new, simple, and affordable method for the detection of these pollutants.

Herein we prepared GQDs using an eco-friendly approach: electrochemical oxidation of graphite electrodes was achieved without the consumption of aggressive and toxic reagents [8]. Dots were purified by dialysis and structurally modified through gamma irradiation. During gamma irradiation, covalent modification of material can be achieved without the consumption of aggressive, toxic reagents. Thus, this method is considered a green tool for modification. By selecting the medium with N-atoms, the incorporation of N-functional groups was achieved. The effect of the herbicide glyphosate, insecticide malathion, and copper (II) ions on the intensity of photoluminescence of GQDs was investigated.

Experimental

GQDs were produced using a previously described procedure [8]. Gamma-irradiation was conducted in a water solution of isopropanol (3 vol%) and ethylenediamine (EDA, 4 vol%) [9]. Before the irradiation, the sample was purged with argon to remove dissolved oxygen. The sample was irradiated at a dose of 50 kGy.

UV-Vis measurements were performed at a Shimadzu UV-2600 UV-Visible spectrophotometer (Shimadzu Corporation, Tokyo, Japan). Spectra were recorded at 20 °C under a normal atmosphere, in the range of 200-800 nm. The concentration of GQD dispersions was 0.25 mg mL-1.

The PL spectra were recorded on Horiba Jobin Yvon Fluoromax-4 spectrometer (Horiba, Kyoto, Japan). GQDs dispersions in methanol (c=0.25 mg mL-1) were placed in a quartz cuvette with 1 cm path length and 4 mL volume. For the excitation, laser wavelengths were 300, 360 and 400 nm. Spectra were collected under room temperature in the air environment.

X-ray Photoelectron Spectroscopy (XPS) was acquired by using a ULVAC-PHI PHI500 VersaProbe II scanning microprobe (ULVAC-PHI, Inc., Chigasaki, Japan), with an Al Kα source (1486.6 eV), 100 μm spot, 25 W power, 15 kV acceleration, and 45° take-off angle. All spectra were collected using a dual neutralization system (both e− and Ar+).

Atomic Force Microscopy (AFM) measurements were performed using Quesant (Agoura Hills, CA, Unites States) microscope operating in tapping mode, in the air, at room temperature. We used the Q-WM300 AFM probe, rotated, monolithic silicon probe for non-contact high-frequency applications. Standard silicon tips (NanoAndMore Gmbh, Wetzlar, Germany) were used, with a force constant of 40 N/m. GQDs were dispersed in MiliQ water in a concentration of 0.25 mg mL-1 and deposited with spin-coated on a mica substrate. Gwyddion 2.53 software was used for image analysis.

Results and discussion

UV-Vis spectroscopy showed that p-GQDs had a peak of absorption centered around 230 nm while after gamma irradiation, this band was narrow, shifted to 205 nm with a shoulder band at 260 nm. The first band was due to π-π* transitions of sp^2 C in aromatic bonds, while the second was assigned to π→n transitions of C=O groups. These results indicated the changes in the amount of O functional groups occurred during gamma irradiation. PL spectra showed that after gamma irradiation the highest intensity of emission band was observed with an excitation wavelength of 400 nm (figure 2c) while for p-GQDs, the highest emission was detected at excitation of 300 nm. The excitation-dependent photoluminescent behavior was observed for both samples. AFM analysis (figure 1d and e) showed that irradiation caused the lowering in the average GQDs height, from 1.73 nm as measured for p-GQDs to 1.25 nm. The average diameter was around 18 nm for p-GQDs, and 15 nm for $_{50}$γ-GQDs. XPS analysis showed that GQDs had C and O atoms, while $_{50}$γ-GQDs had C, O and N atoms in the structure (figure 1f).

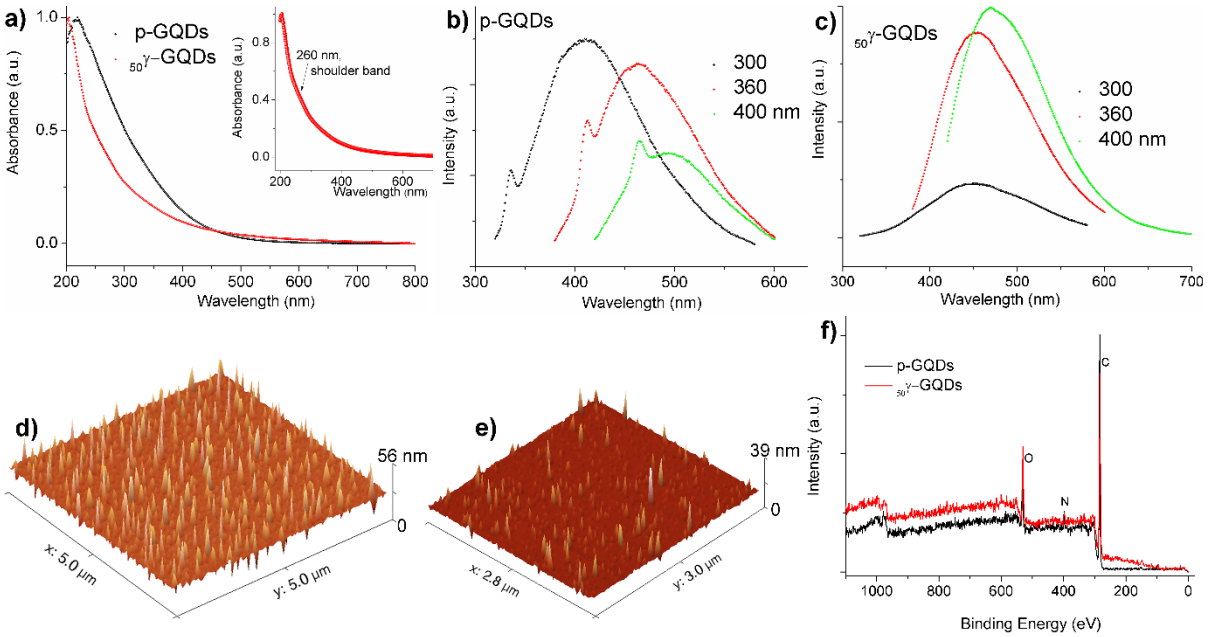

Figure 1. UV-Vis spectra of p-GQDs and $_{50}\gamma$-GQDs (a), PL spectra, and AFM images of p-GQDs (b, d) and $_{50}\gamma$-GQDs (c, e), as well as XPS survey of samples (f).

To investigate the possibility of GQDs application in non-enzymatic PL detection, GQDs were mixed with Cu(II) ions, pesticide malathion and the herbicide glyphosate. After a short incubation time (5 minutes), mixtures of GQDs with analytes were recorded on PL spectroscope and obtained spectra are presented in figure 2. By adding Cu(II) ions, the maximum of the intensity of PL emission spectra was lowered for both p-GQDs and $_{50}\gamma$-GQDs. In the case of malathion which was added in a concentration of 18.1 mM, the PL intensity was increased, while in the case of glyphosate the increase in PL intensity was observed for two concentrations: 10 and 5000 ng mL^{-1}. A higher increase in PL intensity was observed in the case of p-GQDs/malathion while in the case of glyphosate the higher changes were detected for gamma-irradiated GQDs.

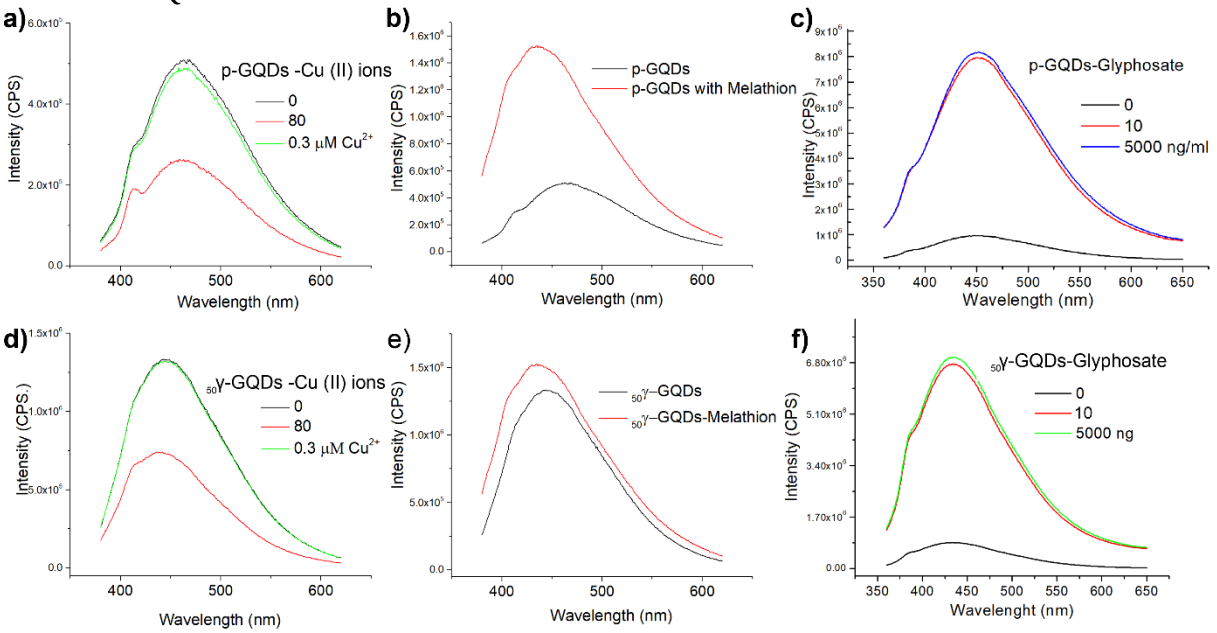

Figure 2. PL p-GQDs with Cu (II) ions (a), malathion (b), glyphosate (c) and $_{50}\gamma$-GQDs with the same analytes at (d), (e) and (f), respectively.

These preliminary results showed that both non-modified and modified GQDs possess the potential for their application in Cu(II) ions, malathion and glyphosate detection. In the case of Cu(II) ions, it was suggested that the lowering in PL intensity was due to the electrostatic destabilization and coagulation of negatively charged GQDs. On the opposite, pesticide malathion and glyphosate induced an increase in PL intensity of GQDs. In future research we will analyze if the increase in pesticide concentration leads to a linear increase of the PL intensity for a wide range of pesticide concentrations.

Conclusion

The potential of GQDs application in the detection of metal ions and pesticides was investigated. GQDs were synthesized in an electrochemical approach and modified by gamma irradiation. This treatment induced the lowering in GQDs height and diameter, and resulted in the incorporation of N atoms in the GQD structure. Both modified and non-modified GQDs were investigated as sensors in PL detection of Cu ions, malathion and glyphosate. A preliminary investigation showed the changes in the PL intensity when these analytes were added: Cu (II) lowered while malathion and glyphosate increased PL intensity.

Acknowledgments

This work was financially supported by the Ministry of Education, Science and Technological Development of the Republic of Serbia (Grant No. 451-03-68/2020-14/2652, 451-03-68/2020-14/200017 and 451-03-68/2020-14/200026). ATeN Center (University
of Palermo; project “Mediterranean Center for Human Health Advanced Biotechnologies (CHAB)” PON R&C 2007–2013) is acknowledged for hospitality and service.

References

[1] S. Jovanovic, Handbook of Graphene Set, 1 (2019) 267.
[2] X. Yuan, Z. Liu, Z. Guo, Y. Ji, M. Jin, X. Wang, Nanoscale Research Letters, 9 (2014) 1.
[3] Z. Gan, H. Xu, Y. Hao, Nanoscale, 8 (2016) 7794.
[4] M. Li, T. Chen, J.J. Gooding, J. Liu, ACS Sensors, 4 (2019) 1732.
[5] R. Mesnage, M.N. Antoniou, Front Public Health, 5 (2017) 316.
[6] L. Niemann, C. Sieke, R. Pfeil, R.J.J.f.V.u.L. Solecki, 10 (2015) 3.
[7] V. Silva, H.G.J. Mol, P. Zomer, M. Tienstra, C.J. Ritsema, V. Geissen, Science of The Total Environment, 653 (2019) 1532.
[8] H.T. Li, X.D. He, Z.H. Kang, H. Huang, Y. Liu, J.L. Liu, S.Y. Lian, C.H.A. Tsang, X.B. Yang, S.T. Lee, Angew Chem Int Edit, 49 (2010) 4430.
[9] S. Jovanović, S. Dorontić, D. Jovanović, G. Ciasca, M. Budimir, A. Bonasera, M. Scopelliti, O. Marković, B. Todorović Marković, Ceram Int, 46 (2020) 23611.

ON-LINE CHARACTERIZATION OF NANOPARTICLES BY SINGLE PARTICLE ICP-MS UTILIZING MICROFLUIDIC DEVICES

Gyula Kajner[1,2], Albert Kéri[1,2], Ádám Bélteki[1,2], Sándor Valkai[3], András Dér[3], Zsolt Geretovszky[2,4], Gábor Galbács[1,2]

[1]Dept. of Inorg. and Anal. Chem., Univ. of Szeged, H-6720 Szeged, Dóm sq. 7, Hungary
[2]Dept. of Mater. Sci., Interdiscip. Excel. Cent., Univ. of Szeged, H-6720 Szeged, Dugonics sq. 13, Hungary
[3]Inst. of Biophys., Biol. Res. Cent., H-6726 Szeged, Temesvári blvd. 62, Hungary
[4]Dept of Opt. and Quantum Elec., Univ. of Szeged, 6720 Szeged, Dóm sq. 9, Hungary
e-mail: galbx@chem.u-szeged.hu

Abstract
In this study, polydimethylsiloxane (PDMS) - glass microfluidic chips (MCs) were designed and fabricated using moulds prepared by a professional 3D printer. The prepared chips were used for the dilution, counting and characterization of nanoparticles (NPs) performing single particle inductively coupled plasma mass spectrometry (spICP-MS) measurements.

Introduction
Single particle inductively coupled plasma mass spectrometry is a novel technique for the rapid characterization of the dispersions of nano- and submicron particles. The technique can provide information on the presence, size and size distribution, number concentration, elemental and isotope composition of nanodispersions [1, 2]. An outstanding advantage of spICP-MS is the low (10^3-10^5 mL^{-1}) optimal particle number concentration (PNC), which can be prepared from sub-microgram amounts of sample [3]. This advantage can be best exploited by a sample introduction system capable for the introduction of low-volume samples. The sample preparation procedure of spICP-MS is simple, requiring only the dilution of nanodispersions. Nevertheless, in case of real-life samples, where the PNC can be hardly estimated accurately, it can be work- and time-consuming to find the right dilution to achieve single particle detection. MCs are well-established state-of-the-art devices suitable for the handling of low-volume solution and dispersion samples. These tools often serve capillary electrophoresis but are exploited in other fields of analytical separation and sample preparation techniques as well. Most microfluidic devices are prepared utilizing polydimethylsiloxane (PDMS) and glass/quartz microscope slides as these materials are cost-effective and easy to produce [4]. MCs also bear the possibility for automation which makes them even more attractive.
The aim of our study was to develop microfluidic devices for on-line spICP-MS sample preparation. In this contribution, we present some of our experimental results.

Experimental
An Agilent 7700X inductively coupled plasma mass spectrometer (ICP-MS) was used in all experiments. Sample introduction was performed by utilizing Gilson Minipuls 3 peristaltic pumps (Gilson Inc. Middleton, WI, USA) and a Micro Mist type nebulizer equipped with a Peltier-cooled spray chamber (standard Agilent 7700x accessories). The sample uptake rate was 600 µL/min. The data acquisition software was used in Time Resolved Analysis (TRA) mode. The integration time was set to 500 ms for the measurement of solution samples and 6 ms for nanodispersions, whereas the acquisition time was set to 60 s. All measurements were repeated three times and the error bars in the following graphs indicate their standard deviation.
The microfluidic chip moulds were fabricated utilizing a Form 3 professional 3D printer using „High Temp” resin material (Formlabs, Somerville, MA, USA). Utilizing the moulds, the MCs

were prepared by using Sylgard 184 silicone elastomer and curing agent (Dow Corning, Midland, MI, USA) and sealing the PDMS to a flat glass microscope slide. Detailed description of the preparation of the MCs can be found in one of our earlier publications [5].
Before dilution and also directly before aspiration into the ICP-MS, the dispersions were sonicated in an ultrasonic bath for 5 min (Bransonic 300, Ney, Danbury, CT, USA) in order to minimize particle aggregation.
Co and Ag sample solutions were prepared from 1000 mg/L CertiPUR monoelemental standards (Merck GmbH, Darmstadt, Germany). In spICP-MS measurements, commercially available NP standard dispersions were used. Ultra uniform polyethylene-glycol-capped 47.8 (1.8) nm gold nanospheres were purchased from Nano-Composix (San Diego, California USA), Pelco NanoXact tannic acid-capped 43.4 (3.2) nm silver NPs were obtained from Ted Pella (Redding, California, USA). Trace-quality de-ionized labwater from a MilliPore Elix 10 device equipped with a Synergy polishing unit (Merck GmbH, Darmstadt, Germany) was used for the preparation of all solutions and dispersions. Ismatec S3 E-LFL Tygon tubings (IDEX Health & Science GmbH, Wertheim, Germany) of 0.27 and 0.48 mm inner diameter were used for the aspiration of liquid samples. To drive the liquid samples to and from the MCs, stainless steel capillaries with 1.2 mm outer diameter, fabricated from medical needles, were placed in the inlet and outlet ports. For the connection of peristaltic tubing, the inlet and outlet needles and the ICP-MS nebulizer, PFA tubing with 0.3 mm inner diameter (part number 5042-0953, Agilent Technologies, Santa Clara, California, USA) and patches prepared from silicone tubing with 1.0 mm inner diameter (Deutsch & Neumann GmbH, Berlin, Germany) were applied.
All data processing was performed within the Agilent MassHunter (Agilent Technologies, Santa Clara, California, USA) and OriginLab Origin (Northampton, Massachusetts, USA) software.

Results and discussion

The design of the MCs (number of inlet ports, the angle between the inlet channels) has a strong impact on flow conditions. Chips with different sample and diluent inlet patterns (presented in Figure 1) were prepared and their performance for the on-line mixing/dilution of solutions was investigated both in computer simulations and in experiments.
In one of the first tests, we investigated how accurately can dilution be performed on the chips. We pumped Co standard solution and water into the input ports in a calculated microflow ratio and monitored the diminishing of the Co ICP-MS signal. According to our results, presented in Figure 2, the achieved dilution showed a good agreement with the theoretical dilution for “W” design, while the other two patterns provided less accurate dilution factors. This phenomenon can be probably explained by less favorable flow conditions at the junction when the diluent is introduced in only one channel. Thus, all further spICP-MS experiments were carried out using only the W design. Please also note the small error bars in the graph (and all later graphs), which indicate that the joint action of the chip, nebulizer and spray chamber, the overall mixing of the liquids in the system take place with very good efficiency.

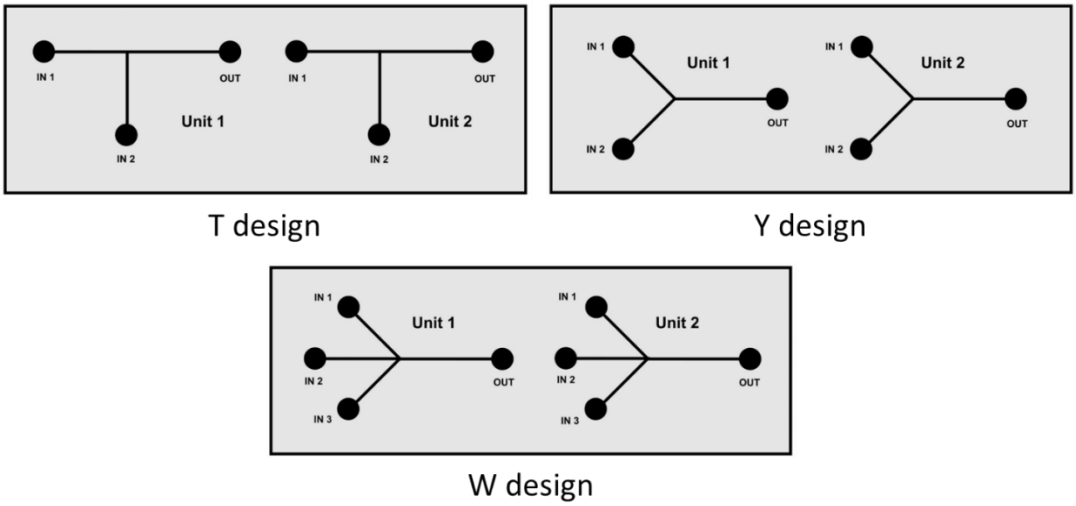

Figure 1. The various designs of the fabricated microfluidic chips

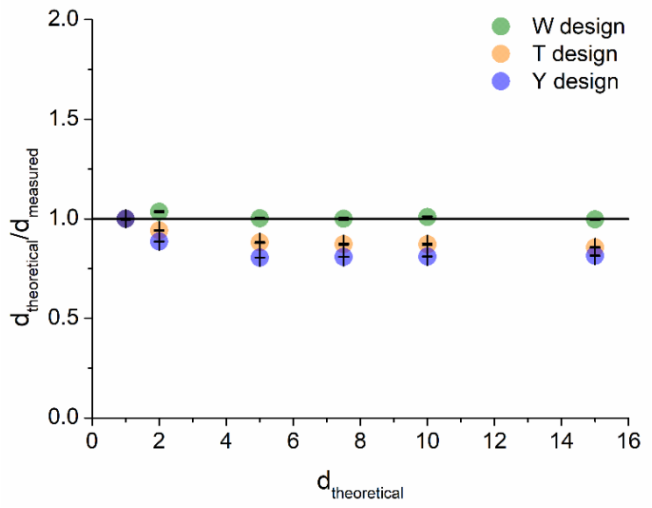

Figure 2. Investigation of the dilution accuracy of the different microfluidic chip designs

A typical task during spICP-MS analysis of unknown dispersions is to find the optimal PNC by performing dilution of the sample. The goal is to find a dilution where the maximum number of particles can be measured to obtain reliable statistical data but individual particle detection is still ensured. In practice this means that several diluted dispersions have to be prepared in relatively large volumes which is a time- and chemical-consuming process. Utilization of MCs for the on-line dilution of nanodispersions can make the process faster and more practical. In order to test this, the online dilution of a gold nanodispersion with 47.8 nm particle size and initial PNC of $1 \cdot 10^5$ mL^{-1} was carried out in the dilution range of 1-100 folds. As Figure 3 shows, there is an excellent linearity between the number of detected NP events and the nominal PNC resulted by the on-line dilution in the range of $1 \cdot 10^3$ and $5 \cdot 10^4$ mL^{-1}. At the highest measured concentration ($1 \cdot 10^5$ mL^{-1}) the number of detected events falls below expectations, which is a clear indication of the detection of more than one NP during the same integration window.

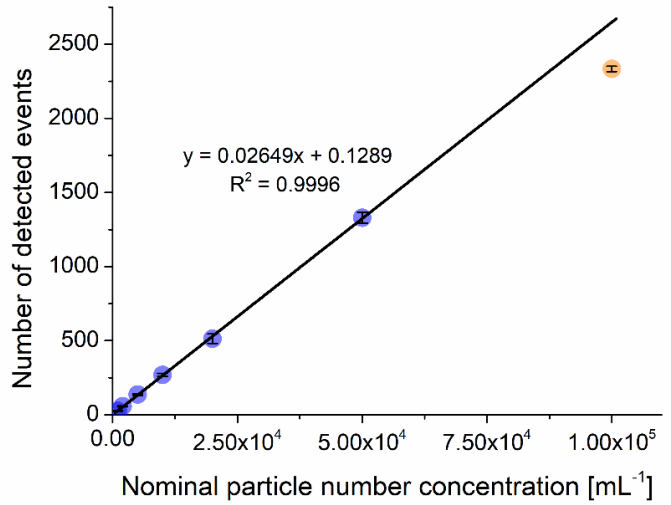

Figure 3. On-line dilution of Au nanodispersion with 47.8 nm particle size and initial PNC of $1 \cdot 10^5$ mL^{-1} in the 1-100 dilution range

Dissolved analyte content in nanodispersions can originate from either the matrix (presence of precursor residues or impurities of other synthesis reagents), or from the partial dissolution of the NPs. In either case, the dissolved analyte content generates a continuous background signal during the time-resolved spICP-MS measurements, which can bury the signal peaks of small NPs. A practical approach to tackle this interference is to dilute the dispersion, as it does not affect the signal originating from individual NPs, but it effectively diminishes the background signal. Utilization of MCs for this purpose is also favorable. Figure 4 shows our experimental results, which demonstrates the above discussed possibilities. A nanodispersion containing 43.4 nm Ag NPs with $1 \cdot 10^5$ mL^{-1} PNC and 1 ppb dissolved Ag was on-line diluted in the range of dilution factors 1 to 10. According to our results, a 5-fold dilution was optimal, as this resulted in a particle peak position that did not shift further to the left with additional dilution. The downside of this technique is that the total measurement time has to be increased in correspondence with the dilution factor in order to maintain the statistical relevance of the collected data.

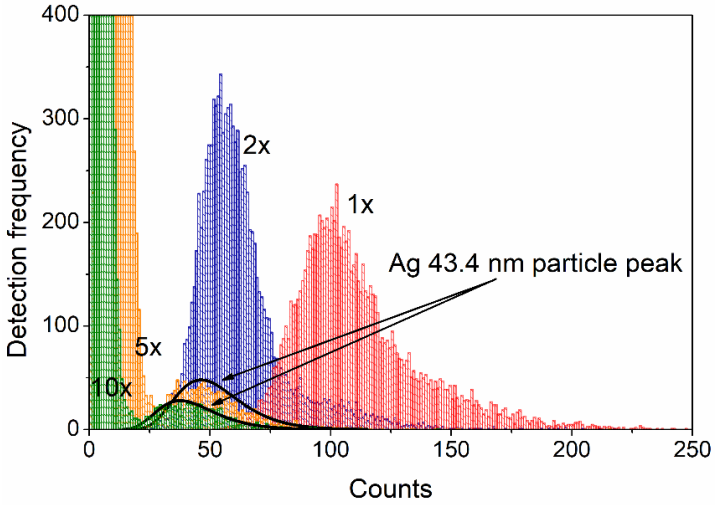

Figure 4. spICP-MS histograms of on-line diluted nanodispersion originally containing 43.4 nm Ag NPs with $1 \cdot 10^5$ mL^{-1} PNC and 1 ppb dissolved Ag

A particularly challenging situation in spICP-MS is when only a small amount of sample is available for analysis. As MCs are capable for handling of µL liquid samples with ease, they could be applied for the analysis of e.g. precious nanodispersion samples. We tested this concept by the injection of a few ten µL sample volumes and studied if the number of detected events is proportional to the PNC. As our results in Figure 5 indicate, the utilization of the fabricated MCs provided a good correlation with a reasonable standard deviation and accuracy.

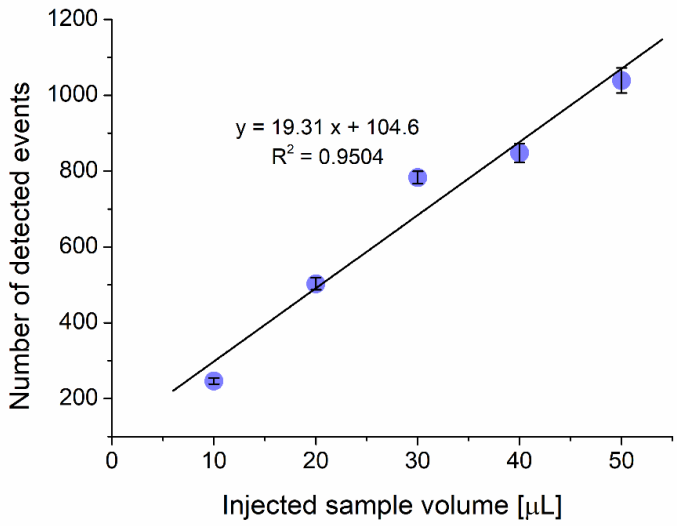

Figure 5. The number of detected events of low volume (10-50 µL) Au nanodispersions with 47.8 nm size and initial PNC of $5 \cdot 10^5$ mL^{-1} with 10-folds online dilution on the MC

Conclusion

PDMS-glass microfluidic chips were successfully applied for the on-line dilution and sample introduction of NPs for spICP-MS analysis. The utilization of the chips provides the prospect of automation (e.g. using electronically actuated microvalves and software control) that makes spICP-MS sample preparation fast and simple. We also demonstrated the feasibility of carrying out spICP-MS measurements on low (only a few tens of µL) sample volumes.

Acknowledgements

The authors gratefully acknowledge the financial support from various sources including the Ministry of Innovation and Technology (No. TUDFO/47138-1/2019-ITM FIKP) and the National Research, Development and Innovation Office (through project No. EFOP-3.6.2-16-2017-00005, GINOP-2.3.3-15-2016-00040 and TKP 2020 Thematic Excellence Program 2020) of Hungary.

References

[1] M.D. Montaño, J.W. Olesik, A.G. Barber, K. Challis, J.F. Ranville, Anal. Bioanal. Chem. 408 (2016) 5053.
[2] D. Mozhayeva, C. Engelhard, J. Anal. At. Spectrom. 35 (2020) 1740.
[3] A. Sápi, A. Kéri, I. Kálomista, D.G. Dobó, Á. Szamosvölgyi, K.L. Juhász, Á. Kukovecz, Z. Kónya, G. Galbács, J. Anal. At. Spectrom. 32 (2017) 996.
[4] M. He, B. Chen, H. Wang, B. Hu, Appl. Spectrosc. Rev. 54 (2019) 250.
[5] A. Metzinger, A. Nagy, A. Gáspár, Zs. Márton, É. Kovács-Széles, G. Galbács, Spectrochim. Acta B 126 (2016) 23.

PHOTOCATALYTIC EFFICIENCY OF ZnFe-MIXED METAL OXIDES IN CORRELATION WITH REACTION PARAMETERS

Milica Hadnadjev-Kostic[1], Djurdjica Karanovic[1], Tatjana Vulic[1]

[1]University of Novi Sad, Faculty of Technology Novi Sad, Bul. cara Lazara 1, 21000 Novi Sad, Serbia.
e-mail: djurdjicakaranovic@uns.ac.rs

Abstract
In the last decade, the interest for the photocatalytic phenomena has rapidly grown due to its great potential for the overall environmental decontamination. Photocatalysts based on ZnFe mixed oxides have been considered to be potentially photocatalyticly efficient in wastewater purification. This investigation is focused on the characterization of the synthesized and thermally treated photocatalysts, on their photocatalytic efficiency in the degradation process of organic dye pollutant Rhodamine B (RhB), as well as on the influence of process parameters on the photocatalytic efficiency. The results showed that the obtained mixed oxides are highly efficient in the RhB degradation. In addition, the pH effect of the reaction system on the photocatalytic activity was observed, which could be explained by the correlation with different textural and structural properties of the photocatalysts.

Introduction
The concern for the exponential increase of environmental pollution with no systematic solution has become overwhelming in the scientific community [1]. Organic dye pollutants from different industries regularly occur in wastewater and initiate vast hazardous environmental problems, considering their toxicity, unpleasant colouring and non-biodegradation [2]. Therefore, the search for the most effective removal method is still in progress and has become a challenging and motivating task with the aim to decrease or completely eliminate environmental problems regarding dye pollutants in wastewater. Zinc oxide (ZnO) has been considered to be a good candidate for the wastewater purification due to its wide band gap (3.2 eV) in the near-UV spectral region, strong oxidation ability, good photocatalytic property and low cost. It has been brought to the attention in scientific publications, that more efficient photodegradation is triggered by coupling of semiconductors with a wide band gap with another semiconductor with a narrow energy band [3]. Therefore, the motivation for this investigation was to develop a simple and inexpensive synthesis method for ZnFe-mixed metal oxides with the desired properties in order to enhance photocatalytic performance in photodegradation of organic dyes, as well as to investigate the influence of the process parameters on the photodegradation efficiency.

Experimental
Mixed metal oxides were synthesized by the coprecipitation method using $Zn(NO_3)_2 \cdot 6H_2O$ and $Fe(NO_3)_3 \cdot 9H_2O$ precursors that were added in the base solution (0.67 M Na_2CO_3 and 2.25 M NaOH) and vigorously stirred at constant temperature (40^{o}C). The precipitates were aged and then washed with deionized water until pH 7 was reached. The products were dried for 24 h at 100°C (sample denoted as ZnFe-100) and thermally treated for 5 h at 300°C (denoted as ZnFe-300).
X-ray powder diffraction (XRD) analysis was used for the identification of the phase composition, conducted by Rigaku MiniFlex 600.
Photocatalytic tests were performed in an open cylindrical thermostated Pyrex reaction vessel using ULTRA VITALUX 300 W lamp, to simulate solar light irradiation. Before illumination,

reaction mixtures (50 mg of catalysts and 100 ml of 10 μmol/l (RhB solution) were stirred in the dark for 30 min to ensure adsorption/desorption equilibrium. The reaction solutions were than submitted to light irradiation while stirred. Aliquots were analysed at the defined time intervals using UV-VIS spectrophotometer. The photocatalytic activity was estimated by RhB photodegradation, monitoring the decrease of the RhB concentration in time.
The effect of the initial pH of reaction solutions on the photodegradation efficiency of RhB was studied in the range of 2-12. Aqueous solutions of HCl and NaOH were applied for the adjustment of the initial pH and the photodegradation efficiency of ZnFe-300 sample was measured after 180 min of light irradiation.

Results and discussion

The results of the structural characterisation are presented in Figure 1 as XRD diffraction peaks of the ZnFe-photocatalysts (ZnFe-100 and ZnFe-300). The XRD diffraction patterns for the ZnFe-100 sample exhibited sharp intense diffraction peaks at 31.79°; 34.4°; 36.25°; 47.5°; 56.6°, 62.85° i 67.97° that correspond to (100), (002), (101), (102), (110), (103) i (112) crystalline lattice for the ZnO phase [4].
After thermal treatment at 300°C the formation of additional spinel phase $ZnFe_2O_4$ with the cubic structure was detected with diffraction peaks at 0.05°, 35.36°, 42.78°, 52.96°, 56.78° and 62.2° [5]. It can be concluded that the thermal treatment at higher temperature initiated the formation of the spinel phase that has been cited as the phase that enhances photocatalytic properties of the photocatalyst.

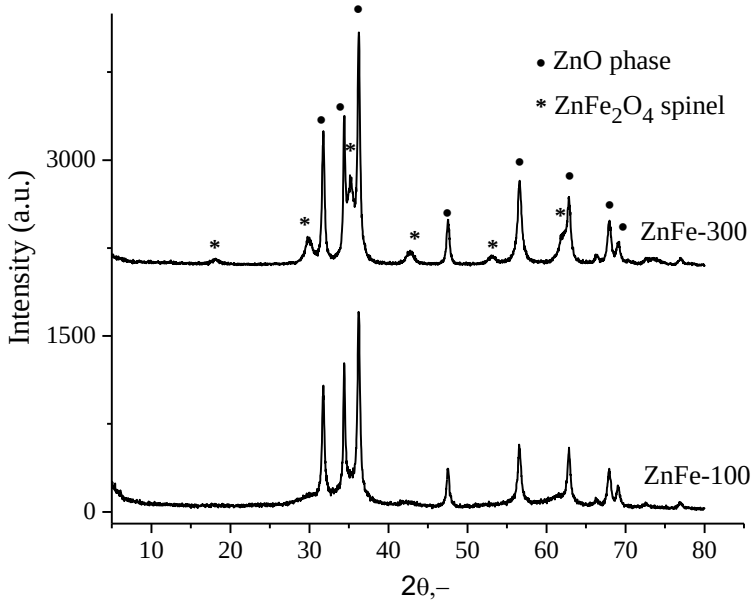

Figure 1. XRD diffraction peaks for sample: ZnFe-100 and ZnFe-300

The results of the RhB photodegradation, presented in Figure 2, show that the photocatalyst activated at higher temperature, ZnFe-300, exhibits higher photocatalytic efficiency (over 91% after 330min of UV irradiation) than photocatalyst treated at lower temperature, ZnFe-100 (around 50% after 330min f UV irradiation). The enhanced photodegradation could be assigned to the formation of the additional $ZnFe_2O_4$ spinel phase after thermal treatment.

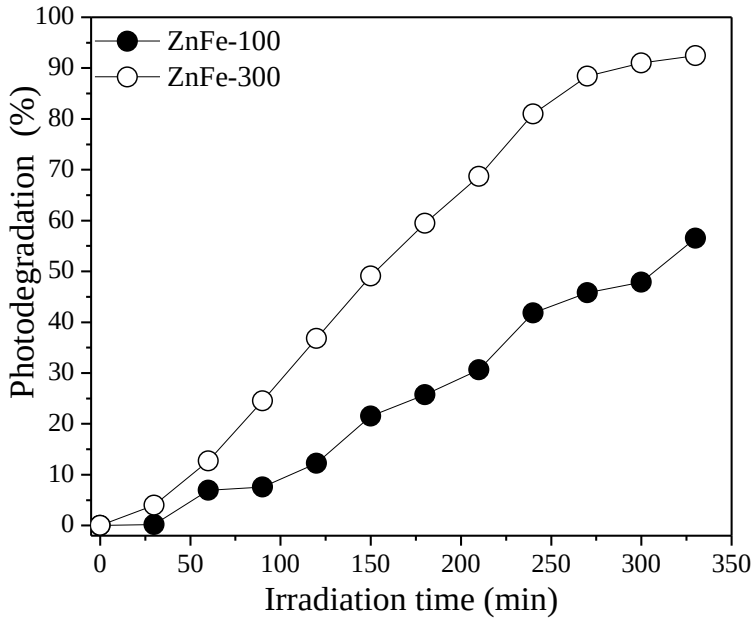

Figure 2. The photodegradation of RhB as a function of light irradiation time

In order to determine the influence of the pH on the photocatalytic effieciency, numerous photodegardation reactions were conducted using better performing photocatalyst (ZnFe-300) at different pH values, measuring the photodegradation efficiency at the same time intervals (Figure 3). The optimal pH resulting in the most efficient photodegradation for ZnFe-300 photocatalyst was observed at pH 6. The photodegradation efficiency increased with the increase of the pH values up to pH 6 and than gradually decreased in the alkaline pH region.

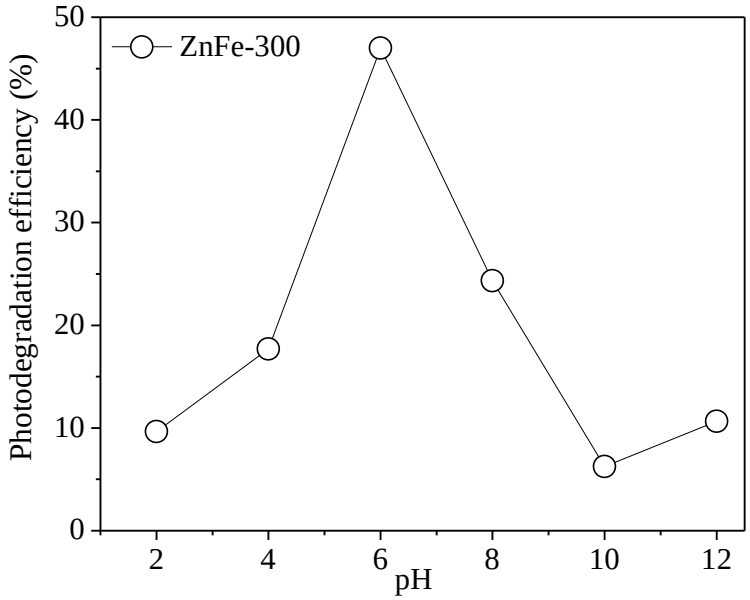

Figure 3. Influence of the pH values on the photocatalytic efficiency of ZnFe-300

Conclusion

In this investigation, ZnFe-mixed oxides were successfully synthesized and thermally treated at 100 and 300°C. The XRD and photocatalytic results confirmed that the ZnFe-300 catalyst, composed of wurzite ZnO and spinel structured $ZnFe_2O_4$ phases, had better crystallinity and enhanced photocatalytic efficiency in the RhB photodegradation compared to ZnFe-100

photocatalyst. The results proved that the $ZnFe_2O_4$ spinel phase conclusively affects the photocatalytic efficiency probably due to the synergic coupling effect of ZnO and $ZnFe_2O_4$. Additionally, the ZnFe-300 photocatalyst exhibited significant loss of activity in the acidic (pH from 2 to 6) and alkaline solutions (pH higher than 7) suggesting that the optimal pH for RhB photodegradation using ZnFe mixed oxides, is around pH 6. This research enabled a better insight into the influence of photocatalyst thermal activation on physico-chemical properties of ZnFe-mixed oxide based photocatalysts in correlation with their photocatalytic performance at various pH reaction conditions.

Acknowledgements
This work was partially supported by the Ministry of education,science and technological development of the Republic of Serbia.

References
[1] M. Hadnadjev-Kostic, T. Vulic, R. Marinkovic-Neducin, D. Loncarevic, J. Dostanic, S. Markov, D. Jovanovic, J Clean. Prod. 164 (2017) 1.
[2] D. Zhang, Acta Chim. Slovaca 6 (1) (2013) 141.
[3] H. Derikvandi, A. Nezamzadeh-Ejhieh, J. Hazard. Mater. 321 (2017) 629.
[4] P. Geetha Devi, A. Sakthi Velu, J Theor Appl Phys 10 (2016) 233.
[5] C.G. Anchieta, A. Cancelier, M. A. Mazutti, S.L. Jahn, R.C. Kuhn, A. Gündel, O. Chiavone-Filho, E. L. Foletto, Materials 7 (2014) 6281.

ADSORPTION KINETICS FOR THE REMOVAL OF METHYL ORANGE USING ADSORBENTS BASED ON Zn Al-LAYERED DOUBLE HYDROXIDES

Djurdjica Karanovic[1], Milica Hadnadjev-Kostic[1], Tatjana Vulic[1] and Marija Milanović[1]

[1]University of Novi Sad, Faculty of Technology Novi Sad, Bul. cara Lazara 1, 21000 Novi Sad, Serbia.
e-mail: djurdjicakaranovic@uns.ac.rs

Abstract
The adsorption phenomena of adsorbents based on ZnAl layered double hydroxides was studied. Methyl orange was used as test pollutant. The emphasis of the study was the analysis of Methyl Orange removal kinetics. The synthesized and thermally treated adsorbents were characterized by X-ray diffraction. The analysis of adsorption kinetics was conducted using the pseudo-second order kinetic model. The results showed that the samples have adsorptive removal properties, particularly the adsorbent derived from thermally treated layered double hydroxides. The findings give an insight into the adsorption phenomena of ZnAl-layered double hydroxides based materials which could be considered as promising adsorbents for the removal of Methyl Orange in wastewaters.

Introduction
From various industries, organic dyes have been detected as one of the toxic pollutants in wastewaters and have recently become a serious concern due to the increased quantity discharged into the environment. Considering their stable nature, these dyes can cause severe problems not only to the environment, but also to humans [1]. Therefore, an urgent need for a rapid and efficient removal method for coloured dyes from water is of essential importance and has been set as a priority in the scientific world. Lately, layered double hydroxides (LDHs) have received considerable attention in the environmental friendly processes. These materials consist of stacked hydroxide layers with charge-balancing anions in the interlayer [2]. Additionally, the properties of the LDHs can be tailored through variation of numerous synthesis methods and parameters enabling abundant possibilities for preparation of materials with targeted characteristics. After thermal treatment, their layered structure collapses triggering the formation of non-stoichiometric metastable mixed oxides with developed surface area and specific acid-base and redox properties. One of the most interesting property of the obtained mixed oxides is the so-called "memory effect" that gives the thermally treated oxides the ability to easily reconstruct the original layered structure in an aquatic environment [3].
Therefore, the motivation for this study was to investigate the behaviour of synthesized ZnAl-LDHs and their mixed oxides (thermally treated at 500°C/5h) in the Methyl Orange (MO) removal processes and to determine the adsorption kinetics of the process.

Experimental
For the synthesis of layered double hydroxides with carbonate anions in the interlayer low supersaturation coprecipitation method at constant pH (9–9.5) was used. Metal salts solution $Zn(NO_3)_2{\cdot}6H_2O$ and $Al(NO_3)_3{\cdot}9H_2O$, were continuously (4 cm^3min^{-1}) added at constant temperature (40°C) maintaining the required constant pH with the base solution of 0.67 M Na_2CO_3 and 2.25 M NaOH. The precipitates were aged for 15 h, thoroughly washed with distilled water until neutral pH = 7. The obtained samples were dried 24 h at 100°C (ZnAl-100) and then calcined for 5 h, at 500°C in air (ZnAl-500).
The phase composition of samples was analysed by X-ray powder diffraction (XRD), using Rigaku MiniFlex 600.

Adsorption experiments were conducted in an open cylindrical thermostated Pyrex reaction vessel containing 100 ml of MO solution (C_0 = 20 mg dm^{-3}) and 50 mg of powdered adsorbents (ZnAl-100 and ZnAl-500). At defined intervals, aliquots were centrifuged and MO concentrations were determined using UV-VIS spectrophotometer at 464 nm.
The pseudo-second-order kinetic model was used for the analysis of the MO adsorption kinetics.

Results and discussion

XRD spectra of the synthesized (ZnAl-100) and thermally treated (ZnAl-500) samples are presented in Figure 1. XRD pattern of ZnAl-100 sample corresponds to the characteristic reflections for the layered structure of the hydrotalcite-like materials (Zinc Aluminium Carbonate Hydroxide Hydrate JCPDS 38-0486) and the observed sharp and highly intensive peaks suggest a well-defined crystal structure [4]. Additional peaks were also detected that could be attributed to the presence of the crystalline ZnO phase in the ZnAl-100 sample [5]. After thermal treatment at 500°C, layered LDH structure collapsed and the formation of the spinel phase $ZnAl_2O_4$ with additional ZnO peaks was detected. Besides that, the intensities of the diffraction peaks are much lower suggesting that the newly formed mixed-oxide phase has lower crystallinity than starting LDH phase. The results of the XRD analysis show that thermal treatment of layered double hydroxides leads to the collapse of the layered structure verified by the formation of new phases detected in sample ZnAl-500.

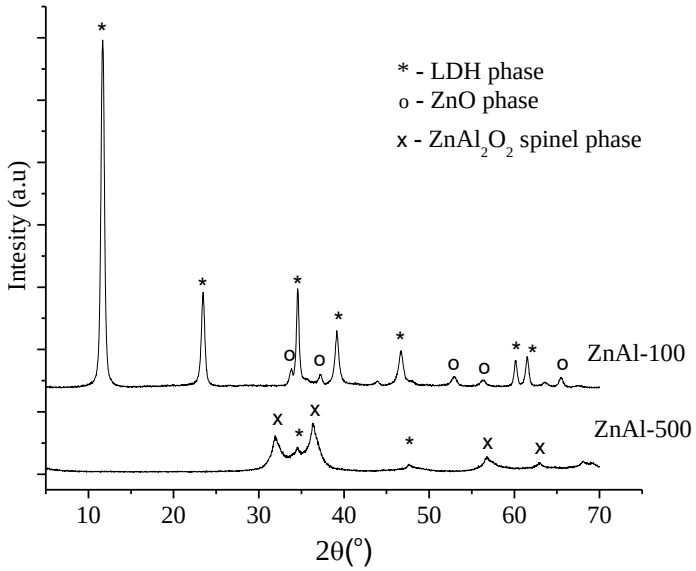

Figure 1. XRD diffraction patterns for samples ZnAl-100 and ZnAl-500

The absorption process of the MO is presented as a function of MO concentration decrease with contact time (adsorbent-pollutant) in Figure 1. It can be observed that the decrease in MO concentration was detected with both adsorbents. The concentration decrease for the sample ZnAl-100 was only around 30% after 120 minutes of adsorbent-pollutant contact, whereas outstanding concentration decrease was observed for sample ZnAl-500. After only 1 min of adsorbent-pollutant contact the MO concentration decreased to complete decolourisation of the pollutant (~0 mg/l). This higher adsorptive capacity of ZnAl-500 sample could be explained by the memory effect. The thermally treated sample probably reconstructed its starting layered structure after contact with the MO aquatic solution, partially intercalating the MO and CO_3^{2-} ions into the interlayer of LDH, leading to complete removal after only 1 minute of contact.

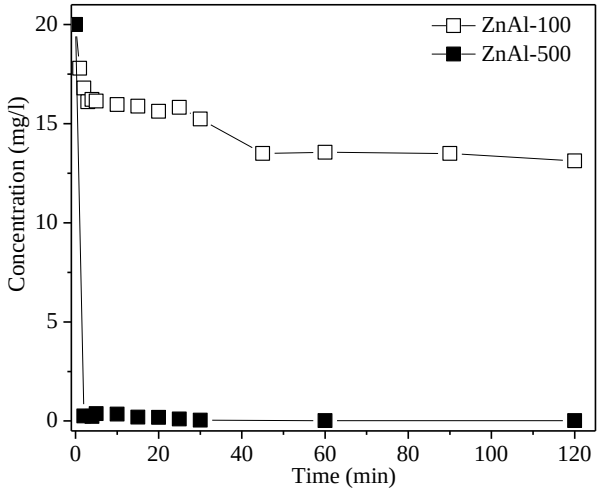

Figure 2. The MO concentration decrease as a function contact time (adsorbent-pollutant)

In order to define the adsorbent efficiency for dye removal processes and to clarify the adsorption mechanism, it is necessary to determine adsorption kinetics. Adsorption kinetics was evaluated using the pseudo-second-order kinetic model given by the following equation:

$$\frac{t}{q_t} = \frac{1}{k_2 q_e^2} + \frac{1}{q_e} t \qquad (1)$$

where q_e (mg g^{-1}) is the adsorption capacity at equilibrium conditions and q_t (mg g^{-1}) is the adsorption capacity at equilibrium at defined time t (min); k_2 (g mg^{-1} min^{-1}) is the equilibrium rate constant for the pseudo-second-order model.

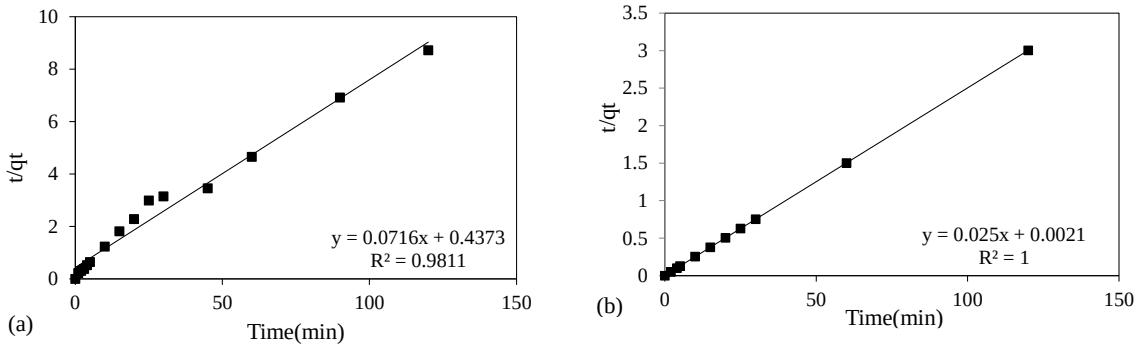

Figure 3. Pseudo-second-order kinetic plot: (a) ZnAl-100 and (b) ZnAl-500

Considering the correlation coefficient (R^2) and the data obtained for MO adsorption, it can be observed that the best fit for both adsorbents was obtained by the pseudo-second-order kinetic model. The results of fitting experimental data for pseudo-second-order kinetic model are given in Table 1. The analysis of data indicates that the pseudo-second-order model is suitable for the explanation of the MO adsorption kinetics on adsorbents based on layered double hydroxides. Considering that the pseudo-second-order model is based on the adsorption loading of the solid phase, the rate-determining step has been described to be the chemisorption [6]. Additionally, it has been suggested that the pseudo-second-order model can predict the behaviour over the whole range of the adsorption process [1].

Table 1. Kinetic parameters and correction coefficient (R^2) for the pseudo-second-order kinetic model

Samples	Pseudo-second order		
	q_e(mg/g)	k_2(g/mgmin)	R^2
ZnAl-100	13.76	0.012078	0.9811
ZnAl-500	39.96	0.2982	1

Conclusion

In this study, ZnAl-LDH and ZnAl-mixed oxides were successfully synthesized and thermally treated at 100 and 500°C. The XRD analysis for ZnAl-100 sample confirmed the presence of the characteristic reflections for the layered structure of the hydrotalcite-like materials with the additional ZnO phase. After thermal treatment at 500°C, sample ZnAl-500 layered LDH structure collapsed and the formation of the spinel phase $ZnAl_2O_4$ with additional ZnO peaks was detected.

The adsorbent treated at higher temperature, ZnAl-500, showed high adsorption properties that could be explained by the memory effect and the ability to intercalate the MO and CO_3^{2-} ions into the interlayer of LDH during the reconstruction of the layered structure. Adsorption kinetics analysis showed that the best fit for both adsorbents was obtained by the pseudo-second-order kinetic model indicating that the rate-determining step is the chemisorption and suggesting possible prediction of the behaviour over the whole range of the adsorption process. These results suggested that the LDHs could be considered as promising adsorbents for the removal of Methyl Orange in wastewaters.

Acknowledgements

This work was partially supported by the Ministry of education, science and technological development of the Republic of Serbia.

References

[1] Z.-M. Ni, S.-J. Xia, L.-G. Wang, F.-F. Xing, G.-X. Pan, J. Colloid Interface Sci. 316 (2007) 284.
[2] H. Laguna, S. Loera, I. A. Ibarra, E. Lima, M. A. Vera, V. Lara, Microporous Mesoporous Mater. 98 (2007) 234.
[3] M. Hadnadjev-Kostic, T. Vulic, R. Marinkovic-Neducin, D. Loncarevic, J. Dostanic, S. Markov, D. Jovanovic, J Clean. Prod. 164 (2017) 1.
[4] M. Hadnadjev-Kostic, T. Vulic, R. Marinkovic-Neducin, Adv. Powder Technol. 25 (2014) 1624.
[5] P. Geetha Devi, A. Sakthi Velu, J Theor Appl Phys 10 (2016) 233.
[6] L. Ai, C. Zhang, L. Meng, J. Chem. Eng. Data 56 (2011) 4217

MICROWAVE-ASSISTED SYNTHESIS OF N-DOPED CARBON QUANTUM DOTS FOR THE PHOTOCATALYTIC REMOVAL OF METHYLENE BLUE FROM WASTEWATER

Dejan Kepić[1], Jovana Prekodravac[1], Bojana Vasiljević[1], Dragana Jovanović[1], Duška Kleut[1], and Biljana Todorović Marković[1]

[1] *Vinča Institute of Nuclear Sciences - National Institute of the Republic of Serbia, University of Belgrade, P.O.B. 522, 11001 Belgrade, Serbia*
e-mail: d.kepic@vin.bg.ac.rs

Abstract
Wastewater treatment is an emerging problem in the industrialized world. The development of new semiconducting materials with the potential to be used in photocatalysis is the focus of the scientific community. Here, we present the synthesis of N-doped carbon quantum dots (N-CQDs) using microwave radiation. N-CQDs were synthesized by irradiation of glucose solution in the presence of ammonia hydroxide as a nitrogen doping agent at low temperature (100 °C), low applied microwave power (100 and 200 W), and for a short period of time (60 s). The possible application of N-CQDs as a catalyst for photocatalytic degradation of Methylene Blue (MB) dye under blue light, green light, red light, and daylight was investigated. The highest values of MB degradation were observed for the samples exposed to red light with a maximum of 58.8 % for N-CQDs sample prepared at the reactor power of 200 W exposed to red light for 2 h.

Introduction
With the rapid industrial development and production of goods, industrial effluents became a big problem for the environment. The release of toxic chemicals in water, soil, and air constantly increases in the past decades, which consequently increases the need for the special treatment of waste material. Various organic dyes commonly used in the industry show mutagen and cytotoxic behavior [1]. Among different methods for the removal of dyes from wastewater, photochemistry has big potential to solve this problem. The size of the bandgap of semiconducting catalysts dictates the wavelength of the absorbed light. Recently, scientists put an effort to find semiconducting material with smaller bandgaps to improve visible light absorption. Besides, to exploit the ability of reactive oxygen species (ROS) to breakdown the dye molecules, it is important to find a catalyst with bandgap close to the redox potential of $H_2O/\cdot OH$ couple. To date, many heterogeneous catalysts are reported for the removal of dyes from wastewater [2-4].
The emerging interest in carbon nanomaterials brought to the scene new materials for the application in photocatalysis [5]. A new zero-dimensional carbon-based nanomaterial, carbon quantum dots (CQDs), recently draw attention due to their extraordinary properties. They are water dispersible, non-toxic, biocompatible, and economically and environmentally friendly, and they possess semiconducting character with a tunable energy bandgap that can be directed by the introduction of selected functional groups or heteroatom into their structure [6,7]. Nitrogen proved to be an effective heteroatom for doping of various carbon nanomaterials since it greatly influences the electronic properties of the material [8-10]. Although many methods for the N-doping of CQDs are reported so far, the majority of them are complex, time-consuming, and expensive. On the other hand, microwave-assisted synthesis accelerates chemical reactions at low temperatures and therefore can be applied for fast and efficient synthesis of N-doped CQDs (N-CQDs).

In this paper, a fast preparation of N-CQDs using microwave irradiation is demonstrated. The synthesis of N-CQDs from glucose solution in the presence of ammonia hydroxide as a nitrogen doping agent was conducted under microwaves with reactor power of 100 and 200 W for 60 s. The possible application of N-CQDs as a catalyst for photocatalytic degradation of Methylene Blue (MB) dye under blue light, green light, red light, and daylight was investigated.

Experimental

For the N-doped CQDs synthesis, 10 wt.% glucose solution in water was mixed with 25 % ammonia hydroxide in ratio 5:1. The reaction mixture was heated in microwave reactor (CEM Discover BenchMate) for 1 minute at a fixed temperature of 100 °C and microwave power of 100 and 200 W. Further in the text the samples are labeled according to the reactor power N-CQDs-100 and N-CQDs-200, respectively. After cooling to room temperature at atmospheric conditions, the samples were dialyzed (300 Da) for 5 days and filtered (membrane pore sizes between 450 and 10 nm). The morphology analysis was performed using TEM JEOL Jem 1210 Electron Microscope operating at 120 kV. For the analysis, the N-CQDs samples were prepared by drop-casting of the samples onto carbon-coated TEM copper grid 200 mesh. ATR FTIR spectra were obtained at Nicolet 8700 spectrometer with spectral resolution of 4 cm^{-1}. The UV-Vis absorption spectra were measured using Avantes UV-Vis spectrophotometer (Apeldoorn, The Netherlands). N-CQDs water solutions with concentration of 1 mg/ml were mixed with MB (0.03 mM) and exposed to blue light (λ=470 nm), green light (λ=530 nm), red light (λ=630 nm), and daylight (solar light on a window ledge without light flux concentration, May 30th, 2018) for 2 and 3 h. UV-Vis measurements were performed immediately after the exposure of the selected time period.

Results and discussion

Water solution of glucose and ammonia hydroxide was irradiated in microwave reactor at two different reactor powers of 100 and 200 W. The formation of N-CQDs formation is indicated by the change of the color of the reaction mixture to light brown for N-CQDs-100, and dark brown for N-CQDs-200. The morphology of the samples was characterized by TEM microscopy and the representative TEM images for samples synthesized at 100 and 200 W are presented in Figure 1 a) and b).

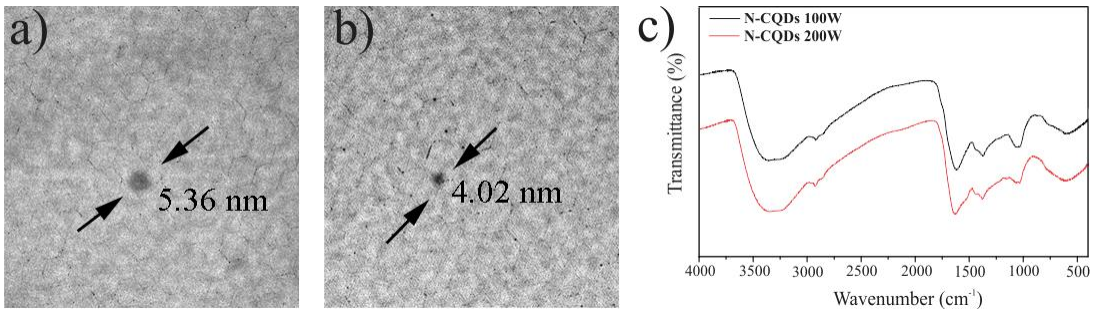

Figure 1. TEM images of N-CQDs samples synthesized at a reactor power of a) 100 W and b) 200 W, and c) FTIR spectra of N-CQDs samples.

The prepared N-CQDs have spherical shapes for both the applied reactor power. According to the microscopy analysis, the majority of particles have diameters of up to 30 nm. The FTIR spectra of N-CQDs synthesized at 100 and 200 W (Figure 1c) show a broad peak at 3400 cm^{-1} that originates from the stretching vibrations of O-H from carboxylic groups. The peak of N-H stretching vibrations from amine group at 3300 cm^{-1} is also present. Among these, peaks that correspond to C-H vibrations at 2929 and 2861 cm^{-1}, C=C vibrations at 1625 cm^{-1}, C-N bonds

from amide groups at 1385 cm^{-1}, and C-O stretching vibrations at 1044 cm^{-1} are also present [11,12]. The presence of polar oxygen-related functional groups in the N-CQDs structure is responsible for their good water dispersibility.

Photocatalytic degradation of MB in the presence of synthesized N-CQDs was evaluated under a broad spectrum of wavelength, including blue light, green light, red light, and daylight. UV-Vis spectra of MB/N-CQDs exposed to these wavelengths are shown in Figure 2.

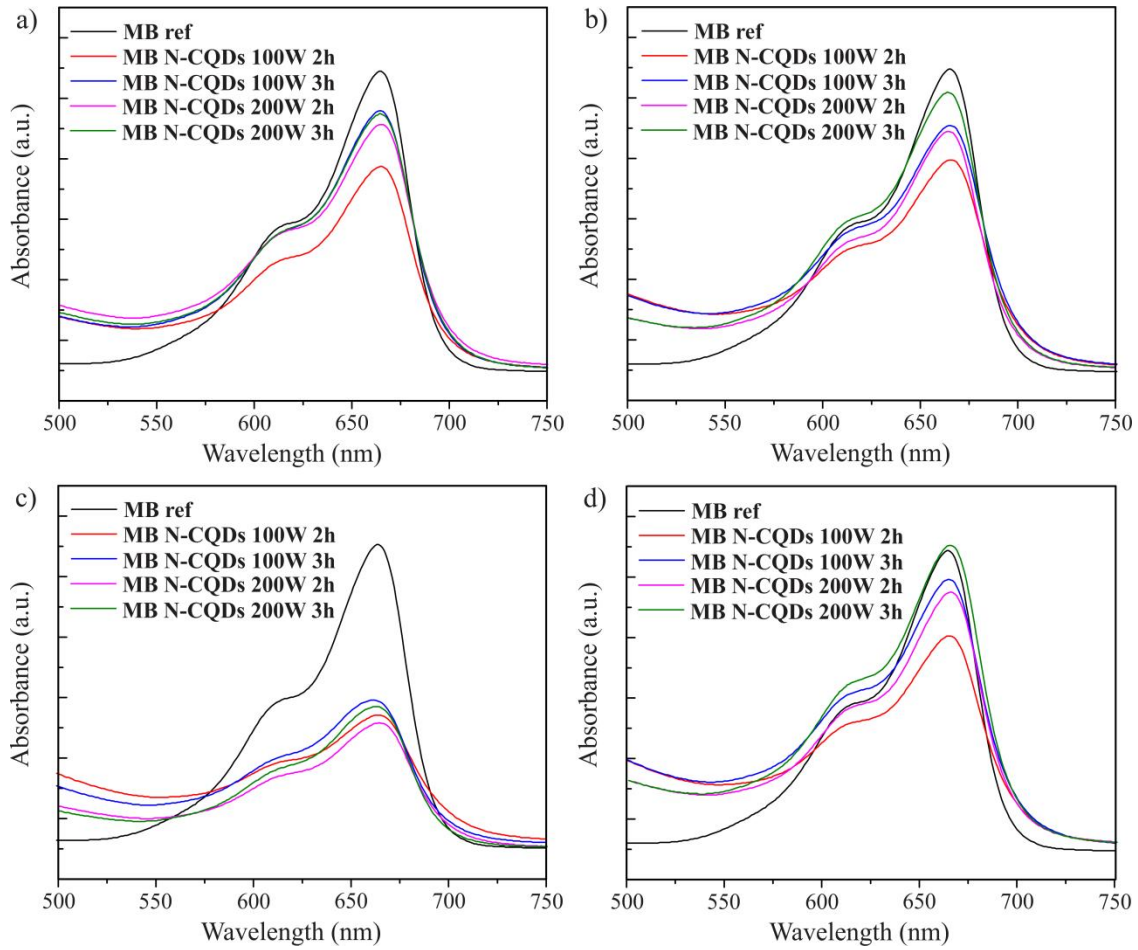

Figure 2. UV-Vis spectra of MB/N-CQDs exposed to a) blue light, b) green light, c) red light, and d) daylight for 2 and 3 h.

Since the concentration of MB is proportional to the absorbance of MB according to Beer-Lambert law, the degradation efficiency of MB can be calculated from the formula:

$$R = (C_0\text{-}C)/C_0 \times 100\ \% = (A_0\text{-}A)/A_0 \times 100\ \%$$

where A_0 and A are the absorbances, and C_0 and C are concentrations of MB in time 0 and t. For the constant amount of MB (0.03 mM), we examined the effect of the exposure time to the degradation of MB. Samples were exposed for 2 and 3 h to the blue light, green light, red light, and daylight. The results are presented in Table 1. As it can be seen, the highest values of MB degradation is observed for red light exposure, reaching values of 56.1 % and 51.5 % for MB/N-CQDs-100, and 58.8 % and 53.1 % for MB/N-CQDs-200. On the other hand, the lowest values of MB degradation is observed for MB/N-CQDs-200 exposed to green light and daylight for 3 h.

Table 1. Calculated degradation efficiency (in %) of MB in the presence of N-CQDs.

	Blue light λ=470 nm	Green light λ=530 nm	Red light λ=630 nm	Daylight
MB/N-CQDs-100 2 h	32.5	30.1	56.1	29.2
MB/N-CQDs-100 3 h	13.9	19.2	51.5	10.5
MB/N-CQDs-200 2 h	18.8	20.8	58.8	15.8
MB/N-CQDs-200 3 h	15.5	7.5	53.1	2.0

Conclusion

In this paper, a fast and efficient method to synthesize N-doped CQDs employing microwaves at two different reactor power of 100 and 200 W is described. N-CQDs were prepared from glucose solution in ammonia hydroxide as a nitrogen doping agent for 60 s of irradiation at 100 °C. Obtained N-CQDs have spherical morphology of up to 30 nm in diameter. The presence of oxygen-related functional groups in the structure makes N-CQDs water dispersible. Photocatalytic degradation of MB was evaluated under the exposure of samples to blue light, green light, red light, and daylight, and degradation efficiency was calculated. It was found that the highest degradation efficiency show samples exposed to red light, with the highest value of 58.8 % for MB/N-CQDs-200 sample exposed for 2 h.

Acknowledgements

The research was supported by the Ministry of Education, Science and Technological Development of the Republic of Serbia (451-03-2/2020-14/20).

References

[1] W.K. Walthall, J.D. Stark, Environ. Pollut. 104 (1999) 207.
[2] R.E.P. Nogueria, W.F. Jardin, J. Chem. Educ. 70 (1993) 861.
[3] R. Ameta, P.B. Punjabi, S.C. Ameta, J. Serb. Chem. Soc. 76 (2011) 1049.
[4] A. Sharma, P. Rao, R.P. Mathur, S.C. Ameta, J. Photochem. Photobiol. A 86 (1995) 197.
[5] S. Perathoner, C. Ampelli, S.M. Chen, R. Passalacqua, D.S. Su, G. Centi, J. Energy Chem. 26 (2017) 207.
[6] S. Jovanović, Z. Marković, M. Budimir, Z. Špitalský, B. Vidoeski, B.Todorović-Marković, Opt. Quant. Electron. 48 (2016) 259.
[7] S. Jovanović, Z. Marković, Z. Syrgiannis, M. Dramićanin, F. Arcudi, V. La Parola, M. Budimir, B. Todorović-Marković, Mater. Res. Bull. 93 (2017) 183.
[8] K. Hola, Y. Zhang, Y. Wang, E.P. Giannelis, R. Zboril, A.L. Rogach, Nano Today 9 (2014) 590.
[9] D. Kepić, S. Sandoval, Á. Pérez del Pino, E. György, L. Cabana, B. Ballesteros, G. Tobias, ChemPhysChem, 18 (2017) 935.
[10] J. Prekodravac, B. Vasiljević, Z. Marković, D. Jovanović, D. Kleut, Z. Špitalský, M. Mičušik, M. Danko, D. Bajuk-Bogdanović, B. Todorović-Marković, Ceram. Int. 45 (2019) 17006.
[11] S. Devi, A. Kaur, S. Sarkar, S. Vohra, S. Tyagi, Integr. Ferroelectr. 186 (2018) 32.
[12] J. Ju, R.Z. Zhang, S.J. He, W. Chen, RSC Adv. 4 (2014) 52583.

GIS-BASED METHODOLOGY FOR COMPLEX UGS PROVISION ASSESSMENT THROUGH THE CASE STUDY OF SZEGED, HUNGARY

Ronald A. Kolcsár[1], Nándor Csikós[1], Péter Szilassi[1]

[1]Department of Physical Geography and Geoinformatics, University of Szeged, H-6720 Szeged, Egyetem u. 2-6, Hungary
e-mail: kolcsar@geo.u-szeged.hu

Abstract

Proper urban green space (UGS) provision is an important attribute of a livable city. For urban planners to delineate areas within the city where improvements on either the quality or the quantity of the green infrastructure are needed, an all-encompassing UGS provision analysis could become an invaluable tool. These analyses need to include all of the three aspects of the UGS provision, namely availability, accessibility and attractiveness, as well as evaluate the affected population.

In this present study the UGS provision analysis of Szeged has been carried out with the involvement of various maps and GIS databases (e.g.: isochrone and vegetation maps, population data), through which we aim to delineate areas within the city that are lacking the proper green infrastructure compared to the population density.

We expect results that will be useable by urban planners in Szeged, and also hope that our methodology will be adaptable by professionals from other cities for their own UGS provision assessments.

Introduction

Urban green spaces (UGS) grant access to various ecological and recreational benefits (ecosystem services) to city dwellers [1]. Because of their significant effects on the human well-being, UGS have come to the forefront of many researchers', practitioners' and city administrators' attention [2]. UGS provision assessments are used to evaluate the quality and quantity of UGS supply within a city.

Several researches aimed to define UGS provision and its components, as well as develop methodologies to properly describe them [3]–[7]. One of the most straightforward categorization of the UGS provision components was described by Biernacka et al., (2020) [7]. They defined three levels of UGS provision: availability, accessibility and attractiveness. By their definition, availability is the existence and quantity of UGS within a defined area regardless of whether these green spaces are accessible to the public or not. Accessibility answers if there are any physical or psychological barriers (fences, prohibitions, dangers) that prevent someone to reach UGS. The road network of a city is also a huge influencing factor of UGS accessibility. Attractiveness describes the willingness of potential visitors to use UGS that is both available and accessible within a reasonable distance. Attractiveness has several influencing factors, like size, services and human perception [7], [8]. When assessing UGS provision or any of its components, researchers frequently use population data as well, to evaluate affected inhabitants and their demographic composition [2], [9], [10].

In this summary we aim to present a complex methdology for UGS provision evaluation incorparating availabity, accessibility and attractiveness analyses, as well as a detailed population database in the study area of Szeged, Hungary.

Materials and methods

Study area

Our research was conducted within the administrative area of Szeged, Hungary. With approximately 161.000 inhabitants, Szeged is the third largest city in the country and the largest settlement (as well as regional center) of the Great Hungarian Plain.

Used databases

Throughout the research, various GIS databases were utilized, including different OpenStreetMap layers, a plot boundary layer and the Urban Atlas land use and land cover (LULC) database.

The analysis of availability, accessibility and attractiveness

As UGS availabilty, the area of available ‚local green spaces' was estimated within the plots of the residents' homes and their human scale proximities (100 m). Based on the building regulations document, we have reproduced the plot boundary layer of Szeged in GIS environment. A manually expanded version of the OpenStreetMap building layer (completed with adress-level population data provided by the Hungarian Ministry of Interior) was used to select plots with permanent population. Buffer zones were generated around each of these plots with a 100 m radius to define their human scale proximities.

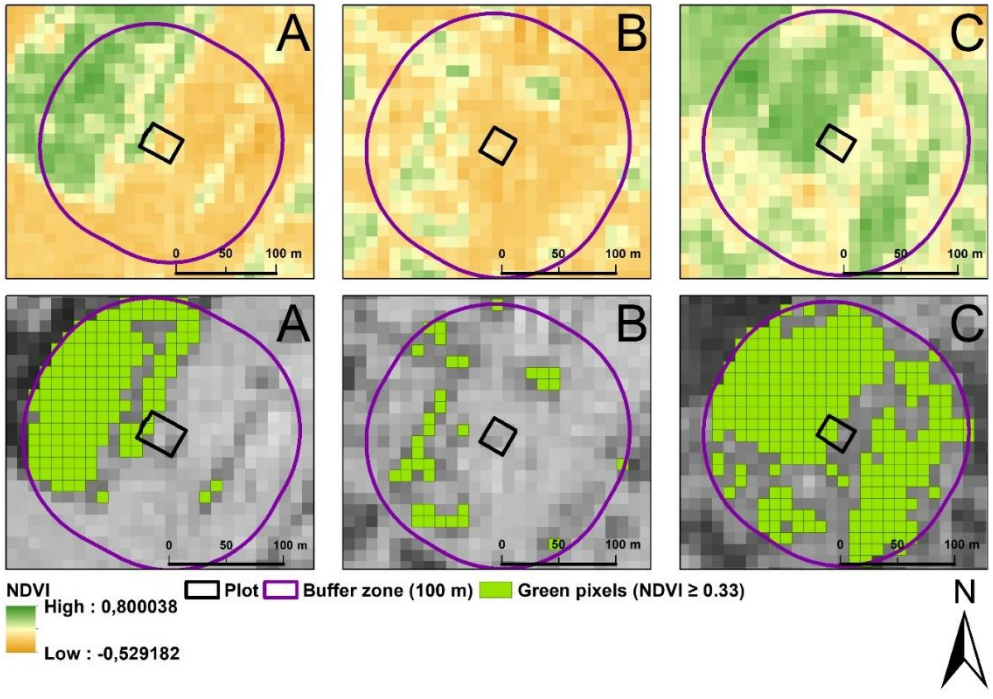

Figure 1. Examples of local green space availability estimations through three randomly selected plots one being close to Széchenyi tér, one of the biggest geen spaces of Szeged (A); one from the downtown with scarce vegetation (B); and one from the suburbian area of Újszeged district (C).

To the availability evaluation an NDVI map was also created based on Sentinel-2 imagey from 2019.08.23. Pixels with vegetation value of 0.33 or higher were selceted and counted within each buffer zone. Knowing the resolution of Sentinel-2 imagery (10 m x 10 m), green space coverage could easily be deduced from the pixel count (Figure 1.).

For the accessibility analysis, UGS polygons were selected from the Urban Atlas LULC database. These areas are mainly categorized by Urban Atlas as Forests or Green Urban Areas. Polygons representing private areas, hence unaccessible to the public were excluded from the

analysis. Using OpenStreetMap's road network layer, entry points were generated where the roads crossed the UGS polygons. With the help of ArcGIS online's Network Analyst tool, we generated service areas around these entry points in one minute resolution (between 1 and 15 minutes). An isochrone map was created from these service areas which shows the accessable public UGS and the required walking time to reach them from any given poit of the city within 15 minutes.

We evaluated the potential attractiveness of the UGS polygons previously selected for the accessibility assessment and modified the maximum considered travel time to their entry points based on their size and functions. The modifications were based on one of the guidelines (National open space guidlines) described by Stessens et al. (2017), but took into account number of point of interests (POI) within these areas as well [8]. For this, the POI layer of OpenStreetMap was used.

Plot-level UGS provision analysis

As the final step of our research we are planning to synthesize the results of the availability, accessibility and attractiveness analyses with the population data at our disposal within the plot layer of Szeged and use the obtained layer to delineate areas within the city, where either the lack of UGS or the high population density justifies the creation of new urban parks or other types of vegetation coverage.

Results, expected results

As partial results, so far the area of availabe ‚local green space' on each plot with permanent residents has been calculated (Figure 2).

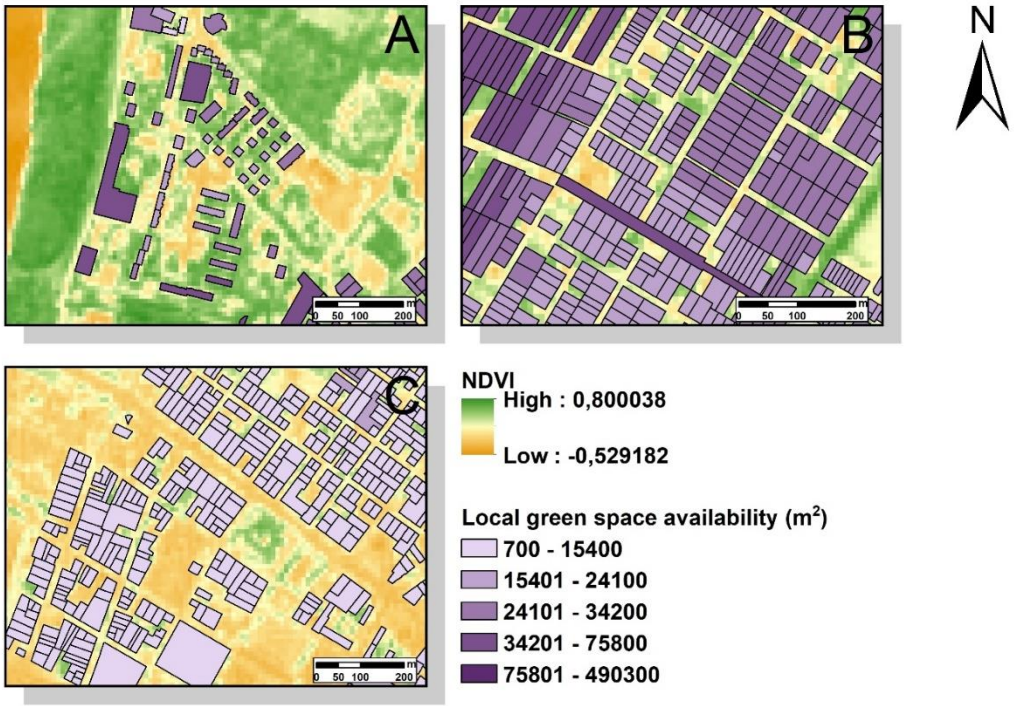

Figure 2. Examples of plot-level local green space availability: (A) in an area close to the urban park, Erzsébet liget and a floodplain forest; (B) in a vegetation-rich suburban area; and (C) in a dense urban area with low vegetation.

These plot-level availability maps provide a good indication about the greeness of the residents' environment and also offers an opportunity to compare them with the population data via additional indicators (e.g.: green area/capita). It can be cleary seen that plots embedded

either in a suburban environment or located close to larger urban parks or forest has better local UGS availability than plots in areas with dense urban fabric.

The acessibility maps of the public UGS weighted by their potential attractiveness was also created (Figure 3). While these maps ignore a significant part of the informal green spces (e.g.: smaller green lots, alleys and private gardens, it shows the pedestrian travel times to the larger and more function rich public UGS which are especially important to residents living in areas which lack proper local green space availability. Based on which aspect of UGS accessibility needs to be emphasized, these maps can be used to define either how long travel time is needed to reach the closest public UGS, or how many public UGS can be reached within a realistic walking duration (1 - 15 minutes) from from any given point of the city.

After the complex analysis with the involvement of these results and the population data, we expect to find areas with the worst overall UGS provision at the northern parts of Móraváros, and the south-western areas of Rókus district.

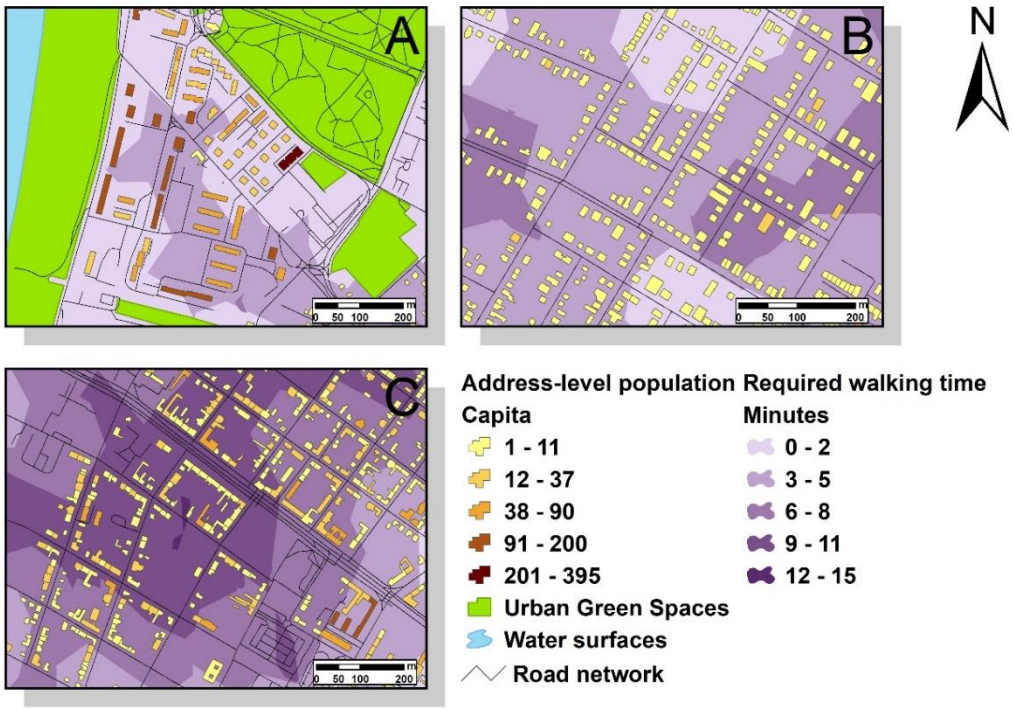

Figure 3. Examples public green space accessibility weighted by attractiveness: (A) in an area close to Erzsébet liget and a floodplain forest, (B) in a vegetation-rich suburban area, and (C) in a dense urban area with low vegetation.

Conclusion

Based on our results so far, we can conclude, that the overall UGS provision of Szeged is in good condition. Our partial result foreshadows the areas of Szeged, where poor UGS provision is expected. In the future further refinement of this methodology is possible through more thorough weighting by the potential attractiveness and the involvement of more attractiveness defining factors next to the size and the POI count. The elaboration of the address level building database and population data by age groups is another possibility to further develop present methodology.

Acknowledgements

We would like to thank the Hungarian Ministry of Interior for providing us with essential detailed population data without which this study would not be possible. We are also thankful to Vanessza J. Kolcsár for proofreading our manuscript.

The financial support of the Ministry of Human Capacities through grant NTP-NFTÖ-20 (R. A. Kolcsár) and TUDFO/47138-1/2019-ITM of the Ministry for Innovation and Technology, Hungary is acknowledged.

References

[1] MEA, *Millennium Ecosystem Assessment | World Resources Institute*. 2005.

[2] H. Zepp, L. Groß, and L. Inostroza, "And the winner is? Comparing urban green space provision and accessibility in eight European metropolitan areas using a spatially explicit approach," *Urban For. Urban Green.*, vol. 49, p. 126603, Mar. 2020, doi: 10.1016/j.ufug.2020.126603.

[3] S. Weldon, C. Bailey, and L. O'Brien, "New pathways for health and well-being in Scotland: Research to understand and overcome barriers to accessing woodlands," 2007.

[4] D. Edwards *et al.*, "A valuation of the economic and social contribution of forestry for people in Scotland," Edinburgh, 2009.

[5] M. Le Texier, K. Schiel, and G. Caruso, "The provision of urban green space and its accessibility: Spatial data effects in Brussels," *PLoS One*, vol. 13, no. 10, p. e0204684, Oct. 2018, doi: 10.1371/journal.pone.0204684.

[6] M. Biernacka and J. Kronenberg, "Urban Green Space Availability, Accessibility and Attractiveness, and the Delivery of Ecosystem Services," 2019.

[7] M. Biernacka, J. Kronenberg, and E. Łaszkiewicz, "An integrated system of monitoring the availability, accessibility and attractiveness of urban parks and green squares," *Appl. Geogr.*, vol. 116, p. 102152, Mar. 2020, doi: 10.1016/j.apgeog.2020.102152.

[8] P. Stessens, A. Z. Khan, M. Huysmans, and F. Canters, "Analysing urban green space accessibility and quality: A GIS-based model as spatial decision support for urban ecosystem services in Brussels," *Ecosystem Services*, vol. 28. Elsevier B.V., pp. 328–340, 01-Dec-2017, doi: 10.1016/j.ecoser.2017.10.016.

[9] J. Bok and Y. Kwon, "Comparable measures of accessibility to public transport using the general transit feed specification," *Sustain.*, vol. 8, no. 3, pp. 1–224, Mar. 2016, doi: 10.3390/su8030224.

[10] H. Poleman, "A walk to the park? Assessing access to green areas in Europe's cities. Update using completed copernicus urban atlas data," 2018.

DETECTION OF THE EFFICIENCY OF ENZYMATIC AND FERMENTATION PROCESSES BY DIELECTRIC MEASUREMENT

Tamás Kovács[1], Cecília Hodúr[1], Zoltán Jákói[1], Sándor Beszédes[1]

[1] *Department of Process Engineering, University of Szeged, H-6725 Szeged, Moszkvai krt. 9, Hungary*
e-mail: kovacstomi16@gmail.com

Abstract
In my work I wanted to investigate, whether measuring dielectric parameters is a proper method to detect the changes during enzymatic hydrolysis and fermentation processes. Besides I wanted to investigate, how the different types of microwaves pre-treatments affected the amount of produced RS content. The results shows that measuring the dielectric constant (ε') is rapid and easy method to detect the changes during enzymatic and fermentation processes. As for the microwave pre-treatment, more reducing sugar were produced with 500 W 1 minute, but the rate of the hydrolysis was higher during 250 W 2 minutes treatment.

Introduction
In the last few decades the importance of using renewable energy sources is increasing. One of the most important source is biomass, because it can be utilized in many ways. One of them are the different types of biofuels, such as bioethanol and biodiesel. Bioethanol can be made of different types of plants, with high carbohydrate contents, for example corn. [1] In my work I used a type of corn cob, which has high cellulose content. The problem with cellulose is that yeasts cannot utilize that. To solve that problem, it has to be degraded in enzymatic hydrolysis. After that, there are lots of glucose molecules that can be utilized by yeasts, so they can produce ethanol during their fermentation.

Experimental
The material with high cellulose content from corn cob was Cobex EU-GRITS. For the enzymatic degradation I used Cellic Ctec2 enzyme blend. The reducing sugar content of samples were measured by spectrophotometric reducing sugar assay (DNSA method). For the microwave pre-treatments Labotron 500 professional equipment operated at a frequency of 2450 MHz with two power level (250 W and 500W) was used in continuous irradiation operation mode. For dielectric measurement a DAK-3.5 (SPEAG, Switzerland) dielectric probe connected to ZVL3 (Rohde&Schwarz, Germany) type Vector Network Analyzer was used in a frequency range of 200 MHz to 2400 MHz.

Results and discussion
In the first parts of the work, I measured the dielectric parameters (dielectric constant and dielectric loss factor) during the enzymatic hydrolysis of grits (GM16). Since the suspension is an aqueous medium, its dielectric behaviour is similar to how water behaves in electromagnetic field.

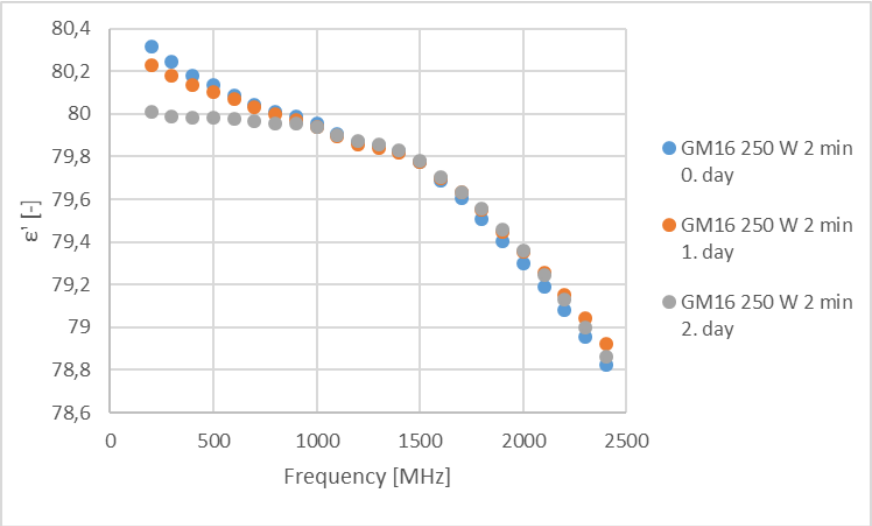

Figure 1. Correlation between dielectric constant and frequency

As Fig.1 shows the dielectric constant is decreased with increasing frequencies. This happened, because the dipoles are not able to follow up the rapid variation of the applied electromagnetic field. [2] The dielectric loss factor is increased with increasing frequencies. The results showed that the dielectric loss factor measured in consecutive days at a given frequency cannot be told apart. As for the dielectric constants of consecutive days at given frequency can be told apart, especially in the frequency range 200 MHz-800 MHz and 2200 MHz-2400 MHz.

Measuring of dielectric constant to detect changes was also effective during fermentation processes.

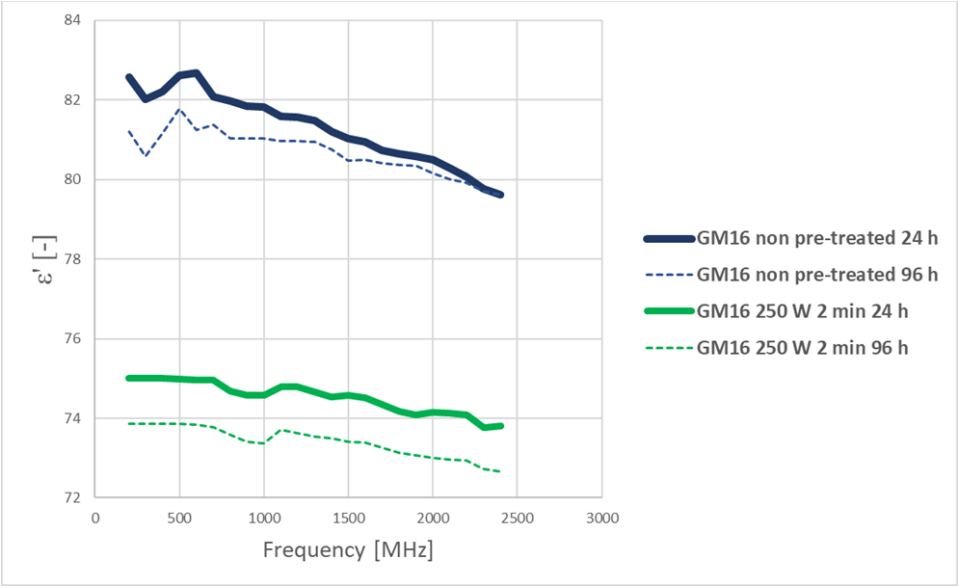

Figure 2. Change of the dielectric constant values of two different types of samples during fermentation process

The result showed that dielectric constant decreased as time progressed (Fig.2). It is because the concentration of ethanol increasing as time progresses, and ethanol's dielectric constant is less, than water's. [3] The dielectric constant values measured in the non-pre-treated samples were higher, than in the samples, which was pre-treated with microwave. This happened, because in the pre-treated samples more reducing sugar were produced because of the treatment,

and there were more fermentable sugar, so more ethanol have been produced by yeasts. It also can be seen that the dielectric constant is decreasing with increasing frequencies. Since these suspensions are also aqueous mediums, their dielectric behaviour is very similar to water's dielectric behaviour.

As for the microwave pre-treatment, the results show that more reducing sugar were produced with 500 W 1 minute, but the rate of the hydrolysis was higher during the beginning of 250 W 2 minutes treatment (Fig.3). The reason behind this is simple, the higher power altered the cellulose-hemicellulose system more than the 250 W 2 minutes pre-treatment, so the samples could have been hydrolysed more by the enzyme.

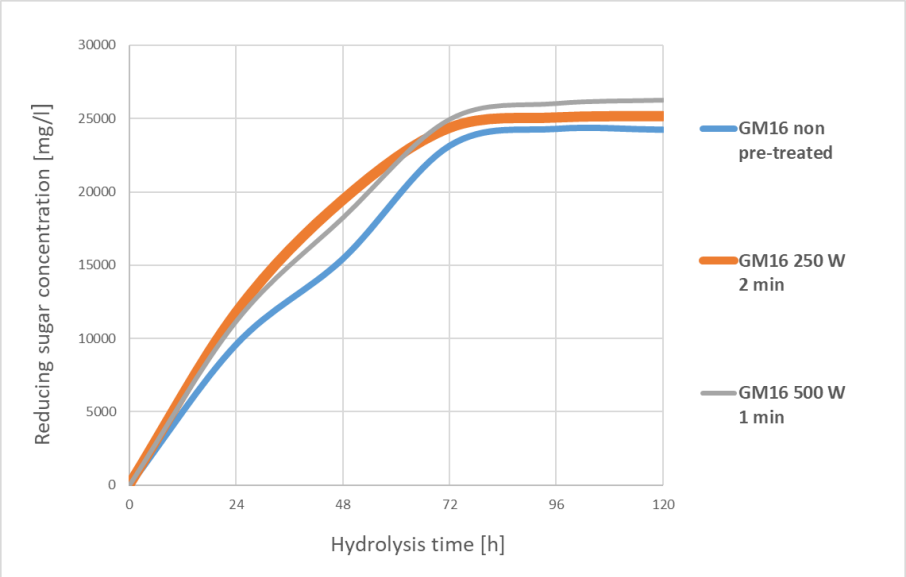

Figure 3. Glucose yields after different types of microwave pre-treatments

Conclusion

My results verified that measuring dielectric parameters (especially dielectric constant) is a proper and easy way to detect the chemical change of the biomass during enzymatic and fermentation processes. The results also verified that more reducing sugar were produced with high power short time microwave pre-treatment, but the rate of the hydrolysis was higher during the beginning of 250 W 2 minutes treatment.

Acknowledgements

The authors are grateful for the financial support provided by the projects EFOP-3.6.2- 16-2017- 00010 – RING 2017; and National Office for Research, Development and Innovation - NKFIH, K115691.

References

[1] Balat M., Balat H., Öz C. (2008): *Progress in bioethanol processing*, Progress in Energy and Combustion Science 34 551–573

[2] Onimisi M. Y.; Ikyumbur J. T. (2015): *Computation of dielectric constant and loss factor of water and dimethylsulphoxide from 0.1 to 13 GHz*, Scientific Review, Vol. 1, No. 4, pp: 79-85

[3] https://depts.washington.edu/eooptic/linkfiles/dielectric_chart%5B1%5D.pdf

MECHACHEMISTRY FOR CATALYSIS: PREPARATION OF PEROVSKITE STRUCTURAL MATERIALS AND MIXTURES OF METAL OXIDES

Gábor Kozma[1], Ákos Kukovecz[1], Zoltán Kónya[1,2]

[1]University of Szeged, Department of Applied and Environmental Chemistry, Szeged, Hungary
[2]MTA-SZTE Reaction Kinetics and Surface Chemistry Research Group, Szeged, Hungary.
e-mail: kozmag@chem.u-szeged.hu

Abstract

The main task of our research was the production and investigation of mechanochemically produced perovskite-structured materials and mixtures of metal oxides. Our goal is to develop a general synthetic method suitable for the large-scale production of many such materials. For this we have at our disposal a high-energy planetary ball mill, as well as an in-situ pressure and temperature measuring system that greatly facilitates the follow-up of the process. In addition we also used a model describing the synthesis conditions in a context suitable for determining the grinding energy developed and verified in part by us.

Introduction

About 85% of industrial processes are based on some kind of catalytic process, which is due to maximizing product yields, speeding up production processes and preventing waste generation. As a result, global catalyst sales have now exceeded $ 35 billion a year. Researchers are only able to satisfy the industry's unquenchable catalyst hunger with continuous improvement, so the basic goal is to produce such materials that can be produced cheaply and in large quantities.

Mechanochemistry is one of the processes in which kinetic work is translated into the transformation of various materials. This is mostly one of the structural synthesis methods that can be used to create particles in the nanometer range. A common feature of perovskites is the structure represented by the general formula $^{XII}A^{2+VI}B^{4+}X^{2-}_3$. Their versatility is due to the fact that many elements can be incorporated into the crystal lattice lattice, so that their properties can be changed. Their application is not only limited to cheaper solar cells, but can also be used as a sensor and even a catalyst. Similarly, metal oxides and their mixtures play a prominent role among catalysts.

Experimental

We pointed to the synthesis of metal-oxide and perovskite nanoparticles by the mechanochemical reaction in a planetary ball mill (Fritsch Pulverisette 6 planetary ball mill) is suited for fast and high-yield production. Besides the metal-salt precursor Na_2CO_3 and NaCl matrix was applied also. The latter bulks large in the separation of the nanoparticles and in the energy transmission. We state by numerous measurement method (XRD, FT-IR, Raman, TEM, SEM) that the products have uniform morphology and monodisperse size distribution (10 ±5 nm) and after preparation extractable by simple washing. We successfully applied this method to synthesise SnO_2, ZnO, TiO_2 metal-oxide and $BaTiO_3$, $ZnTiO_3$ or $NaNbO_3$ perovskite structured nanoparticles.

In the course of our work, our goal was to follow the mechanochemical processes in time with a pressure and temperature measuring head (GTM), which can be mounted specifically on the grinding drum. Thus, the knowledge of the reaction kinetics was expected to be expanded, and a significant shortening of the optimization process was expected with the help of the measuring unit (Fig.1). We tried to prove that the GTM head can trigger the

optimization of the synthesis of a product in one step, which is only possible in several steps with XRD or TG techniques.

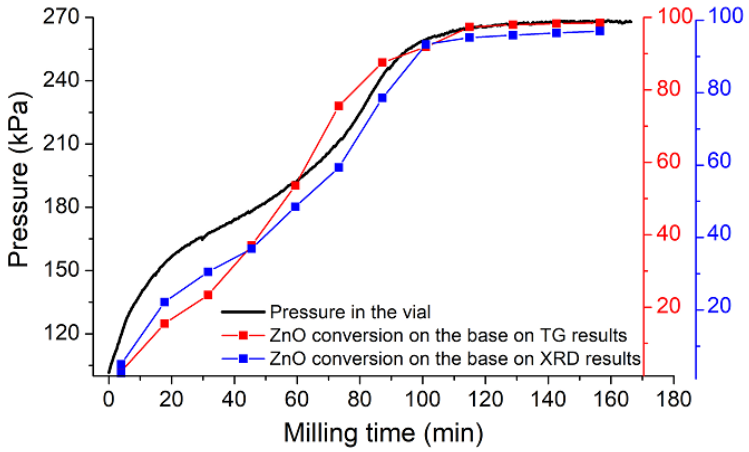

Fig.1: Pressure curve in the vial during the preparation of ZnO, and the conversion of ZnO based on the TG and XRD measurements.

We performed the production of different nanoscale perovskite structures in a planetary ball mill. Each of the produced materials was characterized in detail, their properties and the reproducibility of the mechanochemical process were investigated.

Results and discussion

In the initial phase, $ZnTiO_3$ was prepared in two steps. $ZnCl_2$ is mechanochemically converted to $ZnCO_3$ as an intermediate and then to ZnO by high energy ball milling. TiO_2 was prepared directly from $TiCl_4$ by mechanochemical means. With the precise control of the grinding energy, it was also possible to produce pure anatase and rutile phase TiO_2. We also produced titanate nanofibers and nanotubes from TiO_2 by the method developed in our department by hydrothermal means. This provided us all the starting materials. In the second step, the mechanochemical treatment of samples with different precursor compositions were performed. In all case the product was $ZnTiO_3$. The preparation was monitored by X-ray diffraction measurement (Fig.2).

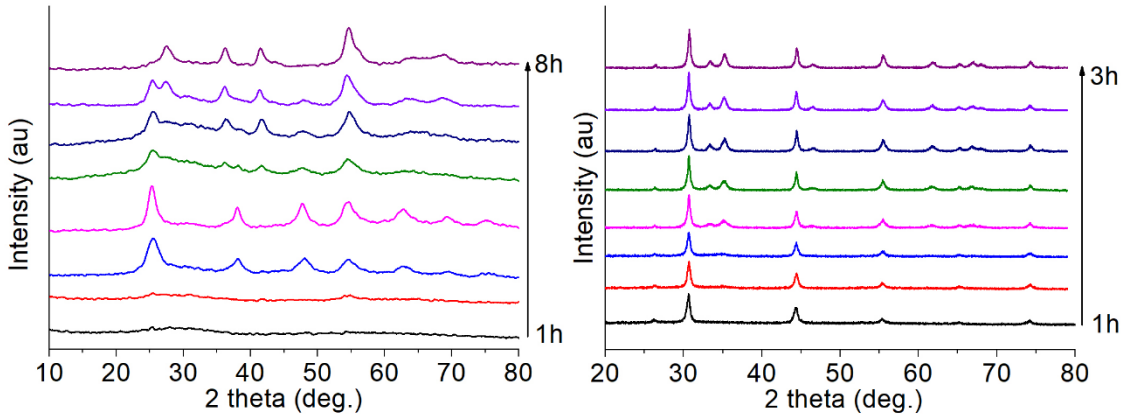

Fig.2: XRD pattern of the as-milled TiO_2 and ZnO samples.

As a result, all titanate sources were suitable for the production of $ZnTiO_3$. Among the grinding parameters, the speed and the number of grinding balls were varied, and several grinding vessels made of different materials were tested. It has been found that a grinding vessel

made of a material of inappropriate density, low speed and ball speed are not suitable for the production of ZnO and $ZnTiO_3$. The same was observed for $NaNbO_3$ and $BaTiO_3$. The high grinding speed and high wear-rate material contaminate our sample, destroying the perovskite structure. After the successful production of $ZnTiO_3$, since the ultimate goal is to determine a general mechanochemical perovskite synthesis, we also tried to generate additional perovskites based on the obtained results. Thus, Mn / Sn / $PbTiO_3$ perovskites were successfully prepared from $MnCl_2$, $SnCl_2$, $PbCl_2$ and $TiCl_4$ precursors. The above materials were also co-milled and prepared from the corresponding metal oxide by a two-step technique.

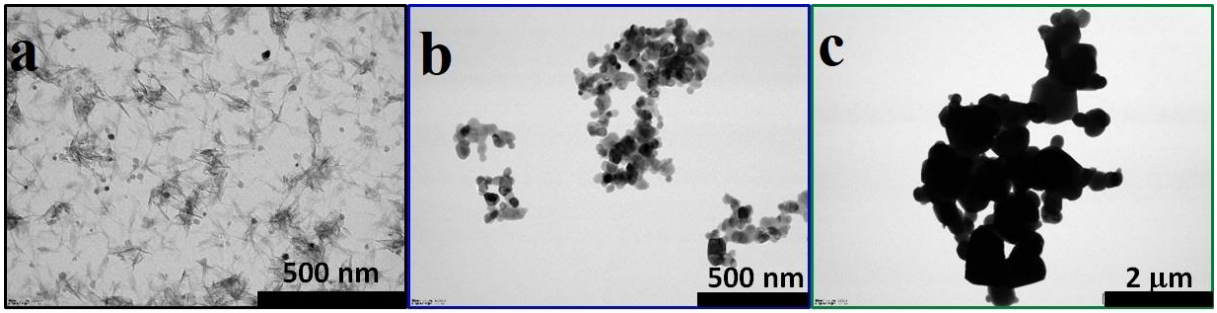

Fig.3: TEM images of $ZnTiO_3$ samples calcined at different temperature (a: non calcined; b: 400 °C; c: 1000 °C)

Conclusion

We have successfully used the high-energy milling to produce perovskite-structured materials and metal-oxide samples. Our proposed conversion from the pressure measured in the closed grinding vessel proved to be correct, which was supported by XRD and TG measurements. The use of milling drums made of different materials was successfully coordinated using the equation we proposed earlier to determine the grinding energy.

Acknowledgements

The work was supported by the János Bolyai Research Fellowship of the Hungarian Academy of Sciences BO/00835/19/7, and by the professional support of the New National Excellence Program of the Ministry of Innovation and Technology ÚNKP-20-5-SZTE-656.

CHLOROPHYLL FLUORESCENCE INSTRUMENTATION FOR A RAPID, *IN SITU* MEASUREMENT OF ALGAL DENSITY

Diána Lázár[1,2], Szandra Klátyik[1], Sándor Lenk[3], Attila Barócsi[3], László Kocsányi[3], Nóra Adányi[4], Eszter Takács[1], András Székács[1]

[1]Agro-Environmental Research Institute, National Agricultural Research and Innovation Centre, H-1022 Budapest, Herman O. út 15, Hungary
[2] Research Group of Limnology, Center for Natural Science, University of Pannonia, H-8200 Veszprém, Egyetem u. 10, Hungary
[3]Department of Atomic Physics, Budapest University of Technology and Economics, H-1111 Budapest, Budafoki út 8, Hungary
[4]Food Science Research Institute, National Agricultural Research and Innovation Centre, H-1022 Budapest, Herman Ottó út 15, Hungary
e-mail: lazar.diana@akk.naik.hu

Abstract

In the project reported, we are developing an instrument for measuring algal density based on the detection of chlorophyll fluorescence. Following the adjustment of several parameters defined during preliminary analyses, measurements were made on different concentrations of model green and blue algal cultures. Fluorescent signal intensities measured by the prototypes of the fluorometer module were compared to values determined by other, widely used methods for estimation of algal density (i.e. Bürker chamber cell counting, optical density measurement and chlorophyll-*a* measurement with ethanol extraction method). Fluorometer results correlated well with the other methods, resulting high correlation coefficients (R^2>0.9%). Limits of detection and limits of quantification showed a decreasing trend during the development phases resulting in a highly sensitive instrument.

Introduction

A common problem affecting surface waters is the load of organic materials and plant nutrients by human activity. This leads to eutrophication and the excessive growth of algae. This influences the aquatic ecosystem of water bodies, their ecological status, and alters water use opportunities. Algae are good indicators of water quality; therefore, their study is an important element in water monitoring. Several methods exist to estimate their abundance, one of which is the measurement of chlorophyll-*a*, the main photosynthetic pigment in algae. Algal species contain various types of pigment, the diversified detection of which on the basis of different light spectra used in the process can be used to estimate algal composition.

The phenomenon of fluorescence can be used to measure chlorophyll, during which the sample is excited by electromagnetic radiation at a given wavelength and in response, it emits light at another, somewhat higher wavelength. The method of fluorescence-based chlorophyll measurement was developed during the early 1970s [1] and several attempts were made later to separate the main algal groups from each other based on their different pigment composition [2, 3]. Fluorescence-based instruments for estimating chlorophyll content and algal composition are available today [4], although their effectiveness is often disputed [5].

Within the framework of a consortium of Project Aquafluosense (NVKP_16-1-2016-0049) [6], we develop a complex, modular instrument for water quality measurements. Our current goal reported here is to develop a module for measuring algal density and composition based on fluorescence, operating with higher sensitivity and efficiency than previous instruments.

Experimental

During the module development, several instrument prototypes were tested with specific characteristics presented in Table 1.

Table 1. Fluorescence measurement instrument prototypes at developmental phases

Instrument characteristics	FluoroMeter Modul (FMM)	Chlorophyll Fluorometer (CFM4Ch)	Fluorometer with dichroic system (FDS)
Excitation source	Laser diode (10 mW)	Laser diode (>25 mW)	LED-light source
Excitation wavelength (nm)	635	637	470, 630
Detection wavelength (nm)	690 (Δλ=10) 735 (Δλ=10)	690 (Δλ=10) 735 (Δλ=10) 716 (Δλ=43) 708 (Δλ=75)	716 (Δλ=43) 708 (Δλ=75)
Number of channels	2	4	2

In order to select optimal excitation wavelengths, the emission fluorescence spectra of species of different algal phyla were recorded at excitation wavelengths of 420, 470, and 630 nm. The test species belonging to the blue-green algae (Cyanophyta) were *Cylindrospermopsis raciborskii* (CR) and *Microcystis aeruginosa* (MA), and test species of green algae (Chlorophyta) were *Desmodesmus subspicatus* (DS), *Pseudokirchneriella subcapitata* (PS) and *Scenedesmus obtusiusculus* (SO). The basis of the separation is that while the photosynthetic system of blue-greens contains only chlorophyll-*a*, green algae additionally contain chlorophyll-*b*. The excitation wavelengths 470 nm and 630 nm were selected for the latest fluorometer prototype. At these excitation wavelengths, emission peaks were detected at 690 and 660 nm, respectively. The detection wavelengths were selected taking into account the emission spectra, as well as other important electrotechnical and optical aspects required by the module development (Table 1.).

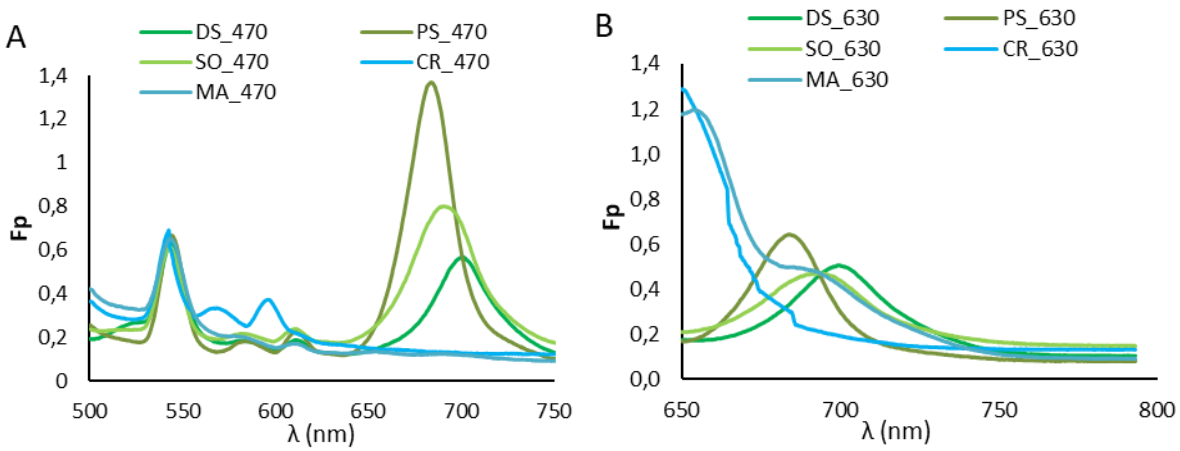

Figure 1. Emission spectra of different algal species at excitation wavelengths of 470 nm (A) and 630 nm (B).

Preliminary experiments were performed to examine and set additional parameters of the module. During these measurements, reflection was measured on microplates of different colors, using a continuous increase of light intensity, in order to find the microplate producing a stronger signal. Additionally, the effect of dark adaptation on the fluorescent signal was studied, during which a period of 10 minutes of dark incubation of a dilution series of samples before their measurement was applied. The fluorescent signals were then compared to those measurements without preceding dark incubation. Reflection was studied on three algal culture media and distilled water, using black and white microplates. Dark adaptation was studied on a dilution series of algal cultures.

Using the parameters set during the preliminary experiments, the applicability of the FluoroMeter Module (FMM), the Chlorophyll Fluorometer (CFM4ch) and the Fluorometer with dichroic system (FDS) prototypes were tested on the monocultures of the green algae *Pseudokirchneriella subcapitata* and the blue-green *Microcystis aeruginosa*.

Results were validated by other methods measuring algal density. These were (i) the detection of optical density measured spectrophotometrically at 750 nm, (ii) microscopic cell counting using a Bürker-chamber and (iii) chlorophyll measurement with the organic solvent (ethanol) extraction method. Finally, the limits of detection (LODs) and limits of quantification (LOQs) of the prototypes were determined and compared.

Results and discussion

The effect of the microplate color on the fluorescence signal is shown in Figure 2. The signal did not increase with increasing light intensity over time and remained constant on the black microplate. In contrast, it showed an increasing trend on the white microplate, along light intensity over time, in all the algae culture media (Z8, Allen, Diat.) and in distilled water (DW). The reason for this is probably that the black microplate absorbs light, whereas the white plate produces a well detectable signal. Based on these results, white the microplate was selected for the subsequent analyses.

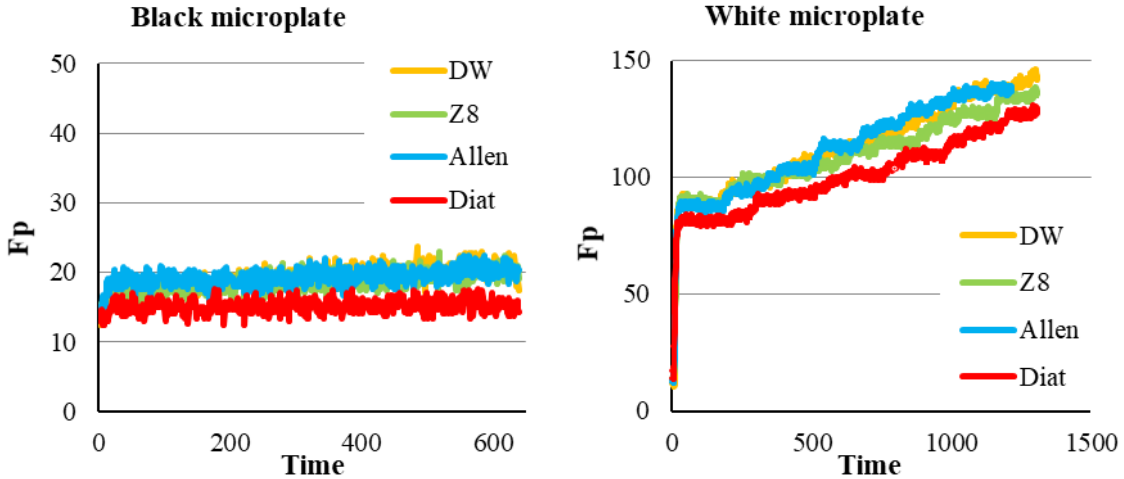

Figure 2. Reflection measured on microplates of different colors with increasing light intensity over time.

Correlation between signals of samples obtained with and without dark adaptation is presented on Figure 3. The R^2 value of the fitted line is 0.99 showing that the two datasets correlated strongly and significantly. Based on these findings, we conclude that the application of dark adaptation has no effect on the extent of the obtained fluorescence signal. Thus, in the future, it is not necessary to apply dark adaptation before our measurements.

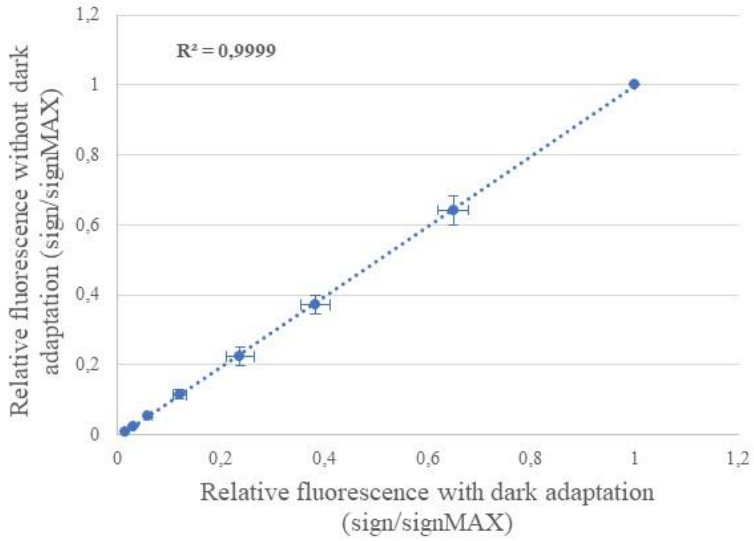

Figure 3. Effect of dark adaptation on the magnitude of the fluorescence signal.

Results obtained with the different abundance-measuring methods on the same samples were compared with the three module prototypes. The R^2 values of the fitted linear models on the correlations are presented in Table 2. Results are presented separately for the monocultures of the two algae species. In each case, we found very strong and significant correlations with R^2 coefficients >0.90, except for one case where it was 0.84.

Table 2. Correlation coefficients between densities of model green and blue algae determined by different methods.

		P. subcapitata			***M. aeruginosa***	
Prototype	**FMM**	**CFM4ch**	**FDS**	**FMM**	**CFM4ch**	**FDS**
OD	0.98	0.97 0.95	0.99 0.98	0.99	0.99 0.98	0.96 0.94
Bürker-chamber	0.98	0.95 0.98	0.94 0.98	0.99	0.99 0.99	0.95 0.92
Chl-*a* extraction	0.99	0.97 0.84	0.90 0.95	0.99	0.99 0.98	0.94 0.94

Calculated LOD and LOQ values for the three module prototypes are shown in Table 3. Based on the correlation with the cell counting method, values are interpreted in cells per milliliter, based on the *P. subcapitata* species. LOD and LOQ values showed a continuous decrease along the development phase of the module with LOD values of $4.01*10^6$, $2.22*10^3$ and $8.12*10^6$ cells/ml, and LOQ values of $8.12*10^4$, $2.65*10^5$ and $6.10*10^3$ cells/ml.

Table 3. Limit of detection and limit of quantification values for the three prototypes of the fluorometer module.

	FMM	**CFM4Ch**	**FDS**
LOD (cells/ml)	$4.01*10^6$	$2.22*10^3$	$3.70*10^3$
LOQ (cells/ml)	$8.12*10^6$	$2.65*10^5$	$6.10*10^3$

Conclusion

We conclude that the present prototype of the module gives good quality results that are validated by other methods used for the quantification of algal biomass. Both the limit of detection and limit of quantification decreased with the development process and the present prototype is considered sensitive and efficient in regard to these parameters. Our further plans for the development contain the improvement of the capacity to separate major algae groups based on their photosynthetic pigment composition, while maintaining detection and quantification limits low. We aim to enlarge its applicability to natural water samples where complex communities are present.

Acknowledgements

This research was supported by project Aquafluosense, NVKP_16-1-2016 0049 funded by the National Research, Development and Innovation Fund of Hungary within the National Competitiveness and Excellence Program.

References

[1] D.A. Kiefer, Marine Biology, 22 (1973) 263-269.

[2] C.S: Yentsch, C.M. Yentsch, J. Mar. Res., 37 (1979) 471-483.

[3] C.S. Yentsch, D.A. Phinney, J. Plankton Res. 7 (1985) 617-632.

[4] M. Beutler, K.H. Wiltshire, B. Meyer, C. Moldaenke, C. Lüring, M Meyerhöfer, U.P. Hansen, H. Dau, Photosynth. Res. 72 (2002) 39-53.

[5] M. Kahlert, B.G. McKie, Environ. Sci. Proc. & Imp. 16 (2014) 2627-2634.

[6] http://aquafluosense.hu

POROUS SNO_2/TI DIMENSIONALLY STABLE ANODE FOR DEGRADATION OF POLLUTANTS FROM WATER: SYNTHESIS AND MORPHOSTRUCTURAL CHARACTERIZATION

Corina Orha[1], Mina Ionela Popescu[1,2], Cornelia Bandas[1], Mircea Nicolaescu[1], Carmen Lazau[1], Florica Manea[2]

[1]National Institute for Research and Development in Electrochemistry and Condensed Matter, Timisoara, Condensed Matter Department, 1 P. Andronescu Street, 300254, Timisoara, Romania
e-mails: orha.corina@gmail.com , mina.popescu37@gmail.com, carmen.lazau@gmail.com , cornelia.bandas@gmail.com, nicolaescu.mircea13@yahoo.com
[2]Department of Applied Chemistry and Engineering of Inorganic Compounds and Environment, Politehnica University of Timisoara, Blv. Vasile Parvan No. 6, 300223, Timisoara, Romania
e-mails: florica.manea@upt.ro;

Abstract
In this work, the protocol based on *Doctor-Blade* method for synthesis of porous SnO_2/Ti dimensionally stable anode suitable for advanced treatment of water/wastewater is presented. Prior to SnO_2/Ti synthesis, SnO_2 was obtained by *sol-gel* method using $SnCl_2$ as Sn precusor and polyethylene glycol. The morpho-structural characterization through X-ray diffraction (XRD) and scanning electron microscopy coupled with energy-dispesive X-ray (SEM/EDX) confirmed an uniform deposition of SnO_2 mesoporous on the Ti surface with typical mud cracked-like structure, which should be suitable for the further water treatment application.

Introduction
Nowadays, the electrochemistry-based processes are tacking ground in the research field of advanced water/wastewater treatment technology. However, it is well-known that for the electrochemical process, besides their advantages, several drawbacks related to the energy consuming and the minimum conductivity required for water have been limited their practical application. To overcome these shortcomings, three-dimensional electrode materials are considered to develop the 3D electrochemical reactor [1]. The 3D electrochemical processes can be designed and customized function on the practical needs [2] and one of the main important element is the electrode material characterized by the specific features, e.g., electrocatalytic activity, high porosity, sorption capacity. Dimensionally stable anodes (DSA) are very well-known for advanced water treatment because of their high-catalytic activity towards pollutants destruction, relatively inexpensive and long life-time. Several types have been tested (e.g., TiO2, SnO2, RuO2, IrO2) in wastewater treatment and the most of them as thin films [3, 4]. Very good performances of the DSA-based electrochemical processes have been reported for the degradation of a large spectrum of organic pollutants from water but with high energy consuming or without their complete mineralization [5].
Three dimensional anodes based on specific configuration consisted of Ti filter electrodes array and activated carbon have been reported for efficient advanced wastewater treatment within 3D electrochemical reactor, considering high electroactive surface area combined with other electrochemical, mechanical and physical characteristics, which is direct linked to the characteristic morphological features [6].
In this work, the morpho-structural characteristics of porous SnO_2 on Ti substrate synthesized through *Doctor-Blade* method using SnO_2 paste prior synthesized from tin chloride precursors, envisaging its further usage in advanced treatment of water containing cystostatics as emerging

pollutants, are presented. The morpho-structural properties of the porous SnO_2/Ti are characterized by scanning electron microscopy coupled with energy-dispersive X-Ray (SEM/EDX) and X-Ray diffraction (XRD) methods.

Experimental

1.Pretreatment of titanium plates surface: First, a titanium plates (1 X 1 cm) was sanded with sandpaper P4000, followed by an ultrasonic treatment in distilled water for 30 min. Next, it was placed in a 10% (wt%) sodium hydroxide solution for 1 h at 80˚C and finally in a 10% (wt%) oxalic acid solution, for 2 h at 80˚C. Lastly, the Ti substrate were rinsed sequentially with acetone, ethanol and distilled water and the dried at 60˚C.

2. Preparation of SnO_2 mesoporous: Anhydrous tin chloride ($SnCl_2$, 99%, Aldrich) was used as a tin source, and polyethylene glycol Pluronic P-123 (Aldrich) was applied as the structure-directing agent. All of the chemicals were used without further purification. SnO_2 samples was synthesized using *sol-gel method* process as following: a solution was prepared by dispersing 1.5 g of Pluronic P-123 in 15 mL ethanol over 1 h at 40 °C. Then solution was mixed with 5 mL of $SnCl_2$, 10 mL distilled water under continuous stirring and then an appropriate amount of HCl was added to adjust the acidity of the solution. After 4 hours mixing the precipate was left standing to age for 48 h in Petri dishes at 40˚C. In order to obtain SnO_2 mesoporous the sample was treated in furnance in air atmosphere at 400˚C for 1 hour at a ramping rate of 1˚C/min.

3. Preparation of SnO_2 paste: SnO_2 solutions were prepared, according to following protocol: 0.3 g crystalline SnO_2 powder was mixed with a solution of ethyl cellulose and 2 ml α-terpinol and ultrasounded for 20 minutes. For a good homogenization, SnO_2 paste was placed in the ball mill (Lab Mills lx QM vertical planetary ball mill) at a frequency of 40 kHz for 12 hours. Finally, SnO_2 paste was deposited on Ti plates using a conventional one deposition of *Doctor-Blade* method. The SnO_2/Ti plate was then dried in air for 30 minutes, and a final annealing was performed at 300˚C for 1 hour at a ramping rate of 1˚C/min.

Results and discussion

In order to determine the crystal phase composition, X-ray diffraction measurements were carried out at room temperature using a PANalytical X'PertPRO MPD Difractometer with Cu tube in the region 2θ = 20–80º.

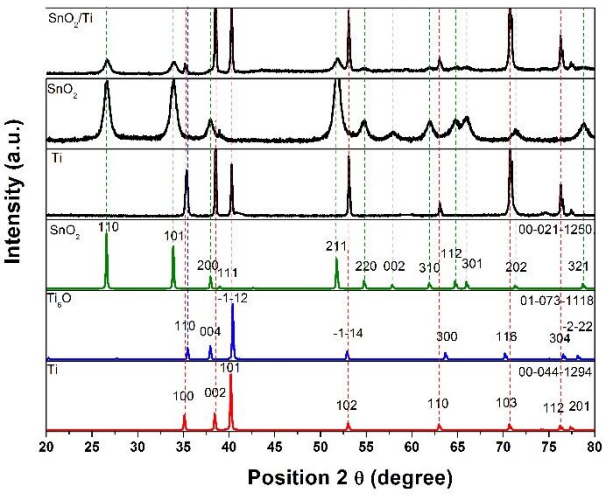

Fig. 1. XRD pattern for Ti plate, SnO_2 powder and SnO_2/Ti plate (electrode)

Figure 1 presents XRD patterns of the Ti plates, SnO_2 powder and SnO_2/Ti plates. The diffraction data at room temperature for SnO_2 compound ((110), (101), (200), (211), (220),

(002), (310), (112), (301), (321) - crystallographic planes, JCPDS card no.00-021-1250) indicates that the sample is well crystallized.

Also, XRD data evidence the presence of Ti peaks of the corroded Ti plates according to standard card JCPDS card no.00-044-1294((100), (002), (101), (102), (110), (103) (112)). The presence of Ti_6O according to standard card JCPDS card no.01-073-1118 (110) appear because of partial oxidation of Ti plate under acidic conditions.

These results show that the electrode composition prepared by *Doctor Blade* method can promote the uniform deposition of SnO_2 onto the Ti surface and SnO_2 mainly exists in its crystalline form.

The morphology of the Ti plates, SnO_2 powder and SnO_2/Ti electrode were examined comparatively through scanning electron microscopy (SEM) coupled with the energy dispersive X-Ray analysis detector (EDX).

From Figure 2 can be seen that the surface of Ti plates after corrosion treatment has a highly disordered, appears very rough and presents a cratered structure which should contribute to the good coating by the SnO_2 paste.

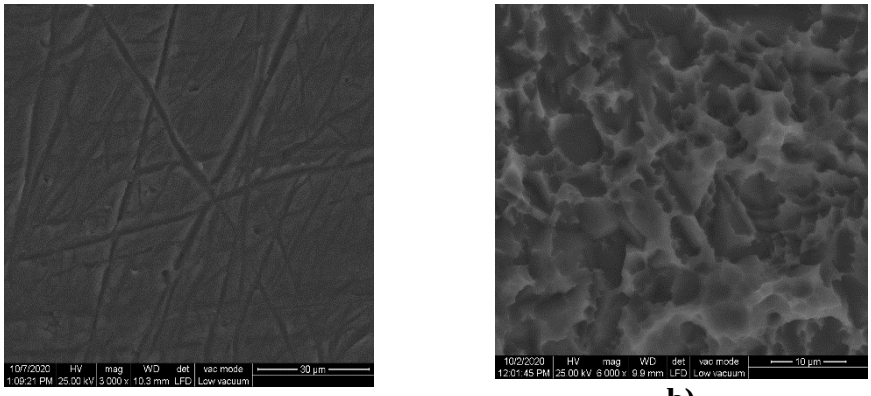

a) **b)**

Fig. 2. SEM images for Ti plates: a-untreated; b-pretreated (corrodated)

Figure 3 presents the SEM images for SiO_2 powder synthesized by sol-gel method and it can be highlight that the material has spongeous porous-mesoporous aspect with the almost equal dimensions. The formation of the chanels which give the spongeous aspect is due to the decomposition of the surfactant from the mesoporous systems during the thermal treatment.

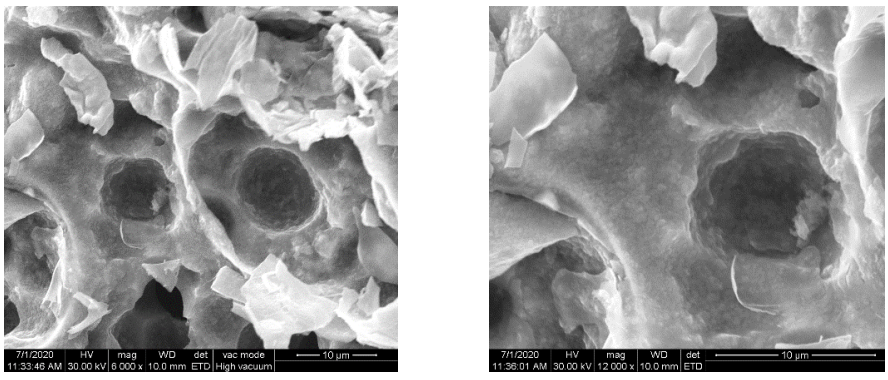

a) **b)**

Fig.3 SEM images for SnO_2 powder at different magnifications:
a)-6000x; b)-12000x

Figure 4 shows the SEM images and EDX spectrum of a SnO_2/Ti electrode prepared after one single layer deposition of *Doctor-Blade* method, which presents a typical mud cracked-like structure. The main reasons are the thermal treatment of the electrode coating and the cratered

structure of titanium substrate. Afer the *Doctor-Blade* method deposition, the SnO_2/Ti maintained its highly porous structure which would facilitate the electroactive surface area increasing combined with a local preconcentration of the pollutant concentration onto the electrode surface, which should improve the overall oxidation/degradation process of the pollutants from water. The Ti and Sn content is evidenced also by EDX microprobe and it is in according with XRD results.

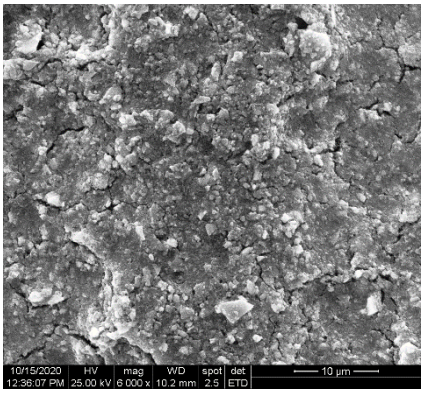

a)

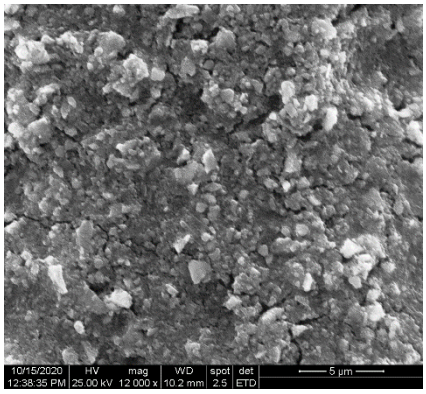

b)

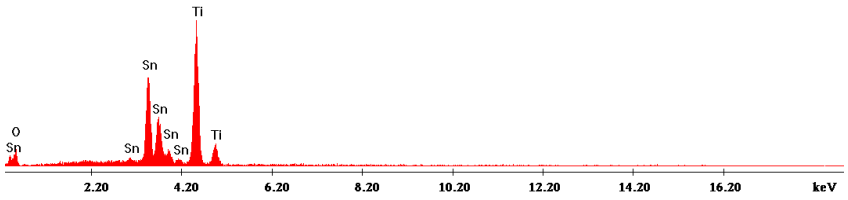

c)

Fig.4 SEM images for SnO_2/Ti electrode at different magnifications: a)-6000x; b)-12000x; c)-EDX image for SnO_2/Ti

Conclusions

The porous SnO_2/Ti dimensionally stable anode material was succesfully synthesized using the protocol based on *Doctor-Blade* method applied for the Ti plate prior corrodated under alkaline/acidic medium using SnO_2 paste. Also, SnO_2 was synthesized by *sol-gel* method using $SnCl_2$ as Sn precusor and polyethylene glycol. An uniform deposition of mesoporous SnO_2 on the Ti surface with typical mud cracked-like structure was found through X-ray diffraction (XRD) and scanning electron microscopy coupled with energy-dispesive X-ray (SEM/EDX). The morphostructural properties show that porous SnO_2/Ti dimensionally stable anode material exhibits great potential for further electrochemical studies envisaging the final water treatment application.

Acknowledgements

This work was supported by a grant of the Romanian Ministry of Education and Research, CCCDI - UEFISCDI, project code PN-III-P2-2.1-PED-2019-4492, contract number 441PED/2020, within PNCDI III.

References

1. C. Zhang, Y. Li, Z. Hu, L. Zhou, M. Zhou, Chem. Eng. J. 228 (2013) 455.
2. M. Uğurlus, S.I. Yilmaz, A.Vazoğullar, Materials Today: Proceedings 18 (2019) 1986.
3. L, Liang, H. Huanhuan, Z. Chao, W. Qian, Z. Minghua, Curr. Org. Chem.16 (2012) 2091.
4. S. Trasatti, Electrochim. Acta 45 (2000) 2377.
5. M. Ihos, C. Bogatu, I. Cristea, F. Manea, R. Pode, Rev. Chim. 67(8) (2016), 1462
6. Z. Liu, F. Wang, Y. L. Tianlong, X. S. Zhu, J. Env. Sci. 23(Supplement) (2011) S70.

PRELIMINARY IDENTIFICATION ON KEY INDICATORS FOR AIR QUALITY RISK ASSESSMENT FROM LANDFILL

Una Marceta[1], Bogdana Vujic[1], Zorica Srdjevic[2], Visnja Mihajlovic[1], Jelena Micic[3]

[1] University of Novi Sad, Technical faculty "Mihailo Pupin", Đure Đakovića bb, Zrenjanin, Serbia
[2] University of Novi Sad, Faculty of Agriculture, Trg Dositeja Obradovića 8, Novi Sad, Serbia
[3]University of Novi Sad, Faculty of Technical Sciences, Trg Dositeja Obradovića 6, Novi Sad, Serbia
e-mail: una.tasovac@tfzr.rs

Abstract
Landfilling is still the most widely used form of waste disposal although it is associated with a number of environmental issues primarily related to unregulated and partially controlled landfills that are numerous in Serbia. Landfill gas, mostly composed of methane, represents a high risk for human health and environment. This paper gives preliminary identification of criteria for quantification of methane risk impact on air in the immediate vicinity of landfills in Serbia. Four types of criteria were defined. Those criteria consist of sub-criteria that must be considered when considering the potential risks to the environment and human health.

Introduction
The basic landfill gas components are methane, carbon dioxide and trace concentrations of a wide variety of other gases that depend on the content of disposed waste. If methane as a by-product of municipal waste disposal is not collected and used as a renewable energy source, it is emitted into atmosphere with high global warming potential that is 23 times higher than carbon dioxide potential [1]. Thus, methane is considered to be one of the most significant greenhouse gases [2]. Each landfill carries certain health and environmental risks which depend on several factors such as the size and the age of the landfill, type of waste, water presence and geological conditions. Groundwater pollution, generation of landfill gas, odors, dust and noise are just some of the potential negative effects of landfills [3], [4]. If not controlled properly, landfill gas can spread below ground and pose a risk of explosion and suffocation in surrounding facilities. Thus, adequate landfill location i.e. maintenance of the distance between landfill and sensitive land is of crucial importance and it is an effective risk management measure [5]. Methane is very effective greenhouse gas and its uncontrolled emission into atmosphere can have an impact on atmospheric chemistry and climate thus significantly affecting ozone levels, water vapor, hydroxyl radicals and other numerous compounds [6]. According to EPA the default buffer requirements are not different for operating and closed landfills. However, the buffer for operating landfills serves to manage landfill gas risk and odor impacts while the buffer for closed landfills serves to manage the risk of landfill gas impacts only [7]. The aim of this paper is to make a preliminary identification of criteria for risk quantification of methane risk impact on air in the immediate vicinity of landfills in Serbia. Based on EPA environmental legislation and the legislation of the Republic of Serbia [8], four criteria types with certain sub-criteria were defined.

Results and discussion
There are 160 controlled and 3500 uncontrolled waste disposal sites in Serbia [9], [10], and only 5% of the total generated amount of the waste is recycled. Landfilling is a dominant waste disposal method. In order to minimize human health and environmental risks, these locations require closure and remediation. However, precisely because there is a large number of landfills

and lack of financial means, it is necessary to categorize the existing landfills based on its risk from the aspect of production and impact of methane on environment. In that sense, a preliminary identification of four criteria types was carried out. Those criteria consist of sub-criteria that are key factors for risk quantification.

The first criterion is related to source emission potential. Methane emission potential form landfill depends on several factors that were in this case taken as sub-categories: 1) **Landfill type -** there are only seven landfills in Serbia that meet the criteria defined by the EU Directive. Other landfills, where more than 80% of generated waste is disposed, have certain characteristics of sanitary landfill; 2) **The amount of landfill waste/ landfill size -** the greater the waste mass is, the greater is the amount of productive methane [11]. Data on dimensions and volume of landfill in the Republic of Serbia are not the most reliable because they are based on estimation and there is no relevant technical documentation for many landfills [10], [12]. The average waste production is 0.76 kg/cap/day; 3) **Landfill age -** this criterion primarily refers to whether the landfill is in the methanogenic decomposition phase; 4) **The composition of landfill waste -** over 50% of generated waste in Serbia contains biodegradable waste (garden waste or food). However, variations in the morphological composition of waste can occur at the local level depending on several factors (economic development and urban characteristics of the municipality, as well as the age and educational background of inhabitants) [12].

The second defined criterion is the landfill infrastructure. Monitoring of possible migrations of landfill gas is very important in order to avoid spreading among site facilities or locations along and accumulation of concentrations that can be hazardous to people or properties due to its inflammability and explosive potential. Thus, three sub-criteria were also defined: 1) **the presence of bottom landfill lining system** which role is to prevent gas penetration below landfill ground level; 2) **landfill cover type** - landfill management in Serbia mainly involves soil application as inert material and 3) **degassing system** - landfills mostly have passive degassing system exclusively due to explosion and fire prevention [12], [13].

The third criterion is related to landfills vulnerability on the environment and human health. Areas where there is a potential landfill impact on surrounding are defined as buffer zones. According to EPA, a reasonable default buffer distance is 500 m. When the distances are less than 500 m, the risk to the environment is considered to be low. According to SEPA surveys, out of the total number of landfills in the territory of the Republic of Serbia, 7.3% are located at distances less than 100 m from the settlements [10].

Potential methane concentration in ambient air is the fourth defined criterion. Given that the measurements are expensive, a preliminary estimation of methane concentration in ambient air could be done in faster and simpler way throughout modelling. The listed landfill characteristics and waste disposal are important factors that must be considered for the estimation of gas emission potential of the landfill site.

Conclusion

One of the biggest obstacles for solving problems related to waste management in developing countries is lack of funds. There is a great number of uncontrolled and non-sanitary landfills in the Republic of Serbia that must be remediated in order to reduce their negative impact on the environment and human health. Based on the defined criteria for environmental risk quantification it is possible to position landfills based on the risk they carry with the aim to firstly remediate the most critical ones. Landfill remediation is an expensive process and it cannot be performed for all landfills at the same time. Therefore, it is necessary to identify preferential landfills and, in that way, distribute funds.

References

[1] N.J. Themelis, P.A. Ulloa, Methane generation in landfills, Renewable Energy, 32, 1243–1257, 2007.
[2] D. Di Trapani, G. Di Bella, G. Viviani, Uncontrolled methane emissions from a MSW landfill surface: Influence oflandfill features and side slopes, Waste Management, 33, 2108–2115, 2013.
[3] EPA 969/12, Landfill gas and development near landfills–advice for planning authorities and developers, 2012.
[4] S. Mor, K. Ravindra, A. De Visscher, R.P. Dahiya, A. Chandra, Municipal solid waste characterization and its assessment forpotential methane generation: A case study, Science of the Total Environment 371, 1–10, 2006.
[5] EPA Guidelines, Environmental management of landfill facilities (municipal solid waste and commercial and industrial general waste), 2007.
[6] D.J. Wuebbles, K. Hayhoe, Atmospheric methane and global change, Earth-Science Reviews, 57, 177–210, 2002.
[7] EPA Draft guideline, Assessing planning proposals near landfills, 2016.
[8] Official Gazette of the Republic of Serbia, No. 92/2010, The Waste Disposal by Landfill Act.
[9] N. Stanisavljević, D. Ubavin, B. Batinić, J. Fellner, G. Vujić, Methane emissions from landfills in Serbia and potential mitigation strategies: a case study, Waste Management & Research, 30, 10, 1095–1103, 2012.
[10] SEPA, http://www.sepa.gov.rs/index.php?menu=9&id=6003&akcija=showAll#a2.
[11] Intergovernmental Panel on Climate Change, IPCC Guidelines for National Greenhouse Gas Inventories, Waste, 5, Chapter 3, 2006.
[12] University of Novi Sad, Faculty of Technical Sciences, Department of Environmental Engineering and Occupational Safety and Health, Utvrđivanje sastava otpada i procene količine u cilju definisanja strategije upravljanja sekundarnim sirovinama u sklopu održivog razvoja Republike Srbije, 2009.
[13] SEPA, http://www.sepa.gov.rs/index.php?menu=207&id=1006&akcija=showExternal.

SCREENING OF DIFFERENT *TRICHODERMA* ISOLATES AS ANTAGONISTS OF VARIOUS MAIZE PHYTOPATHOGENS

Ivana Mitrović*[1], Sonja Tančić Živanov[2], Božana Purar[2], Bojan Mitrović[2]

[1] *Faculty of Technology, University of Novi Sad, Bulevar Cara Lazara 1, Novi Sad 21000, Serbia*
[2]*Institute of Field and Vegetable Crops, Maksima Gorkog 30, Novi Sad 21000, Serbia*
e-mail: tadi@uns.ac.rs

Abstract
The increasing use of chemical plant protection agents in recent years has become a serious problem. Environmental pollution, non-selectivity, the emergence of resistant species, and chemicals in the food chain, has led to need to find new agents with improved characteristics. One of the solutions is certainly the use of beneficial microorganisms. The genus *Trichoderma* is genetically very diverse with a number of capabilities among different strains with agricultural and industrial significance. Maize is an agricultural crop that is susceptible to infections by various phytopathogenic fungi, producers of mycotoxins harmful to humans and animals. Since this agricultural crop has an important place in the human diet, its health safety is very important. In this work, the screening of antagonistic activity of three *Trichoderma* isolates, isolated from the environment, against the most common maize phytopathogens, was examined using dual culture technique. The results showed that there is a statistically very significant difference between the applied *Trichoderma* isolates. Using the Scheffe test, it was determined that the isolate of *Tricoderma harzianum* shows the best effect on the tested phytopathogens of maize by forming Radial Growth Inhibition (RGI) of 100% for *Penicilium* sp., 53.67% for *Helminthosporium carbonum*, 52.33% for *Fusarium graminearum* and 35% for *Aspergillus flavus*. Considering that *Trichoderma* spp. isolates were considered as effective when RGI exceeded 50%, from the obtained results it can be concluded that *T. harzianum* shows a very significant effect on all phytopathogenic isolates. It shows slightly weaker activity only on isolate *A. flavus*. This result once again confirms the great antagonistic potential of *Trichoderma* isolates and their use in biological control would contribute to the development of sustainable agricultural production and would affect the healthier environment.

Introduction
Maize is one of the most important grain crops, with its global production exceeding 1×10^9 t [1]. Also, maize is used for the nutrition of livestock, as well as for the nutrition of adults, children and babies, and the health safety of this food is extremely important. Maize grains can be infected by a variety of toxigenic fungi and the most common are fungi of the genus *Fusarium*, *Aspergillus*, and *Penicillium* [2]. In addition to ear infections, stalk infections can also significantly affect yield reductions.

F. graminearum typically start at the tip of the ear and produce a pink to red fungus growth moving toward the base of the ear. This fungus produces two mycotoxins–vomitoxin and zearalenone, both have detrimental effects on livestock. *Aspergillus* infections may be scattered on the ear and appear as green or gray-green fungal growth. The fungus produces aflatoxin in hot, dry conditions, which harms livestock and humans [3]. In addition, *Penicillium* spp. also belongs to the significant phytopathogens of maize, producers of mycotoxins [4]. On the other hand, phytopathogens of stalks can cause stalk lodging which reduces the yield of this important crop and the genus *Helminthosporium* and *Fusarium* are mentioned as the most common phytopathogen of maize stalk [5].

Protection of the environment is one of the most important issues of politics in many countries. The increasing use of chemical plant protection agents in recent years has become a serious problem. Environmental pollution, non-selectivity, the emergence of resistant species, and chemicals in the food chain, has led to necessity of finding new agents with improved characteristics [6]. One of the solutions is certainly the use of beneficial microorganisms. The largest generator of active agents are living organisms whose natural products have been in human use for thousands of years, and they certainly represent a source that is far from exhausted. *Trichoderma* species are naturally occurring fungi found in soils worldwide, which have been studied mostly for their plant associated biocontrol and growth promotion properties, but also for their important roles in bioremediation. The mechanisms of mycoparasitism and antibiosis are the most important biocontrol mechanism for *Trichoderma* isolates, when direct confrontation with pathogen occurs [7]. All this beneficial effects indicate enormous potential for *Trichoderma* species application in eco-friendly agriculture production.

Therefore, finding an environment-friendly way in maize fungal pathogens control is significant. In this study, we screened the antagonistic activity of three *Trichoderma* isolates against four phytopathogenic fungi (*F. graminearum*, *A. flavus*, *H. carbonum* and *Penicillium* sp.) isolated from maize plants. This step is very important because not all *Trichoderma* isolates have the same efficacy, and some do not show it at all. Considering that, it is very important to test their performance and select the best one.

Experimental

Antagonists. As antagonists, three *Trichodema* isolates, *T. harzianum*, *T. citrinoviride* and *T. capillare*, were used. Microorganisms are stored in the Microbial Culture Collection of the Institute of Field and Vegetable Crops, Novi Sad, Serbia.

Test phytopathogens. In the present work phytopathogenic isolates *F. graminearum*, *A. flavus*, *H. carbonum* and *Penicillium* sp., were used as test microorganisms. Phytopathogens were isolated from maize plants that showed symptoms of infection. Microorganisms are stored at the PDA (Potato Dextrose Agar) medium in the Microbial Culture Collection of Faculty of Technology Novi Sad.

Dual culture technique. Dual culture technique was used for screening antagonistic effect of three *Trichoderma* isolates on four different pathogens *in vitro*. Each *Trichoderma* isolate plug of 7 days old culture (5 mm^2) was confronted with the pathogens isolate plug in 90 mm Petri plates at the 60 mm distance on PDA (Potato Dextrose Agar) in three replicates. Antagonistic abilities of *Trichoderma* isolates were registered periodically on 7^{th}, 14^{th}, and 21^{st} day of incubation in dark at 25 °C. After 14^{th} day of incubation, Radial Growth Inhibition (RGI) was calculated according to Moya et al. [8].

Statistical analysis. The obtained data were processed by factorial ANOVA using Software Statistica, version 13.0 (StatSoft Inc., USA). Scheffe multiple range test was used to test significance of differences ($p \leq 0.05$) between mean values of measured diameter of inhibition zones.

Results and discussion

Since the obtained results measured after 14^{th} days of incubation and 21^{st} day of incubation did not show a statistically significant difference, the results measured after 14^{th} days of incubation were chosen for this study.

Results presented in Table 1. show significant differences between RGI observed as the result of activity of different antagonists, different tested phitopathogenic fungal isolates as well as interaction between these two factors. However, the biggest source of variation of RGI was activity/sensitivity of different test fungi isolates. This was expected given that tested fungi isolated from maize belong to different genera, so it can be assumed that this is the reason for their different sensitivity to applied *Trichoderma* antagonists. On the other hand, the results of Tančić Živanov et al. (2017), showed that differences in sensitivity to applied *Trichoderma* antagonists can exist within the same genus [7].

Table 1. Results of factorial analysis of variance

Source of variation	SS	Degr. of - Freedom	MS	F-value	p-value
Antagonist	1015.8	2	507.9	117.44	0.0000
Test isolate	24839.2	3	8279.7	1914.56	0.0000
Antagonist*Isolate	1160.6	6	193.4	44.73	0.0000
Error	103.8	24	4.3		

SS – sum of squares; MS – mean square

The significant influence of *Trichoderma* isolates and test fungal isolates on RGI was confirmed with $p<0.01$ and $p<0.01$, respectively. Also, the mutual influence of these two factors shows statistical significance ($p<0.01$). In order to obtain more information on the differences in the significance of the obtained RGI (%) resulting from the interaction of antagonist and phytopathogen, a more detailed post-hoc analysis was performed using the Scheffe test.

By applying Scheffe test, it was determined that the isolate of *Tricoderma harzianum* shows the best effect on the tested phytopathogens of maize (Table 2). Given that *Trichoderma* isolates were considered as effective when RGI exceeded 50%, from the obtained results it can be concluded that *T. harzianum* shows a very significant effect on all phytopathogenic isolates compare to *T. citrinoviride* and *T. capillare*.

Therefore, *T. harzianum* shows the best antagonistic activity by forming Radial Growth Inhibition (RGI) of 100% for *Penicilium* sp., 53.67% for *Helminthosporium carbonum*, 52.33 for *Fusarium graminearum* and 35% for *Aspergillus flavus*. Based on this results, it can be concluded that *T. harzianum* shows slightly weaker activity only on isolate *A. flavus*.

On the other hand, for isolate *T. citrinoviride* significant RGI was registrated on isolates *Penicillium* sp. (90.49%) and *H. carbonum* (53.55%). Efficacy on *F. graminearum* is weaker and has value of 31.78 % while on *A. flavus* shows the weakest activity of 25.33 %. At the same time, according to results, it can be concluded that isolate *T. capillare* show the weakest effect on the tested isolates. Certainly, the highest value of RGI is observed in isolates *Penicillium* sp. of 95.08%. The activity on other isolates is not significant, and the obtained mean RGI values are: *F. graminearum* 47.33%, *H. carbonum* 40% and *A. flavus* 9.67%.

Table 2. Mean values of RGI (%) after 14 days of incubation

Antagonist	Test isolate	RGI (%)
Trichoderma harzianum	*Penicillium* sp.	100.00 ^{g}
	H. carbonum	53.67 ^{e}
	F. graminearum	52.33 ^{e}
	A. flavus	35.00 ^{c}
Trichoderma citrinoviride	*Penicillium* sp.	90.49 ^{f}
	H. carbonum	53.55 ^{e}
	F. graminearum	31.78 ^{bc}
	A. flavus	25.33 ^{b}
Trichoderma capillare	*Penicillium* sp.	95.08 ^{fg}
	H. carbonum	40.00 ^{cd}
	F. graminearum	47.33 ^{de}
	A. flavus	9.67 ^{a}

∗Results are means. The mean values with the same lowercase letters in the column RGI (%) are not significantly different at 5% level of probability (Scheffe test).

Observing the results, it can be noticed that all *Tricoderma* isolates show the weakest efficiency on phytopathogenic isolate *A. flavus* while, at the same time, the most sensitive phytopathogenic isolate is *Penicilium* sp.

Conclusion

In vitro results, obtained in this study, have shown that *Trichoderma harzianum* can be successfully used in the biological control of selected phytopathogenic fungi, the causative agents of maize diseases. Additionally, the results confirmed the fact that not all *Trihoderma* isolates have the same activity on certain phytopathogens. Certainly, the use of *Trichoderma harzianum* instead of synthetics agrochemicals in biocontrol of the most common phytopathogens of maize would contribute to the development of sustainable agricultural production and healthier environment.

Acknowledgements

The study is the result of the investigations conducted within the project 142-451-3213/2020-03 funded by Provincial Secretariat for Higher Education and Scientific Research, Autonomous Province of Vojvodina, Republic of Serbia.

References

[1] B. Mitrović, B. Drašković, D. Stanisavljević, M. Perišić, P. Čanak, I. Mitrović, S.Tančić-Živanov, Genetika 52 (2020) 367-378.
[2] V.S. Krnjajal, J.L. Lević, S.Ž. Stanković, T.S. Petrović, M.D. Lukić, Jour. Nat. Sci, Matica Srpska Novi Sad 124 (2013) 111-119.
[3] M.E.H. Thompson, M.N. Raizada, Pathogens 7(81) (2018) 1-16.
[4] B. Udovički, K. Audenaert, S. De Saeger, A. Rajković, Toxins 10(279) (2018) 1-22.
[5] Y. Degefu, K. Lohtander, L. Paulin, Biochimie 86 (2004) 83-90.

[6] Z.X. Lu, G.P. Tu, T. Zhang, Z.Q. Li, X.H. Wang, Q.G. Zhang, W. Song, J. Chen, J. Integr. Agric., 19(1) (2020) 145-152.
[7] S. Tančić Živanov, R. Jevtić, M. Lalošević, D. Živanov, S. Medić Pap, V. Županski, Ratar. Povrt., 54(3) (2017) 104-109.
[8] P. Moya, V. Barrera, J. Cipollone, C. Bedoya, L. Kohan, A. Toledo, M. Sisterna, Biol. Control, 141 (2020) 104152.

ASSESING THE SOIL QUALITY OF A FORMER INDUSTIAL AREA, USING POLLUTION LOAD INDEX AND ENRICHMENT FACTOR

Ana Moldovan[1,2], Anamaria Iulia Török[1], Băbălău-Fuss Vanda[1], Valer Micle[2]

[1] *INCDO-INOE 2000, Research Institute for Analytical Instrumentation, 67 Donath Street, 400293 Cluj-Napoca, Romania;*
[2] *Technical University, Faculty of Materials and Environmental Engineering, 103-105 Muncii Boulevard, 400641 Cluj-Napoca, Romania*
e-mail: ana.moldovan@icia.ro

Abstract
Soil degradation involves the decline of soil quality and fertility due to the acidification, salinization or chemical contamination of soils from agricultural or industrial sources. In this study, spatial changes of topsoil quality were investigated in the lower basin of Arieș River, an area with a wide history of industrial activities. A sampling campaign has been done along the lower Arieș catchment, during a rainy season (November 2019). The topsoils pH and metals content were analysed. In order to asses the quality of the soil samples, soil contamination index C_d and enrichment factor EF were computed. The results of the present study showed that the topsoil samples from the former industrial sites had a high Cu, Pb and As content. According to the C_d, one sample presented a level of concern due to high level of heavy metals content, and EF assigned a considerable degree of soil enrichment - in case of two topsoil samples.

Introduction
Intensive anthropogenic land use activities have a negative impact on the land ecosystem and can lead to the land degradation. The quality of the soil is given by its capacity to function within land-use and ecosystem boundaries, with a balanced chemical composition (Fusaro et al., 2018, Paz-Kagan et al., 2014). The soil is an environmental segment that can store various pollutants, a witness of the historical anthropogenic activities with negative effects on the quality of the environment. Hence, it is crucial that methodologies assessing impacts caused by historical and actual anthropogenic activities to use related impacts in their frameworks (Turran et al., 2019, Ma et al., 2020). To assess soil quality, indicators have been used, evaluating different soil functions, utilizing chemical, physical, and biological attributes (Chavaz et al., 2017).
The present study aims to establish the current quality of the six topsoils sampled from the lower Arieș River basin. Their quality was assessed with the help of two indices: soil contamination index C_d (Rehman et al., 2020) and enrichment factor EF (Siddiqhe et al., 2020).

Experimental
1. Study area
The Arieș River catchment is an area affected by past mining and industrial activities. Although, in the last decade, most of the anthropogenic activities were stopped, the historical pollution is still leaving their mark on the soil quality (Levei et al., 2013, Butiuc-Keul et al., 2012).

The lower basin begins at the border between Cluj and Alba counties and continues until Arieș River joins the Mureș River and overlap entirely to the Transylvanian Depression. The geomorphological substrate of the lower basin is a clay rich area (Costea, 2009).
The history of the studied area is characterized by intense industrial activities, like extractive, chemical (Turda) and metallurgical industries (Câmpia Turzii). In the present, the land use is primarily managed for farming activities in the lower reaches of the Mures river (Frink, 2009).

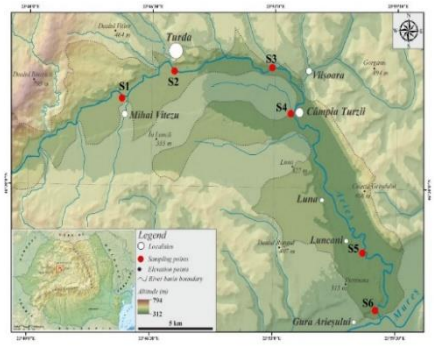

Figure 1. The lower Arieș River basin and sampling points

2. Sampling and testing
Soil samples were collected at the 0.10–0.20 m depths, from 6 different areas (Figure 1), in November 2019. Sampling locations were chosen with respect to the history of anthropic activities carried out in the area.
The soil samples were homogenized, dried at 105 °C for 24 h and passed through a 4 mm sieve. To analyze the pH, the samples were dispersed in water with a soil/water ratio of 1:5. The samples pH was determined using a 350I multiparameter (WTW). 3 g of soil samples were digested in a mixture of HCl and HNO_3 (3:1) prior to measure the concentrations of metals. Fe, Ni, Cr, Cu, Zn, Cd, Pb, Na, Mg, K, Ca, Mn, Ba, Al, Sr, P concentrations were measured using Optima 5300 DV Spectrometer (Perkin Elmer), while As concentration was determined by ELAN DRC II Spectrometer (Perkin-Elmer). All chemicals were of analytical grade (Merck).

3. Soil quality assessment
Two methods to calculate the potential ecological risk were used to evaluate the current quality of the soil samples collected in 2019. To identify the contributions of the heavy metals to soil pollution, soil contamination index $\boldsymbol{C_d}$ (Eqs. 1-2) and enrichment factor $\boldsymbol{EF}$ (Eqs. 3-4) were assessed.

$$C_f = \frac{C_{Ai}}{C_{Ni}} - 1 \quad (1)$$

$$C_d = \sum_{i=1}^{n} (c_f) \quad (2)$$

Where, C_{Ai} is the value of the concentration of ith metal ions in the analyte and C_{Ni} represents the maximum allowable concentration (MAC) of the elements, according to the national legislation (Law 756/1997). $\boldsymbol{C_f}$ and $\boldsymbol{C_d}$ results higher than 1.0 indicate a powerful contamination with metals (Ullah and Muhammad, 2020).

$$EF = Re_{sa}/Re_{bk} \quad (3)$$

$$PER = \sum_{i=1}^{n} EF \quad (4)$$

where, Re_{sa} is the value of the concentration of ith metal ions in the analyte and Re_{bk} is the value of the concentration of ith metal ions in the background sample (Kabata-Pendias, 2011, Kukdrer et al., 2014).

Results and discussion

1. Descriptive statistics of heavy metal concentrations

Soil screening values for pH and metal content are presented in Table 1. The tested soil samples pH was neutral (in the range of 7.5 to 8.0 pH units). The high exceeding rates of heavy metals comparing with intervention threshold for sensitive soil indicated an obvious accumulation in topsoil, especially for Cu, Pb and As. The concentration of Cu was higher than the intervention concentration in S2 and S3, while the Pb and As admissible concentrations were exceeded in the soils sampled from S2 and S4. All other metals content fall within the permissible guideline values. Romanian environmental legislation has not established limiting values for Fe, Na, Mg, K, Ca and Al to soil quality, due to the natural presence of these elements in soils.

Table 1. The analyzed parameters in the tested soil sample

		S1	***S2***	***S3***	***S4***	***S5***	***S6***	***ITSS****	***BK*** **
pH	pH units	8.0	8.0	7.5	7.8	7.8	7.7	-	-
Fe		10287	10428	10785	10677	10912	10426	-	-
Ni		31.6	44.8	42.4	38.5	30.8	24.5	100	15–50
Cr		28.4	43.1	37.2	35.8	48.2	26.1	300	42–200
Cu		146	216	204	175	87.3	82.8	200	11–13
Zn		202	305	291	356	104	111	600	31–90
Cd		<0.20	<0.20	<0.20	<0.20	<0.20	<0.20	5.00	-
Pb		22.3	157	58.3	117	16.8	33.2	100	10–35
Na		410	462	517	427	126	123	-	-
Mg	mg/kg	2456	2103	2871	2603	2737	2503	-	-
K		3274	3311	4279	3612	1654	1216	-	-
Ca		10062	1345	17532	12341	4276	5062	-	-
Mn		785	1127	1254	1096	513	349	2500	310–1007
Ba		100	84.7	124	97.2	49.8	49.7	625	315–500
Al		15262	19473	20004	18006	15312	9818	-	-
Sr		44.3	52.4	75.8	61.6	20.8	13.4	-	-
P		325	265	85.6	192	236	174	-	-
As		18.2	25.1	24.5	27.1	17.2	21.1	25	-

* Intervention threshold for sensitive soils according to Law 756/1997

** Heavy metal concentration (mg/kg) in background soils of the world (Semenkov et al., 2020)

Comparing with the metal concentration background soils of the world, the content of Cu and Zn from all the samples analyzed exceeded, while Pb and Mn were higher than their corresponding background values in the perimeter of the former industrial areas. Ni, Cr and Ba content are similar to the indicated limits for the metals content of the background soils, (Semenkov et al., 2020).

It can be concluded that the topsoil samples with high concentration of metals were obtain near from the former industrial areas of „Chemicals“ from Turda and „Wire Industry“ from Câmpia Turzii. In this study, the metal concentrations observed in soils of the studied area corresponded to base values found in the Iron Quadrangle region from Brazil, which is one of the richest mineral-bearing *regions* in the world (Souza et al., 2015).

2. Soil pollution assessment using C_d *and* ***EF***

The indices C_f and ***EF*** were implemented to evaluate the level of metal pollution in the environment of industrial areas in the lower Arieș River basin. Contamination index C_d was computed for 8 heavy metals: Ni, Cr, Cu, Zn, Pb, As, Cd, Mn and it is presented in Table 2. For S2, C_f for Cu, Pb and As were higher than unity, and the value of C_d (1.53) indicated a powerful contamination with heavy metals. C_f indicated a high contamination for Pb in the sample S3, however the C_d was low (C_d<1), which indicates a moderate metal contamination. For S2 and S3, C_f mean values were observed as Pb > Cu > As > Zn > Ni > Mn > Cr > Cd.

Table 2. The contamination index computed for soil sampled from the lower Arieș River basin

	C_f – Ni	C_f – Cr	C_f – Cu	C_d – Zn	C_f – Pb	C_f – As	C_f – Cd	C_f – Mn	C_d
S1	-0.579	-0.716	0.460	-0.327	-0.554	0.213	-1.00	-0.686	-5.90
S2	-0.324	-0.547	1.12	0.214	1.48	1.07	-1.00	-0.476	1.53
S3	-0.487	-0.642	0.750	0.187	1.340	0.807	-1.00	-0.562	-1.70
S4	-0.435	-0.628	1.040	-0.030	0.166	0.633	-1.00	-0.498	-3.45
S5	-0.589	-0.518	-0.127	-0.653	-0.664	0.147	-1.00	-0.795	-6.65
S6	-0.673	-0.739	-0.172	-0.630	-0.336	0.407	-1.00	-0.860	-6.60

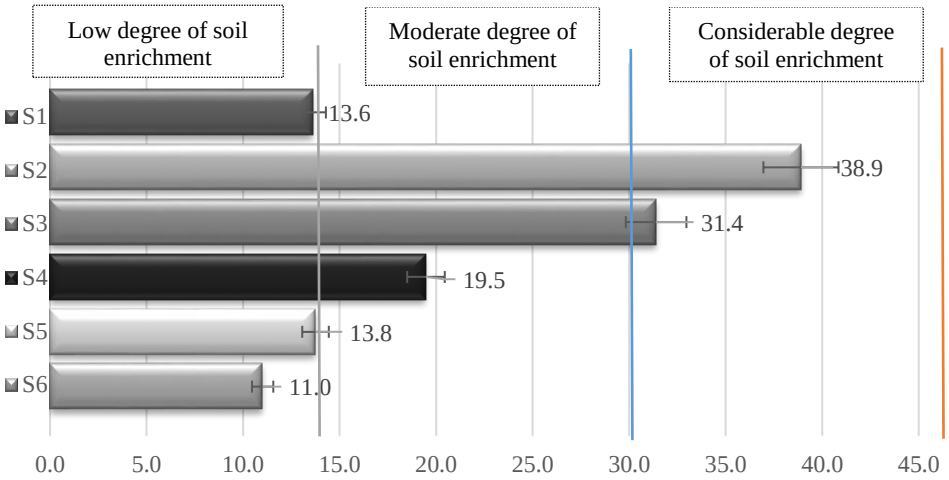

Figure 2. The enrichment factor ***EF*** computed for the soil samples

Enrichment factor (***EF***) is usually employed for differentiating metals originating from natural weathering from parent materials or human-induced processes (Kabala et al., 2020). Figure 2 showed that the values of ***EF*** were very high and varied greatly across different sited. According to Hossain Bhuiyan (2020), S1, S5 and S6 have a low degree of enrichment, S4, a medium degree, S2 and S3, a considerable degree of metal enrichment. The sequence of heavy metals as regards to calculated mean ***EF*** values was Cr > Pb > Ni > As > Zn > Cu > Cd. ***EF*** was an effective tool in proving the initial hypothesis: that the historical pollution is still very present in the topsoil of the studied area. Ciarkowska and Gambus (2020) suggested a high ecological risk in an industrial area from Nowa Huta district of Krakow, generated by the soil accumulation of Cr and Pb. In addition, a change in the management strategies applied to the sites is recommended by the authors.

Conclusion

In the lower basin Arieș River, the geographic position and history of industrial activities carried out in the area had a major impact on the soil quality. The aim of the present study was to assess the current quality state of 6 topsoils sampled of different point from lower Arieș River

basin. Although the neutral pH, the soil samples from S2 and S3 Cu, Pb and As content was higher than the intervention threshold for sensitive soils. Furthermore, some metals content such as Cu, Zn, Pb and Mn, was higher than their corresponding background values. According to C_d, S2 presented a high level of metal contamination, with a computed value of 1.53. ***EF*** divided the 6 topsoil samples into three different enrichment categories: low degree (S1, S5, S6), medium degree (S4) and a considerable degree of soil enrichment (S2, S3). In the mentioned pollution index context, the sequence pollution state of the topsoil tested was S2 > S3 > S4 > S5> S1 > S6.

Acknowledgements
This paper was supported by the Project "Entrepreneurial competences and excellence research in doctoral and postdoctoral programs -ANTREDOC", project co-funded by the European Social Fund.

References
[1] S. Fusaro, F. Gavinelli, F. Lazzarini, M.G., Paoletti, Ecol. Indic. 93 (2018), pp. 1276 – 1292.
[2] T. Paz-Kagan, M. Shachak, E. Zaassy, A. Karnieli, Geoderma 230 – 231 (2014), 171 – 184.
[3] I.D. Turam., O. Dengiz, B., Ozkan, Comput. Electron. Agric. 164 (2019), 104933.
[4] L. Ma., T. Xiao, Z. Ning, Y. Liu, H. Chen, J. Peng, Sci. Total Environ. 724 (2020), 138176.
[5] H.M.L. Chaves, C.M.C. Lozada, R.O. Gaspar, Geoderma Reg. 10 (2017), pp. 18 – 190.
[6] I. Rehman, M. Ishaq, S. Muhammad, I.U. Din, S. Khan, M. Yaseen, Environ. Technol. Innov. 20 (2020), 101155.
[7] A.B. Siddique, K. Alam., S. Ilam, T.M. Digata, A. Akbor, U.H. Bithi, A.I. Chowdhury, A.K.M.A. Ullah, Environ. Nanotechnol. Monit. Manag. 14 (2020), 100366.
[8] E. Levei, T. Frențiu, M. Ponta, C. Tănăselia, G. Borodi, Chem. Cent. J. 7 (2013), 5.
[9] A. Butiuc-Keul, L. Momeu, C. Craciunas, C. Dobrota, S. Cuna, G. Balas, J. Environ. Manage. 12 (2012), S3 – S8.
[10] M. Costea, Transylv. Rev. Syst. Ecol. Res. 7, (2009), pp. 1 – 10.
[11] J.P. Frink, Rev. Syst. Ecol. Res. 7, (2009), pp. 29 – 40.
[12] R. Ullah and S. Muhammad, Environ. Technol. Innov. 19 (020), 100931.
[13] ORDER no. 756 / 1997 for the approval of the Regulation on the assessment of environmental pollution
[14] A. Kabata-Pendias, 10.1201/b10158 (2010).
[15] S. Kükrer, S. Şeker, Z.T: Abacı, B. Kutlu, Environ. Monit. Assess. 186 (2014), pp. 3847 – 3857.
[16] I. Semenkov and T. Koroleva, Geoderma Reg. 21 (2020), e00283.
[17] J.J.L. Leal de Souza, W.A.P. Abrahao, J. da Silva, L.M. da Costa, T.S. de Oliviera, Sci. Total Environ. 505 (2015), pp. 338 – 349.
[18] C. Kabala, B. Galka, P. Jezierski, Sci. Total Environ. 738 (2020), 139918.
[19] M.A. Hossain Bhuiyan, S.C. Karmaker, M. Bodrud-Doza, A. Rakid, B.B. Saha, Chemosphere 263 (2020), 128339.
[20] K. Ciarkowska and F. Gambus, Sci. Total Environ. 740 (2020), 140161.

HEAVY METAL UPTAKE BY *Impatiens walleriana* GROWING IN URBAN SOILS

Dávid Mónok[1], Levente Kardos[1]

[1]*Department Department of Agro-Environmental Studies, Insitute of Environmental Science, Szent István University, H-1118 Budapest, Villányi út 29-43, Hungary*
e-mail: monokdavid27@gmail.com

Abstract
The objective of our research was to evaluate the heavy metal (Cd, Cr, Cu, Ni, Pb, and Zn) transfer from soil to different parts (root, stem, leaf, flower) of *Impatiens walleriana*. For this, we collected soil and plant samples from 5 different sites in the center of Budapest. Based on our analytical measurements, the accumulation and translocation of the studied heavy metals in plants clearly differ from each other. Cd concentration was relatively high in all plant parts, but Ni accumulated primarily in roots and leaves, Cr only in roots, while Pb in stem and flowers. In contrast, the plant accumulated a relatively low amount of Cu and Zn. According to our results, *Impatiens walleriana* is a potentially suitable plant for phytoremediation of Cd, Ni or Cr polluted urban soils.

Introduction
I. walleriana (*Impatiens walleriana*, Hook. f.) is a species of the family *Balsaminaceae*, native to eastern Africa. Nowadays, it is one of the most widely grown ornamental herbaceous annual, found in many regions of the world [1]. It is often planted in urban parks and ornamental gardens, private backyard gardens, and along roadsides. According to previous studies, *I. walleriana* can accumulate large amounts of heavy metals, such as Cd [2,3], Ni [4], and Zn [5]. Therefore, this plant could be a good candidate to be used for phytoremediation purposes in heavy metal contaminated soils.
It is well-known, that heavy metals are one of the main pollutants in urban soils [6,7]. Although they are natural components of soil, most of them are mainly derived from anthropogenic sources (e.g. traffic, industrial, and domestic emissions) [8]. Since these emissions are not expected to decrease considerably in the near future, reducing heavy metals in the soil may become increasingly important in urban areas [6].
In our study, we investigated the heavy metal (Cd, Cr, Cu, Ni, Pb, and Zn) uptake of *I. walleriana* from the soil in Budapest, Hungary. Our objective was to evaluate the plant uptake, accumulation, and translocation of these metals, in order to learn about the suitability of *I. walleriana* for remediation of urban soils. In addition to this, we also investigated whether there is a correlation between the heavy metal concentrations of soil and plant.

Experimental
Soil and plant samples were collected from 5 different sites, which are located in the center of Budapest (Figure 1.). All sample sites were close to the Grand Boulevard (Nagykörút), one of the busiest parts of the city. Within each site, three 1 × 1 m subplots were randomly established. Soil samples were taken from these subplots (from the upper 0-20 cm layer of soil), with a composite of 5 subsamples. 3 plants (along with their roots) were also collected from each subplot.

Figure 1. Location of the study sites

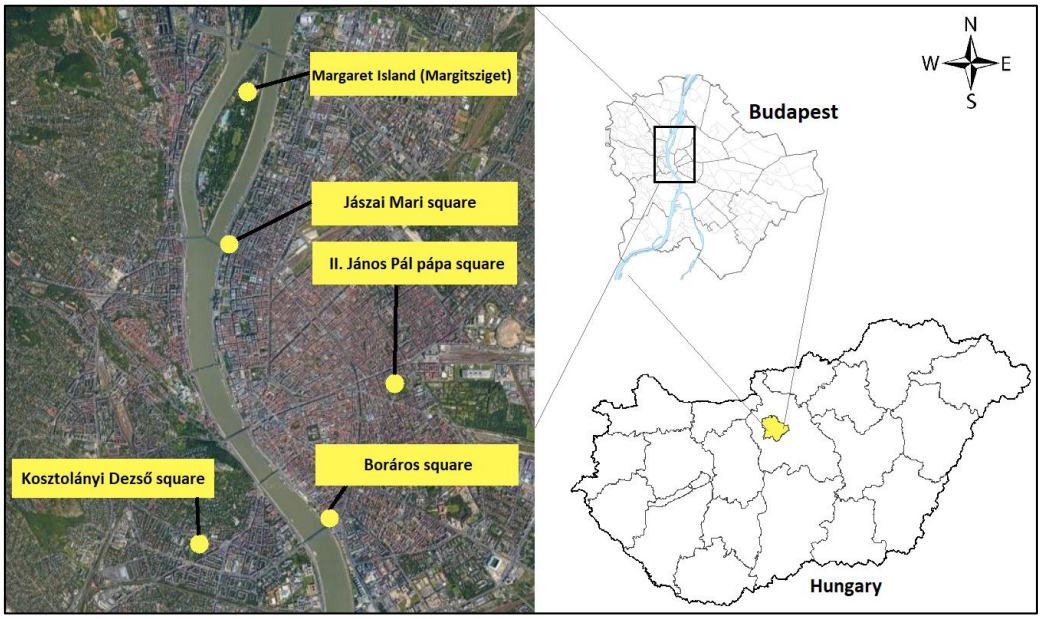

In the laboratory, soil samples were homogenized, air-dried, and manually sieved through a 2 mm sieve. The plants were separated into root, stem, leaf, and flower, then each part was washed, dried at 105 °C, and grounded separately. Heavy metal (Cd, Cr, Cu, Ni, Pb, Zn) concentration of soils and plant parts were measured after HNO_3+H_2O_2 digestion by AAS.
Statistical analyses were performed using GraphPad Prism 8.0.1 software. During this, Tukey's or Games-Howell test ($p<0.05$) was carried out to test for any significant differences between the heavy metal concentrations in soil and different plant parts. Pearson's correlation analysis was also used, to detect if there was any connectivity between the metal concentration of soils and plants. For this, we calculated the average metal concentration of the whole plant, based on the known data (weight and metal concentration of the plant parts).

Results and discussion

The measured heavy metal concentrations are shown in Table 1. *I. walleriana* clearly accumulated Cd in its tissues, as in most cases the metal concentrations in the plant parts were significantly higher than in the soil. This is consistent with the results found in the literature [2,3]. Highest Cd concentrations were observed in plant roots and leaves.
At each site, significantly higher Cr concentrations were measured in plant roots than in soil. However, the concentration of Cr in the above-ground parts of the plant was not very high (except for the leaf samples from Jászai Mari square). This may be because the plant can limit the toxic effect of Cr by the secretion of it in the vacuole of the root cells [9].
In the case of Cu, the results were a little controversial. Relatively high Cu concentration was measured in soil samples from Jászai Mari square and Kosztolányi Dezső square. In contrast, Cu concentration was very low (below 1 mg kg^{-1}) in samples from Margaret Island and II. János Pál papa square. Despite this, the concentration of Cu in plant parts was more or less constant. This can be explained by the fact that Cu is an essential element for plants, so *I. walleriana* took up only the required amount of Cu from the soil [10].
I. walleriana accumulated Ni in its roots and leaves, as the Ni concentration of these plant parts were significantly higher than in soil at all sites. However, there was no remarkable Ni accumulation in stem and flower.
In contrast to Ni, Pb accumulated primarily in the stem and flower of the plant. Moreover, the Pb concentration in leaves was in many cases lower than in soil.

In most cases, there were no significant differences between the Zn concentration measured in plant parts and soil (except for samples from Kosztolányi Dezső square). The Zn concentration in plant parts was varied between a small range, which may be due to its essential role, similar to Cu [10].

Table 1. Mean concentration of heavy metals (mg kg^{-1}) in soil and different plant parts. Different letters mean statistically significant differences according to Tukey's or Games-Howell test ($p<0.05$).

Site	Soil/Plant part	Cd	Cr	Cu	Ni	Pb	Zn
Margaret Island	soil	1.03**a**	20.55**a**	<1.00**a**	34.42**a**	146.76**ac**	59.09**a**
	root	8.73**b**	98.60**c**	<1.00**a**	241.65**b**	125.59**ab**	61.33**a**
	stem	5.96**ab**	29.99**ab**	<1.00**a**	15.10**a**	214.64**ac**	68.73**a**
	leaf	10.97**b**	15.13**a**	10.00**b**	423.90**b**	81.48**b**	80.89**a**
	flower	4.56**a**	34.37**b**	<1.00**a**	30.69**a**	233.88**c**	53.80**a**
Jászai Mari square	soil	<0.1**a**	40.37**a**	178.34**a**	34.99**a**	174.01**a**	73.46**a**
	root	8.21**b**	212.49**c**	37.81**b**	95.21**b**	200.44**ab**	62.83**ab**
	stem	7.67**bc**	37.38**a**	1.95**c**	16.88**a**	255.86**b**	62.33**ab**
	leaf	10.81**c**	115.61**b**	9.69**c**	210.82**c**	138.56**a**	59.76**b**
	flower	6.28**b**	27.11**a**	1.00**c**	47.00**a**	230.25**ab**	65.28**ab**
II. János Pál pápa square	soil	1.01**a**	36.02**a**	<1.00**a**	60.01**ac**	189.86**a**	58.23**a**
	root	8.63**b**	226.30**c**	30.75**b**	121.94**c**	168.77**a**	58.45**a**
	stem	6.49**b**	42.38**a**	<1.00**a**	13.38**b**	223.55**b**	70.73**a**
	leaf	9.11**b**	62.36**a**	14.09**ab**	280.54**c**	131.64**a**	53.53**a**
	flower	7.79**b**	3.08**b**	<1.00**a**	45.23**a**	228.19**b**	50.72**a**
Boráros square	soil	2.83**a**	11.09**a**	30.25**a**	33.18**a**	134.94**a**	48.01**a**
	root	14.05**c**	175.75**c**	2.49**a**	288.78**b**	139.24**a**	72.37**ab**
	stem	13.58**bc**	15.87**a**	<1.00**a**	12.11**a**	333.16**b**	53.29**ab**
	leaf	10.64**bc**	35.12**ab**	6.67**a**	313.46**b**	75.81**a**	82.86**b**
	flower	7.77**b**	39.90**b**	<1.00**a**	26.81**a**	258.08**b**	66.79**ab**
Kosztolányi Dezső square	soil	3.46**a**	13.81**a**	109.54**a**	39.84**a**	162.03**a**	48.61**a**
	root	12.85**b**	99.70**b**	26.27**b**	247.71**d**	142.52**ab**	62.48**c**
	stem	7.44**a**	19.13**a**	1.01**c**	13.85**b**	228.17**ac**	37.42**b**
	leaf	11.00**ab**	37.13**a**	16.47**b**	415.35**d**	66.76**b**	79.29**d**
	flower	6.07**a**	33.74**a**	<1.00**c**	30.24**c**	219.01**c**	52.07**ac**

The results of the correlation analysis are shown in Figure 2. It can be concluded that with the increase of the heavy metal concentration in soil, the metal concentration in the plant also increased. However, this increase was not significant in the case of Ni and Zn. This was not unexpected, as the amount of heavy metal taken up by a plant also depends on a number of other factors besides metal concentration of soil, such as plant physiological factors, soil properties (texture, pH, etc.) or other environmental factors (temperature, precipitation, etc.) [11]. The strongest correlation between soil and plant metal concentrations were found for Cd ($R^2 = 0.58$) and Pb ($R^2 = 0.59$).

Figure 2. Correlation between heavy metal concentration of soil and plant according to Pearson's correlation analysis.

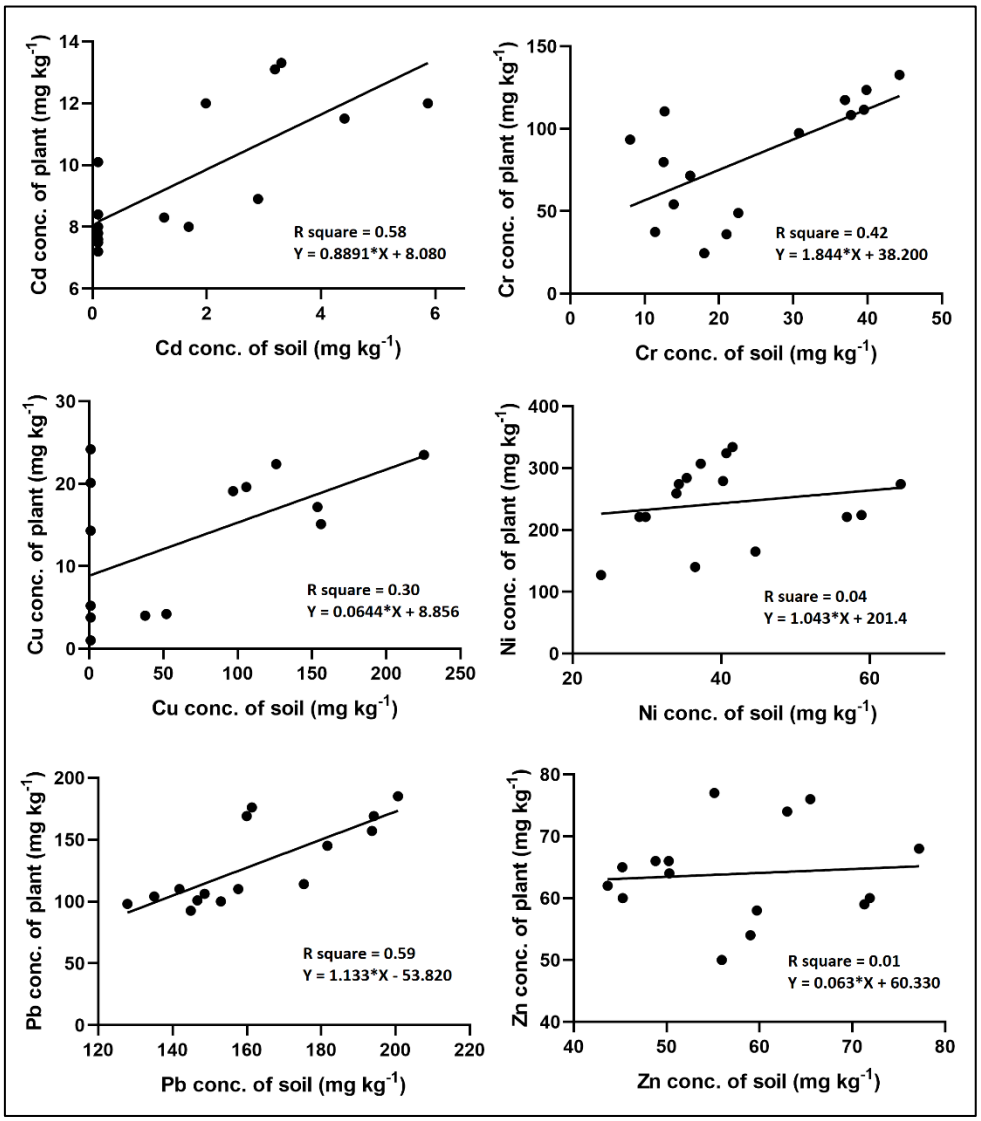

Conclusion

We investigated the heavy metal uptake and accumulation of *I. walleriana* growing in urban soils. It was revealed that the plant can accumulate relatively large amounts of Cd and Ni. In some cases, the concentration of these metals in the leaf was ten times higher than in the soil. Based on these results, *I. walleriana* could be a suitable plant for phytoremediation of Cd and Ni polluted urban soils. In most of the urban green areas, ornamental plants are harvested at the end of the growing season. The entire plant (including roots) is then removed from the area. Since Cr has accumulated in roots, *I. walleriana* can be also used to control the amount of Cr in the soil (besides Cd and Ni) in these areas.

I. walleriana is practically unsuitable for phytoremediation of the other three heavy metals. Although relatively high concentrations of Pb were observed in the stem and flower of the plant, these plant parts make up only a small part of the whole plant. Thus, only a small amount of Pb can be removed from the soil with this technique. Based on our measurements, *I. walleriana* has not accumulated Cu and Zn remarkably, therefore cannot be used for remediation of soils contaminated with these metals.

Acknowledgments
This research has been supported by the ÚNKP-19-3-I-SZIE-34. New National Excellence Program of the Ministry for Innovation and Technology, Hungary.

References
[1] C. Salgado-Salazar, N. LeBlanc, A. Ismaiel, Y. Rivera, C. Y. Warfield, J. A. Crouch, Plant Dis. 102 (2018) pp. 2411-2420.
[2] J. L. Wei, H. Y. Lai, Z. S. Chen, Ecotox. and Environ. Saf. 84 (2012) pp. 173-178.
[3] H. Y. Lai, Chemosphere, 138 (2008) pp. 370-376.
[4] F. Schenato, N. T. Schröder, F. B. Martins, International Conference on Energy, Environment, Ecosystems and Sustainable Development (2008) pp. 366-373.
[5] J. K. Torrecilha, G. P. Mariano, P. S. da Silva, International Nuclear Atlantic Conference (2013) p. 9.
[6] B. Wei, L. Yang, Microchem. J. 94 (2010) pp. 99-107.
[7] L. Madrid, E. Díaz-Barrientos, F. Madrid, Chemosphere 49 (2002) pp. 1301-1308.
[8] C. Su, Environ. Skeptics and Critics. 3 (2014) p. 24.
[9] M. Shahid, S. Shamshad, M. Rafiq, S. Khalid, I. Bibi, N. K. Niazi, M. I. Rashid, Chemosphere, 178 (2017) pp. 513-533.
[10] M. Adrees, S. Ali, M. Rizwan, M. Ibrahim, F. Abbas, M. Farid, S. A. Bharwana, Environ. Sci. Poll. Res. 22 (2015) pp. 8148-8162.
[11] J. R. Peralta-Videa, M. L. Lopez, M. Narayan, G. Saupe, J. Gardea-Torresdey, Int. J. Biochem. Cell Biol. 41 (2009) pp. 1665-1677.

ENVIRONMENTAL ANALYTICAL ASPECTS OF MOSQUITO CONTROL PRACTICE

Mária Mörtl[1*], Zoltán Gulyás[2], László Kovács[3], Béla Darvas[4], András Székács[1]

[1]Agro-Environmental Research Institue of National Agricultural Research and Innovation Centre, Herman Ottó u. 15, H-1022 Budapest, Hungary
[2]Independent expert, Szolnok, Hungary
[3]Institue of Agricultural Engineering, National Agricultural Research and Innovation Centre, Tessedik Sámuel u. 4, H-2100 Gödöllő, Hungary
[4]Hungarian Society of Ecotoxicology, Herman O. u. 15, H-1022 Budapest
** e-mail: mortl.maria@akk.naik.hu*

Abstract
Aerial application of insecticides was monitored by determination of the active ingredient (deltamethrin) using a gas chromatograph coupled to an electron capture detector. The amount of pesticide active ingredient settled to trays after an hour indicated uneven distribution patterns influenced by micrometeorological conditions as well. Maximum half and typically about 30% of the applied insecticide settled in one hour after the treatment. Pesticide drift observed 50 meters away from the target treatment zone was significant in all cases. The measured values ranged between 7% and 31% of the applied deltamethrin and the highest value was observed for K-OTHRIN 10 ULV formulation. Parallel determination of the spray droplet size distribution and specific droplet numbers also confirmed that the drops reach the soil surface and indicated a substantial spray drift.

Introduction
Nowadays pyrethroids are the most widely used insecticide active ingredients to control mosquitoes. Formerly, aerial application of pesticides containing deltamethrin used to be typical in Hungary, and reduction of larvae population by larvicides (*Bacillus thuringiensis* var. *israelensis*) as a targeted biological control has been less significant [1,2]. Adulticides are applied either using aerial applications by aircraft or on the ground by truck-mounted sprayers, which produce small particles by a thermal or a cold (ULV, ultra-low volume) fogger. The authorization of all products formulated for aerial application for imago control was expired in 2019, and only a single product, applied by thermal fog formation, remained temporarily on the market [3]. Ground-based applications are suitable for the treatment of smaller areas, but their drawback is that mosquitoes are easily replaced from nearby regions. Currently a single formulation containing deltamethrin as an active ingredient is provisionally authorized for aerial application [4], and another deltamethrin-based formulation and a formulation containing etofenprox and natural pyrethrins (0.1%) are authorized for ground-based spraying in thermal foggers [1]. Two formulations as spraying agents, restricted for use only by certified experts (category II), containing either cypermethrin or a combination of cypermethrin, tetramethrin and pyriproxyfen are available, the latter also containing piperonyl butoxide as a synergistic additive [5]. In addition, other pyrethroid active ingredients (bioallethrin, cyfluthrin, cyhalothrin, transfluthrin, etc.) are available for home use [1]. According to a European pesticide database [6], deltamethrin, alpha-cypermethrin (aka alphamethrin) and pyrethrins are currently authorized pesticide active ingredients, but tetramethrin is no longer approved in plant protection in the European Union. It is misfortunate that authorization of the active ingredients in mosquito control and agricultural uses are not synchronized, neither in respect of the actual active ingredients, nor for their approval expiration dates.

Gas chromatography (GC) coupled with electron capture detection (ECD) provides a convenient instrumental analytical method with sufficient analytical sensitivity to determine pyrethroids from different matrices [7-9]. In the present work, we studied the settling, drift, as well as the droplet size distribution of the previously used formulations applied in aerial treatments. Settling of the formulation was characterized by laboratory measurement of the active ingredient content (deltamethrin).

Experimental

Eleven trays (size 37.5x26 cm) were placed every 5 meters on the target treatment zone to sample the insecticide settled. Three trays were placed 50 m from the treatment line to determine the pesticide drift. The typical dosages of deltamethrin were between 0.5 and 1.0 g/ha. One hour after application, the material settled to the surface of the trays was dissolved by washing in two subsequent steps by 2x50 ml of a suitably chosen organic solvent. Solutions were stored at 4 °C until instrumental analysis. Several solvents (e.g., hexane, ethanol) were tested for analytical efficacy. Ten milliliters of the organic solutions were evaporated to the dryness in the laboratory and redissolved in 1 ml of isooctane prior to determination.

The active ingredient (deltamethrin) content in ten-fold concentrated samples was measured by the developed GC method. ECD was used for detection; thus, interferences with the white oil matrix used as a carrier for the application or with other components were minimal. The limit of detection is 10 ng/ml, which considering the concentration factor, allows the detection of up to 1 ng of active substance per tray. Sample analyses were carried out on a HP 5890 GC instrument equipped with a HP 7673 autosampler. A Chrompack CP-Sil 8 CB column (30 m x 0.25 mm, 0.25 μm) was used for the separation applying hydrogen 5.0 as a carrier gas and nitrogen 6.0 as make up gas. Injector and detector temperatures were 280 and 300 °C, respectively. The temperature program started with initial oven temperature of 80 °C for 1 min, then increased by the rate of 30 °C/min to 260 °C, followed by the rate of 6 °C/min to 287 °C, and was held for 2 min. Quantification was performed by external calibration with solutions containing 100, 200, 300, 500, 700 and 1000 ng/ml of deltamethrin (Pestanal).

Relative coverage (%) and specific droplet number (number/cm^2) values, as indicators of spray dispersal characteristics, were determined by using oil sensitive papers (TeeJet 52 x 76 mm) placed on the ground along with the sampling trays (see above) to catch the fall-off of the aerial spray reaching ground level. Fifty papers were placed perpendicular to flying direction in every 1 meter, and to follow the spray drift eight papers were placed in every 5 meters up to 50 meters. Result were digitally recorded and statistically (Statistica, ANOVA) evaluated.

Results and discussion

Regarding the solvents to remove the ingredient from the tray surfaces, there were no significant differences between the efficiency of hexane and ethanol, and 4% of water in ethanol did not influence the results either. On-site application of methanol is not recommended due to its toxicity, and in addition resulted in the appearance of a further, unidentified peak in the chromatogram of the extract.

The GC-ECD method allowed a sensitive detection mode of the target analyte and no significant interference with the matrix occurred (Figure 1). In the above concentration range the calibration curve was linear, but calculation in some cases of lower concentrations resulted in negative estimated values due to the nonlinear characteristics of ECD as a function of the analyte concentration. Data were calculated from three parallel injections. Additional points are required in the low region to determine the levels below 100 ng/ml.

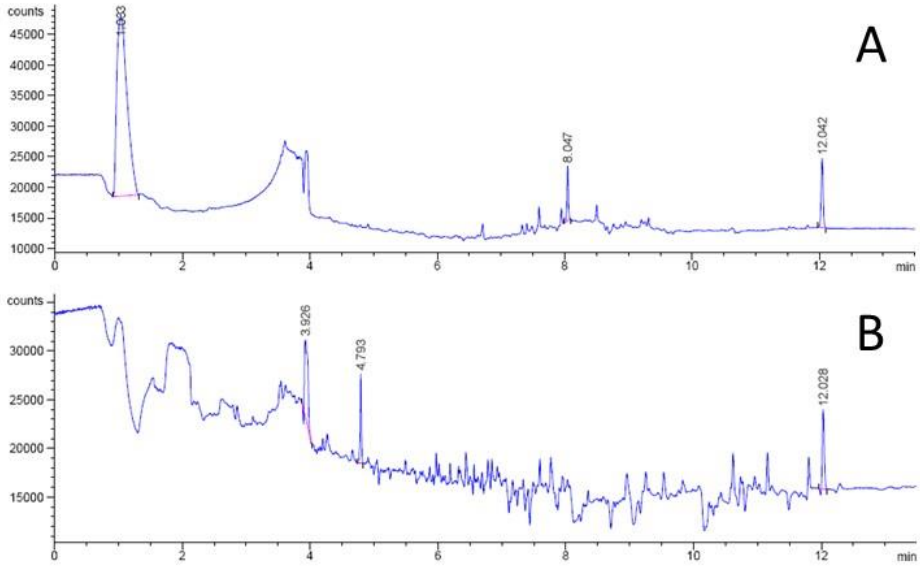

Figure 1. Chromatograms of a calibration solution (A) and a field sample (B), containing 100 and 461 ng/ml of deltamethrin, respectively. The retention time was at 12 min.

Results for a commercially available formulation K-OTHRIN 10 ULV (see Figure 2) showed a smooth distribution pattern indicating a significant drift of deltamethrin. The pesticide drift determined at 50 meters was the highest (31%), whereas 49% of the sprayed active ingredient (0.96 g/ha) settled to the treated area. Thus, this formulation containing oil as carrier medium settled intensively upon 1 hr, and its levels were practically even among the trays, yet this formulation was found to be prone to drift.

Relative coverage values varied between 0.2-0.5%, whereas the specific droplet numbers (see Figure 2) were between 6-27 droplets/cm^2 as an average on the treatment target area. The corresponding values ranged between 0.11-0.42% and 10-22 droplets/cm^2 for non-target areas (50 meters from the flight line). Thus, the untreated area sampled received the same order of magnitude from the spray (and therefore, the active ingredient) than the treated area. Spray drift determined at each point was significant up to 50 meters, which is objectionable from environmental point of view.

Worthy of note that application of large amount of insecticides against the mosquitoes contaminates the aquatic environment and via pesticide drift nearby soils are also polluted. This latter effect gains agricultural importance when the drift settles on cultivated crops. Through this, deltamethrin can occur as an unintended pesticide residue on the crop, which can be problematic in agrochemicals-based technologies, but can cause an irreconcilable problem in organic farming, were to occurrence of synthetic pesticide residues (deltamethrin in this case), even in trace amounts, is strictly prohibited. Although the dosage of deltamethrin for mosquito control is about one tenth (0.96 g/ha) of the recommended dosages in intensive crop protection (7.5-12.5 g/ha), residues may appear e.g. on the surface of organic produce. Thus, spray drift from mosquito control with active ingredients also registered as pesticides can make organic farming, if affected, unmanageable. Moreover, formulating agents (e.g. cyclohexanone added to finished preparations in a proportion as high as 1.7%) or the carrier mineral oil simultaneously appear and pollute the soil surface.

As the investigated compound is highly toxic not only to insects and aquatic organisms but also to humans and vertebrates [5], besides exposure to mosquitoes, its use can damage non-target organisms as well. The determined ecotoxicological parameters, for example the acute EC_{50} values are 0.00056 mg/l and 0.00015 mg/l for for *Daphnia magna* and *Oncorhynchus mykiss*, respectively.

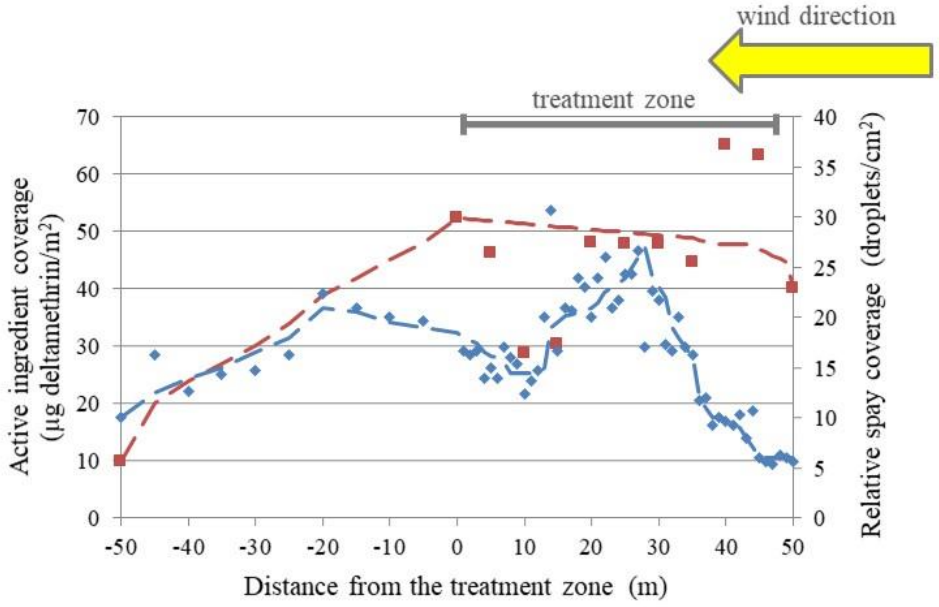

Figure 2. Amounts of deltamethrin (µg/m^2) (■) spray droplet coverage (♦) settled on the ground one hour after the aerial application of K-OTHRIN 10 ULV.

Due to their poor water solubility (e.g., 0.2 µg/l for deltamethrin), pyrethroids are rarely detected in water resources, but contamination of surface waters is more pronounced by the metabolites. Decomposition of deltamethrin results in a smaller compound containing a cyclopropanecarboxylic acid moiety and the remaining phenoxybenzyl derivative, both are enough volatile to be detected by GC-MS. According to our monitoring results, the two corresponding metabolites were observed in June in the Danube River water and in Lake Balaton. Lack of standards prevented the quantification, but they were present not at trace levels.

Conclusion

Physical measurements of the pesticide spray droplet size and their distribution as well as the chemical instrumental analysis of the active ingredient confirmed that spray droplets in aerial application of deltamethrin as an active ingredient adulticide in mosquito control reached the surface of the soil, and the survey also evidenced a substantial spray drift. The amount of the insecticide settled one hour after the treatment varied between 8 and 48%. The results confirmed that the drift of the airborne agent at 50 meters can be significant, up to 31%. In the process, micrometeorological factors play a key role, which is mostly influenced by local vegetation cover. Comparing the two application technologies, it can be concluded that in aerial application, lower concentrations can be measured due to scattering over a larger area, while the thermal foggers (where field dosages maybe higher) result in higher concentrations locally. The large amounts of aerially applied active ingredient pollute surface waters, and despite of its extremely low water solubility, its metabolites were detected in Danube water samples. In addition, in the case of aerial application, the contamination of the agricultural areas over which the aircraft applies or to which the applied agent drifts must not be neglected. Over intensive agricultural areas, this effect is not severe, as the doses used for mosquito control are lower than the dosages of the given active ingredient used against the insects in agriculture, nonetheless, low dosage exposures of pest insects can promote the development of resistance of agricultural pests. However, this type of involvement of organically grown areas is serious, as no synthetic active substance is allowed in this agricultural management practice at all. Formulating agents and solvents of formulations are usually synthetic chemicals, which can also gain significance when they affect organic farming.

Despite of developments in chemical mosquito control technology as well as in spraying machines, pesticide drift upon aerial application is still of concern. Applying the more targeted biological control (reduction of larvae populations), off-target exposure can be eliminated for many aquatic species. Numerous treatments in every year lead to detrimental environmental effects and to unintended contamination of surrounding agricultural areas by synthetic insecticides, which hinders organic farming. Therefore, restriction of aerial applications of insecticide active ingredients is justified and biological control of mosquitoes is recommended.

Acknowledgements
This work was supported by OTKA 112978.

References

[1] B. Darvas, V. Zöldi, M. Mörtl, A. Székács, Abs. IX. Ökotoxikológiai Konf. 9 (2019) 6.
[2] A. Székács, szerk. (2006) Környezetbarát védekezési technológiák csípőszúnyogok ellen. MTA Növényvédelmi Kutatóintézet, Budapest. https://mek.oszk.hu/09900/09992
[3] V. Zöldi (2019) https://index.hu/velemeny/2019/11/28/miert_korszerutlen_a_szunyoggyeritesunk
[4] http://www.hort.hu/2020/szunyogirtas_korlevel_onkormanyzatoknak.pdf
[5] Irtószerek Kereshető Adatbázisa, http://www.oek.hu/ika
[6] Hertfordshire University, Pesticide Properties DataBase, https://sitem.herts.ac.uk/aeru/ppdb/en/atoz.htm
[7] V. Nardelli, F. Casamassima, G. Gesualdo, et al. J Agric. Food Chem. 66(39) (2018)10267 .
[8] A. Kretschmann, N. Cedergreen, J.H. Christensen, Anal. Bioanal. Chem. 408(4) (2016) 1055.
[9] M. Paramasivam, S. Chandrasekaran, Chemosphere 111 (2014)291 .

ENHANCED ELECTROANALYTICAL PERFORMANCE FOR DICLOFENAC DETECTION THROUGH OPTIMIZING VOLTAMMETRIC OPERATING CONDITIONS

Sorina Motoc (m. Ilies)[1], Florica Manea[2], Elisabeta Szerb[1], Sorina Negrea[3,4], Claudia Delcioiu[2,3], Aniela Pop[2]

[1]"Coriolan Dragulescu" Institute of Chemistry Timisoara of Romanian Academy, Mihai Viteazu 24, Timisoara, 300223, Romania;
e-mails: sorinailies@acad-icht.tm.edu.ro; szella73@gmail.com
[2]Department of Applied Chemistry and Engineering of Inorganic Compounds and Environment, Politehnica University of Timisoara, Blv. Vasile Parvan No. 6, 300223, Timisoara, Romania
e-mails: florica.manea@upt.ro;
[3]"Gheorghe Asachi" Technical University of Iasi, Department of Environmental Engineering and Management,Blvd. Mangeron, 67, 700050, Iasi, decanat@chtuiasi.ro, Romania
[4]National Institute of Research and Development for Industrial Ecology - (INCD ECOIND)-Timisoara Branch, Bujorilor 115, 300431, Timisoara, ecoind.tm@gmail.com, Romania

Abstract

In this study, the influence of the operating conditions of the voltammetric techniques, i.e., differential-pulsed voltammetry (DPV) and square-wave voltammetry (SWV) on the electroanalytical performance of fullerene-carbon nanofiber paste electrode (Full-CNF) for diclofenac (DCF) determination is studied. The optimization of the step potential (SP) and the modulation amplitude (MA) were achieved for DPV, which were further applied for SWV technique. The influence of frequency was tested and the SP of 25 mV, an MA of 200 mV, at the scan rate of 0.1 $V \cdot s^{-1}$ and frequency of 5 Hz were found as optimized voltammetric operating conditions related to the sensitivity for the determination of DCF in aqueous solution.

Introduction

Pharmaceuticals and personal care products as pollutants (PPCPs) have been identified in the environment for decades. Pharmaceutical compounds can reach detectable concentrations in rivers and lakes if production and use are sufficiently large and the compounds show some mobility and persistence in the aquatic environment [1]. The major concerns with the ecotoxicities of PPCPs come from prescription and over-the-counter medications due to their specific targets on living tissues. Analgesics are pain-relief drugs that include narcotic analgesics, non-narcotic analgesics, and non-steroidal anti-inflammatory drugs (NSAID). They act in various ways on the peripheral and central nervous systems and are widely used to improve the pain present in almost all diseases [2]. NSAIDs include diclofenac (DCF), fenoprofen, ketoprofen, mefenamic acid, indomethacin, naproxen and ibuprofen [3].

Several methods have been developed for the determination of pharmaceuticals such as chromatographic techniques, spectrophotometry and capillary zone electrophoresis [4-6]. However, most of these methods need expensive and sophisticated instruments and are time consuming, and in many cases, due to their relatively low sensitivities, they need a preliminary pre-treatment step, which is laborious and expensive [7]. The electrochemical methods are known to exhibit a great potential for high-performance analytical methods but their performance is in direct relation to the electrode material and the operating tehniques [8, 9].

Nanotechnology has become very popular in the sensor fields in the recent times. It is thought that the utilization of such technologies, as well as the use of nanosized materials, could well have beneficial effects for the performance of sensors [7]. Nanosized materials have been

shown to have a number of novel and interesting physical and chemical properties. These can have marked differences from those of the bulk material, offering the possibility of new applications and improved performance [10]. Fullerenes have high melting points and boiling points, like other giant molecular substances. The size, hydrophobicity, three-dimensionality, and electronic configurations make the fullerenes an appealing subject in pharmaceutical chemistry [7]. Carbon nanofibers (CNF) are part of carbon materials class, and they are cheaper in comparison with carbon nanotubes due to the synthesis method, and also have excellent electrical conductivity, and a large surface-to-volume ratio [11].

In this study, a voltammetric method for the diclofenac detection using paste electrode consisted of fullerene (Full) and carbon nanofibers (CNF) in paraffin oil, which was reported previously by our research team for the amperometric detection of DCF [8]. Voltammetric techniques, i.e., cyclic voltammetry (CV), differential pulsed voltammetry (DPV), and square-wave voltammetry (SWV), were applied and optimized operating conditions were found to develop enhanced and fast voltammetric methods for DCF determination in aqueous solutions.

Experimental

The composition of the fullerene–carbon nanofiber paste electrode (Full–CNF) was obtained by manual mixing certain amounts of carbon nanofibers, paraffin oil, and fullerene to reach the ratio of 50 wt. % carbon nanofibers, 25 wt. % fullerene, and 25 wt. % paraffin oil, described detailed in our previously reported work [8].

The electrochemical measurements were performed with a classical three-electrode cell system, consisting of a Full–CNF paste working electrode, a platinum counter electrode, and an Ag/ AgCl as reference electrode using an Autolab potentiostat/ galvanostat PGSTAT 302 (Eco Chemie, The Netherlands) controlled with GPES 4.9 software. The Full–CNF paste electrode with disc geometry was obtained by filling a Teflon mold, resulting in an active surface with a diameter of 3 mm. Prior to use, the electrode was electrochemically stabilized through 10 continuous repetitive cyclic voltammograms within the potential ranging between -0.5 V to +1.5 V/Ag/ AgCl in 0.1 M sodium sulfate supporting electrolyte. Na_2SO_4 used was analytical-grade reagent from Merck, and Diclofenac (DCF), was used as received from Amoli Organics Ltd. All solutions were prepared with doubly distilled and deionised water.

The electrochemical techniques applied for electrochemical characterization and the analytical applications in DCF determination were cyclic voltammetry (CV), differential-pulsed voltammetry (DPV), and square-wave voltammetry (SWV).

Results and discussion

A good distribution of carbon nanofibers and fullerene in oil paraffin was assured and the larger electroactive electrode area was found to be 0.249 cm^2 versus s the value of the electrode geometric area of 0.196 cm^2 [8].

Figure 1 present the electrochemical behavior of DCF on Full-CNF paste electrode investigated by cyclic voltammetry (CV) in a supporting electrolyte of 0.1 M Na_2SO_4 and in the presence of increasing DCF concentrations ranged from 3.4 to 17 μM, and the anodic peak corresponding to DCF oxidation recorded at the potential value of about +0.7 V *vs* Ag/AgCl increased linearly with DCF concentration. The calibration plots is presented in the inset of Figure 1, which informed about the diffusion-controlled oxidation process of DCF onto Full-CNF paste electrode. Also, the cathodic peak is noticed at the potential value of about +0.2V *vs* Ag/ AgCl, which are related to the carbon redox system, confirmed by the results already published [8].

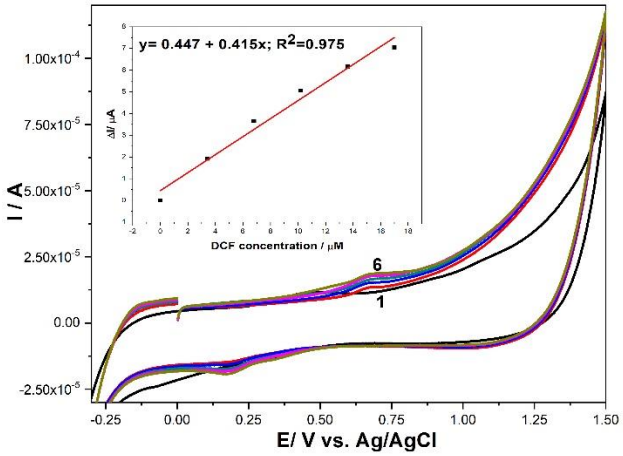

Figure 1. Cyclic voltammogram recorded on Full-CNF electrode in 0.1 M Na_2SO_4 supporting electrolyte (curve 1) and in the presence of various DCF concentrations: curves 2–6: 3.4–17 μM DCF; potential scan rate: 0.05 $V \cdot s^{-1}$; potential range: −0.5 to +1.5 V/Ag/ AgCl. Inset: Calibration plots of the currents recorded at E = +0.7 V Ag/ AgCl versus DCF concentrations.

Due to the method sensisitvity determined by the slope of the calibration plots is low, the advanced voltammetric techniques of DPV and SWV were considered to improve the electroanalytical performance for DCF voltammetric determination. Thus, in order to enhance the sensitivity and the limit of detection (LOD) by voltammetric method, the first voltammetric technique considered in this study is differential-pulsed voltammetry (DPV), and the operating conditions tested are gathered in Table 1.

Figure 2 presents DP voltammograms recorded under the optimized operating parameters (SP of 25 mV, an MA of 200 mV, and at the scan rate of 0.1 $V \cdot s^{-1}$), and enhanced sensitivity was obtained for DCF determination in comparison with those of cyclic voltammetry (2.465 μA/μM). It can be noticed that the second anodic peak appeared at the potential value of about +1.1. V *vs* Ag/AgCl, which was not considered for this DCF single component system.

Table 1. Operating conditions for DPV

SP, mV	MA, mV	Scan rate,Vs^{-1}	Sensitivity, μA/μM
25	100	0.05	0.760
50	100	0.1	2.279
25	**200**	**0.1**	**2.465**
100	200	0.2	Not stable, the scan rate is to high
10	200	0.2	Not stable, the scan rate is to high

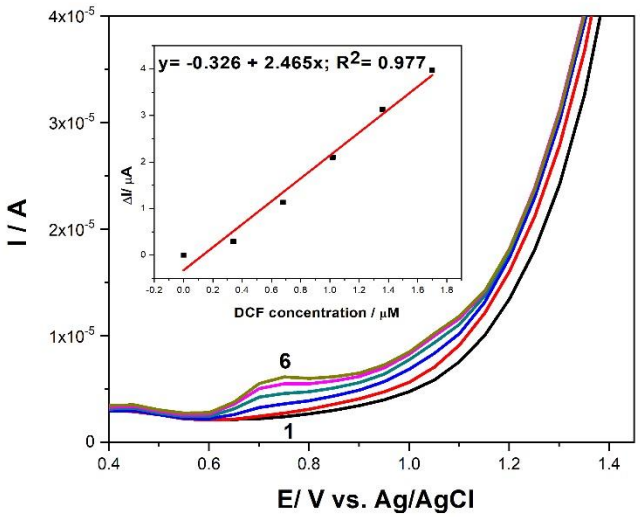

Figure 2. Differential pulse voltammetry recorded on Full-CNF electrode in 0.1 M Na_2SO_4 supporting electrolyte (curve 1) and in the presence of various DCF concentrations: curves 2–6: 0.34–1.7 μM DCF; step potential 0.025V; modulation amplitude 0.2V, potential scan rate: 0.1 $V \cdot s^{-1}$; potential range: 0 to +1.5 V *vs* Ag/ AgCl. Inset: Calibration plots of the currents recorded at E = +0.7 V Ag/ AgCl versus DCF concentrations.

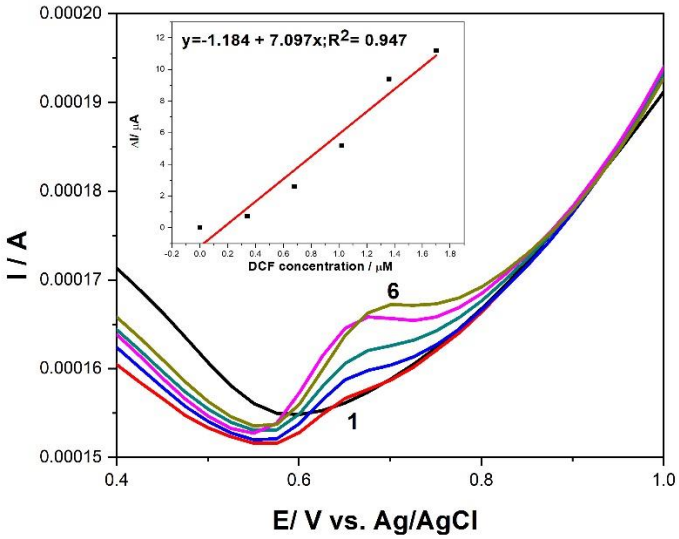

Figure 3. Square-wave voltammetry recorded on Full-CNF electrode in 0.1 M Na_2SO_4 supporting electrolyte (curve 1) and in the presence of various DCF concentrations: curves 2–6: 0.34–1.7 μM DCF step potential 0.025V; modulation amplitude 0.2V, frequency 5 Hz, potential scan rate: 0.1 $V \cdot s^{-1}$; potential range: 0 to +1.5 V/Ag/AgCl. Inset: Calibration plots of the currents recorded at E = +0.65 V Ag/ AgCl versus DCF concentrations.

Also, the SWV technique was tested under similarly optimized operating conditions as the DPV technique, and the results are presented in Figure 3. Using SWV operated under SP of 25 mV, MA of 200 mV at the scan rate of 0.1 $V \cdot s^{-1}$ and frequency of 5 Hz, a good linearity was reached, as can be seen in the inset of Figure 3. About seven times better sensitivity was

reached for optimized operating conditions (7.097 µA/µM *vs* 1.075 µA/µM). All electroanalytical parameters determined for each electrochemical technique were improved under optimized operating conditions using Full-CNF paste electrode and they are summarized in Table 2.

Table 2. Electroanalytical performances of Full-CNF electrode in DCF determination

Technique applied	Detection potential	Sensitivity (µA/µM)	LOD (nM)	Reference
DPV	+0.77V	0.689	10.2	[8]
	+0.7V	2.465	1.2	This work
SWV	+0.75	1.076	0.9	[8]
	+0.65V	7.09	7.4	This work

It can be noticed that the optimized operating variables are related to the sensitivity and the lowest limit of detection depending on the practical needs.

Conclusion

The influence of the operating conditions of the voltammetric techniques on the electroanalytical performance are highlighted in this study. The optimized operating conditions depended on the electrode composition through its electrochemical stability and implicit, the electrochemical response signal. The best sensitivity for DCF determination using Full-CNF paste electrode was achieved through SWV under SP of 25 mV, MA of 200 mV at the scan rate of 0.1 $V \cdot s^{-1}$ and frequency of 5 Hz (7.097 µA/µM) while the lowest limit of detection was achieved for a SP of 2 mV, MA of 10 mV, and frequency of 25 Hz.

Acknowledgements

Funding for this study was provided by a grant of the Romanian Ministry of Research and Innovation, CNCS - UEFISCDI, project number PD 88/2020, project code PN-III-P1-1.1-PD-2019-0676, within PNCDI III.

References

[1] B. Petrie, R. Barden, B. Kasprzyk-Hordern, Water res. 72 (2015) 3.
[2] Q. Xu, A. Yuan, R.Zhang, X. Bian, D. Chen, X. Hu, Curr. Pharm. Anal. 5(2) (2009) 144.
[3] A. Gogoi, P. Mazumder, V. K.Tyagi, G.G. Tushara Chaminda, A.K. An, M. Kumar, Groundw. Sustain. Dev. 6 (2018) 169.
[4] S. Schmidt, H. Hoffman, L.A. Garbe, J. Cromatogr. A 1538 (2018) 112.
[5] S. Battu, V. Gandu, B.P. Nenavathu, Asian J. Biomed. Pharmaceut. Sci. 10 (69) (2020) 19.
[6] L. Suntornsuk, J. Chromatogr. Sci. 45 (2007) 559.
[7] T.A. Saleh, J. Bioenerg. 5(1). (2016) 1.
[8] S. Motoc, F.Manea, C. Orha, A. Pop, Sensors 19 (6) (2019), 1332.
[9] S. Motoc, F.Manea, A. Iacob, A. Martinez-Joaristi, J. Gascon, A. Pop, J. Schoonman, Sensors 16 (10) (2016) 1719.
[10] S. Kurbanoglu, S.A. Ozkan, J. Pharm. Biomed. Anal. 147 (2018), 439.
[11] M. Ardelean, F. Manea, A. Pop, J. Schoonman, J. Ecol. Eng. 10(9) (2016) 1237.

HIGH PRESSURE AND ULTRASOUND-ASSISTED EXTRACTON OF BIOACTIVE COMPOUNDS FROM *Santolina chamaecypatissus*

Zorana Mutavski[1], Jelena Vladić[1], Senka Vidović[1], Milica Aćimović[2]

[1]University of Novi Sad, Faculty of Technology, Bulevar cara Lazara 1, 21000 Novi Sad, Serbia
[2]Institute of Field and Vegetable Crops, Maksima Gorkog 30, 21000 Novi Sad, Serbia
e-mail: zoranamutavski@gmail.com

Abstract
The objective of this study was to determine the most adequate process, using a green approach, which ensures maximal exploitation of *Santolina chamaecypatissus* and attainment of high quality extracts rich in bioactive compounds and with strong antioxidant activity. Two environmentally friendly techniques were applied, supercritical carbon dioxide for isolating volatile compounds and ultrasound-assisted extraction for obtaining extracts rich in polyphenolic compounds.

Introduction
S.chamaecypatissus L. (cotton lavender) is a flowering plant in the family of *Asteraceae* native to the Mediterranean region. It is a herbal special of medicinal significance due to its analgesic, bactericidal, and fungicidal properties. Cotton lavender is rich in volatile components which makes it a reliable source of commercial essential oils. Although it is most commonly for isolating oil, cotton lavender also represents a great source of hydrophilic antioxidant compounds which usually remain unutilized because the common and traditional methods for separating oil are not adequate for isolating non-volatile antioxidant compounds [1].

Experimental
The first step was the extraction with CO_2 in supercritical state at a pressure of 300 bar and a temperature of 40°C. Residue after supercritical CO_2 extraction was subjected to ultrasound-assisted extraction. Extraction parameters for the most optimal quality of extracts were investigated: ethanol at concentrations of 30, 50, and 70% (v/v), temperature 30, 50, and 70°C, and extraction time 10, 20, and 40 min. In obtained extracts the content of total phenols, total flavonoids, and antioxidant activity were determined.

Results and discussion
The yield of supercritical extraction was 3.98% (m/m). The highest ultrasound-assisted extraction yield (28.48%) was achieved by using 50% ethanol at temperature of 50°C during a period of 40 min, while the lowest yield was achieved with 30% ethanol, 50°C, and 20 min. Using the one-variable-at-a-time technique, where one parameter is varied while the other two remain constant, it was recorded that all investigated factors had a positive effect on the extraction yield. The increase of concentration of ethanol resulted in extracts with a higher content of phenols and the highest measured concentration of total phenols was 2.45 mg equivalent of gallic acid/mL of extract. Temperature exerted a negative impact on phenolic fraction content. However, higher content of total flavonoids was obtained with an increase in temperature and decrease in ethanol concentration. The extract with the highest antioxidant activity was the one with the shortest extraction time (10 min, 50°C, and 50% ethanol), while the highest IC_{50} value was measure in the extract obtained with 70% ethanol (20 min and 50°C). Additionally, compared to extracts obtained by ethanolic ultrasound-assisted extractions, the extract obtained by supercritical extraction showed a significantly lower antioxidant activity.

Conclusion

Based on the obtained results, cotton lavender represents a significant and rich source of bioactive compounds with widely ranging polarities. The applied extraction approach including combining different green technologies for isolating volatile and non-volatile compounds proved to be an adequate method for obtaining high-quality extracts of cotton lavender and efficient utilization of this natural material.

References

[1] L.L. Niu, Q. P. Qin, L.T. Wang, Q. Y. Gai, J. Jiao, C.J. Zhao, Y.J. Fu, Chemical profiling of volatile components of micropropagated Santolina chamaecyparissus L. Industrial Crops and Products, (2019) 137, 162-170.

TUNABLE SURFACE WETTABILITY OF CARBON NANOTUBES-NONWOVEN TEXTILE COMPOSITES

Krisztina Anita Nagy[1], Ildikó Y. Tóth[1], Ákos Kukovecz[1]

[1]Department of Applied and Environmental Chemistry, University of Szeged, Interdisciplinary Excellence Centre, H-6720, Szeged, Rerrich Béla tér 1, Hungary
e-mail: n.krisztina@chem.u-szeged.hu

Abstract
Tunable surface wettability of a material may have a valuable role in environmental application. We created a composite material from a nonwoven textile (NW) decorated with carboxylic functionalized carbon nanotubes (*f*-CNT) using a vacuum filtration method. The surface wettability of the composites is tunable by the *f*-CNT amount. Surface wettability was checked by contact angle measurements. The morphology of the samples was observed by scanning electron microscopy. The isoelectric point of *f*-CNT was determined from electrophoretic mobilities measurements. This composite material with tunable wetting properties may be relevant *e.g.* in water purification.

Introduction
Carbon nanotubes are widely known in the sciences since Ijima's work [1]. CNTs have a wide range of application in the wastewater treatment. CNT based materials like the CNT sponges are applicable *e.g.* for oil absorption due to the large surface area and excellent flexibility, furthermore they are light-weight [2]. The functionalization is a good opportunity to tune or modify some property of CNTs [3]. The overlapped nanotubes in a group of CNT make bulges on the surface. The liquid follows or suspends on the highest part of the bulges which eventuates 'Wenzel' or 'Cassie-Baxter' states, respectively [4,5]. The chemical properties (hydrophilic or hydrophobic) of the substance and the extent of surface roughness can control these wetting regimes [6].

Experimental
Materials:
Multiwalled carbon nanotubes (MWCNT) were synthesized and then it was modified with an oxidative functionalization to create carboxylic groups on the outer shell of the tubes. The MWCNTs were synthesized by 2 h of catalytic chemical vapor deposition from a C_2H_4:N_2 (30:300 cm^3/min) gas mixture at 650 °C by using Fe,Co/Al_2O_3 catalyst (metal loading: 2.5-2.5 m/m%). The synthesized materials were purified by repeating 4 h of refluxing in 10 mol/dm^3 aqueous NaOH, then 4 h in cc. HCl solution four times. A part of the as prepared pristine non-functionalized carbon nanotubes (*nf*-CNT) were subjected to oxidative chemical functionalization (8 h reflux of 4 g CNT in 500 cm^3 cc. HNO_3 solution). After that, further functionalization was carried out to facilitate surface carboxyl group formation and improve their hydrophilicity to get so called functionalized carbon nanotubes (*f*-CNT). During this step, the suspension of the previously received nanotubes (10 g/dm^3 CNT) were sonicated in a 0.1 mol/dm^3 solution of $KMnO_4$ in 60% aqueous perchloric acid for 15 minutes. The excess $KMnO_4$ was then reacted with oxalic acid. The fabricated CNTs were washed first in 0.01 mol/dm^3 hydrochloric acid to remove MnO_2, afterward in deionized water, then finally dried in air at 80 °C for 24 h.
A circular piece (d=25 mm) of a needlepunched polyester nonwoven material (fibre length of 48 mm; fibre diameter of 29 μm) was used to prepare fCNT-NW composites. An as-prepared *f*-CNT (in deionized water) suspension was filtrated through the nonwoven material by a dead-

end filtration equipment (see in Fig 1.). Three samples were fabricated with nominal *f*-CNT loadings of 5, 10, and 15 wt%. The corresponding sample IDs were assigned as 'fCNT-5-NW', 'fCNT-10-NW' and 'fCNT-15- NW', respectively. Furthermore, an 'fCNT-film' was also prepared in the same manner, just without NW.

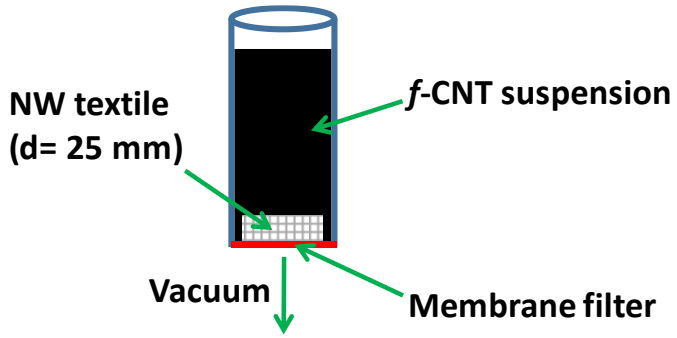

Figure 1. Schematic of the preparation process of the composites.

Methods:

The *f*-CNTs were characterised by **transmission electron microscopy** (TEM). It was performed on a FEI Tecnai G^2 20 X Twin instrument operated at a 200 kV accelerating voltage. The suspension of the sample was dropped onto copper mounted holey carbon standard TEM grids. Several different positions were examined on each sample and images were taken at each position.

Electrophoretic mobilities of the *f*-CNTs were measured in a Nano ZS (Malvern) apparatus with a 4 mW He−Ne laser source (λ = 633 nm) using disposable zeta cells (DTS 1070) at 25±0.1 °C. The zeta-standard of Malvern (−55±5 mV) was used for calibration and the samples were diluted to give an optimal intensity. To get comparable data, the dispersions were homogenized in an ultrasonic bath for 10 s, after which 2 min relaxation was allowed. The effect of pH variation was studied at 10 mM NaCl. The Smoluchowski equation was applied to convert electrophoretic mobilities to electrokinetic potential values. The accuracy of the measurements was ±5 mV.

Morphology of fCNT-NW composites was determined by **scanning electron microscopy** (SEM). For these measurement a Hitachi S-4700 microscope was used equipped with a field emission gun operated with accelerating voltages of 10 kV.

Apparent equilibrium contact angles were measured by placing a 10 µL water droplet (coloured with methylene blue dye) onto the surface investigated. Six independent images (recorded at room temperature by Dino-Lite Edge Digital Microscope; AnMo Electronics Corp.; product code AM4815ZTL) were analyzed for all samples using the ImageJ® system.

Results and discussion

The typical length of the *f*-CNTs was over 10 µm and their outer diameter fell in the 15-25 nm range as determined from TEM image analysis (see in Fig. 2.).

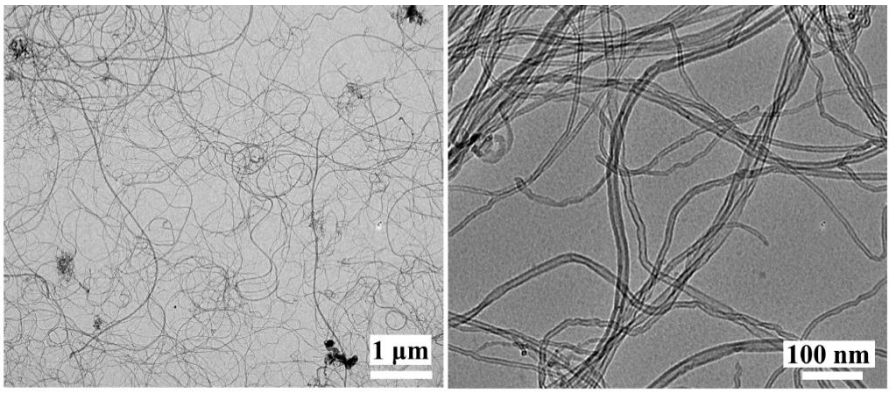

Figure 2. TEM images about *f*-CNT.

Three different composites were prepared, which contain different amount of *f*-CNT. During filtration, a big fraction of *f*-CNT were deposited on the top surface of the nonwoven textile which can be seen in Fig. 3. There is more carbon nanotube on the NW with increasing amount of CNT. While there is some ensemble of *f*-CNT in case of fCNT-5-NW (Fig. 3.b.), however CNTs completely cover the textile surface in case of fCNT-15-NW (Fig. 3.d.). Dual scale surface roughness is experienced on the top of the composites, because the textile fibres are in micron-scale while the CNT is in nano-scale. The top surface of the composites is rough and fractured.

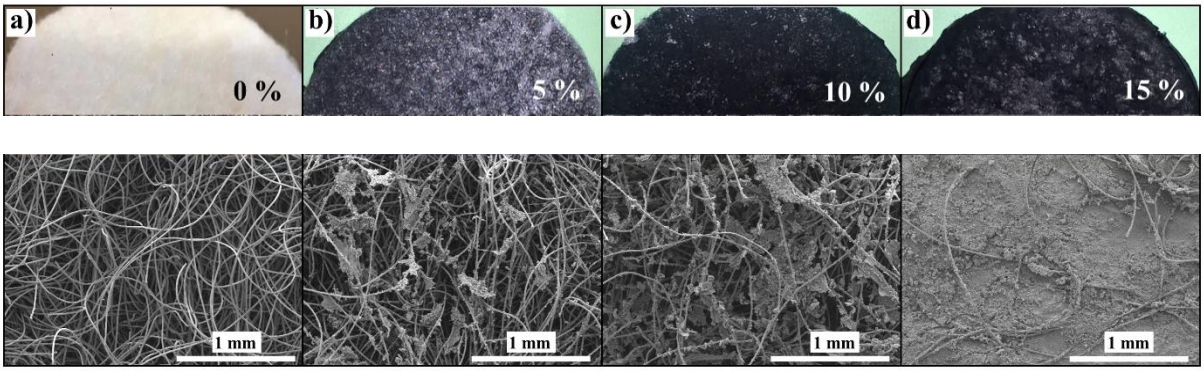

Figure 3. Digital photos (above) and SEM images (below) about fCNT-NW samples.

The zeta potential of the *f*-CNTs is plotted as a function of pH in Fig. 4. The isoelectric point (IEP, at which the net charge of CNT is zero) is at pH~2. The values of zeta potential shift to more negative region with the increasing pH caused by the deprotonation of the –COOH functional group of *f*-CNT.

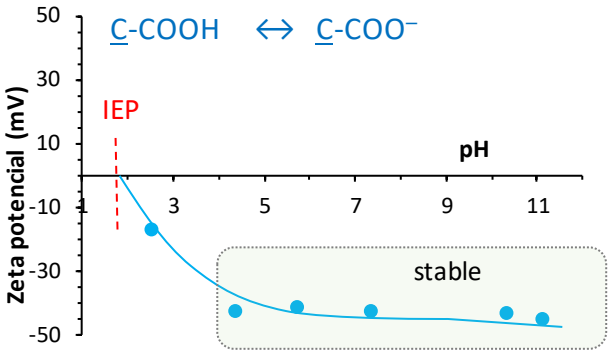

Figure 4. The pH dependent zeta potential of *f*-CNT samples (10 mM NaCl, 25°C).

Apparent contact angles were measured to determine the hydrophilic-hydrophobic nature of the materials. Some representative photos about the water droplets coloured by methylene blue on the surface of pure textile, composite sample and fCNT-film can be seen in Fig. 5.

Figure 5. Some representative photos about the coloured water droplets.

The fCNT-film has the most hydrophilic properties as the average contact angle is found to be 43.3°. The pure NW sample shows hydrophobic nature with contact angle of 132.8°. If the *f*-CNT loading was increased, the contact angle was decreasing in case of composites as it is depicted in Fig. 6. Presumably, there was not a uniform covering with *f*-CNT in case of fCNT-5-NW sample, which leads to the dominance of Cassie-Baxter regime, due to the lower surface energy of the polyester fibres and three dimensional texture of the NW material.

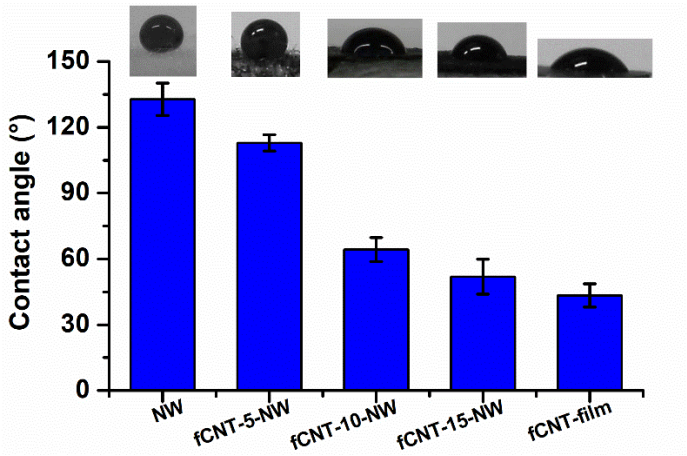

Figure 6. Average contact angles (from 6 droplets, V=10 μL) with digital photos of droplets on the surface of the materials.

Conclusion

In this work it was prepared some composite sample that are carboxylic functionalized MWCNT decorated needlepunched polyester nonwoven textiles by a scalable and inexpensive vacuum filtration process. The carboxylic functionalization of MWCNT results in a more hydrophilic nature of CNT. Apparent contact angles prove, that the functionalized carbon nanotube loading to the nonwoven textiles can tune the hydrophobic-hydrophilic characteristics of the composites. The surface wettability can be controlled by a predefined amount of *f*-CNT. Therefore, it may have a potential role *e.g.* in the wastewater treatment.

Acknowledgements

The financial supports from "Széchenyi 2020" program in the framework of GINOP-2.3.2-15-2016-00013 project and OTKA NKFIH K 112531 grant are acknowledged. I.Y. Toth acknowledge the support by the Ministry of Human Capacities, Hungary through the grant ÚNKP-19-4 New National Excellence Program. We thank Krishn Gopal Rajput for the technical contribution during the preparation.

References

[1] S. Iijima, Nature 354(6348) (1991) 56-58.
[2] X. Gui, J. Wei, K. Wang, A. Cao, H. Zhu, Y. Jia, Q. Shu, D. Wu, Advanced Materials 22(5) (2010) 617-621.
[3] N. Karousis, N. Tagmatarchis, D. Tasis, Chemical Reviews 110(9) (2010) 5366-5397.
[4] R.N. Wenzel, Ind. Eng. Chem. 28(8) (1936) 988–994.
[5] A.B.D. Cassie, S. Baxter, Trans. Faraday Soc. 40(0) (1944) 546–551.
[6] A. Rawal, S. Sharma, V. Kumar, H. Saraswat, Appl. Surf. Sci. 389 (2016) 469–476.

CHANGES IN THE CONTENTS OF HEN EGGS DUE TO POLYPHENOL-RICH SUPPLEMENTATION

Anett Veisz [1], Marietta Fodor[1], Éva Stefanovits-Bányai[1], László Friedrich[1], Csaba Németh [2], Boglárka Kovacs [2], Anna Mária Nagy[3]

[1] St. Stephen's University, Faculty of Food Science, Institute of Food Quality, Safety and Nutrition, H-1118 Budapest, Villányi Street 29-43, Hungary,
[2]Capriovus Ltd. Hungary
[3]Holi-Medic Kft, Hungary
e-mail: holimedic@gmail.com

Abstract

The suspension of *Bábolna Tetra-SL* hen hybrids - the food concentrate ***Flaviva Vasgyúró*** instant drink powder, which is available on the market and is rich in flavonoids, polyphenols and minerals, is mixed into the basic feed. One group of test animals received 200 mg per day and another group received 400 mg of instant vegetable and fruit powder per day mixed in their basic maize feed for 33 days, while the control group received only the basic food containing maize.

In our studies, we measured the cholesterol content and total polyphenol content of the eggs in addition to the physical parameters (weight, length, diameter, color). Our results show that in addition to favorable changes in the physical properties of eggs, the polyphenol content of eggs increased significantly, thus correlating with a significant decrease in the content of cholesterol, which may be of importance from a nutritional point of view in many groups of diseases.

Introduction

One of the most important "common denominants" of diseases with the world's highest morbidity and mortality rates (cardiovascular diseases, tumors, diabetes mellitus, chronic inflammations with various many-organ involved) is the overgrowth of destructive oxidative free radicals and the overturning of redox homeostasis balance (dysbalance). One of the main triggers and maintenance factors for cardiovascular disease is the persistently elevated levels of oxidatively damaged LDL cholesterol (low-density lipoprotein) in the blood plasma, so a significant and sustained reduction in this is important from both individual and public health point of view. Many of our foods contain significant amounts of cholesterol, of which chicken eggs [1-6], which are very valuable food in nutritional value, vitamins, amino acid compositions and minerals [7].

Polyphenol-rich compounds are widely known free radical-catchers (scavangers), so our research has looked for the response to the dose-dependent suspension of hens with complementary nutrients rich in polyphenol components that result in changes in eggs.

Materials and metods

In our research, we observed changes in the eggs of the ***18-week-old hybrid hens of Bábolna Tetra-SL [8],*** which spread in Hungary, in 3 test arms for 33 days, with 3-3-3 eggs per test branch. The control group was fed exclusively with the 'Universal Commodity Feed Mixture II'. In one of the 2 active study strands, hens received a daily dose of 200mg per day and a daily dose of 400mg in the other study arm mixed with flavonoids and polyphenols-rich supplementation to their anesthrax. The basic feed was suppressed by the addition of ***Flaviva Vasgyúró*** instant beverage powder produced by gentle vacuum drying from vegetable and fruit concentrates, which are compared with blackcurrant powder, blackberry powder, organic beet

powder, cherry powder and wild forest cranberry powder (Manufacturer: GPS-Powder Kft., distributor: Szanté Bt.)

In addition to determining ***the physical parameters*** (weight, length, diameter, colour and dry matter content) of the eggs, we also measured the ***total polyphenol content*** of the eggs and the ***content of cholesterol***.

Analytical methods

Measurement of physical parameters: mass (g), diameter (mm), length (mm).

Measuring egg colour changes:Konica Minolta Chroma Meter CR-400 with handheld color measuring instrument (ΔE, ΔL, Δa, Δb).

Sample preparation for analytical tests: 25 mg/ml of the lyophilized egg samples were prepared, centrifuged for 10,000 rpm for 15 minutes (Thermo scientific SORVALL Evolution RC) after 1 hour of ultrasonic exploration, followed by pure supernatant for measurements.

Determination of total phenolic contents (TPC) by Folin-Ciocalteu method: The Folin-Ciocalteu spectrophotometric method by Singleton and Rossi [9], at 760 nm is an electron transfer based assay and shows the reducing capacity, which is expressed as phenolic content. Gallic acid (GA) was used to prepare the standard curve. The results were expressed as μmol GA/g of power.

Cholesterol content was measured from the lyophilized sample using a ***near infrared spectroscopy*** method (Bruker MPA FT-NIR, Ettlingen, Germany). A sample placed in a sample holder with a diameter of a 20 mm was measured by diffuse reflection. The average square error of the estimation function used for the determination is 0.55 mg cholesterol/g and R^2 is 0.96.

All chemicals used in our tests were sourced from Sigma Aldrich Kft.

Results and discussion

I) ***Measurement of the physical parameters of eggs:*** There has been no substantive change in the number of eggs collected. FlaViva Vasgyúró instant drink powder suppressed a dose-dependent, small increase in egg weight, diameter and length, but the extent of the differences was not significant (Table 1, Fig. 1).

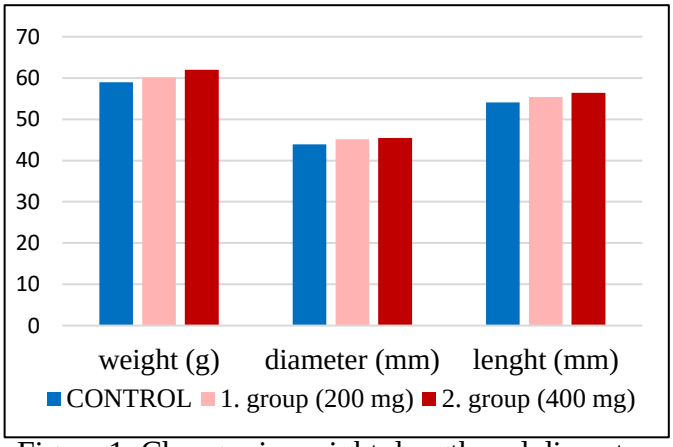

Figure 1. Changes in weight, length and diameter

Table 1. Changes in weight, length and diameter

	Control			**Group 1 (200 mg)**			**Group 2 (400 mg)**		
	weight (g)	**diameter (mm)**	**lenght (mm)**	**weight (g)**	**diameter (mm)**	**lenght (mm)**	**weight (g)**	**diameter (mm)**	**lenght (mm)**
averadge	58,94	43,89	54,10	60,09	45,17	55,38	62,00	45,47	56,39
Sd	**3,51**	0,87	1,85	**3,85**	1,18	1,65	**4,09**	1,73	1,37

II. ***Dry matter measurement***: The dry matter content of the shell and inland eggs has not changed significantly (Table 2).

Table 2. Dry matter (%) of eggs and shell

	eggs			**Shell**		
%	**Control**	**200 mg**	**400 mg**	**Control**	**200 mg**	**400 mg**
dry matter	22.80	22.63	22.48	24.35	23.07	24.88
Sd	1.00	1.42	1.16	2.66	1.93	4.37

(III) Color measurement of lyophilized eggs:

The lightness factor (marked L*) shows that samples of lyophilized eggs of group 2 hens receiving *daily 400 mg doses of the drug* have become darker as experimental time progresses. This hue change, in addition to the carotenoid content of the corn in the basic feed, is mainly due to the significant amount of flavonoid and polyphenols contained in Flaviva Vasgyúró (Table 3). Based on the red-green coloration *(marked with* a*), red hue dominates all samples, but its extent is not significant. According to the measurement of *blue-yellow* colouring (marked with b*), the lyophilized eggs of group *2 receiving* a higher daily dose of additional nutrients resulted in *significantly yellower colours by the end* of the study period , which can be interpreted as a result of the increasing appearance of *polyphenol compounds* in eggs (Table 3. and Fig.2).

Table 3. Results of colour measurements of eggs

	Day 13			**Day 17**			**Day 22**			**Day 32**		
	C	1	2	C	1	2	C	1	2	C	1	2
L*	42.08	45.62	45.01	43.13	46.24	44.25	45.86	44,54	40.33	48.23	44.34	40.15
a*	8.36	5.35	8.91	5.90	4,42	5.23	4.35	5.71	7.61	4.78	4.44	4.55
b*	30.04	33.97	33.78	25.07	33.56	28.33	27.00	27.69	24.04	32.75	25.52	33.56

(IV) Measurement of total polyphenols in eggs:

FlaViva Vasgyúró, rich in polyphenols, increased the polyphenol content of eggs compared to the control group (Fig.2) by adding instant drink powder to the *polyphenols-rich* Flaviva *Vasgyúró.*

The control group supplemented with the "Universal Commodity Egg Laying II compound feed", total polyphenol content of eggs increased by an average of *nearly 30%* from the beginning to the end of the experiment (from 2000 to 3000 on average) due to the polyphenol components of maize in the basic feed.

Compared to the control group, the total polyphenol content of eggs in both active test strands increased even further, but it should be noted that for all measurements in the 400mg group, the study as a whole, but in the 200mg group, only in the first trimester of study time *(measured on days 2-3-4-9), was significant extent of change.*

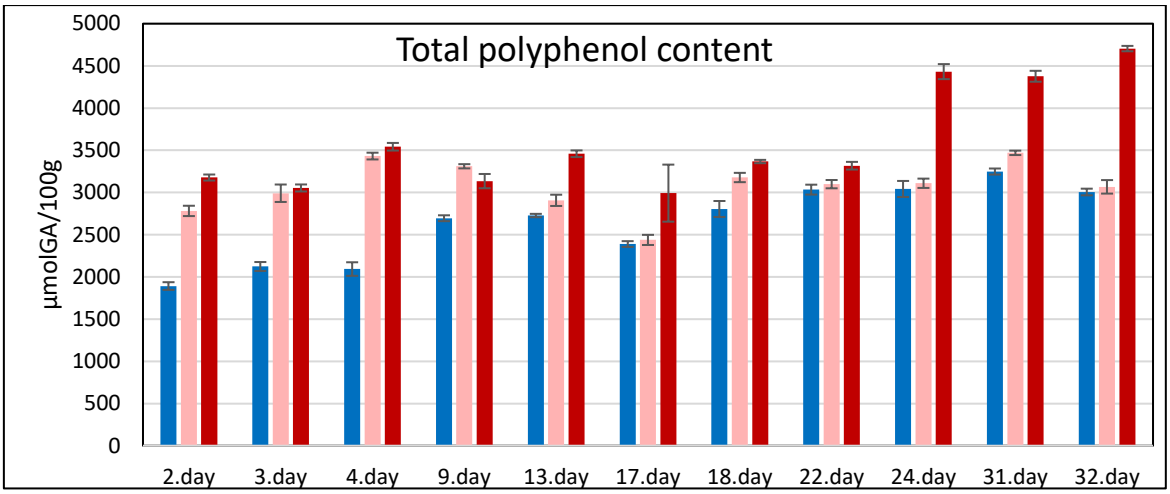

Figure 2. Changes in the total polyphenol content of eggs in the 2 active study groups and the control group with 2 active study groups receiving 2 doses of 200mg/day and 400 mg/day.

When the 2 active study strands were compared to each other, it can be seen that the additional nutrients received daily at 400 mg were obtained in group 2nd over the entire length of the study time, with a higher polyphenol content in each measurement, compared to active group 200 mg, active group 1st, but in the first 3 weeks of the study time this difference was not significant, only at 3 measurements. However, in *the last third of the test period* (24-31-32). days) the total *polyphenol* content increased by *approximately 50% in the 400 mg 2nd group* per day, compared to both the control and 200 mg daily group 1st, which suggests that both the *saturation of the hen's organism with polyphenols* and the selection of polyphenols in eggs, depend on the daily dose and duration of *supplementation.*

These observations may also be useful for human nutrition for medicinal purposes in the proper determination of daily dosing of polyphenol-rich foods on a cure-like basis.

V.) <u>The measurement of cholesterol content in eggs:</u>

The cholesterol content of the control group eggs did not show any significant trend-like changes throughout the study period. The cholesterol content in eggs of hens receiving additional feedings of 200 mg and 400 mg per day showed a *significant increase in cholesterol in the first 3* days of treatment compared to the control group and subsequently stagnated in the mid-term *phases of the experiment (a temporary* increase/decrease was observed undulatingly.

At the end of the experimental period (from 24 days to 32 days), the cholesterol content of the eggs *in both suppressed* active study groups decreased, but the reduction was only observed in the higher (400mg daily) group 2 with an increasing trend. *This correlate with a jump-like (nearly 50%)* significant, sustained increase in total polyphenol content in the same group at the end of the experimental period (Fig.2 and Fig.3). From these measurement results, it can be inferred that regular intake of polyphenols at the right dose can have a beneficial physiological effect not only on maintaining the balance of redox homeostasis in liver cells, but also on bile and cholesterol selection in the liver.

Similarly favourable cholesterol levels are reported by Udvardi [10] and his colleagues when feeding hens with sour cherry. Since *Flaviva* Vasgyúró, used as a supplementation in our study, also contains sour cherry and other highly polyphenol-containing ingredients, therefore, through its supplement, the significantly increased polyphenol content in hens' eggs may have had a positive impact on the antioxidant *capacity and redox homeostasis* balance of the hepatic-biliar organ system in hens, as well as the excretion of bile and cholesterol through the liver, as a result of which a significant decrease in the cholesterol content of eggs may be affected.

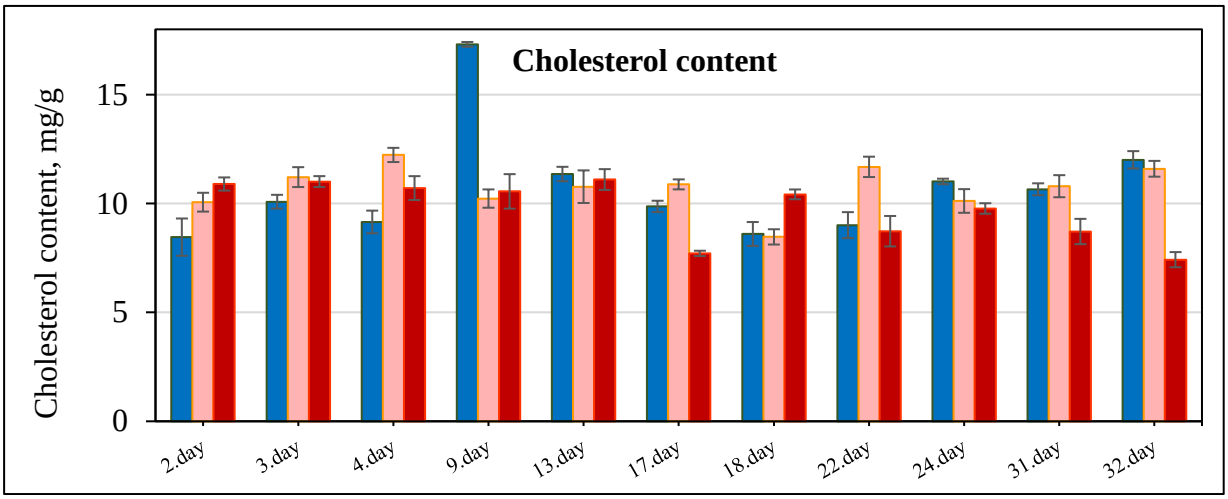

Figure 3. Changes in the cholesterol content of eggs during the feeding test

Conclusion

Flaviva Vasgyúró instant beverage powder, rich in flavonoids, polyphenols and minerals, has a positive effect on egg colour and increased physical parameters when mixed into hybrid hens' feeds, which can have many market sales significance. The significantly higher polyphenol content in eggs compared to the control group significantly increased the antioxidant capacity of the eggs and thus correlated with a significant reduction in the cholesterol content of the eggs, especially in the last week of the study.

Our study may also highlight the role that *feeding hens with polyphenol-rich feed may play a role in* their breeding, not only for healthier meat products, but also that the wider production and consumption of "smart-eggs" with reduced cholesterol content can contribute to the complementary feeding of cardiovascular patients for medicinal purposes.

Acknowledgements

The Project is supported by the European Union and co-financed by the European Social Fund (grant agreement no. EFOP-3.6.3-VEKOP-16-2017-00005).

References

[1] M. Kratz, Azheroclerosis: Diet and Drog (2005) 195-213.
[2] A.von Eckardstein, J.R. Nofer, G. Assmann, Arterioscler Thromb Vasc Biol. (2001).
[3] T.F. Daniels, K.M. Killinger, J.J. Michal, R.W. Wright, Z. Jiang, Int. J Biol Sci. 5(5) (2009) 474-488.
[4] I.Tabas, Clin Invest. 110(5) (2002) 583-590.
[5] C. Garcia-Ruiz, M. Mari, A. Colell, A. Morales, F. Caballero, J. Montero, O. Terrones, G. Basañez, J.C. Fernández-Checa, Histol Histopathol 24 (2009) 117-132.
[6] H. Ma, Nature and Science, 2(4) (2004) 17-21.
[7] Gy. Judge, K.Lindner, nutrient chart. Medicina Publishing House (1998), Budapest
[8] P. Horn P. (Eds.) Poultry, farm pigeon, (2000) Field-host Publisher, Budapest
[9] V.L. Singleton, J.A. Rossi, Am. J. Enol Vitic (1965) 16. 144-158.
[10] E. Udvardi, M. Fodor, N. Papp, É. Stefanovitsné, Bányai, Z.B. Nagy (Eds.), Warming, Ecofootprint, Food Safety, Keszthely, Hungary, (2016) 414-421.

RELATIONSHIPS OF TOTAL POLYPHENOL CONTENT, ANTIOXIDANT CAPACITY AND ANTIBACTERIAL EFFECT IN FRUIT-VEGETABLE INSTANT POWDERS

Ádám Papp[1], Mónika Kovács [1], Éva Stefanovits-Bányai[1], Anna Mária Nagy[2]

[1]St. Stephen's University, Faculty of Food Science, Department, Institute of Food Quality, Safety and Nutritionof Applied Chemistry,
H-1118 Budapest, 29-43 Villányi Street, Hungary,
[2]Holi-Medic Kft, Hungary
e-mail: holimedic@gmail.com

Abstract

Commercially available ***FlaViva Flavurin*** and ***FlaViva*** Vasgyúró instant drink powders produced by vacuum drying from vegetable and fruit juice concentrates, rich in flavonoids, polyphenols and other valuable components, was tested their ***total polyphenol content*** and ***antioxidant capacity*** by spectrophotometric method. In addition, the ***antibacterial effects*** of both products on strains of *bacteria Staphylococcus aureus, Pseudomonas aeruginosa,* and *Escherichia coli* were examined in vitro, by agar hole diffusion method.

Microbiological measurements have shown that *FlaViva FlavUrin* instant drink powder had a significantly higher antibacterial effect than *Vasgyúró for all three bacterias.*

An examination of the antioxidant capacity of the 2 food concentrates – measured by FRAP method – showed that the *antibacterial effect does not correlate with the iron content* of the products, as *the antioxidant capacity of the iron-rich Vasgyúró was 13.77 times higher than FlavUrin.*

The total polyphenol content of the 2 food concentrates did not differ significantly, so this factor alone could not have caused a significant antibacterial effect. Therefore we also measured the *TPC of each ingredients* in both products and we discovered highly ***significant differences between them:*** extremely high TPC values in rosehip powder and cranberry powder present only in FlavUrin, which may have contributed to the significantly higher antibacterial effect. The common ingredients of two food concentrates were elderberry-, blueberry- and blackcurrant powder. Since Vasgyúró also had a lower, but detectable antibacterial effect, these 3 components may have contributed to the antibacterial effects.

In addition to quantitative TPC differences between individual components, it is assumed that different varieties of qualitative individual components, as well as other bioactive components, may be responsible for the significant antibacterial effect and therefore their exploration requires further research.

Analytic and microbiological studies of functional food concentrates and the relationships between their results may draw attention to a number of health and therapeutic options and therefore require further research.

Introduction

It is a widely declared fact, the consumption of the right quantity and quality of fruits and vegetable is essential for a healthy life. At the same time, the inner values of different vegetables and fruits - and their consequent physiological effects - very significantly different from each other, that's why it is very important which one to choose for regular consumption.

The ingredients (cranberry, rosehips, elderberry, blueberry, blackcurrant, beetroot, sour cherry) of 2 complex food-concentrates (FlavUrin and Vasgyúró) we are investigating have very important internal values (carbohydrates, organic acids, minerals). In addition, the scavenger effect, which is their main health protection is due to flavonoids, vitamins and, in

particular - secondary products of plant metabolism - their polyphenol components. Most of them also have a significant amount of anthocyanins [1-8] responsible for their beautiful color.

Many authors have confirmed that some fruits also have significant antimicrobial effects, which have been paralleled by their high polyphenol content. In some examples, a favorable antimicrobial effect was described for black currants [9], cranberries [10], elderberries [11] chokeberry [12], rosehips [13], beetroot [14], sour cherry [15] and blueberries [16].

Materials and methods

FlaViva FlavUrin and Vasgyúró instant fruit-powders produced by vacuum drying have been used for measurements (developed and marketed by Szanté Bt). The ingredients of FlavUrin are cranberry powder, rosehip powder, wild blueberry powder, black elderberry powder, blackcurrant powder. The ingredients of FlaViva Vasgyúró**:** blackcurrant powder, black elderberry powder, bio-beetroot powder, sour cherry powder, wild blueberry powder. (Figure 1).

Fig.1. FlaViva FlavUrin, Vasgyúró

Microbiological methods

The microba strains studied were *Staphylococcus aureus, Pseudomonas aeruginosa, Escherichia coli.*

Antimicrobial effect test by agar hole diffusion method: 50-50 µl samples were sampled in each of the holes in the culture medium containing TGE agar and evaluations were performed after 24 and 48 hours.

Analytical methods

Sample preparation for analytical tests: preparation of 25 mg/ml aqueous solution, 1 hour of UH exploration for 10000 rpm for 15 minutes, then working from the clear supernatant.

Determination of total phenolic contents (TPC) by Folin-Ciocalteu method: The Folin-Ciocalteu spectrophotometric method by Singleton and Rossi [17], at 760 nm is an electron transfer based assay and shows the reducing capacity, which is expressed as phenolic content. Gallic acid (GA) was used to prepare the standard curve. The results were expressed as µMGA/g of powder.

Determination of antioxidant capacities by FRAP (Ferric Reducing Antioxidant Power) method: Measurement of ferric reducing antioxidant power of the fruit extracts was carried out based on the procedure of Benzie and Strain [18], at 593 nm. Ascorbic acid (AA) was used as a standard to prepare the calibration solutions. Results were expressed as µMAA/g of powder.

For microbiological and analytical measurements, all chemicals came from Sigma Aldrich Ltd.

Results and discussion

Agar hole diffusion test results

The largest and most complete inhibitory effect was observed *in staphylococcus* aureus and *escherichia coli* strains: the petri dish had a purification zone of 2 cm around the ***FlavUrin*** sample diffused into the agar gel***, indicating the degree of antibacterial inhibition,*** however, in the case of the Vasgyúró sample, the radius of the purification zone was only 1.5 cm, and the degree of antibacterial inhibition was only partial, because of the small number of bacteria developed within the zone (Table 1).

In *pseudomonas aeruginosa* strain*, the Vasgyúró* sample did not cause a purification zone. ***Similarly, FlavUrin*** was shown to have a purification zone with a ***radius of 2.5 cm, but***

in contrast to the above, the extent of this was only partial, so it inhibited the microbes completely only in the innermost part closest to the samples, but less and less at the edges of the purification zone, so there, in smaller numbers, bacteria had already developed (Table 1).

microbe strain	***FlavUrin*** **Purification zone (cm)**	***Vasgyúró*** **Purification zone (cm)**
Escherichia coli	2	1.5 (partial)
Staphylococcus aureus	2	1.5 (partial)
Pseudomonas aeruginosa	2.5 (partial)	-

Table 1. Agar hole diffusion test results

Figure 2. *E.coli* agar hole diffusion 48 hours (upper row: FlavUrin, lower row Vasgyúró)

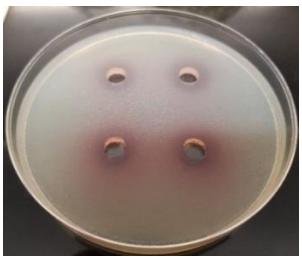

Figure 3. *Staph. aureus* agar hole diffusion 48 hours (upper row: FlavUrin, lower row Vasgyúró)

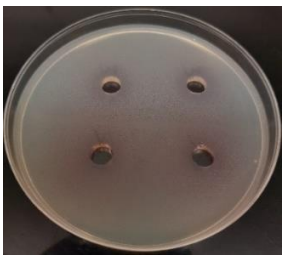

Figure 4. *P. aeruginosa* agar hole diffusion 48 hours (upper row: FlavUrin, lower row Vasgyúró)

Results of the analytical measurements

In determining the total polyphenol content ***(TPC)*** of *FlaViva FlavUrin* and *Vasgyúró* instant drink powders (Fig. 5) despite their different composition, similar results were measured: for *FlavUrin* we obtained values of 84.3 mMol and for *Vasgyúró* we obtained values for 77.9 mMol gallus acid from instant powders per gram.

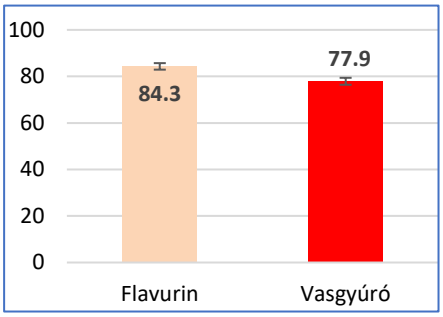

Figure 5*. Total polyphenol content of FlavUrin and Vasgyúró (µMGA/g)*

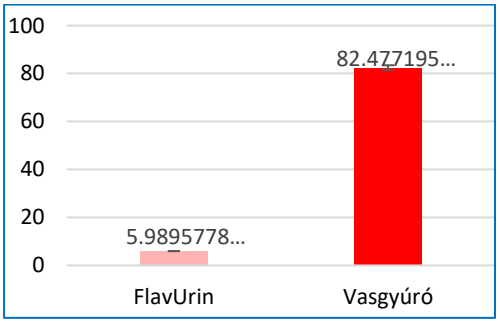

Figure 6*. Antioxidant capacity of FlavUrin and Vasgyúró by FRAP-method (µMAA/g)*

At the same time, the antioxidant capacity test (Fig. 6) measured by FRAP method demonstrated that ***Vasgyúró has 13.77 times more antioxidant capacity than FlavUrin***. Considering that the FRAP measurement method is based on the ability to reduce the iron content in the measured sample, this significant difference is due to the higher iron content of the components ***of the Vasgyúró.*** Since the antibacterial effects of Vasgyúró were significantly lower than FlavUrin, it can be concluded that ***the antibacterial effect is not due to the amount of iron in the ingredients.***

Significant differences were measured in the analysis of the total polyphenol content between the ingredients of two products (Fig.7). The common ingredients in both formulations were: elderberry powder, blueberry powder and blackcurrant powder (indicated in blue color in Fig.7). Since Vasgyúró also had a lower, but detectable antibacterial effect, these 3 components may have contributed to the antibacterial effects.

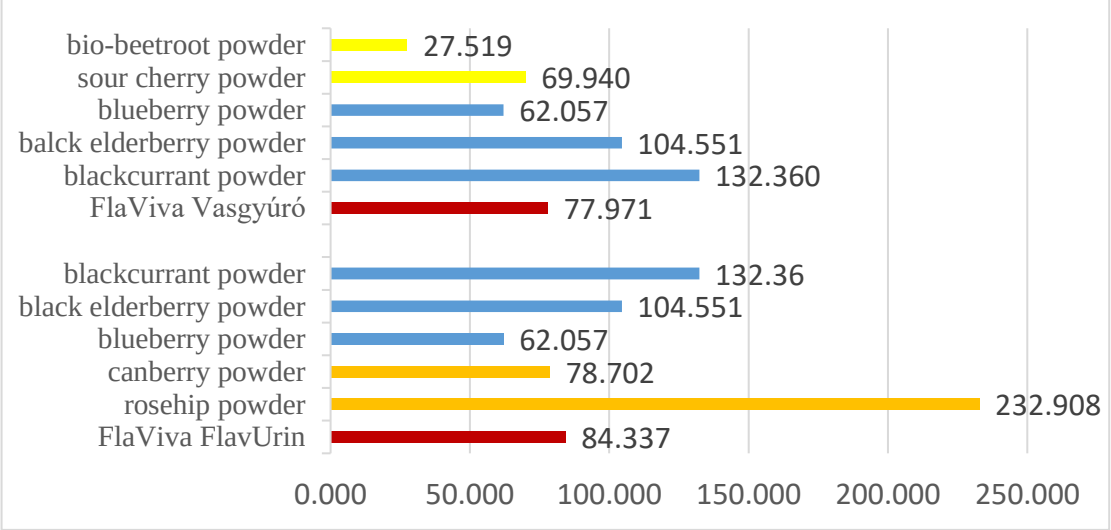

Figure 7. Total polyphenol content of FlaViva FlavUrin and Vasgyúró and their ingredients (uMGS/g)

Sour cherry powder and bio-beetroot powder are only present in the Vasgyúró, while rosehips powder and cranberry powder are exclusively present in the FlavUrin. The latter 2 ingredients have a significantly higher total polyphenol content (rosehips powder of 232.91 uMGS/g, cranberry powder 78.7 uMGS/g) compared to sour cherry powder in Vasgyúró (69.9 uMGS/g) and beetroot (27.5 uMGS/g) ***and therefore these significant differences in TPC may have contributed to a significantly higher antibacterial effect of FlavUrin.***

However, it should be highlighted that since the total polyphenol content (TPC) of the two products do not differ significantly (Fig.5), the antibacterial effect of FlavUrin is not only due to total polyphenol quantitative contents, but presumably also to their different kinds of components (so ***not quantitative, but qualitative differences***) and other bioactive components in its ingredients, the exact detection of which requires further investigations.

Conclusion

FlaViva FlavUrin and *Vasgyúró*, produced by vacuum drying, rich in flavonoids, polyphenols and other valuable components, have been subjected to analytic and microbiological investigations of commercially available products. In our studies, it was found that FlavUrin inhibited the growth of the 3 bacteria tested with significantly higher antibacterial effects *in vitro* (in agar hole diffusion) than Vasgyúró. In the analytic measurements, the antioxidant capacity test measured by FRAP-method gave the Vasgyúró a value more than 13 times higher, which arises from the higher iron content of its components. At the same time, this result also highlights that the antibacterial effect does not correlate with the iron content of food.

Since both products measured almost the same total polyphenol content (TPC, Fig 5.), FlavUrin's significantly higher antibacterial effect ***is not solely due to the quantitative amount of polyphenols***, but also to their ***qualitative different kinds of poliphenols***, and other bioactive components of the ingredients, therefore their accurate exploration requires further research.

Acknowledgements
The Project is supported by the European Union and co-financed by the European Social Fund (grant agreement no. EFOP-3.6.3-VEKOP-16-2017-00005).

References:
[1] V. Ara, Flussiges Obst, (2002) 69 (10), 653-657.
[2] N. Heiberg, F. Maage, in B. Caballero, L. C.Trugo, P.M. Finglas, Encyclopedia of food sciences and nutrition 2003, pp. 1708-17012.
[3] M. Butu, S. Rodino, Natural Beverages (2019) 303-338.
[4] R.Veberic, J. Jakopic, F. Stampar, V. Schmitzer, Food Chemistry, (2009) 114(2), 511-515.
[5] L. Krenn, M. Steitz, C. Schlicht, H. Kurth, F. Gaedcke, Die Pharmazie-An International Journal of Pharmaceutical Sciences, (2007) 62(11), 803-812.
[6] N. Demir, O. Yildiz, M. Alpaslan, A.A. Hayaloglu, Lwt-food science and technology, (2014) 57(1), 126-133.
[7] L. Zoratti, H. Klemettilä, L. Jaakola, Nutritional Composition of Fruit Cultivars, 2016. Elsevier, 83–99.
[8] A. Karlsons, A. Osvalde, V. Nollendorfs, Latvian Journal of Agronomy/Agronomija Vestis, (2009) (12).
[9] S.M. Paunović, P. Mašković, M. Nikolić, R. Miletić, Scientia Horticulturae, (2017) 222. 69-75.
[10] J. Côté, S. Caillet, G. Doyon, D. Dussault, J.F. Sylvain, M. Lacroix, Food Control, (2011) 22 (8), 1413-1418.
[11] C. Krawitz, M.A. Mraheil, M. Stein, C. Imirzalioglu, E. Domann, S. Pleschka, T. Hain, BMC complementary and alternative medicine, (2011) 11(1), 16.
[12] M. Bräunlich, R. Slimestad, H. Wangensteen, C. Brede, K.E. Malterud, H. Barsett, Nutrients (2013) 5, 663-678.
[13] S.O. Yilmaz, , S. Ercisli, Rom Biotech Lett, (2011)16(4), 6407-6411.
[14] M. Nikan, A. Manayi, Nonvitamin and Nonmineral Nutritional Supplements (2019) 153-158.
[15] M. Hevesi, A. Blázovics, E. Kállay, A. Végh, M. Stéger-Máté, G. Ficzek, M. Tóth, Food Technology and Biotechnology, (2012). 50(1), 117.
[16] X. Shen, X. Sun, Q. Xie, H. Liu, Y. Zhao, Y. Pan, V.C. Wu, Food Control, (2014) *35*(1), 159-165.
[17] V.L. Singleton, J.A. Rossi, American Journal of Enology and Viticulture, (1965) (161) 144- 158.
[18] I.F.F. Benzie, J.J. Strain, Analytical Biochemistry, (1996) (239) 70-76.

DIATOMS AND THEIR ROLE IN AQUATIC ECOSYSTEMS

Dorian-Gabriel Neidoni[1], Valeria Nicorescu[1], Sorina Negrea[1], Lidia-Ani Diaconu[1], Dan-Alin Pop[1], Stefania Milarez[1], Iuliana Iordache[1], Anca Tomescu[2]

[1]National Research and Development Institute for Industrial Ecology- ECOIND, Timisoara Subsidiary, 115 Bujorilor Str.,300431, Bucharest, Romania
[2]West University of Timisoara, Faculty of Chemistry, Biology and Geography, Department of Biology, Pestalozzi Str., no. 16A, code 300115, Timisoara, Romania
e-mail: dorian.neidoni@ecoind.ro

Abstract
The present article aimed to determine diversity and abundance of diatoms in the river basin of the Cerna River. In order to achieve the objective, samples were taken from the entire course of the river, from 9 specific points (I, II, III, IV, V, VI, VII, VIII, IX) in spring-summer of 2020. 53 species of diatoms classified in 21 genera were determined.

Introduction
Aquatic ecosystems are open to pollution due to population growth, technological development and increasing industrial activity [1]. Industrial activities are the main source of water pollution due to the generation of effluents with distinct characteristics. Pollutants commonly found in water include pesticides, organic contaminants, heavy metals, nitrogen compounds and sometimes even radionuclides [2]. A versatile and effective biological method in assessing the quality of aquatic environments is the use of diatoms, which are unicellular microscopic algae that live in all aquatic environments with sufficient light and are used worldwide as bioindicators due to their high sensitivity to certain chemical parameters of water, such as would be: mineralization of water, organic matter, nutrients, heavy metals, etc. [3]. Due to their wide distribution, species abundance, ease of storage and sensitivity to environmental changes, diatoms are effective as environmental indicators [4]. They are an important source of oxygen for planet Earth, producing about 25% of the oxygen released into the atmosphere [5]. They are photosynthesizing organisms, but there are some species that can survive in the dark if the environment contains sufficient amounts of organic carbon [6]. They are highly adaptable to different environmental conditions, such as temperature, pH, photoperiod and salinity, and can achieve higher growth rates compared to other groups of algae. Their size varies from 1 to 2000 μm and is known to contribute up to 45% to net primary productivity in the ocean due to their higher growth rate and competitive advantages over other groups of microalgae [7].

Experimental
Study area
For the study of diatoms in the Cerna River, 9 sampling stations were selected. The stations were chosen in such a way as to cover the entire course of the river and to be representative of the different areas through which it passes, and the samples were taken in the spring-summer period of 2020. A point with the highest altitude was chosen, being also the closest to the source of the southern channel - upstream of Gura Bordului. The following stations were selected according to the place of discharge of the tributaries - the stations were chosen before the area of discharge of the tributaries, and upstream of the locality. The only downstream station was represented by station VII - downstream of Hunedoara, because the upstream area of Hunedoara is dammed and arranged to avoid floods during rainfall, especially when the Hasdau stream, a tributary of Cerna, increases in flow.

Figure 1. Graphic representation of sampling points along the Cerna river

Sampling and preservation of samples

The samples were taken in the spring-summer of 2020. At each sampling 3 sub-samples were collected. The final samples for each point are obtained by mixing the 3 sub-samples. For diversity, we looked for three stones with different structure and size (figure 2), taken from places where the water depth remains relatively constant, both in periods of drought and in those with high rainfall.


Figure 2. The substrate from which the diatomic samples were taken

The samples of diatoms were taken by brushing and washing the stones with water. The aim was to brush on a large surface of the stone for the diversity of species. Where the stones were in the muddy substrate, only the accessible surfaces of the stone were brushed. The samples were placed in Falcon tubes and treated with 3 ml of formaldehyde, for preservation and maintenance until processing in the laboratory.

Sample processing

The processing of the diatom samples included several stages. The first of these was the removal of the remaining substrate particles in the samples. This operation was performed by washing and decanting repeatedly. In the second stage, the elimination of organic matter from the samples was followed by successive treatment with HCl (20%) 10 ml and HNO3 (37%) with a volume equal to that of the samples (nitric acid was added in two phases at an interval of 48 hours), respectively burning the samples on a metal plate at a temperature of 80-90 ° C, for 6-8 hours. The degreased lamella were placed on the plate, with a small amount of sample spread very well over its entire surface. The burned lamella were left to dry for 24 hours. In the third stage, the diatom frustules were mounted on microscopic slides using rosin. A thin start of rosin was spread on the heated lamella (at 60-70 ° C). After liquefying the rosin, the lamella was

placed, obtaining the "microscopic preparation". After cooling the "microscopic preparations", the excess rosin was removed. Species identification was performed using the Olympus CX 43 optical microscope (2019), at the 40x objective and at the 100x immersion objective. Online determinants were used to identify the species: https://diatoms.org/species [8] https://www.biodiversitylibrary.org/item/23911#page/1/mode/1up [9].

Results and discussion

Composition of diatom communities in the Cerna river basin

During the Cerna River, 53 species of aquatic diatoms were identified and studied. The taxonomic analysis of the floristic list of diatoms highlights the following aspects, namely: the best represented genera with 6 species are Navicula and Nitzschia, followed by the genera Cymbella and Fragilaria with 5 species. The genus Surirella has 4 species, followed by the genera Cyclotella and Gomphoneis with 3 species, respectively the genera Achnanthes, Amphora, Cocconeis, Diatoma, Diploneis and Gyrosigma with 2 species each. The rest of the genera Aulacoseira, Eunotia, Frustulia, Hannaea, Melosira, Reimeria, Rhoicosphenia, Stauroneis and Synedra have only one species. The graphic representation of the genera is presented in figure 2.

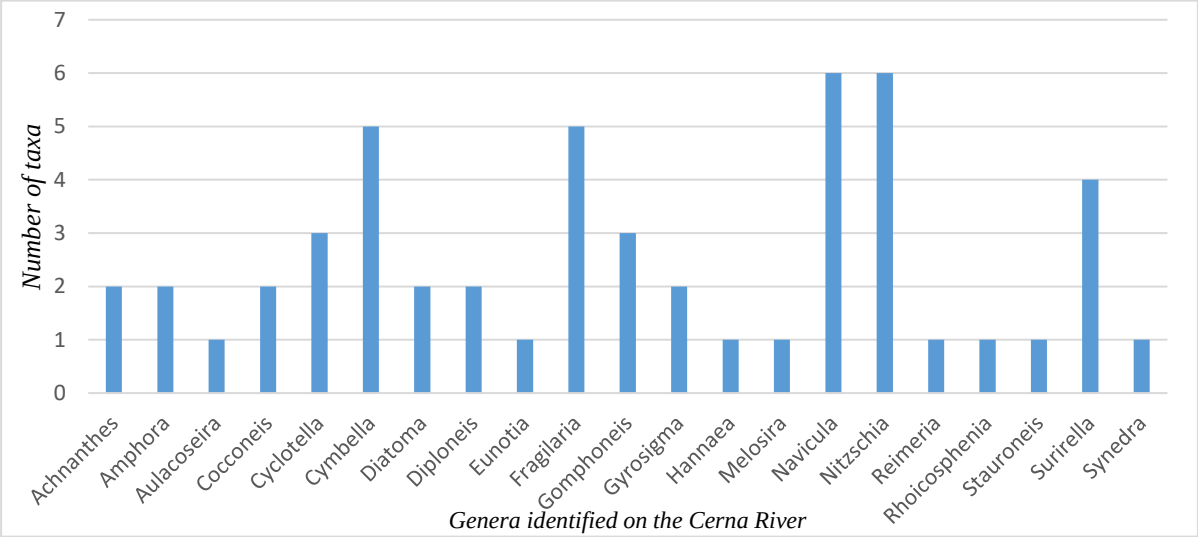

Figure 3. The main types of diatoms with the number of related taxa present in the Cerna river

Based on the absence / presence of the species in the sampling points, the diatoms were divided into four categories: dominant species (found in 7, 8 and 9 sampling points), sub-dominant species (found in 5 or 6 sampling points) , rare species (found in 3 or 4 sampling points) and very rare species, these being found in only 1 or 2 sampling points.

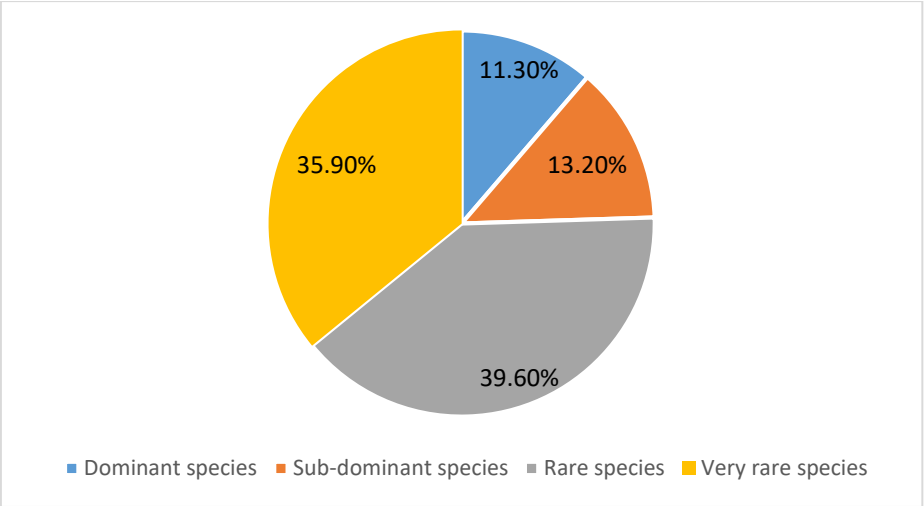

Figure 4. Classification of species in the four categories

The most abundant species present in the Cerna river basin are: *Achnanthes minutissima, Cymbella affinis, Cymbella minuta, Navicula radiosa, Reimeria sinuata* and *Synedra ulna*, and the least common species in the sampling points are: *Aulacoseira crassipunctata, Cymbella hantzschiana, Cymbella tumida, Diatoma moniliformis, Diploneis ovalis, Fragilaria famelica, Fragilaria vaucheriae, Frustulia vulgaris, Gomphoneis olivaceum, Gyrosigma acuminatum, Gyrosigma attenuatum, Melosira varians, Nitzschia brevissima, Nitzschia communis, Nitzschia minuta, Nitzschia palea, Rhoicosphenia abbreviate, Stauroneis obtusa* and *Surirella minuta*.

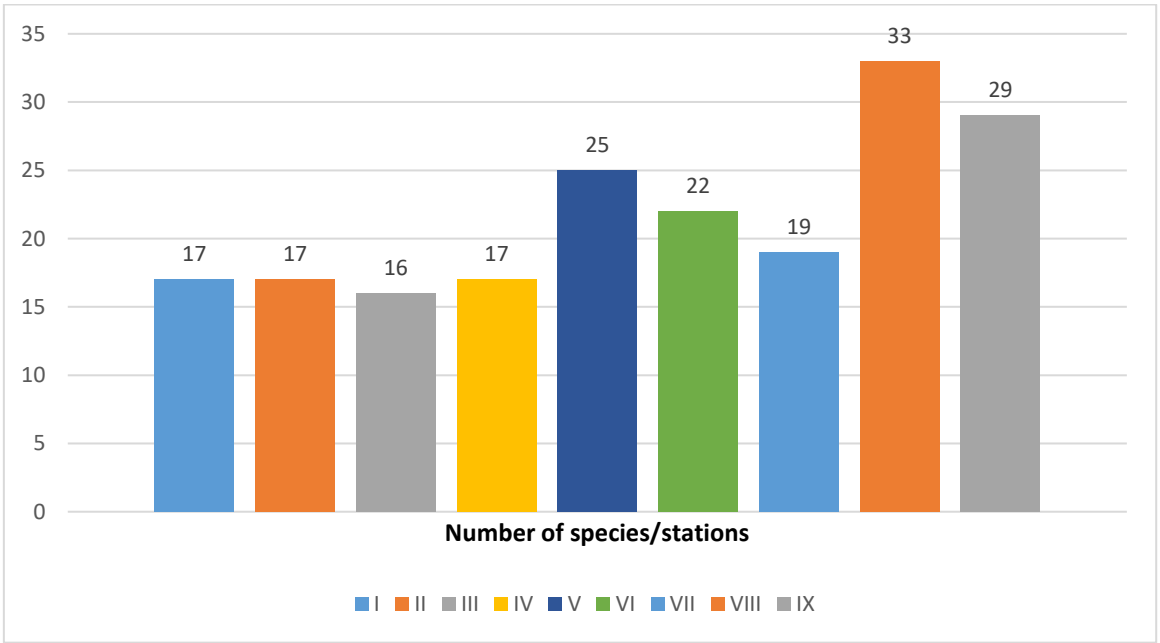

Figure 5. Number of diatomic species for each sampling station

Regarding the number of species from each sampling point, there is a uniformity of species in the first 4 stations, after which in the rest of the areas the abundance of species increases slightly reaching a maximum in the sampling point number VIII. We can attribute these differences to the depth and flow of water which is lower in the lower part of the river than in the upper area where the flow and depth increase with the discharge of tributaries. In addition, points VII, VIII

and IX are close to the cities of Hunedoara and Deva and it seems that the proximity to human communities affects to some extent the diatom communities.
Our relating and interpretations are also supported by Butiuc-Keul et al. 2012 [10], who studied the diatoms present in the Aries river basin and concluded that there are major differences between diatomic communities due in particular to anthropogenic factors and human intervention in the areas.

Conclusion

From the experimental study we can draw some interesting conclusions regarding the diatom communities present in the Cerna river basin. 53 species of diatoms classified in 21 genera were determined. The most abundant genera determined were the genera Navicula, Nitzschia, Fragilaria and Cymbela. The first two genera have 6 species in each component, and the next two genera have 5 species each. The stations where diatom species abound are stations VIII and IX with 33 and 29 taxa, respectively. .

Acknowledgements

The present research was financially supported by the Romanian National "Nucleu" Program, project code PN 19 04 01 02.

References

[1] D.G. Neidoni, V. Nicorescu, L. Andres, M. Ihos, C.B. Lehr, Book Of Abstracts- Section Pollution Control and Monitoring, (2018) 78.
[2] F. Zarpelon, D. Galiotto, C. Aguzzoli, L. N. Carli, C. A. Figueroa, I. J. R. Baumvol, G. Machado, J. da S. Crespo, M. Giovanela, J. Environ. Chem. Eng. 4 (2016) 137.
[3] D. Carayona, A. Eulin-Garrigue, R. Vigouroux, F. Delmas, Ecol. Indic., 113 (2020) 106248.
[4] M. Chen, H. Qi, W. Intasen, A. Kanchanapant, C. Wang, A. Zhang, REG. STUD. MAR. SCI., 34 (2020) 100991.
[5] https://cordis.europa.eu/article/id/31381-research-shows-diatomic-ability-to-process silicon
[6] F.E. Round, R.M. Crawford, D.G. Mann, Cambridge University Press, New York., 747, 1990
[7] T. K. Marella, A. Saxena, A. Tiwari, Bioresour. Technol., 2020.
[8] https://diatoms.org/species
[9] https://www.biodiversitylibrary.org/item/23911#page/1/mode/1up
[10] A. Butiuc-Keul, L. Momeu, C. Craciunas, C. Dobrota, S. Cuna, G. Balas, J. Environ. Manage., 95 (2012) 3.

ANALYTICAL INVESTIGATION TECHNIQUES IN THE SERVICE OF LIPOSOME DEVELOPMENT

Zsófia Németh[1], Dorina Gabriella Dobó[1], Edina Pallagi[1], Ildikó Csóka[1]

[1]Institute of Pharmaceutical Technology and Regulatory Affairs, University of Szeged, H-6720 Szeged, Eötvös u. 6., Hungary
e-mail: zsofia.nemeth@pharm.u-szeged.hu

Abstract
The quality of the liposome formulations differs based on the features of the compositions. Several investigation methods help with their results to make the right decision to achieve an optimised preparation. During these sets of experiments to prepare liposomes via the thin-film hydration technique, dynamic light scattering (DLS) and zeta potential measurements, thermogravimetric analysis (TGA), differential scanning calorimetry (DSC) investigations, and Fourier-transformed infrared (FT-IR) studies were used to select the more optimal compositions. The formulations differed in the phospholipid-cholesterol ratio, the type of the applied PEGylated phospholipid, the quality of the solvent, the hydration media and the cryoprotectant.

Introduction
The investigation of nanocarrier systems, such as the liposomes, is one of the core points of pharmaceutical research and development fields [1]. Liposomes are described as artificially prepared vesicles composed of one or more concentric lipid bilayers that are enclosing one or more aqueous compartments by the European Medicine Agency [2]. Due to their bilayer structure, liposomes provide a sufficient opportunity for targeted drug delivery in case of both hydrophobic and hydrophilic compounds over the body. As the number of information and novelties increases, the options of developments raise as well to get a high-quality product.
The goal of this study was to find the optimal phospholipid-cholesterol ratio, solvent, hydration media and cryoprotectant for liposomal formulations made from different types of PEGylated phospholipids (DPPE-PEG2000, DSPE-PEG3000).

Experimental
The liposomes were prepared via the thin-film hydration method [3] using different combinations of phosphatidylcholine, cholesterol, and PEGylated phospholipids. The particle size and size distribution values were determined via dynamic light scattering (DLS) technique and the zeta potentials of the vesicle surfaces measured with a zetasizer. Additionally, thermogravimetric analyses (TGA) and differential scanning calorimetry (DSC) investigations were done. The interactions between the compounds of the liposomes were studied via Fourier-transform infrared (FT-IR) spectroscopy measurements.

Results and discussion
Liposome samples with size under 200 nm and polydispersity index lower than 0.30 proving homogeneity were prepared while the zeta potential values were slightly negative. The particular TG and DSC curves showed that the weight of the samples does not change above 250°C. Alternations between the formulations prepared with different phospholipid combinations were detected. The measured spectra were identical in case of the samples prepared from compositions with the same ratios but different PEGylated phospholipids. The traces of the FT-IR curves were consistent.

The results showed that the usage of 60:40 phospholipid-cholesterol weight ratios led to more stable formulations than that of the 80:20. The properties of the liposomes made with ethanol 96% were better than samples prepared with the chloroform-methanol mixture. The higher ionic strength of the hydration media maintained more negative zeta potential. Liposomes made from formulations prepared with trehalose as cryoprotectant were smaller than those with inulin; however, the inulin-containing formulations were less polydisperse. Samples containing DPPE-PEG2000 had smaller liposome with more negative surface charge than the ones with DSPE-PEG3000.

Conclusion

It has been shown that the usage of different PEGylated phospholipid compositions influences the quality of the liposomes and that those factors should be considered when the formulation is optimised. The results of the study set examples for analytical monitoring during the decision-making process of a liposomal development procedure.

Acknowledgements

This work was supported by the Gedeon Richter's Talentum Foundation, the Hungary grant 20391 3/2018/FEKUSTRAT, the construction EFOP 3.6.3-VEKOP-16-2017-00009, and the UNKP-19-3-SZTE-61 New National Excellence Program of the Ministry for Innovation and Technology.

References

[1] V.P. Torchilin, Nat. Rev. Drug Discov. 4 (2005) 145–160.
[2] European Medicine Agency. EMA/Committee Hum Med Prod 806058/2009/Rev 02. (2013) 1–13.
[3] H. Zhang, in: G. D'Souza (Eds.), Liposomes, Methods Mol. Biol., Humana Press, New York, 2017, pp. 17-22.

OBTAINING TiO_2 WITH NANOPOROUS STRUCTURE BY CHEMICAL CORROSION AND THERMAL OXIDATION OF TI FOILS

Nicolaescu Mircea[1,2], Carmen Lazau[1], Corina Orha[1], Bandas Cornelia[1], Mina Popescu[1,2], Viorel Aurel Serban[2]

[1]National Institute for Research and Development in Electrochemistry and Condensed Matter, no 144, A. PaunescuPodeanu Street, Timisoara 300569
[2]Politehnica University of Timisoara, P-ta Victoriei, No. 2, Timisoara
mircea.nicolaescu@student.upt.ro

Abstract

Over the past years, titanium dioxide (TiO_2) has known an increased interest in different applications such as gas sensors, photocatalysis, solar cells, etc, due to its vast properties. An improvement of the catalytic properties can be obtained by the increased surface area of the nanoporous titanium oxide. The thermal oxidation process is a very well-studied field, for the growth of nano and micro oxide structures, having several advantages over other methods based on chemical techniques, such as low production cost and large-scale production of metal oxide.

In this study an aqueous mixture of HF was used as a corrosive solution, having the role of increasing the surface area by chemical corrosion in the surface of the titanium foils. Due to the intergranular boundaries, as well as the crystalline defectsof the metal, the corrosive solution attack differently the surface of the 99.99% purity Ti foils, resulting in a nanoporous titanium structure on the surface. After the chemical corrosion process, the titanium plate was washed with distilled water, then dried in vacuum. For the achievement of titanium oxide with nanoporous structure having a ligament form morphology, thermal oxidation process has been applied, in a controlled atmosphere consisting in a mixed gas flow of Ar and O_2, at a temperature of 500 ℃. In this study we followed the variation of titanium oxide nanoporosity depending on the corrosion time (1h and 2h) in the 0.5 M HF and chemical concentration of HF aqueous solution (0.05 and 0.01 M HF) at 24 h holding time keeping both the temperature and the holding time of the thermal oxidation process constant, at 500 ℃ for 4h. Scanning electron microscopy (SEM), X-ray diffraction (XRD), and UV-Vis spectroscopy were used to characterize the TiO_2 nanostructure.

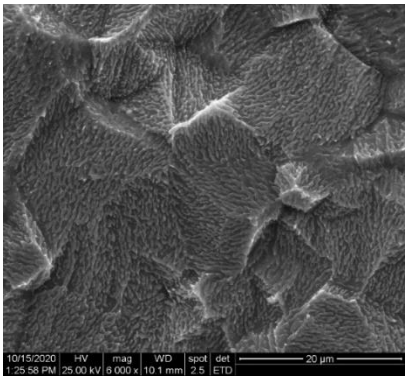

Figure 1. Scanning electron microscopy (SEM) image of TiO_2 grown by thermal oxidation (500℃/4h) on corroded Ti foils (0.5 M HF/2h)

Acknowledgements

This work was supported by a grant of the Romanian Ministry of Research and Innovation CCCDI-UEFISCDI, project number 40PCCDI/2017 and 40N/2018.

DETERMINATION OF DDT AND ITS METABOLITES IN SOIL, TREE BARK AND EARTHWORM SAMPLES NEAR THE BUDAPEST CHEMICAL WORKS

Marianna Oláh[1], Mária Mörtl[1], Béla Darvas[2] and András Székács[1]

[1]Agro-Environmental Research Institute, National Agricultural Research and Innovation Centre, Herman O. u. 15, H-1022 Budapest, Hungary
[2]Hungarian Society of Ecotoxicology, Herman O. u. 15, H-1022 Budapest
e-mail: szekacs.andras@akk.naik.hu

Abstract

An abandoned industrial site of the former Budapest Chemical Works (BVM) company has been found to contain 2000-3000 tonnes of leaking industrial waste and dangerous chemicals in corroded barrels on bare ground. The waste lot includes general industrial reagents and intermediates, some 100-200 tonnes of sulphuric acid, several hundred tonnes of 1.2 dichlorobenzene and isopropanol, and numerous other substances falling into toxicity categories from toxic to very toxic or carcinogenic, such as dinitrobenzoic acid, as well as chemical wastes from the pesticide production of the company. BVM used to manufacture numerous pesticide active ingredients, including chlorinated hydrocarbons. Thus, it produced the insecticide DDT in large quantities until the ban of the compound in 1968 and derogated approval for sales until 1974.

The premises of the company has been reported previously to be contaminated, therefore, in the scope of our pesticide residue monitoring surveys between 2015 and 2019, we carried out sampling in its immediate vicinity. In our study, soil (8 samples), surface water (2 samples), tree bark (*Robinia pseudoacacia*, *Sambucus nigra*, *Populus nigra*) and common reed (*Phragmites australis*, (6 samples), as well as earthworms (*Lumbricus terrestris*; 1 sample) sampled next to BVM were analyzed for DDT and metabolite (~DDT) levels. Exceedingly high ~DDT levels above the accepted limit (0.1 mg/kg) were detected in soil samples: nearly 1.5 mg/kg in one sample and 0.11-0.484 mg/kg in other 5 cases. Among the biological samples (tree bark, common reed and earthworm) 0.184 and 0.190 mg/kg concentrations of ~DDT were determined in a black poplar and in an earthworm sample. These findings indicate that the well-known persistency problem related to chlorinated hydrocarbon insecticides, particularly to DDT remains actual to our days.

Introduction

The chemical work premises of BVM (Budapesti Vegyiművek) were constructed in the 19th century, in the outskirts of Budapest at that time. Upon a rugged business history, in 1948 the legal predecessor of BVM [1] began manufacturing the two leading chlorinated hydrocarbon insecticides of the time, 1,1'-(2,2,2-trichloroethane-1,1-diyl)bis(4-chlorobenzene) or by its outdated chemical name dichloro-diphenyl-trichloroethane (from which it earned its acronym DDT) and hexachlorocyclohexane (HCH). A comprehensive study published in 2003 on persistent organic pollutant (POP) compounds manufactured and sold between 1950-2000 by the Hungarian pesticide industry, detailed information is available on the production of BVM as well [2]. Being unaware of the hormonal and other detrimental effects of DDT and particularly its metabolites (~DDT) on warm-blooded organisms, discovered only a decade later, the compound was listed as non-hazardous [3]. This, along with the outstanding economy of the chemical technology resulted in a boost in the production and sales. In turn, driven by the precautionary warning by Hungarian toxicologists, Hungary was the first country banning DDT in 1968. Turnover statistics [2] clearly indicate the above: sales of DDT showed an

increase from 1950 to 1970 with a total of 39 476 tons of the active ingredient sold in two decades (Figure 1).

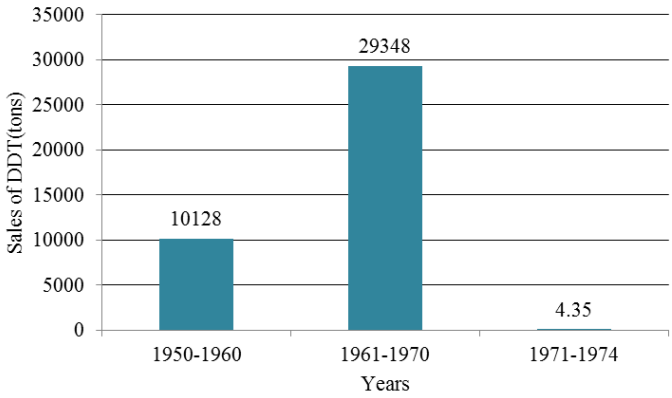

Figure 1. Sales of DDT by Hungary between 1950 and 1974 [2].

The production process, however, doesn't end at the finished product. Waste management is also a fundamental issue in any technology, particularly in the case of substances of high persistence. In addition, in spite of the 6-year derogation period after the ban of DDT, substantial lots of DDT remained on BVM premises, stored mostly in steel drums with expected lifespans of 13-30 years. Long-term storage of obsolete pesticides is a worldwide problem [4] that in sustained time often leads to occupational and environmental risks. Leaching of chemicals from corroded, ballooned or otherwise severely damaged steel drums has occurred also at BVM. Soil contamination by chlorinated hydrocarbons has been detected in the vicinity of the BVM premises quite soon after the bankruptcy of the corporation in 2007. Certain levels of non-systematic contamination is legally tolerated, but residue levels above the maximum residue limit (MRL), defined as the highest overall concentration of a compound and its metabolites officially permitted, call for subsequent legal measures.

In 2011, ELGOSCAR-2000 Kft. started a remediation project by groundwater purification, in a seemingly useless exercise as the cracked barrels causing the pollution have not been removed from the spot. Remediation greatly reduced contaminant levels in groundwater, but recontamination has risen to baseline levels within 2-3 years. 2011 measurements prior to remediation indicated concentrations of benzene and chlorobenzene in groundwater at peak levels of 100 mg/l at some points, which in case of benzene is 100 000 times of the permissible limit [5-7]. The scope of the ELGOSCAR project did not include DDT. A study by WESSLING Hungary Ltd. in 2015, which already focused on chlorinated hydrocarbon insecticides among industrial chemical pollutants, indicated that groundwater pollution had already escaped from the premises of the former BVM [8]. High ~DDT levels (0.16 and 0.22 mg/kg) were detected in two soil samples [9], exceeding the 0.1 mg/kg MRL. Another survey by Greenpeace monitoring ~DDT in house dust and in the eggs of household-raised chicken (*Gallus gallus domesticus*) in the region showed that ~DDT contaminants appeared in nearby homes. Chemical analysis revealed an extremely high level of ~DDT concentration of 1.69 mg/kg in egg [10].

Experimental

The aim of our study was to determine residue levels of DDT (~DDT) in samples collected nearby the former BVM. The sampling regime study included soil (8 samples) and surface water from Illatos ditch (2 samples), as well as biological samples, tree bark (*Robinia pseudoacacia*, *Sambucus nigra*, *Populus nigra*) and common reed (*Phragmites australis*, 6 samples), as well as earthworms (*Lumbricus terrestris*; 1 sample) near or within a 2 km vicinity of the BVM premises.

Preparation of solid samples was carried out by solvent extraction [11], while surface water samples were processed by solid phase extraction [12]. The concentrations of DDT and metabolites in the sample extracts were determined by instrumental analysis, gas chromatography coupled with electron capture detection (GC-ECD).

Results and discussion

Levels of ~DDT were measured in all these samples, as shown along with sample information in Table 1.

Table 1. Sampling points with code, GPS coordinate, type, and place of sampling and the results of the ~DDT measurement

Sample code	GPS coordinate (latitude, longitude)		Type of sample	Place of sampling	DDT content (mg/kg)
BVM1	47.45322	19.10800	soil (10 cm depth)	BVM	1.43
BVM2	47.45321	19.10760			0.345
BVM3	47.45311	19.10727			0.416
BVM4	47.45320	19.10667			0.484
BVM5	47.45323	19.10732	earthworm		0.190
BVM6	47.45455	19.11147	tree bark (*Robinia pseudoacacia*)		0.0109
BVM7	47.45474	19.11167	tree bark (*Populus nigra*)		< LOD*
BVM8	47.45469	19.11137	soil (10 cm depth)		0.0745
BVM9	47.45469	19.11137	soil (60 cm depth)		0.110
BVM10	47.45469	19.11137	soil (30-40 cm depth)		0.0963
BVM11	47.45451	19.11059	tree bark (*Sambucus nigra*)		0.0591
BVM12	47.45365	19.11129	tree bark (*Populus nigra*)		0.184
BVM13	47.45365	19.11129	tree bark, wood chips (*Populus nigra*)		0.0169
BVM14	47.45560	19.10558	surface water (Illatos ditch I.)		< LOD*
BVM15	47.45560	19.10558	surface water (Illatos ditch II.)		< LOD*
BVM16	47.45560	19.10558	common reed (Illatos ditch)		0.0488
BVM17	47.44576	19.12961	soil (10 cm depth)	164. Kisfaludy St.	0.144
BVM18	47.44571	19.12961	tree bark (*Salix* sp.)		0.0440
BVM19	47.44571	19.12955	tree bark (*Tilia* sp.)		0.0206

* below the limit of detection (LOD) of the analytical method, 0.01 mg/l.

An exceedingly high (nearly 1.50 mg/kg) ~DDT level was measured in a soil sample collected near the fence of the BVM premises along the rail cargo tracks, and high concentrations were determined in 5 cases (0.110-0.484 mg/kg) (Figure 2). The ~DDT concentration in 2 soil samples remained below the MRL for ~DDT is soil, 0.1 mg/kg. This indicates MRL violation if 75% of the soil samples, on one occasion by 15 times.

The concentration of ~DDT remained below the LOD of the GC-ECD instrumental analytical method applied, 0.01 mg/l, in both surface water samples collected, [13] however, substantial amounts of metolachlor was detected. Metolachlor (it was officially used until 2003 in

Hungary) is a chloroacetanilide-type herbicide active ingredient with a high potential for runoff into surface water [14], also manufactured by BVM. Exceedingly high levels (0.750-1.279 µg/l) of metolachlor were detected in these samples, quite atypical in the winter period.

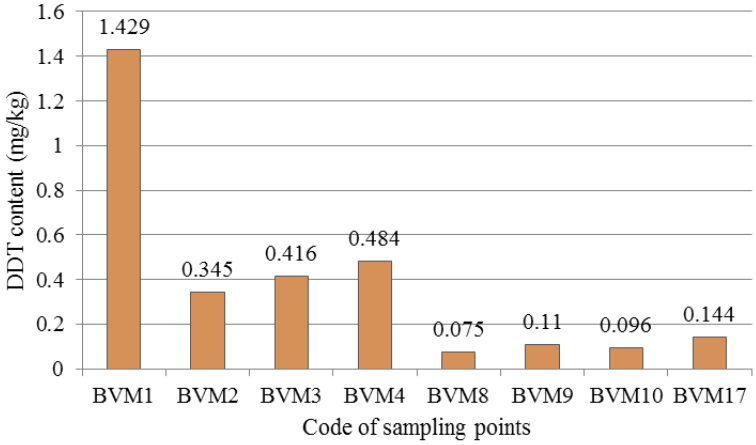

Figure 2. ~DDT content in soil samples.

Among the tree bark and common reed samples, high concentration (0.1837 mg/kg) of ~DDT was measured in a black poplar sample (Figure 3). A similarly high level of ~DDT (0.19 mg/kg) was determined in the earthworm sample studied (Figure 3), indicating substantial soil-borne exposure.

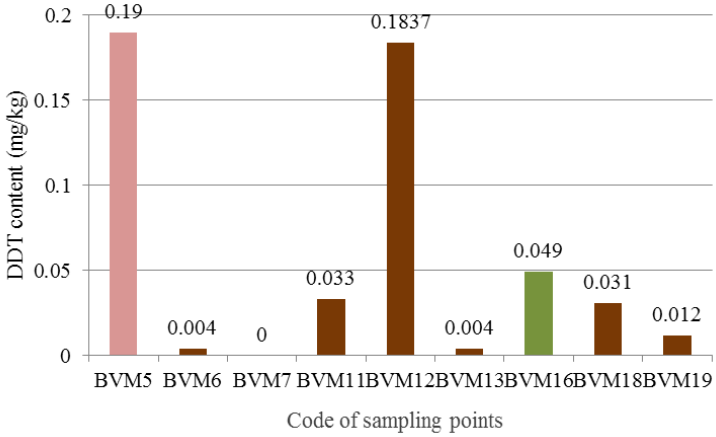

Figure 3. ~DDT content in tree bark (brown), common reed (green) and earthworms (pink) samples.

Conclusion

Along with several former studies, our survey also demonstrated that ~DDT residues remain to be an actual problem nearby Illatos road in Budapest close to residential areas. Almost 2,500 tons of extremely hazardous materials were stored in appalling conditions. Heavily eroded barrels were lying on bare ground, with often unidentifiable chemicals leaching into the soil and groundwater. Upon pressure by Greenpeace, finally all of the 2,493 tons of toxic waste has been removed from the area, and reassessment, including a detailed analysis of the soil and groundwater, are planned with remediation plans to follow [15], although the removal of the hazardous waste barrels ceased the ongoing pollution of the area, natural dissipation for these persistent pollutants is very slow, and the alleged remediation has not started to this date.

Acknowledgements

This research was supported by project OTKA K109865.

References

[1] Ferencváros Önkormányzata (2009) Integrált Városfejlesztési Stratégia. *http://www.ferencvaros.hu/doks/FOE_FoepiteszIroda/IVS_1_5_fej_20091216.pdf*

[2] Á. Pethő, Z. Ocskó (2003) POP hatóanyagot tartalmazó növényvédőszerek hazai felhasználása 1950-2000, In: A környezetben tartósan megmaradó szerves szennyező anyagok (POP) országos leltára a Stockholmi Egyezményben előírt intézkedési terv készítéséhez- GEF/UNIDO projekt száma: GF/HUN/01/005 (Lotz T, Tátrai I.szerk.) Környezetgazdálkodási Intézet, Budapest.

[3] B. Darvas, (2000) Egy Nobel-díjas: a DDT. pp. 131-135. In *Virágot Oikosnak*. l'Harmattan http://mek.oszk.hu/09800/09886/

[4] FAO (1996) Disposal of bulk quantities of obsolete pesticides in developing countries. *http://www.fao.org/fileadmin/user_upload/obsolete_pesticides/docs/w1604e.pdf*

[5] ELGOSCAR-2000 Környezettechnológiai és Vízgazdálkodási Kft. (2011) Vizsgálati jegyzőkönyv, Talaj- és talajvíz-tisztítás, kármentesítés a Bp. Illatos úti telephelyen. *http://kimittud.atlatszo.hu/request/4413/response/7394/attach/4/30%20130%202015%203mell%20klet.pdf*, *http://www.fava.hu/siofok2010/eloadasok/2nap/1215_illesnesa_magyarb.pdf*

[6] G. Simon(2015). V. Ökotoxikológiai Konferencia (Darvas B. szerk.) 5, 34-35. http://www.ecotox.hu/ecotox2/download/konf/2015/motkonf2015.pdf

[7] Nemzeti Élelmiszerlánc-biztonsági Hivatal (Nébih) (2015) Összefoglaló értekezés a Budapest Illatos árok és Ráckevei Dunaág növényvédőszeres szennyezettségével kapcsolatos panaszbejelentéséről. Ikt: 04,2/6297-1/2015.

[8] Wessling Hungary Kft. (2015) Szakértői vélemény, Budapest IX. kerület Talaj-, talajvíz, felszíni víz vizsgálat.

[9] KvVM-EÜM-FVM (2009) A földtani közeg és a felszín alatti víz szennyezéssel szembeni védelméhez szükséges határértékekről és a szennyezések méréséről, 6/2009 (IV.14.) KvVM-EÜM-FVM együttes rendelet.

[10] Greenpeace (2020) Mérgezett örökségünk. *https://hu.greenpeace.org/mergezett-oroksegunk/bvm*

[11] S. Sporring, S. Bøwadt, B. Svensmark,, E. Björklund (2005) *J. Chromatogr. A*, 1090, 1-9.

[12] E. Maloschik, A. Ernst , G. Hegedűs, B. Darvas, A. Székács, (2007) *Microchem. J.* 85, 88-97.

[13] Vidékfejlesztési Minisztérium (2010) a felszíni víz vízszennyezettségi határértékeiről és azok alkalmazásának szabályairól, 10/2010 (VIII.18.) VM rendelet

[14] Y.-J. Lin,, M. Karuppiah,, A. Shaw,, G. Gupta, (1999) *Ecotox. Environ. Saf.* 43 (1), 35-37.

[15] Pest Megyei Kormányhivatal (2016) Folytatódik az Illatos út rendbetétele. http://www.kormanyhivatal.hu/hu/pest/hirek/folytatodik-az-illatos-ut-rendbetetele

EVAPORATION FROM CARBON NANOTUBE BUCKYPAPERS WITH DIFFERENT FUNCTIONALIZATION: ANALYTICAL POSSIBILITIES OF THE MASS MEASUREMENTS

I. Y. Tóth[1], J. Papp[1] and Á. Kukovecz[1]

[1]*Department of Applied and Environmental Chemistry, University of Szeged, Interdisciplinary Excellence Centre, H-6720, Szeged, Rerrich Béla tér 1, Hungary*
e-mail: kolozska@citromail.hu (J.P.); ildiko.toth@chem.u-szeged.hu (I.Y.T.)

Abstract
The evaporation of liquids from porous films is a very complex phenomenon, which can be followed by simultaneous weight monitoring, electric resistance measurement, infrared imaging and contact angel measurement. The appropriate evaluation of these measurement results can carry both quantitative and qualitative analytical information. The aim of our recent work is to demonstrate this opportunity through the example of the evaporation of simple solvents from porous buckypapers prepared from carbon nanotubes with different functionalization. In this work the focus will be on the analytical possibilities of the mass measurements.

Introduction
Recent developments in nanotechnology have highlighted the importance of the classical topics of wetting, droplet spreading and evaporation due to their pronounced effect in technological applications (*e.g.*, air/fuel premixing, micro-fluidics, oil recovery, etc.) [1,2]. Multiple phenomena take place simultaneously when a liquid droplet contacts a porous surface: wetting, spreading, capillary filling, gravity induced convective flow, adsorption, evaporation from the surface, evaporation from the pores, etc. The evaporation of a sessile droplet can be studied by several experimental methods: transmission electron microscopy, environmental scanning electron microscopy, contact angle measurement, high speed camera recordings, thermal imaging, just to name a few. The evaporation of sessile droplets can be followed by an equipment assembled at the Department of Applied and Environmental Chemistry, University of Szeged: this equipment can guide simultaneous weight monitoring, electric resistance measurement and infrared imaging at a controlled temperature (typically at 50 °C). There are several experimental results characteristic for the evaporation process, the most important ones being the total evaporation time, time of evaporation only from the surface, full width at half maximum of the time-dependent mass and resistance curves, evaporation rate, initial area of the droplet, and the wetted area at the moment of total evaporation from the surface, etc. [3-6]. The main goal of this work was to demonstrate the analytical possibilities of the mass measurements through the example of sessile droplet evaporation (water and ethanol) from porous buckypapers (BP) prepared from pristine non-functionalized carbon nanotubes (*nf*-CNT), from –COOH functionalized CNT (*f*-CNT) and from their mixtures.

Experimental
Materials: The multiwall carbon nanotubes were synthesized by 2 h of catalytic chemical vapor deposition from a C_2H_4:N_2 (30:300 cm^3/min) gas mixture at 650 °C over Fe,Co/Al_2O_3 catalyst (metal loading: 2.5-2.5 m/m%). The synthesized materials were purified by repeating 4 h of refluxing in 10 mol/dm^3 aqueous NaOH, then 4 h in cc. HCl solution four times. Some pristine non-functionalized carbon nanotubes (*nf*-CNT) were subjected to oxidative chemical functionalization (8 h reflux of 4 g CNT in 500 cm^3 cc. HNO_3 solution) to facilitate surface carboxyl group formation and improve their hydrophilicity to get so called functionalized

carbon nanotubes (*f*-CNT). The typical length of CNTs was over 10 μm and their outer diameter fell in the 15-25 nm range as determined from TEM image analysis. CNTs were converted into buckypaper (BP) by filtering 70 cm^3 of their 0.1 g/dm^3 suspensions through a 0.45 μm nominal pore diameter Whatmann nylon membrane filter. The *nf*-CNTs and *f*-CNTs were suspended by 40 min ultrasonication in N,N-dimethylformamide and water, respectively [3,4]. The functionality (ration of the *f*-CNT) of the BP samples were 0.00; 0.25; 0.50; 0.75 and 1.00, prepared by the filtration of the *nf*-CNT's and *f*-CNT's physical mixtures.

Methods:

Electrophoretic mobilities of the CNTs were measured in a Nano ZS (Malvern) apparatus with a 4 mW He−Ne laser source (λ = 633 nm) using disposable zeta cells (DTS 1070) at 25±0.1 °C. The zeta-standard of Malvern (−55±5 mV) was used for calibration and the samples were diluted to give an optimal intensity. To get comparable data, the dispersions were homogenized in an ultrasonic bath for 10 s, after which 2 min relaxation was allowed. The influence of the functionality and the effect of pH variation were studied at 10 mM NaCl. The Smoluchowski equation was applied to convert electrophoretic mobilities to electrokinetic potential values. The accuracy of the measurements was ±5 mV.

Liquid droplet evaporation (distilled water and ethanol) was studied from the buckypaper films. The droplets (5 μL, 25 °C) were instilled with an Eppendorf Xplorer electronic pipette on the surface of the porous films. The temperature, the electric resistance and weight variations could be simultaneously monitored by the equipment assembled at the Department of Applied and Environmental Chemistry, University of Szeged.

Buckypaper was placed onto a purpose-built sample holder and kept in place by a top piece that had a 1.4 cm diameter circular opening in it for placing the liquid droplet. The setup included a type K thermocouple in contact with the non-wetted part of the BP. The distance between the porous film and the heater was 1 cm. Data from the thermocouple was fed back to the temperature controller that maintained a base BP temperature of 25 ± 0.5 °C by continuously adjusting the heater power using fuzzy logic control.

The sample holder was placed on a Sartorius Cubis microbalance with 0.01 mg readability and the weigh variation during droplet evaporation was recorded.

For thermal imaging a FLIR A655sc infrared (IR) camera was used. This unit has a thermal sensitivity of 30 mK, an accuracy of ±2 °C for temperatures up to 650 °C at 640x480 resolution. Its uncooled microbolometer detector has a spectral range of 7.5-14.0 μm. The IR camera is equipped with a 2.9x (50 μm) IR close-up lens, with 32x24 mm field of view and 50 μm spatial resolution. The recorded images are transferred to a PC with FLIR ResearchIR Max software. Sessile droplet evaporation movies were acquired at maximum resolution with 50 Hz frame rate. Each CNT film's emissivity (ε_{film}) was determined by calibration at the initial film temperature (25 °C) with a black electrical tape (ε = 0.95). During liquid surface evaporation the temperature was determined by taking into account the emissivity of the liquid (ε_L = 0.95); after surface evaporation, the emissivity of the wetted film was calculated as the average between the emissivities of the studied liquid and the porous film.

The sample holder plastic plate with the 0.7 cm radius gap in the center was equipped with two copper electrical connections at the opposite edges of the gap on the bottom of the sheet. The BP was fixed to the bottom of the plastic section with magnetic clips. The copper electrodes were contacted to the source meter by 0.3 mm diameter copper wires. The rigidity of these wires did not affect the balance because of the large inertia of the whole assembly mounted on the balance plate. This was confirmed by independent experiments before the evaporation profile (electrical resistance variation as a function of time) measurements. The computer recorded the electrical resistance of the buckypaper as measured by a Keithley 2612A Source Meter.

Before the measurements, the BP film was mounted in the assembly and heating at initial temperature was applied until the electrical resistance and the sample weight both stabilized. Then all three recordings (resistivity, IR imaging and sample weight) were started a few seconds before dropping. The evaporation was studied by dropping a single droplet of a selected solvent to the center of the BP film and simultaneously recording the IR video, the mass and electrical resistance until they returned to their original values.

The schematics of the equipment is presented in Fig. 1. The ambient air temperature and the relative humidity of the ambient atmosphere were kept constant (at 25 °C and 55 RH%, respectively) [3-6]. In our experiments the electric resistance and weight variations were simultaneously monitored, but in this work we will focus only on the results of the mass measurements.

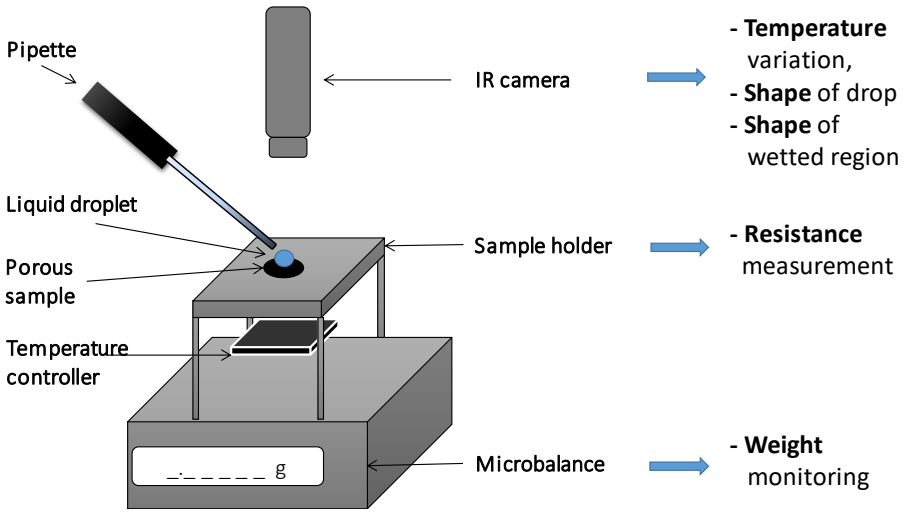

Figure 1. Evaporation monitoring equipment schematic.

Results and discussion

The zeta potentials of different CNTs are plotted as a function of pH in Fig. 2. The isoelectric point (IEP, at which the net charge of CNT is zero) shifts gradually to more acidic pH with the increasing functionality. The values of zeta potential shift to more negative region with the increasing pH and/or with the increasing amount of –COOH.

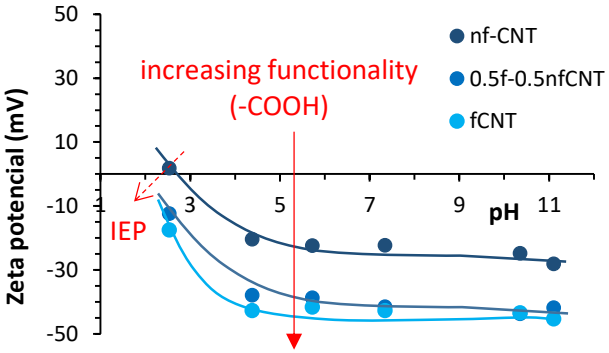

Figure 2. Functionality and pH dependent zeta potential of CNT samples (10 mM NaCl, 25°C).

In general at the moment we drop the liquid on the buckypaper film (t_0), the liquid starts to diffuse immediately into the pores of the BP, but a part of it remains spread on the surface of the film. The evaporation of this liquid from the surface takes place together with the diffusion. Once all liquid evaporates from the surface, namely the primary surface evaporation is complete (t_s), liquid is left only in the pores. The solvent gradually evaporates from the pores as well. The

complete evaporation of the solvent (t_t) was confirmed by the fact that the mass of the buckypaper returned to the baseline.
One typical mass variation is illustrated in Fig. 3. where t_0 marks the time when the drop was instilled. The mass of the BP increased as soon as the solvent was dropped to the film and this is followed by a quasi-linear weight decrease. Once the primary surface evaporation is complete (t_s), the mass of the buckypaper decreases as linear (within experimental error) functions of time due to the continuous evaporation of the solvent. The total evaporation time (t_t) was at the moment when the mass of the BP returned to the baseline. At the linear weight decreasing ranges, the rate of evaporation (-dm/dt) is constant. The change of -dm/dt value suggests the change of the dominant evaporation process, *e.g.*, evaporation of the droplet sitting on the surface of the BP, evaporation of the condensed water from the porous system or the evaporation of the adsorbed water from the microscopical surface of the porous system (see the linear ranges in Fig. 3.). From this type of measurement, the typical experimentally determined data are the shape of the curve: m_{max}, area, FWHM; the t_s and t_t, the evaporation rate -dm/dt and its change. These data are characteristic for the measured system and can be used to identify them [3-6].

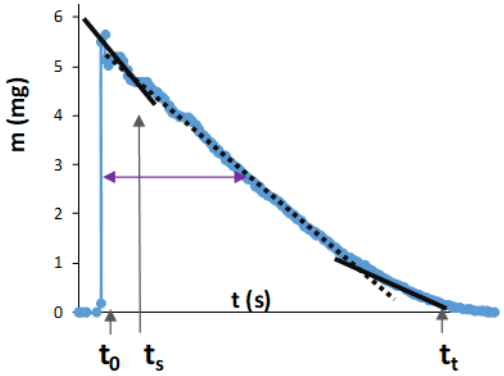

Figure 3. Illustration: weight variation of a buckypaper as a functions of time during the evaporation process.

The evaporation of water and ethanol from the surface of CNT buckypapers with different functionality can be seen in Fig. 4. It is clear that ethanol evaporates faster than water in case of all solid materials. Based on the detailed analysis the t_t, the area, the FWHM, the evaporation rate for the condensed water in the porous system and for the adsorbed water can be determined.

Conclusion

The weight monitoring of the evaporation of liquids from porous films can provide information about the mechanism of wetting and vaporization which is a significant area of the basic researches. Furthermore, it can be proved by using appropriate statistical methods (*e.g.*, matrix of Pearson correlation coefficients, hierarchical cluster analysis, functional analysis, etc.), that the experimentally determined characteristic values are specific for the physical properties of the solvents, and they are also dependent on the quality of the solid materials, therefore, they can be used for qualitative chemical and quantitative analysis via the estimation of physical properties. The results allow us to presume the possibility of this experimental setup and theoretical approach for a potential future application in the field of analytics.

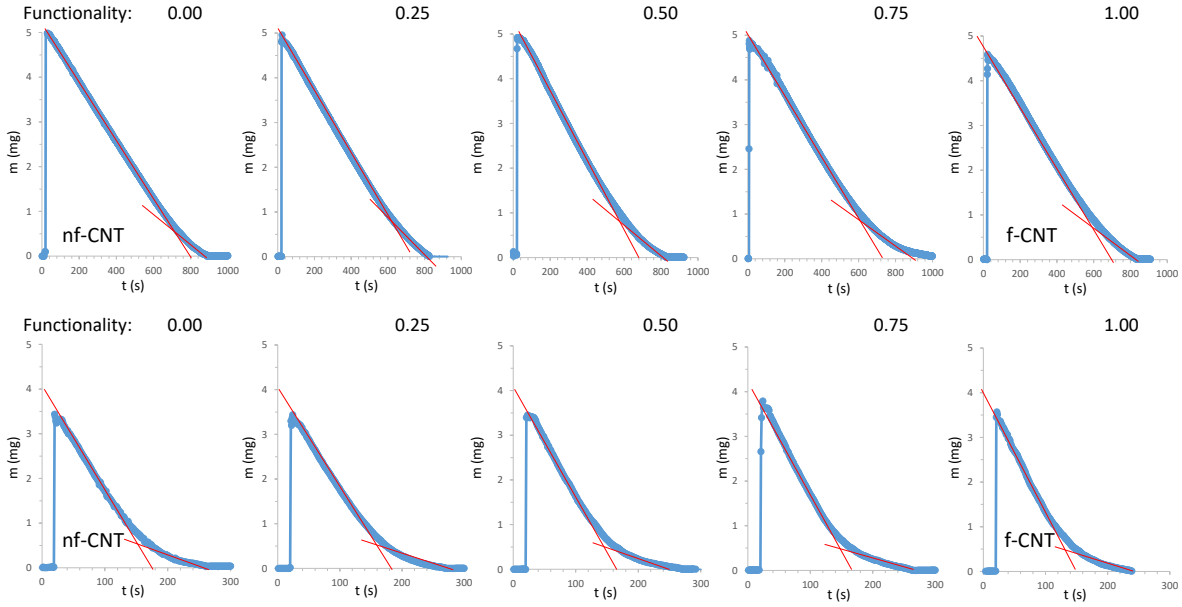

Figure 4. Evaporation of water (1st row) and ethanol (2nd row) from CNT buckypapers with different functionality (5 µL, 25°C).

Acknowledgements

We thank Krisztina Nagy for the technical contribution during the measurements. Financial support from the Hungarian National Research, Development and Innovation Office through the GINOP-2.3.2-15-2016-00013 "Intelligent materials based on functional surfaces−from syntheses to applications" project is acknowledged. I.Y. Toth also acknowledge the support by the János Bolyai Research Scholarship of the Hungarian Academy of Sciences and the Ministry of Human Capacities, Hungary through the grant ÚNKP-19-4 New National Excellence Program.

References

[1] D. Bonn, J. Eggers, J. Indekeu, J. Meunier, E. Rolley, Mod. Phys. 81(2) (2009) 739−804.
[2] H.Y. Erbil, Adv. Colloid Interface Sci. 170(1-2) (2012) 67−86.
[3] G. Schuszter, E.S. Bogya, D. Horváth, Á. Tóth, H. Haspel, Á. Kukovecz, Mic. Mes. Mat. 209 (2015) 105–112.
[4] E.S. Bogya, B. Szilagyi, Á. Kukovecz, Carbon 100 (2016) 27–35.
[5] Á. Kukovecz, Egydimenziós nanoszerkezetek és hálózataik létrehozása, módosítása és néhány felhasználási lehetősége, MTA értekezés, Szeged, 2018
[6] I.Y. Tóth, L. Janovák, E.S. Bogya, Á. Deák, I. Dékány, A. Rawal, Á. Kukovecz, J. Mol. Liquids 305 (2020) 112826

EFFECTS OF STEPWISE TERMINAL NH_2-METHYLATION OF ESTRONE-SALICYLALDEHYDE–THIOSEMICARBAZONE AND COPPER COORDINATION, SOLUTION SPECIATION, ANTICANCER ACTIVITY AND REDOX ACTIVITY.

Tatsiana V. Petrasheuskaya,[1,2] Debora Wernitznig,[3] Márton A. Kiss,[4] Nóra V. May,[5] Dominik Wenisch,[3] Bernhard K. Keppler,[3] Éva Frank,[4] Éva A. Enyedy[1,2]

[1]Department of Inorganic and Analytical Chemistry, Interdisciplinary Excellence Centre, University of Szeged, Dóm tér 7, H-6720 Szeged, Hungary. Email: enyedy@chem.u-szeged.hu
[2]MTA-SZTE Lendület Functional Metal Complexes Research Group, University of Szeged, Dóm tér 7, H-6720 Szeged, Hungary
[3]Institute of Inorganic Chemistry and Research Cluster 'Translational Cancer Therapy Research', University of Vienna, Währinger Straße 42, Vienna, Austria
[4]Department of Organic Chemistry, University of Szeged, Dóm tér 8, H-6720 Szeged, Hungary
[5] Chemical Crystallography Research Laboratory, Research Centre for Natural Sciences, Magyar tudósok körútja 2, H-1117 Budapest, Hungary
petrashevtanya@chem.u-szeged.hu

Thiosemicarbazones (TSCs) as excellent metal chelators are a class of organic compounds with structural diversity and broad spectrum of pharmacological activities, such as antiproliferative, antiviral, antibacterial, antimalarial and antifungal effect [1]. Also, their metal complex can be more active than the free ligand, and some side effects may decrease upon complexation. In addition, the complex can exhibit bioactivities, which are not shown by the free ligand. Previously, a tridentate estrone-salicylaldehyde TSC hybrid molecule (estrone-TSC) was developed in addition to an analogous bicyclic derivative (thn-TSC), which were cytotoxic against the hormone-responsive MCF-7 breast cancer cell lines (IC_{50}: thn-TSC: 3.7 μM, estrone-TSC: 6.4 μM). Their Cu(II) complexes showed more significant cytotoxicity than the ligands as 1-2 orders of magnitude lower IC_{50} values were obtained for the complexes against a series of human cancer cell lines [2]. Disubstitution of the terminal NH_2 groups in case of several α-N-pyridine thiosemicarbazones could result in highly increased anticancer activity (e.g. dimethylated Triapine, DpC, Dp44mT) [3]. Based on this finding in this work the *N*-terminally mono- and dimethylated derivatives of estrone-TSC and thn-TSC (Chart 1) and their Cu(II) complexes were aimed to prepare to obtain more effective compounds.

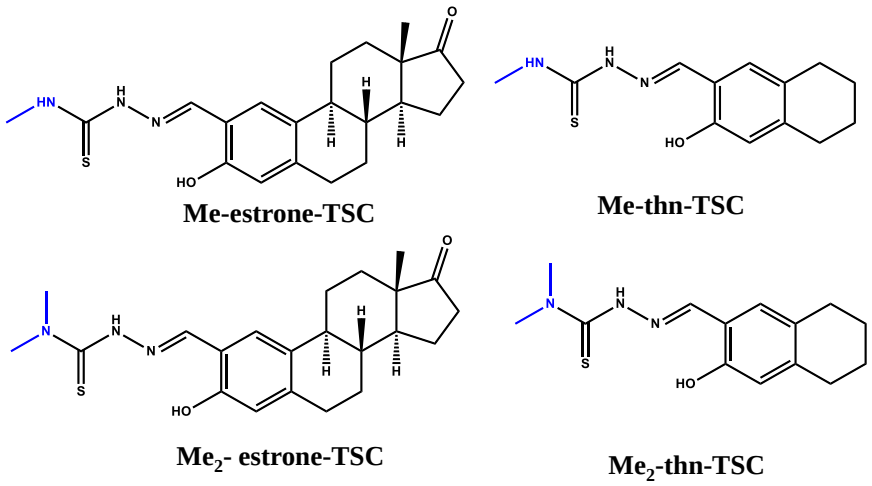

Chart 1. Chemical structures of the investigated ligands.

The solution stability and structure of the complexes were determined using UV-visible spectrophotometry and electron paramagnetic resonance spectroscopy. Due to the limited water solubility of the compounds UV-titrations were performed in a 30% (v/v) DMSO/H_2O solvent mixture in order to determine the pK_a values of the ligands and the stability constants of the complexes. Additionally, their anticancer activity was studied via *in vitro* cytotoxicity and ROS generation assays, and the cell proliferation, apoptosis and its caspase-dependence were also screened on 3D cancer spheroids, which are considered to mimic better the main features of human solid tumours compared with traditional 2D cultures.

Acknowledgements:
National Research, Development and Innovation Office-NKFIA projects GINOP-2.3.2-15-2016-00038, FK 124240 and Ministry of Human Capacities, Hungary grant, TKP-2020. Visegrad Scholarship 52010752 (T. V. P.).

References

[1] D. S. Kalinowski, P. Quach and D. R. Richardson, Future Med. Chem. 1 (2009) 1143.
[2] T. V. Petrasheuskaya, M. A. Kiss, O. Dömötör, T. Holczbauer, N. V. May, G. Spengler, A. Kincses, A. Čipak Gašparović, É. Frank and É. A. Enyedy, New J. Chem. 44 (2020) 12154.
[3] C. R. Kowol, W. Miklos, S. Pfaff, S. Hager, S. Kallus, K. Pelivan, M. Kubanik, É. A. Enyedy, W. Berger, P. Heffeter and B. K. Keppler, J. Med. Chem. 59 (2016) 6739.

WASTE-WOOD DERIVED BIOCHAR AS A SUPPORT FOR HORSERADISH PEROXIDASE IMMOBILIZATION

Mirjana Petronijević[1], Sanja Panić[1], Nataša Đurović-Mladenović[1], Saša Savić[2]

[1]Faculty of Technology, University of Novi Sad, 21000 Novi Sad, Bulevar cara Lazara 1, Serbia
[2]Faculty of Technology, University of Niš, 16000 Leskovac, Bulevar Oslobođenja 124, Serbia
e-mail: mirjana.petronijevic@uns.ac.rs

Abstract
In this paper, the suitability of waste-wood derived biochar particles as a support for the horseradish peroxidase (HRP) immobilization by adsorption method was investigated. The change in enzymatic activity of the immobilized enzyme at different values of pH and temperature, as well as stability over time, was measured. The results showed that HRP can efficiently bind to biochar particles by adsorption. The immobilized enzyme shows high activity (>80%) at a wide range of pH (7-9) and temperature (20-50°C). The immobilized enzyme retains 22% and 40% of its activity during storage at temperatures of 25 and 10°C after a period of 30 days, respectively.

Introduction
Peroxidases represent a large group of enzymes that have been used for environmental remediation purposes [1]. However, the application of enzymes in industry has certain disadvantages due to their instability during time and non-reusability, which could be avoided by binding the enzyme on a suitable solid support. Biochar is an attractive alternative material for enzyme immobilization due to its low cost and readily available starting materials. Also, due to its porous carbon nature and large surface area these materials are very useful as a support for enzyme immobilization [2]. The aim of this work was to investigate the suitability of waste-wood derived biochar particles as a support for the HRP immobilization by adsorption method.

Experimental
Wood biochar (BC) was obtained from sawdust of beech and oak wood mixture by pirolysis at 700°C under atmospheric pressure (Basna doo, Čačak, Serbia). In order to introduce the oxidative functional groups on the surface of BC, their functionalization with concentrated nitric acid was performed according to the method given in Naghdi et al [3]. HRP was extracted from horseradish root and immobilized onto functionalized BC by adsorption method. The enzyme activity was measured according to Worthington method [4]. Surface morphology characteristics of BC and immobilized HRP onto BC were investigated by using scanning electron microscopy (SEM) JEOL JSM-6460LV on 25 kV. The impact of different temperature (30–80°C) on enzyme activity was measured at constant pH7, and impact of different pH (4-9) on enzyme activity was measured at ambient temperature. The storage stability of immobilized HRP was evaluated by measuring their peroxidase activity during one month period. Results for enzyme activity were presented as relative values (%).

Results and discussion
Enzyme immobilization by adsorption (with hydrophobic interactions) provides binding of the enzyme onto the surface of the support. The activity of immobilized HRP onto BC was 11.2±1.4 U/g BC at pH 7.
The surface morphology of the following samples: a) BC, b) functionalized BC and c) functionalized BC after enzyme immobilization, are present in Figure 1. All samples are

characterized by a heterogeneous surface and a developed porous structure. The pore size is in range 7.81-13.0 μm. After treatment with nitric acid during the functionalization process, no visible changes on the surface of BC were observed (Figure 1b). The size of HRP is only 2-4 nm, so it can easily be incorporated into the pores of BC (Figure 1c).

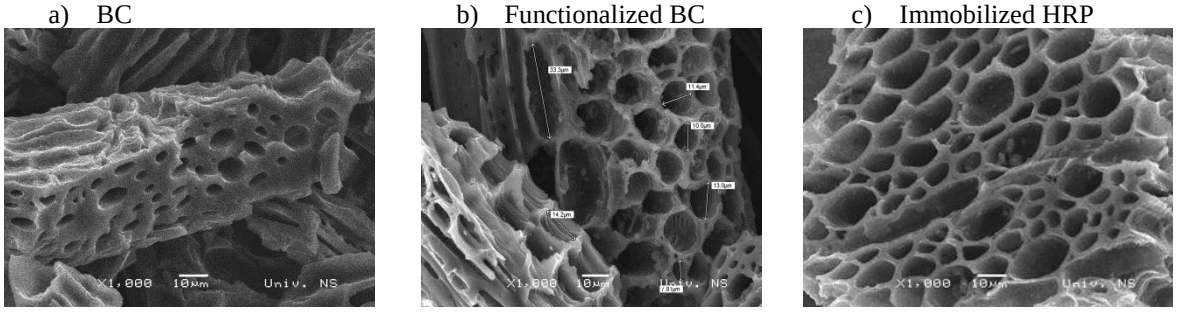

Figure 1. Scanning electron micrographs of a) non-functionalized biochar, b) functionalized biochar and c) HRP immobilized onto functionalized biochar

The activities of HRP immobilized onto functionalized BC at different a) temperatures and b) pH values are present in Figure 2. It could be seen that the activity of investigated enzyme equally depends of both factors. The immobilized enzyme shows high activity (> 80%) at temperatures 20-50°C, while further increasing in temperature decreases the enzyme activity due to their denaturation. On the other hand, the immobilized enzyme is more active in neutral and base than acid conditions, with the highest activity recorded at pH 9.

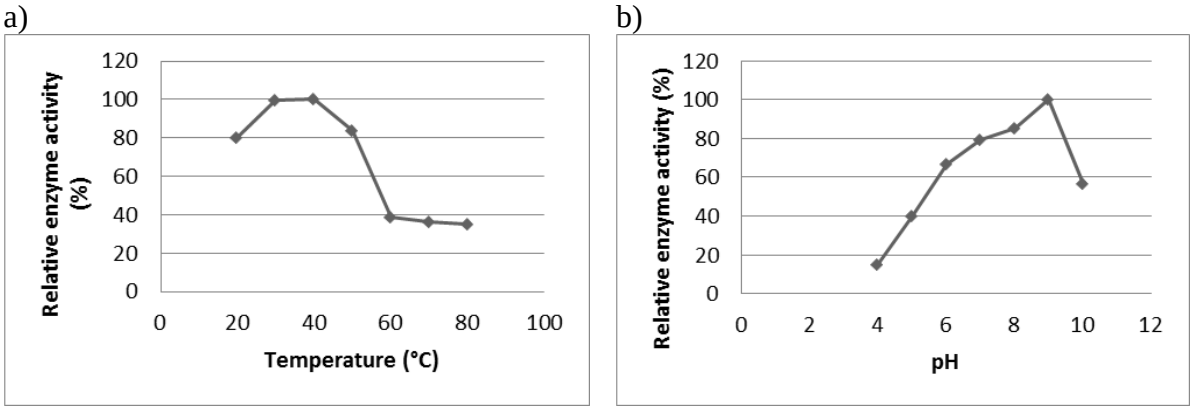

Figure 2. The impact of a) temperature and b) pH values on activity of immobilized HRP

The change in enzyme activity over a period of one month at 10 and 25°C is shown in the Figure 3. The HRP immobilized onto functionalized BC retains around 80% of its activity in the first 5 days at both temperatures. After a period of one month the activity decreases up to 40% and 22% during storage at temperatures 10°C and 25°C, respectively.

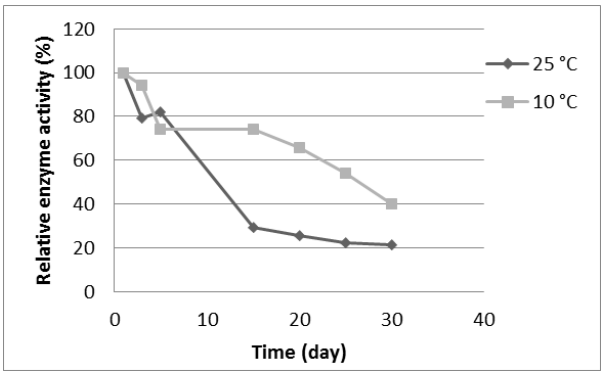

Figure 3. The stability of immobilized HRP during time

Other researchers come to the same conclusion that the immobilized HRP exhibits higher thermal stability, pH stability, storage stability than the free HRP [2,5].

Conclusion

Immobilization of HRP onto BC via hydrophilic interactions yields an enzyme with high activity, stable to various variations of pH and temperature. The immobilized enzyme remains stable for a longer period if stored at a temperature of 10°C. Hence, biochar is proved as a carbon material with a great potential to improve enzyme immobilization efficiency.

Acknowledgements

This work was supported by the Ministry of Education, Science and Technological Development of Republic of Serbia (Project 451-03-68/2020-14/200134).

References

[1] S. Savić, S. Stojmenović, M. Petronijević, Ž. Petronijević, Appl Biochem Micro. 50 (2014) 214.
[2] M. Naghdi, M. Taheran, S.K. Brar, A. Kermanshahi-pour, M. Verma, R.Y. Surampalli, Int. J. Biol. Macromol. 115 (2018) 563.
[3] M. Naghdi, M. Taheran, S.K. Brar, A. Kermanshahi-pour, M. Verma, R.Y. Surampalli, Sci. Total Environ. 584 (2017) 393.
[4] K. Worthington, V. Worthington, Worthington Enzyme Manual. Worthington: Biochemical Corporation, 2011.
[5] M.B. Vineh, A.A. Saboury, A.A. Poostchi, A.M. Rashidi, K. Parivar, Int. J. Biol. Macromol. 106 (2018) 1314.

ANTICANCER 8-HYDROXYQUINOLINE-AMINO ACID HYBRIDS AND THEIR HALF-SANDWICH Ru AND Rh COMPLEXES: SOLUTION CHEMISTRY AND INTERACTION WITH BIOMOLECULES

Tamás Pivarcsik[1,2], Orsolya Dömötör[1,2], János P. Mészáros[1,2], Nóra V. May[3], Oszkár Csuvik[4], Ferenc Fülöp[4], Gabriella Spengler[2,5], István Szatmári[4], Éva A. Enyedy[1,2]

[1]Department of Inorganic and Analytical Chemistry, Interdisciplinary Excellence Centre University of Szeged, H-6720 Szeged, Dóm tér 7, Hungary
[2]MTA-SZTE Lendület Functional Metal Complexes Research Group, University of Szeged, H-6720 Szeged, Dóm tér 7, Hungary
[3]Chemical Crystallography Research Laboratory, Research Centre for Natural Sciences, Magyar Tudósok Körútja 2, H-1117 Budapest, Hungary
[4]Institute of Pharmaceutical Chemistry, University of Szeged, H-6720 Szeged, Eötvös u. 6, Hungary
[5]Department of Medical Microbiology and Immunobiology, Faculty of Medicine, University of Szeged, H-6720 Szeged, Dóm tér 10, Hungary
e-mail: pivarcsik.tamas@chem.u-szeged.hu

Abstract

Development of novel chemotherapeutic agents aims to obtain more effective and selective compounds. Platinum(II)-containing chemotherapeutics have been widely used for decades in cancer therapy against solid tumors due to their effectiveness; although, their use is accompanied by drawbacks such the serious side-effects and resistance [1]. To overcome these problems, efforts have been made to find better alternatives such as the complexes of other platinum metals. 8-hydroxyquinolines and their metal complexes are widely investigated due to their anticancer properties [2,3]; however, they often have limited water solubility. In this work two novel water-soluble 8-hydroxyquinoline-D-amino acid hybrids, [(R)-1-((5-chloro-8-hydroxyquinolin-7-yl)methyl)pyrrolidine-2-carboxylic acid (8HQCl-D-Pro) and its homologue 8HQCl-D-hPro (Chart 1), and their $[Ru(\eta^6\text{-}p\text{-cymene})(H_2O)_3]^{2+}$ and $[Rh(\eta^5\text{-}C_5Me_5)(H_2O)_3]^{2+}$ complexes were developed.

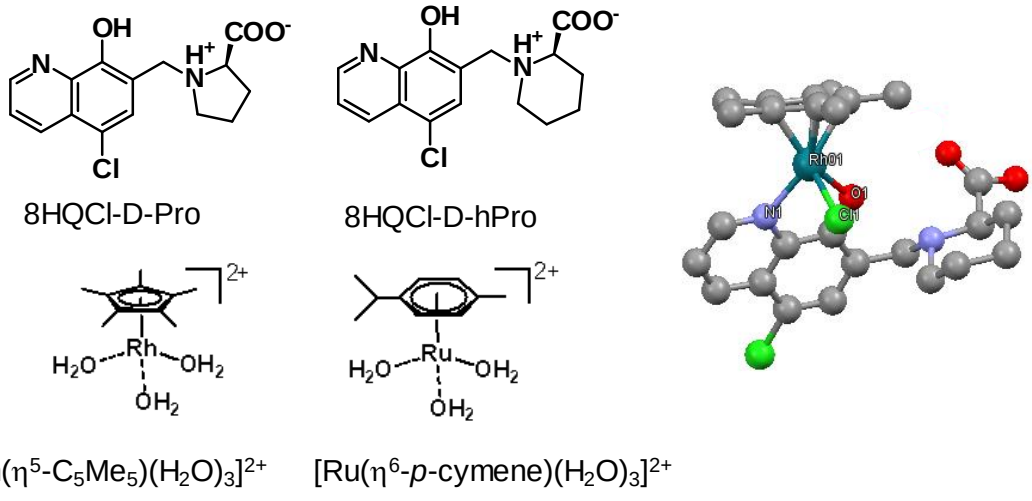

Chart 1. Chemical structure of the ligands and the organometallic triaqua cations and ORTEP view of the complex $[Rh(\eta^5\text{-}C_5Me_5)(8HQCl\text{-}D\text{-}hPro)Cl]$

An 8-hydroxyquinoline-L-proline hybrid and its half-sandwich complexes have already been investigated in our group [4]; herein, we aimed to investigate (i) the impact of changing the structure (proline *vs.* homoproline) and chirality (L *vs.* D) of the ligand on the anticancer activity, (ii) solution chemical properties, (iii) complex formation with $[Ru(\eta^6\text{-}p\text{-cymene})(H_2O)_3]^{2+}$ and $[Rh(\eta^5\text{-}C_5Me_5)(H_2O)_3]^{2+}$ (Chart 1) as well as (iv) the interactions with biomolecules such as human serum albumin (HSA) and calf-thymus DNA (ct-DNA).

The coupling of 5-chloro-8-hydroxyquinoline with D-proline or D-homoproline was achieved via a modified Mannich reaction in methanol under reflux conditions. The ligands and the metal complexes were synthesized similarly as the analogous 8HQCl-L-Pro and its complexes in our previous work [4].

Proton dissociation processes of the ligands and complex formation equilibria were characterized using pH-potentiometry, UV-visible spectrophotometry and ^{1}H NMR spectroscopy in pure water in the absence of chloride ions. Based on the pK_a values determined for 8HQCl-D-Pro and 8HQCl-D-hPro, it was concluded that these ligands are neutral at physiological pH; however, due to their zwitter-ionic structure at the proline moiety they possess excellent water-solubility. The complex formation process was much slower with $[Ru(\eta^6\text{-}p\text{-cymene})(H_2O)_3]^{2+}$ in comparison to $[Rh(\eta^5\text{-}C_5Me_5)(H_2O)_3]^{2+}$, and all the metal complexes were characterized by high solution stability in the whole pH range studied. The ligand coordinates via (N,O) donor atoms to the metal centers, which was confirmed by the X-ray crystallographic analysis of the complex $[Rh(\eta^5\text{-}C_5Me_5)(8HQCl\text{-}D\text{-}hPro)Cl]$ (Chart 1). The proton dissociation of the coordinated water and the non-coordinated proline-NH^+ of the bound ligand was characterized by such high pK_a values that their deprotonation does not take place at pH 7.4. The logK' values determined for the H_2O/Cl^- exchange process were significantly higher in case of the $Rh(\eta^5\text{-}C_5Me_5)$-complexes representing their stronger chloride ion affinity. Lipophilicity of the homoproline derivative 8HQCl-D-hPro was higher than 8HQCl-D-Pro, and the same trend was observed for the metal complexes as well. The higher chloride ion concentration of the medium increases the lipophilicity of the complexes due to the higher fraction of the neutral chlorido complex.

Interaction of the organometallic complexes of 8HQCl-D-Pro and 8HQCl-D-hPro with HSA and ct-DNA was investigated using of UV-visible spectrophotometry, spectrofluorometry, ^{1}H NMR spectroscopy and capillary zone electrophoresis (CZE), and results were compared to those of the analogous 8HQCl-L-Pro compounds. Formation of the complex-HSA adducts was much slower for $Ru(\eta^6\text{-}p\text{-cymene})$ complexes. No ligand release was found upon the protein binding. Our studies suggest the coordination nature of the binding, most likely a histidine nitrogen donor atom of the protein coordinates to the metal center. This suggestion was supported based on the results obtained with histidine-containing model oligopeptides. The complexes have similar and strong affinity towards HSA according to the fluorometric and CZE measurements. They also interact with ct-DNA however, significant differences were found between the complexes of the D-proline and the L-proline derivatives.

Cytotoxicity of the ligands as well as their complexes was measured *in vitro* against human cancer cells and normal cells. Both ligands showed significant cytotoxicity in Colo 205 and Colo 320 adenocarcinoma cells (IC_{50} = 12 – 17 μM). The $Rh(\eta^5\text{-}C_5Me_5)$-complexes display similar or a somewhat lower toxicity (IC_{50} = 19 – 34 μM) than the ligands; however they were more selective against the cancer cells. The $Ru(\eta^6\text{-}p\text{-cymene})$ complexes were ineffective against both cancer cell lines, possibly due to the loss of the arene ring.

Acknowledgements
This work was supported by the National Research, Development and Innovation Office-NKFIA through projects GINOP-2.3.2-15-2016-00038, FK 124240 and Ministry of Human Capacities, Hungary grant, TKP-2020.

References
[1] C.S. Allardyce, P.J. Dyson, Dalton Trans. 45 (2016) 3201.
[2] M.C. Ruiz , J. Kljun, I. Turel, A.L. Di Virgilio, I.E. León, Metallomics 11 (2019) 666.
[3] M. Kubanik, H. Holtkamp, T. Söhnel, S.M.F. Jamieson, C.G. Hartinger, Organometallics34 (2015) 5658.
[4] J.P. Mészáros, J.M. Poljarevic, I. Szatmári, O. Csuvik, F. Fülöp, N. Szoboszlai, G. Spengler, É.A. Enyedy, Dalton Trans. 49 (2020) 7977.

DANGEROUS AND HARMFUL MATERIALS IN AGRICULTURAL SOIL AND CULTIVATED CROPS IN THE MUNICIPALITY OF PROKUPLJE

Radmila Pivić[1], Jelena Maksimović[1] Aleksandra Stanojković-Sebić[1], Zoran Dinić[1]

[1]Institute of Soil Science, Belgrade, Teodora Drajzera 7, Republic of Serbia
e-mail: drradmila@pivic.com

Abstract
In the area of the Municipality of Prokuplje in the Republic of Serbia, in the period July-November 2019, 26 samples of soil and aboveground part of plant material found at the research sites were sampled. In the laboratory of the Institute of Soil Science, Belgrade, a test of the content of hazardous and harmful substances in the sampled soil and plant material was conducted. The analyzed plant cultures are used partly for human consumption (fruits), one part is used for human and animal nutrition (cereals, corn), and one part belongs to animal feed (grass mixture). The study was aimed to examine the possibility that hazardous and harmful substances enter the food chain. The obtained values of the tested trace elements in the plant material are low at most of the examined localities, even on plots with increased content of total forms of tested elements in the soil, there are no increased contents in plant material, except at one locality where Pb content was found in wheat. In this specific sample, value was above (MPC) the maximum permitted concentrations (Pb=0.94 $mg \cdot kg^{-1}$), which is recommended to be excluded for human consumption.

Key words: soil, plant material, hazardous and harmful substances

Introduction
Heavy metals are present in traces in all unpolluted soils as a result of decomposition of the parent substrate and are therefore widespread in soils, plants and animals. Studies have shown that especially in urban and industrial areas there has been a significant increase in the content of heavy metals in the soil [1]. A special problem is represented by metals that accumulate in the human body through food, through the food chain, such as cadmium and lead. Land is a dynamic system in balance with the environment and needs to be protected from further degradation. Plants are a mediator through which elements from the soil, and partly from water and air, are transmitted to the human body. Some of the elements are necessary for the growth and development of plant cultures and without them they cannot survive, some have a stimulating effect, while one group of elements at higher concentrations has a very toxic effect on plants.

Material and Methods
The total number of locations where the composite soil sample was sampled in the period July-November 2019 was 26. Number of samples of found plant material (aboveground part of the vegetative mass) was 32. From total number of samples, three samples of corn plant mass were sampled in milky and waxy maturity. The plant material at location 24 consisted of four fruit species, so that the chemical properties were tested for each plant species found at the sampling site. Figure 1 shows the layout of the sampling sites. In the laboratory, composite soil samples were dried and passed through a Ø 2 mm sieve [2]. Determination of trace elements in ICP-AES soil extracts - Total concentrations of the most significant hazardous (As, Cd, Cr, Ni, Pb, Co) and harmful elements (Cu, Zn, Fe), by the method of ISO 22036: 2008; Available forms of Fe, Mn, Zn, Cu - DTPA buffer solution extraction and determination by ICP using method: SRPS ISO 14870: 2005. Analyzed aerial parts of the study plant species were dried for 2 hours

at 105°C, using gravimetric method for determination of dry matter content of plant tissue. The dry matter determination is used to correct the sample element concentration to an absolute dry matter basis [3]. The content of heavy metals (Pb, Ni, Cr and Cd) in selected plants was determined with an inductively coupled plasma optical emission spectrometer ICAP 630 (ICP-OES), after the samples were digested with concentrated HNO_3/H_2O_2 for total form extraction.

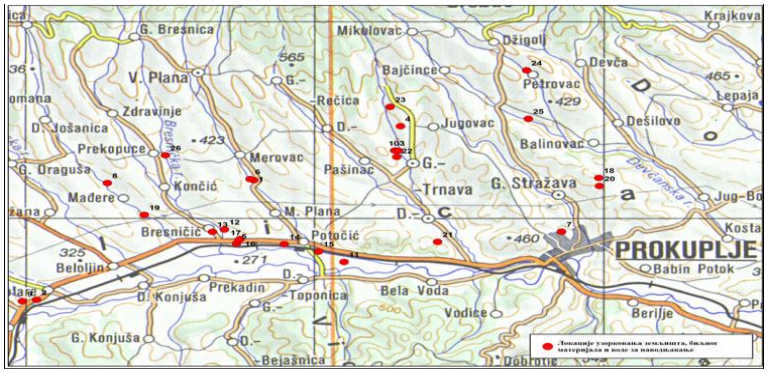

Figure 1. Sampling sites (source: Institut of Soil Science, 2019.)

Results and discussion

For interpretation of the maximum allowable concentrations (MPC) of the total forms of the tested elements, for soil samples, the values shown in Table 1 were used.

Table 1. Maximum permitted concentrations (MPC) of total forms of hazardous and harmful substances in the soil in the Republic of Serbia

Element/Rule book	Cd	Co	Cr	Mn	Ni	Pb	Zn	Cu	As
	(mg kg^{-1}) absolutely dry matter								
Official Gazette 23/1994 [4]	3		100		50	100	300	100	25
Kastori et al.(1997) [5]				400*					
Ordinance - Official Gazette 51/2002 [6]		30*							

Tables 2 and 3 show the mean value, the range of the analyzed total forms of the examined elements and the number of locations where the content above the MPC was determined in the soil samples at both sampling depths (0-30 cm and 30-60 cm).

Table 2. The content of total forms trace elements in soil samples (0-30 cm)

Element	Cd	Co	Cr	Mn	Ni	Pb	Zn	Cu	As
	(mg kg^{-1})								
Range	0,21 - 0,42	9,93 - 18,2	19,2 - 84,3	354-890	15,9-97,6	9,28-74,6	37,2-78,8	12,2-89,2	2,06-24,4
Average	0,30	14,9	56,8	579	54,1	18,3	56,7	25,4	8,04
Nº of location Above MPC	0	0	0	25	17	0	0	0	1

Table 3. The content of total forms trace elements in soil samples (30-60 cm)

Element	Cd	Co	Cr	Mn	Ni	Pb	Zn	Cu	As
	(mg kg^{-1})								
Rang	0,20 - 0,43	10,3 - 18,5	19,6-91,6	391 - 955	16,8 - 101	7,06 - 66	38,4-99,4	11,3-69,9	1,68-20,7
Average	0,30	15,2	58,6	581	55,6	17,8	58,7	25,3	7,66
Nº of location Above MPC	0		0	25	16	0	0	0	1

In all examined soil samples, the content of total forms of Mn above the maximum permissible concentrations (MPC) was determined at both sampling depths (0-30 cm and 30-60 cm), except at location 21, where it was in the permitted concentrations. Ni content was above MPC at

location number 1 in the first sampling depth, location no. 2 in the second sampling depth, and at both sampling depths at locations no. 4, 8, 9, 14, 15, 17, 18, 19, 20, 21, 22, 24. The content of As was above the MPC at both sampling depths only at location Nº 24. The content of other examined elements is within the limits of the MPC. The appearance of the content of individual elements above the MPC can be partly caused by geophysical origin and partly by anthropogenic factors, therefore, research the causes of the occurrence of these concentrations aove the permitted values should be investigated in more details.
Table 4 shows the levels of content provision of accessible forms of the tested elements in the soil samples and in Tables 5 and 6 the contents at the test depths.

Table 4. Limit values of accessible microelements in soil

Limit values	Cu	Zn	Fe	Mn
		(mg kg^{-1})		
very low	<0,3	<0,5	0-5	0-4
low	0,3-0,8	0,5-1	5-10	4-8
medium	0,9-1,2	1-3	11-16	9-12
high	1,3-2,5	3-6	17-25	13-30
very high	>2,5	>6	>25	>30

Table 5. The content of available forms trace elements in soil samples (0-30 cm)

Grade	Cu	Nº samples	Fe	Nº samples	Mn	Nº samples	Zn	Nº samples
very low	<0,3	0	0-5		0-4	0	< 0,5	2
low	0,3-0,8	0	5-10	0	4-8	0	0,5-1	12
medium	0,9-1,2	0	11-16	3	9-12	3	1-3	11
high	1,3-2,5	14	17-25	2	13-30	9	3-6	1
very high	>2,5	12	>25	21	>30	14	>6,0	0
Rang		1,54 – 18,5		11,0 – 87,5		7,60 – 54,2		0,35 – 3,67
Average		3,52		45,2		30,1		1,10

Table 6. The content of available forms trace elements in soil samples (30-60 cm)

Grade	Cu	Nº samples	Fe	Nº samples	Mn	Nº samples	Zn	Nº samples
very low	<0,3	0	0-5	0	0-4	0	< 0,5	5
low	0,3-0,8	0	5-10	0	4-8	0	0,5-1	8
medium	0,9-1,2	0	11-16	1	9-12	3	1-3	12
high	1,3-2,5	12	17-25	2	13-30	6	3-6	1
very high	>2,5	14	>25	23	>30	17	>6,0	0
Rang		1,07 – 24,1		11,5 - 144		11,0 – 69,6		0,13 – 4,80
Average		3,93		54,5		35,1		1,13

The content of accessible forms of Cu in the tested soil samples at a depth of 0-30 cm in 88% of the tested samples is very high while in 12% it is high; the content of available Fe is very high in 96% of the samples and high in 4%; the content of accessible Mn in 72% of samples is very high, 24% high, 4% medium; the content of available Zn is high in 12% of samples, 68% medium, 12% low and 8% very low. At a depth of 30-60 cm, the content of accessible forms of Cu is very high in 76% of the examined samples, 24% high; affordable Fe 96% very high, 4% high; accessible Mn 64% very high, 32% tall, 4% medium; affordable Zn 4% very high, 40% medium, 48% low and 8% very low.

The obtained values of the tested trace elements in the plant material are low at most of the examined localities, even on plots with increased content of total forms of tested elements in the soil there are no increased contents in the plant.
The exception is the content of the examined trace elements registered at locality number 13, where wheat was sampled. The Pb content above the MPC (Pb = 0.94 mg kg-1) was determined in the tested plant material.The results of chemical analyzes of plant mass were compared with the limit values taken from the literature [8-10]. The classifications are shown in Table 7.
Based on the limit values for human and animal nutrition, wheat should not be used in human nutrition but can be used for animal nutrition. Other tested elements in the examined plant material were within the maximum permitted concentrations.

Table 7. Optimal values of tested elements in samples of plant material for human and animal nutrition

Type of use	Plant species	MPC in plant material				
		Pb	Ni	Cr	Cd	Fe
		(mg kg^{-1})				
Values for human consumption	plum	0,1	0,1-5*	0,1-1*	0,05	30
	cherry	0,1	0,1-5*	0,1-1*	0,05	30
	strawberry	0,1	0,1-5*	0,1-1*	0,05	30
	blackberry	0,1	0,1-5*	0,1-1*	0,05	30
	raspberry	0,1	0,1-5*	0,1-1*	0,05	30
	cereals	0,2	0,1-5*	0,1-1*	0,2	/
	corn	0,2	0,1-5*	0,1-1*	0,1	/
Values for animal feed	grass mixture	40	50	/	1	/
	cereals	40	50	/	1	/
	corn	40	50	/	1	/

* Optimal values of trace element content

Table 8 shows the individual values of the examined content of trace elements in the plant material in the study area.

Table 8. Content of trace elements in plant material

Location	Plant species	Content of trace elements in plant material				
		Pb	Ni	Cr	Cd	Fe
		(mg kg^{-1})				
1	2	3	4	5	6	7
1	Plum	0,02	0,07	0,014	0,028	0,96
2	Plum	0,03	0,09	0,007	0,017	1,06
3	Plum	0,05	0,09	BLMD	0,009	0,74
4	Plum	0,01	0,07	0,012	0,003	1,08
5	Plum	0,03	0,16	BLMD	0,012	1,25
6	Cherry	0,00	0,02	0,007	0,003	1,63
7	Cherry	0,02	0,05	BLMD	0,002	2,38
8	Cherry	0,02	0,03	BLMD	0,019	2,68
9	Cherry	0,03	0,11	BLMD	0,015	2,54
10	Cherry	0,02	0,03	0,003	0,008	2,25
11	Grass mixture	0,28	2,15	0,772	0,064	136
12	Strawberry	0,09	0,10	0,041	0,014	14,0
13	Weath/ Cereals	0,94	0,86	0,122	0,088	39,7
1	2	3	4	5	6	7
14	Grass mixture	0,71	1,97	1,755	0,045	216
15	Blackberry	0,02	0,12	0,183	0,005	3,52
16	Raspberry	0,01	0,34	0,080	0,010	3,34

17	Raspberry	0,03	0,60	0,006	0,015	4,71
18	Cereals	0,18	0,36	0,468	0,034	31,5
19	Grass mixture	0,38	2,29	2,855	0,015	546
20	Grass mixture	0,60	3,44	4,525	0,035	1442
21	Grass mixture	0,31	3,66	1,267	0,198	224
22	Corn-tree	0,24	0,66	1,045	0,085	70,1
	Corn-grain	BLMD	0,32	0,081	0,111	14,7
23	Corn-tree	0,08	0,80	1,435	0,120	98,9
	Corn-grain	BLMD	0,55	0,225	0,081	16,2
24	Plum	BLMD	0,193	BLMD	BLMD	3,66
	Apple	BLMD	0,019	BLMD	BLMD	1,41
	Plum	BLMD	0,091	BLMD	BLMD	1,14
	Pear	BLMD	0,148	0,054	BLMD	1,89
25	Corn-tree	0,26	0,97	1,79	0,065	129
	Corn-grain	BLMD	0,60	0,213	0,085	13,5
26	Cereals	0,086	0,49	0,262	0,074	28,6

BLMD-below the limit of the method detection

Acknowledgment: This research was financially supported by the Ministry of Education, Science and Technological Development, Republic of Serbia [Project To 451-03-68/2020-14].

References

[1] Z., Dinić, J., Maksimović, A.,Stanojković-Sebić, R., Pivić (2018): The content of trace elements in forage crops grown on diverse soils of the Mali Zvornik municipality in Serbia, 11th International Scientific/Professional conference Agriculture in nature and environment protection, Vukovar, Hrvatska, P58.
[2] R., Džamić, D., Stevanović, M., Jakovljević (1996): Agrochemistry Manual. Faculty of Agriculture, University of Belgrade, Serbia, (in Serbian).
[3] R.O., Miller (1998): Determination of dry matter content of plant tissue: gravimetric moisture, In: Kalra Y.(ed.) Handbook of reference methods for plant analysis, CRC Press, Taylor&Francis Group, Boca Raton,Florida, USA, pp.51-52.
[4] Official Gazette of Republic Serbia, 23/94, (1994).
[5] R. Kastori, N. Petrović, I. Arsenijević-Maksimović (1997): Heavy metals and plants. In Heavy Metals in the Environment. Kastori R (Ed). Institute of Field and Vegetable Crops, Novi Sad, Serbia, 196-257.
[6] Ordinance - Official Gazette of Republic Serbia 51/2002, (2002).
[7] Kloke A., Sauerbeck D.R. and Vetter H. (1984): The contamination of plants and soils with heavy metals and the transport of metals in terrestrial food chains. In: Nriagu, J.O. (ed.) Changing metal cycles and human health. Dahlem Konferenzen, Springer-Verlag, Berlin, Heidelberg, New York, Tokyo, 113-141.
[8] Kabata-Pendias, A. and H. Pendias (2000): Trace Elements in Soils and Plants. 3rd edition. London, England. CRC Press.
[9] NRC (2003, 2005, 2016): Mineral Tolerance of Animals, National Research Council of the National Academies, The National Academies Press, Washington D.C.
[10] Ordinance - Official Gazette of Republic Serbia ("Sl. glasnik RS", br. 4/2010, 113/2012, 27/2014 and 25/201539/2016, 54/2017.).

MICROWAVE SYNTHESIS OF N–CQDs: EFFECT OF WAVELENGTH ON DEGRADATION OF ORGANIC POLLUTION IN WATER

Jovana Prekodravac[1], Bojana Vasiljević[1], Dragana Jovanović[1], Dejan Kepić[1], Svetlana Jovanović Vučetić[1], Milica Budimir[1] and Biljana Todorović Marković[1]

[1]*Vinča Institute of Nuclear Sciences – National Institute of Republic of Serbia, University of Belgrade, Belgrade, Serbia*
e-mail: prekodravac@vin.bg.ac.rs

Abstract
Industries today realis high amounts of different hazards into the environment without any pre–treatment, which is why the remediation from organic pollution still represents one of the most important issues in waste water treatment. Organic dyes from textile industry are one of the extremely geno–toxic and cyto–toxic pollutants. Thus, finding the appropriate photocatalyst for the treatment of contaminated water under sunlight is still a challenging work from economical and green chemistry approach. Here we present a microwave assisted synthesis of nitrogen doped carbon quantum dots with high efficiency in degradation of Rose Bengal organic dye from water under visible, blue, green and red light irradiation in batch system. The effect of microwave irradiation power and time on size and photocatalytic activity of synthesized dots were also investigated.

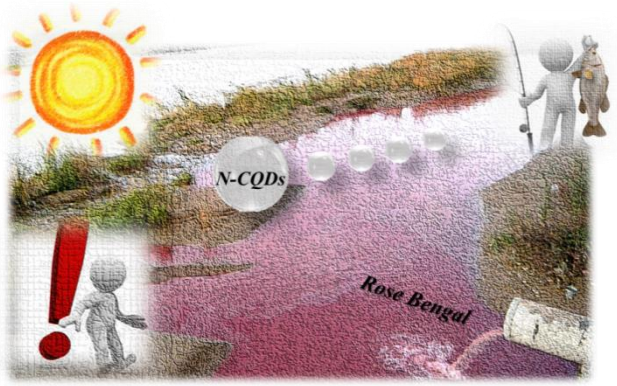

Introduction
Organic dyes, as waste materials released daily into the environment without special treatment from the textile industry, are causing significant environmental issues [1]. Dyes such as Rose Bengal (RB), Methylene Blue (MB), Congo Red (CR) and Methyl Orange (MO) are extremely gene–toxic, mutagenic and cytotoxic organic dyes [2–4]. Therefore, the researchers are focused on developing different methods for overcoming these difficulties. Semiconductor heterogeneous photocatalysis proved to be an encouraging method for the degradation of industrial dyes. However, photocatalysis still requires research efforts in finding new semiconducting materials with smaller bandgaps for enhancing visible light absorption [5]. Carbon quantum dots (CQDs) come from carbon based nanomaterial family with significant attention from economic and environmental aspects. CQDs are water dispersible materials, due to a large number of oxygens–related groups (carbonyl, carboxyl and hydroxyl) whose properties could be significantly influenced through chemical modification [6–10]. Most of synthetic methods for synthesis and doping of CQDs are complex, economically affordable or time consuming [11, 12], quite the reverse, microwave (MW) assisted method can accelerate chemical reactions at milder reaction conditions. Here we report MW assisted synthesis of N–

CQDs with potential application in water treatment for removal of toxic organic dye RB through exposure to the visible light as well as the blue, green and red light illumination.

Experimental

The MW synthesis of N–CQDs was performed as we described in our previous work [13]. The 10 wt% of glucose water solution containing ammonia hydroxide as a nitrogen doping agent were heated in microwave reactor for 1 min, at fixed temperature (100 °C) and with applied microwave power of 100W and 200 W. The color of the MW treated solutions changed from transparent brown as a result of the N–CQDs formation. The samples were dialyzed (300 Da) for several days and filtrated through filters with different pore sizes. The synthesized N–CQDs were dispersed in RB water solution and exposed to visible light irradiation from window ledge as well as to blue, green and red light illumination using lamp (3W).

Results and discussion

The morphology of synthesized N–CQDs was examined by AFM microscopy. The top view AFM images of synthesized samples presented in Figure 1 a, c, show that N–CQDs have spherical like shapes. Measurements of particles thickness showed 1.2 nm for 100W samples and 0.9 nm for 200W samples indicating the single layer dots formation [13]. The real particle diameters of the particles measured by AFM, over more than 100 dots for each sample were in the range from 7 to 30 nm. Thus, increasing the MW power during synthesis resulted in formation of 90% N–CQDs with diameter lower than 18 nm.

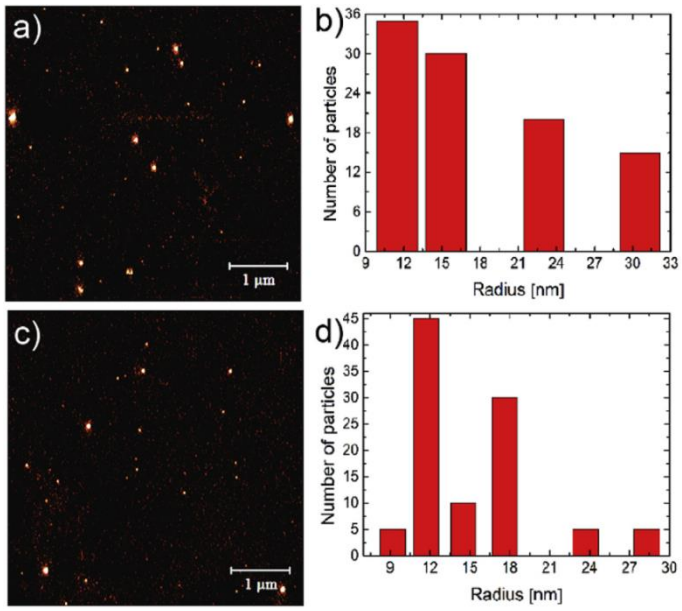

Figure 1. AFM analysis of synthesized N–CQDs samples: top view AFM image and real particle distribution for samples synthesized under 100W (a, b) and 200W (c, d).

The XPS results resolved that increase of applied MW power induces the increase of C sp^3 comparing to the sp^2 domains (Table 1), suggesting that synthesized dots are carbon nanodots consisting of sp^3 carbon matrix with sp^2 domains. The increase of applied MW power induced the decrease of pyrrolic–N and graphitic–N bonds while there is an increase of pyridinic/NH_2 bonds. The content of oxygen functional groups decreases, which could indicate the lowering of surface defects in the samples.

Table 1. The detail XPS analysis of the samples synthesized at 100W and 200W.

	Sample at 100W		**Sample at 200W**	
Name	***Peak BE (eV)***	***Atomic %***	***Peak BE (eV)***	***Atomic %***
C1s	285.8	66.4	285.5	69.2
O1s	532.2	23.5	532.1	19.1
N1s	400.0	10.1	399.9	11.8
C1s sp^2	284.5	18.9	284.5	18.8
C1s sp^3	285.1	22.7	285.1	28.2
C1s C–O	286.1	43.0	286.0	37.5
C1s C=O	286.9	5.6	286.9	5.0
C1s O–C=O	288.8	3.2	289.2	0.6
C1s NC=O	287.9	6.6	287,9	10.0
N1s pyrrolic	400.4	23.4	400.4	20.8
N1s pyridinic/NH_2	399.4	64.6	399.4	69.3
N1s graphitic/NH_3^+	401.7	12.0	401.6	9.8

The photocatalytic activity of synthesized materials was examined for photocatalytic degradation of one of the most dominant dye in textile industry (RB). The photocatalytic degradation efficiency of RB by N–CQDs material was monitored through decrease in the absorption peak intensity designated at 549 nm with a shoulder at 520 nm, both characteristic for pure RB dye. In our previous work we presented the decomposition of RB in the presence of N–CQDs under visible light irradiation explaining the effect of medium pH, contact time and catalyst concentration. Therefore here we have decided to explore how irradiation under different wavelengths affects the decomposition rate after 2h of irradiation. After performing reactions under the same reaction conditions such as using catalyst in concentration of 1 mg/ml, adjusting reaction medium to pH 7 and by exposing samples to the visible light (380–780 nm) or its components: blue light (380–500 nm), green light (500–570 nm) and red light (625–740 nm), different results were confirmed (Figure 2.). Exposure to the wavelengths shorter (Figure 2a) than absorption wavelength of pure RB resulted in the lowest values of degradation percentages, comparing to the green and red light experiments (Table 2). Similar observations were made comparing results after irradiation at longer wavelengths above 600 nm, and irradiation under wavelength region for RB absorption between 500 and 570 nm. However, the highest degradation percentage was observed after performing experiments under visible light irradiation where over 94% of RB dye was successfully decomposed (Figure 2d).

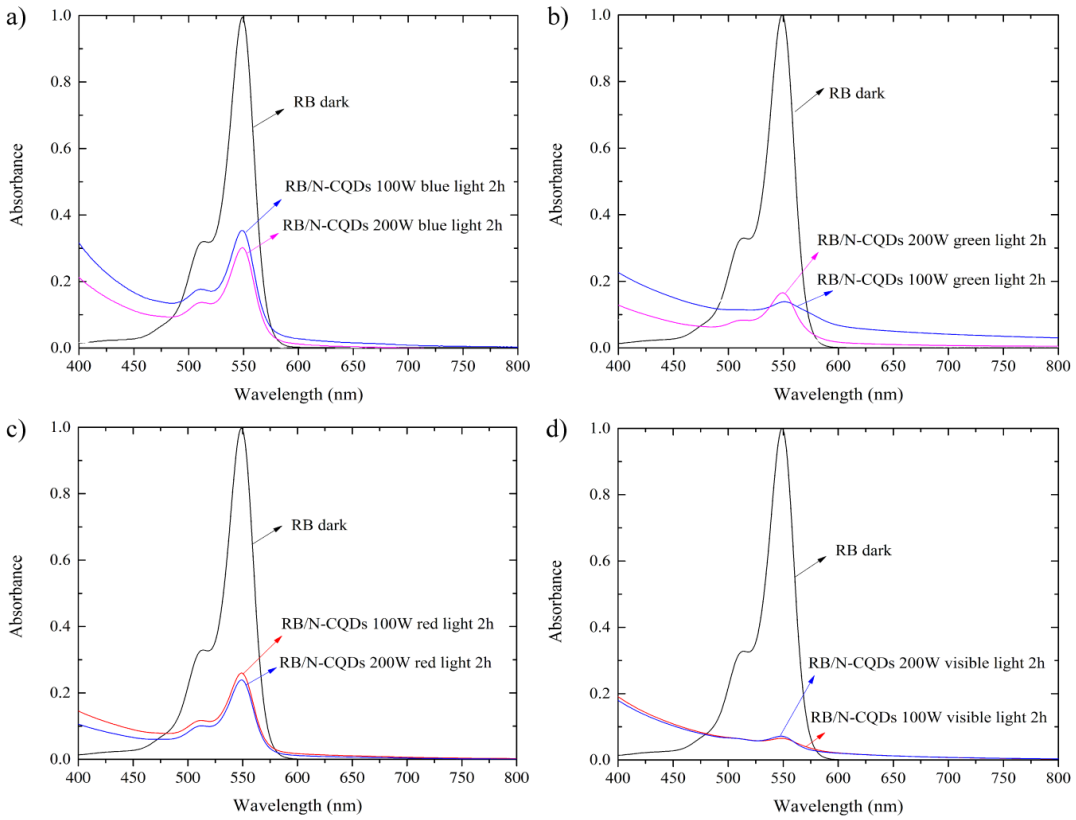

Figure 2. Degradation of RB dye in the presence of N–CQDs samples synthesized under 100W and 200W: a) blue light, b) green light, c) red light and d) visible light.

Table 2. Decomposition percentage of RB under different wavelength irradiations.

Irradiation wavelength (nm)	***N–CQDs 100W Degradation***	***N–CQDs 200W Degradation***
Blue light (380–500 nm)	65%	70%
Green light (500–570 nm)	86%	84%
Red light (625–740 nm)	74%	76%
Visible light (400–700 nm)	93%	94%

Conclusion

Presented study demonstrates the effect of the light irradiation wavelength on the decomposition efficiency of organic dye pollutant such as RB in water medium. The decomposition was examined in the presence of N–CQDs semiconductor photocatalyst with approximately 10 to 11% of attached nitrogen, synthesized by fast and easy method using microwave reactor. Successful decomposition was obtained under every examined wavelength with slight diversity inside the visible range. The highest decomposition efficiency was observed however while irradiating samples containing RB/N–CQDs under visible light comparing to irradiation with separate parts of visible light spectrum.

Acknowledgements

This work was financially supported by the Ministry of Education, Science and Technological Development of the Republic of Serbia (Grant No. 451-03-68/2020-14/200017).

References

[1]. Chequer FMD, Venâncio V de P, Bianchi M de LP, Antunes LMG. Genotoxic and mutagenic effects of erythrosine B, a xanthene food dye, on HepG2 cells. Food Chem Toxicol. 2012 Oct;50(10):3447–51.

[2]. Mpountoukas P, Pantazaki A, Kostareli E, Christodoulou P, Kareli D, Poliliou S, et al. Cytogenetic evaluation and DNA interaction studies of the food colorants amaranth, erythrosine and tartrazine. Food Chem Toxicol. 2010 Oct;48(10):2934–44.

[3]. Allen MJ, Tung VC, Kaner RB. Honeycomb Carbon: A Review of Graphene. Chem Rev. 2010 Jan 13;110(1):132–45.

[4]. Lee M, Chen B-Y, Den W. Chitosan as a Natural Polymer for Heterogeneous Catalysts Support: A Short Review on Its Applications. Appl Sci. 2015 Nov 17;5(4):1272–83.

[5]. Colmenares JC, Xu Y-J, editors. Heterogeneous Photocatalysis. Berlin, Heidelberg: Springer Berlin Heidelberg; 2016. (Green Chemistry and Sustainable Technology).

[6]. Sun D, Ban R, Zhang P-H, Wu G-H, Zhang J-R, Zhu J-J. Hair fiber as a precursor for synthesizing of sulfur- and nitrogen-co-doped carbon dots with tunable luminescence properties. Carbon N Y. 2013 Nov;64:424–34.

[7]. Hu Y, Yang J, Tian J, Jia L, Yu J-S. Oxygen-driven, high-efficiency production of nitrogen-doped carbon dots from alkanolamines and their application for two-photon cellular imaging. RSC Adv. 2015;5(20):15366–73.

[8]. Prekodravac JR, Jovanović SP, Holclajtner-Antunović ID, Peruško DB, Pavlović VB, Tošić DD, et al. Monolayer graphene films through nickel catalyzed transformation of fullerol and graphene quantum dots: a Raman spectroscopy study. Phys Scr. 2014 Sep 1;T162:014030.

[9]. Prekodravac JR, Marković ZM, Jovanović SP, Holclajtner-Antunović ID, Kepić DP, Budimir MD, et al. Graphene quantum dots and fullerenol as new carbon sources for single–layer and bi–layer graphene synthesis by rapid thermal annealing method. Mater Res Bull. 2017 Apr;88:114–20.

[10]. Jovanović SP, Syrgiannis Z, Marković ZM, Bonasera A, Kepić DP, Budimir MD, et al. Modification of Structural and Luminescence Properties of Graphene Quantum Dots by Gamma Irradiation and Their Application in a Photodynamic Therapy. ACS Appl Mater Interfaces. 2015 Nov 25;7(46):25865–74.

[11]. Saud PS, Pant B, Alam A-M, Ghouri ZK, Park M, Kim H-Y. Carbon quantum dots anchored TiO2 nanofibers: Effective photocatalyst for waste water treatment. Ceram Int. 2015 Nov;41(9):11953–9.

[12]. Liu R, Li H, Duan L, Shen H, Zhang Y, Zhao X. In situ synthesis and enhanced visible light photocatalytic activity of C-TiO 2 microspheres/carbon quantum dots. Ceram Int. 2017 Aug;43(12):8648–54.

[13]. Prekodravac J, Vasiljević B, Marković Z, Jovanović D, Kleut D, Špitalský Z, et al. Green and facile microwave assisted synthesis of (metal-free) N-doped carbon quantum dots for catalytic applications. Ceram Int. 2019;

COMPLEX FORMATION OF COPPER(II) WITH A PROLINE SUBSTITUTED 8-HYDROXYQUINOLINE: SOLUTION STUDIES AND STRUCTURAL CHARACTERIZATION

Inna Safyanova[1], Nóra V. May[2], Oszkár Csuvik[3], Ferenc Fülöp[3], István Szatmári[3], Eva A. Enyedy[1]

[1]Department of Inorganic and Analytical Chemistry, Interdisciplinary Excellence Centre and MTA-SZTE Lendület Functional Metal Complexes Research Group, University of Szeged, H-6720 Szeged, Dóm tér 7, Hungary
[2]Chemical Crystallography Research Laboratory, Research Centre for Natural Sciences, Magyar Tudósok Körútja 2, H-1117 Budapest, Hungary
[3]Institute of Pharmaceutical Chemistry, University of Szeged, H-6720 Szeged, Eötvös u. 6, Hungary
e-mail: sssafyanova@gmail.com

Abstract

8-hydroxyquinoline and its substituted derivatives are a well-known class of bidentate ligands widely used in bioanalytical and supramolecular chemistry due to wide specter of their applications and high coordination binding activity [1, 2]. 8-hydroxyquinolines and their metal complexes often exhibit anticancer activity [2], and the most prominent example is orally active tris(8-hydroxyquinolato)gallium(III), which is tested under clinical trials phase I and II [3]. The cytotoxicity of 8-hydroxyquinolines is also related to complexation with endogenous metals such as the redox active copper and iron ions [4]. 8-Hydroxyquinolines generally suffer from limited water solubility, and in this work a more water soluble D-proline hybrid molecule, (D)-5-chloro-7-((proline-1-yl)methyl)8-hydroxyquinoline (8HQCl-D-Pro, Fig. 1.a), was developed and its complexation with copper(II) was investigated.

.

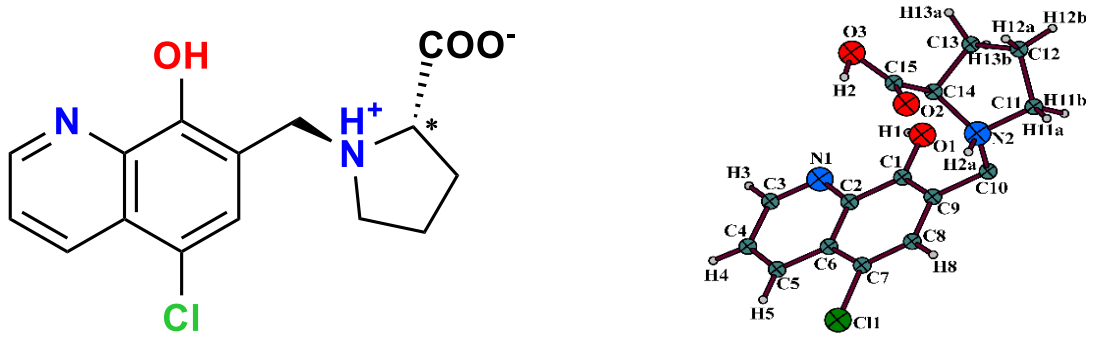

a **b**

Figure 1. a) Scheme of 8HQCl-D-Pro ligand; b) Crystal structure of 8HQCl-D-Pro.

The ligand was synthesized similarly as the analogous 8HQCl-L-Pro in our previous work [5].The solution equilibrium processes of 8HQCl-D-Pro, whose crystal structure was obtained and determined by X-ray analysis (Fig. 1.b), with copper(II) was investigated in a 30% (v/v) dmso/water solvent mixture using pH-potentiometry and UV-visible spectroscopy. A model containing mononuclear $[Cu(LH)]^+$, $[Cu(L_2H)]^-$ and $[Cu(LH)_2]$ species is proposed (Fig. 2).

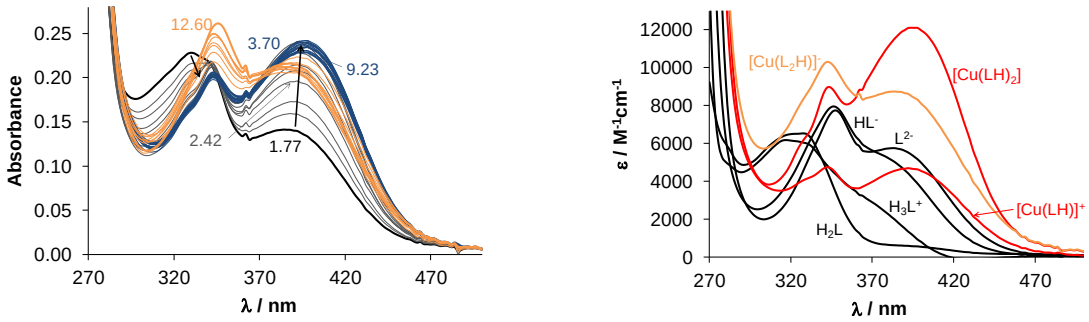

a **b**

Figure 2. a) a) UV-visible absorption spectra of 8HQCl-D-Pro at pH range 1.9–12.6 in a 30% (v/v) DMSO/H_2O solvent mixture; b) individual UV-visible absorption spectra of the different complexes (red lines) and ligand species (black lines) calculated for the Cu(II) – 8HQCl-D-Pro system (c_{ligand} = 42,5 μM; $c_{Cu(II)}$ = 23 μM; T = 25.0 °C; I = 0.1 M (KCl), l = 1 cm).

Acknowledgements

This work was supported by the National Research, Development and Innovation Office-NKFIA through project GINOP-2.3.2-15-2016-00038 and Ministry of Human Capacities, Hungary grant, TKP-2020. Visegrad Scholarship 52010718 (I. S.).

References

[1] Y. Song, H. Xu, W. Chen, P. Zhan and X. Liu, Med. Chem. Commun. 6 (2015) 61.
[2] A. R. Timerbaev, Metallomics. 1 (2009) 193.
[3] U. Jungwirth, J. Gojo, T. Tuder, G. Walko, M. Holcmann, T. Schöfl, K. Nowikovsky, N. Wilfinger, S. Schoonhoven, C.R. Kowol, R. Lemmens-Gruber, P. Heffeter, B.K. Keppler, W. Berger, Mol. Cancer Ther. 13 (2014) 2436.
[4] V. Oliveri and G. Vecchio, Eur. J. Med. Chem. 120 (2016) 252.
[5] J. P. Mészáros, J. M. Poljarevic, I. Szatmári, O. Csuvik, F. Fülöp, N. Szoboszlai, G. Spengler, É. A. Enyedy, Dalton Trans. 49 (2020) 7977.

INFLUENCE OF *Cannabis sativa* L. ON GUAIACOL PEROXIDASE ACTIVITY IN *Ambrosia artemisiifolia* L.

Konstantinović Bojan[1], Kojić Mirjana[2], Šućur Jovana[3], Samardžić Nataša[1], Koren Anamarija[4], Senka Vidović[5]

[1] University of Novi Sad, Faculty of Agriculture, Department of Environmental and Plant Protection, Trg Dositeja Obradovića 8,21000 Novi Sad, Serbia
[2]PhD grant student of Ministry of education science and technological development, Nemanjina 22-26, 11000 Belgrade, Serbia
[3] University of Novi Sad, Faculty of Agriculture, Department of field and vegetable crops, Trg Dositeja Obradovića 8,21000 Novi Sad, Serbia
[4]Institute of field and vegetable crops, Maksima Gorkog 30, 21000 Novi Sad, Serbia
[5] Univerzity of Novi Sad, Faculty of Technology, Bulevar cara Lazara 1, 21000 Novi Sad, Serbia
e-mail: natasa.samardzic@polj.uns.ac.rs

Abstract

Agricultural research is increasingly focused on finding alternative, biological methods of pest control. It is known that many plant species have allelopathic properties and allelopathy may be one of the mechanisms of biological weed control in the future. Allelopathic substances responsible for biochemical interactions between plants are secondary metabolites of plants. Unlike many pesticides on natural bases present on the market, the number of preparations based on allelochemicals with herbicidal action is insufficient. Therefore, it is necessary to investigate the influence of allelochemicals on weed plant species.

Cannabis sativa L., as a type of confirmed allelopathic properties, has a significant impact on cultivated and weed plant species. Finding allelopathic substances that would have negative effect on *A. artemisiifolia* L. is very important due to its invasiveness. Changes in guaiacol peroxidase activity are one of the indicators of oxidative stress in plants produced by allelochemicals.

Key words: alleopathy, *Cannabis sativa* L., *Ambrosia artemisiifolia* L., guaiacol peroxidase

Introduction

Allelopathy is a relationship between two organisms in wich one organism affects the other positively or negatively with its secondary metabolites [1]. Allelopathic substances can have a significant effect on changing the composition of weed flora but also on crop growth and yield, and can potentially be used as a weed control [2]. The allelopathic properties of different organisms are an important mechanism for the spread of invasive plant species [3]. The lack of coevolutionary tolerance and resistance of autochthonous vegetation to new allelopathic substances produced by introduced invasive weed species can negatively affect the dominant species of autochthonous biocenoses [4]. Although allelopathic interactions of *Cannabis sativa* L. and other plant species have been known for a long time, it is necessary to investigate in detail the mechanisms of action of allelopathic *C. sativa* L. substances on other plant species [5]. *Ambrosia artemisiifolia* L. is a very invasive weed species in Europe and finding new compounds for its suppression is becoming increasingly important [6].

Aim of this study was to determine allelopathy effect of *C. sativa* extract on the activity of guaiacol peroxidase in leaves of *A. artemisiifolia*.

Experimental

In the experiment was used a milled dry plant material of *C. sativa* collected at the ripening stage. Extract was obtained by classic extraction (20g in 200ml water). Applied concentrations of extract was 100%, 50%, 25% and 10%. Plants of *A. artemisiifolia* were treated under field conditions in initial stages. Sampling was performed after 6h and 24h. Fresh leaf samples (2g) were homogenized in 10ml phosphate buffer and then centrifuged. After dissolving 20□l of sample in 3ml of guaiacol solution and 20□l of 1% H_2O_2, absorbance at □=436nm was read, after addition of H_2O_2 at 1min intervals. Activity of guaiacol peroxidase was determined on basis of transformation of guaiacol into tetragvaiacol over 1 minute. The activity was expressed in U/g fresh weight (U/g FW)

Result and discussion

In untreated plant samples, control plants, activity of guaiacol peroxidase was 19,9 U/g FW after 6h, while in variant with application of 100% of the *C. sativa* extract it was 20,7 U/g FW. An experiment variant with 50% *C. sativa* extract activity was 20,8 U/g FW, with a 25% *C. sativa* extract value was 24,5 U/g FW and with a 10% *C. sativa* extract value was 14,1 U/g FW. After 24h, guaiacol peroxidase activity in control variant was 22,5 U/g FW, in variant with 100% *C. sativa* extract was 22,7 U/g FW, with 50% *C. sativa* extract was 24,3 U/g FW, with 25% *C. sativa* extract was 19,5 U/g FW and with 10% *C. sativa* extract was 17,02 U/g FW.
The *C. sativa* applied extract increased guaiacol peroxidase activity after 6h in the treatment with 25%. After 24h guaiacol peroxidase activity were increased in variant with 50% while in variant with 25% and 10% were decreased.

Conclusion

Changes in activity of guaiacol peroxidase indicate the presence of oxidative stress in treated plants of *A. artemisiifolia* compared to control group of plants. Based on the results it can be concluded that *C. satiava* extract, in concentration 25% and 50%, possess a negative effect against *A. artemisiifolia.*

Acknowledgements

This study was carried out with support and financing of Ministry of education, science and technological development of Republic of Serbia.

References

[1] Farooq M., Bajwa A., Cheema S., Cheema Z. Application of allelopathy in crop production, International Journal of Agriculture & Biology, 2013 15, pp 1367-1378

[2] Singh, H.P., Batish, D.R., Kohli, R.K. Allelopathy in Agroecosystems: an overview Journal of Crop Production, 2001, 4(2): 1-41

[3] S. Akhtar, N. Bangash, R. Asghar, M. Munir, N. Khalid, Allelopathic assessment of selected invasive species of Pakistan, Pak. J. Bot., 2014, 46(5): 1709-1713

[4] Hierro, J.L., Callaway, R.M. Allelopathy and exotic plant invasion. Plant and Soil. 2003, 256: 29-39.

[5] J. M. McPartland, *Cannabis* as repellent and pesticide, Journal of the International Hemp Association 1997, 4(2): 87-92

[6] Vladimirov V.,Valkova M., Maneva S., Milanova S. Supressive potential of some perennial grasses on the growth and development of Ambrosia artemisiifolia. Bulg. J. Agric. Sci, 2017, 23 (2): 274-279

STIMULATING EFFECT OF MICROALGAE ON GERMINATION AND INITIAL GROWTH OF RED RADISH (*Raphanus sativus* L. *var. Radicula* Pers.)

Vladimira Seman[1], Timea Hajnal-Jafari[1], Dragana Stamenov[1], Simonida Đurić[1]

[1]Department of Field ang Vegetable Crops, University of Novi Sad, 21000 Novi Sad, Trg Dositeja Obradovića 8, Serbia
e-mail: vladimira.seman@polj.edu.rs

Abstract
Microalgal application in plant producton are becoming promising alternative practice aiming to enhance seed germination performance. Red radish is one of the most commonly eaten vegetables in early spring in Serbia. The effect of two microalgae on red radish germination and growth promotion was tested. Two concentrations (1 and 2%) of *Chlorella sp.* (strains 71 and 72) suspension were prepared. The root and shoot length, weight of fresh biomass and germination percentage were assessed. The highest germination, root and shoot length were determined after *Chlorella sp.* strain 71 treatment with 2% concentrated suspension. Lower concentration of the same microalga led to the highest fresh shoot biomass. Red radish root (+106 %) and shoot length (+27%) were increased by 1 % and 2% *Chlorella sp.* (72) water suspension, respectively.

Introduction
Healthy and good quality product can be obtained by microalgae application while respecting the environment and maintaining soil fertility through the optimal use of resources. Algal biofertilizers contain live or dormant (metabolically inactive) cells. They can be applied to the soil, used for seed priming [1], or foliarly [2]. Plant growth stimulation is achieved throughout microbes mechanisms such as symbiotic associations, biological control (by production of antibiotics, siderophores, volatile substances or parasitism) and by direct delivery of growth hormones to plants [3].
Regarding the use of biofertilisers, recent published works indicate the positive effect of microalgae on seed germination and plant development. Results of [4], showed enhancement of wheat, maize, bean and lettuce growth parameters for 7.9 to 34.2%. The usage of microalgal based biofertilizers enhanced the growth parameters, fruit yield and vitamin C content in tomato plants [5].
Considering that *Chlorella vulgaris* have been successfully applied as a biostimulant to several crops ([6]; [1]; [7]), this microalga was used in our experiment. This study has been undertaken to estimate the ability of two *Chlorella sp.* strains to stimulate the initial plant growth of red radish. Their effect on red radish germination, fresh biomass and length of root and shoot was evaluated.

Experimental
Two strains of single celled green algae *Chlorella sp.* (strain 71 and 72) form Algae Collection, Faculty of Agriculture, University of Novi Sad, Serbia were used for experiment. *Chlorella sp.* has an ellipsoid cell shape, cell size ranging between 4 to 10μm.
Red radish (*Raphanus sativus* L. *var. Radicula* Pers.) seeds (variety Verica, NSSeme, Institute of field and vegetable crops, Novi Sad, Serbia) were sterilized and then germinated on Whatman filter paper in Petri dishes. Sterilized distilled water (dH_2O) was used as control treatment, while *Chlorella sp.* treatments were prepared as 1 and 2 % suspensions, respectively. Algal strains were grown in BG11 medium for three weeks with periodically added fresh medium. Semi-controlled conditions were obtained during algal growth. Day:night photoperiod 14:10, room

temperature (25°C) and aeration with an aquarium air pump (Champion CX-0088) were maintained. Stock cultures were prepared after centrifugation, using fresh algal biomass. Final algal treatments were prepared by dilution of biomass in dH_2O to the concentration of 1% and 2%.

The experiment was carried out in three replications and completed after 12 days. Germination percentage (%), length (cm) and fresh weight (g) of roots and shoots were measured. According to the ISTA [8], 100 grains were used per replicate for germination assay. Four days after sowing, germination (%) was determined. 100 seedlings were placed in thermostat at 28 °C on wet wadding for initial growth measurements. Eighth days after, fresh weight, roots and shoots lengths were measured.

The data were statistically processed using R software (ver. 4.0.2). The significance of the difference between the applied treatments was determined using Fisher's LSD test ($p<0.01$).

Results and discussion

This research showed that microalgal suspensions stimulated red radish germination and initial growth. Measured parameters average values with standard deviations were determined and presented in Table 1.

The results showed that algal water suspension enabled better germination of treated radish seeds. Lower concentration of algal suspensions led to an increase of 4.67-10 % while higher concentration led to 14.33-21.33 % higher germination than the control. Germination increased as the algal suspension concentrations of both strains increased. Microalgae produce a wide array of biologically active compounds responsible for germination related processes improvement [1]. Our results are supported by the results of other researchers. [14] reported that *Chlorella sp.* strain 56, could enhance germination of barley and wheat seeds, respectively. [7] confirmed that 1 and 2 mg/L of *Chlorella sp.* extract significantly increased the germination percentage of beet. Higher dosages of the same extract did not significantly affect the germination. Our data suggested that the algal suspensions positively affected the germination process at both investigated concentrations. [9] also stated that *Chlorella sp.* extract stimulated the germination of cress.

Table 1. Average values of germination (%), root and shoot length (cm) and fresh biomass (g) of red radish seedlings

Treatments	Germination (%)	ROOT				SHOOT			
		Length (cm)	Min. Length (cm)	Max. Length (cm)	Fresh biomass (g)	Length (cm)	Min. Length (cm)	Max. Length (cm)	Fresh biomass (g)
H_2O	69.33%±2.88 ***c***	3.65±0.61 ***c***	0.8	9.3	1.12±0.01 ***e***	3.41±0.28 ***d***	1	6.3	4.68±0.11 ***d***
Chlorella sp. **71 (1%)**	79.33%±7.02 ***ab***	7.52±0.61 ***a***	2.4	11	2.02±0.06 ***bc***	4.48±0.07 ***b***	2.5	6	8.09±0.14 ***a***
Chlorella sp. **71 (2%)**	90.66%±4.16 ***a***	8.12±0.20 ***a***	3.5	15	2.30±0.03 ***a***	5.40±0.11 ***a***	3	9	6.83±0.09 ***c***
Chlorella sp. **72 (1%)**	74.00%±5.29 ***bc***	7.84±0.19 ***a***	3.2	14	1.95±0.04 ***c***	4.81±0.02 ***ab***	3.1	6.4	8.03±0.13 ***a***
Chlorella sp. **72 (2%)**	83.66%±2.52 ***ab***	7.23±0.23 ***a***	2.8	13.4	2.04±0.02 ***b***	4.26±0.02 ***bc***	2.5	5.6	7.52±0.08 ***b***
Fisher's LSD test *	***p***<0.01**; lsd=12.28	***p***<0.01**; lsd=1.13			***p***<0.01**; lsd=0.084	***p***<0.01**; lsd=0.613			***p***<0.01**; lsd=0.356

* Means with Fisher's lsd test results for which statistically significant difference (p<0.01**) occurred are marked in italics (means with the same letter are not significantly different)

Foliar spraying with the 2% *Chlorella sp.* strain 71 suspension led to significantly (p≤0.01) highest values of root and shoot length and fresh root biomass of red radish seedlings. The lowest values were measured in control treatment. Root (+106.08 and +122.40 %) and shoot length (+31.38 and +58.36 %) of red radish seedlings increased by application of 1% and 2% suspensions concentration, respectively.

Increase in growth of shoot was more even than root within each treated group since disparity between the lowest and the highest values of growth parameters was minor for shoot length. However, increase in growth of roots was more intense than of shoot at each treatment.

According to [10], 10% suspension of live *Acutodesmus dimorphus* triggered faster seed germination (2 days earlier) and greater lateral root development (>5) in comparison to 10% and 100% extract of the same microalga. Components such as polysaccharides, amino acids, cytokinins, auxins and gibberellins affect cellular metabolism processes, led to enhance seed germination, seedling growth and stimulate plant vegetative growth ([11]; [12]; [13]). *Chlorella sp.* cell suspension increased the barley and wheat seed growth compared to those of control (sterilized culture medium). The best treatments were 0.06 g/L and 0.23 g/L of algal suspension for the root and shoot lengths of barley and wheat seeds, respectively [14]. [7] reported that concentration of 2mg/L of *Chlorella sp.* extract could enhance plant length of sugar beet by 500%. Higher dosages (>2mg/L) of the same *Chlorella sp.* extract did not negatively affect plant length and root development of sugar beet. They tested five concentrations and every concentration of applied algal formulations provided enhanced root development. [13] gained enhancement of red radish roots fresh weight by application of seaweed (*Sargassum vulgare*) extract at 1 and 2% by about 11.15 and 24.06%, respectively. Fresh weight of shoot was increased by 35.96 and 70.25% over the control treatment, respectively. On the contrary, [15] reported that brown seaweed (*Ascophyllum nodosum*) extract did not affect yield of two broccoli cultivars.

Conclusion

Germination tests using red radish seeds were conducted to test whether algal suspensions could have stimulating effect on the initial phase of plant growth. Both microalgae strains affected root and shoot of red radish seedlings. Changes of root and shoot length were indicators of promising plant growth promotion based on microalgae. The best results were obtained with 2% concentration of *Chlorella sp.* strain 71. Accordingly, this alga proved to be better for further application as an efficient biostimulator on red radish seed germination.

Acknowledgements

This research was supported by the Ministry of Education, Science and Technological Development, Republic of Serbia.

References

[1] L. Tuhy, A. Saeid, K. Chojnacka, Encyclopedia of Marine Biotechnology, 2020, pp. 105.
[2] T. Hajnal-Jafari, V. Seman, D. Stamenov, S. Djuric, Pol J Microbiol. 69 (2020) 235.
[3] B.J.J. Lugtenberg, L.A. Weger, J.W. De Bennett, L.A. Deweger, Curr. Opin. Biotechnol., 2 (1991) 457.
[4] T. Hajnal-Jafari, S. Djuric, D. Stamenov, Zbornik Matice Srpske za Prirodne Nauke, 130 (2016) 29.
[5] N. Abdel-Raouf, A. Al-Homaidan, I. Ibraheem, Afr. J. Biotechnol. 11 (2012) 11648.
[6] A. Dmytryk, and K. Chojnacka, Algae Biomass: Characteristics and Applications, 2018, pp. 115.
[7] I. Puglisi, V. Barone, F. Fragalà, P. Stevanato, A. Baglieri, A. Vitale, Plants, 9 (2020), 675.
[8] International Seed Testing Association (2020): International Rules for Seed Testing, Chapter 2, i–2-44 (52), https://doi.org/10.15258/istarules.2020.02
[9] D. Ronga, E. Biazzi, K. Parati, D. Carminati, E. Carminati, A. Tava, Agronomy 9 (2019) 192.
[10] J. Garcia-Gonzalez, M. Sommerfeld, J. Appl. Phycol.. 28. (2015) 1051.
[11] R. Yusuf, P. Kristiansen, and N. Warwick, Acta Hortic. 958 (2012) 133.
[12] R.W. Khan, U.P. Rayirath, S. Subramanian, N.J. Mundaya, P. Rayorath, D.M. Hodges, A.T. Critchley, J.S. Craigie, J. Norrie, B. Prithiviraj, J. Plant. Growth Regul., 28 (2009) 386.
[13] H.S. Mahmoud, D. Salama, A. El-Tanahy, E. El-Samad, Ann. Agric. Sci. 64 (2019) 167.
[14] B. Odgerel, and D. Tserendulam, Proc. Mong. Acad. Sci. 56 (2017) 26.
[15] T. Lola-Luz, F. Hennequart, M. Gaffney, Agric. Food Sci. 23 (2014) 28.

EFFECT OF SUBTOXIC DOSE, EXTREME LOW FREQUENCY (ELF) ELECTROMAGNETIC FIELD (EMF) TREATMENTS ON LIVER ENZYME CHANGES IN *IN VIVO* TURKEY MODEL EXPERIMENTS

Péter Hausinger and Krisztián Sepp, Andrea Csikós, Marianna Radács, Zsolt Molnár and Márta Gálfi

Institute of Applied Natural Science, Faculty of Education, University of Szeged Hungary, Department of Environmental Biology and Education, Juhász Gyula Faculty of Education, University of Szeged
e-mail: galfi.marta@szte.hu, molnar.zsolt@szte.hu

Abstract
Natural electromagnetic field background radiation in Earth is 20-30 μT, which is a condition in terrestrial evolution. Today, however, in the technosphere-determined environment, intermittent extreme low-frequency electromagnetic fields are predominant. In the present work, we aim to investigate this topic area by *in vivo* systematic study of subtoxic and chronic electromagnetic field exposures in a turkey model.

Introduction
Spontaneous electromagnetic radiation (20–30 μT) showed no significant change in the pre-social time interval of biological evolution provided by terrestrial conditions. Significant changes in natural electromagnetic background radiation in terrestrial habitat were begun in the 20th century with the extensive use of electrical devices. All this resulted in locally increased electromagnetic fields (EMF). A few publications on the study of the biological effects of EMF (radio frequency, microwaves) examine the question of how low frequency (0 and 300 Hz) electromagnetic radiation can affect living organisms, consequently humans [1, 2, 3, 4]. Evidence suggests that cell processes can be influences by EMF, it appears that EMF represent global stress. Changes in animal behaviour occur in response to a variety of electric field types [3]. The effects of noise and extreme low frequency (ELF) EMF are well documented on psychological mood and mental disorders. Many animal and human studies have reported various effects on the central nervous system and cognitive disorders from exposure to electromagnetic fields emitted by mobile phones [5, 6, 7, 8].

Aims
In the present work, we intend to investigate this topic area with *in vivo* model studies of subtoxic and chronic ELF EMF exposures. We place particular emphasis on a more in-depth study of subtoxic effects, with the aim of possibly proving a hypothesis that environmental exposure in the absence of a specific sensor may elicit more extensive response mechanisms.

Methods
Test animals
Adult (♀, certified) turkeys- *Meleagris gallopavo* (b.w.: 5000–5200 g) were included in our studies according to animal care and research protocols (5 animals per group). The turkeys were kept together in the experimental protocol, except for treatment time intervals. Prior to the start of the experiments, the turkeys were conditioned for 1 week. The animals were identified by unique numbering.

Extremely low frequency (ELF) electromagnetic field (EMF) exposures

The exposure was provided by a device capable of producing an intermittent ELF EMF (8 ms energy exposure - 2 ms energy-free pause). During the treatment, the cages were covered with a 200 cm × 80 cm "magnetic blanket". In operating mode, the parameters of the Hungarian electrical service system (U = 220 V, ν = 50 Hz) were provided. Turkeys were treated with ELF EMF exposure at ν = 50 Hz every 8 hours for 20 minutes for 3 weeks after a one-week conditioning period. The treatment protocol was followed by a 5-week regeneration phase, i.e., a treatment-free time zone. The technical safety of the treatments was controlled by the electromagnetic equipment: ME3951A low frequency (NF) analyser, Gigahertz Solutions, Germany, B = 10 μT checked: PCE-EMF823 electromagnetic field was performed with a radio tester (Tursdale Technicale Services Ltd, UK).

In vivo experimental model

The experimental protocol was 9 weeks in which we worked with 5 animals per group. In this time band, the first week after the conditioning period, ELF EMF (U = 230V, ν = 50Hz, B = 10 μT) treatment was performed for 3 weeks (in the treatment group), followed by an additional five weeks in the time band without treatment the evolution of data patterns of regeneration enzymes. Control groups designed for treatments: (AC) absolute control that was not treated; (C +) positive control for which the equipment was set in standby mode; (C-) negative control for which the machine was turned off mode; and (SC) stress control, in which the entire experimental protocol was performed but using an ELF EMF-free blanket. During the experiments, blood samples were taken every seven days (in sterile samples of heparin and citrate from the subclavian vein), toxicity enzyme parameters were determined.

Enzyme measurement

Toxicity parameters of the model animals participating in the experimental protocol were detected by Dialab methods (DIALAB, Austria). For toxicological monitoring, serum biochemical enzyme parameters of blood samples obtained from the subclavian vein: serum aspartate aminotransaminase (AST, EC 2.6.1.1) according to Remaley and Wilding, 1989 [9], serum alanine aminotransferase (ALT, EC 2.6.1.2) according to Matsuzawa et al., 1997 [10], and gamma-glutamyl transpeptidase (γGT: EC 2.3.2.2.) Were measured (3 technical replicates and at least 5 replicates). Data were evaluated with ANOVA.

Results

In our work, our results were related to the absolute control (AC) values, because there was no significant difference within the control system (AC, + C; -C; SC), only discrete modulation, so the results were presented in the average kinetic relations of the AC controls.

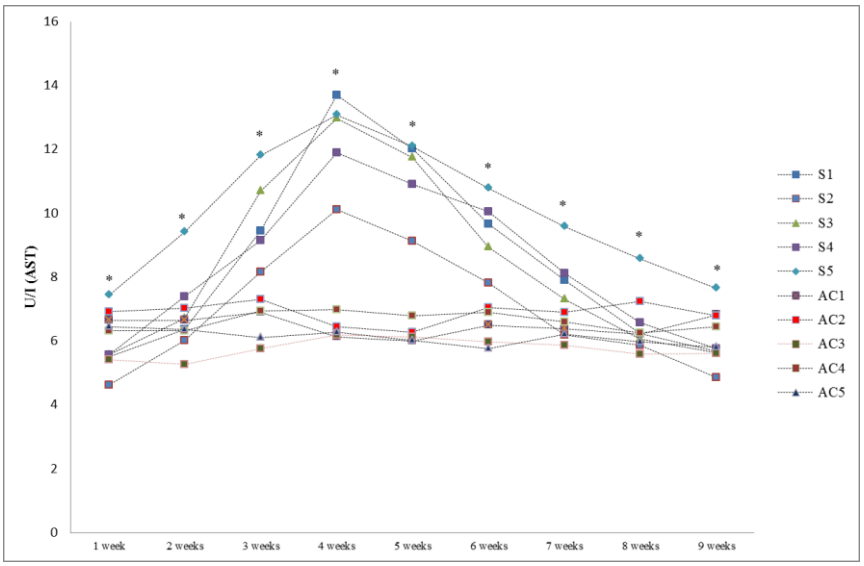

Figure 1. Changes in AST values as a result of ELF EMF treatments and changes in the AST enzyme during the regeneration phase (n=3, S: samples, AC: absolute controls, *: $p<0.05$ /related to ACs/)

It can be seen that the levels of individual AST enzymes were significantly shifted by ELF EMF treatments (2-4 weeks) after the conditioning period (1 week). However, the differences shown did not exceed the limits of normal enzyme levels (normal range: 1-40 U/L). AST enzyme levels returned to baseline during an additional 5 weeks of treatment-free, regenerative experimental period.

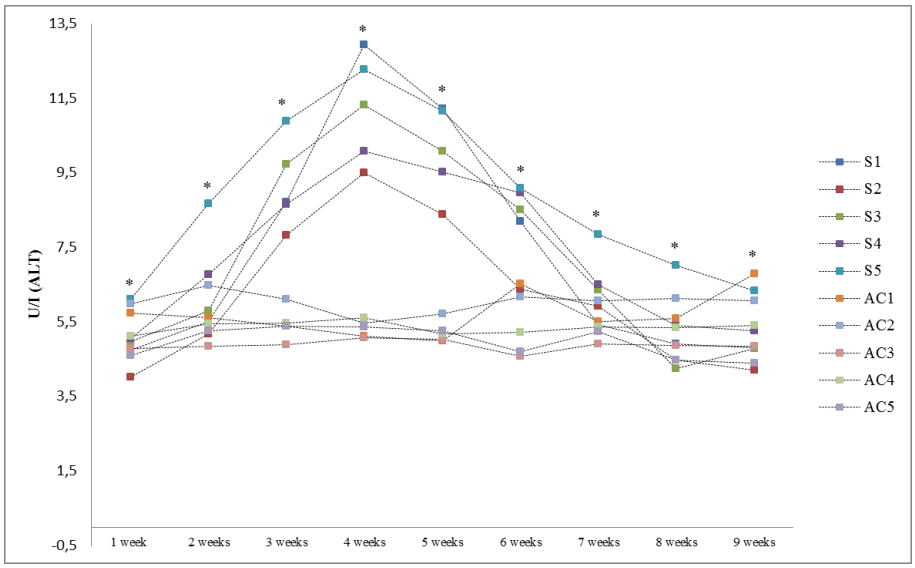

Figure 2. Changes in ALT values as a result of ELF EMF treatments and changes in the level of this enzyme during the regeneration phase (n=3, S: samples, AC: absolute controls, *: $p<0.05$ /related to ACs/)

It can be seen that the individual ALT kinetics were significantly modified by ELF EMF, although they remained within normal physiological range (1-50 U/L). Serum ALT enzyme levels returned to baseline during the treatment-free, regenerative experimental period.

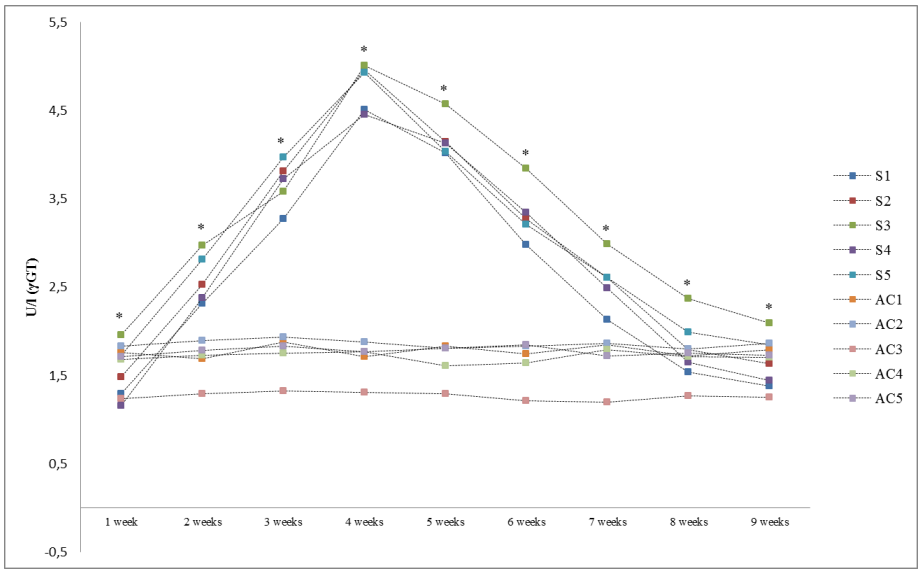

Figure 3. Changes in γGT enzyme levels as a result of ELF EMF treatments and changes in this enzyme level during the regeneration phase (n=3, S: samples, AC: absolute controls, *: $p<0.05$ /related to ACs/)

The figure shows that *in vivo* ELF EMF exposure significantly altered γGT enzyme levels, which returned to baseline levels during the untreated regenerative experimental period. The detected enzyme level changes varied within the physiological normal γGT (1-30U/L), enzyme level limits.

Discussion and conclusion

In our previous studies, we have described that the ELF EMF space altered noradrenaline-activated β-adreneregic receptor functions in the time dimension and dose we used. Because the aim was to study subtoxic doses, we could also describe that liver enzymes indicating toxicity did not leave the normal physiological range. In the present work, however, we specifically investigated whether it is possible to find ELF EMF effects following the individual liver enzyme kinetics within the range of physiological enzyme levels considered to be very broad-spectrum normal.

The presented kinetic curves clearly demonstrate that *in vivo* ELF EMF treatments had a direct effect on the synthesis results of enzymes signaling the functional function of the liver, pancreas, bile, and kidneys. As the ALT / AST ratio was below 1 in all cases, hepatotoxicity could be ruled out, so we performed our studies with truly subtoxic doses.

Acknowledgements

This research was supported by the European Union and the State of Hungary, co-financed by the European Social Fund in the framework of TÁMOP-4.2.4.A/2-11/1-2012-0001 'National Excellence Program', TÁMOP-4.2.6-15/1-2015-0002, TÁMOP-6.1.5-14-2015-0004 and EFOP-3.6.1-16-2016-00008 and EFOP-3.4.3-16-2016-00014.

References

[1] M. T. Santini, G. Rainaldi, P. L. Indovina, Cellular effects of extremely low frequency (ELF) electromagnetic fields. Int. J. Radiat. Biol., 2009, 85,–313.

[2] M., J. Cifra, Z. Fields, A. Farhadi, Electromagnetic cellular interactions. Progr. Biophys. Mol. Biol., 2011, 105, 223–246.

[3] M. Feychting, A. Ahlborn, L. Kheifets, EMF and health. Annual Review of Public HealthAnnual Reviews, 2005, 169-189, Palo Alto.
[4] R. H. W. Funk, T. Monsees, N. Ozkucur. 2009. Electromagnetic effects - From cell biology to medicine. Progress in Histochemistry and Cytochemistry, 2009, 43:177-264.
[5] A. Bellossi, C. Rocher, M. Ruelloux, Exposure of mice to pulsed magnetic fields: long-term observations. In Vivo., 1996, 10, 357-360.
[6] R. M. Berman, M. Narasimhan, G. Sanacora, A. P. Miano, R. E Hoffman, X. S.Hu, D. S.Charney, N. N. Boutros, A randomized clinical trial of repetitive transcranial magnetic stimulation in the treatment of major depression. Biol. Psychiat., 2000, 47, 332-337.
[7] G. A. Boorman, D. L. McCormick, J. C. Findlay, J. R. Hailey, J. R. Gauger, T. R. Johnson, R. M. Kovatch, R. C. Sills, J. K. Haseman, Chronic toxicity/oncogenicity evaluation of 60 Hz (power frequency) magnetic fields in F344/N rats. Toxicol. Pathol., 1999, 27, 267-278.
[8] A. M. Laszlo, M. Ladanyi, K. Boda, J. Csicsman, F. Bari, A. Serester, Zs. Molnar, K. Sepp, M. Galfi, M, Radacs, Effects of extremely low frequency electromagnetic fields on turkeys. Poultry Science, 2018, 97, 634-642.
[9] A. T.Remaley, P. Wilding, Macroenzymes: biochemical characterization, clinical significance, and laboratory detection. Clin. Chem., 1989, 35, 2261–2270.
[10] T. Matsuzawa, Y. Hayashi, M. Nomura, T. Unno, T. Igarashi, T. Furuya, K. Sekita, A. Ono, Y. Kurokawa,. A survey of the values of clinical chemistry parameters obtained for a common rat blood sample in ninety-eight Japanese laboratories. J. Toxicol. Sci., 1997, 22, 25–44.

Curcuma longa L: PULSED ELECTRIC FIELD PRETREATMENT FOLLOWED BY SUBCRITICAL WATER EXTRACTION WITH ADDITION OF ACIDIC MODIFIER

Siniša Simić[1], Jelena Vladić[1], Thomas Fauster[2], Hoang Le Tan[2], Tina Gerhart[2], Henry Jaeger[2]

[1]Faculty of Technology, University of Novi Sad, Novi Sad, Serbia
[2]Department of Food Science and Technology, University of Natural Resources and Life Sciences (BOKU), Vienna, Austria
e-mail: vladicjelena@gmail.com

Abstract
In this study, subcritical water extraction (SWE) was applied to the *Curcuma longa* that was subjected to the pulse electric field (PEF) pretreatments. In addition, to investigate the possibility of improving the stability of curcuminoids and considering that curcuminoids are stable in an acidic environment, the addition of the HCl acid as an extraction modifier was investigated.

Introduction
Turmeric (*Curcuma longa* L.) is a perennial herb widely spread in tropical and subtropical regions of the world. Moreover, turmeric is very common in the food industry and also represents one of the most extensively studied plant species because it possesses a large number of pharmacological activities. It has been proven that turmeric has antiinflammatory, antioxidative, antibacterial, hepatoprotective, neuroprotective, cardioprotective, antidiabetic, and anticancer activities [1,2]. Considering its high pharmacological potential, there is a constant need to improve the techniques for obtaining bioactive components of turmeric. At the same time, it is essential to focus on the quality of products and the impact on the environment.

Experimental
In this study, subcritical (100 - 160°C) as well as liquid (80°C) water extraction with added HCl as a modifier (1%) were applied on turmeric powder to obtain extracts with high polyphenolic content. Additionally, for further improvement of the extraction process, pretreatment with PEF with a specific energy input of 14 kJ/kg and field strength 2 kV/cm was applied. The extraction of the sample that was not pretreated (control) was also performed to determine the efficiency of the applied PEF pretreatment. The content of total phenols and flavonoids in the obtained extracts was determined using spectrophotometric methods, as well as the antioxidant activity of the extracts.

Results and discussion
The obtained PEF-treated turmeric extracts had the content of total phenols in the range from 0.538 to 2.141 mg GAE/mL, and the content of total flavonoids was from 0.168 to 0.492 mg CAT/mL. As the extraction temperature increased, an increase in the content of total polyphenols was noted, therefore, the highest yield of polyphenols was measured at a temperature of 160°C. The 80°C was the lowest extraction temperature at which water had the properties of a polar solvent and achieved the lowest yield of polyphenols. The application of PEF pretreatment had a positive effect on the total content of phenols and flavonoids in all extracts obtained with modified water in the subcritical state.
With an increase in extraction temperature, a rise in the antioxidant activity of the PEF extracts was observed, therefore, the highest antioxidant activity was recorded at a temperature of 160°C (1.38 µL/mL). It has been shown that antioxidant activity of the extracts correlates to the content

of total phenols and total flavonoids. Moreover, the application of PEF pretreatment had a positive effect on antioxidant activity of the extracts obtained at temperatures 100 and 160°C.

Conclusion

PEF demonstrated to be an effective pretreatment for enhancing polyphenolic extraction and, in combination with SWE, it represents a green alternative approach for obtaining turmeric extracts. However, further detailed analyses of the chemical profile of extracts are required, as well as the possible presence of contaminants generated during SWE, to ensure the safe application of the obtained extracts.

Acknowledgements: This work was conducted with the support of the Austrian Academy of Sciences.

References

[1] V. Krup, L.H. Prakash, A. Harini, J. Homeop. Ayurv. Med. 2 (2013), 2167-1206.
[2] L. Labban, Int. J. Pharm. Biomed. Sci. 5 (2014), 17-23.

NANOFILTRATION OF ACID WHEY AFTER ULTRFILTRATION PROTEIN RECOVERY PROCESS

Marjana Simonič[1]

[1]*Faculty of Chemistry and Chemical Engineering, University of Maribor, Smetanova 17, Maribor, Slovenija*
e-mail: marjana.simonic@um.si

Abstract
After the ultrafiltration of acid whey, nanofiltration of permeate was performed. The use of NFT-50 membrane for whey nanofiltration was studied. Whey flux was measured, and fouling potential was determined. Some general chemical parameters of whey were measured. The results showed that chemical parameters decreased after the treatment. Filter cake was formed, and reversible fouling prevailed at 40 bar.

Introduction
Whey has been classified into sweet, which is a by-product of cheese manufacturing, and acid whey from production of fresh and cream cheese, Greek Yogurt and caseinates (Chandrapala, 2016). There is interest in new applications of whey and its derivatives (de Souza, 2010). Lactose represent 5-6 % share in whey and can be used for production of glucose and galactose by hydrolysis.
Disposal of acid whey is complicated due to its high biological oxygen demand as well as high organic matter content (COD) that leads to the need for costly water treatment facilities prior the discharge into the environment. (Chandrapala, 2016). Several methods are available for whey concentrating, such as membrane technologies (de Souza). Most researchers focus on protein fractionation. Two nanofiltration membranes were tested for lactose separation from whey (Cuartas Uribe, 2009). The best results were achieved at 2 mPa at volume dilution factor 2.06, since lactose losses were not high. Fouling problems were not detected for the performed NF tests, however, longer experiments in larger scale plant were suggested to evaluate the economic feasibility of such nanofiltration process.
The main objective of the present research was to study the fouling properties of chosen NFT-50 membrane by separating. The aim of the research was to determine optimal conditions for lactic acid whey nanofiltration using NFT-50 membrane. The results would be used for evaluation of the feasibility of a semi-industrial scale-up. Lactic acid whey permeate would be further tested for skin moisturizing application.

Experimental
Lactic acid whey at 6,32 g/100 g of dry mass (DM) was provided by Slovene dairy factory. The product was stable, stored at 4 ºC. An Osmo Nanofiltration device was used to demineralize lactic acid whey at constant temperature. Membrane NFT-50 (Osmonics) was used with MWCO 150 g/mol, an isoelectric point close to 4.00 and water permeability 2.2 L/(h.m^2.bar). Some membrane properties are seen from Table 1.

Table 1. The NFT-membrane characteristics

Parameter	NFT-50
Producer	Alfa Laval (Sveden)
pressure	1 – 55 bar
T max	50°C
pH	2-10
MWCO	150 Da
Pore	0,43 nm
Kontaktni angle	21°
Morphology	Thin film polyamide
Support	polyesther

Transmembrane pressure (TMP) was varied between 20 and 50 bar. The water permeate flux was checked every time when transmembrane pressure was increased. The chemical analysis of water was performed according to ISO standards in three replicates. The standard methods are gathered in Table 2.

Table 2. The methods used for water analyses

Parameter	Standard method	Apparatus
T (°C)	ISO 10523	Thermometer
pH	ISO 10523	pH-meter, MA 5740
A	SIST EN ISO 7887	Spectrophotometer
Turbidity (NTU)	ISO 2027-1	Turbidity-meter

Reversible fouling Fr was determined after eq.1:

$$Fr = (Jw-Js)/Jw \quad (1)$$

Irreversible fouling *F*ir was determined after eq.2:

$$Fir = (Jw-Jwe)/Jw \quad (2)$$

Where

*J*w = water flux through virgin membrane
*J*we = water flux through membrane after sample filtration
*J*s = sample flux

Models were determined according to Hermia (Salahi et al, 2010). *J* and *J*o are final and initial flux, *K* is constant and *t* time.

Equation (3) regarding complete pore blocking: $\ln(J^{-1}) = \ln(Jo^{-1}) - K.t$ (3)

Equation (4) regarding standard pore blocking: $J^{-0.5} = Jo^{-0.5} - K.t$ (4)
Equation (5) regarding intermediate pore blocking: $J^{-1} = Jo^{-1} - K.t$ (5)

Equation (6) regarding cake layer formation: $J^{-2} = Jo^{-2} - K.t$ (6)

Graphs were drawn where the slope represents constant *K*.

Results and discussion

The UF permeate pH was 4.75, conductivity 7.91 mS/cm and turbidity 886 NTU were determined in untreated whey. Analyses after NFT-50 filtration showed that turbidity decreased to 0.4 NTU to and we assume that fats were mostly removed, pH remained unchanged. Absorbance at 436 nm was completely removed. Measured fluxes are presented in Figure1.

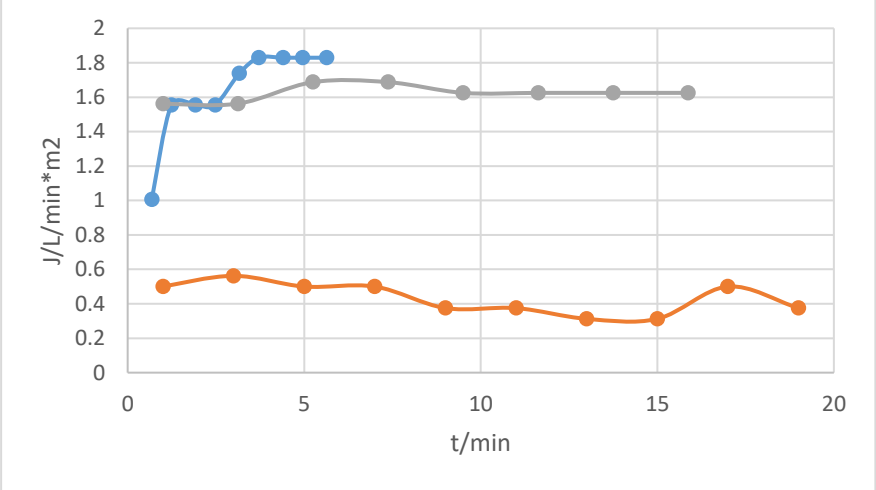

Figure 1. Flux in dependence of time: blue: millipore water, red: whey, green: millipore water after whey

Millipore water flux was determined at transmembrane pressure *TMP* from 20 bar to 50 bar using NFT-50 membrane. The reversible and irreversible fouling were determined at each TMP. The results are presented in Table 3.

Table 3: Reversible and irreversible fouling

***TMP* (bar)**	***Fr***	***Fir***
20	0.61	0.4
30	0.71	0.5
40	0.79	0.11
50	0.72	0.27

It is seen that the lowest irreversible fouling was determined at 40 bar. Therefore, the experiments were continued at 40 bar in order to determine the model of clogging and physico-chemical analyses were performed at the same *TMP*.

Graph was determined according the result of eq. 3-6. Flux in dependence of time was drawn. The constant value K (the slope) while r^2 was the highest with filter cake, therefore only this kind of graph is represented (others not shown). It is seen from Figure 2 that the slope *K* was determined at 0.56 and R^2 equals 0.95.

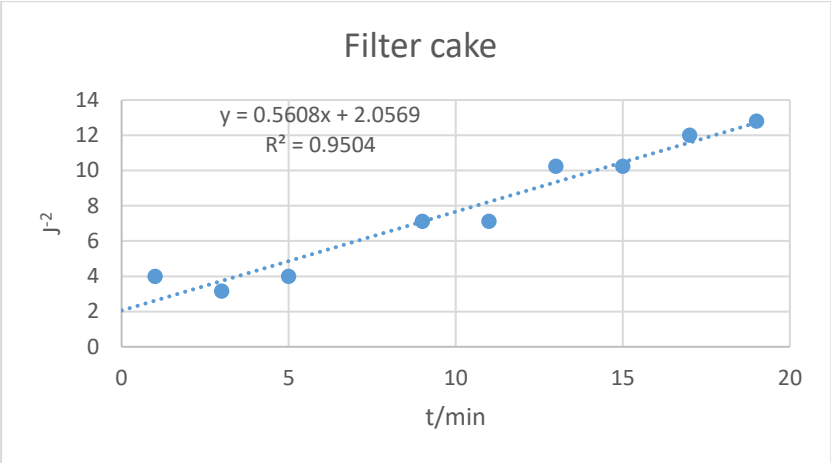

Figure 2. Flux (expressed as J^{-2}) in dependence of time representing filter cake model

The model is in accordance to cleaning: only milli pore water was used for cleaning and the flux of millipore water reached the same level as before nanofiltration started at 40 bar.

Conclusion

NFT-50 could be used in scaling up process in semi-industrial plant. Fouling was determined. The lowest irreverible fouling was observed at TMP 40 bar.

Acknowledgements

The research work was produced within the framework of the project Fractionation and processing of whey proteins and exploitation of the residue for the formation of new functional foods and food supplements (LAKTIKA).

References

[1] B. Cuartas-Uribe, M. Alcaina-Miranda, E. Soriano-Costa, A. Bes-Pia. Comparison of the behavior of Two Nanofiltration membranes for Sweet whey demineralization. Journal of Dairy Science, 90 (2007) 1094-1101.

[2] S. A. Mourouzidis-Mourouzis, A. J. Karabelas. Whey protein fouling of microfiltration ceramic membranes - Pressure effects. Journal of Membrane Science, 282 (2006) 124-132.

[3] J. Chandrapala et al., Nanofiltration and nanodiafiltration of acid whey as a function of pH and temperature, Separation and Purification Technology, 160 (2016) 18-27.

[4] M. Simonič, D. Vnučec. Coagulation and UF treatment of Pulp and paper Mill wastewater in comparison. Central European Journal of Chemistry, 10 (2012) 127–136.

[5] T. Steinhauer, M. Marx, K. Bogendörfer, U. Kulozik. Membrane fouling during ultra- and microfiltration of whey and whey proteins at different environmental conditions: The role of aggregated whey proteins as fouling initiators. Journal of Membrane Science, 489 (2015) 20-27.

[6] Salahi A., Mohsen A., Mohammadi T. Permeate flux decline during UF of oily wastewater: experimental and modeling. Desalination, 251 (2010) 153-160.

[7] Cuartas Uribe B., et al, A study of the separatioon of lactose from whey ultrafiltration permeate using nanofiltration, Desalination, 241 (2009) 244-255.

VOLTAMMETRIC DETECTION OF TETRACYCLINE IN WATER AT BORON-DOPED DIAMOND ELECTRODE

Sorina-Claudia Negrea[1,2], Lidia Ani Diaconu[1], Valeria Nicorrescu[1], Dorian Neidoni[1], Claudia Licurici[2,3], Sorina Motoc (m. Ilies)[4], Florica Manea[3*]

[1] National Institute of Research and Development for Industrial Ecology - (INCD ECOIND)-Timisoara Branch, Bujorilor 115,300431,Timisoara, ecoind.tm@gmail.com, Romania
[2]Department of Environmental Engineering and Management, "Gheorghe Asachi" Technical University of Iasi, Blvd. Mangeron, 67, 700050, Iasi, decanat@chtuiasi.ro, Romania
*[3]Department of Applied Chemistry and Engineering of Inorganic Compounds and Environment, Faculty of Industrial Chemistry and Environmental Engineering, Politehnica University of Timisoara, V. Parvan 6, 300223, Romania, * correspondence author: e-mail: florica.manea@upt.ro, Phone: +40256-403-071; Fax: +40256-403-069*
[4]"Coriolan Dragulescu" Institute of Chemistry Timisoara of Romanian Academy, Mihai Viteazu 24, Timisoara, 300223, Romania

Abstract

In this work a voltammetric based protocol for detection of tetracycline (TC), considered as emergent pollutant in water, was developed. The electrochemical behavior of TC studied by cyclic voltammetry was considered to optimize operating conditions of advanced voltammetric tehniques, e.g., differential-pulsed voltammetry (DPV) and square-wave voltammetry (SWV). The best electroanalytical parameters for TC detection of 2,29 μA/μM sensitivity and limit of detection (LOD) were achieved using SWV under SP of 0.05V, MA of 0.1V and frequency of 10 Hz.

Introduction

According to the Norman Network (2016), over 1000 substances combined in 16 classes (pharmaceuticals, personal care products, pesticides, perfumes) are part of the category of emerging pollutants present in the environment due to the combined effects of both natural processes and human activities [1-3].The presence of emerging pollutants in the environment is due to excessive results of chemicals and/or biological substances used in everyday life, whose toxicity and / or persistence is able to alter the metabolism of a living being. Among the various antibiotics frequently used, more attention is paid to tetracycline, as it presents serious environmental problems, including environmental risks and damage to the human health. Tetracycline (TC) belongs to the main groups of antibiotics used for veterinary purposes, for human therapy and for agricultural purposes. Due to their widespread use, most of the real evidence suggests that tetracycline based antibiotics are ubiquitous compounds found in various ecological compartments [4]. The antibiotic quantification procedure usually involves solid phase extraction (SPE), followed by instrumental analysis usually using liquid chromatography coupled with mass spectrometry (LC-MS / MS), which provides sensitivity, selectivity and reliability of results [5,6]. The disadvantages of conventional methods of detecting emerging pollutants are well known and include increased labor, operating time and high costs in terms of purchasing equipment and reagents needed to carry out the detection method. To complete the list of instruments for the detection of these emerging pollutants, efforts have been made to develop electrochemical methods for the electrochemical detection of TC [7]. Electrochemical methods are powerful and versatile tools that offer high sensitivity, excellent selectivity, fast response, time saving, simple operation and high accuracy in detecting emerging pollutants in water [8]. In this context, it is necessary to develop simple, reliable and fast methods to allow a fast and selective detection of emerging pollutants without high costs. Due to their high

sensitivity, ease of use, short operating time (provides analyte detection in just a few seconds) and the ability to analyze complex samples, the enhancement of electrochemical sensors has attracted great attention in recent decades. The use of electrochemical sensors has become a powerful tool in various fields, such as environmental monitoring, biotechnology and industrial control processes [9]. Also, the electrode material is the key to the performance of electrochemical methods in the detection of emerging pollutants. Due to its remarkable potential window, low background currents and long-term stability, the boron-doped diamond electrode (BDD) is recognized as one of the most versatile electrode materials used in electroanalytical applications [10,11]. The aim of the research study was to develop a detection protocol based on certain voltammetric techniques for the detection of TC in aqueous solution using the boron diamond electrode (BDD). Detection based on the direct oxidation of tetracycline were investigated by cyclic voltammetry (CV), differential pulsed voltammetry and square-wave voltammetry (SWV) techniques.

Experimental

Electrochemical studies were performed using a potentiostat - galvanostat Autolab PGSTAT 302 (Eco Chemie, The Netherlands), controlled by a computer using GPES 4.9 software and a cell with three electrodes. The cell structure includes a boron-doped diamond electrode (BDD) as the working electrode with a diameter of 3 mm, a platinum counter-electrode and a saturated calomel electrode (SCE) as the reference electrode. The BDD electrode was produced by Windsor Scientific Ltd. for electroanalytical use, being a doped polycrystalline industrial diamond polished like a mirror (with a boron content of about 0.1%). All measurements were performed at room temperature without its control. The working electrode was mechanically cleaned using 0.2 μm alumina powder (Al_2O_3) and then washed with distilled water. The support electrolyte of 0.1 M Na_2SO_4 solution was prepared using analytical purity Na_2SO_4 (Merck, Germany) and distilled water. The electrode surface was renewed after each experiment by a light mechanical cleaning, washing and application of an electrochemical treatment by repeating the cyclic scanning voltammetry between 0 and +1.25 V/SCE in the 0.1M Na_2SO_4 support electrolyte. Standard tetracycline solution was prepared using distilled water and 0.1 M NaOH solution (Merck, Germany) in a 1: 1 volume ratio to get a 1 mM TC solution.

Results and discussion

For the elaboration of the tectracycline detection protocol (TC), the electrochemical characterization of the BDD electrode in the present TC using the cyclic voltammetry (CV) technique is studied in a first stage. The electrochemical behavior of the BDD electrode in the presence of TC was studied using CV technique in 0.1 M Na_2SO_4 as support electrolyte to simulate closely the real water composition. Figure 1 shows the cyclic voltammograms recorded for the BDD electrode in the presence of different TC concentrations at the scan rate of 0.05 Vs^{-1}.

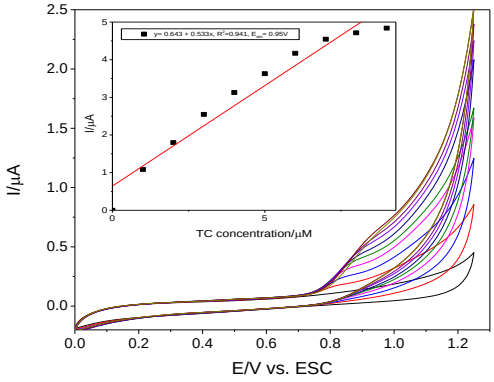

Figure 1. Cyclic voltammograms recorded at the BDD electrode in the 0.1 M Na_2SO_4 solution electrolyte and in the presence of 10-90 µM TC; potential range: 0-1.25 V / SCE. Inset: the calibration plots of the currents recorded at E = +0.95V/SCE vs. TC concentrations

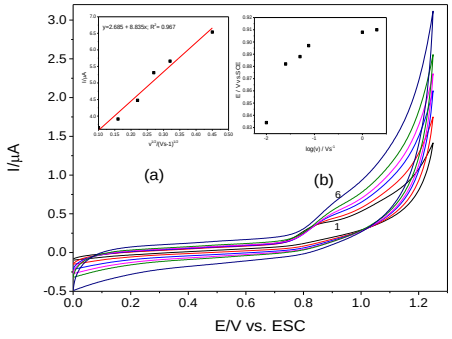

Figure 2. Cyclic voltamograms recorded at the BDD electrode in 0.1 M Na_2SO_4 solution support electrolyte at different scan rates (curves 1-6). Inset: (a) The liniar current dependance vs. the square root of the scan rate; (b) The potential variation vs. scan rate logarithm

It is observed that the oxidation process starts at the potential value of about +0.8 V / SCE at low concentrations, and as the concentration increasing the oxidation potential shifts to more positive values. The oxidation peak current increases with increasing TC concentration, and a linear dependence between the oxidation peak current and the TC concentration was achieved. For concentrations higher than 70 µM clogging the electrode appeared and the oxidation peak current reached a plateau. The cathodic branch of the cyclic voltamogram does not show any peak, which would lead to the hypothesis of the irreversibility of the oxidation process of TC on the BDD electrode. In order to elucidate some aspects related to the mechanism of the TC oxidation process, the influence of the scanning rate on the profile of cyclic voltamograms recorded on the BDD commercial electrode in the presence of 50 µM TC is studied. The evolution of cyclic voltamograms recorded on the BDD electrode at different scan rates (0.01; 0.025; 0.05; 0.075; 0.1; 0.2 Vs^{-1}) is presented in Figure 2. The linear dependence of the anodic peak current recorded in the presence of TC as a function of the square root of the scanning rate suggests that the reaction is controlled by mass transfer, which is promising for electrochemical detection protocol development. Moreover, the shift of the peak potential to a positive potential as the scanning rate increases indicates that the process of electro-oxidation of TC is irreversible (Inset of Figure 2).

Pulsed voltammetric techniques are very suitable for the development of enhanced detection methods, due to their specific characteristics related to the minimization of the background current and the improvement of the faraday component and implicit, the electrochemical response. The use of differential-pulsed voltammetry (DPV) requires to set up the optimal operating parameters, the potential step (SP) which represents the increase of the potential between two consecutive values and the value of the modulation amplitude (MA). Two operating conditions of the DPV technique were tested, MA of 0.1V and 0.2 V, respectively, for the potential step SP = 0.05V.The series of differential pulse voltammograms obtained at different TC concentrations are presented in Figure 3 a and Figure 3 b.

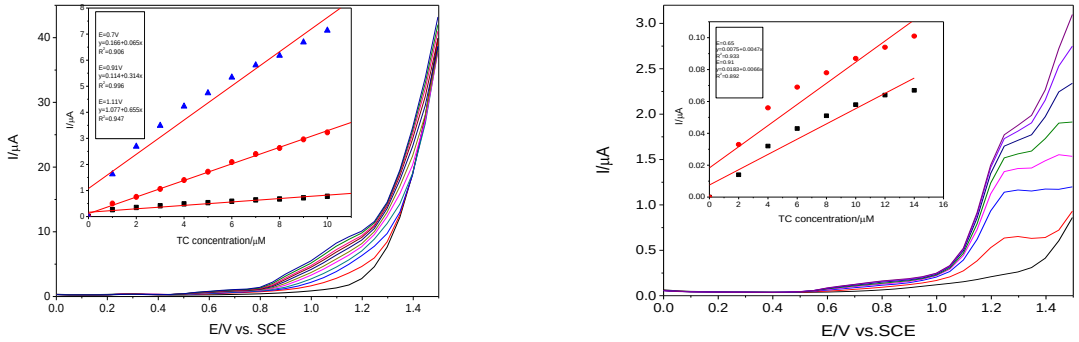

(a) (b)

Figure 3. Differential-pulsed voltamograms recorded under the conditions: SP = 0.05V, v = 0.05Vs^{-1} at the BDD electrode in electrolyte support 0.1 M Na_2SO_4 solution in the potential range: 0 -1.5 V / SCE: (a) MA = 0.1V and in the presence of 1-10 μM TC; (b) MA = 0.2V and in the presence of 1-10 μM TC, Inset: The calibration plots of the currents vs. TC concentrations.

It is noticed that the different operating conditions of DPV lead to modified shapes of the voltamograms. Although voltamograms appear to be better defined and differentiated for MA of 0.2V, however, the best sensitivity is obtained for MA = 0.1 (Figure 3a). Based on the results obtained for these operating conditions, the best results were obtained at the potential step of 0.05 V and the modulation amplitude of 0.1 V, which are better in comparition with CV related to the electroanalytical parameters involving the detection potentials.

Square wave voltammetry (SWV) technique was tested at the both above presented DPV conditions regarding SP and MA for the frequency of 10 Hz. The results are presented in Figure 4 a and Figure 4 b.

For the detection potential value of 1.17 V/SCE the best sensitivity was obtained compared to the previously presented techniques.

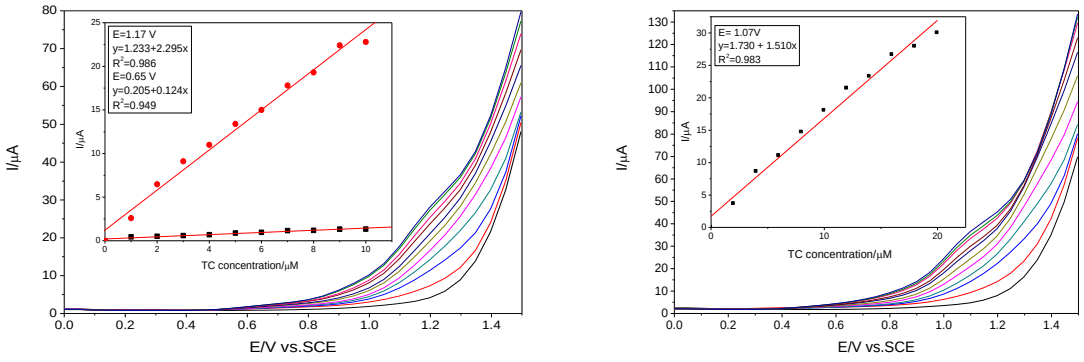

(a) (b)

Figure 4. Square wave voltamograms recorded at the frequency f = 10Hz, having MA = 0.1V, SP = 0.05V, v = 0.5Vs^{-1} at the electrode BDD in the electrolyte support 0.1 M Na_2SO_4 solution in the potential range: 0 -1.5 V / SCE: (a) MA = 0.1V and in the presence of 1-10 μM TC; (b) MA = 0.2V and in the presence of 2-20 μM TC, Inset: The calibration plots of the currents vs. TC concentrations.

The comparative results regarding the electroanalytical parameters (sensitivity, detection limit, quantification limit) obtained for the application of the BDD electrode in the detection of tetracycline using the techniques presented above, are presented in Table 1.

Table 1. Analytical parameters obtained at the BDD electrode using various electroanalytical techniques

Tehnique	***Conditions operating***	**E_{det} (V/SCE)**	***Sensitivity (μA/μM)***	***R^2***	**RSD (%)**	**LOD (μM)**	**LQ (μM)**
CV	v 0.05Vs^{-1} v	1	0.034	0.933	4.47	0.841	2.81
DPV	0.05V SP 0.1V MA	0.7	0.065	0.906	11.4	1.87	6.22
		0.91	0.317	0.996	9.07	0.580	1.94
		1.11	0.655	0.947	11.7	0.849	2.83
	0.05V SP 0.2V MA	0.65	0.004	0.933	5.75	1.69	5.63
		0.91	0.006	0.892	3.83	1.72	5.72
SWV	0.05V SP 0.2V MA, 10Hz f	1.07	1.510	0.983	3.59	0.315	1.05
	0.05V SP 0.1V MA, 10Hz f	0.65	0.124	0.949	5.94	1.30	4.33
		1.17	2.29	0.986	6.43	0.320	1.07

Conclusion

The protocol based on the advanced voltammetric techniques using commercial BDD electrode was proposed for the detection of TC, as emergent pollutant in water. The mechanistic aspects regarding TC oxidation onto BDD were determined using CV technique, which were considered as references for optimizing the detection protocol. The optimization of the operating conditions for DPV, allowed to propose a SWV based protocol which assure a great sensitivity of 2.29 μA/μM and LOD of 0.32 μM TC.

Acknowledgements

The present research was partially finaces by the Romanian National "Nucleu" Program, contract no. 20 N/2019, AA4/2019 (Project code PN 19 04 01 02) and partially by a grant of the Romanian Ministry of Research and Innovation, CNCS - UEFISCDI, project number PD 88/2020, project code PN-III-P1-1.1-PD-2019-0676, within PNCDI III.

References

[1] I. Stefanakis, J. A. Becker, IGI Global, E. McKeown, G. Bugyi (Eds), Impact of Water Pollution on Human Health and Environmental Sustainability, 2015, pp.57.
[2] C. Pena-Guzman, S.Ulloa-Sanchez, K. Mora, R. Helena-Bustos, E. Lopez-Barrera, J. Alvarez, M. Rodriguez-Pinzon**,** J. Environ Manage. 273 (2019) 408.
[3] C. Teodosiu, A. F. Gilca, G. Barjoveanu , S. Fiore, J. Clean. Prod. 197 (2018) 1210.
[4] R. Daghrir, P. Drogui, Environ. Chem. Lett. 11 (2013) 209.
[5] A. Puga, E. Rosales, M. A. Sanroman, M. Pazos, Chemosphere. 248 (2020) 125995.
[6] A. Sultana, K Sazawa, M. S. Islam, K. Sugawara, H. Kuramitz, Anal. Lett. 52 (2018) 1153
[7] Y. Zhou, Y. Yang, D. Zhang, N. Gan, Q. Li, J. Cuan, Sens. Actuator B-Chem. 262 (2018) 137.
[8] M. Ardelean, R. Pode, J. Schoonman, A. Pop, F. Manea, WIT Trans. Ecol. Environ. 216 (2017) 213.
[9] R. Islam, H. T. Le Luu, S. Kuss, Electrochem. Soc. 167 (2020) 045501.
[10] A. Baciu, M. Ardelean, A. Pop, R. Pode, F. Manea, Sensors. 15 (2015) 14526.
[11] A. Pop, F. Manea, A. Flueras , J. Schoonman, Sensors. 17 (2017) 2033.

NATURAL COMPOUNDS FOR *ECO-FRIENDLY* CORROSION INHIBITION OF STEEL PIPELINES

Mariana Nela Ştefănuţ [1*], Adina Cãta [1], Bogdan Ţăranu[1], Paula Sfirloaga[1], Ioana Maria Carmen Ienaşcu [1,2]

[1]National Institute of Research and Development for Electrochemistry and Condensed Matter, Dr. A. P. Podeanu 144, 300569 Timişoara, Romania

**Corresponding author's email address: mariana.stefanut@gmail.com*

[2]"Vasile Goldiş" Western University of Arad, Faculty of Pharmacy, 86 Liviu Rebreanu, 310045, Arad, Romania

Abstract

Steel pipes are used for industrial fluids transport. Extracts with natural compounds from some ***Brassicaceae*** sources showed important anticorrosion effects on steel material. Extracts of broccoli, cabbage, black radish, rapeseed and cauliflower were electrochemically tested in H_2SO_4 0.5M, in a conventional glass three-electrode cell with a Pt counter electrode, saturated calomel (SCE) as reference electrode and steel working electrode (WE). Electrochemical experiments (Tafel curves) were performed with a Voltalab 80 (Radiometer, Copenhagen) equipped with a Volta Master7 software. The potentiodynamic measurements were started at -600 mV cathodic potential to anodic potential +250 mV, at a scan rate 1 mV/s and room temperature. Before each experiment, open circuit (OPC) was applied to WE during 30 minutes.

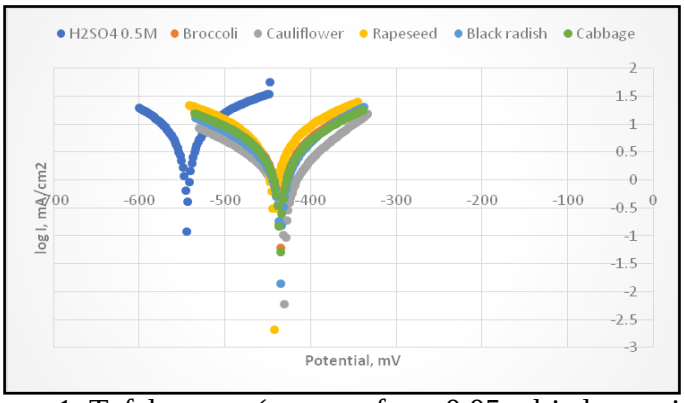

Figure 1. Tafel curves (extracts from 0.05g dried material)

The corrosion rate decreased from 119 mm/year in case of sulfuric acid 0.5M to about 2-7 mm/year when concentrated extracts were used. Surface morphology of WE were studied after work using a SEM method (Scanning Electron Microscope Inspect S + EDAX Genesis XM 2i (FEI, Holland), at HV = 30.00 kV and at magnification 3000, in vacuum mode.

[1] Ngobiri N.C., Oguzie E.E., Li Y., Liu L., Oforka N.C., Akaranta O., Eco-friendly Corrosion Inhibition of pipeline steel using *Brassica Oleracea*, Hindawi Publishing Corporation, International Journal of Corrosion, vol.2015, http://dx.doi.org./10.1155/2015/404139.

ISOLATION OF PHENANTHRENES FROM *JUNCUS ENSIFOLIUS*

Dóra Stefkó[1], Norbert Kúsz[1], Judit Hohmann[1,2], Andrea Vasas[1]

[1] *Department of Pharmacognosy, University of Szeged, Eötvös u. 6, H-6720 Szeged, Hungary*
[2] *Interdisciplinary Centre of Natural Products, University of Szeged, Eötvös u. 6, H-6720 Szeged, Hungary*
e-mail: stefko.dori@gmail.com

Introduction

Juncaceae species are good sources of phenanthrenes. To date, more than 100 phenanthrenes were isolated from ten Juncaceae species, approximately 60 from *Juncus effusus*.[1] As almost all identified phenanthrenes are substituted with vinyl group, these constituents are serve as chemotaxonomic markers. According to the literature data, phenanthrenes possess diverse biological activities (e.g. antiproliferative, antimicrobial, anti-inflammatory and spasmolytic).[1-3] In continuation of our work dealing with the phytochemical and pharmacological investigation of Juncaceae species occur in the Carpathian Basin, *Juncus ensifolius* (swordleaf rush) was chosen with the aim of the isolation of biologically active secondary metabolites, especially phenanthrenes from the plant.

Results and discussion

The dried plant material was extracted with methanol. After evaporation, the extract was dissolved in 50% methanol and then subjected to solvent–solvent partition with *n*-hexane, chloroform and finally with ethyl acetate. Phenanthrenes accumulated in the $CHCl_3$ fraction; therefore, it was separated by a combination of different chromatographic methods, including vacuum liquid chromatography, medium pressure liquid chromatography, gel filtration, and high performance liquid chromatography.
With a combination of different chromatographic techniques, nine compounds were isolated from *J. ensifolius*, eight of them are phenanthrenes. The structures of the pure components were determined by 1D and 2D NMR spectroscopy, and MS measurements. Five compounds are new natural products. All components were isolated for the first time from swordleaf rush.

Conclusion

Phenanthrenes can be valuable chemotaxonomic markers due to their limited occurrence. Our investigation is in progress. After isolation process, the antiproliferative activity of the pure compounds will be tested. The active compounds can serve as starting materials for semi synthetic transformations and further pharmacological investigations.

Acknowledgements

The work was supported by the UNKP-20-3 New National Excellence Program of the Ministry of Human capacities, EFOP 3.6.3-VEKOP-16-2017-00009 and the Economic Development and Innovation Operative Program GINOP-2.3.2-15-2016-00012.

References

[1] C. Bús, B. Tóth, D. Stefkó, J. Hohmann, A. Vasas, Phytochem. Rev. 17 (2018) 833–851.
[2] D. Stefkó, N. Kúsz, A. Csorba, G. Jakab, P. Bérdi, I. Zupkó, J. Hohmann, A. Vasas, Tetraherdron 75 (2019) 116-120.
[3] D. Stefkó, N. Kúsz, A. Barta, Z. Kele, L. Bakacsy, Á. Szepesi, C. Fazakas, I. Wilhelm, I. Krizbai, J. Hohmann, A. Vasas, Journal of Natural Products 83 (2020) 3058-3068.

EVAPORATION FROM CARBON NANOTUBE FOREST: ANALYTICAL POSSIBILITIES OF THE MASS MEASUREMENTS

I. Y. Tóth[1], I. Sütő[1] and Á. Kukovecz[1]

[1]Department of Applied and Environmental Chemistry, University of Szeged, Interdisciplinary Excellence Centre, H-6720, Szeged, Rerrich Béla tér 1, Hungary
e-mail: suto.istvan94@gmail.com (I.S.); ildiko.toth@chem.u-szeged.hu (I.Y.T.)

Abstract
The evaporation of liquids from porous materials is a very complex phenomenon, which can be followed by simultaneous weight monitoring, electric resistance measurement, infrared imaging and contact angel measurement. The appropriate evaluation of these measurement results can carry both quantitative and qualitative analytical information. The aim of our recent work is to demonstrate this opportunity through the example of the evaporation of simple solvents from a carbon nanotube forest. In this work the focus will be on the analytical possibilities of the mass measurements.

Introduction

Recent developments in nanotechnology have highlighted the importance of the classical topics of wetting, droplet spreading and evaporation due to their pronounced effect in technological applications (*e.g.*, air/fuel premixing, micro-fluidics, oil recovery, etc.) [1,2]. Multiple phenomena take place simultaneously when a liquid droplet contacts a porous surface: wetting, spreading, capillary filling, gravity induced convective flow, adsorption, evaporation from the surface, evaporation from the pores, etc. The evaporation of a sessile droplet can be studied by several experimental methods: transmission electron microscopy, environmental scanning electron microscopy, contact angle measurement, high speed camera recordings, thermal imaging, just to name a few. The evaporation of sessile droplets can be followed by an equipment assembled at the Department of Applied and Environmental Chemistry, University of Szeged: this equipment can guide simultaneous weight monitoring, electric resistance measurement and infrared imaging at a controlled temperature (typically at 50 °C). There are several experimental results characteristic for the evaporation process, the most important ones being the total evaporation time, time of evaporation only from the surface, full width at half maximum of the time-dependent mass and resistance curves, evaporation rate, initial area of the droplet, and the wetted area at the moment of total evaporation from the surface, etc. [3-6]. The main goal of this work was to demonstrate the analytical possibilities of the mass measurements through the example of sessile droplet evaporation (water-ethanol mixtures) from a carbon nanotube forest (CNT forest).

Experimental

Materials: The carbon nanotube forest (vertically aligned CNTs) was grown on Si/SiO_2 substrate by 30 minutes of catalytic chemical vapor deposition (CCVD) at 890 °C in a single zone tube furnace from ferrocene/xylene (0.5 g / 25 mL) precursor solution (0.1 mL/min ferrocene/xylene, 44 mL/min Ar).

Methods:

Scanning electron microscopy (SEM) was used for the determination of the general structure and morphology of the prepared carbon nanotube forest. For these measurement a Hitachi S-4700 microscope was used equipped with a field emission gun operated with accelerating voltages of 10 kV.

Liquid droplet evaporation (distilled water - ethanol mixtures) was studied from the CNT forest. The droplets (5 µL, 50 °C) were instilled with an Eppendorf Xplorer electronic pipette on the surface of the solid. The temperature, the electric resistance and weight variations could be simultaneously monitored by the equipment assembled at the Department of Applied and Environmental Chemistry, University of Szeged.

The CNT forest was placed onto a purpose-built sample holder. The setup included a type K thermocouple in contact with the non-wetted part of the solid. The distance between the solid and the heater was 1 cm. Data from the thermocouple was fed back to the temperature controller that maintained a base solid temperature of 50 ± 0.5 °C by continuously adjusting the heater power using fuzzy logic control.

The sample holder was placed on a Sartorius Cubis microbalance with 0.01 mg readability and the weigh variation during droplet evaporation was recorded.

For thermal imaging a FLIR A655sc infrared (IR) camera was used. This unit has a thermal sensitivity of 30 mK, an accuracy of ±2 °C for temperatures up to 650 °C at 640x480 resolution. Its uncooled microbolometer detector has a spectral range of 7.5-14.0 µm. The IR camera is equipped with a 2.9x (50 µm) IR close-up lens, with 32x24 mm field of view and 50 µm spatial resolution. The recorded images are transferred to a PC with FLIR ResearchIR Max software. Sessile droplet evaporation movies were acquired at maximum resolution with 50 Hz frame rate. The CNT forest's emissivity (ε_{film}) was determined by calibration at the initial solid temperature (50 °C) with a black electrical tape (ε = 0.95). During liquid surface evaporation the temperature was determined by taking into account the emissivity of the liquid (ε_L = 0.95); after surface evaporation, the emissivity of the wetted material was calculated as the average between the emissivities of the studied liquid and the CNT forest.

The sample holder plastic plate with the 0.7 cm radius gap in the center was equipped with two copper electrical connections at the opposite edges of the gap on the bottom of the sheet. The copper electrodes were contacted to the source meter by 0.3 mm diameter copper wires. The rigidity of these wires did not affect the balance because of the large inertia of the whole assembly mounted on the balance plate. This was confirmed by independent experiments before the evaporation profile (electrical resistance variation as a function of time) measurements. The computer recorded the electrical resistance of the solid as measured by a Keithley 2612A Source Meter.

Before the measurements, the CNT forest was mounted in the assembly and heating at initial temperature was applied until the sample weight both stabilized. Then all recordings (IR imaging and sample weight) were started a few seconds before dropping. The evaporation was studied by dropping a single droplet of a selected solvent to the center of the solid and simultaneously recording the IR video and the mass until they returned to their original values. The schematics of the equipment is presented in Fig. 1. The ambient air temperature and the relative humidity of the ambient atmosphere were kept constant (at 25 °C and 55 RH%, respectively) [3-6]. In our experiments the weight and IR video were simultaneously monitored, but in this work we will focus only on the results of the mass measurements.

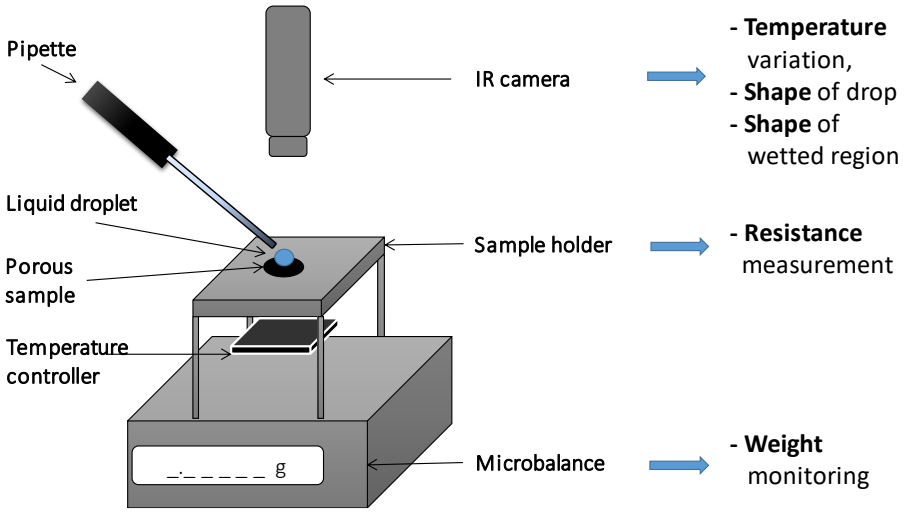

Figure 1. Evaporation monitoring equipment schematic.

Results and discussion

The SEM image of the CNT forest can be seen in Fig. 2. The height of the forest (*i.e.* the length of the vertical alligned carbon nanotubes) is ~1200 µm.

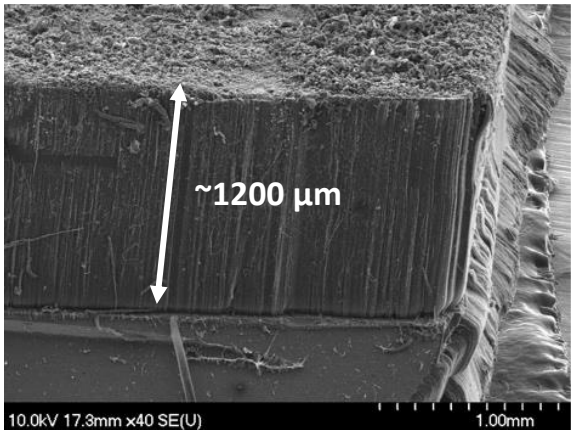

Figure 2. SEM image of the CNT forest.

In general at the moment we drop the liquid on the solid (t_0), the liquid starts to diffuse immediately into the pores, but a part of it remains spread on the surface of the material. The evaporation of this liquid from the surface takes place together with the diffusion. Once all liquid evaporates from the surface, namely the primary surface evaporation is complete (t_s), liquid is left only in the pores. The solvent gradually evaporates from the pores as well. The complete evaporation of the solvent (t_t) was confirmed by the fact that the mass of the solid material returned to the baseline.

One typical mass variation is illustrated in Fig. 3. where t_0 marks the time when the drop was instilled. The mass of the sample increased as soon as the solvent was dropped to the solid and this is followed by a quasi-linear weight decrease. Once the primary surface evaporation is complete (t_s), the mass decreases as linear (within experimental error) functions of time due to the continuous evaporation of the solvent. The total evaporation time (t_t) was at the moment when the mass of the solid returned to the baseline. At the linear weight decreasing ranges, the rate of evaporation (-dm/dt) is constant. The change of -dm/dt value suggests the change of the dominant evaporation process, *e.g.*, evaporation of the droplet sitting on the surface of the solid, evaporation of the condensed water from the porous system or the evaporation of the adsorbed water from the microscopical surface of the porous system (see the linear ranges in Fig. 3.).

From this type of measurement, the typical experimentally determined data are the shape of the curve: m_{max}, area, FWHM; the t_s and t_t, the evaporation rate -dm/dt and its change. These data are characteristic for the measured system and can be used to identify them [3-6].

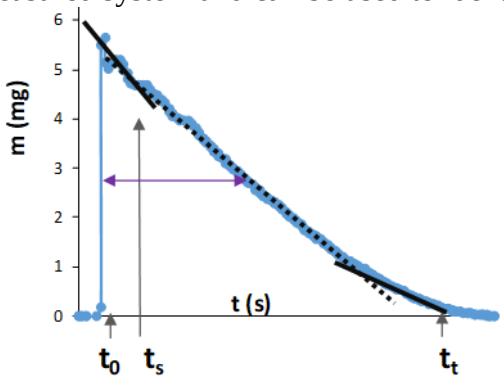

Figure 3. Illustration: weight variation of a representative solid material as a functions of time during the evaporation process.

The evaporation of water-ethanol mixtures from the surface of the CNT forest can be seen in Fig. 4. It is clear that the liquids with ethanol-content evaporate faster than the pure water. Based on the detailed analysis the t_t, the area, the FWHM, the evaporation rate for the condensed water in the porous system and for the adsorbed water can be determined. The t_t and area are plotted as a function of ethanol-content in Fig. 5.

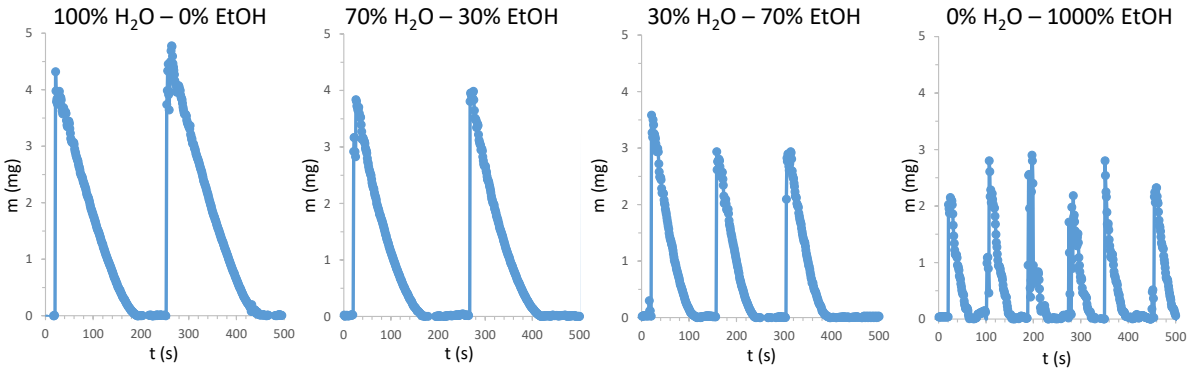

Figure 4. Evaporation of water-ethanol mixtures from CNT forest (5 µL, 50°C).

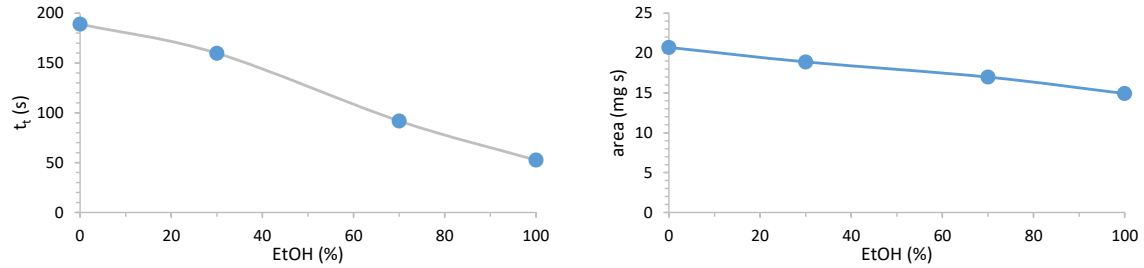

Figure 5. Analytical possibilities of the mass measurements. (Evaporation of water-ethanol mixtures from CNT forest, 5 µL, 50°C.)

Conclusion

The weight monitoring of the evaporation of liquids from porous materials can provide information about the mechanism of wetting and vaporization which is a significant area of the basic researches. Furthermore, it can be proved by using appropriate statistical methods (*e.g.*, matrix of Pearson correlation coefficients, hierarchical cluster analysis, functional analysis,

etc.), that the experimentally determined characteristic values are specific for the physical properties of the solvents, and they are also dependent on the quality of the solid materials, therefore, they can be used for qualitative chemical and quantitative analysis via the estimation of physical properties. The results allow us to presume the possibility of this experimental setup and theoretical approach for a potential future application in the field of analytics.

Acknowledgements
We thank Krisztina Nagy for the technical contribution during the measurements and Imre Szenti for the preparation of the carbon nanotube forest and for the SEM measurement. Financial support from the Hungarian National Research, Development and Innovation Office through the GINOP-2.3.2-15-2016-00013 “Intelligent materials based on functional surfaces−from syntheses to applications” project is acknowledged. I.Y. Toth also acknowledge the support by the János Bolyai Research Scholarship of the Hungarian Academy of Sciences.

References
[1] D. Bonn, J. Eggers, J. Indekeu, J. Meunier, E. Rolley, Mod. Phys. 81(2) (2009) 739−804.
[2] H.Y. Erbil, Adv. Colloid Interface Sci. 170(1-2) (2012) 67−86.
[3] G. Schuszter, E.S. Bogya, D. Horváth, Á. Tóth, H. Haspel, Á. Kukovecz, Mic. Mes. Mat. 209 (2015) 105–112.
[4] E.S. Bogya, B. Szilagyi, Á. Kukovecz, Carbon 100 (2016) 27–35.
[5] Á. Kukovecz, Egydimenziós nanoszerkezetek és hálózataik létrehozása, módosítása és néhány felhasználási lehetősége, MTA értekezés, Szeged, 2018
[6] I.Y. Tóth, L. Janovák, E.S. Bogya, Á. Deák, I. Dékány, A. Rawal, Á. Kukovecz, J. Mol. Liquids 305 (2020) 112826

PRODUCTION OF CNT FORESTS BY A SIMPLE LAYER BUILDING METHOD ON A CONDUCTIVE SUBSTRATE

Anna Szabó[1], Lilla Nánai[1], Zsejke-Réka Tóth[1], Klára Hernádi[1]

[1]Department of Applied and Environmental Chemistry, University of Szeged, H-6720 Szeged, Rerrich Béla tér 1, Hungary
e-mail: szabo.anna@chem.u-szeged.hu

Abstract
The carbon nanotubes (CNTs) play an important role in nanotechnology research today because the CNT have outstanding properties. Many substrates can be used to fabricate carbon nanotube forests (CNT forests); however, it is important that the desired structure is achieved on a conductive substrate, and for these reasons, carbon nanotube forests have been synthetized on a titanium substrate in this research. Environmental protection is highly discussed nowadays, therefore it is necessary to be able to produce CNT forests with less energy investment and cost-effectively. For these reasons, we used dip-coating method, which is a simple process and without heat-treatments step to save energy in achieving the forest structure. Therefore, this research uses a dip-coating method to form a catalyst layer on the surface of the substrate, and to investigate the effect of heat-treatment of the substrate to produce CNT forests directly on the titanium substrate.

Introduction
The CNTs are used in different aera today due to their prominent properties. One type of CNTs is 3D-structured vertically aligned carbon nanotubes (VACNT), often referred to in as CNT forests, which have outstanding electrochemical properties. This structure was first produced in 1996 by a Beijing research team [1]. Nowadays, it is important to produce CNT forests on a conductive substrate, such as aluminum [2], copper [3], and titanium [4] substrates are often used in researched. In addition, it is possible to form a catalyst thin film on the substrate surface with several layer building methods such as spin-coating [5], spray-coating [6], PLD [4], and dip-coating [2], however, it is increasingly important to use a simple method to make forest structure more cost effective. Another important factor is to produce CNT forests directly on the surface of the substrate without the oxide support layer [7], which requires better catalyst adhesion for many substrates and allows the production of CNT forests in fewer steps. In this research, we would like to produce CNT forests on a titanium substrate using a simple layering method such as dip-coating. Then we want to investigate whether it is possible to directly achieve the CNT forest structure on the titanium substrate without the absence of the support oxide layer, and whether the heat-treatment phases used during the layer construction are necessary to fix the catalyst layer on the substrates.

Experimental
During the syntheses, a titanium substrate was used, for which layer building was a simple process, which was dip-coating. The catalyst was Fe- and Co-nitrate mixed in absolute ethanol at a concentration of 0.11 M and the catalyst ink ratio was Fe:Co = 2:3. The substrate was heat-treated in different phases, before and after the catalyst construction, and in some cases an Al-nitrate layer was built on the surface of the substrate due to the formation of the support oxide layer. The samples containing catalyst layer were synthesized by the quartz reactor already containing the sample in a pre-heated tube furnace at 700°C and synthesized at this temperature. The role of the carrier gas in the system was to provide a nitrogen as well as an oxygen free

environment, hydrogen was used to reach the reduction environment, and the carbon source was ethylene.

Results and discussion

In the research, a thin layer was formed on a titanium substrate by dip-coting method based on the parameters described in the experimental section. Before the catalyst layer building, the substrate was subjected to heat-treatment in some cases, to observe whether a native oxide layer formed on the substrate surface during heat-treatment is necessary to achieve the desired structure, and an alumina-oxide layer was also built on the substrate surface to see how these parameters affect the growth of CNT forests.

In addition, in all cases the structure characteristic of the CNT forest appeared on the substrate, even in the case when the heat-treatment did not take place after the substrate or the catalyst. This may be due to the fact that the synthesis took place at high temperatures and it was possible for the iron- and cobalt-nitrate in the reactor to decompose to oxide at the beginning of the synthesis, after which carbon detachment on the catalyst particles may occur. However, in cases where alumina-oxide was present on the substrate surface, the height of the CNT forests was significantly higher and the carbon nanotube forests did not appear uniformly on the substrate, while without support oxide, the CNT forest structure appeared more ordered on the substrate. In the sample without heat-treatment, the height of the CNT forests was only 5 μm, and it should be taken into account that if without heat-treatment is applied at all, in that case the production can be made more cost-effective.

Conclusion

Summarizing it can be concluded that it was possible to produce CNT forests with a simple catalyst layer building method. Also, there is no need for the presence of a support oxide layer on the surface of the substrate, could be produce CNT forests directly on the substrate. In addition, there is no need for a heat-treatment phase to stabilize the catalyst thin film on the surface of the substrate, thus making the production of carbon nanotube forests more cost-effective.

Acknowledgements

SUPPORTED BY THE ÚNKP-20-3-SZTE-557 NEW NATIONAL EXCELLENCE PROGRAM OF THE MINISTRY FOR INNOVATION AND TECHNOLOGY FROM THE SOURCE OF THE NATIONAL RESEARCH, DEVELOPMENT AND INNOVATION FUND.

References

[1] Li, W. Z., Xie, S. S., Qian, L. X., Chang, B. H., Zou, B. S., Zhou, W. Y., et al. (1996). Sci. 274, 1701–1703.

[2] A. Szabó, E. Kecsenovity, Z. Pápa, T. Gyulavári, K. Németh, E. Horvath, K. Hernadi, (2017). Sci. Rep., 7, 9557.

[3] G. Atthipalli, Y. Tang, A. Star, J.L. Gray, Thin Solid Films (2011), 520, 1651–1655.

[4] A. Szabó, P. Andricević, Z. Pápa, T. Gyulavári, K. Németh, E. Horvath, L. Forró, K. Hernadi. (2018). Front. Chem. 6, 1–9.

[5] Ph. Mauron, Ch. Emmenegger, A. Züttel, Ch. Nützenadel, P. Sudan, L. Schlapbach, (2002) Carbon, 40, 1339.

[6] L. Nánai, A. Szabó, T. Gyulavári, J. Budai, K. Hernadi, (2019) Thin Solid Films, 689, 137491.

[7] Noda, S., Hasegawa, K., Sugime, H., Kakehi, K., Zhang, Z., Maruyama, S., et al. (2007). J. Appl. Phys. Part 2 Lett. 46:3.

NANOFILTRATION-ASSISTED REMOVAL OF ACRIFLAVINE FROM AQUEOUS SOLUTIONS

Péter Gyenes[1], Tamás Szabó[1], Alberto Tiraferri[2]

[1] *Department of Physical Chemistry and Materials Science, University of Szeged, Rerrich B. tér 1, Szeged, H-6720, Hungary*
e-mail: sztamas@chem.u-szeged.hu
[2] *Department of Environment, Land and Infrastructure Engineering, Politecnico di Torino, Corso Duca degli Abruzzi 24, Torino, 10129, Italy*

Abstract

Nanofiltration membranes were modified using Layer-by-Layer method. Different number of polycation/graphene oxide bilayers was deposited on the surface of the membranes. The structure of modified membranes was studied under optical microscope. The structure of graphene oxide was investigated using transmission electron microscopy and dynamic light scattering. The experimental properties of modified membranes were determined using acriflavine solution in a bench scale setup. The retention of the membranes increased with an increasing number of bilayers to a point, similar to a saturation curve. The flux of the permeate decreased slightly, converging to a lower limit with increasing number of bilayers. The results show that nanofiltration membranes can be effectively modified using polycation/colloid particle bilayers.

Introduction

The use of pharmaceuticals in the world increases year-by-year. Pharmaceutical products are released in wastewater streams from manufacturing sites. The production and use of a comprehensive portfolio of pharmaceutical products results in wastewater with a complex composition which is difficult to treat to levels in compliance with regulation from industry authorities. Reverse osmosis (RO) and nanofiltration (NF) have proved to be effective in the removal of various pharmaceuticals [1]. Three factors affect the efficiency of RO and NF in the removal of organic compounds (membrane, molecular, and background fluid characteristics) via three main mechanisms: size exclusion, adsorption, and electrostatic repulsion/attraction [2]. The use of acridines as antimicrobial agents was first proposed in 1912, and the first clinical use of these agents already occurred in 1917. Many compounds containing the acridine chromophore were synthesized and tested, and the aminoacridines bound wide use, both as antibacterial agents and as antimalarials, during World War II. The emergence of the penicillins eclipsed the acridines in antisepsis due to the greater therapeutic efficacies of the former. However, with the current massive increases in drug-resistant bacterial infection, new acridine derivatives may be of use[3]. In addition, the topical utilization of aminoacridines in conjunction with directed low-power light offers bactericidal action at much lower doses. This study focuses on the removal of acriflavine, using commecially available NF membranes, in a crossflow setup. We also modified the employed NF270 membranes with carbon nanosheets and studied their effects on the key performance parameters.

Experimental

Graphene oxide was synthesized using modified Hummers method. The resultant graphene oxide suspension was thoroughly dialyzed to remove any impurity that can modify the layer-by-layer deposition.

The membranes were modified using Layer-by-Layer method. The membrane was immersed in poly(diallyldimethylammonium chloride) solution and graphene oxide dispersion 10 minutes each per bilayer.

The membranes were tested in a crossflow experimental setup (Figure 1.) using the model molecule acriflavine. The retention was determined from the absorption of feed and permeate solutions. The flux of the permeate was measured using a measuring cylinder. The experimental setup was operated at 100 psi and 50 liter per hour crossflow. The active area of the membrane was 42 cm^2.

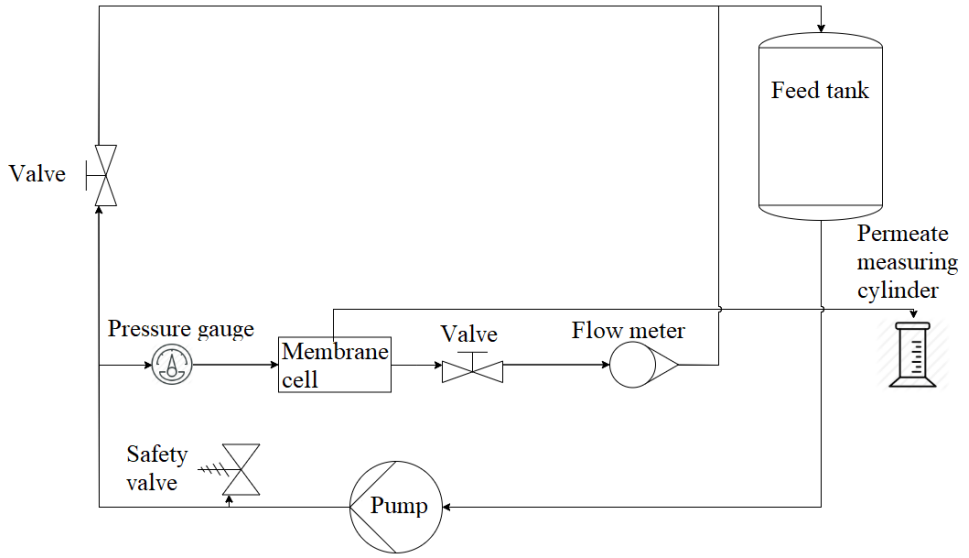

Figure 1. The scheme of the experimental setup

Results and discussion

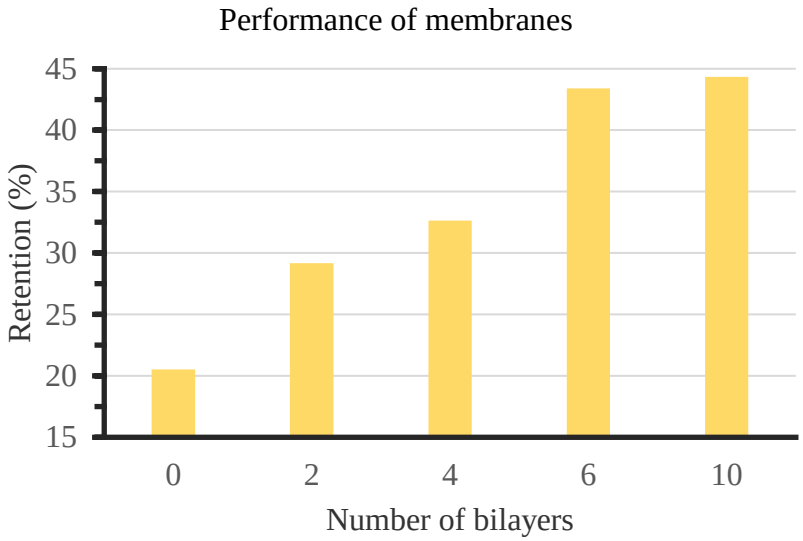

Figure 2. Effect of the number of bilayers on the acriflavine retention of membranes

As Figure 2. shows the Layer-by-Layer modification changed the retention of the membranes in a bilayer number dependent manner. The retention of membranes increases with increasing number of bilayers. After 6 bilayers the retention increase is non-significant. The retention values follow a saturation curve. This shows that the bilayer is not a standard filtration layer, because then it would show an exponential increase.

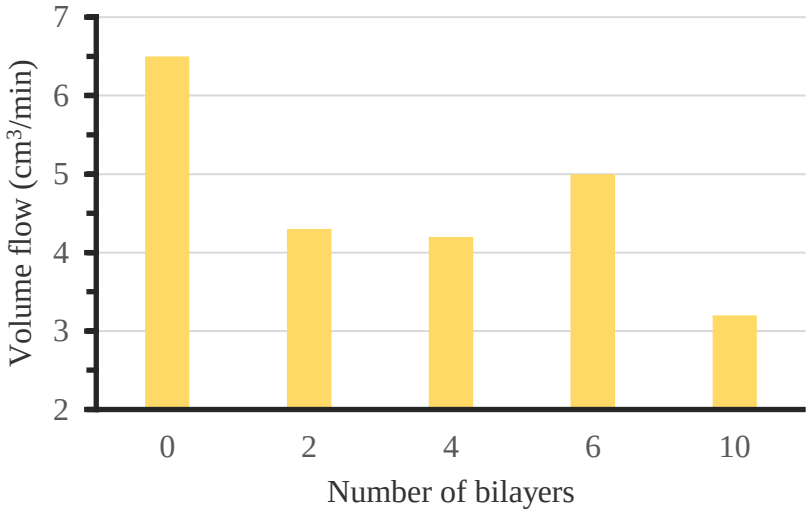

Figure 3. Effect of the number of bilayers on permeate volume flow

The Layer-by-Layer modification decreased the volume flow of the membranes as seen in Figure 3. The volume flow of the membranes decreases with increasing number of bilayers. The volume flow of membrane with 6 bilayers is probably anomalous and too high. The volume flow values converge to a lower limit. Similar to retention values this indicates that this is not a standard filtration layer, because then the trend would be an exponential decrease.

Conclusion

Poly(diallyldimethylammonium chloride)/graphene oxide bilayers increased acriflavine retention and slightly decreased the flux of the permeate. The modified membranes have improved properties for acriflavine removal. The properties of bilayers warrant further research using different polymers/nanoparticles/pH.

Acknowledgements

Project no. 126498 has been implemented with the support provided from the National Research, Development and Innovation Fund of Hungary, financed under the KH funding scheme. T. S. also acknowledges the support by the János Bolyai Research Scholarship of the Hungarian Academy of Sciences (No. BO/00131/19/7) and the support from the ÚNKP-20-5 New National Excellence Program of the Ministry for Innovation and Technology.

References

[1] V. Homem and L.J. Santos, J. Environ. Manag., 92: 2304-2347, **2011**.
[2] B. Van der Bruggen, J. Schaep, D. Wilms and C.J. Vandecasteele, J. Membr. Sci., 156: 29-41, **1999**.
[3] M. Wainwright, J. Antimicrobial Chemotherapy, 47: 1-13, **2001**.

TRANSITION METAL-CATALYZED SYNTHESIS OF 13α-ESTRONE DERIVATIVES WITH POTENTIAL ANTICANCER PROPERTIES

Péter Traj,[1] Ali Hazhmat Abdolkhaliq,[2] Anett Németh,[1] Sámuel Trisztán Dajcs,[1] István Zupkó,[2] Erzsébet Mernyák[1]

Department of Organic Chemistry, University of Szeged, H-6720 Szeged, Dóm tér 8, Hungary[2]
Department of Pharmacodynamics and Biopharmacy, University of Szeged, Eötvös u. 6., H-6720 Szeged, Hungary
e-mail: trajpeter@chem.u-szeged.hu

Abstract
Synthesis of 3-(*N*,*N*-dimethylcarbamoyl)-13α-estrone and its 17-deoxy counterpart has been carried out. The dimethylcarbamoyl directing group enabled the regioselective ortho arylation of the steroidal starting compounds. The microwave-assisted, palladium-catalyzed phenylations led to 2-substituted 13α-estrones in a one-pot, tandem process. The Suzuki-Miyaura cross coupling reactions of the carbamates with phenylboronic acid resulted in 3-phenyl-3-deoxy-13α-estrone. Certain newly synthesized compounds displayed potent antiproliferative action against human reproductive cancer cell lines of gynecological origin.

Introduction
At the beginning of 2000s, the synthetic chemistry has completely changed. In recent years more attention is paid to the principles of green chemistry. Application of halogen-free reagents, effective energy transfer methods and fast catalytic circles displaced the traditional preparative chemical processes. That is why transition metal-catalyzed cross-coupling reactions are becoming increasingly popular [1-4]. These new methods facilitate reactions with higher nuclear efficiency, which were previously available with much lower yields. The combination of transition metal-catalysis with microwave irradiation is a promising approach in the modern synthetic organic chemistry. The major advantages of the microwave irradiation methods are: higher selectivities, lower reaction temperatures and shorter reaction times. Concerning the transition metal-catalyzed cross coupling reactions, phenol esters are increasingly used as electrophile partners instead of aryl halides [5-7]. Phenol esters are of great importance even in the C-H activation processes, depending on the nature of the directing group [8] (Scheme 1.).

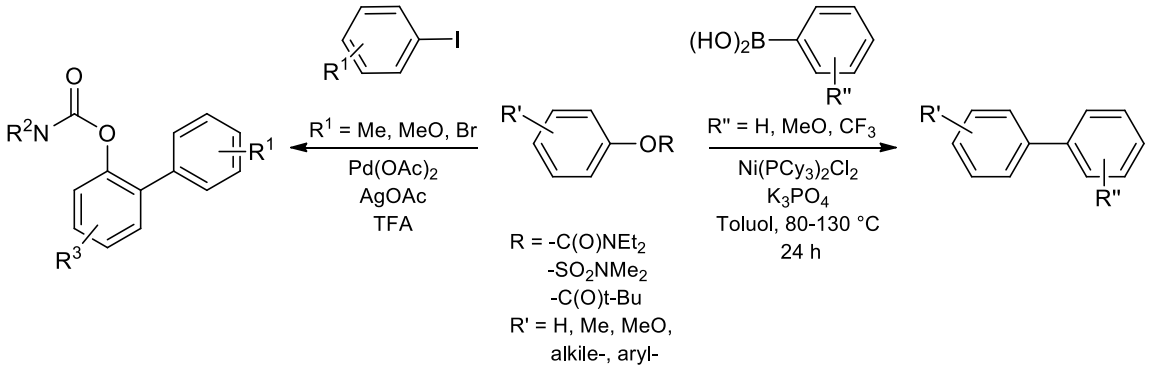

Scheme 1.: Cross coupling and C-H activation reactions of phenol esters.

Aims

The introduction of the *N*,*N*-dimethylcarbamoyl group on the phenolic hydroxy function of 13α-estrone and its 17-deoxy derivative was planned. Transition metal-catalyzed reactions of carbamates were aimed in order to synthesize 2- or 3-phenyl 13α-estrone derivatives. The newly introduced function might serve as a leaving or a directing group in the transformations (Scheme 2.). The determination of the antiproliferative properties of the newly synthesized derivatives against human adherent cancer cell lines was also planned.

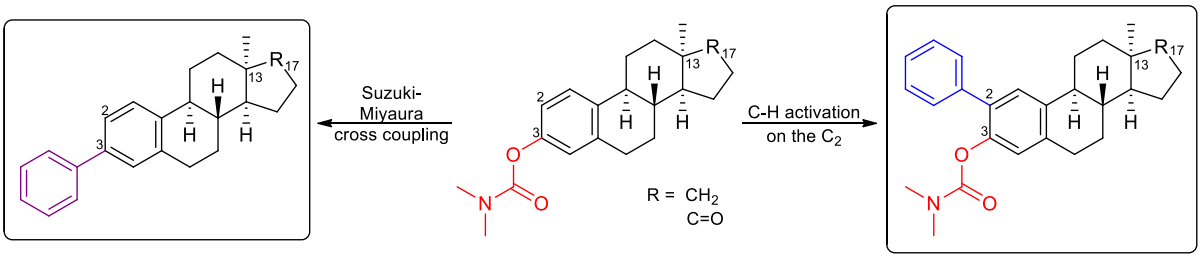

Scheme 2.: Carbamoyl group as a good leaving and directing group in transition metal-catalyzed reactions.

Results and discussion

Firstly, carbamates were synthesized, using *N*,*N*-dimethylcarbamoyl-chloride as a reagent and sodium hydride as a base (Scheme 3.). The reactions were performed at room temperature and the products were isolated with high yields.

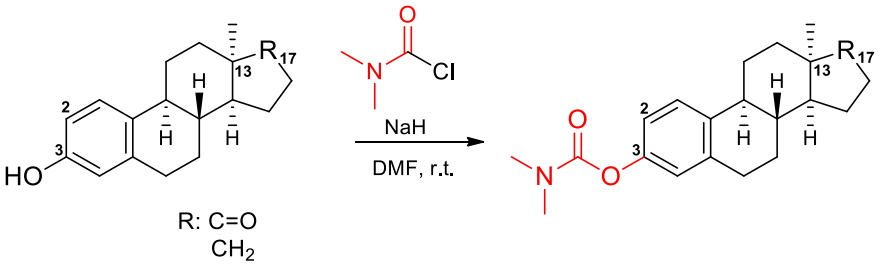

Scheme 3.: Synthesis of the carbamates

As a next step, carbamates were used in Suzuki-Miyaura cross coupling reactions as starting compounds (Scheme 4.). $NiCl_2(PCy_3)_2$ was chosen as a selective and environmentally friendly catalyst. The microwave-assisted couplings of the steroidal carbamates with phenylboronic acid as a reagent furnished the desired 3-phenyl-3-deoxy derivatives in moderate yields.

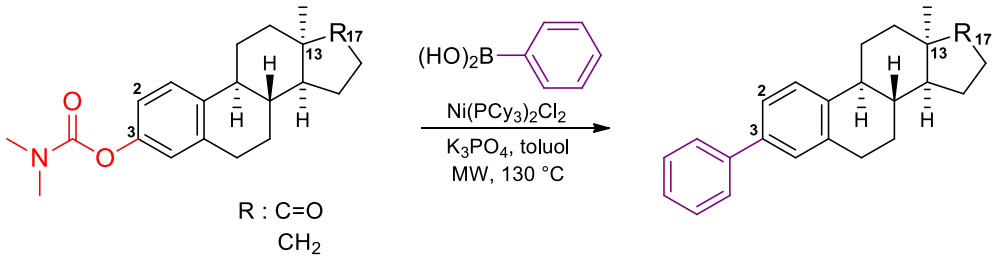

Scheme 4.: Suzuki-Miyaura cross couplings in the 13α-estrone series

As a continuation of our work, the steroidal carbamates were subjected to palladium-catalyzed C-H activation reactions (Scheme 5.). 4-Iodobenzene, 1-iodo-4-methylbenzene and 1-chloro-

4-iodobenzene were chosen as reagents. The reactions were performed in the presence of silver-acetate and trifluoroacetic acid. Application of microwave irradiation led to the formation of the desired products in high yields. Due to the presence of the directing group, ortho substitution occured exclusively at the C-2. Substitution at C-4 was not observed, probably due to the steric hindrance of the B-ring.

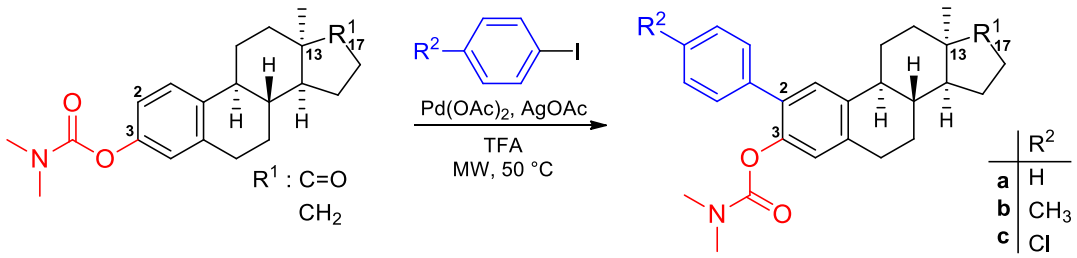

Scheme 5.: C-H activation at the ortho position

The C-H activation and the removal of the directing group could be performed in one step by varying the conditions of microwave irradiation. (Scheme 6.). Literature reveals that the removal of the directing group should be carried out in a further reaction step, thus reducing the efficiency of the process. Our microwave-assisted process allows the introduction of the phenyl group and the cleavage of the directing group in a one-pot, tandem reaction.

The antitumoral properties of the novel 13α-estrone derivatives against a panel of human adherent breast (MCF-7 and MDA-MB-231), cervical (HeLa and SiHa), and ovarian (A2780) cancer cell lines were determined by means of MTT assay. Structure-activity investigations reveal that the antiproliferative action greatly depends of the substitution pattern or A-ring. Certain compounds displayed substantial cell growth-inhibitory actions. The ortho-phenylation overally improved the activity of the 3-modified derivatives.

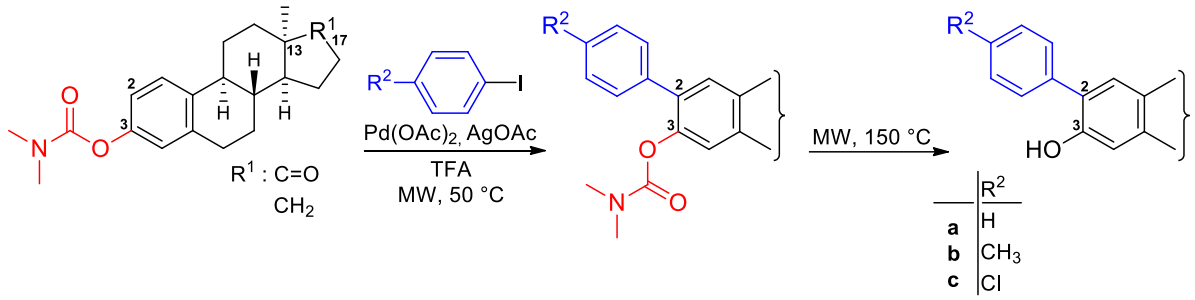

Scheme 6.: Phenylation at C-2 and cleavage of the directing group

Conclusion

In summary, steroid carbamates have been prepared from 13α-estrone and its 17-deoxy derivative. Carbamates proved to be suitable for nickel- and palladium-catalyzed phenylations at C-2 or C-3. Steroidal phenol esters are “greener” alternatives to steroidal aryl halides in cross coupling reactions. We have developed an efficient, microwave-induced, one-pot, tandem C-H activation and deprotection method for the synthesis of biphenyl derivatives starting from phenol carbamates.

Acknowledgements

This work was supported by National Research, Development and Innovation Office-NKFIH through projects GINOP-2.3.2-15-2016-00038 and OTKA SNN 124329. The authors thank for support from the Ministry of Human Capacities, Hungary grant 20391-3/2018/FEKUSTRAT.

The work of Péter Traj was supported by NTP-NFTÖ-19C.

References

[1] C. C. C. J. Seechurn, M. O. Kitching, T. J. Colacot, V. Snieckus, Angew. Chem. Int. Ed., 51 (2012) 5062 –5085.
[2] Guram, A. S.; Buchwald, J. Am. Chem. Soc., 116 (1994) 7901−7902.
[3] Paul, F.; Patt, J.; Hartwig, J. Am. Chem. Soc., 116 (1994) 5969−5970.
[4] Hirao, T.; Masunaga, T.; Ohshiro, Y.; Agawa, T., Tetr. Lett., 21 (1980) 3595−3598.
[5] T. Mesganaw, N. K. Garg, J. Am. Chem. Soc., 17 (2013) 29−39.
[6] K. W. Quasdorf, M. Riener, K. V. Petrova, N. K. Garg,, J. Am. Chem. Soc., 131 (2009) 17748−17749.
[7] K. W. Quasdorf, X. Tian, N. K. Garg, J. Am. Chem. Soc., 130 (2008) 14422–14423.
[8] R. B. Bedford, R. L. Webster, C. J. Mitchell, Org. Biomol. Chem., 7 (2009) 4853-4857.

HYDROGENATION EFFECT ON THE PHOTOVOLTAIC PERFORMANCE OF COPPER OXIDE BASED P-TYPE DSSC

Melinda Vajda[1, 2], Daniel Ursu[1], Cristina Mosoarca[1], Narcis Duteanu[2], Marinela Miclau[1]

[1] *National Institute for Research and Development in Electrochemistry and Condensed Matter, Dr. A. Păunescu-Podeanu Street 144, 300569 Timisoara, Romania*
[2] *Politehnica University Timisoara, Piata Victoriei Street 2, 300006 Timisoara, Romania*
e-mail: melinda.vajda@student.upt.ro

Abstract

Justified by 20% of the theoretically predicted power conversion efficiency (PCE) of DSSCs (dye-sensitized solar cells), along with their low production cost, transparency and flexibility [1,2], an extensive research has been focused on DSSCs. In order to improve the efficiency and to augment the commercialization of DSSC, the idea of tandem-DSSCs has been proposed by its theoretical photon to energy conversion efficiency of over 40% [3]. The development of tandem cells is conditioned by a further progress in *p*-type DSSCs which still have a limited efficiency of ~2%, far below *PCE* of their *n*-type counterparts [4].

Hydrogenation has emerged as a novel approach to effectively modify the properties of crystalline solids, which has been able to introduce important structural changes improving their optical, photocatalytic and electronic properties. Hydrogenation of photoanodes has proved to be an effective method to improve the performance of *n*-type dye-sensitized solar cells (DSSCs). Based on unfavorable assumptions given by the theoretical simulations [5,6], no hydrogenation of photocathodes (nickel, delafossite or copper oxides) and its effect on the conversion efficiency of in *p*-type DSSCs are reported. While the theoretical works have addressed the study of the electronic structure of hydrogenated Cu_2O, our experimental work aims to highlight the features of hydrogenated Cu_2O/dye interface which are critical in DSSC and still unexplored. We report the beneficial effect of hydrogen in Cu_2O on anchoring of the dye leading to an improvement by 98% for J_{SC} and thus, improving the solar energy conversion efficiency of *p*-type DSSC. Even in 2% H_2 atmosphere, the significant increase in J_{SC} had demonstrated the suitability of hydrogenation in the case of *p*-type semiconductors as an effective and low-cost way to augment the efficiency of *p*-DSSCs.

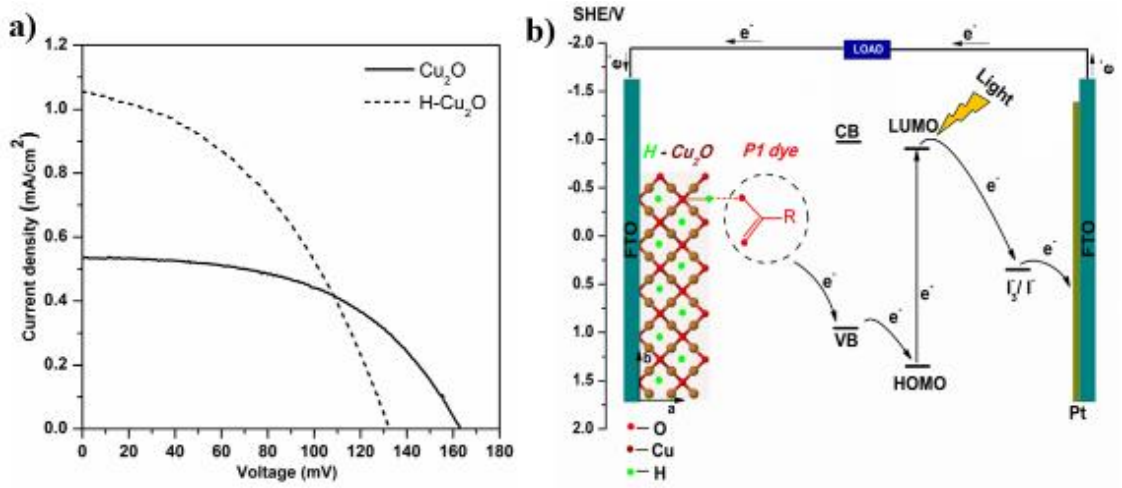

Figure 1. a) J-V curve of the *p*-type DSSC based on Cu_2O and H-Cu_2O photocathodes; b) Schematic energy diagram of the DSSC composed of the H-Cu_2O photoelectrode on FTO, a Pt counter electrode, P1 dye and the I_3^-/I^- redox couple**.**

Acknowledgements
This work was supported by a grant of the Romanian National Authority for Scientific Research and Innovation, the project number PN 19 22 01 03, within PNCDI III.

References
[1] H.J. Snaith HJ. Advanced Functional Materials, 20 (2010)13-19.
[2] A. Hagfeldt, G. Boschloo, L. Sun, L. Kloo, H. Pettersson, Chem Rev.110 (2010) 6595–6663.
[3] F. Odobel, Y. Pellegrin, E.A. Gibson, A. Hagfeldt, A.L. Smeigh, L. Hammarström, Coordination Chemistry Reviews, 256 (2012) 2414-2423.
[4] F. Odobel, L. Le Pleux, Y. Pellegrin, E. Blart, Acc Chem Res. 43 (2010) 1063-1071.
[5] D.O. Scanlon, G.W. Watson, Phys Rev Lett. 106 (2011) 186403.
[6] A. Larabi, A. Mahmoudi, M. Mebarki, M. Dergal, Condensed Matter Physics. 22 (2019) 23702.

SYNTHESIS OF BILE ACID AMINES VIA MICROWAVE IRRADIATION

Vasiljević Bojana[1], Jovana Prekodravac[1], Dragana Jovanović[1]

[1] *Vinča Institute of Nuclear Science-National Institute of Republic of Serbia, University of Belgrade, Belgrade, Serbia*
e-mail: bojana.vasiljevic@vin.bg.ac.rs

Abstract
Herein, we present microwave-assisted reductive amination of oxo derivative of deoxycholic acid with morpholine in the presence of sodium-cyanoborohydride. These chemical transformation produces a majority of the 3β-amino isomer **5** as a new compound after five minutes of irradiation. In addition, formylated bile acid have been proved as excellent starting material for the synthesis of bile acid`s *N*-morpholino amine. Microwave-assisted reactions of formylation in the absence of catalyst, selective deformylation, as well as further oxidation with N-bromosuccinimide gained 3-oxo derivatives of deoxycholic acid acid in high yield. Compared to the conventional protocol a remarkable reduction in overall processing time from hours to a few minutes was achieved.

Introduction
Microwave-assisted organic synthesis has revolutionized organic chemistry [1]. These new technique is considered as an important approach toward green chemistry, medicinal chemistry and drug development, since small molecules can be built in a fraction of time required by conventional heating methods [2].
In the chemistry of bile acids there are significant advantages in the replacement of hydroxyl group by amino functionality [3]. Till date various aminosterols have been discovered, but their synthesis usually need longer heating time and tedious apparatus setup, which resulted in the higher cost of the process and the excessive use of solvents [4-6]. Only few reports on the use of microwave irradiation in chemistry of bile acids confirmed its efficiency in synthesis of various bile acids derivatives [7]. Furtheremore, synthesis of bile acids oxo derivatives as well as insertion of protecting groups presents one of the time consuming steps in organic synthesis. The acetyl protecting group has generally been more widely used than any other function-protecting group due to its stability in various reaction conditions and its ease of removal. However, reactions of acetylation are usually accompanied with unpure products and demand for further purification. Neverthelles, formylated bile acid have been proved as excellent starting material for the synthesis of different bile acid derivatives [8,9]. Taking that under consideration our goal is in investigating and expanding microwave technology in the chemistry of bile acids.
Herein we reported the synthesis of new bile acid amine, 3β-(*N*-morpholino)-12α-hydroxy-5β-cholanoic acid, via fast and efficient microwave irradiation. In-core microwave heating lead to pure formylated and partially deformylated 3α,12α-dihydroxy-5β-cholanoic acid (deoxycholic acid, DCA).

Experimental
All reagents and solvents were obtained from commercial suppliers and used without further purification. Microwave-assisted reactions were carried out in a CEM Discover BenchMate single-mode microwave reactor (300 W max magnetron power output) in 10 mL sealed process Pyrex vials with magnetic stirring. Reaction temperatures were monitored by an external infrared (IR) sensor. Reaction cooling is performed by compressed air automatically after the heating period has elapsed. Reactions were monitored by thin layer chromatography (TLC) on

silica gel plates (Silica gel 60 F_{254}). Purification of products was carried out by flash column chromatography using Kieselgel 60 (0.040-0.063, Merck). NMR spectra were recorded on a Bruker AC 250 E spectrometer operating at 250 MHz (^{1}H) and 62.5 MHz (^{13}C). Chemical shifts are expressed as ppm downfield from TMS using $CDCl_3$ as solvent. All organic extracts were dried with anhydrous Na_2SO_4. Organic solutions were concentrated in a rotary evaporator under reduced pressure at a bath temperature above 30 °C.

3α,12α-diformyloxy-5β-cholanoic acid 1

Starting compound 3α,12α-dihydroxy-5β-cholanic acid (500 mg, 1.27 mmol) and metanoic acid (2 mL, 52 mmol) were placed into a 10 mL microwave process vial equipped with a magnetic stir bar. The reaction mixture was heated in a microwave reactor at 60 °C for 30 min. After the reaction time elapsed, reaction mixture was cooled by gas jet cooling. Acetic anhydride was then added dropwise until a large quantity of bubbles appeared. The solution was then poured into 50 mL of cold water with stirring and the reaction product was extracted with chloroform (3 x 20 mL). After removing the solvent under *vacuo*, the TLC chromatography (chloroform : acetone = 6 : 4) confirmed high purity of compound **1**, as white crystals (562 mg, 98 %).
1H NMR ($CDCl_3$, δ, ppm): 0.75 (s, 3H, CH_3-18); 0.83 (d, 3H, CH_3-21); 0.93 (s, 3H, CH_3-19); 1.09-2.40 (m, 27H, CH, CH_2); 4.83 (m, 1H, H-3); 5.25 (s, 1H, H-12); 8.04 (s, 1H, CHO-3); 8.14 (s, 1H, CHO-12). 13C NMR ($CDCl_3$, δ, ppm): 12.33 (CH_3-18); 17.43 (CH_3-21); 22.92 (CH_3-19); 23.43, 25.74, 25.89, 26.47, 26.77, 27.34, 30.47, 30.87, 32.09, 34.02, 34.20, 34.66, 34.77, 35.60, 41.73, 45.01, 47.35 and 49.25 (C-1, C-2, C-4, C-5, C-6, C-7, C-8, C-9, C-10, C-11, C-13, C-14, C-15, C-16, C-17, C-20, C-22, C-23); 74.10 (C-3); 76.49 (C-12); 160.56 (CHO-3); 160.69 (CHO-12); 179.78 (CO_2H).

12α-formyloxy-3α-hydroxy-5β-cholanoic acid 2

To a stirred solution of 3α,12α-diformyloxy-5β-cholanoic acid **1** (100 mg, 0.22 mmol) in acetone (1.12 mL) was added 0.2 M NaOH (0.48 mmol, 2.4 mL) dropwise. The reaction mixture was heated in a microwave reactor at 60 °C for 5 min. After the reaction time elapsed, the solution was cooled by gas jet cooling and acidified with dilute acetic acid (13 µL glacial acetic acid in 102 µL of water). The reaction product was extracted with chloroform (3 x 20 mL). After removing the solvent under *vacuo*, the TLC chromatography (chloroform : acetone = 6 : 4) confirmed high purity of compound **2**, as white crystals (89 mg, 95 %).
1H NMR ($CDCl_3$, δ, ppm): 0.75 (s, 3H, CH_3-18); 0.83 (d, 3H, CH_3-21); 0.91 (s, 3H, CH_3-19); 1.12-2.39 (m, 28H, CH, CH_2); 3.59 (m, 1H, H-3); 5.24 (s, 1H, H-12); 8.12 (s, 1H, CHO-12).

12α-formyloxy-3-oxo-5β-cholanoic acid 3

Solution of 12α-formyloxy-3α-hydroxy-5β-cholanoic acid **2** (0.25 mmol, 103 mg) in *t*-butanole (2 mL) and solution of *N*-bromosuccinimide (0.46 mmol, 82 mg) in water (1 mL) were placed into a 10 mL microwave process vial equipped with a magnetic stir bar. The reaction mixture was heated in a microwave reactor at 80 °C for 1 min. When the reaction time elapsed, reaction mixture was cooled by gas jet cooling. After removing the most of *t*-butanole under *vacuo*, the reaction product was extracted with chloroform (3 x 20 mL). TLC chromatography (chloroform : acetone = 6 : 4) confirmed high purity of compound **3**, as white crystals (95 mg, 92 %).
1H NMR ($CDCl_3$, δ, ppm): 0.79 (s, 3H, CH_3-18); 0.84 (d, 3H, CH_3-21); 1.01 (s, 3H, CH_3-19); 1.17-2.17 (m, 27H, CH, CH_2); 5.29 (s, 1H, H-12); 8.13 (s, 1H, CHO-12). 13C NMR ($CDCl_3$, δ, ppm): 12.38 (CH_3-18); 17.44 (CH_3-21); 22.27 (CH_3-19); 23.41, 25.36, 26.08, 26.39, 27.31, 30.45, 30.87, 34.27, 34.54, 34. 77, 35.33, 36.58, 36.89, 42,17, 43.95, 45.07, 47.37 and 49.21 (C-1, C-2, C-4, C-5, C-6, C-7, C-8, C-9, C-10, C-11, C-13, C-14, C-15, C-16, C-17, C-20, C-22, C-23); 160.47 (CHO-12); 179.65 (CO_2H); 212.93 (C-3).

12α-hydroxy-3-oxo-5β-cholanoic acid 4

Starting compound 12α-formyloxy-3-oxo-5β-cholanoic acid **3** (0,38 mmol, 150 mg) and 0.2 M NaOH (0.77 mmol, 3.84 mL) were placed into a 10 mL microwave process vial equipped with a magnetic stir bar. The reaction mixture was heated in a microwave reactor at 60 °C for 2 min. After the reaction time elapsed, reaction mixture was cooled by gas jet cooling and poured into dilute acetic acid (13 μL glacial acetic acid in 102 μL of water). The reaction product was extracted with chloroform (3 x 20 mL). TLC chromatography (chloroform : acetone = 6 : 4) confirmed high purity of compound **4**, as white crystals (104 mg, 74 %).

1H NMR ($CDCl_3$, δ, ppm): 0.67 (s, 3H, CH_3-18); 0.96 (d, 3H, CH_3-21); 1.21 (s, 3H, CH_3-19); 1.26-2.75 (m, 27H, CH, CH_2); 4.01 (s, 1H, H-12); 5.97 (br s, 2H, OH i CO_2H). 13C NMR ($CDCl_3$, δ, ppm): 12.59 (CH_3-18); 17.11 (CH_3-21); 23.49 (CH_3-19); 26.40, 27.36, 28.66, 29.17, 29.54, 30.60, 31.61, 32.70, 33.60, 35.53, 36.70, 42.13, 44.14, 46.40, 48.18, 53.68, 36.91 and 54.81 (C-1, C-2, C-4, C-5, C-6, C-7, C-8, C-9, C-10, C-11, C-13, C-14, C-15, C-16, C-17, C-20, C-22, C-23); 73.22 (C-12); 178.77 (CO_2H); 213.97 (C-3).

3β-(*N*-morpholino)-12α-hydroxy-5β-cholanoic acid 5

Starting compound 12α-hydroxy-3-oxo-5β-cholanoic acid **4** (0.97 mmol, 380 mg), MeOH (2 mL), morpholine (9.74 mmol, 0.843 mL), sodium-cyanoborohydride (5 mmol, 0.314 g) and glacial acetic acid (100 μL) were placed in a 10 mL microwave process vial equipped with a magnetic stir bar. The reaction mixture was heated in a microwave reactor at 100 °C for 5 min. After the reaction time elapsed, reaction mixture was cooled by gas jet cooling. The reaction mixture was added saturated solution of $NaHCO_3$ and then extracted with methylene chloride (3 x 20 mL). The residue was purified by flash column chromatography affording pure compound **5**, as white crystals (140 mg, 31 %).

1H NMR ($CDCl_3$, δ, ppm): 0.68 (s, 3H, CH_3-18); 0.97 (s, 3H, CH_3-19); 0.99 (d, 3H, CH_3-21); 1.01-1.80 (m, 24H, CH, CH_2); 2.0-2.3 (1H, H-3 i 2H, CH_2-23), 2.4-2.5 (m, 4H, CH_2NCH_2), 3.60-3.80 (m, 4H, CH_2OCH_2); 3.99 (s, 1H, H-12); 6.30 (br s, 2H, OH and CO_2H).

13C NMR ($CDCl_3$, δ, ppm): 12.77 (CH_3-18); 17.48 (CH_3-19); 21.21 (CH_3-21); 22.61, 23.66, 23.68, 23.78, 26.19, 27.32, 27.51, 28.69, 28.91, 30.38, 31.82, 33.58, 34.07, 34.67, 35.38, 36.05, 36.74 (C-1, C-2, C-4, C-5, C-6, C-7, C-8, C-9, C-10, C-11, C-13, C-14, C-15, C-16, C-17, C-20, C-22, C-23); 50.63 (CH_2NCH_2); 59. 89 (C-3); 67.29 (CH_2OCH_2); 73.36 (C-12); 180.34 (CO_2H).

Results and discussion

The significance of hydroxyl-protected groups in the chemistry of bile acids turned our attention to finding more appropriate and greener reactions conditions for synthesis of bile acid formates. Herein, we developed a simple method of formylation, that involves heating of bile acid in methanoic acid under microwave irradiation (Scheme 1).

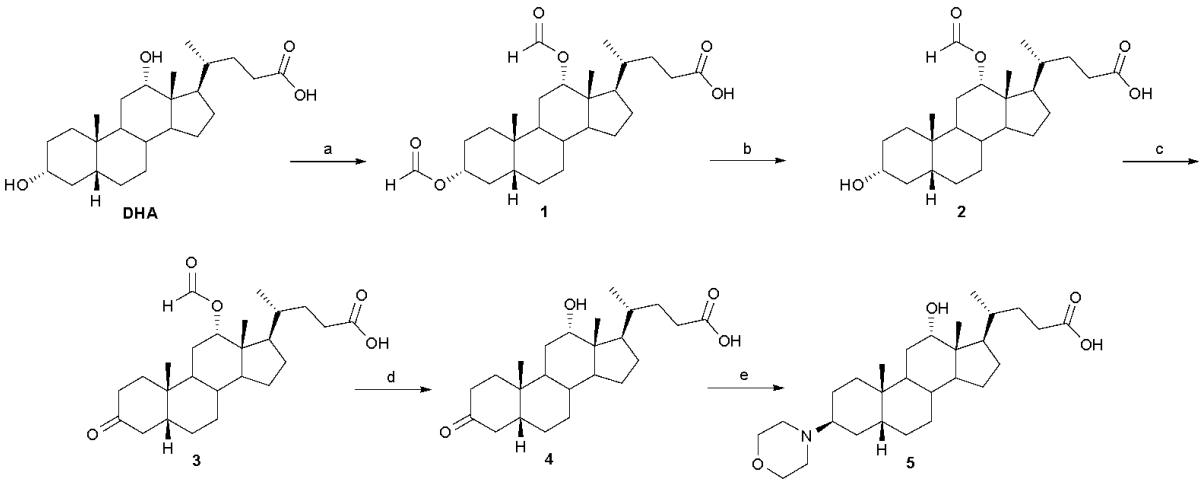

Scheme 1 Reagents and conditions: MW (a) HCOOH, , 60 °C, 30 min, 98 % (b) 0.2 N NaOH, $(CH_3)_2CO$, 60 °C, 5 min, 95 % (c) NBS, $CH_3(CH_2)_3OH$, 80 °C, 1 min, 92 % (d) 0.2 N NaOH, 60 °C, 2 min, 74 % (e) $O(CH_2CH_2)_2N$, MeOH, CH_3COOH, $NaBH_3CN$, 100 °C, 5 min, 31 %

Pure product of 3α,12α-diformyloxy-5β-cholanoic acid **1** was obtained in high yield from DCA after 30 minutes of microwave iradiation. The TLC chromatography confirmed only trace amounts of starting material. Pure performilated bile acids are isolated simply by diluting the reaction mixture with water. Compared to the conventional heated reacton of DCA formilation, the presence of an acidic catalyst was unnecessary [8]. In the next phase, a partial deformylation of 3α,12α-diformyloxy-5β-cholanoic acid **1** with sodium-hydroxide in acetone was achieved at 60 ºC during 5 minutes of MW exposure.
Microwave-assisted selective oxidation with *N*-bromosuccinimide in *t*-butanol (80 °C, 1 min) and further deformylation (60 °C, 2 min) gave 12α-hydroxy-3-oxo-5β-cholanoic acid **4** in high yield and purity. Compared to the conventional protocol a remarkable reduction in overall processing time from hours to a few minutes was achieved. Structures of synthesized bile acid derivatives have been confirmed by ^{1}H- and ^{13}C- NMR spectroscopic data.

Finally, we have report efficient synthesis of new compound, 3β-(*N*-morpholino)-12α-hydroxy-5β-cholanoic acid **5** under high intensity of microwave irradiation. Target compound **5** was obtained by reductive amination of 3-oxo-12α-hydroxy-5β-cholanoic acid **4** with morpholine in the presence of $NaBH_3CN$ (Scheme 1), after 5 min of MW heating.
The resulting 3-hydroxy formyl bile acid proved to be the best starting materials for the synthesis of bile acids derivatives with specific modification at 3-hydroxyl group, such as the synthesis of bile acid`s *N*-morpholino amine. The structure of synthesized bile acid`s *N*-morpholino amine was confirmed by the presence of a signal at 2.54 ppm in the 1H NMR spectrum derived from hydrogen at C-3. Coupling constants are not observed on the given signal, indicating the equatorial position of the mentioned hydrogen.

Conclusion

In summary, we have shown that the use of bile acid formates, obtained in high yield and purity by a new formylation procedure, resulted in a much cleaner product and hence in higher yields and simplified procedures. Microwave irradiation has once again confirmed its efficiency within synthesis of new bile acid derivative, 3β-(*N*-morpholino)-12α-hydroxy-5β-cholanoic acid **5** in very short reaction time.

References

[1] J.M. Kremsner, A. Stadler, A Chemist's Guide to Microwave Synthesis, Anton Paar GmbH, Austria, 2018.
[2] C.O. Kappe, D. Dallinger, S.S. Murphree, Practical Microwave synthesis for Organic Chemists, Wiley-VCH Verlag GmbH & Co. KGaA, Weinheim, 2009.
[3] M. Blanchet, J. M. Brunel, Curr. Org. Chem., 25 (2018) 3613.
[4] B. Brycki, H. Koenig, T. Pospieszny, Molecules 20 (2015) 20887.
[5] S. Jones, W. Kinney, X. Zhang, L. Jones, B. Selinsky, Steroids 61 (1996) 565.
[6] M. Zasloff, W. Kinney, S. Jones, United States Patent number 5,856,535, 1999.
[7] Lj.M. Grbović, K.J. Pavlović, S.S. Jovanović-Šanta, B.R. Vasiljević, Curr. Org. Chem. 23 (2019) 256.
[8] K.-Y. Tserng, P. D. Klein, Steroids 25 (1977) 635.
[9] W. Kozanecka-Okupnik, B. Jasiewicz, T. Pospieszny, M. Matuszak, L. Mrówczyńska, Steroids 126 (2017) 50.

SPRAY DRYING OF INDUSTRIAL HEMP WITH MALTODEXTRIN AND GUM ARABIC

Danilo Šarčević,[1] Andrijana Dragodan,[1] Simona Višnić,[1] Milica Aćimović,[2] Jelena Vladić[1]

[1]Faculty of Technology, University of Novi Sad, Bilevar cara Lazara 1, 21000 Novi Sad, Serbia
[2]Institute of Field and Vegetable Crops, Maksima Gorkog 30, 21000 Novi Sad, Serbia
e-mail: vladicjelena@gmail.com

Abstract
The goal of this study was to obtain industrial hemp powder that is stabile and high-quality with regard to physical-chemical properties. The impact of two different carriers in spray drying and their concentrations on the quality and stability parameters of extracts from aerial parts of *Cannabis sativa* L. was investigated.

Introduction
Industrial hemp (*C. sativa* L.) belongs to the family of *Cannabaceae* and originates from humid and hot climates of central and southern Asia. Industrial hemp represents an important material in the production of paper and construction materials. Moreover, it is present in folk medicine for treating different disorders and medical conditions. *C. sativa* has long been in focus of the scientific community, therefore, its numerous pharmacological properties have been confirmed, such as: antimicrobial, antioxidant, antiemetic, antiproliferative, and analgetic activity. The most significant components of industrial hemp with attributed pharmacological potential are cannabinoids. Apart from cannabinoids, industrial hemp possesses other significant bioactive components of non-cannabinoid structure [1].

Experimental
Liquid plant extract was dried using spray drying with inlet temperature 120-130°C and outlet temperature 80°C. Drying was conducted without carriers and with addition of carriers ((MD and GA) in two concentrations (50 and 120%). The obtained powders were characterized in term of physical and chemical properties (moisture content, higroscopicity, bulk volume, WAI, WSI, total phenols, and flavonoids content).

Results and discussion
Drying without carrier was not efficient and the produced powder was sticky, while it was noticed that the efficiency of drying increased with the addition of both MD and GA. Furthermore, drying with 50% GA resulted in 58% process efficiency, whereas higher GA concentration increased the efficiency up to 72.3%. In addition, using MD 120% was significantly less adequate compared to 120% GA with achieved efficiency of 47.73%.
It was recorded that powders prepared with 120% of carrier had an approximately two-fold lower moisture content than powders obtained with 50% of carrier (3.82% and 4.38%, for MD and GA, respectively). These results confirmed the stability of powders and demonstrated their lower affinity to microbiological contamination. Additionally, it was observed that the addition of MD and GA decreased phenols content due to the dilution effect. GA demonstrated to be a more adequate encapsulation carrier as it preserved a higher amount of phenolic compounds. An opposite trend was observed with the flavonoids content where a higher concentration of the carrier was more appropriate.

Conclusion

Obtained hemp powders with a higher carrier concentration were of better quality with respect to moisture content making their storage, packaging, and distribution easier compared to powders with 50% carrier. Moreover, GA demonstrated to be a more favorable agent for obtaining industrial hemp powders.

Acknowledgements

This research was funded by Serbian Ministry of Education and Science; Project No. 451-03-68/2020-14/200134.

References

[1] H.P. Rupasinghe, A. Davis, S.K. Kumar, B. Murray, V.D. Zheljazkov, Molecules, 25 (2020), 4078.

EXAMINING SUBMERGED AND SOLID-STATE CULTIVATION COURSE OF HYDROLYTIC ENZYMES PRODUCTION FROM WHEAT CHAFF

Damjan Vučurović[1], Bojana Bajić[1], Siniša Dodić[1]

[1]*University of Novi Sad, Faculty of Technology Novi Sad, Department of Biotechnology and Pharmaceutical Engineering, Bulevar cara Lazara 1, 21 000 Novi Sad, Serbia*
e-mail: dvdamjan@uns.ac.rs

Abstract
Agricultural waste represents an interesting raw material for biotechnological processes nowadays, due to its low price, favorable composition and availability. Wheat chaff, as a lignocellulosic by-product of wheat processing could be a suitable renewable source for producing hydrolytic enzymes for second generation ethanol production technologies. The aim of this work was to investigate the course of *Trichoderma reesei* cultivation for hydrolytic enzymes production by submerged and solid-state techniques on medium based on wheat chaff. Results show that the monitored values (hydrolytic enzymes activities, total protein content and reducing sugars content) vary significantly with cultivation time, thus there is a need for further optimization of this process parameter.

Introduction
With its composition, wheat chaff is a very attractive raw material for the production of enzymes [1]. On the other hand, the previous use of this by-product of grain processing was only as fodder for cattle. Therefore, the question arises of the possibility of obtaining greater economic and environmental benefits by using a given raw material for the production of a high value product, such as enzymes, with the valorization of other process outputs to achieve the concept of cleaner production, or zero emission concept. It is the simulation models of production plants that represent an auxiliary tool for performing economic analysis and other calculations related to bioprocess, which are important for their design [2]. For the purposes of generating such models, and later the control of the bioprocess itself, it is necessary to know the kinetics and kinetic parameters related to a given process. Determining these kinetic equations only makes sense when the bioprocess is performed under optimal conditions [3]. In order to optimize the process, it is necessary to study in detail the production of enzymes by cultivating fungi on by-products of grain processing at different process parameters [4].

The aim of the research completed within this work is to investigate the submerged and solid-state cultivation course for producing hydrolytic enzymes by cultivating fungi on media that contain wheat chaff as a basis for nutrient media. The results obtained will provide data on which process parameters will need to be further optimized.

Experimental
Trichoderma reesei QM 9414, which are kept in the collection of cultures at the Faculty of Technology Novi Sad, was used as a producing strain. Refreshing of the fungi was carried out on the potatoes dextrose agar (PDA) by incubating them for 3-4 days at 28 °C. The inoculation of the nutrient media was carried out with a pre-prepared spore suspension in a sterile saline solution containing 10^6 spores/g. For the purpose of experiments, 10 % of the inoculum was added to the liquid substrates, and for the solid-state substrates, the same volume of the spore suspension was sprayed over their surface.

For the purpose of research, the by-product of wheat processing (wheat chaff) was used to prepare nutrient media. The raw material was obtained from the local wheat processing plant (mill) "Žitopromet - Mlin" a.d. Senta.

The composition of liquid substrates for the submerged cultivation technique (SmF) on wheat chaff with the aim of selecting the producing strain was 3 g of wheat chaff, 0.5 % $(NH_4)_2SO_4$ and 1.36 % K_2HPO_4 in 100 mL of distilled water.

For cultivation on solid substrates (SSF) with the aim of selecting the producing strain, the same amount of raw material (3 g) was suspended in the same amount (100 mL) of a water solution containing 0.5 % $(NH_4)_2SO_4$ and 1.36 % K_2HPO_4 like for the liquid media. After 15 minutes of mixing, the pH value was checked and corrected to 4.5 ± 0.1 by adding 1 % NaOH or 1 % H_2SO_4. After an additional 15 min of stirring, the suspension was allowed to stand still so that the solid phase could settle in the gravitational field. The liquid phase was decanted and the residue used as a solid substrate for the production of enzymes. In this way enzymes have been produced from the same amount of raw material used, i.e. 3 g of wheat chaff, as well as the same preparation method (100 mL of prepared salt solution), so that the obtained results could be comparable [5].

Sterilization of the prepared media was carried out in an autoclave at a temperature of 121 °C and a pressure of 2.1 bar for 20 min.

Production of enzymes by fungi cultivation for both submerged and solid-state techniques was carried out in 300 ml Erlenmeyer flasks for 7 days at a temperature of 28 ± 1 °C.

After cultivation on solid media, the products of strain metabolism were extracted with 100 mL 0.1 M acetate buffer (pH 5.0) with constant mixing at 200 rpm during 30 min at a constant temperature, in order to equal the liquid volume with the submerged cultivation broths. Separation of solid and liquid phase after extraction of solid media as well as the submerged cultures was carried out by filtrating through a qualitative filter paper. Obtained filtrates were subjected to the standard analysis of cultivation media.

The intensity of hydrolytic action of the cultivation liquids and solid extracts towards cellulose and xylan were assayed separately for each substrate by measuring the release of reducing sugars using the DNS (3,5-dinitrosalicylic acid) method [2].

Results and discussion

In addition to the appropriate nutrient medium and production microorganism, the success of fermentation also depends on the knowledge of the values of the desired parameters in certain phases of the process, i.e. the knowledge of the cultivation course [6]. Knowing the course of a bioprocess helps in its better understanding, facilitates its translation on a larger scale (scale-up) to the final industrialization, and thus its control and management. For this reason, experiments were performed using submerged and solid-state cultivation of *Trichoderma reesei* on a substrate based on wheat chaff, with the aim of analyzing the activity of hydrolytic enzymes (amylase, cellulase and xylanase), total protein content and reducing sugars at defined time intervals of bioprocesses. Figures 1 and 2 show the results of cultivation course tests for submerged and solid-state techniques, respectively.

Based on the results shown in Figure 1, it can be seen that the activities of the tested hydrolytic enzymes in the culture medium have an intense increase in the first 48 h, followed by a slight

increase or stagnation until the end of cultivation. According to the same principle of the sigmoidal curve, which is characteristic for enzyme systems [7], the total protein content also changes, with the moment of transition from sudden to weaker intensity of increase of this value a little earlier in relation to the activities of tested enzymes, i.e. about 32 h. The content of reducing sugars in the first four hours has an intensive growth, when it reaches its maximum value of 12.4895 mg/mL, then sharply decreases to about 2 mg/mL at 24 h and by the end of cultivation this value does not change drastically.

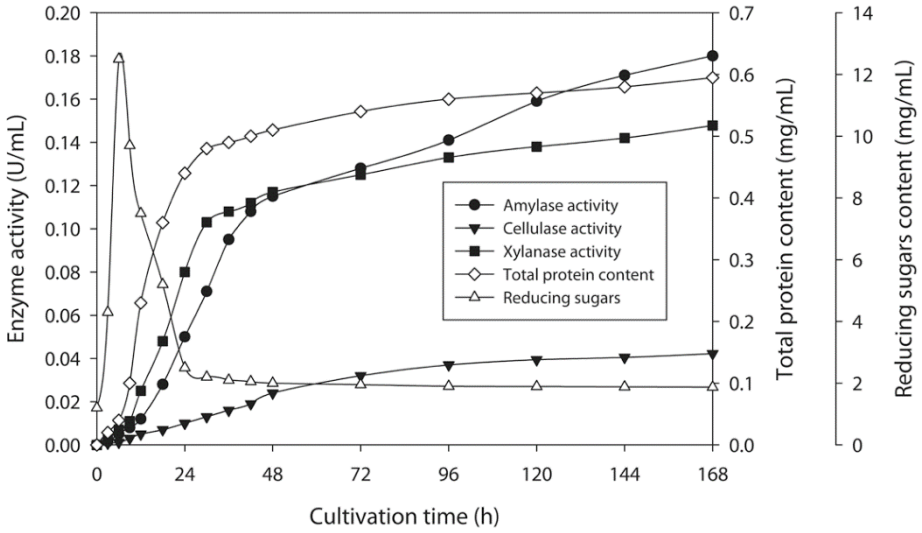

Figure 1. Enzyme activity (amylase, cellulase and xylanase), total protein and reducing sugars content as functions of submerged cultivation time of *Trichoderma reesei* on a nutrient medium with wheat chaff

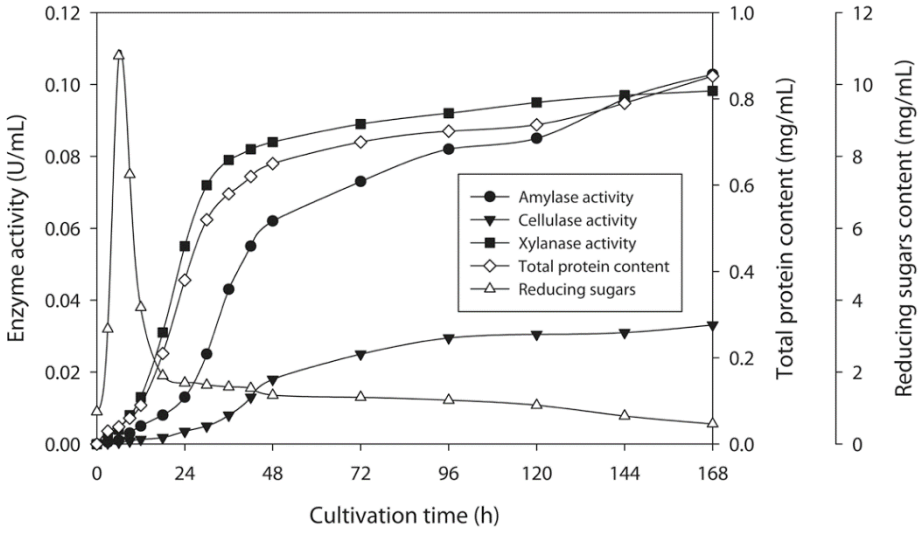

Figure 2. Enzyme activity (amylase, cellulase and xylanase), total protein and reducing sugars content as functions of solid-state cultivation time of *Trichoderma reesei* on a nutrient medium with wheat chaff

Analysis of amylase, cellulase and xylanase activity in samples taken during fungi cultivation on a solid nutrient medium based on wheat chaff (Figure 2) shows that the values first increase intensively up to 48 h, then increase slightly until the end of cultivation. As with submerged cultivation, the total protein content first has a sharp increase, but this time up to 48 h, and then

a slight increase up to 168 h. The maximum value of the reducing sugar content was reached already in 4 h of cultivation, after which it falls to a value below 2 mg/mL already in 18 h of cultivation and continues to fall to a value of 0.5 mg/mL until the end.

Conclusion

Examining the course of two cultivation techniques for producing hydrolytic enzymes by fungi on a nutrient medium based on wheat chaff, it was pointed out that there is a possibility of shortening the cultivation time, i.e. the need for further optimization in the form of process parameters.

Acknowledgements

This study is part of the project which is supported by the Ministry of Education, Science and Technological Development of the Republic of Serbia (Grant no. 451-03-68/2020-14/200134).

References

[1] M. Jovanović, D. Vučurović, S. Dodić, B. Bajić, J. Dodić, V. Vlajkov, R. Jevtić-Mučibabić, Rom. Biotech. Lett. 25 (2020) 1938.
[2] M. Jovanović, D. Vučurović, B. Bajić, S. Dodić, V, Vlajkov, R. Jevtić-Mučibabić, J. Serb. Chem. Soc. 85 (2020) 177.
[3] D. Vučurović, M. Jovanović, B. Bajić, S. Dodić, 1st International Conference on Advanced Production and Processing – ICAPP 2019 (2019) 284.
[4] D. Vučurović, K. Lisickov, S. Dodić, Z. Rončević, J. Dodić, J. Grahovac, B. Bajić, 43rd International Conference of Slovak Sociegty of Chemical Engineering – SSCHE 2016 (2016) 922.
[5] 14. G. Hansen, M. Lübeck, J. Frisvad, P. Lübeck, B. Andersen, Process. Biochem. 50 (2015) 1327.
[6] P. Stanbury, A. Whitaker, S. Hall, Adv. Biosci. Biotechnol. Principles of Fermentation Technology (3rd edn), Butterworth-Heinemann, Amsterdam, 2016, pp. 487.
[7] S. Pan, G. Chen, J. Zeng, X. Cao, X. Zheng, W. Zeng, Z. Liang, Biochem. Eng. J. 141 (2019) 268.

INFLUENCE OF EXTRACTION TECHNIQUES ON THE CHARACTERISTICS OF SAMBUCUS NIGRA L. EXTRACTS

Milena Vujanović[1], Tatjana Majkić[2], Ivana Beara[2], Aleksandra Cvetanović[1], Mirjana Petronijević[1], Alena Tomšik[3], Gokhan Zenhin[4], Miloš Radosavljević[1], Marija Radojković[1]

[1]Faculty of Technology Novi Sad, Bulevar cara Lazara 1,21000 Novi Sad, Serbia
[2]Faculty of Sciences, Trg Dositeja Obradovića 3, 21000 Novi Sad, Serbia
[3]Institute of Food Technology, Bulevar cara Lazara 1, 21000 Novi Sad, Serbia
[4]Science Faculty, Selcuk University, Department of Biology, Campus, Konya, Turkey
e-mail: milenavujanovic@uns.ac.rs

Abstract

Sambucu nigra L. belongs to the group of plants recognizable by its strong biological activity which was well-known in traditional medicine. However, modern science has confirmed many of its activities such as antimicrobial, antioxidant, immunomodulatory, etc. The biological ability of the plant is closely related with its chemical composition, in the first place with its polyphenolic constituents. The content of individual components in extracts is strongly influenced by isolation technique, as well as the type of solvent. Therefore, the aim of this study was to investigate the influence of modern (microwave-assisted extraction, MAE) and traditional (maceration, MAC) extraction techniques on polyphenol yield in *S.nigra* extracts, as well as on their biological activity. At the same time, the influence of the two most commonly used solvents (water and ethanol) on the mentioned outputs was also examined. The obtained extracts were analyzed spectrophotometrically in order to determine the content of total phenols and flavonoids, while the content of individual polyphenolic components was measured chromatographically using the LC-MS/MS technique. The biological potential of the obtained extracts was determined by measuring their antioxidant and enzyme-inhibitory activities. The obtained results showed that in all examined extract 15 different components were identified, while the two analyzed compounds were under the LoD. Among the identified components the most dominant was quinic acid as well as rutine. It was noticed that MAE was the more prominent technique for the isolation of target compounds, while ethanol was marked as a solvent with better solvating properties towards to polyphenols in comparison to water. Antioxidant assays showed that all examined extracts were capable to act as free-radical scavenges and antioxidants. By applying in vitro assays the ability of the extracts to inhibit the activity of amylase and acetylcholinesterase was determined, and it was showed that they were much more active towards to amylase (2.18-7.14 mg ACAE/mL) than to acetylcholinesterase (0.09-0.11mg GALAE/mL).

Acknowledgements

The present work was carried out within the project financed by Provincial Secretariat for High Education and Scientific Research AP Vojvodina, Serbia (Project No. 142-451-3240/2020-03). The authors are grateful to the Science Fund of the Republic of Serbia for financial support within the Promis Project (Project No. 6060592) as well as to the Ministry of Education, Science and Technological Development of Republic of Serbia (grant contract no. 451-03-68/2020-14/200134).

DETERMINATION OF ATROPINE AND SCOPOLAMINE IN POPCORN BY THE LC-MS/MS

Gorica Vuković[1], Vojislava Bursić[2], Tijana Stojanović[2], Aleksandra Petrović[2], Bojan Konstantinović[2], Nikola Puvača[5], Dušan Marinković[2]

[1]Institute of Public Health, Bulevar despota Stefana 54a, Belgrade, Serbia
[2]University of Novi Sad, Faculty of Agriculture, Trg Dositeja Obradovića 8, Novi Sad, Serbia
[3]University of Belgrade, Faculty of Agriculture, Nemanjina 6, Belgrade, Serbia
[4]Institute of Field and Vegetable Crops, Maksima Gorkog 30, 21000 Novi Sad, Serbia
[5]University Business Academy in Novi Sad, Faculty of Economics and Engineering Management, Cvećarska 2, Novi Sad, Serbia
e-mail: tijana.stojanovic@polj.edu.rs

Abstract
Tropane alkaloids are secondary metabolites produced mainly by the genera of the *Solanaceae* family - *Hyoscyamus*, *Datura* and *Atropa*. For determination and quantification of the atropine and scopolamine in 12 samples of popcorn the validated rapid and sensitive liquid chromatography-tandem mass spectrometry (LC-MS/MS) was used. Out of the studied popcorn samples 41.67% were contaminated with atropine and scopolamine, while in 58.33% of the tested samples tropane alkaloids were not detected, or the present concentrations were below the limit of detection (<1 µg/kg). Atropine was present in the range from 5.3 to 28 µg/kg, while scopolamine ranged from 2.1 to 6.3 µg/kg.

Key words: tropane alkaloids, atropine, scopolamine, LC-MS/MS, popcorn

Introduction

Animals, plants and organisms produce natural toxins which, although they are not toxic to them, may be present in food and be toxic to humans when ingested. As a possible health hazards World Health Organisation (WHO) highlighted the monitoring importance in case of relevant natural food toxins by the national authorities [1].
Those natural toxins represent the secondary metabolites which are produced, among others, by the weeds present in the fields, where they contaminate the food crops. Namely, the seeds and parts of plant organs of weeds which contain tropane alkaloids end up in the crops such as sunflower, buckwheat and maize, as well as in their products as the accidental impurities. The main weeds genera containing tropane alkaloids are the genera from the *Solanaceae* family – *Hyoscyamus*, *Datura* and *Atropa* [2].
The maximum levels of residues of the tropane alkaloids are still not determined, due to which all tropane alkaloids containing samples with concentrations above the Limit of Quantifications (LOQs) are not considered suitable for the consumption [3]. The maximum levels have not been established in case of popcorn either. That can be considered alarming since the KiESEL study ("The Children's Nutrition Survey to Record Food Consumption") done by the German Federal Institute for Risk Assessment (BfR - Bundesinstitut für Risikobewertung) determined that the single consumption intake of popcorn in children aged between 3 and 5 years can be up to 100 g [4].
The above-mentioned problems led to the liquid chromatography with tandem mass spectrometry (LC-MS/MS) determination of the atropine and scopolamine in 12 popcorn samples collected during 2020 which was done in this research.

Experimental

Chemicals and apparatus. Atropine and scopolamine reference standards were obtained from Sigma-Aldrich. The mixture working standard solution was prepared at 5 mg/L with methanol and stored in the dark at -20℃. Carbofuran D3 was used as an internal standard (IS). HPLC grade methanol and acetonitrile were obtained from J.T. Baker Chemicals. Formic acid was purchased from Fisher Scientific UK. The Agilent Bond Elut EN Buffered Extraction kit and Bond Elut QuEChERS EN Dispersive SPE kits for Fruits and Vegetables with fats and waxes were purchased from Agilent. An Agilent series 1200 HPLC system (Agilent Technologies) equipped with a G1312B binary pump, a G1367D autosampler, a G1379B degasser and G1316B column compartment temostat. The HPLC system was coupled to an Agilent triple quadrupole mass spectrometer (6410 B) coupled to an electrospray ionization source (ESI+). A Zorbax XDB C18 column (50x4.6 mm, 1.8 µm particle size) from Agilent was employed for the separation. The chromatographic determination of atropine and scopolamine was carried out employing a binary mobile phase with methanol (A) and an aqueous solution of formic acid (0.1%, v/v) (B). A gradient elution started at 90% of B and held 4 min at flow rate of 0.4 mL/min. This composition was reduced to 5% B in 10 min, and held for 5 min. The composition of the mobile phase returned to the initial conditions in 2 min and the stationary phase was equilibrated during 2 min. The total running time was 17 min. The injection volume was 5 µL and column temperature was kept at 25 ºC. The ESI source values were as follows: drying gas (nitrogen) temperature 350 °C, drying gas flow rate 10 L/min, nebulizer pressure 40 psi and capillary voltage 3500 V. The detection was performed using the multiple reactions monitoring mode (MRM). The Agilent MassHunter software (version B.06.00 Agilent Technologies, 2012) was used for the optimization and quantification.

Sample collection. All analyses samples were popcorn from the local shops. The sampling was performed in accordance with 2002/63/EC for establishing MLs in the food commodities. All 12 samples were placed in polythene bags, labelled and transported to the laboratory for processing. The samples were ground into powder prior to the analysis. The blank samples were used for the preparation of fortified samples during the optimization of sample extraction procedure and method validation.

Sample preparation. A 5 g of homogenized sample was placed into a 50-mL centrifuge tube with adding of 100 µL of IS and 10 mL of water to each tube and vortexed for 1 min and equilibrated for 10 min. Next, 10 mL aliquot of acetonitrile containing acetic acid (1%, v/v) was added and shaken by vortex for 1 min. The QuEChERS EN extraction salt packet was added directly to each tube. The tubes were sealed tightly and shaken vigorously for 20 seconds by hand and 15 min/250 rpm by orbital shakers. The sample tubes were centrifuged at 4000 rpm for 5 min. The supernatants were then transferred to 15-mL QuEChERS d-SPE kits consisting of C18 and $MgSO_4$, vortexed for 5 min and centrifuged at 4000 rpm for 10 min. The obtained mixtures were transferred and dried under the nitrogen gas at 45 ºC until the volume was <0.3 mL. The residues were reconstituted in the mixture methanol/water up to 2 mL, vortexed, centrifuged at 7000 rpm and filtered prior to the LC-MS/MS analysis.

Results and discussion

The ionization was achieved using electrospray in the positive ionization mode. For each compound the detection was related to four daughter ions (atropine: m/z 290.2 to 124.2, 93.2, 77.1 and 67.1; scopolamine: m/z 304.1 to 156.1, 138.2, 103.2 and 77.1).

Validated LC-MS/MS method for the determination of atropine and scopolamine was used for the analyses of 12 popcorn samples. The validation was done according to the SANTE/1183/2017 [3]. The average recoveries of scopolamine and atropine were 87.4 and 69.2%, respectively, with the relative standard deviation (RSD) lower than 15%. The matrix–matched calibrations were with the R^2>0.99 in the calibration range from 2 to 20 µg/kg. LOQs

(limit of quantification) of atropine and scopolamine were set at 5 µg/kg. These limits were checked in terms of the recovery and repeatability.
The TIC chromatograms of popcorn samples number 7 (A) with the atropine, scopolamine and IS (carbofuran – D3) detections and blank popcorn samples (B) with only detection of IS, are shown in Figure 1.

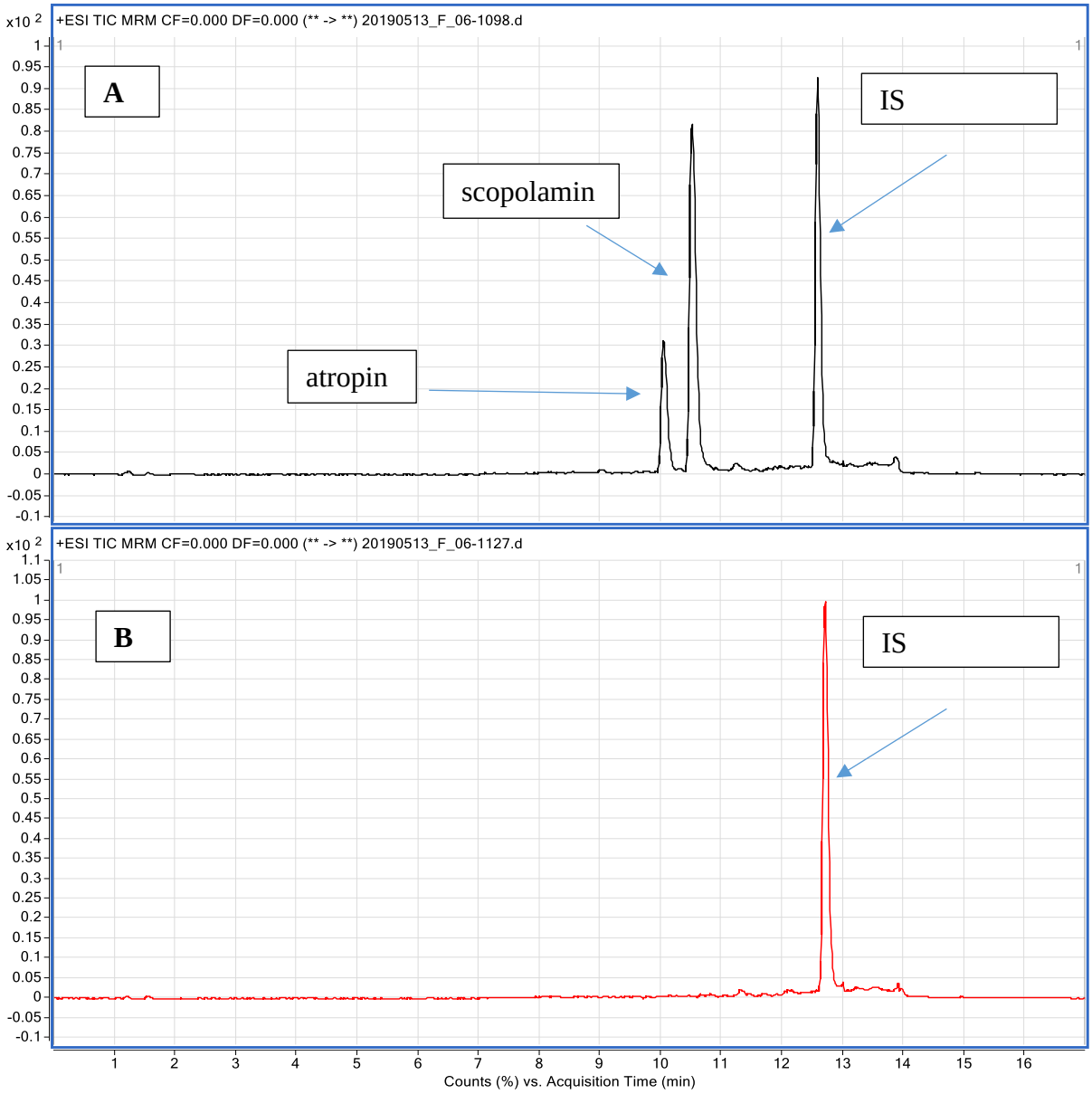

Figure 1. TIC chromatograms of samples

Table 2. Atropine and scopolamine residues in popcorn samples (µg/kg)

Sample	**1**	**2**	**3**	**4**	**5**	**6**
Atropine	< 1	5.4	5.3	< 1	< 1	< 1
Scopolamine	< 1	2.8	2.1	< 1	< 1	< 1
Sample	**7**	**8**	**9**	**10**	**11**	**12**
Atropine	16.3	28	< 1	18.8	< 1	< 1
Scopolamine	3.3	6	< 1	6.3	< 1	< 1

In almost half of the tested samples (5 out of 12 in total) atropine and scopolamine were detected in concentrations above the LOD (1 μg/kg). Atropine was present in the range from 5.3 to 28 μg/kg, while scopolamine ranged from 2.1 to 6.3 μg/kg. The obtained results may be considered alarming since the RASFF (Rapid Alert System for Food and Feed) reported three cases of atropine and/or scopolamine in popcorn in similar concentrations to those detected in our research, which ended with the withdrawal from the market in every of the mentioned cases. Namely, in 2015 in microwave popcorn from Spain atropine was detected in the concentration of 29 μg/kg, while scopolamine was present with 6 μg/kg. In 2018 two incidents were noted. In the first 6.6 μg/kg of atropine and 1.8 μg/kg of scopolamine were detected in popcorn from France, while in the second incident 10.3 μg/kg of scopolamine was detected in popcorn from Argentina [5]. Since Perharič et al. [6] reported loss of atropine (37%) and scopolamine (58%) during cooking, it is unknown how much of these substances actually remains in the popcorns.

The European Food Safety Authority (EFSA) determined 0.016 μg/kg body weight as the acute reference dose for the sum of atropine and scopolamine [7]. As the maximum concentration for atropine and scopolamine in the infants and young children food 1 μg/kg has been established by the EU Regulation 2016/239, while the preferred LOQ for the same tropane alkaloids in agricultural commodities is below 5 μg/kg and not above 10 μg/kg and below 2 μg/kg for the finished foods (e.g. breakfast cereals), as stated by the EU commission recommendation 2015/976 [8].

Conclusion

In almost half of the tested samples (5 out of 12 in total) atropine and scopolamine were detected in concentrations above the LOD (1 μg/kg) Atropine was present in the range from 5.3 to 28 μg/kg, while scopolamine ranged from 2.1 to 6.3 μg/kg. The obtained results may be considered alarming since the RASFF (Rapid Alert System for Food and Feed) reported three cases of atropine and/or scopolamine in popcorn in similar concentrations to those detected in our research, which ended with the withdrawal from the market in every of the mentioned cases. The concentrations of atropine were from ~2 to ~5 times higher than the ones of scopolamine. Considering the results obtained by this research there is an urging need for the determination of the tropane alkaloids maximum concentrations in popcorn, as well as in other maize-based products for the human consumption, since they have not been established to this day.

Acknowledgements

The authors acknowledge the financial support of the Ministry of Education and Science, Republic of Serbia.

References

[1] N. Casado, J. Gañán, S. Morante-Zarcero, I. Sierra, New advanced materials and sorbent-based microextraction techniques as strategies in sample preparation to improve the determination of natural toxins in food samples, Molecules. 25(702) (2020) 1, 2.
[2] C. Gonçalves, E. Cubero-Leon, J. Stroka, Determination of tropane alkaloids in cereals, tea and herbal infusions: exploiting proficiency testing data as a basis to derive interlaboratory performance characteristics of an improved LC-MS/MS method, Food Chemistry (2020).
[3] G. Vuković, V. Bursić, T. Stojanović, A. Petrović, S. Gvozdenac, M. Starović, S. Kuzmanović, G. Aleksić, LC-MS/MS determination of tropane alkaloids in maize crop, Contemporary Agriculture. 67(3-4) (2018) 222, 223.
[4] BfR, Popcorn quantities consumed by toddlers as basis for assessment of possible health risks (2020) 1.

[5] RASFF Portal. https://webgate.ec.europa.eu/rasff-window/portal/?event=SearchByKeyword&NewSearch=1&Keywords=popcorn
[6] L. Perharič, K. A. Juvan, L. Stanovnik, Acute effects of a low dose atropine/ scopolamine mixture as a food contaminant in human volunteers. Journal of Applied Toxicology, 33 (2013) 980–990.
[7] A. Romera-Torres, R. Romero-González, J. L. Martínez Vidal, A. Garrido Frenich, Comprehensive tropane alkaloids analysis and retrospective screening of contaminants in honey samples using liquid chromatography-high resolution mass spectrometry (Orbitrap), Food Research International. 133 (2020) 1.
[8] M. Martinello, A. Borin, R. Stella, D. Bovo, G. Biancotto, A. Gallina, F. Mutinelli, Development and validation of a QuEChERS method coupled to liquid chromatography and high resolution mass spectrometry to determine pyrrolizidine and tropane alkaloids in honey, Food Chemistry. 234(1) (2017) 295-302.

POTENTIAL OF CRUDE GLYCEROL UTILIZATION IN BIOTECHNOLOGICAL PRODUCTION OF XANTHAN: A MINI REVIEW

Ida Zahović, Zorana Trivunović

University of Novi Sad, Faculty of Technology Novi Sad, Department of Biotechnology and Pharmaceutical Engineering, Bulevar cara Lazara 1, Novi Sad 21000, Serbia
e-mail: idaidaza@gmail.com

Abstract
Xanthan is extracellular secondary metabolite of bacteria from the genus *Xanthomonas* and the most important microbial polysaccharide as well as significant industrial biopolymer. Commercial xanthan is relatively expensive due to usage of glucose or sucrose as carbon sources in the xanthan production media. On the other hand, the production of biodiesel in the world is in the rise. The main effluent generated by the biodiesel industry is crude glycerol. The high costs of crude glycerol purification and degradation of environmental quality caused by its disposal in untreated form are the reasons for the increase in research about alternative methods that can be potentially used to convert crude glycerol into a valuable product. The promising alternative is microbial conversion of crude glycerol. The purpose of this study is to discuss data from available scientific and professional literature related to the possibility of using crude glycerol as a substrate for the production of xanthan.

Keywords: Biodiesel industry, crude glycerol, waste utilization, biotechnological xanthan production

Introduction
Fossil fuels in limited reserves are concentrated in certain regions of the world that are shortening day by day. They are being consumed more rapidly than they are being created so they are considered as non-renewable [1]. The rise in oil prices and the enlarge substitution of liquid fossil fuels with renewable energy sources have led to an increase of biodiesel production worldwide. Biodiesel presents a diesel-equivalent, processed fuel derived from biological sources such as plant and animal oils [2]. There are four primary ways to produce biodiesel but transesterification of animal fats or vegetable oils is the most commonly used method for biodiesel production [3]. The main advantages of biodiesel as a diesel biofuel are its portability, availability, renewability, higher combustion efficiency, lower sulfur and aromatic content, higher biodegradability and environmentally friendliness. Another important advantage of biodiesel lies in the fact that the risks of handling, transporting, and storing biodiesel are much lower than those associated with petro diesel [2]. Considering the environmental concerns about pollution coming from the fossil fuels and all advantages of biodiesel, it is evident why biodiesel has become a developing area of high concern. The world's biodiesel supply grew from 3.9 billion liters in 2005 to 18.1 billion liters in 2010 and is expected to reach 41.4 billion liters in 2025 [4].

Expansion of biodiesel production results in the accumulation of significant amount of effluents such as wastewater used to wash the catalyst from the ester phase, unused catalyst, crude glycerol, methanol, soaps, as well as peptides, lecithin, proteins and phospholipids in small quantities [5, 6]. Considering that crude glycerol is generated in the amount of 10-20% of the total volume of biodiesel produced, it presents the main by-product of the biodiesel industry [7]. The glycerol derived from biodiesel production is impure and requires some form of treatment prior to discharging into environmental receptors. The significant cost of

crude glycerol purification that increases the cost of biodiesel production and health risks prevents its use in food and pharmaceutical industries [5]. Thus, new effective and environmentally safe methods for the utilization of crude glycerol are urgently needed.

The composition of crude glycerol depends on several factors, which is why it is difficult to define it precisely. Glycerol generated during biodiesel production is usually about 55-90% purity and contains residues such as unconverted triacylglycerol, methanol, ethanol, biodiesel, soap and other compounds [8]. The results of several studies indicate that glycerol represents an excellent carbon source for numerous bioconversions into value added products such as succinic acid, ethanol, hydrogen, polyhydroxybutyrate polymers, clavulanic acid, citric acid and xanthan [9, 10]. Among all aforementioned value added products, xanthan stands out due to its extraordinary characteristics.

Xanthan is a non-toxic, biocompatible and biodegradable microbial biopolymer. This water soluble heteropolysaccharide is biosynthesized by *Xanthomonas campestris* and by other *Xanthomonas* species on a culture medium of appropriate composition. Xanthan is industrially produced using the reference strain *Xanthomonas campestris* ATCC 13951 under optimal conditions, discontinuously, by submerged aerobic biosynthesis in bioreactors with a volume of 100,000 L [11]. The chemical structure of xanthan is composed of repeated units formed by two glucose units, two mannose units, and one glucuronic acid unit, in the molar ratio 2.0:2.0:1.0. [9]. Molecular weight of xanthan macromolecules ranges from $2 \cdot 10^6$ Da to $20 \cdot 10^6$ Da and its distribution depends on the association between chains, i.e. formed aggregates of several individual chains [12].

Exceptional rheological characteristics and stability over a wide range of temperature and pH value make xanthan widely used in a broad range of industries, such as food, pharmaceutical, cosmetic, chemical, oil recovery and textile. Xanthan is reported as GRAS by United States drug and food administration on the basis of toxicology tests in human foods. Hence, the most advanced application of xanthan is in food industry as a suspending and thickening agent and in pharmaceutical industry in controlled drug delivery system [13, 14].

Glucose and sucrose have been used for decades as the most suitable carbon sources in cultivation media for xanthan production, but rising prices and increasing demand for these sugars indicate the necessary exploitation of alternative substrates of lower market value. Results from several researches indicate the possibility of using crude glycerol as a raw material for production of xanthan of satisfactory quality [5, 15]. However, the main disadvantage of the application of this significant waste stream in the production of xanthan is reflected in the limited ability of the reference strain to metabolize glycerol as a carbon source [9]. Thus, there is a need for isolation of new strains that exhibit tolerance against crude glycerol impurities and produce xanthan. The purpose of this review is to discuss the possibility of xanthan production on a medium containing crude glycerol by different strains of *Xanthomonas campestris.*

Material

The available scientific publications were used as a primary material for this paper. The collated data were selected, systematized, compared and critically discussed.

Discussion

Despite the fact that development and improvement of xanthan production have been studied during the years, there are a small number of studies based on the biotechnological xanthan production on crude glycerol containing media. One of the first studies focused on the possibility of using crude glycerol for xanthan production is performed by Reis et al. and aimed to investigate the possibility of using glycerol, obtained from biodiesel industry, as substrate for xanthan production by *Xanthomonas* C1 and *Xanthomonas* C9 strains isolated in Brazil [16]. The following carbon sources were used in cultivation medium: only sucrose, only glycerol or a glycerol-sucrose mixture in the ratio of 50:50%. Incubation was performed at 28±2°C with stirring at 180 rpm for 96 h. The obtained results showed that crude glycerol as unique carbon source is not a media adequate for xanthan production in applied experimental conditions. However, when supplemented with sucrose were not detectable significance differences with the medium containing only sucrose. The highest yield of xanthan of 0.0038 g/L·h among the three media was obtained using glycerol with supplementation of the sucrose (25:25, w/w) by the wild-type isolate *Xanthomonas* C1 and C9. The best results of productivity and apparent viscosity were accomplished when the media containing glycerol was used. Therefore, the results obtained in this study suggest that the crude glycerol is an adequate substrate for the production of xanthan.

One more confirmation that *Xanthomonas* isolates can be employed to convert crude glycerol is obtained by Brazlilan team of researchers. Brandão et al. also investigated the possibility of using residual crude glycerol from biodiesel production as an alternative substrate for xanthan biosynthesis by *X. campestris mangiferaeindicae 2103* using a fermentation medium supplemented with 0.01% urea and 0.1% K_2HPO_4 [5]. Batch fermentation was carried out at 250 rpm and 28±2°C for 120 h. The amount of xanthan obtained using crude glycerol as substrate in applied experimental conditions was 7.23 g/L. This value is approximately 70% higher than the production obtained from the conventional substrate sucrose (4.21 g/L) under the same operating conditions. The solutions of obtained xanthan (2.0% w/v) exhibited a pseudoplastic rheological behavior, with a viscosity of up to 642.57 mPa·s at 25°C. The viscosity was 30% higher than the viscosities found for the solution of xanthan obtained from the sucrose media. The xanthan's molecular weight varied from $28.2 \cdot 10^6$ Da to $36.2 \cdot 10^6$ Da. From the obtained results it can be noted that the molecular weight of xanthan produced from glycerol presented a similar value to xanthan obtained from sucrose. The findings of this study indicate that crude glycerol presents great promise as a substrate for the efficient production of xanthan.

Another study focused on the production of xanthan on crude glycerol media was performed in Brazil. de Jesus Asis et al. investigated xanthan production from crude glycerol biodiesel (CGB) by *Xanthomonas campestris mangiferaeindicae* 2103 [17]. The xanthan was produced from CGB in a 4.5 L bioreactor containing production medium consisting of 2.0 % (v/v) CGB, 0.01 % (w/v) $(NH_2)_2CO$, 0.1 % (w/v) KH_2PO_4, and 0.1 % (v/v) antifoam at 28°C for 120 h. The obtained results showed that low agitation speed increases the production of xanthan, biomass concentration, apparent viscosity of xanthan solutions, glucose and pyruvic acid concentrations in the xanthan chain, and molecular mass in applied experimental conditions. The results also showed that decreasing the aeration contributes to increased xanthan production and higher concentrations of glucose and mannose in the polymeric chain. According to the results obtained in this study it can be concluded that the highest content of xanthan of 5.59 g/L was achieved when biosynthesis was performed on medium with crude glycerol at aeration of 0.97 vvm and agitation speed of 497.76 rpm. The findings of this research indicate that the studied

crude glycerol have strong potential and promising properties for the efficient and cost-effective production of xanthan.

In the work of Trinidade et al. the possibility of crude glycerol (81.92%) utilization for xanthan biosynthesis by *Xanthomonas campestris* pv. *mangiferaeindicae* IBSBF 1230 was examined [18]. Following the idea of Reis et al. [16], sucrose and crude glycerol were used as single and mixed (1:1) carbon sources in cultivation media. The highest amount of xanthan of 4.98 g/L was obtained when crude glycerol was used as the only carbon source in cultivation media in applied experimental conditions. Similar to the results obtained in research performed by Reis et al. [16], results from this study indicate that the use of sucrose and a mixture of sucrose and crude glycerol did not represent significant differences in xanthan yield. Thus, it was shown that crude glycerol is a potential alternative carbon source for substituting sucrose in the biotechnological production of xanthan.

Research performed in Serbia in 2015 confirmed that commercial glycerol is viable as a carbon source in the applied experimental conditions using the reference strain *Xanthomonas campestris* ATCC 13951 and eight strains isolated from different vegetables grown in Vojvodina for the production of xanthan [15]. The authors suggested that further research should encompass the optimization of the glycerol-based media in order to increase yield and quality of the desired product. This research was great background for the later research conducted in Serbia in 2019 [19] and 2020 [20]. Yield of xanthan of 6.68 g/L was achieved when *Xanthomonas campestris* ATCC 13951 was cultivated for 168 h on crude glycerol containing medium under aerobic conditions. This value is higher comparing to yield achieved in several previous studies [17, 18]. Later, the same authors examined the possibility of xanthan biosynthesis using four *Xanthomonas campestris* strains isolated from different cruciferous plants (CB, CF, 12-2 and Xp3-1) on a crude glycerol-based medium. Xanthan production was carried out in a batch mode under aerobic conditions (an air flow rate of 1 vvm in the first 48h, and 2 vvm afterwards) for 168 h. In the first 48 h, the temperature was 25°C and the agitation rate was 200 rpm, which thereafter increased to 30°C and 300 rpm, respectively. The results obtained in this study indicate that all the strains considered can be used for xanthan production on a crude glycerol-based medium. The values of produced xanthan were in range from 5.22 g/L to 7.67 g/L. The values of xanthan yield obtained in this research are the highest values ever reported when *Xanthomonas* spp. were cultivated on crude glycerol-based media. High values of all the indicators of bioprocess success suggest that *Xanthomonas campestris* Xp 3-1 isolate represents the most appropriate producing strain for xanthan biosynthesis on crude glycerol-based media under the set experimental conditions.

Conclusion

This paper provides valuable information on the possibility of biotechnological xanthan production on a medium containing crude glycerol as a carbon source by different strains of *Xanthomonas campestris*. The results discussed above indicate that crude glycerol has strong potential for the efficient and cost-effective production of xanthan. All the results presented in this study can be used for selecting the producing strain and optimum medium composition for economically justified xanthan production. Besides the significance for industrial process development, studies focused on crude glycerol usage in biotechnological xanthan production are also a precious tool for great social, economic and environmental benefits for society.

Acknowledgements
This study is part of the project (451-03-68/2020-14/ 200134) funded by the Ministry of Education, Science and Technological Development of the Republic of Serbia.

References
[1] G. Sivakumar, D.R. Vail, J. Xu, D. Burner, J. Lay, X. Ge, P. Weathers, Eng. Life Sci. 10 (1) (2010) 8-18.
[2] A. Demirbas, Energy Convers. Manag. 50(1) (2009) 14–34.
[3] D.Y.C. Leung, X. Wu, M.K.H. Leung, Appl. Energy 87(4) 2010 1083–1095.
[4] P. Purohit, S. Dhar, AIMS Energy 6 (2018) 453–486.
[5] L.V. Brandão, D.J. Assis, J.A. López, M.C.A. Espiridião, E.M. Echevarria, J.I. Druzian, Braz. J. Chem. Eng. 20 (2013) 737-746.
[6] A. Hejna, P. Kosmela, K. Formela, L. Piszczyk, J. T. Haponiuk, Renew. Sust. Energ. Rev. 66(C) (2016) 449-475.
[7] C.A.G. Quispe, C.J.R. Coronado, J.J.A. Carvalho, Renew. Sust. Energ. Rev. 27(C) (2013) 475-493.
[8] I. Contreras-Andrade, E. Avella-Moreno, J.F. Sierra-Cantor, C.A. Guerrero-Fajardo, J.R. Sodré, Fuel Process Technol. 132 (2015) 99-104.
[9] Z. Wang, J. Wu, L. Zhu, X. Zhan, Bioresour Technol. 211 (2016) 390-397.
[10] V. K. Garlapati, U. Shankar, A.Budhiraja, Biotechnol. Rep. 9 (2016) 9−14.
[11] M. Ozdal, E.B. Kurbanoglu, J Genet Eng Biotechnol. 16 (2018) 259–263.
[12] F. Garcia-Ochoa, V.E. Santos, J.A. Casas, E. Gómez, Biotechnol. Adv. 18(7) (2000) 549–579.
[13] I.K. Sherley, R.D. Priyadharshini, Int. J. Chemtech Res. 8 (2) (2015) 711-717.
[14] A. Lachke, Resonance 9 (2004) 25–33.
[15] B. Bajić, Z. Rončević, S. Dodić, J. Grahovac, J. Dodić, Acta Period. Technol. 46 (2015) 197-206.
[16] E.C. Reis, M. Almeida, J.C. Cardoso, M.A. Pereira, C.B.Z. de Oliveira, E.M. Venceslau, J.I. Druzian, R. Mariano, F.F. Padilha, Macromol. Symp. 296 (1) (2010) 347-353.
[17] D. de Jesus Assis, L.V. Brandão, C.L.A. de Sousa, T.V.B. Figueiredo, L.S. Sousa, F.F. Padilha, J.I. Druzian, Biotechnol. Appl. Biochem. 172 (2014) 2769-2785.
[18] R.A. Trindade, A.P. Munhoz, C.A.V. Burkert, Biocatal. Agric. Biotechnol. 15 (2018) 167-172.
[19] I. Zahović, Z. Rončević, S. Dodić, J. Grahovac, J. Dodić, Proceedings, 8th Memorial Scientific Meeting on Environmental Protection 'Docent Dr Milena Dalmacija' (2019) UO-04.
[20] Z. Rončević, I. Zahović, N. Danilović, S. Dodić, J. Grahovac, J. Dodić, Journal on Processing and Energy in Agriculture 24 (2020) DOI:10.5937/jpea24-25506.

EFFECT OF DROUGHT STRESS ON ANTIOXIDANT STATUS OF WHEAT SEEDLINGS

Ružica Ždero Pavlović[1], Bojana Blagojević[1], Milan Mirosavljević[2], Boris Popović[1]

[1]Faculty of Agriculture, University of Novi Sad, Trg Dositeja Obradovića 8, 21000 Novi Sad, Serbia
[2]Institute of Field and Vegetable Crops, Maksima Gorkog 30, 21000 Novi Sad
e-mail: ruzica.zdero@polj.uns.ac.rs

Abstract

The aim of this experiment was to study antioxidant status of two wheat varieties under drought stress. Investigated parameters were: relative water content (RWC), lipid peroxidation, proline content, and activity of antioxidant enzymes (SOD, CAT, and POD). The plants were grown for 3 weeks before drought was imposed by completed withheld of watering for 6 days. The results showed that ability of some wheat varieties to enhance enzymatic antioxidant activities might be an important attribute linked to drought tolerance. This could limit cellular damage caused by active oxygen species during water deficit.

Introduction

Wheat is one of the most important food staples in Serbia with an average annual production of 2.5 million tons. In the EU, wheat accounts for 47% of cereals with an annual production of over 140 million tons. Apart from the economic importance, wheat have significant place in human diets because of its high amount of carbohydrates, minerals, proteins, vitamins, and phenolic compounds [1].

Drought is the most important limiting factor for plant growth and productivity and it is becoming an increasingly severe problem in many regions of the world. It is estimated that drought causes an annual loss of 20% in wheat yield [2]. Under unfavorable conditions, such as drought, plants suffer from oxidative stress that affects numerous metabolic process and cause damages to DNA, proteins, and lipids. Accumulation of reactive oxygen species (ROS) and activation of antioxidant system in plants is observed by many authors [3, 4]. Major ROS-scavenging enzymes are superoxide dismutase (SOD), catalase (CAT), peroxidase (POD), and glutathione-reductase (GR). Antioxidants of low molecular weight such as ascorbic acid, tocopherol, and glutathione are also present in wheat. Active together they contribute to maintaining redox balance in cells.

There is a much variation in drought tolerance among wheat genotypes. Comparative investigations of Paul et al. [5] have shown that observed wheat cultivar –dependent differences can be related to plants antioxidant capacity.

The aim of this work was to study the variation in antioxidative enzymes activity (SOD, CAT, and POD), level of lipid peroxidation, proline content and electrolyte leakage in wheat leaves imposed to drought stress.

Experimental

Wheat seeds (*Triticum aestivum* L. cv. ‘NS 40S’, cv. ‘Renesansa’) were obtained from Institute of Field and Vegetable Crops, Novi Sad, Serbia and stored in refrigerator. Seeds were surface sterilized with 70% ethanol for 5 min and then with 5% NaOCl for 15 min and then rinsed with tap water several times. Seeds were sawn in pots with mixture of soil and send (7:2). Drought stress was imposed on 20 day-old wheat seedlings by stop watering pots for 5 days. The seedlings (green part) were excised, rapidly weight (1 g) and ground with pestle in an ice

cold mortar with 10 ml of 100 mM phosphate buffer, pH 7. One part of plant material was frozen and stored at -70°C until use for determination of free proline content.

For determination of relative electrolyte leakage, ten pieces of fresh leaf samples were washed in deionized water and then were soaked in tubes with 20 ml of deionized water at 25°C. Electrical conductivity of bathing solution was measured after 24 h (L_1) using conductivity meter (model EL30, Mettler Toledo, USA). The tubes with samples were then incubated in a boiling water bath (100°C) for 25 min and a final conductivity reading (L_2) was taken after cooling to room temperature. Relative electrolyte leakage was calculated according to formula: REL (%) = (L_1/L_2) • 100% [6]. Lipid peroxidation (LP) was estimated by measuring the concentration of malodialdehyde (MDA) [7]. Absorbance was read at 532 and 600 nm and MDA content was calculated using an extinction coefficient 155 mM^{-1} cm^{-1} by subtracting the absorbance at 532 nm from that at 600 nm. The concentration of protein was measured according to Bradford [8]. The content of free proline was determined as describe earlier by Bates [9]. The superoxide dismutase activity was determined according to the method described by Giannopolitis and Ries [10] by measuring the ability of the enzyme extract to inhibit the photochemical reduction of nitro-blue tetrazolium. One unit of SOD activity was defined as the amount of enzyme required to produce a 50% inhibition of reduction of NBT at 560 nm. Catalase (CAT) activity was assayed according to Aebi [11]. The decomposition of H_2O_2 was followed spectrophotometrically by the decrease in absorbance at 240 nm. One unit of catalase activity corresponded to the amount of enzyme that decomposes 1 μmol of H_2O_2 per minute. The activity of POD was determined using oxidation of guaiacol, as described by Diaz et al. [12].

Results of the biochemical parameters represent data expressed as means of determinations made in triplicates and tested by ANOVA followed by comparisons of means by the Duncan's test ($p < 0.05$). Data were analyzed using software STATISTICA version 13.2 (StatSoft, Inc., USA).

Results and discussion

The results obtained in this study are presented in one figure and one table. The relative electrolyte leakage and lipid peroxidation are presented in Figure 1. Under drought stress relative electrolyte leakage and lipid peroxidation significantly increase, when compared to the controls (Fig.1). In general, lipid peroxidation, assayed as malondialdehide (MDA) formation, was higher in control leaves of cultivar 'Renesansa' (42.8 nmol MDA/g FW) than in control cultivar 'NS 40S' (29.9 nmol MDA/g FW). An increase in relative electrolyte leakage indicates deterioration in cellular membrane systems. Also, observed higher levels of MDA under drought conditions indicate oxidative damage of membrane lipids, resulting from uncontrolled free radical production. This result is in agreement with those of Popovic et al. [3], who investigated the responses of poplar clones to drought and reported significant increase of reactive oxygen and nitrogen species and lipid peroxidation.

Drought stress is associated with increased oxidative stress and induction of antioxidant enzymes is a general mechanism of adaptation strategy which plant use to overcome oxidative stresses [13]. In this study, activities of SOD, CAT, and POD were analyzed and presented in Table 1. The activity of SOD enzyme decreased under the drought stress conditions in the cultivar 'Renesansa', which is in agreement with findings of Tian and Lei [14] who found that SOD under severe drought stress decreased a lot. In the cultivar 'NS 40S' the values of SOD activity under stress were significantly above the control levels. The activity of CAT stayed at control level. The activity of POD had similar trends at both cultivars and did not significantly change under drought stress.

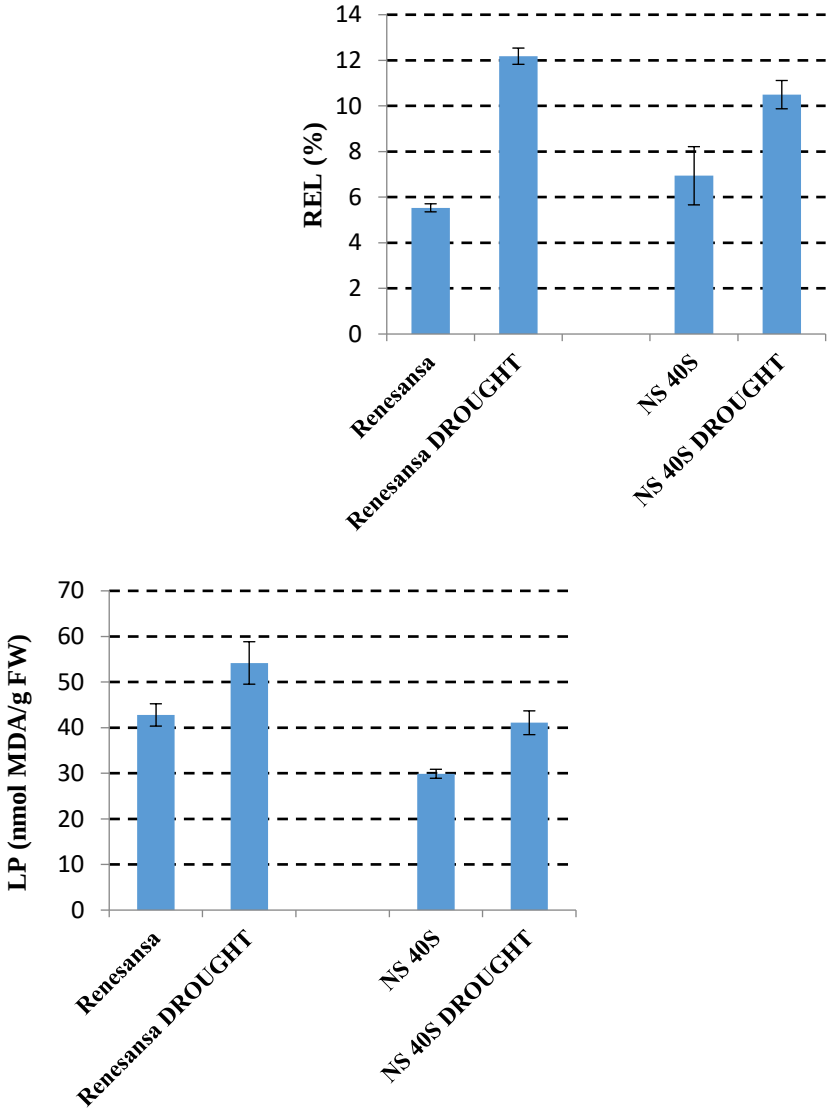

Figure 1. Effect of drought stress on relative electrolyte leakage (REL) (A) and lipid peroxidation (LP) (B) in wheat seedlings. Values are the means of the three different experiments. Error bars represent SD with $n = 3$. The bars with different letters indicate significance of difference at $p < 0.05$ level by Duncan's test.

Table 1. Antioxidant enzyme activities and PRO levels in wheat seedlings leaves of control and stressed plants

	cv.	control	drought
SOD (U mg^{-1} protein)	Renesansa	46.97^{a}	29.05^{b}
	NS 40S	29.95^{b}	47.49^{a}
CAT (nmol H_2O_2 mg^{-1} protein min^{-1})	Renesansa	2.92^{a}	2.97^{a}
	NS 40S	3.94^{a}	3.45^{a}
POD (µmol guaiacol mg^{-1} protein min^{-1})	Renesansa	5.48^{b}	5.81^{b}
	NS 40S	7.46^{a}	7.33^{a}
PRO (mg g^{-1})	Renesansa	10.07^{d}	60.72^{a}
	NS 40S	31.11^{c}	50.86^{b}

*Values marked with same letter do not differ significantly at $p < 0.05$ (Duncan's test)

Table 1 also shows the results concerning free proline accumulation in wheat seedlings. The highest free proline quantity was detected in drought stressed seedlings of cultivar 'Renesansa'. The proline content in our study is in consistency with results obtained by Paul et al. [5]. It is interesting to observe that proline induction was smaller in cultivar 'NS 40S' which showed the higher SOD activity under drought treatment. This indicate that cultivar 'NS 40S' was effectively preventing the formation of ROS by antioxidant systems without the need for a large extent of proline production. This is in agreement with previous investigations of Babić et al. [15] who indicated cultivar 'NS 40S' as drought tolerant cultivar. In contrast, cultivar 'Renesansa' suffered large electrolyte leakage under drought conditions also showed very high level of proline production, indicating the inefficiency of other antioxidant protective mechanisms.

Conclusion

Water stress is one of the most important environmental factors that regulate plant growth and development, and limit plant production. In our study, obtained data showed that drought stress caused oxidative damage to wheat seedlings through excessive generation of ROS. In both investigated cultivars drought stress increased electrolyte leakage and lipid peroxidation, as well as proline accumulation. In cultivar 'NS 40S' was observed higher activation of antioxidant system, so the use of this wheat cultivar in dry land conditions is supported by these results.

Acknowledgements

This work was supported by the Ministry of Education, Science and Technological Development of the Republic of Serbia, grant number 451-03-68/2020-14/200117.

References

[1] Zhu, Y., Sang, S. (2017). Phytochemicals in whole grain wheat and their health-promoting effects. *Molecular Nutrition & Food Research*, *61*(7): 1600852.

[2] Daryanto, S., Wang, L., Jacinthe, P-A. (2016). Global synthesis of drought effects on maize and wheat production. *PloS ONE, 11(5):* eo156362.

[3] Popović, B.M., Štajner, D., Ždero Pavlović, R., Tari, I, Csiszár, J., Gallé, A., Poór, P., Galović, J., Trudić, B., Orlović, S. (2017). Biochemical response of hybrid black poplar tissue culture (*Populus* × *canadensis*) on water stress. *Journal of Plant Research, 130*: 559–570.

[4] Štajner, D., Orlović, S., Popović, B.M., Kebert, M., Galić, Z**. (**2010). Screening of drought oxidative stress tolerance in Serbian melliferous plant species. *African Journal of Biotechnology, 10*: 1609–1614.

[5] Paul, K., Pauk, J., Kondic-Spika, A., Grausgruber, H., Allahverdiyev, T., Sass, L., Vass, I. (2019). Co-occurrence of mild salinity and drought synergistically enhances biomass and grain retardation in wheat. *Frontiers in plant science*, *10*: 501.

[6] Xiao, X.W., Yang, F., Zhang, S., Korpelainen, H., Li, C.Y. (2009). Physiological and proteomic responses of two contrasting *Populus cathayana* populations to drought stress. *Physiologia Plantarum, 136*: 150–168.

[7] Heath, R.L., Packer, L. (1968). Photoperoxidation in isolated chloroplast I. Kinetics and stoichiometry of fatty acid peroxidation. *Archives of Biochemisty Biophysics,* 25: 189–198.

[8] Bradford, M.M. (1976). A rapid and sensitive method for the quantitation of microgram quantities of protein utilizing the principle of protein-dye binding. *Analytical Biochemistry*, *72*: 248–253.

[9] Bates, L. S., Waldren, R. P., Teare, I. D. (1973). Rapid determination of free proline for water-stress studies. *Plant Soil*, *39*: 205–207.

[10] Giannopolitis, C.N., Ries, S. K. (1977). Superoxide dismutases. I. Occurrence in higher plants. *Plant Physiol*ogy, *59*: 309–314.
[11] Aebi, H. (1984). Catalase *in vitro*. *Methods in enzymology*. 105, p. 121–126.
[12] Díaz, J., Bernal, A., Pomar, F., Marino, F. (2001). Induction of shikimate dehydrogenase and peroxidase in pepper (*Capsicum annuum* L.) seedings in response to copper stress and its relation to lignification. *Plant Sciences, 161*: 179–188.
[13] Gill, S.S., Tuteja, N. 2010. Reactive oxygen species and antioxidant machinery in abiotic stress tolerance in crop plants. *Plant Physiology and Biochemistry* 48: 909–930.
[14] Tian, X., Lei, Y. (2006). Nitric oxide treatment alleviates drought stress in wheat seedlings. *Biologia plantarum, 50(4)*: 775-778.
[15] Babić, Lj., Babić, M., Turan, J., Matić-Kekić, S., Radojčin, M., Mehandžić-Stanišić, S., Pavkov, I., Zoranović, M. (2011). Physical and stress-strain properties of wheat (*Triticum aestivum*) kernel. *Journal of the Science of Food and Agriculture, 91*: 1236-1243.

COMPUTATIONAL AND EXPERIMENTAL INVESTIGATIONS ON A TUNEABLE SPATIAL HETERODYNE SPECTROMETER

Dávid Jenő Palásti[1,2], Miklós Veres[3], Miklós Füle[4,5], Zsolt Geretovszky[2,6], Gábor Galbács[1,2*]

[1]*Department of Inorganic and Analytical Chemistry, University of Szeged, H-6720 Szeged, Dóm tér 7, Hungary*
[2]*Department of Materials Science, Interdisciplinary Excellence Centre, University of Szeged, 6720 Szeged, Dugonics sq. 13, Hungary*
[3]*Department of Applied and Nonlinear Optics, Wigner Research Institute for Physics, H-1121 Budapest, Konkoly-Thege Miklós út 29-33, Hungary*
[4]*Faculty of Engineering, University of Szeged, H-6724 Szeged, Mars square 7, Hungary*
[5]*ELI-ALPS Laser Research Institute, H-6728 Szeged, Wolfgang Sandner street 3, Hungary*
[6]*Department of Optics and Quantum Electronics, University of Szeged, H-6720 Szeged, Dóm tér 9, Hungary*
e-mail: galbx@chem.u-szeged.hu

Abstract
Spatial heterodyne spectrometers (SHS) are interference based instruments for obtaining spectroscopic information in the UV and visible ranges. In this current study we are representing our experimental and computational findings about a tuneable SHS instrument.

Introduction
Although SHS concept was first described in the 1960s and 1970s [1], but the practical applications of this type of spectrometers only came in the early 1990s, when Harlender et al. demonstrated its potential in high resolution spectroscopic observation of faint, distant objects in astronomy [2]. Recently we built and used an SHS spectrometer for qualitative and quantitative Raman spectroscopy [3].

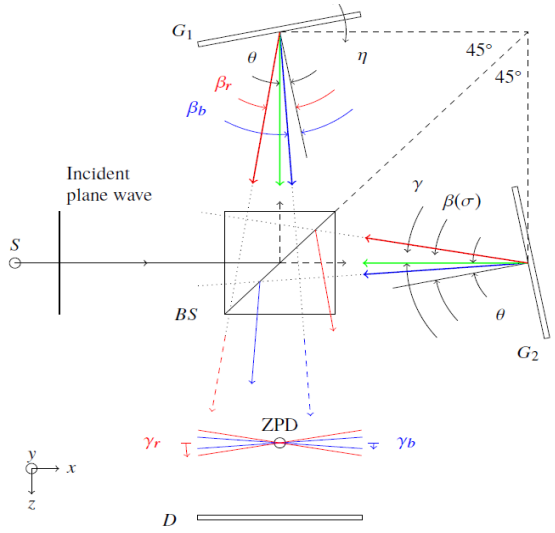

Figure 1. The schematic and working principle of spatial heterodyne spectrometers

Fig. 1. shows the basic arrangement and working principle of SH spectrometers. The collimated incident wave is split by the beamsplitter (BS) and illuminates two gratings (G_1, G_2), where the spectral components are diffracted at different β angles. The combination of these diffracted wavefronts creates an interference pattern. Each spectral components create its own Fizeau fringes with a spatial frequency characteristic of the γ angle between the two wavefronts. The superposition of the individual fringes may create a very complex pattern. All lines of this pattern contains spectral information, which can be extracted by Fourier-transformation.

SHS has many unique features, which can be advantageously utilized in atomic spectroscopy. It has high light throughput, which improves the sensitivity and robustness of the instrument. It is easy to achieve high resolution in any wavelength region. It is a "one shot" technique, that is the whole covered spectral range can be extracted from a single interference pattern.

As it is obvious from the drawing, γ can be changed by the rotation of the gratings, thus the observed spectral range can be shifted which provides a tuning feature. It creates a possibility to record very high resolution spectra in a wider spectral range by splicing adjacent spectrum segments. Our final goal with this project is the construction of an automatic, self-tuning SHS, capable of providing high resolution and a wide spectral coverage at the same time. To achieve our goal, it is essential to understand the tuning characteristics and the instrumental function of the setup, thus we carried out a thorough computational and experimental analysis.

Experimental

The optical model of the double greating SHS arrangement (Fig 2.) was constructed in Comsol Multiphysics, using the geometrical optics interface and the ray tracing module. During the modeling of the sensitivity, and free spectral range of the setup, parametric sweeps of non-sequential ray tracings were performed using hexapolarly arranged, unpolarized, monochromatic and collimated input light beam consisting of 331 individual rays, with plane wave approximation. The fundamental experimental variables of the SHS setup were the groove density of the gratings, the grating arm lengths (distance of the grating surface from the active plane of the beamsplitter), grating rotation angle (around an axis oriented along the *z* direction and placed at the grating surface), input beam wavelength, and input beam diameter.

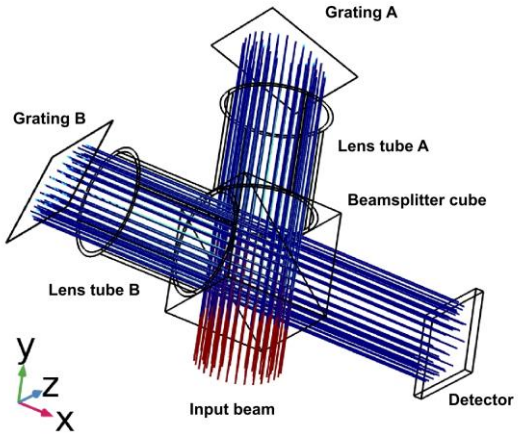

Figure 2. Conceptual ray tracing model of the SHS setup in Comsol. Please note that the number of rays plotted here is much smaller than the number of rays used in the modeling.

In our experimental setup (Fig. 3.), the light from the source (Hg-Ar spectral calibration lamp) was led by a fiber optics into a reflective collimator, which feeds the light into a bandpass filter (this eliminates some spectral interferences) towards the 50:50 beamsplitter. The splitted light beams go through irises then reach the diffractive ruled gratings sitting in grating holders.

One of the gratings were placed on the top of a motorized rotation stage, able to provide sub-minute precision rotation. The gratings were oriented in such a way that the first order of diffraction was sent back towards the camera. The gratings were also slightly tilted in order to make the interpretation of the Fourier transform easier. Further spectral filters were also applied in the beam path for the purpose of eliminating order overlap. Spectral calibration was achieved by a mercury-argon calibration lamp (Ocean Optics Hg1).

The camera objective and some additional lens image the plane of the gratings onto the an Andor iSTAR iCCD camera. Lens tubes were also employed to protecting the lightpath from scattered ambient light.

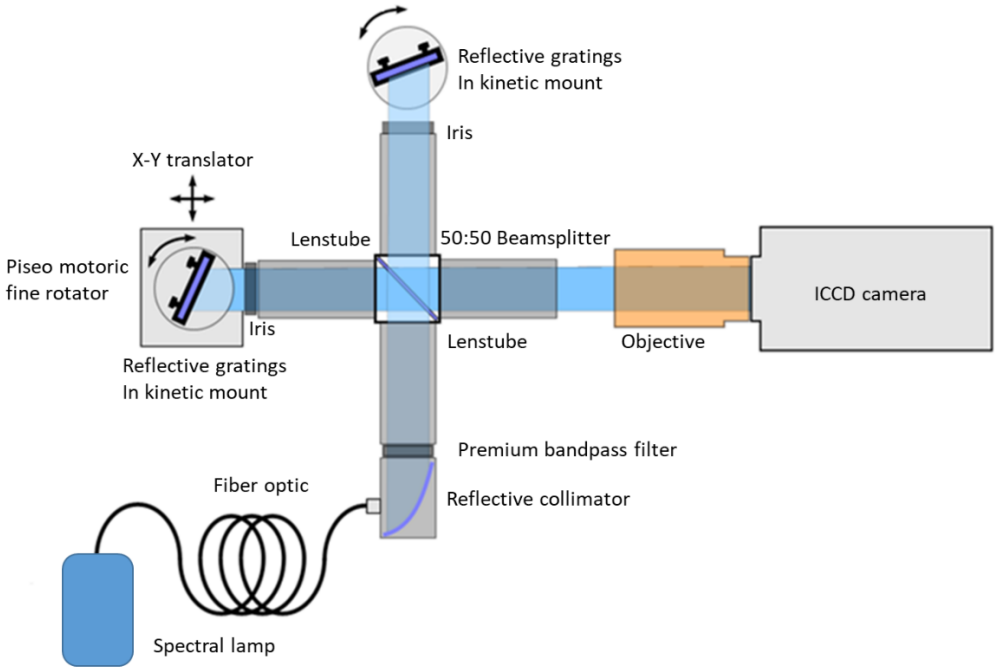

Figure 3. Schematic of our experimental setup

Results and discussion

The ray tracing simulations revealed, not entirely surprisingly, that the sensitivity of the recorded spectral lines depend on how far they are from the blaze wavelength of the grating. Since the setup is constructed in such a way that it uses the first order reflection, therefore for maximum sensitivity the rotation angle has to be adjusted to coincide with the blaze angle. The relative sensitivity decreases rapidly, if the gratings are rotated concertedly; a few degree rotation results in a sensitivity drop of about 50%. We simulated the sensitivity surves for three different gratings (with different grating density) and the results can be seen in Fig 4.

A similar parameter sweep was executed to estimate the spectral coverage of the spectrometer. This time, the rotation angle was fixed, and the wavelength of the incident light was changed between 400 and 700 nm in the geometrical optics simulation. The simulations showed that with 50 mm armlength, it is possible to achieve at least 150 nm free spectral ranges. The calculations also revealed the possibility for an overlap between the first and second order diffracted beams, which emphasized the importance of adequate filtering.

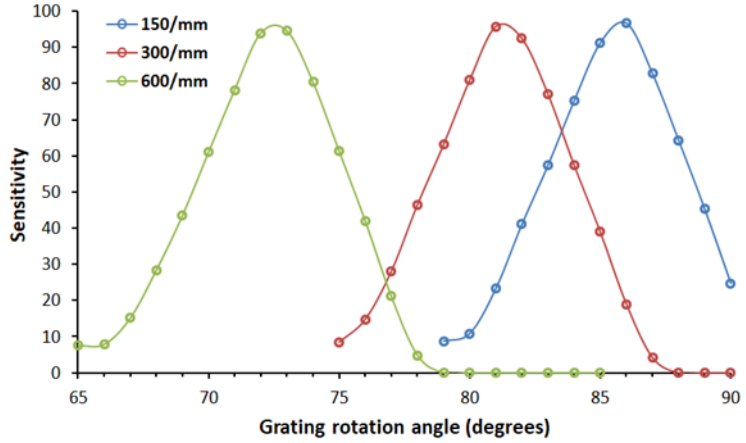

Figure 4. Effect of concerted grating rotation on the relative sensitivity of the SHS arrangement, at the 500 nm blaze wavelength. Arm length is 50 mm.

We experimentally assessed the spectral resolution of our SHS for a set of 300 mm^{-1} and 600 mm^{-1} gratings and values of 0.03 and 0.015 nm/pixel were achieved. These values are excellent considering the compact size of the instrument. Similar resolutions can only be obtained with regular, dispersion monochromators if the arm length (focal length) is on the order of 750-1000 mm and by using a holographic grating (1800 or higher grooves/mm)

The tuneability of the system was also investigated experimentally. One of the gratings was rotated by the piezo rotation stage, while the other was fixed. According to our observations, the spectral lines emitted by the calibrating Hg-Ar light source shifted linerally with the angle of rotation as it is demonstrated in the Fig 5. The effect of the rotation was found to be similar in case of both applied grating sets.To move a spectral peak with a certain amount of pixels into one direction the same rotation is needed, thus the rotation angle needed to move the observed range with a certain value is double in case of the 600 mm^{-1} compared to the 300 mm^{-1} one. It was found that the system is very sensitive for the rotation angle, a sub-degree rotation shifts the recorded spectral range with 20-40 nm.

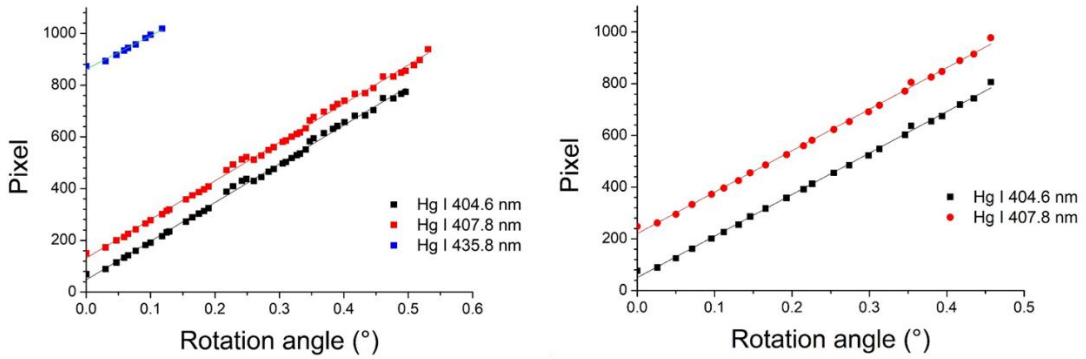

Figure 5. The shift of the observed pixel position of spectral lines as a function of the rotation angle. Left graph: 300 mm^{-1} gratings, right graph: 600 mm^{-1} gratings.

Conclusions

A capable geometrical optics model of an SHS was constructed using the Comsol Multiphysics software package. Using this model, a wavelength dependence of the spectrometer sensitivity as well as the spectral coverage was investigated. Experiments were carried out to assess the spectral resolution which resulted in 0.03 and 0.015 nm/pixel values, which are remarkable for such a compact spectrometer. We also studied the tuning characteristics of the SHS and it was

found that the system is very sensitive for the rotation angle, a sub-degree rotation shifts the recorded spectral range with 20-40 nm.

Acknowledgements
The financial support received from various sources including the Ministry of Innovation and Technology (through project No. TUDFO/47138-1/2019-ITM FIKP) and the National Research, Development and Innovation Office (through projects No. K_129063, EFOP-3.6.2-16-2017-00005, TKP 2020 Thematic Excellence Programme 2020) of Hungary is kindly acknowledged. It was also supported by the ÚNKP-20-3 - New National Excellence Program of The Ministry for Innovation and Technology from the source of The National Research, Development and Innovation Fund.

References
[1] G. W. Stroke, A. T. Funkhouser, Physics Letters, 16 (1965) 272-274.
[2] J. Harlender, R.J. Reynolds, F.L. Roesler, The Astrophysical Journal, 396 (1992) 730-740.
[3] A.B Gojani, D.J. Palásti, A. Paul, G. Galbács, I.B. Gornushkin, Applied Spectroscopy, 73 (2019) 1409-1419.

BIOETHANOL PRODUCTION FROM MILLING INDUSTRY BY-PRODUCT IN A LABORATORY-SCALE BIOREACTOR

Jovana Gucunski[1], Bojana Bajić, Vesna Vučurović, Đurđina Belić, Damjan Vučurović, Siniša Dodić

[1] *University of Novi Sad, Faculty of Technology Novi Sad, Biotechnology and Pharmaceutical Engineering, Bulevar cara Lazara 1, 21000 Novi Sad, Republic of Serbia e-mail: jgucunski@uns.ac.rs*

Abstract

Bioethanol produced by biomass fermentation is a renewable and environmentally friendly energy source and has significant potential as a replacement for liquid fossil fuels. Due to the world moving toward more sustainable energy sources, the production of bioethanol has been steadily increasing. This research aims to investigate the efficiency of bioethanol fermentation from a milling industry by-product in a laboratory-scale bioreactor. Prior to fermentation in a bioreactor, for preparation of a milling industry by-product, two different thermo-enzymatic procedures were investigated and compared, and based on the obtained results the more efficient procedure was selected and used for the experiment in a bioreactor. The bioethanol fermentation was carried out in a 14-litre bioreactor in batch mode under anaerobic conditions at 30°C. The obtained results showed that this by-product can be used for the production of bioethanol but that further optimization is necessary to improve the overall efficiency of the bioprocess.

Introduction

As industrial development and the worldwide population increase, the need for energy consumption in the world is growing. The expected environmental threats such as global warming, acid rain and urban smog have caused humanity to move toward utilizing a variety of renewable energy resources, such as bioethanol, that are less toxic for the environment [1]. Bioethanol is mostly produced by fermentation of sugar or starch based raw materials as first generation bioethanol. Usage of these raw materials competes with their use as food sources and has led to the development of bioethanol production from various other sources such as agro-industrial wastes and by-products [2]. There are different by-products and waste materials rich in sugars that have been presented as great raw materials for fermentation processes and a by-product made in the milling industry with a high percentage of starch can be used as a raw material for bioethanol production [3,4]. The aim of this paper was to examine the efficiency of the bioethanol fermentation using a milling industry by-product, which consists of shrunken and damaged wheat grains as well as a small portion of other impurities, and cannot be used as a raw material in the milling industry for the production of wheat flour. The application of this by-product as a raw material in bioethanol production is of great importance considering its high value and wide application, as well as the fact that this bioprocess produces stillage that has the potential to be used as animal feed.

Experimental

Milling industry by-product, i.e. shrunken and damaged wheat grains were ground and mashed with water (at the hydromodule of 1:3, temperature 55°C and pH 6.5). Thermo-enzymatic preparation of the raw material was performed by the following procedure: the addition of Termamyl SC enzyme (keeping the mixture for 30 min at 50°C), heating and keeping the mixture for 30 min at a temperature of 65°C (for experiment 1) or 90°C (for experiment 2),

cooling the mixture to the temperature of 55°C, addition of SAN Super 360 L enzyme and after 30 min cooling to the temperature of 30°C.

The first set of experiments (experiment 1 and experiment 2), i.e. the experiment that was used to select the appropriate temperature of the thermo-enzymatic preparation of the raw material was conducted in the Erlenmeyer flasks of 1 L. The second experiment, i.e. the experiment used to investigate the efficiency of the bioethanol fermentation was performed in the 14-litre laboratory scale bioreactor (Chemap AG). After hydrolysis, 1 mL of 10% (m/v) $(NH_4)_2HPO_3$ solution was added, pH was set to 5.0, and fermentation medium was inoculated with *Saccharomyces cerevisiae* (Voronejskiye, Russia). The fermentation process was performed at 30°C with continuous mixing (200 rpm) under anaerobic conditions.

For determination of dry mass, starch in raw material, protein content in raw material and stillage and bioethanol content in the distillate obtained after destilation of fermentation broth, the standard AOAC methods were used [5].

Results and discussion

In order to properly formulate fermentation media based on the milling industry by-product, it is necessary to characterize the raw material or determine the parameters that are important for bioethanol production. This raw material is characterized by high dry matter content (89.75±0.19 g/100g) and it can be concluded that it has good stability and the possibility of safe storage over a long period of time, without a high risk of contamination. The amount of starch (54.26±0.83 g/100g) and proteins (8.34±0.20 g/100g) shows that this raw material is viable for bioethanol production because it will provide yeast cells with sufficient amounts of nutrients and energy necessary for growth and production of the desired product.

The results obtained after the first set of experiments (experiment 1 and experiment 2) showed that when using lower temperature of liquefaction, i.e. 65°C, the bioethanol yield (g/100g of raw material) is higher by about 5% compared to the experiment conducted under liquefaction temperature of 90°C. Therefore, it is more efficient to use the conditions from experiment 1, due to the higher concentration of the desired product, as well as energy savings due to the application of lower liquefaction temperature.

The results obtained after bioethanol fermentation in a 14-liter bioreactor, content of bioethanol as well as reducing sugars [6] obtained after hydrolysis of starch were measured during the course of fermentation and the obtained results are shown on the figure 1.

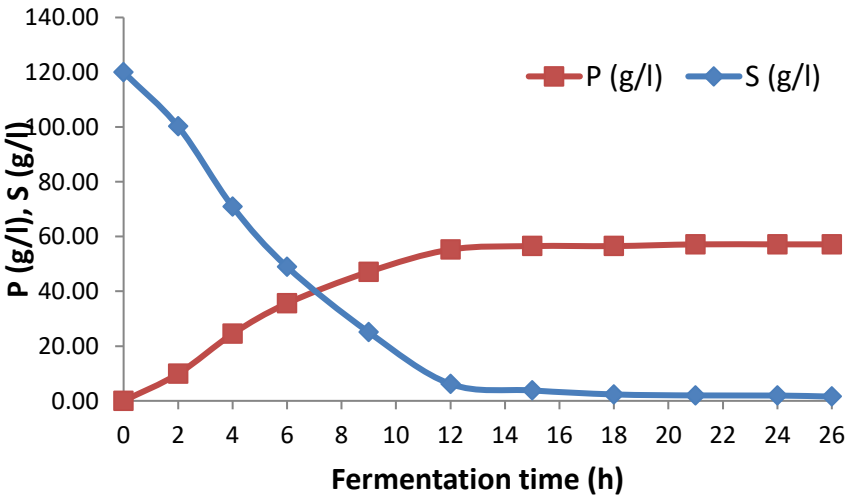

Figure 1. Bioethanol (P) and reducing sugar (S) content obtained during bioethanol fermentation with *Saccharomyces cerevisiae* in a laboratory-scale bioreactor

Under applied experimental conditions, the obtained concentration of bioethanol was 57.1 g/L. The conversion of reducing sugars is 98.7%, while the yield of sugar to ethanol is 89.5%. Changes in the concentration of substrates and products are intense during the first 14 hours of fermentation, after which the intensity decreases and based on the course of fermentation, it can be concluded that it is necessary to shorten the fermentation time. The content of nitrogen in stillage obtained after distillation of fermentation broth was determined and has a value of 4.3 (% m/m).

Conclusion

The obtained results showed that shrunken and damaged wheat grains as a milling industry by-product can be used as raw material for the production of bioethanol, during which bioprocess stillage is obtained that can potentially be used as animal feed. Further research should encompass further optimization of pretreatment and hydrolysis of raw material, optimization of milling industry by-product based media as well as fermentation parameters in order to increase yield and quality of the desired products.

Acknowledgements

This study is part of the project (451-03-68/2020-14/200134) funded by the Ministry of Education, Science and Technological Development of the Republic of Serbia.

References

[1] M. Vohra, J. Manwar, R. Manmode, S. Padgilwar, S. Patil, Bioethanol production: Feedstock and current technologies. Journal of Environmental Chemical Engineering. (2014);2(1):573-584.

[2] A. Bušić, N. Mardetko, S. Kundas, G. Morzak, H. Belskaya, M.I. Šantek, D. Komes, S. Novak, B. Šantek, Bioethanol production from renewable raw materials and its separation and purification: A review. Food Technol Biotechnol. (2018);56:289–311.

[3] P. K. Sadh, S. Duhan, J. S. Duhan, Agro-industrial wastes and their utilization using solid state fermentation: a review. Bioresour Bioprocess. (2018);5(1).

[4] V. Micić, M. Jotanović, Bioethanol as fuel for internal combustion engines, Zastita Materijala. (2015);56(4):403 – 408.

[5] Associattion of official Analitical Chemists International, 17th edition, Gaithersburg, AOAC, 2000. Official Methods: 966.20, 968.28, 970.57, 969.37, 977.08, 969.36, 942.06.

[6] G.L. Miller, Use of Dinitrosalicylic Acid Reagent for Determination of Reducing Sugar. Anal Chem., 31, 426-428.

INVESTIGATION OF THE TRANSFORMATION OF 5-FLUOROURACIL CYTOSTATICS BY UV AND VUV PHOTOLYSIS

Dávid Dercze, Luca Farkas, Tünde Alapi

Department of Inorganic and Analytical Chemistry, University of Szeged, H-6720 Szeged, Dóm tér 7, Hungary
email: derczedavid0905@gmail.com

Abstract

In this work, UV (254 nm), UV/VUV$_{185\ nm}$, and VUV$_{172\ nm}$ photolysis of 5-fluorouracil (5-FLU), a cytostatic drug were investigated. For the water treatments three type of lightsources were applied: a low-pressure mercury vapour lamps emitting only 254 nm UV light, an other low-pressure mercury vapour lamps emitting both 254 nm UV and 185 nm VUV light, and a Xe excimer light source emitting 172 nm VUV photons. In parallel, with the transformation of 5-FLU, H_2O_2 formation was detected and measured. During UV/VUV$_{185\ nm}$ photolysis, the formation of H_2O_2 follows a maximum curve, while in the case of UV photolysis, it shows a saturation curve. Its concentration reached higher value in the case of UV/VUV$_{185\ nm}$ than in UV radiation. To enhance the efficiency of the reactors, we used air, O_2 and N_2 gases and assessed their effect to the photolysis of 5-FLU to see wich parameters are the most suitable for transforming it.

Introduction

5 Fluorouracil (5-FLU) is an antineoplastic drug that is being used in a wide variety of cancer treatments such as breast cancer, colon cancer, stomach cancer and some types of skin cancer. 5-FLU is a genotoxic compound, it builds into the DNA and by alkalinizing it, it also inhibits the thimidilate sinthase enzime resulting in fatal DNA errors [1]. In some countries (depending on the size of the population and the incidence of cancer), several kilogram of 5-FLU is used each year, which can result in up to 100 µg in hospital effluents [2]. 5-FLU is a potential contaminant of natural waters through hospital wastewater and its metabolites selected by the human body can pose an environmental risk in the sewer system. Due to its low absorbance above 290 nm, it does not or slowly transform with direct photolysis under the influence of sunlight, so it is likely accumulate in surface waters. On the other hand, 5-FLU has low Henry's law constant (1.66×10^{-10} atm L mol^{-1} [3]) , and it has low logK_{ow} (-0.89 [4]), and neither hydrolysis nor volatilization is typical. Consequently 5-FLU can be disposed primarily by photolysis, so it is very important to investigate the efficacy of AOPs in the conversion of 5-FLU and its degradation products.

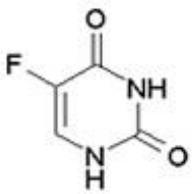

Figure 1. Chemical structure of 5-fluorouracil

One of the most efficient technologies for persistant water pollutant are the advanced oxidation processes wich use electromagnetic radiation (like gamma-, UV-and/or VUV radiation) in some instances alongside oxidating agents such as H_2O_2 and ferrous ions to create highly reactive species (H• and OH• radicals) to transform organic molecules.

UV photolysis is widely used in water treatment for disinfection due to its germicidal effect. In most cases, for UV photolysis low-pressure mercury vapour lamp is used, emitting at 254 nm, both on a laboratory and industrial scale. The efficiency of the method is mainly determined by the molar absorbance of the target compound and the quantum efficiency for its transformation. During its discharge the majority of the emitted photons (approximately 90%) have a wavelength of 254 nm, the rest of them has a wavelength of 185 nm, which is absorbed on the lamp made of traditional quartz. In the case of lamp made of synthetic quartz, it able to emit both 254 nm UV and 185 nm VUV photons.

There are two main sources of $VUV_{172\ nm}$ radiation. The low pressure mercury vapour lamp (mentioned above) and the excimer lamps. The excimer lamps contain noble gases, which form dimers in response to an electric impulse with the sufficient energy. These dimers dissociate afterwards emitting VUV photons that can be taken as quasi monochromatic light. Excimer lamps have a number of advantages such as no warmup time, quasi monochromatic light emission, high spectral power density, low heating (''cold lamps'').

Experimental

Two types of low-pressure mercury vapour lamps was used as light sources: a LightTech GCL307T5L light source for UV (254 nm) photolysis, a GCL307T5VH type light source for UV/VUV (254/185 nm) photolysis, and a Radium Xeradex^{TM} lamp for VUV (172 nm) photolysis. The envelope of the UV lamp emitting at 254 nm was made of commercial quartz, while the UV/VUV (254/185 nm) lamp's envelope was made of synthetic quartz to be able to transmit the 185 nm VUV photons. The intensity of 185 nm VUV light radiation is about 6-8% of UV light radiation.

5-FLU (Sigma-Aldrich, ≥99%) solutions (500 mL) with 1.0×10^{-4} mol L^{-1} initial concentration was made in ultrapure MILLI-Q water (MILLIPORE Milli-Q Direct 8/16).

Separation of the organic substances of the treated samples and determination of 5-FLU concentration was performed by liquid chromatography using Agilent 1100 type HPLC (High Performance Liquid Chromatography) equipped with a diode array UV (DAD) detector. The column (Aminex HPX-87H, 300×7.5 mm) was thermostated at 30 °C, the flow rate of eluent was 0.9 mL min^{-1}, and 20 µL sample was injected.

Total organic carbon (TOC) measurements were performed using an Analytik Jena N/C 3100 analyzer. The concentration of H_2O_2 was measured with a cuvette test by Merck, with a 0.015 - 6.00 mg L^{-1} measuring range.

Results and discussion

At first, transformation rates of 5-FLU were compared in the cases of UV, $UV/VUV_{185\ nm}$, and $VUV_{172\ nm}$ irradiated solutions (table 1). Direct photolysis was effective in the transformation of 5-FLU, which is supported by several literatures [4, 5], but using $UV/VUV_{185\ nm}$ photolysis it increases the transformation rate at least one and a half times (Fig 2.). In the case of 254 nm UV radiated solution, UV photons are absorbed by the organic substances, direct photolysis of 5-FLU takes place, which efficiency depends on the molar absorbance of the target substance ($\varepsilon_{254\ nm}$=5296.6 M^{-1} cm^{-1}) at 254 nm and the quantum yield of its transformation. In the case of VUV photons, it is absorbed by water to form radicals,

$$H_2O + h\nu\ (<190\ nm) \rightarrow H\bullet + HO\bullet \qquad \Phi(HO\bullet)_{185\ nm} = 0.33 \quad \Phi(HO\bullet)_{172\ nm} = 0.42$$

$$H_2O + h\nu\ (<200\ nm) \rightarrow \{e^-, H_2O^+\} + H_2O \rightarrow \{e^-, H_2O^+\} + (H_2O) \rightarrow e_{aq}^- + HO\bullet + H_3O^+$$

$$\Phi(e_{aq}^-)_{185\ nm} = \Phi(e_{aq}^-)_{172\ nm} = 0.05$$

so the transformation of 5-FLU is initiated by H• and/or HO•.

Table 1. *Initial transformation rates of 5-FU at 1.0×10^{-4} M initial concentration*

	UV air	UV N_2	UV/VUV$_{185nm}$ O_2	UV/VUV$_{185nm}$ N_2	VUV$_{172nm}$ O_2	VUV$_{172nm}$ N_2
r_0 ($\times10^{-7}$ M s^{-1})	1.99	1.81	2.73	4.47	1.45	1.55
Φ	0.054	0.049	0.23	0.82	0.014	0.014

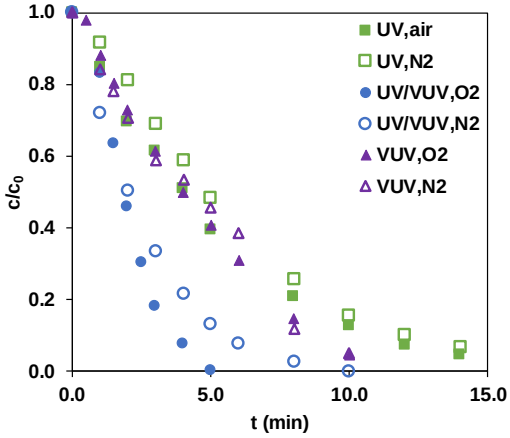

Fig 2. Relative concentration of 5-FLU versus time of irradiation in the case of UV UV/VUV$_{185\ nm}$ and VUV$_{172\ nm}$ photolysis

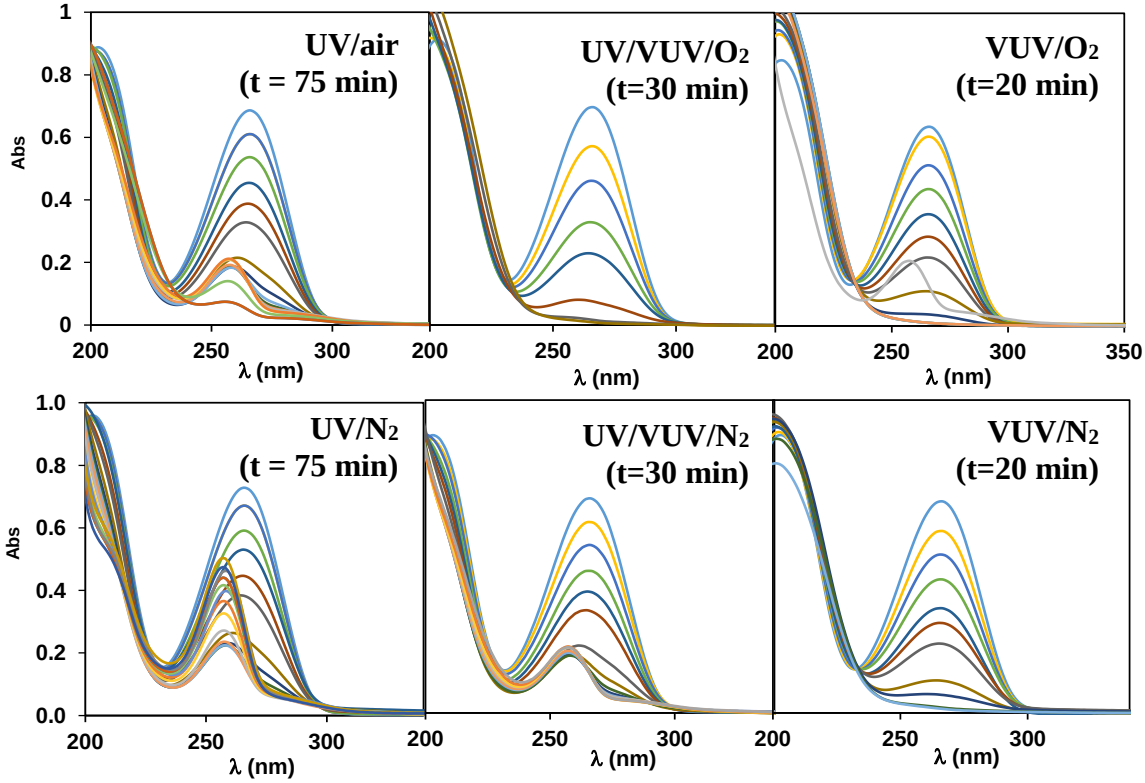

Fig 3. The change of absorbance of the treated 5-FLU solutions

In most cases, the dissolved O_2 has a positive effect on the transformation rate as during 5-FLU UV photolysis (Fig 2). In the case of UV/VUV$_{185\ nm}$ photolysis, dissolved O_2 reduced the transformation of 5-FLU (Fig 2), while it had no significant effect on VUV$_{172\ nm}$ photolysis

(Fig 2). During UV/VUV$_{185\ nm}$ and VUV$_{172\ nm}$ photolysis, dissolved O_2 reacts with H•, reducig the concentration of one of the primary radicals formed during water photolysis, but opens a new way for the transformation of organic substances through the formation of peroxyl radical. The importance of O_2 is demostrated by the change of the spectra of the treated solutions, which is affected by the O_2 concentration in the case of UV and VUV photolysis too.

In the case of toxic or biologically active compounds, it is important to achieve not only to transformation of the parent compound, or if it is, to mineralize it. During UV photolysis, the TOC value of the treated solution slowly decreased (Fig. 4a), while in the case of UV/VUV$_{185\ nm}$ photolysis, the degree of mineralization is significant, the TOC value decreased by approx. 70% (Fig. 4a). Although 172 nm VUV photons did not increase the transformation rate compared to UV photolysis (Table 1.), the mineralization was much more efficient, TOC decreased by approx. 85%. During the oxidative transformation of 5-FLU and its degradation products, through the formation and transformation of organic peroxyl radicals, quite a lot of HO_2•/O_2•$^-$ is formed. These low reactivity radicals or radical ions do not play a significant role in the direct conversion of organic matter. Radicals are mainly recombining to form H_2O_2. Thus, a change in the concentration of H_2O_2 formed indicates the intensity of the transformation of organic substances.

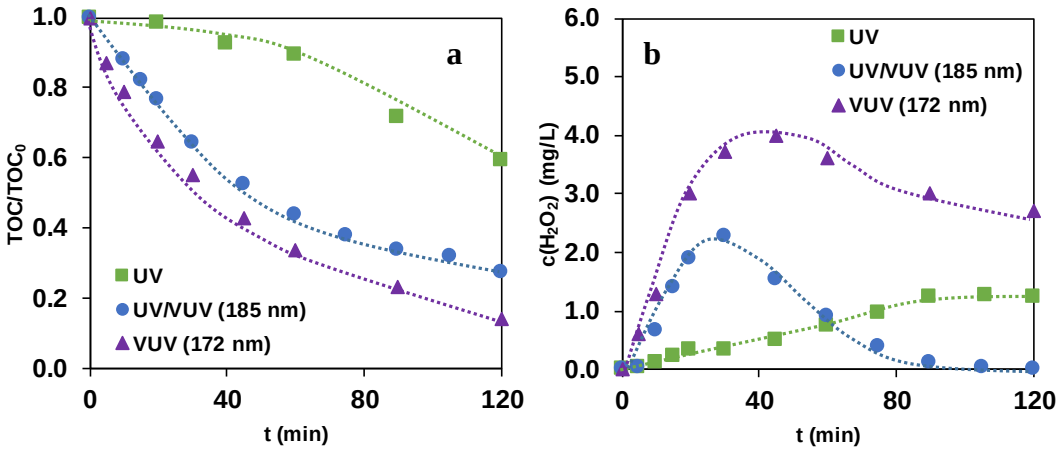

Fig 4. The relative concentration of TOC (a) and the concentration of H_2O_2 (b) versus time of irradiation in the case of UV UV/VUV$_{185\ nm}$ and VUV$_{172\ nm}$ photolysis of 5-FLU

During UV photolysis, a small decrease in TOC and, accordingly, a slow accumulation of H_2O_2 were observed. (Fig. 4). In the case of UV/VUV$_{185\ nm}$ photolysis, the H_2O_2 concentration varies according to a maximum curve, which indicates a more intensive transformation of organic compounds. The H_2O_2 concentration reaches the highest value in the case of VUV$_{172\ nm}$ photolysis, which suggests, as does the TOC, that the intermediates can be transformed most efficiently in this case.

Conclusion

The UV, UV/VUV$_{185\ nm}$, and VUV$_{172\ nm}$ photolysis are effective for the elimination of 5-FLU from aqueous solutions, the highest transformation rate was measured in the case of UV/VUV$_{185\ nm}$ photolysis. Dissolved O_2 has no significant effect on the transformation rate even in the case of VUV$_{172\ nm}$ photolysis. The highest mineralization rate was observed in the case of VUV$_{172\ nm}$ photolysis. Although the photon flux of 172 nm light is much higher than of 185 nm light, the transformation is slower, partly because of the contribution of 254 nm in the case of UV/VUV$_{185\ nm}$ photolysis, and partly because of the extreme inhomogeneity of 172 nm radiated aqueous solution.

Acknowledgements

This publication was supported by the János Bolyai Research Scholarship of the Hungarian Academy of Sciences, and new national excellence program of the Ministry for Innovation and Technology (ÚNKP-20-5-SZTE-639 and ÚNKP-20-3-SZTE-459). The authors thanks the financial support from the project Hungarian Scientific Research Fund (NKFI contract number FK132742)

References

[1] Araújo, A. P. da C., Mesak, C., Montalvão, M. F., Freitas, Í. N., Chagas, T. Q., & Malafaia, G., Science of The Total Environment, 2019, 650, 2284–2293

[2] Mahnik, S. N., Lenz, K., Weissenbacher, N., Mader, R. M., Fuerhacker, M., Chemosphere, 2007, 66 (1), 30-7

[3] Lin, A. Y.-C., Wang, X.-H., Lee, W.-N., Environ. Sci. Technol. 2013, 47, 9, 4104–4112

[4] U.S. National Library of Medicine. http://www.nlm.nih.gov/.

[5] Zhang, Y., Xiao, Y., Zhang, J., Chang, V. W. C., Lim, T.-T., J Environ Chem Eng, 2017, 5, 1, 1133-1139

HETEROGENEOUS PHOTOCATALYSIS OF SULFONAMIDES USING TiO_2 AND ZnO PHOTOCATALYSTS WITH MERCURY-VAPOR AND LED LIGHT SOURCES

Máté Náfrádi, Gellért Farkas, Benjámin Vas, Tünde Alapi

Department of Inorganic and Analytical Chemistry, University of Szeged, H-6720 Szeged, Dóm tér 7, Hungary
e-mail:nafradim@chem.u-szeged.hu

Abstract

Sulfonamides are one of the most often used antibiotics worldwide. The spread of antibiotic-resistant bacteria and the serious health problems caused by them justify the importance of removing antibiotics and their metabolites from water. Heterogeneous photocatalysis is one of the promising methods for elimination of trace organic pollutants from water. This work aims at the investigation of heterogeneous photocatalytic removal of two sulfonamide antibiotics, sulfamethazine and sulfamethoxypyridazine. Commercially available TiO_2 and ZnO were used as photocatalysts, and a mercury vapor lamp (300-400 nm) and UV-LEDs (398 nm) were used as light sources. The efficiency and cost-effectiveness of heterogeneous photocatalysis in the removal of sulfonamides were compared, using TiO_2 and ZnO, in suspensions irradiated with mercury vapor lamp and LEDs. The mercury vapor lamp was found to be more effective due to the better utilization of UV light by the photocatalysts. The LED light source was also worse in terms of operating costs, and TiO_2 with mercury vapor lamps was the most efficient at removing the total organic carbon content.

Introduction

Countless recalcitrant organic pollutants, like pesticides and pharmaceuticals have been detected in the wastewater, and in natural waters worldwide [1]. The water pollution caused by different antibiotics is especially alarming, since they are responsible for the emergence of antibiotic-resistant bacteria. Sulfonamides are a family of antibiotics that are widely used in both veterinary medicine and human healthcare. Some of them are endocrine disrupting, and highly resistant to biological degradation [2, 3].

Advanced Oxidation Processes (AOPs) have been investigated for a long time to remove organic pollutants, which cannot be eliminated via conventional biological water treatment processes. Probably the most researched method is heterogeneous photocatalysis. When a semiconductor is irradiated with photons, having energy higher than the band gap of the catalyst, photogenerated charge separation occurs. The formed conduction band electron (e_{cb}^-) and valence band hole (h_{vb}^+) may react with the organic pollutants, or with O_2 and H_2O, resulting in the formation of other reactive species. Hydroxyl radicals (HO•) are the most important due to their high reactivity and low selectivity.

TiO_2 and ZnO are well-known and widely investigated photocatalysts, due to their efficiency, stability, low price and negligible toxicity. Their band gaps energy are similar; 3.2 eV for TiO_2 and 3.1 eV for ZnO, therefore UV radiation (<400 nm) is required to generate charge separation [4]. Most often a mercury-vapor lamp (MV lamp), emitting in the 300-400 nm range, is applied for excitation of these photocatalysts. Nowadays, due to their intensive development and several advantageous properties, there has been an increased interest in the application of LED light sources in the field of water treatment, even in the case of processes which require UV radiation. [5, 6].

The goal of this study was to investigate the removal efficiency of two sulfonamide antibiotics, sulfamethazine (SMT) and sulfamethoxypyridazine (SMP), using TiO_2 and ZnO photocatalysts under mercury-vapor lamp and commercial UV-LEDs as light sources. The

comparison was based on the initial transformation and mineralization rates. The comparison was also made on the basis of the electrical energy required to operate the light sources (cost efficiency) and on the basis of the photon flux emitted by them (photon efficiency).

Experimental

During the photocatalytic experiments, two reactors were used. In the case of LED light sources, 100 cm^3 suspension was irradiated in a cylindrical glass reactor (volume: 100 cm^3, inner diameter: 45 mm). As light source, UV (LEDmaster, 288 lumen, 4.6 W; λ = 398(±15) nm) LED tape was used, its length was 1 meter, which contains 60 LED pieces. The reactor was equipped with a water cooling system. The LED tape was fixed on the inner wall of the cooling jacket, which was made from an aluminum tube, having 66 mm inner diameter.

Photocatalytic experiments with MV lamp (GCL303T5/UVA, LightTech, 15 W), were performed in a cylindrical glass reactor (56 mm inner diameter). The volume of the irradiated suspension was 500 cm^3. The lamp (20.5 mm diameter and 305 mm length) was immersed into the suspension.

The photon flux of both light sources were determined by ferrioxalate actinometry [7] and found to be 4.83×10^{-6} mol_{photon} s^{-1} for MV lamp and 1.02×10^{-6} mol_{photon} s^{-1} for UV-LEDs. The emission spectra are shown on Fig. 1.

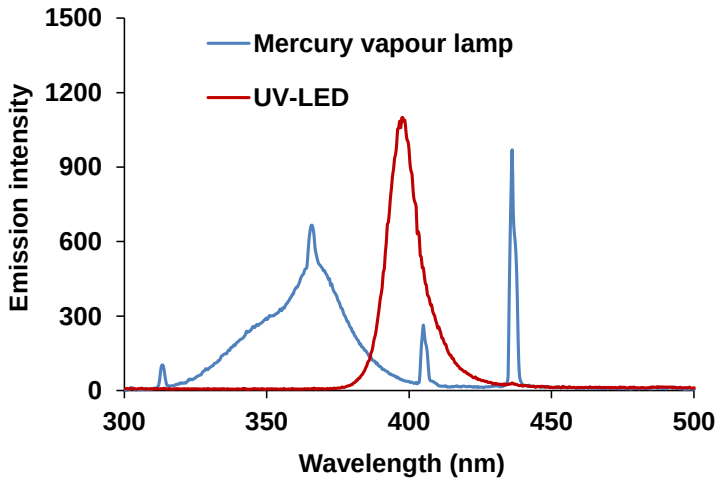

Figure 1. The emission spectra of the light sources

TiO_2 Aeroxide P25 (Acros Organics) and ZnO (Sigma Aldrich) nanoparticles were added to the solutions of sulfonamides, and suspended via ultrasound exposure. The concentration of photocatalysts was 1.0 g dm^{-3}, while the concentration of sulfonamides was 1.0×10^{-4} M in each case. The suspensions were saturated with synthetic air for 15 minutes in the dark, then the photocatalytic experiments were started with switching on the light sources.

Before analysis, samples were centrifuged at 15000 RPM, and filtered using 0.22 µm syringe filters (FilterBio PVDF-L). The concentration of SMT and SMP was measured by HPLC (Agilent 1100 HPLC device, equipped with DAD detector). Licrosphere 100 RP-18 column was used. The eluent contained 30 % methanol and 70 % formic acid solution (0.10 %), the flow rate was 1.0 ml min^{-1}. The detection wavelength was 266 nm for SMT, and 261 nm for SMP. The Total Organic Carbon (TOC) content was measured by Analytik Jena N/C 3100 device.

Results and discussion

Adsorption plays a crucial role in heterogeneous photocatalysis. Thus, the adsorption of both sulfonamides (SMT and SMP) was determined and found to be negligible in each case. (< 1.0 %). The optima of the catalysts loads were determined in the case of both light sources. The linear part of the kinetic curve (until 15 % conversion) was used to determine the initial transformation rate of sulfonamides. Over 0.5 g dm^{-3} catalyst load, no significant increase in the reaction rates was observed, therefore 1.0 g dm^{-3} catalyst load was used in the further experiments. The role of direct photolysis of both SMT and SMP was determined without photocatalyst. The transformation rate was found to be much slower in the case of MV lamp and negligible in the case of LEDs, comparing to the transformation rates determined in the presence of photocatalyst (Table 1).

Table 1. Initial transformation rate and apparent quantum yield of the transformation

	r_0 (mol dm^{-3} s^{-1})		**apparent quantum yield**	
	SMT	**SMP**	**SMT**	**SMP**
MVL	**1.18×10-8**	**1.24×10-8**	**0.0012**	**0.0013**
TiO_2/LED	**5.07×10^{-8}**	**8.69×10^{-7}**	**0.0050**	**0.0852**
ZnO/LED	**6.13×10^{-8}**	**4.80×10^{-8}**	**0.0060**	**0.0047**
TiO_2/MVL	**1.16×10^{-7}**	**1.49×10^{-7}**	**0.0120**	**0.0154**
ZnO/MVL	**1.27×10^{-7}**	**1.13×10^{-7}**	**0.0130**	**0.0117**

The apparent quantum yields were significantly lower in the case of LEDs emitting at 398 nm than is the case of MV lamp, emitting 300-400 nm light. Its reason is the less effective utilization of photons with lower energy by TiO_2 and ZnO. There was no significant difference between the quantum yields determined for ZnO and TiO_2, except when TiO_2 and LEDs were used to eliminate SMP, which was extremely fast (Table 1).

The comparison was also performed on the basis of the electrical energy consumption to treat a unit volume (1.0 dm^3) suspension, which was calculated using the electrical power of the light sources (4.6 W for LEDs and 15 W for MV lamp). The electrical energy, required for the transformation is much higher in the case of LEDs than in the case of MV lamp, expect for SMP, using TiO_2.

The mineralization (complete transformation to CO_2, H_2O, and inorganic ions) of the organic content is also important during water treatment, as the degradation products may also have a similar, or even higher biological effect than the parent compound. Due to the high stability of TiO_2 and the high HO• formation rate, the TOC was reduced by 75% after 120 minutes. ZnO was less effective in the mineralization, despite the similar initial reaction rates, as only 44% TOC content was removed after 120 minutes. In the case of LEDs, only 13% TOC content was removed in TiO_2 containing suspension, while in ZnO containing suspension the decrease was 34%.

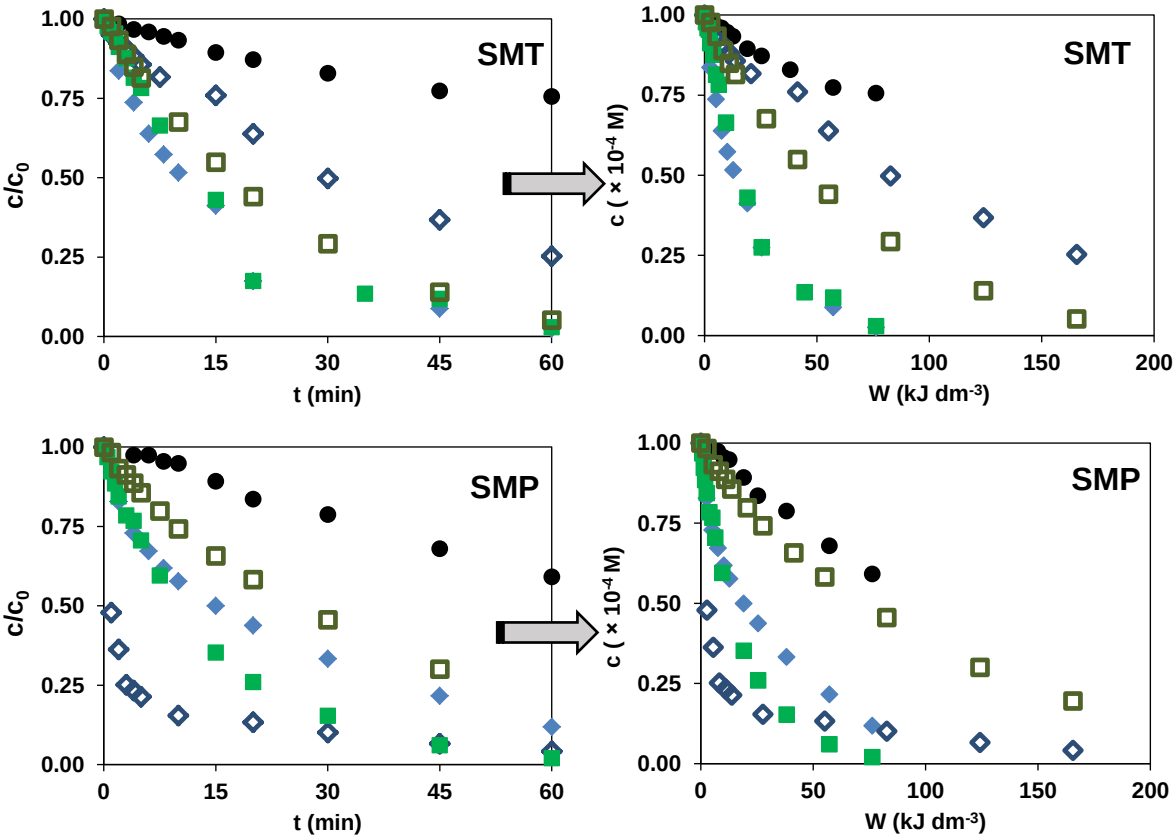

Figure 2. The relative concentration vs. the time of treatment and concentration vs. the electrical power input per volume
●: MV lamp (no photocatalyst); ◆:TiO_2 and MV lamp; ◇: TiO_2 and LEDs; ■: ZnO and MV lamp; □: ZnO and LEDs

The comparison was also performed on the basis of the electrical energy consumption to treat a unit volume (1.0 dm^3) suspension. Similar to the initial reaction rates, using MV lamp is more cost-effective compared to the LEDs, expect for SMP using TiO_2. In this case, TOC decrease was comparable to using MV lamp (Fig. 3).

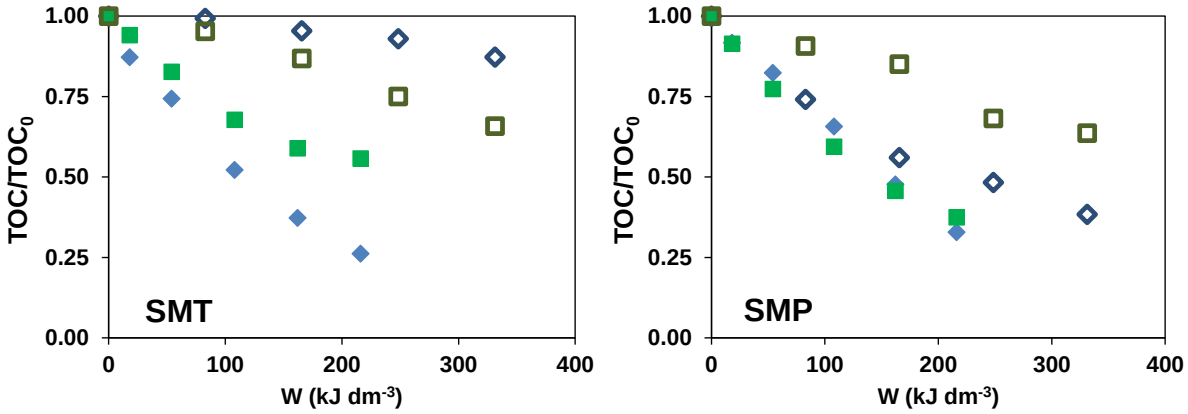

Figure 3. The relative TOC values vs. the electrical energy input
●: MV lamp (no photocatalyst); ◆:TiO_2 and MV lamp; ◇: TiO_2 and LEDs; ■: ZnO and MV lamp; □: ZnO and LEDs

Conclusions

The transformation of SMP and SMT can be performed effectively using both TiO_2 and ZnO photocatalysts, using MV lamp (300-400 nm) and LEDs (398 nm). The apparent quantum yields of the transformation were calculated and compared. It was found to be higher in the case of 300-400 nm radiation than in the case of 398 nm. The electric energy consumption of the MV lamps was significantly lower during the transformation of the sulfonamides, except for SMP. Similar tendencies can be seen for the complete removal of organic content. The behavior of SMP in the presence of TiO_2 irradiated with LEDs is very interesting and needs further investigation.

Acknowledgements

This work was supported by the János Bolyai Research Scholarship of the Hungarian Academy of Sciences, and new national excellence program of the Ministry for Innovation and Technology (ÚNKP-20-3-SZTE 548, and ÚNKP-20-5-SZTE 639). This work was sponsored by the National Research, Development and Innovation Office-NKFI Fund OTKA, project number FK132742.

References

[1] I.T., Carvalho and L. Santos, Environ. Int. **94** (2016) 736-757.
[2] M. De Liguoro, B. Fioretto, C. Polronieri, G. Gallina, Chemosphere, **75** (2019) 1519-1524.
[3] M. Biosic, , M. Mitrevski, S. Babic, Environ Sci Pollut Res Int. **24** (2017) 9802-9812.
[4] Kian Mun Lee, Chin Wei Lai, Koh Sing Ngai, Joon Ching Juan, Water Research **88** (2016) 428e448
[5] M. Khademalrasool, M. Farbod, M. D. Talebzadeh, Journal of Science: Advanced Materials and Devices, **1** (2016) 382-387
[6] J. Zhang, Y. Nosaka, J. Phys. Chem. C, **117** (2013) 1383–1391
[7] C. G. Hatchard, C. A. Parker, Proc. Royal Soc. A, **235** (1956) 518-536.

BiOCl/BiOI COMPOSIT PHOTOCATALYSTS – INVESTIGATION OF THEIR EFFICIENCY USING UV AND VISIBLE LED LIGHT SOURCES

Tamás Hlogyik[1], Máté Náfrádi[1], Klára Hernádi[2], Tünde Alapi[1]

[1]Department of Inorganic and Analytical Chemistry, University of Szeged, H-6720 Szeged, Hungary Dóm tér 7., Hungary
[2]Department of Applied and Enviromental Chemistry, University of Szeged, H-6720 Szeged, Rerrich Béla tér 1.
e-mail: tamas.hlogyik@gmail.com

Abstract
Due to its unique layered structure, bismuth oxyhalide (BiOX, where X=F, Cl, Br, I) has potential applications as a photocatalytic material in clean energy utilization and environmental purification. In this work, BiOI, BiOCl, and their composites with various BiOI:BiOCl molar ratios were synthesized and characterized for their heterogeneous photocatalytic applications. The methyl orange was used as a model pollutant and UV and visible LED light sources were applied. Adsorption measurements and photocatalytic tests proved that, the BiOI/BiOCl composite, which contains 80% BiOI and 20% BiOCl, showed the best activity. The composite catalyst showed good activity under visible light and was particularly better than pure BiOI and BiOCl under UV radiation. The transformation mechanism of methyl orange is initiated by direct charge transfer processes, via photosensitization.

Introduction
The removal of trace amounts of organic pollutants from drinking water is one of the great challenges in water treatment technologies. Advanced oxidation processes (AOPs) based on the formation of reactive particles, as additive water purification methods can offer a solution to remove these substances. Heterogeneous photocatalysis is a widely studied process, mainly for the removal of organic pollutants having low concentration. The process is based on the excitation of a semiconductor, resulting in the formation of excited conduction band electrons (e_{cb}^-) and valence band holes (h_{vb}^+) [1]. The degradation of pollutants can be initiated by the direct charge transfer photogenerated charges and substrates adsorbed on the surface, and/or via radical based reactions. The photosensitization can also play a significant role [2].
Besides the well-known photocatalysts, such as TiO_2 and ZnO [3], a number of new photoactive materials have been developed and studied during the last decades, especially for the harvesting of visible light, as sunlight is the cheapest light source. The synthesis, characterization and activity analysis of new types of photocatalysts are particularly important, as the most common TiO_2 and ZnO require UV radiation (<400 nm).
Bismuth oxyhalide (BiOX, where X=F, Cl, Br, I) photocatalysts have been extensively studied in the last few years as potential photocatalysts, some of them can be excited with visible light. [4]. Bismuth oxyiodide (BiOI) shows the best photocatalytic activity in the visible region, which is explained by the relatively small band gap of the semiconductor (1.8 eV). To increase their stability and activity, various BiOX catalysts were prepared. Li et al. [5] and Zhong et al. [6] used BiOCl/BiOI composites, and successful applied for the elimination of various dyes from aqueous solutions under visible light radiation.
An important technical part of heterogeneous photocatalysis is the selection of the appropriate light source. In the recent years, the use of Light Emitting Diode (LED) has become more and more popular, due to their lower prices, longer lifetime (with proper operation), higher mechanical tolerance and lower electrical energy consumption, they represent a promising alternative to mercury vapor and xenon lamps.

The main goal of this work was the synthesis of BiOI/BiOCl composite catalysts for operation in the visible light region. The transformation of a widely used test compound, methyl orange was investigated. The commercially available LED light sources were used as light source: the application of UV-LED (398 nm) and two other LED light sources, which emit visible light (Cool white and warm white), were investigated and compared.

Experimental

The BiOI/BiOCl photocatalysts were prepared as described in the literature by Bárdos et al. [7]. $Bi(NO_3)_3 \times 5\ H_2O$ (Alfa Aesar, 98 %), KCl and KI (Molar Chemicals, 99.7 %) were used and the photocatalysts were prepared via solvothermal method. The $Bi(NO_3)_3 \times 5\ H_2O$, KCl and KI (in the appropriate proportions) were dissolved in 50 ml ethylene glycol (Sigma-Aldrich, 99.95%). The crystallization was performed at 120 °C in a PTFE autoclave for 3 hours. The solid material was washed with distilled water and ethanol (VWR, 96%), then filtered through 0.1 µm pore size filter (Durapore®, hydrophilic PVDF). The solid material was dried for 24 hours of at 40 °C.

During the photocatalytic experiments, 100 cm^3 suspension was irradiated in a cylindrical glass reactor (inner diameter: 45 mm). The concentration of BiOI/BiOCl photocatalysts was 0.5 g dm^{-3}. Methyl orange (2.0×10^{-4} M) was used as a model compound, in each cases. As light source, UV (LEDmaster, 288 lumen, 4.6 W), cool white (LEDmaster, 390 lumen, 4.6 W), and warm white (LEDmaster, 600 lumen, 4.6 W) LED tapes were used, their emission spectra are shown on Fig. 1. The length of the LED tape was 1 meter in each case. The reactor was equipped with a water cooling system. The LED tape (60 LED/m) was fixed on the inner wall of the cooling jacket, which was made from aluminum tube, having 66 mm inner diameter.

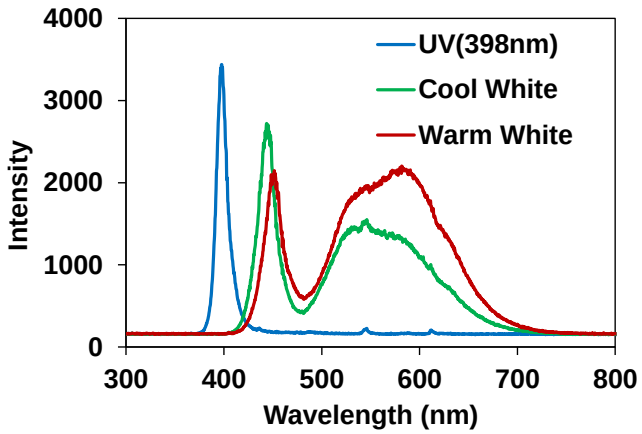

Figure 1. Emission spectra of the LED light sources

Methyl orange is adsorbed well on the photocatalysts surface. After sampling, 0.5 cm^3 NaF solution (0.5 M) was added to 1.0 cm^3 sample for desorption of methyl orange from the surface of the photocatalyst. The samples were centrifuged (Dragonlab, 15000 RPM) and catalysts were filtered with syringe filters (0.22 µm, FilterBiO, PVDF-L).

An Agilent 8453 UV-Vis spectrophotometer was used for spectrophotometry measurements. The absorbance of the samples was measured at 464 nm (the maxima of the methyl orange spectrum) in a 2.0 mm quartz cuvette. For separation of the intermediates and determination of methyl orange concentration in treated solution HPLC (Agilent 1100 HPLC equipped with a DAD detector) was used. As a stationary phase, a Kinetex 2.6u XB-C18 100A (Phenomenex) reverse phase column was applied, while the mobile phase consisted of 40 v/v% acetonitrile (VWR, UPLC-grade) and 60 v/v% formic acid solution (0.1%).

Results and discussion

Pure BiOCl, BiOI and BiOI/BiOCl photocatalysts with different molar ratios have been synthesized. In the case of the composites, the BiOI content changed from 5% to 95%. Adsorption generally has an important role during heterogeneous photocatalysis, especially in the case of dyes. The adsorption capacity of photocatalysts was determined in 0.5 g dm^{-3} suspension containing 1.0×10^{-4} M methyl-orange, after 2 h stirring in the dark. Adsorption equilibrium was reached after 30 min. The adsorption capacity of BiOI (29 % of the initial concentration of methyl orange; 1.16×10^{-3} mol/g) is highly exceed that of BiOCl (11 % of initial concentration methyl orange; 4.3×10^{-4} mol/g). The amount of adsorbed methyl orange increased with increasing the BiOI content, up to 80:20 molar ration of BiOI:BiOCl, when 37 % of methyl orange was adsorbed. After that, it slightly decreased (Fig. 2).

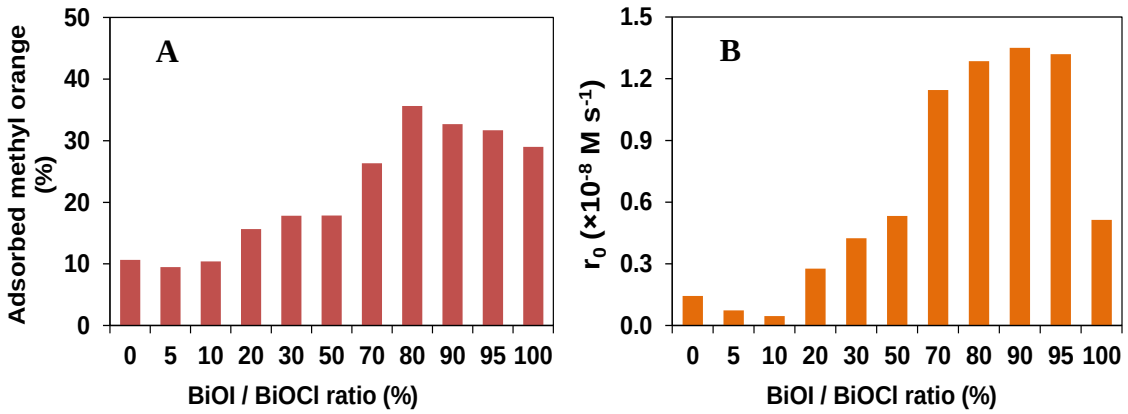

Figure 2. Adsorption capacity for methyl orange (A), and the transformation rates in the case of different BiOCl/BiOI composites

The photocatalytic activity of the synthetized materials were investigated under UV-LED radiation for 2 hours. The pure BiOCl showed negligible activity due to its wide band gap (3.2 eV), but methyl orange was effectively transformed in the case of BiOI. The highest transformation rates (r_0) were measured in the case of catalysts with 70-95 % BiOI/BiOCl molar ratios, as the initial reaction rates were nearly 3 times higher, than for BiOI. For further experiments, the sample containing 80:20 BiOI:BiOCl molar ratio was used.

The UV-Vis absorption spectra of the samples shifted to the shorter wavelengths during the transformation of methyl orange (Fig. 3/A). Due to the formation of products having significant absorbance at 464 nm, the concentration of methyl orange was determined by HPLC-DAD method. The transformation rate determined from chromatographic data was significantly higher, than the rate of absorbance decrease (Fig. 3/B).

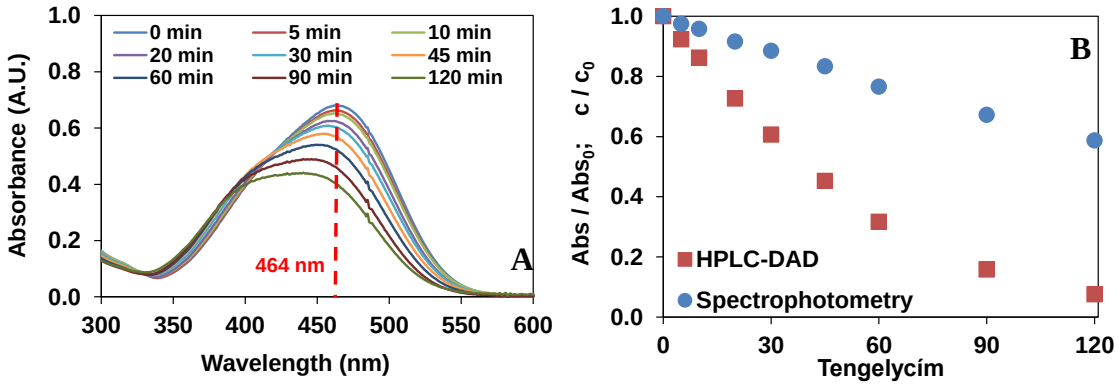

Figure 3. The absorption spectra (A), the relative absorbance of the treated solution and the relative concentration of methyl orange determined by HPLC-DAD method (B) in the case of 80:20 BiOI:BiOCl composite, under UV (398 nm) radiation

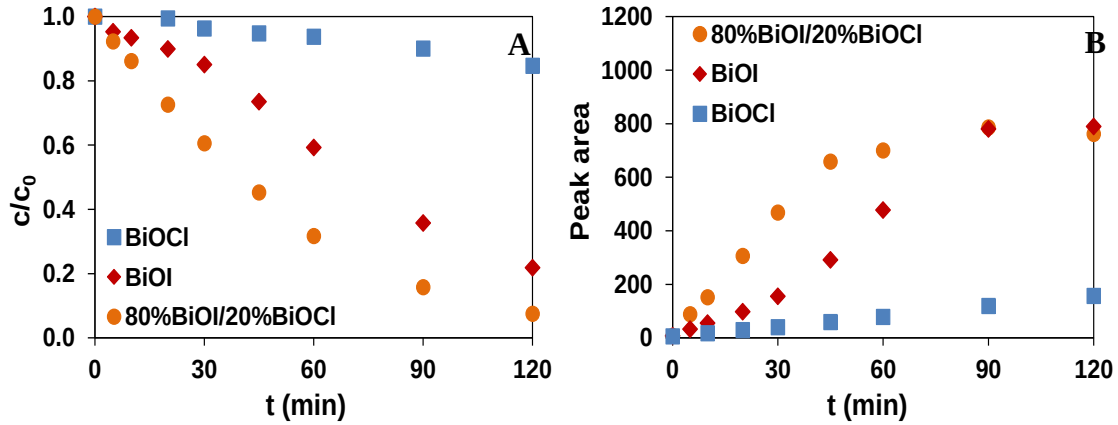

Figure 4. The relative concentration of methyl orange (A) and the peak area of its degradation product (B) as a function of time in the case of BiOI, BiOCl and 80:20 BiOI:BiOCl composite, under UV (398 nm) radiation

The transformation of methyl orange and the formation of its main product were compared in the case of BiOI, BiOCl, and the composite catalysts having 80:20 BiOI:BiOCl molar ratio (Fig. 4.). The activity of BiOCl was negligible, while BiOI and the composite showed similar results after 120 minutes. However, the transformation of methyl-orange, and the formation of the product started much slower in the case of BiOI than in the case of the composite catalyst: In the case of BiOI an induction period can be observed on the kinetic curve.

The measurements were performed with the cool white and warm white LED light sources (Fig. 5.). The composite photocatalyst was found to be the most effective in the case of each LEDs, but two times higher transformation rate was determined in the case of the UV radiation. Despite its wide band gap, BiOCl showed some photocatalytic activity, even under visible light radiation, which refers to the photosensitization in the transformation of methyl orange.

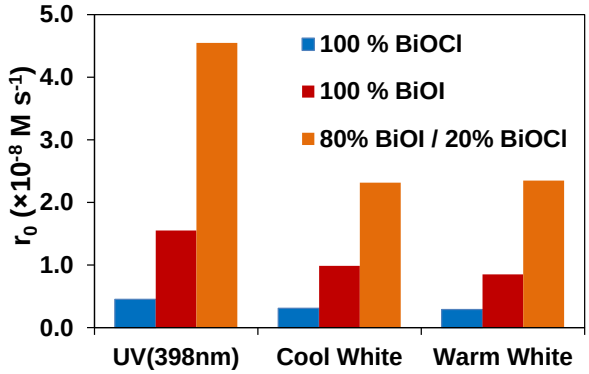

Figure 5. Reaction rate of methyl orange transformation in the case of BiOI, BiOCl and 80% BiOI-20% BiOCl and different UV and Vis-LED irradiation

Conclusions

BiOCl, BiOI and BiOCl/BiOI composite catalysts were synthetized with different molar ratios. The composite catalyst having 80:20 molar ratio of BiOI:BiOCl showed the best activity under both UV and visible irradiation. The adsorption capacity of the composite was similar to BiOI. The transformation of methyl orange was about two times higher for the composite photocatalyst than in the case of BiOI. The transformation rate of methyl orange was about two times higher under 398 nm irradiation, than under cool white or warm white irradiation.

Acknowledgements

This work was supported by the János Bolyai Research Scholarship of the Hungarian Academy of Sciences, and new national excellence program of the Ministry for Innovation and Technology (ÚNKP-20-2–SZTE-409, and ÚNKP-20-5-SZTE 639). This work was sponsored by the National Research, Development and Innovation Office-NKFI Fund OTKA, project number FK132742.

References

[1] A. S. Stasinakis, Global NEST J. (2008) **10**(3), 376-385.
[2] V. Vamathevan, R. Amal, D. Beydoun, G. Low, S. McEvoy, Journal Photochem. Photobiol A, (2002) 148, 233-245.
[3] F. Shen, L. Zhou, J. Shi, M. Xing J. Zhang, RSC Adv. (2015) 5, 4918-4925.
[4] S. Yao, J. Wang, X. Zhou, S. Zhou, X. Pu, W. Li, APTI (2020).
[5] T. B. Li, G. Chen, C. Zhou, Z. Y. Shen, R. C. Jin, J. Xue Sun, Dalton Trans. (2011) 40, 6751.
[6] Y. Zhong, Y. Liu, S. Wu, Y. Zhu, H. Chen, X. Yu, Y. Zhang, Frontiers in Chemistry (2018) 6, article 58.
[7] E. Bárdos, A. K. Király, Zs. Pap, L. Baia, S. Garg, K. Hernádi, Appl. Surf. Sci. (2019) 479, 745–756.

TRANSFORMATION OF SULFADIMETHOXINE AND TRIMETHOPRIM IN VUV RADIATED AQUEOUS SOLUTIONS

Luca Farkas, Máté Náfrádi, Anett Čovic, Tünde Alapi

Department of Inorganic and Analytical Chemistry, University of Szeged, H-6720 Szeged, Dóm tér 7, Hungary
email: fluca@chem.u-szeged.hu

Abstract

The combination of trimethoprim and sulfonamides (e.g., sulfadimethoxine) is often used as a growth promoter and antibiotic in animal husbandry. In this work, the efficiency of the low pressure mercury vapour (LPM) lamp, emits at 254 and 185 nm (UV/$VUV_{185\ nm}$ lamp) and Xe-excimer lamp, emits at 172 nm ($VUV_{172\ nm}$) photons were compared in the transformation of sulfadimethoxine (SDM) and trimethoprim (TRIM). Both light sources were effective on the transformation of both components. Although the VUV photon flux of the excimer lamp was significantly higher than of LPM lamp, there was no significant difference between the transformation rates of organic substances. The reason was most probably the extreme inhomogeneity of 172 nm radiated solution. $VUV_{185\ nm}$ photolysis increased the initial rate of transformation comparing to that determined in UV (254 nm) radiated solution mainly in the case of TRIM, and just slightly for SDM, probably because the direct UV photolysis is also effective for SDM transformation, opposite to the TRIM. The $VUV_{172\ nm}$ photolysis was found to be more effective in mineralization, for both compounds than UV/$VUV_{185\ nm}$ photolysis. Dissolved O_2 has significant effect only in the case of the UV/$VUV_{185\ nm}$ photolysis of TRIM.

Introduction

In recent decades, environmental protection has placed increasing emphasis on preventing the release of persistent, biologically active pollutants into the environment, in particular antibiotics, the inappropriate or excessive use of which poses a serious risk to public health. Human medicine are excreted from the urine and faces and discharged into wastewater, where conventional wastewater treatment plants are often unable to remove these biologically active organic contaminants [1]. Even though, the drug residues are present in very low concentrations in wastewater. Due to the limitations of conventional biological water treatment process, antibiotics can return to drinking water bases, so the drug loading of living organisms through water become continuous. Consequently, it is particularly important to investigate and develop additive water treatment processes, which are able to effectively remove the active pharmaceutical ingredients, and their residues from pre-treated wastewater.

In this study UV/$VUV_{185\ nm}$ and $VUV_{172\ nm}$ photolysis of SDM and TRIM were investigated and compared. The combination of SDM with TRIM is widely used for the treatment of infections in animal husbandry.

Trimethoprim is a widely used antibiotic drug since 1960's. It is commonly used with various sulfonamides together to treat urinary tract infections and it is effective to treat ear infections and diarrhea. Due to its extensive use, and hard biodegradability, it was detected in various waters e.g. rivers [2] or domestic wastewater [3].

Sulfadimethoxine is a long lasting sulfonamide antibiotic, which is used as a veterinary drug to treat urinary tract, enteric, or soft tissue infections. Due to the excessive use of sulfonamides (e.g. sulfadimethoxine), sulfadimethoxine was detected in many cases in various waters such as wastewater, ground water, or surface waters [4-6].

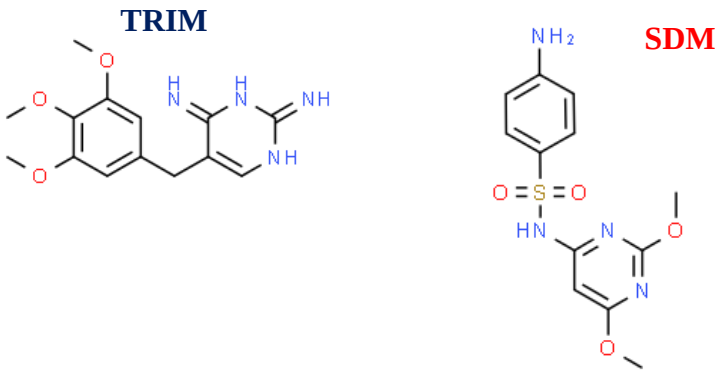

Fig. 1. Chemical structures of TRIM and SDM

Experimental

For the $VUV_{172\ nm}$ radiation Xe_2* excimer lamp (Radium Xeradex™, 130 mm long, 46 mm diameter, 20 W) was used, which was centred in a high purity silica quartz envelope (53 mm diameter), able to transmits the 172 nm light. The aqueous solution was circulated continuously (375 mL min^{-1}) between the reactor and the reservoir. Double walled, water cooled reactor was used, the temperature was set to 25 ± 0.5 °C. Samples were taken from the reservoir. The volume of the treated solution was 500 mL, the thickness of radiated water layer was 5 mm.

The low-pressure mercury vapour (LPM) lamp ($UV/VUV_{185\ nm}$ lamp GCL307T5VH/CELL, 227 mm arc length, produced by LightTech) was used for the UV/VUV (254 nm/185 nm) photolysis. The $UV/VUV_{185\ nm}$ lamp's envelope was made of synthetic quartz to be able to transmit the $VUV_{185\ nm}$ photons. Another LP lamp (UV lamp, GCL307T5L/CELL, 227 mm arc length, produced by LightTech) was used for UV photolysis. The parameters of the UV and $UV/VUV_{185\ nm}$ lamps were the same, but the envelope of UV lamp was made from commercial quartz, which absorbs the 185 nm light, but transmits the 254 nm UV light.

In the case of UV (254 nm), $VUV_{172\ nm}$ and $UV/VUV_{185\ nm}$ photolysis, O_2 or N_2 gas was bubbled continuously trough the solution. Gas bubbling was started at least 20 min before the measurement. SDM (Sigma-Aldrich, ≥98%) and TRIM (Sigma-Aldrich, ≥98.5%) solutions with initial 1.0×10^{-4} mol L^{-1} concentration were made in ultrapure MILLI-Q water (MILLIPORE Milli-Q Direct 8/16).

Separation of the aromatic components in the treated solutions was performed by Agilent 1100 type HPLC, equipped with diode array detector (DAD). For the analysis of sulfadimethoxine and its degradation products, Lichrospher 100, RP-18; 5 µm coloumn was used at 30 °C, the flow rate of eluent was 1.0 mL min^{-1}, and 20 µL sample was injected. The wavelength of the detection was 269 nm. For the analysis of trimethoprin and its degradation products, Kinetex 2.6u XB-C18 100A (Phenomenex) coloumn was used at 30 °C, the flow rate of eluent was 0.75 mL min^{-1}, and 20 µL sample was injected. The wavelength of the detection was 285 nm.

Results and discussion

In the case of the VUV photolysis, the 172 nm and 185 nm VUV light is absorbed by water to form reactive species, such as hydrogen radical (H•), hydroxyl radical (HO•) and with lower yield hydrated electron (e_{aq}^-) [2].

$$H_2O + h\nu\ (<190\ nm) \rightarrow H\bullet + HO\bullet \qquad \Phi(HO\bullet) = 0.33$$

$$H_2O + h\nu\ (<200\ nm) \rightarrow \{e^-, H_2O^+\} + H_2O \rightarrow \{e^-, H_2O^+\} + (H_2O) \rightarrow e_{aq}^- + HO\bullet + H_3O^+$$

$$\Phi(e_{aq}^-) = 0.045 - 0.05$$

There is a significant difference between the aqueous systems, radiated with 185 nm and 172 nm light. The molar absorbance of water at 172 nm, highly exceed (10.0 $M^{-1}cm^{-1}$) its molar absorbance at 185 nm (0.032 $M^{-1}cm^{-1}$). Consequently the 185 nm VUV photons are absorbed within 11 mm, while the 172 nm VUV photons are absorbed within 0.04 mm thin water layer. The VUV photon flux was determined with methanol actinometry, and was found to be 32 times higher (1.04×10^{-5} mol_{photon} s^{-1}) for the excimer lamp than for the LPM lamp (3.23×10^{-7} mol_{photon} s^{-1}). The UV photon flux was 3.70×10^{-6} mol_{photon} s^{-1}.

Table 1. shows the initial transformation rates and apparent quantum yields of TRIM and of SDM transformation, determined in UV, UV/$VUV_{185\ nm}$ and $VUV_{172\ nm}$ radiated solutions at 1.0×10^{-4} M initial concentration. The UV photolysis was effective for transformation of SDM; its transformation rate was almost the same than in UV/$VUV_{185\ nm}$ radiated solution. The TRIM practically does not transform in UV radiated solution. It can be explained by the significant difference between the molar absorbance of these compounds at 254 nm: TRIM: $\varepsilon_{254\ nm}$=4477.5 M^{-1} s^{-1} and SDM: $\varepsilon_{254\ nm}$=16050 M^{-1} s^{-1}. The transformation rate determined not only by the molar absorbance but also the quantum yield of the transformation, which is relatively high of SDM. The presence of 185 nm photons, which have a photon flux one magnitude higher than that of 254 nm light, dramatically increased the transformation rate of TRIM, but only slightly increased that of SDM, probably due to the contribution of the direct UV photolysis.

Table 1: The initial transformation rates of sulfadimethoxine (SDM) and trimethoprim (TRIM) at 1.0×10^{-4} M initial concentration

		UV O_2	UV N_2	UV/VUV O_2	UV/VUV N_2	VUV O_2	VUV N_2
SDM	r_0 ($\times10^{-7}$ M s^{-1})	1.35		1.70	1.46	1.39	1.21
	Φ	0.036		0.11	0.03	0.013	0.012
TRIM	r_0 ($\times10^{-7}$ M s^{-1})	0.07	0.004	0.93	0.46	1.39	1.39
	Φ	0.002	-	0.27	0.14	0.013	0.013

In the case of VUV photolysis, dissolved O_2 reacts with H•. By this way, H• transforms to less reactive HO_2/O_2•$^-$:

$$O_2 + H\bullet \rightarrow HO_2\bullet \qquad k = 2.1\times10^{10}\ M^{-1}\ s^{-1}$$

$$HO_2\bullet + H_2O \leftrightarrow H_3O^+ + O_2\bullet^- \qquad pK_a = 4.8$$

At the same time, through the formation of organic peroxyl (ROO•) radicals, O_2 opens up a new ways to transform organic substances, and generally increases the transformation rate. The transformation rate increases just slightly for SDM in the presence of O_2 (Fig 2 and Table 1). Probably the negative effect (elimination of H•) and the positive effect (formation of peroxyl radical) compensates each other's in this case. In contrast, dissolved O_2 doubled the transformation rate of TRIM in the case of UV/$VUV_{185\ nm}$ photolysis, while in the case of $VUV_{172\ nm}$ photolysis, O_2 has no effect (Fig 2 and Table 1). It has to be mention that, in 172 nm radiated aqueous solutions of organic substances, due to the extremely high HO• concentration close to the wall of the lamp, an O_2-depletion layer forms. Thus, the positive effect of O_2 via peroxyl radical formation is less pronounced, and the relative negative effect (due to the H• elimination) can be amplified.

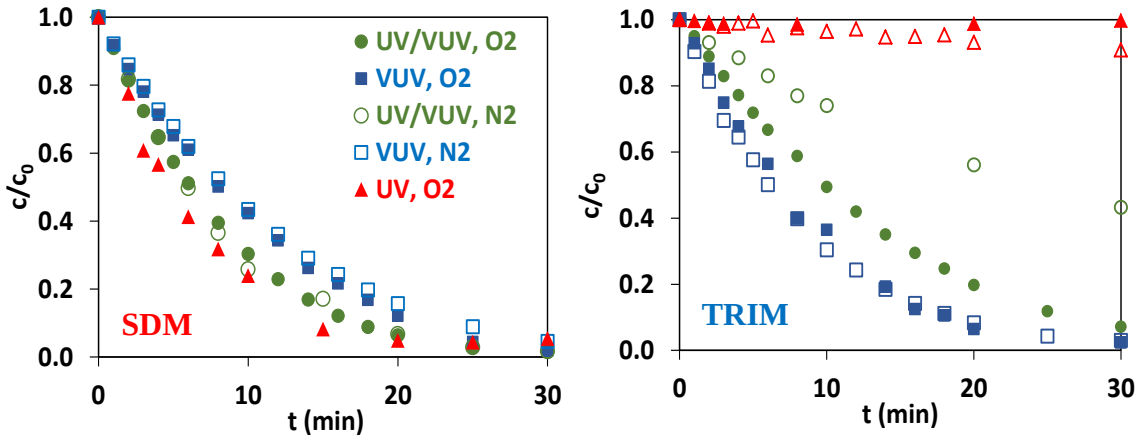

Fig 2. Relative concentration of SDM (a) and TRIM (b) versus time of irradiation in the case UV, UV/VUV$_{185\ nm}$ and VUV$_{172\ nm}$ photolysis

172 nm VUV photolysis enhanced the transformation comparing to the UV/VUV$_{185\ nm}$ photolysis in the case of TRIM, but in the case of SDM, the transformation was faster in UV/VUV$_{185\ nm}$ radiated solution. Results can be explained by the relative high contribution of the direct UV photolysis to the transformation of SDM in UV/VUV$_{185\ nm}$ radiated solution. There is no significant difference between the rate constants of these compounds with HO• ($k_{HO•+TRIM}$=8.13×10^9 M s^{-1} [7] and $k_{HO•+SDM}$=8.13×10^9 M s^{-1} [8]). The apparent quantum yield suggests that, the recombination of H• and HO• radicals in the photoreactive zone (0.04 mm) in the 172 nm irradiated solution is preferable to their reaction with organic matter, probably due to the extremely high concentration of these radicals and the lack of dissolved O_2. Both effects are negligible in 185 nm radiated solutions.

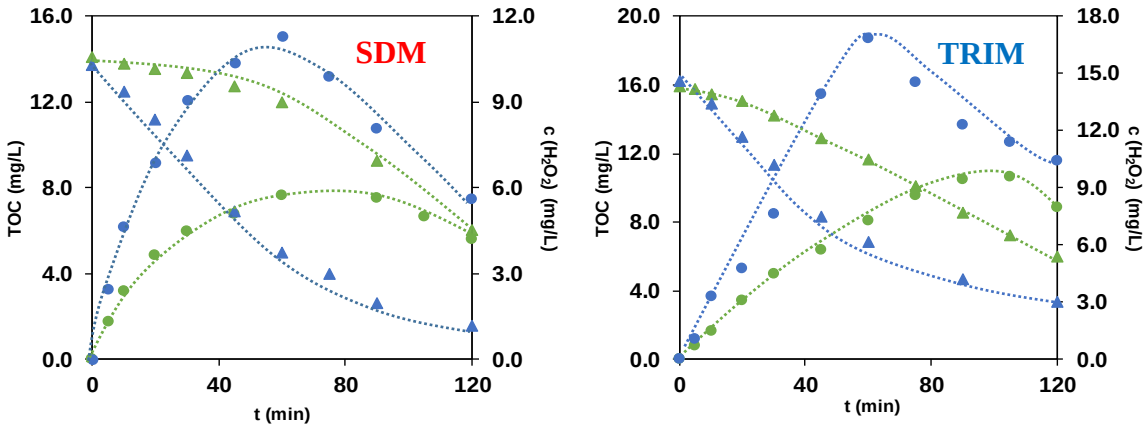

Fig 3. The concentration of TOC and H_2O_2 versus time of irradiation in the case of UV/VUV$_{185\ nm}$ (green) and VUV$_{172\ nm}$ (blue) photolysis of SDM (a) and TRIM (b)

In the case of UV/VUV$_{185\ nm}$ photolysis the decrease of TOC content starts with an induction period, which is much more pronounced for SDM (Fig. 3a). During this time in VUV$_{172\ nm}$ radiated solution the TOC decreases intensively. In both cases the VUV$_{172\ nm}$ photolysis was more effective for mineralization. The maximum value of H_2O_2 concentration is also higher in the case of the excimer lamp, than in the case of LP light, which proves a more intensive mineralization of the organic substances.

Conclusion

The UV, UV/VUV_{185nm}, and VUV_{185nm} photolysis are effective for the elimination of 5-FLU from aqueous solutions, the highest transformation rate was measured in the case of UV/VUV_{185nm} photolysis. Dissolved O_2 has no significant effect on the transformation rate even in the case of VUV_{172nm} photolysis. The highest mineralization rate was observed in the case of VUV_{172nm} photolysis. Although the photon flux of 172 nm light is much higher than of 185 nm light, the transformation is slower, partly because of the contribution of 254 nm in the case of UV/VUV_{185nm} photolysis, and partly because of the extreme inhomogeneity of 172 nm radiated aqueous solution.

Acknowledgements

This publication was supported by the János Bolyai Research Scholarship of the Hungarian Academy of Sciences, and new national excellence program of the Ministry for Innovation and Technology (ÚNKP-20-5-SZTE-639 and ÚNKP-20-3-SZTE-459). The authors thanks the financial support from the project Hungarian Scientific Research Fund (NKFI contract number FK132742)

References

[1] Zhang, R, Sun, P, Boyer, T.H., Zhao, L., Huang, C.H., Environ Sci Technol, 2015, 49 (5) 3056-3066
[2] Gałwa-Widera, M, Eds: Narasimha M., Prasad V., Vithanage M, Kapley A, Plant-based technologies for removal of pharmaceuticals and personal care products, Butterworth-Heinemann, 2019, 297-319
[3] Karthikeyan, K.G., Meyer, M.T., Sci Total Environ, 2006, 361(1–3), 196–207
[4] Wang, Z., Zhang, X.H., Huang, Y., Wang, H., China Environ. Pollut. 2015. 204, 223–232.
[5] García-Galán, M. J., Díaz-Cruz, S., Barcelo, D., Environ. Intern., 2011. 37 (2), 462–473.
[6] Pailler, J. Y., Krein, A., Pfister, L., Hoffmann, L., Guignard, C., Sci. Total Environ. 2009. 407, 4736–4743.
[7] Wojnárovits, L., Tóth T., Takács, E.; Crit Rev Environ Sci Technol, 2018, 48 (6) 575-613
[8] Boreen A.L., Arnold W.A., McNeill K., Environ Sci Technol, 2005, 15, 39 (10) 3630-3638

HERBS' PRODUCTS USED IN ANTIVIRAL PROTECTION AND THERAPY

Mirela Ahmadi, Ioan Peț, Lavinia Ștef, Nicolae Păcală, Gabi Dumitrescu, Liliana Ciochină-Petculescu, Dorel Dronca

Department of Biochemistry, Faculty of Bioengineering of Animal Resources, University of Agricultural Sciences and Veterinary Medicine of Banat "King Michael I of Romania", Calea Aradului No. 119, Timişoara - 300645, Romania
e-mail: *mirelaahmadi@gmail.com; ioan.petz@yahoo.com; ddronca@animalsci-tm.ro*

Abstract
Nowadays the existing antiviral prevention and/or treatments mostly lead sooner or later to viral resistance, viral re-emergence or viral lethargy. Thus, the present paper tries to find natural phytochemical products which can be used as an alternative and/or complementary protection and treatment in viral diseases. To be more effective, the essential oils and distilled products are proposed, because these are products richer in phytonutrients with potent antiviral activity. To be more trustful, the experiments follow the *in vivo* and *in vitro* tests, have to reveal the antiviral mechanisms, the involvement in the virus life cycle, and also to be tested for short-term and long-term positive and negative effects. Thus, different herbal medicines, spices, essential plants' oils and distilled products can be used in antiviral protection and/or treatment. Literature published data prove the benefic effects of some medicinal and aromatic plants' extracts as a phyto-therapeutic approach, even to SARS-CoV-1 (Severe Acute Respiratory Syndrome Coronavirus from 2013), MERS-CoV (Middle East Respiratory Syndrome Coronavirus from 2018), and also to the novel SARS-CoV-2 strains (Severe Acute Respiratory Syndrome Coronavirus from 2019). The complete work that has to be done remain the optimum composition of herbs extracts, the concentration, the extraction technique, the *in vivo a*nd *in vitro* tests – for short- and long-term effects. There have to be evaluated also the positive effects on the virus strains, and also the harmful action for the human and animal organisms.

Key words: plants' extracts, antiviral

FISH AND OTHER SPECIES WERE PERISHED FOR SOILING AND ECONOMY CLEARING IN TISZA RIVER AT LATEST DECADES

Viktoria Szuts[1, 2*], Fanny Wéber[1], Ferenc Otvos[3], Dimitra Eirini Farmaki[1,2], Ildikó Domonkos [2], András Blastyák [5], Kitty Berczes [2], Zita Szegletes[2], Bettina Ughy[2], Ottó Zsíros[2], Fanny Balog-Vig[2], József Csanádi[1], Antal Véha[1], Katalin Halasy[6], Ferenc Szabó[4], József Gál[4]

[1] *Department of Food and Engineering, Faculty of Engineer, University of Szeged, Szeged, Hungary,* [2] *Institute of Plant Biology, Biological Research Centre, Szeged, Hungary;* [3] *Institute of Biochemistry, Biological Research Centre, Szeged, Hungary,* [4] *Department of Economic and Rural Development, Faculty of Engineer, University of Szeged, Szeged, Hungary,* [5] *Institute of Genetics, Biological Research Centre, Szeged, Hungary;* [4] *Department of Anatomy and Histology, University of Veterinary Medicine, Budapest, Hungary.*
E-mail: szutsv@hotmail.com

Keywords: contamination, fresh water, bioremediation, Tisza River, heavy metal, bioindication

Abstract

Water pollution and remediation options for multi-source contaminations in freshwaters are happening sometimes, particularly in River Tisza after the cyanide and heavy metals spills of Romanian origin in 2000. The eco-toxicological effects, degradation and bioaccumulation rates of heavy metals have been followed in the next two years. Here the aim was to follow the bioremediation program and present the renewed economy of River Tisza. High concentration of arsenic, lead, mercury and cadmium was measured in the periphython and sediments samples both of the Rivers Tisza and Szamos. International rehabilitation program was planned and accomplished. Here we demonstrate the renewed economy of Tisza with living flora and fauna after 20 years, and the birth of day of May-fly again.

Introduction

Water pollution and remediation options for multi-source contaminations in fresh-waters are happening sometimes, particularly in River Tisza after the cyanide and heavy metals spills of Romanian origin in 2000. Chronic eco-toxicological effects, degradation and bioaccumulation rates of heavy metals have been followed in the next two years.

Changes in the composition of the phytoplankton are also in support of the affect that the algae do not only utilize mineral salts but also amino acids, carbohydrates, vitamins of decomposing organic materials as well as plant hormones. This should be also considered when establishing the indicator value of algae. Saprophytes and trophity are mutually related not only because the organic materials producing saprophytes increase trophity, but also because the algae are able to directly incorporate some of the organic materials. Mixotrophy can also exhibit differences within species [1].

Periphyton plays role in bio-accumulation. Furthermore, its suitability in bioindication biological monitoring is also applied. This is an essential nutrient source for the zoo-organisms, *i.e.* for the animals of other heterotrophic communities, such as some fish. In the Körtvélyes and Mártély backwaters of the River *Tisza* the alga flora have been studied from 1940 and 1982 sezonaly because the *alga* population changed. Periphyton is a complex of organisms that produce organic material and oxygen by binding light energy and taking up inorganic plant nutrients. Periphyton plays a bioaccumulation role, as well as on its suitability for bioindication and applied in biological monitoring. This is an essential nutrient source for the zoo-organisms, *i.e.* for the animals of other heterotrophic communities, such as some fish.

The littoral zone of Tisza and Szamos, as a transitional region between watercourses and lands, had remarkable conservational and environmental significance too. In the Körtvélyes and Mártély backwaters of the Tisza *River*, the alga flora has been studied from 1940 and 1982 seasonally because the alga population changed but also the fauna. Periphyton is a complex of organisms that produce organic material and oxygen by binding light energy and taking up inorganic plant nutrients.

In this work our aim was to follow the bioremediation program and present the renewed economy of River Tisza with living flora and fauna after 20 years. Furthermore we are looking into the data given on the results of eco-toxicological tests from sediment and water samples nowadays.

Results

Here we demonstrate the renewed economy of *Tisza* with living flora and fauna after 20 years. International rehabilitation program was planned and accomplished. They monitored several contamination effects where the aquatic ecosystem was considered of top priority. High concentration of arsenic, lead, mercury and cadmium was measured in the periphython and sediments samples both of the Rivers Tisza and Szamos. We also followed the birth of May-fly from the bridge in Szeged again (Figure 1 and 2).

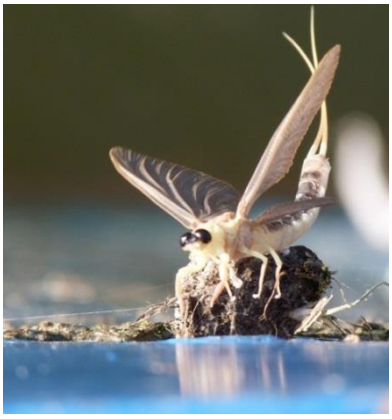

Figure 1: The birth of day, May-fly (*Palingenia longicauda L.)* in Szeged, 2011.

Some metals, hormones or their derivatives can serve as a stress pollution causing disaster in the rivers. After the disaster of Tisza River it was monitored several contamination effects where the aquatic ecosystem was considered of top priority. The littoral zone of Tisza and Szamos, as a transitional region between watercourses and lands, had remarkable conservational and environmental significance too. 17beta-Estradiol (E2) and 17alpha-ethinyl estradiol (EE2), which are environmental estrogens, have been determined with LC-MS in fresh water [2]. Their sensitive analysis needs derivatization and therefore it is very hard to achieve in multiresidue screening. Samples were analyzed from all the large and a few small rivers (River Danube, Drava, Mur, Sava, Tisza, and Zala) of the Carpathian Basin and from Lake Balaton in Hungary. Average levels of E2 and EE2 were 0.61 and 0.084 ng/L, respectively, in rivers, and Lake Balaton together (without city canal water). EE2 was less abundant, but it was still present in almost all of the samples.

Figure 2: The Tisza River at 2018.

The contamination of heavy metals was measured by Sakan et al. [3] in the sediments taken from the Tisza River and its tributaries. The chemical fractionation of Ni, Cu, Zn, Cr, Pb, Fe, and Mn, carried out by using the modified Tessier method, points to different substrates and binding mechanisms of Cu, Zn and Pb in sediments of the tributaries and sediments of the Tisza River. The calculated enrichment factors (EF) indicated that metal contamination (Cu, Pb, Zn and Cr) was recorded in the sediments of the Tisza River, while no indications of pollution were detected in the tributaries of the Tisza River and the surrounding pools. The maximum values of the EF were close to 6 for Cu and Pb and close to 4.5 for Zn (moderate enrichment). [4] The final conclusion is that the contamination of the Tisza River from the mining area in Northern Romania has been continuous and is still ongoing.

The elements were measured using microwave plasma-atomic emission spectrometry (MP-AES): Cu, Cr, Ba, Fe, Mn, Pb, Sr, and Zn by Balogh et al. [5] Among the oxbows studied, one was a protected oxbow, three were used for fishing, and one was contaminated with sewage. Our results indicated that the year of contamination is still observable in the vertical profile of the sediment cores. In the case of Cu, Pb, and Zn, the contamination which originated in year 2000 was detected in the layers of the sediment cores. The contamination levels of Cu, Pb, and Zn were high or moderate in the studied oxbows. All oxbows were moderately contaminated by Mn, and for Fe in the protected oxbow, one fishing oxbow, and the sewage-contaminated oxbow. In the fishing oxbows, a low level of was found for Fe and Sr. The level of Sr was low in the protected oxbow. The pollution index scores indicated that the contamination level for Ba and Cr was low in the sediment cores of the oxbows. These results indicated that the contamination of the Tisza River from the mining area in Northern Romania has been continuous and is still ongoing [6].

Nowadays we have a possibility using new insight into the biological and physiological cellular responses to arousal stress.

In the beach of river pollutants, arousal stress can significantly modify the antioxidative defense system (AOS) response of hibernators during recovery from hibernation (i.e., frogs, in spring). Prokić et al. [7] have determined the relationship between seasonal variations of accumulated metals and AOS parameters in the skin and muscle of two frog species from the *Pelophylax esculentus* complex (*P. ridibundus and P. esculentus*) inhabiting two localities (the Danube-Tisza-Danube canal and the Ponjavica River) with different levels of pollution during pre- and post-hibernation periods, respectively, in autumn and spring. The results showed that even though there were differences in the concentrations of accumulated metals and antioxidative defense system, the AOS parameters of localities and species, the frogs displayed the same patterns of AOS variations during seasons, with a higher AOS response observed in spring. The parameters, *i.e.* SH groups, GSH, GR and SOD had contributed most rather than others. This indicates that the oxidative stress during the post-hibernation period was mainly caused by the organisms' recovery from hibernation, and the accumulated metals did not significantly modify the AOS response. Besides Hungarian resources, significant amount of

support was received from foreign countries to recover the flora and fauna, from algae through higher animals, of a living river.

Conclusion

The cleanness of *Tisza River* is satisfying momentary because after 10 and 20 years of the disaster as shown by most of the species of flora and fauna as indicators of living river. The more thorough study of the backwaters of the River Tisza is ongoing. It would be more useful to compare the phytoplankton of the backwaters of the Tisza with plants, one another, with that of the river itself.. In the latest years several studies have been conducted to investigate the state of the River Tisza. Scientist evaluated background values which may affect assessing the anthropogenic heavy metal pollution in sediments from Tisza River in Serbia. This paper is underlining the significance of the *River Tisza* in our life. This is maybe the same situation in the area of Szeged and Csongrad county sides in Hungary too.

Acknowledgement

This work was supported by the projects NKFIH-112688, OTKA K112688 and EFOP-3.6.2-16-2017-00009. The authors are thankful for Prof. Dr. Győző Garab for advice in collecting data and supporting the project. We are glad to thank to many people for their continuous efforts to save and improve the quality of the nicest piece of our environment, River Tisza.

References

[1] Kiss I. Tiscia (Szeged) 1982, Vol. XVII, pp. 51-65

[2] Avar P, Zrínyi Z, Maász G, Takátsy A, Lovas S, G-Tóth L, Pirger Z. Environ Sci Pollut Res Int. 2016; 23(12):11630-8

[3] Sakan SM, Dordević DS, Manojlović DD, Predrag PS. J Environ Manage 2009, 90(11):3382-90

[4] Gál József, IV.KÁRPÁT-MEDENCEI KÖRNYEZETTUDOMÁNYI KONFERENCIA, 2008, I Kötet, Debrecen

[5] Balogh Z, Harangi S, Gyulai I, Braun M, Hubay K, Tóthmérész B. Simon E. Environ Sci Pollut Res Int. 2017; 24(5):4851-4859

[6] Štrbac S, Kašanin Grubin M, Vasić N. Environ Geochem Health. 2018;40(4):1247-1263

[7] Prokić MD, Borković-Mitić SS, Krizmanić II, Mutić JJ, Gavrić JP, Despotović SG, Gavrilović BR, Radovanović TB, Pavlović SZ, Saičić ZS. Comp Biochem Physiol C Toxicol Pharmacol. 2017; 202:19-25

TRANSPORT STUDY OF KYNURENIC ACID AND ITS NEWEST DERIVATIVES THROUGH AN IN VITRO MODEL OF THE BLOOD-BRAIN BARRIER USING TARGETED UHPLC-MS\MS

Noémi Kmetykó[1], Imola Wilhelm[2], István Ilisz[1], Róbert Berkecz[1]

[1]*Institute of Pharmaceutical Analysis, University of Szeged, H-6720, Szeged, Somogyi u. 4, Hungary*
[2]*Institute of Biophysics, Biological Research Centre, H-6726, Szeged, Temesvári krt. 62, Hungary*
e-mail: berkecz.robert@pharm.u-szeged.hu

Abstract
We have developed a targeted UHPLC-ESI–MS/MS method for the quantification of kynurenic acid (KYNA) and its derivatives from biological samples. The samples were gained from in vitro permeability assay. We have found that the transportation of the derivatives through the blood-brain barrier is better than KYNA.

Introduction
Since kynurenic pathway has a great influence on the central nervous system, interruption of its chemical balance could lead to the development of neurodegenerative diseases. The kynurenics that have positive effect can get through the blood-brain barrier only in a very minimal rate, so restoring the balance is difficult. Nowadays best possible therapy seems to be the use of derivatives of **KYNA** as active ingredient.

Experimental
The method development and its application was preceded by an *in vitro* permeability assay using primary rat brain endothelial cells. The level of **KYNA** and its derivatives (**SZR104, SZR72**) that has passed through the assay was determined by a targeted ultra-high performance liquid chromatography combined with electrospray ionisation triple quadrupole tandem mass spectrometry (UHPLC-ESI-MS/MS) method. For quantitative analysis, external calibration was applied using **SZR73** as an internal standard.

Results and discussion
The main parameters of the sample preparation and the targeted UHPLC-ESI-MS/MS method were optimized. The developed procedures were successfully applied for quantification of **KYNA**, **SZR104** and **SZR72** in the biological samples. Overall, the derivatives **have** significantly better transportation through the blood-brain barrier than the **KYNA**. The amount of the transferred compounds was the following in descending order: **SZR104**, **SZR72** and **KYNA.**

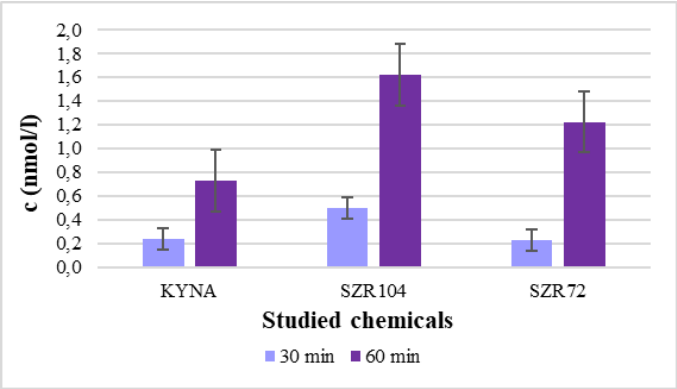

Figure 1. The amount of transferred chemicals *in vitro* permeability assay

Conclusion

Using the developed method on the biological samples, we have found that the amount of transported kynurenics is linked to the duration of the assay and the chemical modification of **KYNA** improved the permeability.

Acknowledgements

This research was supported by the EU-funded Hungarian grant EFOP-3.6.1-16-2016-00008 and GINOP-2.3.2-15-2016-00034 EU.